

NANO-(BIO)CATALYSIS IN LIGNOCELLULOSIC BIOMASS VALORIZATION

EDITED BY: Rafael Luque, Christophe Len and Konstantinos Triantafyllidis
PUBLISHED IN: Frontiers in Chemistry





frontiers

Frontiers Copyright Statement

© Copyright 2007-2019 Frontiers Media SA. All rights reserved.

All content included on this site, such as text, graphics, logos, button icons, images, video/audio clips, downloads, data compilations and software, is the property of or is licensed to Frontiers Media SA ("Frontiers") or its licensees and/or subcontractors. The copyright in the text of individual articles is the property of their respective authors, subject to a license granted to Frontiers.

The compilation of articles constituting this e-book, wherever published, as well as the compilation of all other content on this site, is the exclusive property of Frontiers. For the conditions for downloading and copying of e-books from Frontiers' website, please see the Terms for Website Use. If purchasing Frontiers e-books from other websites or sources, the conditions of the website concerned apply.

Images and graphics not forming part of user-contributed materials may not be downloaded or copied without permission.

Individual articles may be downloaded and reproduced in accordance with the principles of the CC-BY licence subject to any copyright or other notices. They may not be re-sold as an e-book.

As author or other contributor you grant a CC-BY licence to others to reproduce your articles, including any graphics and third-party materials supplied by you, in accordance with the Conditions for Website Use and subject to any copyright notices which you include in connection with your articles and materials.

All copyright, and all rights therein, are protected by national and international copyright laws.

The above represents a summary only. For the full conditions see the Conditions for Authors and the Conditions for Website Use.

ISSN 1664-8714

ISBN 978-2-88945-772-4

DOI 10.3389/978-2-88945-772-4

About Frontiers

Frontiers is more than just an open-access publisher of scholarly articles: it is a pioneering approach to the world of academia, radically improving the way scholarly research is managed. The grand vision of Frontiers is a world where all people have an equal opportunity to seek, share and generate knowledge. Frontiers provides immediate and permanent online open access to all its publications, but this alone is not enough to realize our grand goals.

Frontiers Journal Series

The Frontiers Journal Series is a multi-tier and interdisciplinary set of open-access, online journals, promising a paradigm shift from the current review, selection and dissemination processes in academic publishing. All Frontiers journals are driven by researchers for researchers; therefore, they constitute a service to the scholarly community. At the same time, the Frontiers Journal Series operates on a revolutionary invention, the tiered publishing system, initially addressing specific communities of scholars, and gradually climbing up to broader public understanding, thus serving the interests of the lay society, too.

Dedication to Quality

Each Frontiers article is a landmark of the highest quality, thanks to genuinely collaborative interactions between authors and review editors, who include some of the world's best academicians. Research must be certified by peers before entering a stream of knowledge that may eventually reach the public - and shape society; therefore, Frontiers only applies the most rigorous and unbiased reviews.

Frontiers revolutionizes research publishing by freely delivering the most outstanding research, evaluated with no bias from both the academic and social point of view. By applying the most advanced information technologies, Frontiers is catapulting scholarly publishing into a new generation.

What are Frontiers Research Topics?

Frontiers Research Topics are very popular trademarks of the Frontiers Journals Series: they are collections of at least ten articles, all centered on a particular subject. With their unique mix of varied contributions from Original Research to Review Articles, Frontiers Research Topics unify the most influential researchers, the latest key findings and historical advances in a hot research area! Find out more on how to host your own Frontiers Research Topic or contribute to one as an author by contacting the Frontiers Editorial Office: researchtopics@frontiersin.org

NANO-(BIO)CATALYSIS IN LIGNOCELLULOSIC BIOMASS VALORIZATION

Topic Editors:

Rafael Luque, Universidad de Córdoba, Spain; Peoples' Friendship University of Russia (RUDN University), Russia

Christophe Len, Chimie ParisTech, CNRS, Institut de Recherche de Chimie Paris, PSL Research University, Université de Technologie de Compiègne (Sorbonne Universités), France

Konstantinos Triantafyllidis, Aristotle University of Thessaloniki, Greece

The valorization of lignocellulosic biomass, in the form of forest and agricultural wastes, industrial processing side-streams, and dedicated energy crops, toward chemicals, fuels and added-value products has become a major research area with increasing exploitation potential. The efficient and tailored depolymerization of biomass or its primary structural components (hemicellulose, cellulose, and lignin) to platform chemicals, i.e., sugars, phenolics, furans, ketones, organic acids, etc. is highly dependent on the development of novel or modified chemo- and bio-catalytic processes that take into account the peculiarities and recalcitrance of biomass as feedstock, compared for example to petroleum fractions.

The present Research Topic in *Frontiers in Chemistry*, Section of Green and Sustainable Chemistry, entitled "Nano-(bio)catalysis in lignocellulosic biomass valorization" aims to further contribute to the momentum of research and development in the (bio) catalytic conversion of biomass, by featuring original research papers as well as two review papers, authored and reviewed by experts in the field. The Research Topic addresses various representative reactions and processes in biomass valorization, highlighting the importance of developing novel, efficient and stable nano-(bio) catalysts with tailored properties according to the nature of the reactant/feedstock and the targeted products.

Citation: Luque, R., Len, C., Triantafyllidis, K., eds. (2019). Nano-(Bio)Catalysis in Lignocellulosic Biomass Valorization. Lausanne: Frontiers Media.

doi: 10.3389/978-2-88945-772-4

Table of Contents

- 05 Editorial: Nano-(Bio)Catalysis in Lignocellulosic Biomass Valorization**
Rafael Luque, Christophe Len and Konstantinos Triantafyllidis
- 08 Lignocellulosic Biomass Transformations via Greener Oxidative Pretreatment Processes: Access to Energy and Value-Added Chemicals**
Walter Den, Virender K. Sharma, Mengshan Lee, Govind Nadadur and Rajender S. Varma
- 31 Hydrolysis of Hemicellulose and Derivatives—A Review of Recent Advances in the Production of Furfural**
Frederic Delbecq, Yantao Wang, Anitha Muralidhara, Karim El Ouardi, Guy Marlair and Christophe Len
- 60 Mechanocatalytic Depolymerization of Cellulose With Perfluorinated Sulfonic Acid Ionomers**
Ayman Karam, Prince N. Amaniampong, José M. García Fernández, Claudio Oldani, Sinisa Marinkovic, Boris Estrine, Karine De Oliveira Vigier and François Jérôme
- 69 Fine-Tuned Enzymatic Hydrolysis of Organosolv Pretreated Forest Materials for the Efficient Production of Cellobiose**
Anthi Karnaouri, Evangelos Topakas, Leonidas Matsakas, Ulrika Rova and Paul Christakopoulos
- 86 Silylated Zeolites With Enhanced Hydrothermal Stability for the Aqueous-Phase Hydrogenation of Levulinic Acid to γ -Valerolactone**
Hue-Tong Vu, Florian M. Harth and Nicole Wilde
- 95 Vapor-Phase Hydrogenation of Levulinic Acid to γ -Valerolactone Over Bi-Functional Ni/HZSM-5 Catalyst**
Margarita Popova, Petar Djinović, Alenka Ristić, Hristina Lazarova, Goran Dražić, Albin Pintar, Alina M. Balu and Nataša Novak Tušar
- 107 Physico-Chemical Properties of MgGa Mixed Oxides and Reconstructed Layered Double Hydroxides and Their Performance in Aldol Condensation of Furfural and Acetone**
Oleg Kikhtyanin, Libor Čapek, Zdeněk Tišler, Romana Velvarská, Adriana Panasewicz, Petra Diblíková and David Kubička
- 124 Temperature Dependence of Single Step Hydrodeoxygenation of Liquid Phase Pyrolysis Oil**
Klara Treusch, Nikolaus Schwaiger, Klaus Schlackl, Roland Nagl, Peter Pucher and Matthäus Siebenhofer
- 132 Catalytic Fast Pyrolysis of Kraft Lignin With Conventional, Mesoporous and Nanosized ZSM-5 Zeolite for the Production of Alkyl-Phenols and Aromatics**
Polykarpos A. Lazaridis, Apostolos P. Fotopoulos, Stamatia A. Karakoulia and Konstantinos S. Triantafyllidis

153 One-Pot Enzymatic Production of Lignin-Composites

Sabina Ion, Cristina Opris, Bogdan Cojocaru, Madalina Tudorache, Irina Zgura, Aurelian C. Galca, Adina M. Bodescu, Madalin Enache, Gabriel-Mihai Maria and Vasile I. Parvulescu

162 Efficient Mechanochemical Bifunctional Nanocatalysts for the Conversion of Isoeugenol to Vanillin

Somayeh Ostovar, Ana Franco, Alain R. Puente-Santiago, María Pinilla-de Dios, Daily Rodríguez-Padrón, Hamid R. Shaterian and Rafael Luque



Editorial: Nano-(Bio)Catalysis in Lignocellulosic Biomass Valorization

Rafael Luque^{1,2}, Christophe Len^{3,4} and Konstantinos Triantafyllidis^{5*}

¹ Departamento de Química Orgánica, Universidad de Córdoba, Córdoba, Spain, ² Peoples' Friendship University of Russia (RUDN University), Moscow, Russia, ³ Chimie ParisTech, CNRS, Institut de Recherche de Chimie Paris, PSL Research University, Paris, France, ⁴ Centre de Recherche Royallieu, Université Technologie de Compiègne (Sorbonne Universités), Compiègne, France, ⁵ Department of Chemistry, Aristotle University of Thessaloniki, Thessaloniki, Greece

Keywords: lignocellulosic biomass, (bio)catalysis, biofuels, platform chemicals, added value products

Editorial on the Research Topic

Nano-(bio)catalysis in Lignocellulosic Biomass Valorization

The valorization of lignocellulosic biomass, in the form of forest and agricultural wastes, industrial processing side-streams, and dedicated energy crops, toward chemicals, fuels and added-value products has become a major research area with increasing exploitation potential (Lange, 2007; Zhou et al., 2011; Tuck et al., 2012). The efficient and tailored depolymerization of biomass or its primary structural components (hemicellulose, cellulose, and lignin) to platform chemicals with varying functionalities, i.e., sugars, phenolics, furans, ketones, organic acids, etc. is highly dependent on the development of novel or modified chemo- and bio-catalytic processes that take into account the peculiarities and recalcitrance of biomass as feedstock, compared for example to petroleum fractions (Gallezot, 2008; Serrano-Ruiz et al., 2011). In many cases, in order to reach the final product, a series of catalytic reactions/process should be applied in a cascade or “one-pot” mode. A representative example is the bio-based polymer PEF (polyethylene furanoate) which can replace petroleum-derived PET (polyethylene terephthalate) for the production of plastics, where the following sequence of reactions should occur: hydrolysis of cellulose to glucose, isomerization of glucose to fructose, dehydration of fructose to hydroxymethylfurfural (HMF), oxidation of HMF to 2,5-furandicarboxylic acid (FDCA), poly-condensation with ethylene glycol (Avantium¹).

The most important reactions in biomass conversion include hydrolysis, isomerization, dehydration, hydrogenation, hydrodeoxygenation, hydrogenolysis, oxidation, esterification, ketonization, condensation, and others. Different types of homogeneous and heterogeneous catalysts, as well as biocatalysts (enzymes), with single or dual functionalities (i.e., acidic and hydrogenating, as for example in the acidic zeolite supported Pd, Pt, Ni, etc. catalysts) have been reported so far in the literature, ranging from fundamental catalyst design, to combined optimization of catalyst properties and reaction conditions, to pilot scale validation (Serrano-Ruiz et al., 2011; Zhou et al., 2011; Triantafyllidis et al., 2013). Photocatalysis, as well as alternative energy sources (plasma, microwave, and ultrasound) have also been explored for the catalytic conversion of biomass and its derivatives (Colmenares and Luque, 2014; Granone et al., 2018).

Based on these premises, the present Special Issue in *Frontiers in Chemistry, Section of Green and Sustainable Chemistry*, entitled “Nano-(bio)catalysis in lignocellulosic biomass valorization” aims to further contribute to the momentum of research and development in the (bio)catalytic conversion of biomass, by featuring original research papers as well as two review papers, authored and reviewed by experts in the field.

¹Avantium. Available online at: <https://www.avantium.com/xy/xy-technology/>

OPEN ACCESS

Edited by:

Steve Suib,
University of Connecticut,
United States

Reviewed by:

Renato Grillo,
Universidade Estadual Paulista Júlio
de Mesquita Filho (UNESP), Brazil

*Correspondence:

Konstantinos Triantafyllidis
ktrianta@chem.auth.gr

Specialty section:

This article was submitted to
Green and Sustainable Chemistry,
a section of the journal
Frontiers in Chemistry

Received: 23 September 2018

Accepted: 06 November 2018

Published: 27 November 2018

Citation:

Luque R, Len C and Triantafyllidis K
(2018) Editorial: Nano-(Bio)Catalysis in
Lignocellulosic Biomass Valorization.
Front. Chem. 6:577.
doi: 10.3389/fchem.2018.00577

The first review paper provided a comprehensive overview of the recent research on chemical oxidative techniques for the pretreatment of lignocellulosics with the explicit aim to rationalize the objectives of the biomass pretreatment step and the problems associated with the conventional processes (Den et al.). The mechanisms of reaction pathways, selectivity and efficiency of end-products obtained using greener processes such as ozonolysis, photocatalysis, oxidative catalysis, electrochemical oxidation, and Fenton or Fenton-like reactions, as applied to depolymerization of lignocellulosic biomass were summarized with deliberation on future prospects of biorefineries with greener pretreatment processes in the context of the life cycle assessment.

The second review paper discussed the hydrolysis of hemicellulose and the recent advances in the production of furfural (Delbecq et al.). More specifically, the review discussed advances obtained in major production pathways recently explored, splitting them in the following categories: (i) non-catalytic routes, like use of critical solvents or hot water pretreatment, (ii) use of various homogeneous catalysts like mineral or organic acids, metal salts, or ionic liquids, (iii) feedstock dehydration making use of various solid acid catalysts; (iv) feedstock dehydration making use of supported catalysts, (v) other heterogeneous catalytic routes. The paper also briefly overviewed current understanding of furfural chemical synthesis and its underpinning mechanism.

The topic of efficient and controlled cellulose hydrolysis, not using enzymes or strong inorganic acids, has attracted considerable interest. To this end, one of the original research papers of this Special Issue focused on the mechanocatalytic depolymerization of cellulose with perfluorinated sulfonic acid ionomers (Karam et al.). Very high yields of water soluble sugars (90–97%), mostly as oligosaccharides with a degree of polymerization (DP) up to 11, were obtained under optimized conditions using Aquivion PW98 and PW66, respectively, as solid acid catalysts.

Although, homogeneous and heterogeneous chemo-catalysis can offer high reaction rates as well as other benefits, enzymatic catalysis provides exceptionally high selectivities to the desired products. In a related paper of this issue, it was shown how the enzymatic hydrolysis of organosolv pretreated forest materials can be fine-tuned toward the efficient production of cellobiose, a non-digestible oligosaccharide (NDO), which together with other cello-oligosaccharides (COS), are considered as prebiotic candidates that have been related to the prevention of intestinal infections and other disorders for both humans and animals (Karnaouri et al.). In this work, the heterologous expression and characterization of two Cellobiohydrolases (CBHs) from the filamentous fungus *Thermothelomyces thermophila*, and their synergism with endoglucanases (EGs) for cellobiose release from organosolv pretreated spruce and birch, was systematically studied and discussed.

Levulinic acid, being produced from HMF, has been recognized as a very important platform chemical that can be catalytically converted further to a series of functional chemicals. In the present special issue, two papers have focused on the hydrogenation of levulinic acid toward γ -Valerolactone, another

very important chemical with a wide range of uses. The first paper deals with the development of silylated zeolitic catalysts (3 wt.% Pt on zeolite Y) with enhanced hydrothermal stability for the aqueous-phase hydrogenation of levulinic acid to γ -Valerolactone (GVL) (Vu et al.). It was shown that by the use of trichlorosilanes as silylating agents, the hydrothermal stability of zeolite Y can be improved significantly, although an inhibition in the yield of GVL was observed due to blockage of the pores by the silane. The second relevant paper presents a study of nickel modified zeolite optimization as bi-functional catalyst (Ni/HZSM-5) for the vapor-phase hydrogenation of levulinic acid to GVL (Popova et al.). The content and state of nickel and its interaction with the zeolite were critical parameters affecting both the acidity of the zeolite as well as the reducibility of Ni. At the best case, the authors reported 99% conversion of levulinic acid and 100% selectivity to GVL at 320°C.

Aldol condensation and C-C coupling reactions in general are also very important in biomass valorization, especially when the targeted products are hydrocarbon based transportation fuels, such as gasoline and diesel. In a relevant paper of this issue, the physico-chemical properties of MgGa mixed oxides derived from the corresponding Layered Double Hydroxides (LDHs), as well as of their reconstructed layered analogs, were studied and correlated to their performance in aldol condensation of furfural and acetone (Kikhtyanin et al.). It was shown that the basicity and the textural properties of the MgGa materials determined their catalytic activity and selectivity while their properties resembled those of MgAl hydrotalcite-based materials.

Fast pyrolysis is one of the most promising thermochemical processes for the direct conversion of biomass into a liquid product, the so called pyrolysis oil or biooil, with gases and char being formed to a lesser extent. Biooil contains water and its organic fraction consists of phenolics, ketones, aldehydes, acids, sugars, and other compounds in minor amounts. It is relatively acidic, unstable and not miscible with petroleum fractions, and needs to be upgraded, usually via (hydro)deoxygenation. One of the papers in this issue, describes the continuous hydrodeoxygenation (HDO) of biooil with an *in situ* sulfided metal oxide catalyst and the effect of reaction temperature (350, 375, and 400°C) on the deoxygenation activity (Treusch et al.).

Lignin has gained increased interest within the biorefinery concept as it can act as source of high added value phenolics and aromatics. It can be depolymerized via various types of hydrothermal processes, such as reductive or oxidative hydrogenolysis, or by fast pyrolysis which produces a biooil that contains essentially various alkoxy-phenols. In a relevant paper, the fast pyrolysis of a kraft lignin (byproduct of the production of cellulose pulp from biomass via the Kraft processes) was compared to the catalytic fast pyrolysis using conventional, mesoporous, and nanosized ZSM-5 zeolite, aiming at the production of a partially deoxygenated biooil, enriched in alkyl-phenols and aromatics (BTX and naphthalenes) (Lazaridis et al.). The effect of ZSM-5's acidity and hierarchical porosity on product yields, selectivity of

various compounds and resistance to coking was studied and discussed. In another paper of this issue, monolignols such as sinapyl (SA) and coniferyl (CA) alcohols were linked together with caffeic acid (CafAc) via enzymatic catalysis affording a polymeric network similar with natural lignin (Ion et al.). The production of the valuable compound vanillin from isoeugenol under mild conditions was investigated in another paper included in this special issue, using bifunctional nanocatalysts (iron on sulphonated SBA-15) which were prepared by an alternative mechanochemical method (Ostovar et al.).

In summary, the present special issue addresses various representative reactions and processes in biomass valorization, highlighting the importance of developing novel, efficient and stable nano-(bio)catalysts with tailored properties according to the nature of the reactant/feedstock and the targeted products.

AUTHOR CONTRIBUTIONS

All authors listed have made a substantial, direct and intellectual contribution to the work, and approved it for publication.

REFERENCES

- Colmenares, J. C., and Luque, R. (2014). Heterogeneous photocatalytic nanomaterials: prospects and challenges in selective transformations of biomass-derived compounds. *Chem. Soc. Rev.* 43, 765–778. doi: 10.1039/C3CS60262A
- Gallezot, P. (2008). Catalytic conversion of biomass: challenges and issues. *ChemSusChem*. 1, 734–737. doi: 10.1002/cssc.200800091
- Granone, L. I., Sieland, F., Zheng, N., Dillert, R., and Bahnemann, D. W. (2018). Photocatalytic conversion of biomass into valuable products: a meaningful approach? *Green Chem.* 20, 1169–1192. doi: 10.1039/C7GC03522E
- Lange, J.-P. (2007). Lignocellulose conversion: an introduction to chemistry, process and economics. *Biofuels Bioprod. Biorefin.* 1, 39–48. doi: 10.1002/bbb.7
- Serrano-Ruiz, J. C., Luque, R., and Sepúlveda-Escribano, A. (2011). Transformations of biomass-derived platform molecules: from high added-value chemicals to fuels via aqueous-phase processing. *Chem. Soc. Rev.* 40, 5266–5281. doi: 10.1039/C1CS15131B
- Triantafyllidis, K. S., Lappas, A. A., and Stöcker, M. (eds.). (2013). “Preface,” in *The Role of Catalysis for the Sustainable*

ACKNOWLEDGMENTS

The conception of this Special Issue and its realization with regard to the three guest editors and most of the contributing authors have their bases on the European COST Action FP1306 Valorisation of lignocellulosic biomass side streams for sustainable production of chemicals, materials & fuels using low environmental impact technologies (LIGNOVAL) which was implemented in 2014–2018 under the frame of Horizon 2020. The main objective of LIGNOVAL was to develop a solid European multidisciplinary network of researchers able to provide a range of innovative alternatives to the valorisation of lignocellulosic residues to chemicals, fuels and materials making use of environmentally sound protocols from pretreatment/fractionation to conversion to valuable end products. The administrative and editorial support of the Frontiers team has been excellent from the point of designing the issue and throughout its implementation and completion. The time and effort devoted by the reviewers of the articles and their constructive comments are also highly appreciated. The publication has been also prepared with support from RUDN University Program 5-100.

Production of Bio-fuels and Bio-chemicals. (Amsterdam: Elsevier), 9–10.

- Tuck, C. O., Pérez, E., Horváth, I. T., Sheldon, R. A., and Poliakoff, M. (2012). Valorization of biomass: deriving more value from waste. *Science* 337, 695–699. doi: 10.1126/science.1218930
- Zhou, C.-H., Xia, X., Lin, C.-X., Tong, D.-S., and Beltramini, J. (2011). Catalytic conversion of lignocellulosic biomass to fine chemicals and fuels. *Chem. Soc. Rev.* 40, 5588–5617. doi: 10.1039/C1CS15124J

Conflict of Interest Statement: The authors declare that the research was conducted in the absence of any commercial or financial relationships that could be construed as a potential conflict of interest.

Copyright © 2018 Luque, Len and Triantafyllidis. This is an open-access article distributed under the terms of the Creative Commons Attribution License (CC BY). The use, distribution or reproduction in other forums is permitted, provided the original author(s) and the copyright owner(s) are credited and that the original publication in this journal is cited, in accordance with accepted academic practice. No use, distribution or reproduction is permitted which does not comply with these terms.



Lignocellulosic Biomass Transformations via Greener Oxidative Pretreatment Processes: Access to Energy and Value-Added Chemicals

Walter Den^{1*}, Virender K. Sharma², Mengshan Lee³, Govind Nadadur² and Rajender S. Varma^{4*}

¹ Department of Environmental Science and Engineering, Tunghai University, Taichung, Taiwan, ² Department of Environmental and Occupational Health, School of Public Health, Texas A&M University, College Station, TX, United States, ³ Department of Safety, Health and Environmental Engineering, National Kaohsiung First University of Science and Technology, Kaohsiung, Taiwan, ⁴ Regional Centre of Advanced Technologies and Materials, Faculty of Science, Palacký University, Olomouc, Czechia

OPEN ACCESS

Edited by:

Rafael Luque,
Universidad de Córdoba, Spain

Reviewed by:

Konstantinos Triantafyllidis,
Aristotle University of Thessaloniki,
Greece
Alina Mariana Balu,
Universidad de Córdoba, Spain
Germán Sanz Lobón,
Universidade Federal de Goiás, Brazil

*Correspondence:

Walter Den
wden@thu.edu.tw
Rajender S. Varma
varma.rajender@epa.gov

Specialty section:

This article was submitted to
Green and Sustainable Chemistry,
a section of the journal
Frontiers in Chemistry

Received: 05 December 2017

Accepted: 12 April 2018

Published: 27 April 2018

Citation:

Den W, Sharma VK, Lee M,
Nadadur G and Varma RS (2018)
Lignocellulosic Biomass
Transformations via Greener Oxidative
Pretreatment Processes: Access to
Energy and Value-Added Chemicals.
Front. Chem. 6:141.
doi: 10.3389/fchem.2018.00141

Anthropogenic climate change, principally induced by the large volume of carbon dioxide emission from the global economy driven by fossil fuels, has been observed and scientifically proven as a major threat to civilization. Meanwhile, fossil fuel depletion has been identified as a future challenge. Lignocellulosic biomass in the form of organic residues appears to be the most promising option as renewable feedstock for the generation of energy and platform chemicals. As of today, relatively little bioenergy comes from lignocellulosic biomass as compared to feedstock such as starch and sugarcane, primarily due to high cost of production involving pretreatment steps required to fragment biomass components via disruption of the natural recalcitrant structure of these rigid polymers; low efficiency of enzymatic hydrolysis of refractory feedstock presents a major challenge. The valorization of lignin and cellulose into energy products or chemical products is contingent on the effectiveness of selective depolymerization of the pretreatment regime which typically involve harsh pyrolytic and solvothermal processes assisted by corrosive acids or alkaline reagents. These unselective methods decompose lignin into many products that may not be energetically or chemically valuable, or even biologically inhibitory. Exploring milder, selective and greener processes, therefore, has become a critical subject of study for the valorization of these materials in the last decade. Efficient alternative activation processes such as microwave- and ultrasound irradiation are being explored as replacements for pyrolysis and hydrothermolysis, while milder options such as advanced oxidative and catalytic processes should be considered as choices to harsher acid and alkaline processes. Herein, we critically abridge the research on chemical oxidative techniques for the pretreatment of lignocellulosics with the explicit aim to rationalize the objectives of the biomass pretreatment step and the problems associated with the conventional processes. The mechanisms of reaction pathways, selectivity and efficiency of end-products obtained using greener processes

such as ozonolysis, photocatalysis, oxidative catalysis, electrochemical oxidation, and Fenton or Fenton-like reactions, as applied to depolymerization of lignocellulosic biomass are summarized with deliberation on future prospects of biorefineries with greener pretreatment processes in the context of the life cycle assessment.

Keywords: lignocellulosic biomass, depolymerization, biorefinery, greener oxidation, mild pretreatment, life cycle analysis

INTRODUCTION

The shift from petroleum- to biomass-derived materials appears to be the plausible long-term pathway to ensure sustainable supply of the carbon feedstock for energy and chemical industry (Bairamzadeh et al., 2018). The use of biomass as a sustainable feedstock, however, does not assure a successful transition without adapting processes designed with green chemistry and cost-competitive manufacturing processes. In this regard, the concept of integrated biorefineries encompassing green chemistry principles for production, enhanced energy and material efficiency, reduced waste generation and toxicity, and the increased reusability of the products at the end of their lives, has drawn particular interests and discussion (Clark et al., 2009; De Bhowmick et al., 2017). Greener processes incorporating concepts such as use of heterogeneous catalysis, water-based reactions, environmentally-friendly oxidants substituting for less efficient processes using volatile organic solvents and materials with high environmental burden (Dick et al., 2017; Pelckmas et al., 2017). Similarly, alternative activation methods such as microwave (MW) and ultrasound technologies should replace energy-intensive heating to facilitate efficient chemical reactions.

Identifying routes of production for both energy and value-added chemicals are imperative, and their idealistic pathways have been discussed in numerous reports (Laurichesse and Averous, 2014; Abdelaziz et al., 2016). For example, biomass feedstocks often containing valuable extractable chemicals, of interest to pharmaceutical and agricultural commodity chemicals, can be isolated using greener processes such as supercritical carbon dioxide extraction. The oxidative polymerization of the extract-free lignocellulosic materials can also produce polyfunctional monomeric compounds that can be used as an alternative or replacement for fossil fuel-derived building blocks, including aromatics, amino acids, biofunctional molecules (e.g., lactic acid, succinic acid), and fatty acids. Selective functionalization of natural lignin polymer has been studied to improve its compatibility in composite and copolymer materials (Crestini et al., 2010).

Increased production of biomass for energy, besides being a promising renewable energy source, has several potential benefits in offsetting substantial use of fossil fuels, heightening energy security in regions without abundant fossil fuel reserves, increasing supplies of liquid transportation fuels, and decreasing net emissions of carbon into the atmosphere per unit of energy delivered (Field et al., 2008). However, the over-exploitation of biomass, especially consumed by animals, as alternative energy sources also could threaten food security and generate

environmental problems, such as introducing invasive species by the plantation of foreign energy crops. In this context, energy conversion from lignocellulosic biomass as feedstock is particularly attractive because they do not compete with food crops and are abundant in native vegetation. Lignocellulosic feedstock can be derived from discarded agricultural residues and even municipal sludge comprising high organic contents.

The most common forms of bioenergy chemicals using existing technologies are ethanol (biofuel) and methane (biogas). Sugarcane as feedstock can be easily converted to bioenergy through fermentation and distillation because sugar in the form of monosaccharides and disaccharides are both highly digestible. Starch as feedstock (e.g., corn kernels, potatoes) requires enzymatic hydrolysis to convert polysaccharides (glucose polymer in which glucopyranose units are bonded by α -linkages) to monosaccharides (glucose). Of the two components of starch (amylose and amylopectin), amylopectin presents the greater challenge to enzymatic hydrolysis due to the presence of α -1,6-glycosidic branch points which make up about 4–6% of the glucose. Most hydrolytic enzymes are specific for α -1,4-glucosidic branches, yet the α -1,6-glucosidic links must also be broken for complete hydrolysis of amylopectin to glucose.

Cellulose, conversely, is a linear polysaccharide polymer of glucose disaccharide with β -1,4-glucosidic linkages; a cellulose molecule normally consists of a few hundreds to thousands of glucoses. The unbranched cellulose chains are very densely packed via inter-chain hydrogen bonds. Beneficiary of dense packing, cellulose form strong supports for plants in the presence of microfibrils with high tensile strength. Hydrolysis of cellulose is henceforth a critical step for biofuel production to decompose complex organic polymers (proteins, lipids, carbohydrates) into simpler molecules. These molecules can then undergo acidogenesis (converting long-chain fatty acids into volatile fatty acids and sugars), and acetogenesis (converting volatile fatty acids into acetic acid, carbon dioxide and/or hydrogen). The products of acetogenesis provide substrate for methanogenesis, which converts acetic acid into methane and carbon dioxide. Other simple soluble molecules such as amino acids and fatty acids can also be converted into methane by a sequence of fermentative bacteria. For ethanol fermentation, saccharin materials such as glucose, fructose and sucrose are metabolized, normally by yeasts, to produce ethanol and carbon dioxide.

Ironically, as of today, relatively little bioenergy originates from lignocellulosic biomass as compared to feedstock such as starch and sugarcane, primarily due to high cost of production encompassing biomass pretreatment steps to biomass components (i.e., lignin, cellulose, and hemicellulose) and to

disrupt the natural recalcitrant structure of these rigid polymers; complex structure of celluloses renders the molecules resistant to biological degradation. The bottleneck step for either biogas or biofuel pathway remains the same: the low efficiency of enzymatic hydrolysis of the feedstock due to the recalcitrant nature of lignin and cellulose. In fact, pretreatment of lignocellulosic raw materials has been considered the second most expensive unit in the biomass-to-energy cost structure (Mosier et al., 2005). In particular, lignin is notoriously resistant to oxidative, hydrolytic, and biological degradation, and is often regarded as a waste fraction of biomass, despite the presence of rich chemical functionalities (Elizabeth et al., 2016). The full valorization of the lignin into energy products or chemical products is dictated by the effectiveness of selective depolymerization of the pretreatment processes. Existing dissolution methods of lignin involve harsh pyrolytic and solvothermal processes abetted with corrosive acids or alkaline reagents. These methods unselectively decompose lignin into many products that may not be energetically or chemically valuable, or even biologically active. Identifying milder and greener processes that can selectively depolymerize lignocellulosic materials, therefore, is a subject of immense interest for exploration. The primary objective of this work, therefore, is to review the studies performed in recent years for the depolymerization via some of the advanced oxidative processes. Section Present Processes for Biomass Conversion Process to Fuel, Refinery, and Pharmaceutical Precursors of the article provides the necessary background pertaining to the functionalities of pretreating lignocellulosic biomass, as well as the modern physical, chemical, and biological pretreatment processes that have been developed or even practiced industrially. Section Greener Oxidative Processes for Biomass Conversion-Selectivity and Mechanism narrows the discussion into oxidative biomass pretreatment processes that are considered both greener and milder, including ozonolysis, photocatalysis, oxidative catalysis, electrochemical oxidation, Fenton and Fenton-like reactions. The last section, intended to provide an outlook of future biorefineries, summarizes the results from life-cycle assessment studies and discusses the interlinking techno-socio-economic impacts of biorefineries.

PRESENT PROCESSES FOR BIOMASS CONVERSION PROCESS TO FUEL, REFINERY, AND PHARMACEUTICAL PRECURSORS

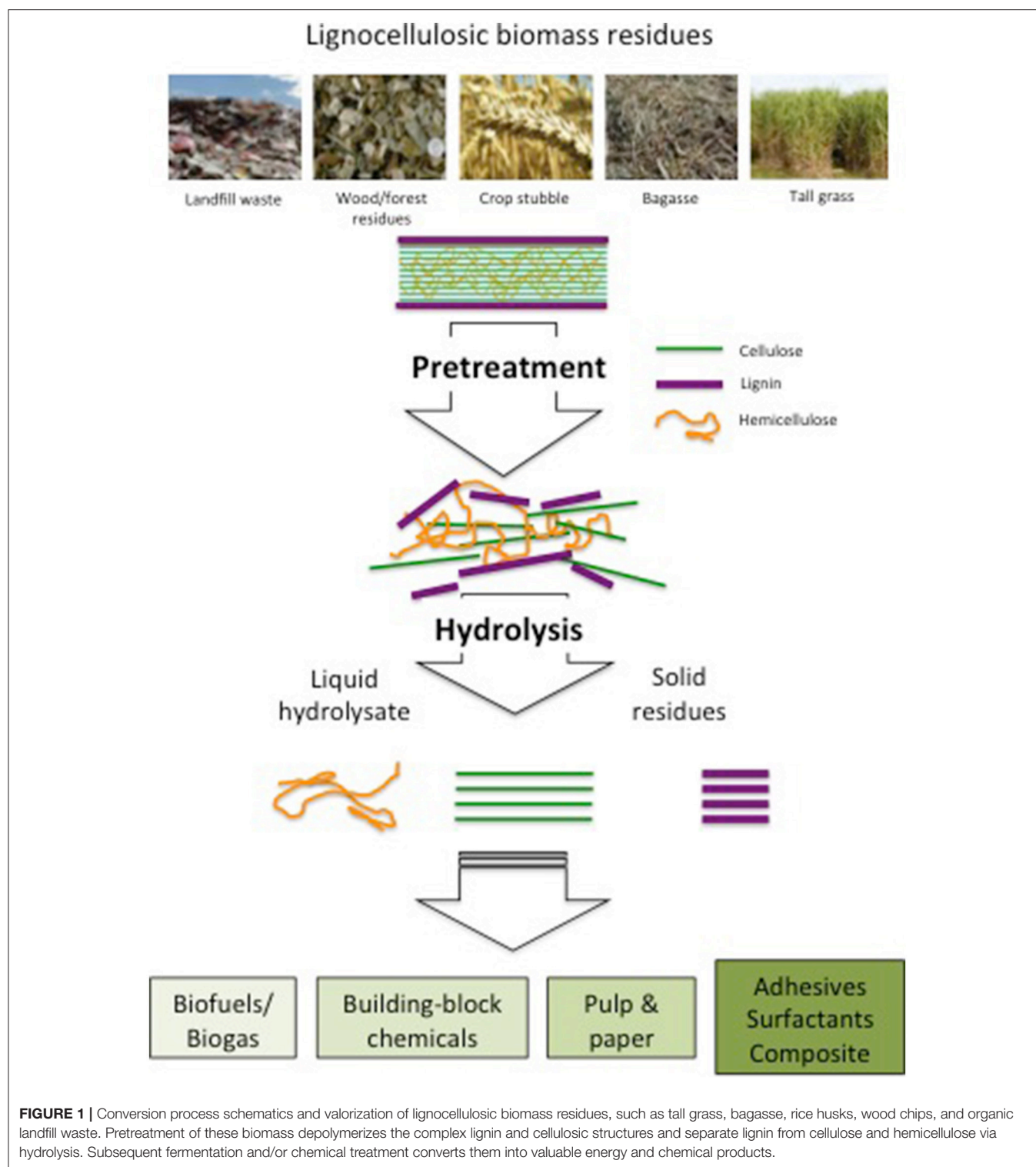
Lignocellulosic biomass generally comprises three types of biopolymers, namely cellulose, hemicellulose, and lignin. While the high polysaccharide contents in cellulose and hemicellulose make the two components valuable feedstock for bioenergy production, lignin is composed of polyphenols connected by a complex network of monomeric phenyl propanoic units with different inter-unit bonds. By cross-linking between cellulose and hemicellulose to make the cell walls rigid and three-dimensional, the complex structure of lignin constitutes the most recalcitrant component and therefore presents the greatest barrier for lignocellulosic biomass to become an economically

viable energy feedstock. Industrially, lignin has been considered as a manufacturing by-product with no commercial values. For example, pulping process removes a major portion of lignin from biomass to separate the cellulosic components and generates fibrous pulp needed to manufacturing downstream products, such as papers and boards. Lignin components, on the other hand, are either combusted to produce heat value or discharged as wastewater. Consequently, many early studies on chemical and biological oxidation of lignin concerned only to removal of lignin and cellulosic residues from process effluents to comply with the environmental mandates. Lignin, the second most abundant biopolymer accounting for 15–30% of biomass, is presently limited to thermovalorization processes as filler in composites and coating materials; its chemical heterogeneity is major reason for the lack of valorization. Accordingly, pretreatment of lignocellulosic components of biomass becomes a critical step for their conversion into useful materials, as indicated in the **Figure 1**.

Lignin consists primarily of complex phenolic heteropolymers. The most common bonding types in lignin, as shown in **Figure 2**, are the β -O-4' aryl glycerol ether bond ($\sim 45\%$) and the β -5 phenyl coumaran bond ($\sim 10\%$), among others (Crestini et al., 2010). Consequently, the lack of specific bonding and subunit patterns in a lignin structure makes it challenging to decompose into selected desired compounds. Lignin is a major barrier to the use of lignocellulosic biomass in biological conversion process to bioenergy. In general, softwood possess the highest lignin matter, followed by hardwood and grasses. The intertwined spatial network of lignin is formed from three major phenylpropane units, namely syringyl (S), guaiacyl (G), and p-hydroxyphenyl (H). These units differ in the number of methoxyl groups on the benzene's aromatic backbone. Softwood lignin is primarily comprised of G ($\sim 90\%$) whereas hardwood lignin predominantly contains G and S while the grass lignin has all the three units. Since hardwood generally contains less lignin than softwood, it is technically and economically more feasible to apply anaerobic digestion process for energy conversion. Agricultural residues typically contain even less lignin (10–20% lignin, 20–30% hemicellulose, and 40–50% cellulose), and are thus more suitable as biomass feedstocks.

Functionalities of Biomass Pretreatment

The intrinsic properties of lignocellulosics make it essentially non-biodegradable without any pretreatment to disrupt the lignin shield of biomass; such pretreatment helps open up the carbohydrate components so that they are accessible to microbial and/or enzymatic attacks. The changes in the physical and chemical characteristics can be detected microscopically, spectroscopically, or thermodynamically. For example, conventional scanning electron microscopy (SEM) and transmission electron microscopy (TEM) provide powerful tools to analyze the topography and distribution of lignin and cellulose in biomass samples (Fromm et al., 2003). Alternatively, environmental SEM (ESEM) enables microscopic observation of biomass samples, which are typically moist and electrically insulating, in a non-destructive manner (Turkulin et al., 2005). Furthermore, techniques using near-infrared spectroscopy



have been applied to effectively quantify the individual components of lignocellulosic matrices (Xu et al., 2013; Li X. et al., 2015). Recently, taking advantage of the unique binding affinities of a luminescent oligothiophenes to lignin, cellulose and hemicellulose in various forms, a technique combining

spectrofluorometric method and fluorescence confocal laser microscopic method was developed (Choong et al., 2017). This technique offers a real-time, non-destructive, visual method to analyze the chemical composition of a biomass sample during its treatment and production process.

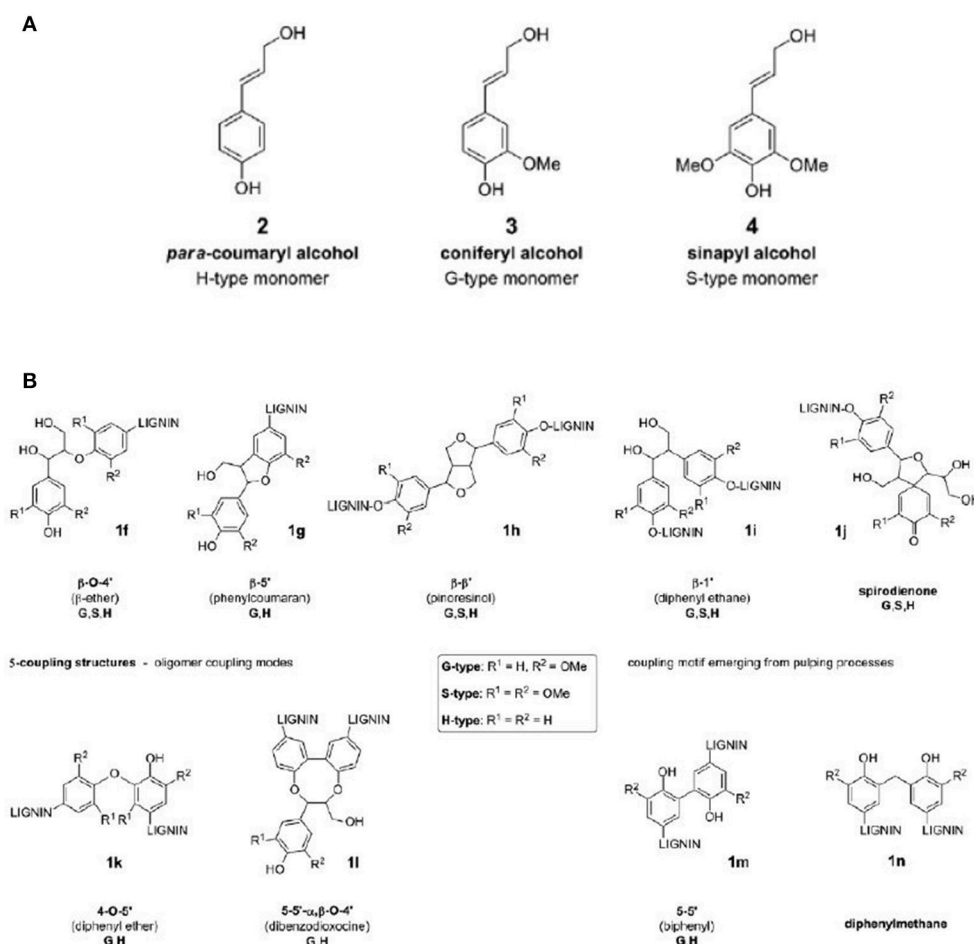


FIGURE 2 | Various common bonding and linkage schemes in lignin. The figure demonstrates **(A)** three major phenylpropane units in lignin structure; and **(B)** the various types of C–O ether bonds and C–C bonds between aromatic monomer units of lignin. The figure is reproduced, without change, from Abdelaziz et al. (2016). The article is supported under the CC BY-NC-ND license (<http://creativecommons.org/licenses/by-nc-nd/4.0/>).

Below is summary of pretreatment approaches used by researchers including two reviews on this topic (Alvira et al., 2010; Zhang et al., 2014).

- Decrystallization of cellulose: Degree of polymerization and cellulose crystallinity are important factors in determining the rate of hydrolysis. Cellulosic molecules have different orientations throughout the structure, leading to altered levels of crystallinity. In general, cellulose consists of amorphous (low crystallinity) and crystalline (high crystallinity) regions; the more crystalline the structure, the less biodegradable the molecules become. The reduction of crystallinity generally has been shown to increase biogas yield, but the inverse case may also occur. Therefore, this parameter should not be considered as the sole factor in determining a pretreatment step.
- Reduction of lignin content: Lignin restricts the enzymatic hydrolysis rate by acting as a physical barrier thus preventing the digestible parts of the substrate to be hydrolyzed. Therefore, decreased lignin content generally leads to increased biogas yield. Treatment processes to reduce lignin

contents can involve melting and lignin restructuring by steam explosion, disruption of lignin-carbohydrates linkages, or solubilization of lignin.

- Increase in accessibility of microbes and enzymes to cellulose and hemicellulose: Accessibility of the substrate to the cellulolytic microbes or enzymes can be enhanced by increasing the available surface area for the enzymatic attack. This may be achieved by the particle size reduction of the biomass feedstock and enhancing the porosity to allow better accessibility of enzymes. Although mechanical treatment such as grinding and milling precedes other processes, nearly all physical and chemical pretreatment methods are capable of increasing the accessibility of microbes and enzymes by disrupting the hemicellulose matrix which limits the pore size in the substrate.
- Formation of inhibiting compounds: Excessive decomposition of lignocellulosics sometimes leads to the generation of fermentation inhibitors namely furfural and hydroxymethylfurfural (HMF), either during the

pretreatment step or in the ensuing anaerobic digester. For example, acidification via heated concentrated acidic solutions typically yields these inhibitory compounds that adversely affect the bioenergy conversion performance.

In summary, a successful pretreatment process ought to attain the following criteria:

- Improve the anaerobic digestibility of feedstock.
- Minimize degradation of carbohydrates to prevent conversion yield loss.
- Avoid formation of inhibitory compounds during pretreatment.
- Curtail the consumption of water, energy, and toxic chemicals.
- Reduce the process footprint (e.g., waste disposal, low toxicity, resource consumption).

Pretreatment Processes of Lignocellulose Biomass

The performance in terms of meeting the criteria by some of the existing pretreatment technologies is discussed hereinafter by broadly dividing the processes into those of physical-chemical methods and biological processes. It is worth noting that many of the methods involve alternation of both physical and chemical characteristics of the raw materials, hence they are generically categorized as physical-chemical processes.

Physical-Chemical Processes

Comminution

Comminution of biomass can be accomplished by using milling or grinding machines. Reduction of biomass particle size can modify the inherent ultrastructure of lignocellulosic biomass, increase the surface area for enzyme accessibility, reduce the degree of cellulose crystallinity, and decrease the degree of cellulose polymerization for enhanced digestibility (Kratky and Jirout, 2011). Schell and Harwood (1994) concluded that particle size must be reduced to 1–2 mm to eliminate limitations to hydrolysis; however, size reduction via mechanical forces is an expensive operation that consumes about 33% of the total electricity demand for the whole process. Another disadvantage of comminution is its inability to remove the lignin, a critical barrier to the access of microbes and enzymes to cellulose.

Hydrothermolysis

In this process using hot water, biomass undergoes high temperature cooking in water at an elevated pressure. During pretreatment, water can penetrate into the biomass cell structure, hydrating cellulose, solubilizing hemicellulose, and slightly removing lignin (He et al., 2016). It is an effective method for enlarging the susceptible surface area of cellulose and improving cellulose degradability, and thus has been extensively practiced to improve biogas yield from various lignocellulosic feedstock, including both energy crop (sunflower stalks, sugarcane bagasse) (Badshah et al., 2012) and biomass wastes (paper residuals, municipal solid wastes) (Qiao et al., 2011).

Catalytic pyrolysis

Pyrolysis refers to heating or thermally degrading organic materials in the air-free environment (Ringer et al., 2006) and may comprise a five-step process: (1) biomass heating; (2) carbonization of volatiles escaping from organic matters; (3) hot volatiles flows toward solids resulting in heat transfer to the cooler portion; (4) volatiles condensed to liquid form with incondensable gas, and (5) the autocatalytic secondary reactions (decomposition or re-polymerization). The weaker chemical bonds in lignin begin to break at lower temperatures. For examples, the hydroxyl group linked to β - or γ -carbon in aliphatic side-chain forms water as a result of fracturing. The cleavage of β - or γ -carbon bond on the alkyl side chain releases formaldehyde. Alkyl ether bond (α - or β -O-4-bond) are also cleaved. As temperature increases, stronger bonds are fractured with the exception of γ -carbon ether bond; above 500°C, the aromatic ring is depolymerized into hydrogen (Brebou and Vasile, 2010).

Conventional pyrolysis of lignin typically involves the use of catalysts, such as zeolite minerals and metallic compounds, to enhance the yields and selectivity of ensuing products from lignin pyrolysis. The metallic catalysts have been reported to increase the overall transformation of lignins into degraded products and suppress the formation of inhibitory chemicals (Maldhure and Ekhe, 2013). Other catalysts such as zeolite, are effective in promoting the cracking reactions of oxygen-containing compounds which diminish the char formation (Li et al., 2014; Kim et al., 2015).

Alternative activation via irradiation-microwave

Irradiation pretreatment processes pertain to alternate energy input systems via various mechanisms, such as MW, ultrasound, gamma ray and electron beam. Except for MW process, other irradiation technologies are either cost prohibitive or non-scalable; consequently, MW technology is by far the most common type of irradiation pretreatment process studied so far (Bundhoo, 2018). However, similar to traditional thermal pretreatment, MW processing can produce heat-induced inhibitors such as phenolics and furfural. Additionally, the beneficial effects of MW pretreatment of lignocellulosic biomass have not been consistently verified. For example, MW pretreatment was applied to the organic solid waste in the temperature range of 115–145°C, yielding only a 4–7% improvement in biogas production (Shahriari et al., 2012). MW treatment with temperatures of 200 or 300°C did not improve biogas production, and an increase in temperature led to lower biogas production levels (Sapci, 2013). For this reason, MW has not been used individually for lignocellulosic biomass pretreatment, but could be deployed to provide necessary heat for aiding the chemical pretreatment at relatively low temperatures without compromising pretreatment effects.

Microwave (MW) technology has been widely applied in lignin extraction from pulp industry, which substantially encourages the development of environmentally benign, innovative, and highly effective lignin conversion processes (Wang et al., 2016). Such MW-assisted technologies contain both thermal effect (i.e., fast heating) and non-thermal effect, and thus

can be grouped into two major pathways: MW-assisted pyrolysis (thermal) of lignin without oxygen, and MW-assisted solvolysis (non-thermal) under milder conditions. MW-assisted pyrolysis can significantly reduce both the reaction time and temperature for lignin conversion into valuable chemicals. For example, the MW heating process for the production of bio-oil from sewage sludge has also been demonstrated using a pilot-scale MW heating apparatus (Lin et al., 2012). Maximum bio-oil yield of 30.4% was attained under the MW irradiation power of 8.8 kW and at the final pyrolysis temperature of 773°K (500°C). MW-assisted pyrolysis of various types of alkali (kraft) lignin also afforded chemical feedstock such as guaiacols (900–1240°K, 1.5–2.7 kW) and phenol (582–864°K, 700 W) (Bu et al., 2014; Farag et al., 2014).

The non-thermal effects play an important role in the chemical reactions, leading to an increase of the pre-exponential factor and a diminution of the activation energy in the Arrhenius equation. Consequently, the breaking of the β -O-4 ether bonds and C-C bonds in lignin structure can be facilitated under the MW irradiation conditions. Some studies have validated the positive effect of MW-assisted solvolysis, culminating in improved chemical yields during liquefaction processes of various agricultural residues such as wheat straw (Ouyang et al., 2015), pine sawdust (Xu et al., 2012), and bamboo (Fu et al., 2014). However, the effect of MW irradiation on the performance of biogas conversion from lignocellulosic biomass has rarely been reported.

Alkaline pretreatment

The method uses bases such as NaOH, KOH, $\text{Ca}(\text{OH})_2$, Na_2CO_3 , and liquid ammonia to remove lignin, hemicellulose, and cellulose. The function of alkaline pretreatment is saponification and cleavage of lignin-carbohydrate linkages (Tarkow and Feist, 1969). Alkaline pretreatment increases porosity and internal surface area by promoting structural swelling, decreases degree of polymerization and crystallinity, thus breaking down lignin structure. NaOH is the most extensively used base to improve biogas yield from lignocellulosic biomass including agricultural residue such as wheat straw, rice straw, corn stover, woody material, and sunflower stalk. The pretreatment can be accomplished at low (0.5–4 wt % NaOH) or high (6–20 wt % NaOH) concentrations (Mirahmadi et al., 2010). Generally, at low NaOH concentration, the pretreatment aims at lignin and hemicellulose removal and is operated at higher temperature and pressure, without recycling NaOH. Contrarily, at higher NaOH concentration, process occurs at atmospheric pressure and low temperature wherein only cellulose dissolution ensues, without significant delignification. The downside of alkaline pretreatment is the possible formation of inhibitory phenolic compounds, and the higher costs of downstream processing for pH control.

Acid pretreatment

Acid pretreatment can be conducted either under concentrated acid (e.g., 30–70%) and at low temperature (e.g., 40°C) or under diluted acid (e.g., 0.1%) and high temperature (e.g., 230°C). Organic and inorganic acids including H_2SO_4 , HCl, HNO_3 , H_3PO_4 , acetic acid, and maleic acid have all been used for acid

pretreatment, with H_2SO_4 being the most commonly used acid. The concentration of phosphoric acid beyond a critical value prompts a phase transition from swelling to cellulose dissolution (Mancini et al., 2016). The regenerated cellulose after dissolution in concentrated phosphoric acid has the dual benefit of having an amorphous form and high reactivity to cellulose (Sathitsuksanoh et al., 2012). For example, Nieves et al. (2011) achieved 40% enhancement (283 mL $\text{CH}_4/\text{g VS}$) of the methane yield by employing concentrated H_2SO_4 (85.7 wt %) for the pretreatment of oil palm empty fruit bunches within 30 days of anaerobic digestion. Nevertheless, a pretreatment of the identical initial substrate with 8 wt % NaOH ensued in a 100% improvement (i.e., 404 mL $\text{CH}_4/\text{g VS}$) of the methane generation compared to the untreated material. Similar to alkaline pretreatment, the main shortcoming of employing acid pretreatment is the deployment of a corrosive reagent, which necessitates special materials for the construction of reactor and downstream neutralization.

Ionic liquids (ILs)

ILs are a comparatively new class of solvents, made up of organic salts with varying melting points, high thermal stability, high polarity and the main benign attribute, barely measurable vapor pressure. Some ILs are regarded as efficient and “green” solvents for dissolution of cellulosic components. They are also attractive because large amounts of cellulose can be dissolved under mild conditions with low energy inputs, and it is feasible to recover nearly quantitatively the used IL and leave minimum residues for the downstream process (Heinze et al., 2005). The dissolution mechanism includes the oxygen and hydrogen atoms comprising cellulose hydroxyl groups, which form electron donor/electron acceptor complexes intermingling with the ILs. The cleavage of hydrogen bonds leads to an opening of the lignocellulosic network, culminating in cellulose dissolution (Feng and Chen, 2008). For example, Gao et al. (2013) showed that the lignocellulosic structure and composition were chiefly modified by the pretreatment with the IL [i.e., a mixture of 1-*N*-butyl-3-methylimidazolium chloride ([Bmim]Cl)/dimethyl sulfoxide (DMSO)], ensuing in a 28% increase of the cellulose matter in the regenerated water hyacinth and a 49% removal of lignin, with a final biogas production of 170 mL/g VS; equivalent to an enhancement by 98% compared with the untreated feedstock. Various ILs, including *N*-methylmorpholine-*N*-oxide monohydrate (NMMO), 1-*n*-butyl-3-methylimidazolium chloride (BMIMCl), 1-allyl-3-methylimidazolium chloride, 3-methyl-*N*-butylpyridinium chloride (MBPCL), and benzyldimethyl (tetradecyl) ammonium chloride, have been studied for pretreatment of lignocellulosic biomass to enhance enzymatic digestibility (Schell and Harwood, 1994). The main shortcomings of ILs are the associated higher costs and their inhibitory effect on the hydrolytic enzymes, even at lower concentrations. In particular, chloride bearing imidazolium cations can cause problems of corrosion and toxicity. Furthermore, the total removal of ILs after the pretreatment step requires the use of large amounts of water and involved recycling systems, which could make the process economically unsustainable (Nguyen et al., 2010).

Organosolv

Pretreatment of lignocellulosic materials with a mixed aqueous-organic or an organic solvent at elevated temperatures (i.e., 100–250°C) comprise the organosolv process which depends on the chemical collapse of the lignin macromolecule by breaking of ether linkages and its successive dissolution (McDonough, 1993). The most deployed solvents often used in this process are ethanol, methanol, acetone, organic acids (such as formic and acetic acid) (Papatheofanous et al., 1995) and higher boiling alcohols. Mirmohamadsadeghi et al. (2014) used organosolv pretreatment (75% ethanol at 150 and 180°C for 30 and 60 min, respectively) on three different lignocellulosic biomass varieties; 55 days of anaerobic digestion, 54.6, 79.5, and 135.2 mL CH₄/g VS ensued from pinewood (softwood), Elmwood (hardwood) and rice straw, respectively. Methane production increased by 84, 73 and 32% with pinewood, elmwood and rice straw, respectively, in relation to the corresponding untreated entities, showing that the organosolv pretreatment is more efficient for biomass with higher initial lignin contents. Organosolv mixtures are combined with acid catalysts (H₂SO₄, HCl, oxalic- or salicylic acid) to cleave hemicellulose bonds in some other studies. Removal of solvents from the system is essential using suitable extraction and separation techniques (e.g., evaporation and condensation), as their recycling would reduce the operational costs; solvent separation is crucial because they might be inhibitory to enzymatic hydrolysis and fermentative microorganisms (Sun and Cheng, 2002).

Wet oxidation

Wet oxidation in its broad sense includes the use of oxidizing agents such as oxygen, ozone, and hydrogen peroxide. The presence of oxygen can increase the reaction rates and production of free radicals; these processes are usually performed under high temperature (125–300°C) and pressure (0.5–20 MPa). Although faster reaction rates can be achieved with high oxygen concentrations, using pure oxygen results in high operating costs. When applying a wet oxidation process to lignocellulosic biomass, all three components are affected. Hemicellulose is extensively broken into monomeric sugars and degraded into organic acids, cellulose is partly degraded, and lignin undergoes both cleavage and oxidation (Hendriks and Zeeman, 2009). Consequently, wet oxidation increases the accessibility of cellulose to biological attack via the removal of lignin and hemicellulose; pretreatment with H₂O₂ alone achieved 50–120% higher methane yield from rice straw (Song et al., 2012) using 1–4% H₂O₂, and 33% improvement for sunflower (Monlau et al., 2012) using 4% H₂O₂. Cesaro and Belgiorio (2013) studied the effect of ozonolysis pretreatment on biogas production from organic municipal solid waste wherein an ozone dose of 0.16 g O₃/g TS achieved the highest biogas yield, which was 37% more than that of untreated material. Ozonolysis is a milder process as it is generally carried out at ambient temperature and pressure, and does not generate inhibitors such as furfural and soluble aromatic compounds derived from lignin oxidation unlike other wet oxidation methods. However, the non-selective nature of all wet oxidation process bears the risk of significant loss of organic matter (e.g., hemicellulose).

Biological Processes

Fungal treatment of lignocellulosic materials for paper production is known historically. This environmentally friendly approach has received renewed attention as a pretreatment method for enhancing enzymatic saccharification of lignocellulosic biomass; cellulose is especially more recalcitrant to fungal attack than other components. Several fungi classes, including brown-, white-, and soft-rot fungi, have been used for pretreatment of lignocellulosic biomass for biogas production, with white-rot fungi (e.g., *Phanerochaete chrysosporium*, *Ceriporia lacerata*, *Cyathus stercoleris*, *Ceriporiopsis subvermispota*, *Pycnoporus cinnabarinus*, and *Pleurotus ostreatus*) (Kumar and Wyman, 2009) being the most effective (Gao et al., 2013). For example, a wood-decaying fungus (*Auricularia auricula-judae*) was applied to pretreat sweet chestnut leaves and hay for 4 weeks; pretreated mixture of leaves and hay in 1:2 ratio resulted in a 15% improvement of biogas production. Amirta et al. (2006) employed four fungi to pretreat Japanese cedar wood chips, and found that a strain of *Ceriporiopsis subvermispota* produced the highest methane yield that was four times higher than that of the untreated sample. In general, bio-pretreatment processes offer advantages such as low-capital cost, low energy, no chemicals requirement, and mild environmental conditions. The main drawback is the low hydrolysis rate attained in most biological protocols in comparison with physical and chemical processes.

Apparently, no pretreatment processes applied to lignocellulosic biomass are optimal. The process of choice depends on the types of the biomass treated, as well as the cost effectiveness of the process. Nevertheless, an improvement of 50% pertaining to biogas yield appears to be a reasonable goal for a functional biomass pretreatment step. To attain this objective, the pretreatment will not only improve the anaerobic digestibility of feedstock, but must also minimize degradation of carbohydrates content and avoid formation of inhibitory compounds.

GREENER OXIDATIVE PROCESSES FOR BIOMASS CONVERSION-SELECTIVITY AND MECHANISM

Greener endeavors as applied to biorefinery concept for lignocellulosic biomass conversion can be broadly classified in to two types namely, biomass transformation into energy products, and generation of valuable chemicals from biomass-derived components (e.g., lignin, cellulose, and hemicellulose). For bioenergy conversion, the key criteria for biomass pretreatment are to effectively decompose the complex lignocellulosic matrix, yet preserving the sugar content while preventing formation of inhibitory compounds to the ensuing enzymatic hydrolysis and fermentation process. In contrast, the ability of an oxidative process to selectively produce target compounds from a biomass-derived component becomes a critical criterion. For example, lignin contains a wide range of monomeric and polymeric phenolic compounds like vanillin, syringaldehyde, *p*-hydroxybenzaldehyde, vanillic acid, acetovanillone, syringic

acid, among others. However, these compounds exist in low concentration amidst a complex mixture of phenolic compounds that ensue from lignin oxidation. Most of these phenolic compounds share similar molecular weights, acid dissociation constants in water, densities and melting points thus questioning their industrial application at the present time in view of the effective separation and purification challenges. Consequently, milder oxidation processes with high level of selectivity and reasonable yields are of higher research priority.

Ozonolysis

Ozone has been accepted as an environmental-friendly oxidant with excessive oxidative power capable of non-selectively decomposing organic substrates especially for compounds containing conjugated double bonds and functional groups with high electron densities (von Gunten, 2003). Ozone is unstable in water and the pH of the water is important as the decomposition of ozone in alkaline medium results in highly reactive hydroxyl radicals ($\bullet\text{OH}$) which is a powerful oxidizing agent with an oxidation potential of 2.33 V (vs. the standard hydrogen electrode, SHE). Therefore, ozone exhibits a faster rate of oxidation reaction for lignin degradation as compared to the conventional oxidants such as hydrogen peroxide or potassium permanganate (Kreetachat et al., 2007; Sharma and Graham, 2010). Recently, kinetics and mechanism of the oxidation of organic compounds by ozone has been discussed in detail (Lee et al., 2017).

Ozone attacks lignin more than cellulosic and hemicellulosic components of lignocellulosic material and releasing soluble compounds of lower molecular weights such as organic acids (Mulakhudair et al., 2017). Traditionally, ozonation has been used mostly for pulp “bleaching” process. The decomposition of lignin in remediating wastewater generated from pulp and paper industry and textile industry via ozonation mineralizes the complex chemicals in the effluents. However, the higher cost of ozone generation has hindered its acceptance as an oxidant in the primary treatment alternative even when the organic content of the wastewater is highly recalcitrant.

Though early studies on ozone delignification sporadically existed in the 1980's, the potential of ozonolysis for the pretreatment of lignocellulosic biomass prior to enzymatic hydrolysis and in the subsequent fermentation processes has picked up steam. The high oxidative power for decomposing the lignin component, the ease of onsite generation and utilization of ozone, and the non-inhibitory reaction products of ozonolysis, are some of the major reasons that render this greener oxidant as an attractive biomass pretreatment alternative. Ozonolysis of various biomass has been reported in the past decades, that includes cereal straws (Aljibouri et al., 2015; Garcia-Cubero et al., 2016), wood and sawdust (Mamleeva et al., 2009), sugarcane bagasse (Barrera-Martinez et al., 2016), grass, and cotton stalks (Kaur et al., 2012; Travaini et al., 2016); the comprehensive progress made on ozonolysis of lignocellulosic biomass has been reviewed recently (Travaini et al., 2016).

For ozonolysis to be effective in structural alteration of lignin, several operating factors need to be understood and controlled especially depending on the type of biomass to be

treated. These elements principally include the moisture content (MC) of the biomass, the ozone dosage, and the removal of ozonolysis by-products. Biomass MC plays a critical role in the ozonation performance, as the distance between carbohydrate fibers increases in the presence of moisture, causing biomass to swell to a different extent; swelling can expose a greater surface area with reactive functional groups subject to ozone reaction, thus enhancing the degree of lignocellulosic ozonolysis. As water content increases near or beyond fiber's water saturation, one may observe conflicting results because a typical gaseous-phase ozonation becomes more complicated as dissolution into water creates an aqueous-phase reaction with the biomass surface. For example, in the study with Aspen sawdust, the wood sample was moisturized by adding water vapor to air-dried samples to create a MC ranging between 8 and 160% w/w; at near saturation, the swollen wood contained abundance of pores filled with water molecules condensed in wood capillaries wherein the dissolved ozone allowed for a greater kinetics of ozone consumption and a faster reduction rate of lignin content. Also, as opposed to attacking the lignin component by the soluble fraction of ozone, gaseous ozone tends to react with hemicellulose components and the delignified products. Thus, an extended retention of water was favorable for more complete lignocellulosic oxidation by ozone. Conversely, in using ozone to treat ground wheat and rye straw, Garcia-Cubero et al. (2016) reported a reduction of acid insoluble lignin content (AIL) (i.e., lignin fraction resistant to enzymatic hydrolysis) as MC increased up to 30%, but further moisturization did not improve AIL reduction.

The major setback for ozonolysis of biomass pretreatment are the higher ozone generation costs, and the poor energy balance stemming from the energy required to produce ozone (2.38 MJ per 100 g O_3) as compared to the energy ensued (2.67 MJ per 100 g ethanol). Other than continuing to develop more energy-efficient ozone generation technology, several options could make ozonolysis more competitive, including reduced ozone dosage for biomass pretreatment, improved ozonolysis efficiency for energy conversion, and identifying value-added chemicals that could be generated from ozone-pretreated biomass.

Individual studies on the effect of ozone dosages typically report ozonolysis performance using a range of ozone concentration, while other parameters are fixed. Therefore, it is difficult to compare their performance without an equal basis of ozone loading rate and other environmental conditions. Nevertheless, Barrera-Martinez et al. (2016) in their ozonolysis study of alkaline lignin solution (1.0% w/v) and wetted sugarcane bagasse (1 g in 1 ml distilled water), found that even with a very low ozone concentration ($<0.056\%$ v/v), noticeable changes in lignin structure and enhancement in its solubilization occurred. The increase in lignin dissolution corresponded well with the results of the ensuing acid and enzymatic saccharification experiments for the bagasse sample ozonated for 90 min. In another study using low-dose ozone ($<3.5\%$ w/v) to treat steam-conditioned Norway spruce slurry, Cavka et al. (2015) reported that increases in ozone dosage led to a reduction of phenolic content and a proportional increase of acid content. The steam-generated inhibitors such as furfural and HMF, were also proportionally reduced with

increased ozone dosage. In conclusion, low ozone dosages were beneficial for the fermentation of steam-pretreated Norway spruce, while high dosages decreased the inhibition of cellulolytic enzymes by soluble components in the sample. These studies demonstrated that low ozone concentration can still be effective for delignification of biomass, though the optimum ozone dosage to be applied largely depends on whether enzymatic saccharification or microbial fermentation follows.

Silva et al. (2013) compared the detoxification performance of several combinations of advanced oxidative processes including H_2O_2 , UV-C, O_3 , and Fe^{2+} , under acidic (pH 3) and alkaline (pH 8) conditions, for rice straw hydrolysate conditioned with sulfuric acid and heat. The conditioned hydrolysate contained a wide spectrum of mono- and poly-phenolic compounds, including vanillin, coumaric acid, vanillic acid, syringic acid, hydroxybenzoic acid-compounds that are valuable building block chemicals but potentially inhibitory to microbial metabolism in the fermentation process to convert sugar content into bioethanol. Results are presented in **Figure 3** (Silva et al., 2013) which depicts the role of varying treatment conditions on the sugar (glucose and xylose) depletion by the yeast *P. stipitis* in hydrolysates. It appears the pH was a critical factor in affecting hydrolysate fermentability. As shown in **Figure 3A**, the acidic pH 3.0, yeast cultured in hydrolysates treatment did not show improved sugar consumption compared to untreated hydrolysates except treatment A7 (e.g., yeast cultivated in assays A4, A6, A13, and A16 had similar or lower sugar consumption compared to those cultivated in the untreated hydrolysate. Significantly, no sugar consumption in assays A1, A10, and A11 was seen (**Figure 3A**). Under alkaline condition (i.e., pH 8.0), hydrolysate treatment ensued in sugar degradation (**Figure 3B**). Assays A3, A5, A9, A12, A14, and A15, consumption of sugar was more than 80% in 96 h.

Results from the aforementioned study suggest that hydroxyl radicals have higher affinity to aromatic rings, which contain much greater electron density than sugar molecules in the lignocellulosic matrix. Additionally, oxidation conditions in the presence of ozone resulted in the greater reduction in the total phenolic concentration (35–47 %), total furan (33–55 %), and low-molecular-weight phenolic compounds (60–96 %). In particular, ozone-based oxidation ($\text{Fe}^{2+}/\text{H}_2\text{O}_2/\text{O}_3$, and $\text{Fe}^{2+}/\text{UV}/\text{O}_3$) were the most effective experimental groups in alkaline pH, which generate phenolate ions due to dissociation of the hydroxyl proton of benzene rings, thus increasing their electron density and becoming more susceptible to hydroxyl free radical attack. Hydrolysate samples treated under oxidation conditions afforded the highest value of ethanol volumetric productivity of 0.36 g/l-h with a yield efficiency as high as 98% (against theoretical maximum content of fermentable sugars) using *Pichia stipitis* as the yeast inoculum for fermentation.

Alternatively, process design can improve the effectiveness of ozonolysis for energy conversion as exemplified by Al jibouri et al. (2015) in a two-step process for pretreatment of humid wheat straw; an intermediate washing procedure was sandwiched between two ozonation processes which was critical to re-exposing lignin functional groups by washing away organic acid molecules generated from the initial ozonation period, thus

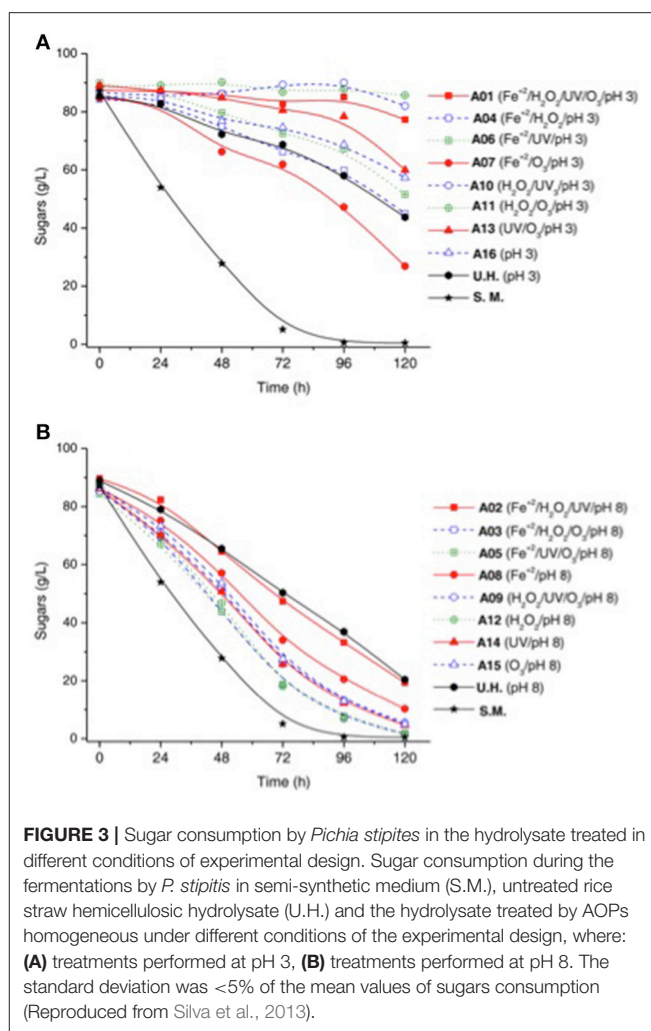


FIGURE 3 | Sugar consumption by *Pichia stipitis* in the hydrolysate treated in different conditions of experimental design. Sugar consumption during the fermentations by *P. stipitis* in semi-synthetic medium (S.M.), untreated rice straw hemicellulosic hydrolysate (U.H.) and the hydrolysate treated by AOPs homogeneous under different conditions of the experimental design, where: (A) treatments performed at pH 3, (B) treatments performed at pH 8. The standard deviation was <5% of the mean values of sugars consumption (Reproduced from Silva et al., 2013).

sustaining the effectiveness of the process. Under an optimized condition with initial MC of 45%, ozone concentration of 3% wt., washing start time of 20 min after initial ozonation and washing time of 80 s, the fermentable sugar yield by the ensuing hydrolysis process improved by 30% as compared to a one-step ozonolysis without intermediate washing, and 4 times better than untreated wheat straw. Since MC exceeding 45% adversely affected the ozonolysis performance, it is prudent to adjust the MC of the washed sample in the second-stage ozonation to 45% or less.

Adapting the multi-step pulp bleaching sequence, (Perron et al., 2016) studied the individual effect of applying ozonation, alkaline washing, and ultrasound radiation in sequence to enhance the enzymatic hydrolysis of sugarcane bagasse. The ozone feed rate was 32 mg/min for 60 min to 20 g of dry sample moistened with 10 ml of water, whereas the 0.1 M NaOH was used to for alkaline washing. They reported that ozonation alone yielded 0.8 ± 0.2 mg/g of soluble fraction in total phenolic content, whereas ozonation followed by alkaline washing significantly improved the yield up to 6.7 ± 0.1 mg/g. Correspondingly, the glucose and xylose yields after enzymatic hydrolysis for samples pretreated with ozonation alone were 16

and 12%, respectively, whereas those treated by ozonation and alkaline washing were 85 and 38%, respectively. The effect of ultrasonication as the final stage further improved the glucose and xylose yields to 94 and 55%, respectively though the extent of sugar yield enhancement was less obvious. The higher yields of fermentable sugar suggested that the initial ozonation step was a mild delignification process while maintaining the cellulose component. Ultrasonication was not effective in improving the yield performance and was energy intensive, though its potential role as an initial pretreatment technique was not deliberated.

Photocatalysis

Photocatalysis is considered one of the most sustainable processes for various applications because it initiates selective oxidation by harvesting abundant light energy (Ong et al., 2018; Patnaik et al., 2018). In general, photocatalysis can be provoked by photo-sensitization and photo-excitation. Photosensitizing molecules can be activated by absorbing ultraviolet or visible region of electromagnetic radiation, gaining sufficient energy to ionize the molecule and then transferring it to the adjacent molecules. For lignocellulosic biomass pretreatment, it has the potential to generate milder decomposing conditions and execute selective depolymerization of biomass-derived molecules into valuable chemicals. Nguyen et al. (2014) demonstrated a room-temperature lignin degradation strategy consisting of a chemoselective benzylic oxidation of a lignin model compound containing a β -O-4 linkage, followed by a photocatalytic reductive C–O bond cleavage, using an Ir-based photocatalyst to efficiently afford benzoic acid and other products. Alternatively, Gazi et al. (2015) developed a pathway to selectively initiate C–C cleavage of the same lignin model compounds using a milder and naturally more abundant vanadium oxo complex irradiated with visible light (>420 nm); pathway converted the model compound into products including an aryl aldehyde and an aryl formate, valuable building block chemicals in organic synthesis.

In photo-excitation, light energy equal or greater than the band-gap energy of a solid-state material promotes an electron (e^-) and simultaneously creates a hole (h^+) from the valence band. In the presence of water moisture, e^- and h^+ migrate along solid surface and react with water molecules to generate strong oxidizing radicals such as hydroxyl radicals ($HO\cdot$), superoxide radicals ($O_2^-\cdot$), and hydroperoxyl radicals ($HO_2\cdot$). Among an array of semiconducting metal-oxides, titanium dioxide (titania) remains the most studied material forming the basis of photocatalytic oxidation, stemming from the extended experience from titania-based application of wastewater purification containing lignin compounds (Ohnishi et al., 1989; Ksibi et al., 2003; Chang et al., 2004). Yasuda et al. (2011) studied the effect of the TiO_2 pretreatment of two types of tropical grass on the ethanol conversion via enzymatic saccharification (*Acetomyces cellulase*) and fermentation (*Saccharomyces cerevisiae*). Photocatalytically pretreated grass samples improved the reaction rate of both the enzymatic and fermentative processes, but the conversion yield of hemicellulose into ethanol did not change noticeably.

Lu et al. (2014) depolymerized pulverized rice husks ($<180\ \mu m$) using TiO_2 photocatalysts irradiated by ultraviolet

light with a primary emitting wavelength ~ 365 nm in 30% peroxide solution. The depolymerized products extracted from both the aqueous solutions and solid cakes, under various photocatalytic exposure times, produced a wide array of soluble organic products including alkanes, alkenes, arenes, alkanols, alkenols, phenols, alkanals, alkenals, benzaldehydes, ketones, carboxylic acids, alkanates, phthalates, and other nitrogen- and sulfur-containing organic compounds. They observed that alkanes, phthalates, ketones, and carboxylic acids were relatively more abundant, but there were no apparent abundance pattern of the products correlating to the time of reaction (20–100 min). The role and effect of peroxide was not discussed.

Prevention of electron-hole recombination to sustain their oxidative activities is another challenge when semiconductor-based materials are used as photocatalysts. Providing an intermediate electrode with an external anodic bias can suppress the recombination between the photogenerated charge carriers. For this purpose, Tian et al. (2010) combined the Ti/TiO_2 nanotubes electrode and the $Ti/Ta_2O_5-IrO_2$ electrode into a working photoelectrochemical electrode ($TiO_2/Ti/Ta_2O_5-IrO_2$), and tested its applicability in lignin decomposition. Individually, the reported photocatalytic degradation of lignin on the Ti/TiO_2 electrode, irradiated with UV (365 nm) but in the absence of the anodic potential bias, resulted in the lowest reaction rate, with a first-order rate constant of $0.0025\ min^{-1}$. In comparison, the electrochemical oxidation on the $Ti/Ta_2O_5-IrO_2$ by applying an electrode potential of +600 mV in the absence of the electrocatalyst yielded a reaction rate that was 3-folds greater than that of the photochemical oxidation. The photochemical-electrochemical oxidation on the $TiO_2/Ti/Ta_2O_5-IrO_2$ electrode returned the highest rate constant ($0.021\ min^{-1}$), demonstrating the possible synergetic effect of the combined photochemical and electrochemical oxidation; vanillin and vanillic acid were the two major oxidation products.

To improve the viability and yield efficiency of semiconductor-based photocatalysis for biomass pretreatment, efforts have been made to narrow the bandgap energy so that the light energy in the visible wavelength would be sufficient to induce photocatalysis, and to sustain the reactivity by effectively separating e^-/h^+ . An Ag–AgCl/ZnO photocatalyst was synthesized by photo-reducing Ag^+ to Ag 0 from AgCl deposited on ZnO particles (Li H. et al., 2015). The photocatalyst demonstrated complete lignin (alkali) degradation at an initial lignin concentration <50 mg/l upon irradiation with solar light for 150 min; evolution of total organic carbon (TOC) from the solution was linearly correlated with lignin degradation. The methane and biogas production yields from lignin degradation reached as high as 184 and 325 ml/g-TOC.

Recently, Gong et al. (2017) applied titania photocatalysts co-decorated with bismuth- (Bi) and platinum- (Pt) to depolymerize lignosulfonate under an simulated solar light. They reported that Bi(1%)/Pt(1%) on TiO_2 achieved higher lignin conversion rate than Bi(1%)- TiO_2 , Pt(1%)- TiO_2 , and pure anatase TiO_2 ; major reaction products being guaiacol, vanillin, vanillic acid, and 4-phenyl-1-buten-4-ol. Neither Bi nor Pt altered the crystalline structure of the anatase TiO_2 , but their presence with TiO_2 may play an important role in controlling the e^-/h^+ transfer during

photocatalysis. While lignin conversion rate was insensitive to the amount of Pt and Bi on anatase TiO₂, pH and Bi:Pt ratio markedly affected the selective yield of the oxidation products. For example, the highest guaiacol yield occurred near neutral range, whereas the maximum production of vanillic acid occurred at pH 2.5. In response to the quantitative change of the Pt and Bi modifiers, the guaiacol yield peaked when an equivalent amount (1%) of Bi and Pt was added. Yields of vanillic acid maximized, however, when the amount of Bi doubled that of Pt [i.e., Bi(2%)/Pt(1%)-TiO₂]. The addition of Pt on TiO₂ increased the number of active sites culminating in more effective e⁻/h⁺ separation and hence the improved lignin oxidation. The presence of Bi, conversely, helped regulate the Pt active sites and favored the selective degradation of lignin into guaiacol.

Recently, Luo et al. (2015, 2017) have prepared carbazolic porous organic frameworks (POFs) possessing varying redox potential for degrading the lignin β-O-4 models under the visible-light irradiation. They fine-tuned the redox potentials of POFs in order to achieve high efficiency to oxidize benzylic β-O-4 alcohols and high yield of reductive cleavage of β-O-4 ketones; synthesized POFs showed excellent stability and recyclability. Overall, findings obtained in this study exhibited the use of visible light POF photocatalysts to generate fine chemicals from lignocellulosic biomass.

Wakerley et al. (2017) proposed a photocatalytic system based on semiconducting CdS quantum dots (QDs), which could photoreform cellulose, hemicellulose and lignin into H₂ at room temperature (**Figure 4**); structures of cellulose, hemicelluloses, lignin, and lignocellulose are presented in **Figure 4A**). CdS is inexpensive and can absorb visible-light (a bulk electronic bandgap and potential of conduction band are ~2.4 eV and -0.5 V vs. the normal hydrogen electrode (NHE) (Yong and Schoonen, 2000). This suggests feasibility of reduction of the proton. Additionally, oxidation of saccharide is feasible due to the +1.9 V (vs. NHE) of CdS valence band (Shimura and Yoshida, 2011). This indicates that photocorrosion of CdS and evolution of H₂ depends on applying easily oxidized sacrificial reagents (Xu et al., 2016). Wakerley et al. (2017) used highly alkaline conditions which could form Cd(OH)₂/CdO (henceforth CdO_x) on the CdS surface (see **Figure 4B**). Significantly, the ensuing CdS/CdO_x QDs had capacity to achieve visible light photocatalysis to generate H₂ without photo-corrosion (see **Figure 4C** for the oxidation of unprocessed lignocellulosic substrates). Importantly, high dissolution of lignocellulosic at high pH could produce the synergistic effect to evolve H₂ with high rates.

A common component from lignin, 4-hydroxy-3-methoxybenzaldehyde (vanillin), can be hydrogenated to 2-methoxy-4-methylphenol, a potential future biofuel but only at high-pressure hydrogenation of vanillin to the upgraded biofuel (2-methoxy-4-methylphenol). Formic acid, a remarkable bio-derived source of hydrogen is readily accessible from renewable resource such as sugars and their oligomers. The larger scale production of biofuels can benefit immensely from the use of formic acid as hydrogenating agent in view of its ease of transportation and as the reactions can now be conducted at ambient atmosphere. Varma and co-workers have developed a

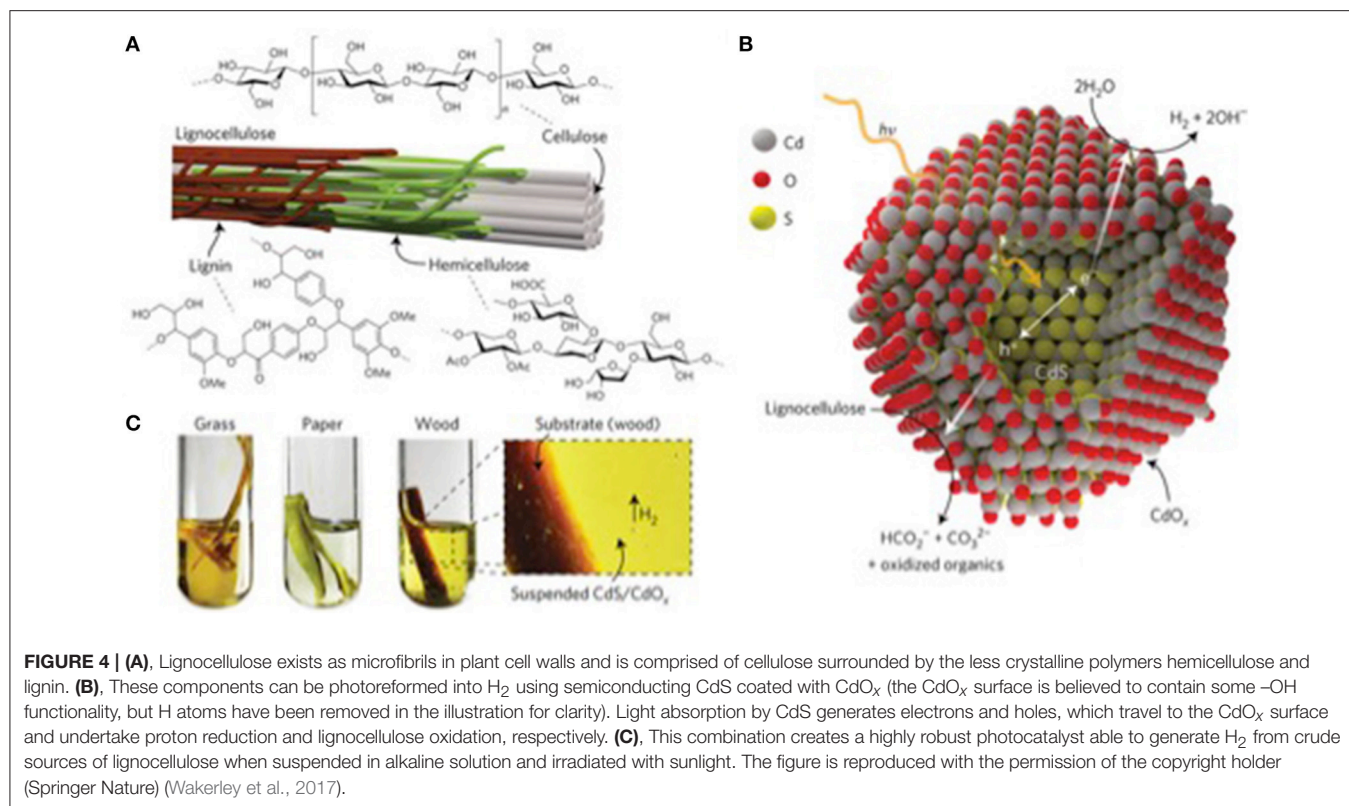
bimetallic catalyst supported on easily accessible and inexpensive graphitic carbon nitride (g-C₃N₄) catalyst, AgPd@g-C₃N₄, which accomplishes the hydrogenation of vanillin using formic acid as hydrogen source to upgrade the biofuels under visible light irradiation (Verma et al., 2016a); graphitic carbon nitride was chosen due to its ability to absorb visible light energy. The same catalyst was exploited in a novel sustainable approach to highly valuable entity, γ-valerolactone, wherein visible light mediated conversion of biomass-accessible levulinic acid occurs readily on AgPd@g-C₃N₄ (Verma et al., 2016b).

Photocatalysis, however, remains an inherently unselective process, especially in water and requires approaches for enhancement in selectivity that is applicable to wide ranging chemical transformations. Comprehensive and successful strategies for enhancing such selectivity in photocatalysis have been summarized recently which may help reinvigorate and stimulate future investigations (Kou et al., 2017). A recent tutorial review envisions approaches for attaining higher selectivity and yield of value-added chemicals from lignin using nanocatalysts that are embedded in the inner portions of a photomicroreactor (Colmenares et al., 2017). The development of such futuristic photocatalytic systems for lignin depolymerization in a continuous microreactor could be an exceptional approach for the production of high-value entities starting from lignin depolymerization and the fruitful accomplishment of such approaches may help in commercialization of bio-based chemicals.

Oxidative Catalysis

In recent years, several investigations have been conducted to explore different catalytic processes to obtain high value chemical from biomass. The main focus has been on overcoming the unreactive feedstock by applying acid-catalyzed depolymerization and then seeking oxidative-cleavage in the molecule. Xiong (Xiong et al., 2015, 2016) utilized bimetallic and metal carbide catalysts to have selectivity achieve C-O/C-O and C-C bond-scission; kinetic, spectroscopy, and computational approaches were applied to demonstrate the efficient biomass conversion. The synthesis of 5-hydroxymethylfurfural from carbohydrate sugars using solid catalysts has been reviewed (Agarwal et al., 2017). The formation of lactic acid from hemicellulosic biomass via a non-toxic heterogeneous catalysts-water system has been elucidated (Yang et al., 2015).

The emerging utility of polyoxometalate (POM) catalysts to convert lignocellulosic biomass to useful chemicals is noteworthy (Huber et al., 2006; Chheda et al., 2007; Alonso et al., 2010; De Gregorio et al., 2016; Romero et al., 2016; Albert, 2017; Bertleff et al., 2017; Reichert and Albert, 2017). Albert's group has shown the selective oxidation of biomass to formic acid, using tailor-made polyoxometalate (POMs) catalysts, termed OxFA process; the strategy entails conversion of biomass to formic acid (FA) in aqueous media under oxygen pressure without pretreatment of biomass (Albert, 2017). Studies on the conversion of well-defined substrates (e.g., glucose, cellobiose, xylose, arabinose, mannose, galactose, and cellulose) to FA using Keggin-type POMs with various degrees of metal substitution, soluble vanadium salts (NaVO₃ and VOSO₄), Anderson- and



Wells-Dawson-type POM ($Na_4Cu_2V_8O_{24}$ and $K_8P_2V_2W_{16}O_{62}$), Lindqvist-type POMs ($K_2W_6O_{19}$ and $K_3VW_5O_{19}$) have been performed. Keggin-type POMs had the highest yields of FA, but all model substrates could be oxidized thereby suggesting that these POMs are not suitable for fractionated biomass conversion. In case of the water-soluble vanadium precursors $NaVO_3$ and $VOSO_4$, same catalytic performance like Keggin-type POMs was observed thus limiting their ability for the desired conversion. The Anderson-type POM $Na_4Cu_2V_8O_{24}$ displayed no catalytic activity under the studied reaction conditions. Comparatively, the Wells-Dawson type POM $K_8P_2V_2W_{16}O_{62}$ demonstrated a little undesired conversion of glucose and cellobiose. Among the various POMs, a fractionated oxidation of biomass was only observed with the Lindqvist-type catalyst $K_2W_6O_{19}$, however the yield of FA was low. More research is needed to optimize the reaction conditions to achieve fractionated conversion (Albert, 2017).

The use of ionic liquids in combination with POMs has been investigated to conduct oxidative depolymerization of lignin (Cheng et al., 2014; De Gregorio et al., 2016; Ozdokur et al., 2016; Shatalov, 2016). De Gregorio et al. (2016) applied the ionic liquid (IL), 1-butylimidazolium hydrogensulfate, in combination with vanadium-based POM under oxygen rich environment (oxygen and hydrogen peroxide) to achieve oxidative depolymerization of lignin from pine and willow. Heteropoly compounds (free acids and salts of heteropolyanions, HPAs) possess high Brønsted and Lewis acidity and can perform multi-electron transfer processes efficiently. HPAs-containing homogeneous and heterogeneous

reaction systems can act as bi-functional catalysts to perform oxidative delignification of lignocellulosic biomass by dioxygen (Shatalov, 2016); wood dissolution in HPAs was enhanced in ionic liquids and dioxygen facilitated the biomass delignification in this system. Role of oxygen in enhancing delignification of Southern yellow pine was also noticed in POMs-ionic liquid reaction system (Cheng et al., 2014).

Catalysts, both heterogeneous as well as homogeneous, have shown limited success in terms of cost-efficiency and productivity. The search, therefore, continues for highly acidic and relatively inexpensive and benign material which could easily convert carbohydrates to furanics in an efficient manner preferably with the possibility of total recyclability. Heterogeneous organo-catalysis appears to be an ideal choice as it is devoid of any metals. An organic sulfonated graphitic carbon nitride has been synthesized by Varma and co-workers which demonstrated its prowess in the conversion of carbohydrates to furanics and related value-added chemicals. The salient feature of the material is the high acidity and its stability which could be harnessed even at higher temperatures for cleaving carbohydrates and transforming them into biologically important scaffolds and platform chemicals (Verma et al., 2017a).

Research and development advancements in chemical processing have enabled expeditious reactions that can be accomplished in short span of time and with minimum energy requirements via innovative intensification techniques. The aforementioned photocatalytic conversion of biomass-derived materials into value-added platform chemicals (Verma et al.,

2016a,b) could be improved immensely to provide a potential source of biofuels, solvents and pharmaceutical feedstocks. This could be achieved via a continuous flow reactor using the bimetallic catalyst, comprising Ag and Pd nanoparticles supported on graphitic carbon nitride surface (AgPd@g-C₃N₄). The sustainable feature of the approach is that formic acid used is also accessible from biomass origin and serves as the safer hydrogen source while the photoactive graphitic carbon nitride support is readily available from inexpensive urea (Tadele et al., 2017).

Chitosan derived from marine waste is rich in nitrogen and is an abundant biopolymer often discarded as landfill material. A porous nitrogen-enriched carbonaceous carbon nitride catalyst (PCNx) has been prepared by Varma and co-workers using this discarded material and its utility shown in a metal-free heterogeneous selective oxidation of HMF to 2,5-furandicarboxylic acid (FDCA) (Figure 5); the process uses aerial oxygen under mild conditions to achieve highly useful conversion (Verma et al., 2017b).

Electrochemical Processes

Electrochemical process is one of the promising greener approaches for oxidative pretreatment of lignocellulosic biomass, as it is a reagent-free process (Frontana-Urbe et al., 2010) and entails electrochemical generation of oxidizing agent such as hydroxyl radical to decompose organics or polymers to their mineralization (Sires et al., 2014). It is highly dependent on type of solvent and supporting electrolyte, nature of electrode and the electrode potential (Chum et al., 1985). The process provides means of valorization of lignin to high value compounds such as fine chemicals or biofuels, an essential feature of future biorefinery industries (Tuck et al., 2012; Luque and Triantafyllidis, 2016). For instance, kraft black liquor (wastewater from wood chip washing) is particularly satisfactory for electrochemical process in view of its sufficiently high conductivity (Di Marino et al., 2016).

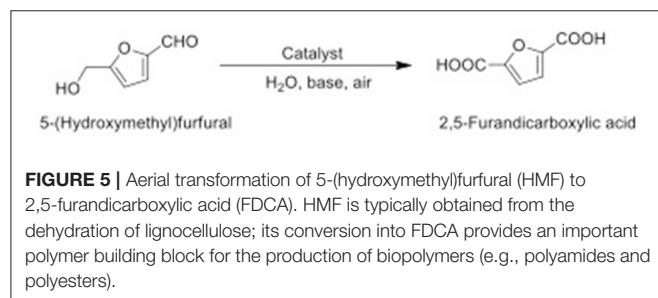
Electrochemical oxidation has been explored for the degradation of lignin, but it suffered from electrode fouling problem caused by polymerization. Recent efforts for the oxidation have moved forward to the development of high activity electrocatalysts (Tolba et al., 2010); nickel-based anode for electrochemical degradation of lignin resulted in yield of high-value fine chemicals like vanillin and acetovanillone (Schmitt et al., 2015). The Ni electrode exhibited high stability and little corrosion issue. 3D materials such as stainless steel

net and Ni form have been employed to improve the yield of vanillin. Possible lignin degradation mechanism was proposed using titanium-based electrodes (Ti/Sb-SnO₂ and Ti/PbO₂) (Shao et al., 2014) wherein decomposition pathway include opening loop of quinoid structure, damage of alkyl-aryl ether bond and demethylation. This study also showed selective and non-selective oxidation models from the studied electrodes.

IrO₂-based electrodes (Ti/Ta₂O₅-IrO₂, Ti/SnO₂-IrO₂, Ti/RuO₂-IrO₂, and Ti/TiO₂-IrO₂) have been fabricated for electrochemical oxidation of lignin to primary products, vanillin and vanillic acid (Di Marino et al., 2016). Among all of the tested electrodes, Ti/Ta₂O₅-IrO₂ showed the highest electrochemical active surface area, while Ti/RuO₂-IrO₂ exhibited the highest stability, long lifetime (40 days) and activity for lignin degradation. The estimated apparent activation energy for the electrode at 20 kJ/mole is similar to the energy for hydroxyl radical reactions (Labat and Gonçalves, 2008). Influence of current density on the oxidation of lignin has been investigated; increase in the current density (200–500 mA/cm²) showed increase in apparent rate constant, but further increase in current density resulted in oxygen evolution reaction and electricity waste. TiO₂ nanotube/PbO₂ electrode was used for the treatment of kraft lignin, taking the advantages of high oxidativity and increased usable surface area (Pan et al., 2012); deposition of PbO₂ nanoparticles onto the TiO₂ nanotube apparently enhanced the electrocatalytic activity of the electrode. The oxidation process followed the pseudo first order kinetic with estimated activation energy of about 16.04 kJ/mole; vanillin and vanillic acid being characterized as the two primary products of the process. These studies suggested that the optimization of current efficiency would greatly benefit the energy- and cost-effectiveness of the process.

Another key electrochemical technology for depolymerization or oxidation of lignocellulosic biomass is electrodialysis that utilizes electric potential as driving force to separate ions or species through an ion exchange membrane. The technique has been widely used in desalination and wastewater treatment processes, and is now a newer area of focus for bio-separation process (Lee et al., 2013). Electrodialysis using bipolar membrane has been utilized to assist acidification pretreatment to extract lignin by precipitation from the kraft black liquor (Haddad et al., 2017) which seemingly used fewer chemicals than conventional acidification pretreatment and could be used to simultaneously produce caustic soda. Electrodialysis has been investigated to integrate with oxalic acid pretreatment of waste mushroom medium (Lee et al., 2013); the method was aimed to remove inhibitory compounds from the process, which consequently increased ethanol production by about three times.

Novel approaches integrating electrochemical process with other pretreatment protocols have garnered attention for biomass processing. Electrochemical depolymerization of lignin has been achieved using the ionic liquids, (1-ethyl-3-methylimidazolium trifluoromethanesulfonate and triethylammonium methanesulfonate) (Dier et al., 2017) which could simultaneously degrade lignin and help assist in the recovery of the electrolyte material. The formation of H₂O₂ played an important role for the lignin degradation. A proposed



mechanism of the degradation of lignin is presented in **Figure 6**. The formation of low molecular weight fractions proposed in the mechanism was confirmed by liquid chromatography-high resolution mass spectrometry (PC-HRMS) and gas chromatography-mass spectrometry (GC-MS) techniques.

Pure deep eutectic solvents (choline chloride with urea or ethylene glycol) coupled with an electrochemical process was investigated to dissolve and process electrochemical oxidative depolymerization of kraft lignin (Di Marino et al., 2016) wherein guaiacol and vanillin were detected as the most abundant products. Electrochemical technology has been deployed to enhance biogas formation via aerobic digestion (Song et al., 2010; Katsoni et al., 2014). Electrochemical process for pretreatment of waste activated sludge showed relatively low specific energy input with improved methane production when compared to other pretreatment methods involving microwave, ultrasound, thermal, Fenton, and ozone (Ye et al., 2016).

Fenton and Fenton-Like Reactions

Fenton reaction involves hydrogen peroxide (H_2O_2) and ferrous iron that generate highly reactive species $\bullet\text{OH}$ [$\text{Fe(II)} + \text{H}_2\text{O}_2 \rightarrow \text{Fe(II)} + \bullet\text{OH} + \text{OH}^-$] (Ganzenko et al., 2017; Jain et al., 2017). Fenton reaction is commonly used to oxidize contaminants such as dyes, trichloroethylene (TCE) and perchloroethylene (PCE) (Diagne et al., 2014; Lin et al., 2017) and generally works efficiently in the pH range from 2.5 to 3.5. Other limitation of the Fenton reaction is the production of iron-containing sludge as secondary pollutants. To overcome this disadvantage of the Fenton reaction, heterogeneous iron-containing catalysts are applied to produce Fenton-like reactions (Barhoumi et al., 2016; Ouiriemmi et al., 2017; Steter et al., 2018); such reactions have been extensively sought to degrade and mineralize numerous organic pollutants (Feng et al., 2017; Mirzaei et al., 2017; Sharma and Feng, 2017; Li et al., 2018).

Zhang and Zhu (2016) studied the synergistic effects of pretreatment of sugarcane bagasse (SCB) using Fenton reaction and NaOH extraction on sugarcane bagasse. Sugarcane bagasse (5 g) was added to a solution of Fe^{2+} (50 mL) to make for a solid-liquid ratio of 5%. Enzymatic hydrolysis and fermentation was done using SHY07-1 yeast (inoculum dosage of 10% v/v) and glycerol stock in YPX medium. Sugar analysis along with SEM and XRD analysis was performed. The optimum Fe^{2+} concentration was found to be 20 mM and the concentration of hydrogen peroxide was fixed at 10% (w/w). Similarly, the pH and temperature were optimized to 2.5 and 55°C respectively. It was found that initial NaOH extraction followed by Fenton reaction had little or no effect on the sugarcane bagasse structure. On the other hand, Fenton reaction first followed by NaOH extraction resulted in the enhanced erosion of the structure by subsequent NaOH extraction step (de Almeida et al., 2013).

Simultaneous saccharification fermentation (SSF) is considered a process to decrease cellulase inhibition by glucose and simplify the operation via the integration of saccharification and fermentation steps, thereby increasing the fermentation efficiency (Hasunuma and Kondo, 2012). It was discovered that the NaOH extraction as compared to Fenton reaction resulted in greater ethanol production. Apparently, Fenton reaction

causes high accumulation of Fe^{3+} ions which inhibit the activity of β -glucosidase culminating in less conversion of glucose to ethanol.

An ideal pretreatment step is one in which the cellulose is left unharmed while a majority of the lignin and hemicellulose are removed (Gabhane et al., 2015). In the case of Fenton pretreatment, there was an 18.3% removal of lignin component, a 16% increase in cellulose and a slight decrease in hemicellulose; total cellulose being 55.8% which was still higher than that of the raw sugarcane bagasse (52.8%). Conventional alkaline pretreatment had a lignin removal rate of 42%. NaOH extraction achieved more total cellulose content and less residual lignin in the pretreated sugarcane bagasse than Fenton pretreatment. The combination of the two methods (NaOH extraction followed by Fenton pretreatment), however, showed a synergistic performance, with about 50% of lignin removal and almost 100% increase in cellulose content. There was a large hemicellulose loss with only 6.8% remaining after the synergistic performance. When the sequence order was reversed, there was a steady increase of 59.8% in lignin removal, a slightly lower cellulose content but less hemicellulose loss.

Jung et al. (2015) studied the effect of Fenton pretreatment of rice straw on the increase in the enzymatic digestibility for the saccharification of lignocellulosic biomass wherein the Fenton's reagent (FeCl_3 and H_2O_2) was used. This was the first reported application of the Fenton reaction for lignocellulose pretreatment at a modest temperature of 25°C and with a relatively higher biomass loading of 10% (w/v). The concentrations of FeCl_3 and H_2O_2 were altered between 0.01–0.1 and 0.5–4.0 M, respectively, to afford varying ratios of Fe^{3+} to H_2O_2 in the range of 1:10–1:100. A temperature of 25°C was maintained and the mixture was shaken at 200 rpm. The various byproducts namely HMF, furfural, acetic acid, levulinic acid, formic acid and glycerol, formed in the dissolved fraction of the pretreated rice straw slurry were quantified by HPLC measurements.

For a fixed FeCl_3 concentration, the enzymatic digestibility of rice straw pretreated with the Fenton's reagent usually enhanced with an increased H_2O_2 concentration possibly due to the greater oxidizing ability of H_2O_2 under acidic environments. Higher digestibility values, 88.7 and 87.5% of the theoretical maximum glucose yield, were obtained after pretreatment using the two diverse concentrations of the Fenton's reagents comprising 0.03 M FeCl_3 and 2.25 M H_2O_2 and 0.05 M FeCl_3 and 2.5 M H_2O_2 , respectively. An analysis of the rice straw after pretreatment with the Fenton's reagent for 24 h showed that the amounts of both, the lignin and xylan were substantially reduced to 9.3 and 3.6%, respectively. When either H_2O_2 or FeCl_3 was used as the only reagent for pretreatment, the amount of lignin was reduced to 16.2 and 15.7%, respectively. Additionally, when ~40% of the initial amounts of lignin and glucan were solubilized after pretreatment using various compositions of the Fenton's reagent, higher values of enzymatic digestibilities i.e., > 70% were observed. This significant solubilization, in conjunction with breakdown of sugar in the rice straw could be due to the indiscriminate oxidation of lignocellulose by engendered reactive oxygen species in the Fenton reaction.

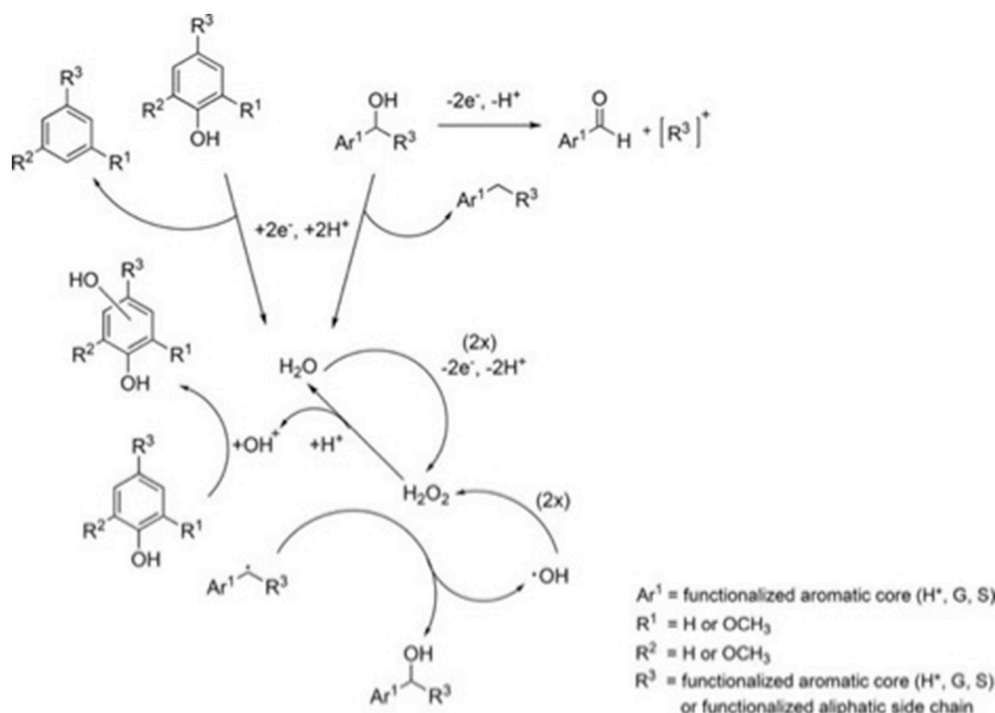


FIGURE 6 | Abbreviated reaction scheme showing proposed electrochemical/radical mechanisms during lignin degradation. The numbers in parentheses give the equivalents of raw material needed for the reaction. Aromatic core units are defined as follows: (H*) 4-hydroxybenzyl, (G) 3-methoxy-4-hydroxybenzyl, (S) 3,5-dimethoxy-4-hydroxybenzyl. The figure is reproduced, without change, from Dier et al. (2017). The article is supported under the CC BY-NC-ND license (<http://creativecommons.org/licenses/by/4.0/>).

The whole mechanism of the Fenton reaction in the pretreatment of rice straw is as follows. The presence of Fe³⁺ and H₂O₂ yield an array of reactive oxygen species, e.g., hydroxyl-, perhydroxyl radicals, organic peroxy radicals, and iron ion conjugates namely ferrous- and ferryl-binding compounds which attack lignin and hemicellulose on the outer surface of lignocellulose, and generate demethylated, oxidized, or fragmented lignin and polysaccharides (Koenigs, 1974; Kirk et al., 1985).

Kato et al. (2014) studied the effect of Fenton pretreatment on the total organic carbon (TOC) and lignin composition of four biomass feedstocks miscanthus (*Miscanthus giganteus*), switchgrass (*Panicum virgatum*), wheat straw (*Triticum aestivum*) and corn stover (*Zea mays*). Enzymatic saccharification showed a significant increase in glucose production upon Fenton pretreatment across all four feedstocks as well as an increase in cellulose bioavailability to *in vitro* cellulase exposure. The latter suggests a reduction in the recalcitrant nature inherent to lignocellulosic materials. A lignin assay analysis was performed on all four samples which showed that there was a decrease in the acid-insoluble lignin (AISL) content in miscanthus (6.63%), corn stover (14.1%) and wheat straw (8.76%) while switchgrass (3.59%) produced no statistically significant decrease ($P < 0.05$). In the case of acid soluble lignin (ASL) content, switchgrass (22.6%) and wheat straw (16.8%) showed a statistically significant ($p < 0.05$) decrease while both miscanthus

(4.61%) and corn stover (0%) showed no decrease relative to the untreated biomass. The aforementioned results show that solution phase Fenton pretreatment may not be degrading lignin as seen in *in vivo* Fenton chemistry of white-rot fungi. It is however, altering the biomass in a way that allows cellulose to be bioavailable as observed by the significant increase in enzymatic saccharification. It has been postulated that Fenton pretreatment may possibly clip or alter the macrostructure of lignin analogous to ammonia fiber explosion (AFEX), thus enabling cellulase enzymes better access to cellulose (Kumar et al., 2009). Aforementioned studies suggest that Fenton reaction can be effective in fragmenting the surface structure but less likely to selectively oxidize the lignocellulosic components into desirable chemical derivatives without other means of oxidative intervention.

OUTLOOK AND PERSPECTIVE ON THE CONVERSION OF BIOMASS INTO VALUE-ADDED CHEMICALS

Techno-Economic Assessment

The concept of biorefineries using lignocellulosic biomass residues as raw feedstocks has been defined and discussed extensively over the past decade in an effort to accelerate the commercialization process to provide a sustainable alternative

to the growing demand of energy. Earlier studies have focused on supply chain modeling and optimization for biomass harvesting, collection, inventory, preprocessing, production, and distribution of the biofuel system to provide tools for strategic analysis and tactical planning that aimed to minimize cost of production (Zamboni et al., 2009; Kim et al., 2011; Rincón et al., 2015). This is mostly because biomass is characterized by seasonal and geographical fluctuations, hence the conventional, vertically integrated feedstock supply system where feedstock is obtained from local growers, and delivered in low-density format to the centralized conversion facility can be cost prohibitive. Additionally, feedstock supply scarcities and price instabilities due to reduced harvests and competition from other industries can also pose risks to investment and plant operation (Lamers et al., 2015). Studies have shown that the cost of pretreatment of heterogeneous biomass residues and the charges for collection, inventory and transportation can take up as much as 50% of the production cost distribution of lignocellulosic biofuels and biochemicals. Kurian et al. (2013) reviewed these aspects addressing the feedstocks supply chain and logistics system for lignocellulosic biorefineries, aiming to reduce the cost and improve profit distribution for the economical production from low density lignocellulosic biomass. One of the models to help the causes is to form decentralized depots of on-site biomass collection and preprocessing. The approach is built on the concept of having a network of biomass supply chain for the operation of a biorefinery by pretreating biomass into various intermediate products. These transitional products can meet the biomass supply for the production of biofuels and biochemicals, and the local demands for electricity and animal feed. The decentralized biomass pretreatment that densifies the feedstocks can then be transported to a centralized biorefinery for the conversion into fuels and chemicals. This strategy can effectively reduce the transportation cost and increase the production capacity, while addressing the local resource demands and environmental issues. In brief, the options to reduce negative impacts on resource and environment include: i) native sourcing of lignocellulose; ii) improving crop traits; and iii) developing a biorefinery model. Both options (ii) and (iii) can potentially aim to attain higher yield of energy and value-added products, and to reduce the resource and environmental impacts. In this regard, replacing conventional pretreatment processes involving abrasive chemicals and energy-intensive conditions with milder physical and chemical processes are in line with the future visions of the biorefinery technologies.

Life-Cycle Perspective

Life cycle assessment (LCA) of environmental impacts is of particular interest for biomass-related studies. It is a fundamental analytical approach to understand the actual contributions to climate change or other environmental issues thus identifying opportunities for environmental improvements (Gnansounou et al., 2009; Singh et al., 2010). It is also an important step for sustainability improvement of green chemistry technologies before scale up or implementation (Tufvesson et al., 2013). LCA of lignocellulosic biofuel have been primarily studied for the converting biomass into ethanol. Lignocellulosic ethanol

was generally reported to have lower greenhouse gas (GHG) emissions than gasoline and conventional grain-based ethanol (Gerbrandt et al., 2016). Morales et al. (2015) and Borrión et al. (2012) also concluded a clear reduction in GHG emissions and ozone layer depletion for lignocellulosic ethanol studies, with highest reduction for corn stover and wheat straw, while other impacts such as acidification, eutrophication, human health and photochemical smog were positively or negatively affected. Most of the LCA studies on lignocellulosic ethanol production appear to be energetically sustainable, with energy balance ratio (heat content of the fuel to non-renewable primary energy input for the fuel) > 1, partly due to the possibility of using by-products as fuel in a cogeneration system (Gerbrandt et al., 2016).

As most of the lignocellulosic biomass pretreatment methods are still under development, there is a limited understanding on their environmental impacts (Prasad et al., 2016). Pretreatment of wheat straw using steam explosion without acid catalyst (SE), liquid hot water (LHW) and wet oxidation (WO) were environmentally favorable over dilute acid (DA) and steam explosion with acid catalyst (SEAC), from LCA results. Pretreatments of SEAC and DA that employed sulfuric acid and ammonia as reagents resulted in comparable contributions in global warming, acidification, eutrophication, ozone layer depletion and ecotoxicity impacts (Wang et al., 2013). Similarly, for a LCA study of corn stover-based ethanol pretreated by LHW, DA, SEAC and organosolv, LHW demonstrated the highest sugar conversion rates and significant reduction in CO₂ emissions but slightly higher water depletion rates, whereas DA was the least preferable choice due to long processing duration (12 h) and intensive electricity use (Gnansounou et al., 2009). Relatively higher acidification potential was also discerned in that study, as a consequence of significant SO₂ emissions from electricity production for the lime pretreatment step (Gnansounou et al., 2009). Electrochemical oxidation of lignin consumes considerably low electricity and is regarded as an environmentally friendly pretreatment method (Shao et al., 2014).

The use of acidic and basic reagents as well as energy demands for processing seemed to determine the contribution of environmental impacts of conversion of lignocellulosic biomass into products. To this end, development of green and sustainable pretreatment and treatment of the lignocellulosic biomass is generally encouraged. Future efforts in energy-intensive approaches such as SEAC and DA can be improved by substituting their energy being supplied using greener or renewable energy sources (Gnansounou et al., 2009). A modified DA pretreatment for woodchip-based bioethanol was proposed to reduce environmental impacts of land use by 18.5% and ecosystem quality by 17% (Shadbahr et al., 2015). Electrodialysis was investigated for a multistage of oxalic acid-based pretreatment to recover and reuse of the acid (Pan et al., 2012). Deep eutectic solvent as an inexpensive environmentally reagent (Khandelwal et al., 2016) was investigated for selective generation of vanillin by electrochemical process (Tuck et al., 2012). Synergistic benefits have been demonstrated for combinative pretreatment systems (Kavitha et al., 2015). These propositions incorporate the green chemistry principles with

improvements to prevent waste and use of hazardous materials, improve material and energy efficiencies, use of renewable resources and, design for reusing/recycling (Tabone et al., 2010).

Socio-Economic Impact of Valorizing Biomass Residue

While LCA framework and methodology provides quantitative indicators that can adequately address the techno-economic and environmental impacts of a developing technology such as lignocellulosic biofuels, the socio-economic and cultural impacts are engaging more subjective arguments given the value conflicts of any given society. For example, Malik et al. (2016) developed an input-output (IO) analysis combining LCA criteria to assess the “triple bottom line” (i.e., social, economic and environmental impacts) of lignocellulosic biofuel production in South Australia. They concluded that gains in economic activities and employment outweigh the losses, in that the biofuel industry would increase the productivity and economic growth in rural part of the regional Australia. The study also showed that the lignocellulosic biofuel industry would result in net carbon-negative (i.e., the amount of CO₂ emitted will be less than the amount sequestered for obtaining the wood biomass), and that the energy return on investment (EROI) for all the cellulose-refining scenarios gave a net gain in energy. Diamantopoulou et al. (2016) evaluated the socio-environmental impacts of fermented biofuels with two different feedstocks (wheat bran and barley straw) in Greece by formulating a metric tool named “biomass sustainability index” (BSI) consisting of three vectors (i.e., preserving natural resource, maintaining natural cycle and ecosystem, social acceptance) that are further expanded into 12 indicators. The scoring system based on three-level (positive, negative, neutral) feedbacks from participants gives a mapping analysis how the public perceive the biofuel industry. The BSI of each of the first-generation ethanol received low scoring and did not appear sustaining as compared with ethanol generated from various biomass residues. Briefly, the study concluded that the “best-practice” scenario with barley straw as the biofuel feedstock received markedly higher score than it did with wheat bran, whereas both feedstocks received low and similar scores under the scenario of “maximum profit”, primarily attributed to perceived concern of irreversible resource and environmental harms. Neither of the feedstock BSIs showed any significantly impact on local employment and regional development, implying the stakeholders in the region did not expect a major economic contribution from the biomass-to-bioenergy industry.

To close the gap in the dimension of social impact of biofuels, Ribeiro and Quintanilla (2015) applied the Delphi survey technique to explore the perception of biofuel experts from diverse countries on prospective social impacts of cellulosic ethanol. The study devised two technological pathways to address the technical aspects of a transition of cellulosic ethanol from conventional feedstock (e.g., starchy and sweet crops) to second-generation lignocellulosic feedstock (e.g., dedicated energy crops, residues, municipal organic solid waste). The participants were surveyed for their opinions on the potential impacts pertaining to social dimension (e.g., negative impacts on food security,

the inclusion of small-scale farmers, exclusion of low-skilled workers, exclusion of small-scale producers in the supply chain) and environmental dimension (e.g., negative impacts on water security, negative impacts on biodiversity security) with several scenarios involving different regions, type and source of feedstocks. The opinions of expert panelists indicated that using non-edible raw material in place of food crops to produce cellulosic ethanol might not be the answer to overcome food security concerns. They considered the lignocellulosic feedstock for ethanol production rests in the same agricultural paradigm to that of conventional ethanol. However, the use of municipal solid waste and residues as feedstock for cellulosic ethanol production was considered favorable over the use of selected energy crops. Also, given that cellulosic ethanol is still being produced on an experimental stage, the contribution of cellulosic ethanol to rural development (supply chain comprising predominately small landholders and small-scale producers) is uncertain. This study shows that experts were skeptical on the prospect of transitioning bioethanol production from convention to lignocellulosic feedstocks, especially when production is based in poorer countries.

To bring the debate of social value into more systematic discussion, Raman et al. (2015) applied the framework of responsible innovation, which emphasizes developing a shared understanding of how to bring forth societal and value questions on a technology innovation, to sustainability assessment. The value-based questions, such as the valuation of land, of biomass, and of nature, often dictate how the members of a regional-specific society assess the potential impacts of lignocellulosic biofuels on environment (i.e., GHG emissions, biodiversity, water, soil, and air) and access to resources (i.e., food, water, energy). These potential impacts by the life-cycle components (e.g., crops, residues, processing, conversion, and distribution) can be individually identified and evaluated in either global scope or regional scope. Furthermore, the basis with which the core values are compared must be defined. For example, the core value pertaining to the techno-economic proficiency of lignocellulosic biofuels is compared with the first-generation biofuels and fossil fuels, whereas the yardstick for socio-economic justice is the impacts on global agricultural economy as compared to the existing system. One such argument is that, while first-generation biofuels imposes concerns on food competition, the question of whether producing second-generation biofuels (lignocellulosic biofuels) would distribute socio-economic impacts more fairly than the first-generation biofuels (or fossils) lingers. This is because biomass is characterized by seasonal and geographical variations, reflecting that lignocellulosic biomass residues could be an indispensable source of energy, food, animal feeds, or other uses in different regions of the world, especially in the developing countries. In summary, each stakeholder inherently prioritizes its own interests and needs, adding a great deal of uncertainties to the steady supply of biomass residues (Perez et al., 2017). Therefore, even with multitude of drivers, commercializing biofuel production from lignocellulosic biomass does not guarantee the eventual economic benefits for farmers or biomass producers, unless a well-thought management and logistics are implemented.

AUTHOR CONTRIBUTIONS

WD took the lead in coordinating the review study and drafting the manuscript. WD, VS, RV, ML, and GN all performed critical reviews and contributed to the writing of sections Greener Oxidative Processes for Biomass Conversion-Selectivity and Mechanism. ML also contributed part of section Outlook and Perspective on the Conversion of Biomass into Value-Added Chemicals. RV and VS critically revised the article and helped

shape the final version of the article. All authors provided comments on the manuscript and approve the final version to be published.

ACKNOWLEDGMENTS

One of the authors, WD, thanks the Ministry of Science and Technology (Taiwan) for the financial support through project 106-2918-I-029-002.

REFERENCES

- Abdelaziz, O., Brink, D. P., Prothmann, J., Ravi, K., Sun, M., Garcia-Hidalgo, J., et al. (2016). Biological valorization of low molecular weight lignin. *Biotechnol. Adv.* 34, 1318–1346. doi: 10.1016/j.biotechadv.2016.10.001
- Agarwal, B., Kailasam, K., Sangwan, R. S., and Elumalai, S. (2017). Traversing the history of solid catalysts for heterogeneous synthesis of 5-hydroxymethylfurfural from carbohydrate sugars: a review. *Renew. Sust. Energ. Rev.* 82, 2408–2425. doi: 10.1016/j.rser.2017.08.088
- Albert, J. (2017). Selective oxidation of lignocellulosic biomass to formic acid and high-grade cellulose using tailor-made polyoxometalate catalysts. *Faraday Discuss.* 202, 99–109. doi: 10.1039/C7FD00047B
- Al jibouri, A. K. H., Turcotte, G., Wu, J., and Cheng, C. H. (2015). Ozone pretreatment of humid wheat straw for biofuel production. *Energ. Sci. Eng.* 3, 541–548. doi: 10.1002/ese3.93
- Alonso, D. M., Bond, J. Q., Serrano-Ruiz, J. C., and Dumesic, J. A. (2010). Production of liquid hydrocarbon transportation fuels by oligomerization of biomass-derived C9 alkenes. *Green Chem.* 12, 992–999. doi: 10.1039/c001899f
- Alvira, P., Tomás-Pejó, E., Ballesteros, M., and Negro, M. J. (2010). Pretreatment technologies for an efficient bioethanol production process based on enzymatic hydrolysis: a review. *Bioresour. Technol.* 101, 4851–4861. doi: 10.1016/j.biortech.2009.11.093
- Amirta, R., Tanabe, T., Watanabe, T., Honda, Y., Kuwahara, M., and Watanabe, T. (2006). Methane fermentation of Japanese cedar wood pretreated with a white rot fungus, *Ceriporiopsis subvermispora*. *J. Biotechnol.* 123, 71–77. doi: 10.1016/j.jbiotec.2005.10.004
- Badshah, M., Lam, D. M., Liu, J., and Mattiasson, B. (2012). Use of an automatic methane potential test system for evaluating the biomethane potential of sugarcane bagasse after different treatments. *Bioresour. Technol.* 114, 262–269. doi: 10.1016/j.biortech.2012.02.022
- Bairamzadeh, S., Saidi-Mehrabad, M., and Pishvaei, M. S. (2018). Modelling different types of uncertainty in biofuel supply network design and planning: a robust optimization approach. *Renew. Energ.* 116, 500–517. doi: 10.1016/j.renene.2017.09.020
- Barhoumi, N., Oturan, N., Olvera-Vargas, H., Brillas, E., Gadri, A., Ammar, S., et al. (2016). Pyrite as a sustainable catalyst in electro-Fenton process for improving oxidation of sulfamethazine. kinetics, mechanism and toxicity assessment. *Water Res.* 94, 52–61. doi: 10.1016/j.watres.2016.02.042
- Barrerra-Martinez, I., Guzman, N., Pena, E., Vazquez, T., Caron-Camacho, R., Folch, J., et al. (2016). Ozonolysis of alkaline lignin and sugarcane bagasse: structural changes and their effect on saccharification. *Biomass Bioenerg.* 94, 167–172. doi: 10.1016/j.biombioe.2016.08.010
- Bertleff, B., Claußnitzer, J., Korth, W., Wasserscheid, P., Jess, A., and Albert, J. (2017). Extraction coupled oxidative desulfurization of fuels to sulfate and water-soluble sulfur compounds using polyoxometalate catalysts and molecular oxygen. *ACS Sustain. Chem. Eng.* 5, 4110–4118. doi: 10.1021/acssuschemeng.7b00087
- Borrión, A. L., McManus, M. C., and Hammond, G. P. (2012). Environmental life cycle assessment of lignocellulosic conversion to ethanol: a review. *Renew. Sustain. Energ. Rev.* 16, 4638–4650. doi: 10.1016/j.rser.2012.04.016
- Brebu, M., and Vatile, C. (2010). Thermal degradation of lignin-a review. *Cell. Chem. Technol.* 44, 353–363.
- Bu, Q., Lei, H., Wang, L., Wei, Y., Zhu, L., Zhang, X., et al. (2014). Bio-based phenols and fuel production from catalytic microwave pyrolysis of lignin by activated carbons. *Bioresour. Technol.* 162, 142–147. doi: 10.1016/j.biortech.2014.03.103
- Bundhoo, Z. M. A. (2018). Microwave-assisted conversion of biomass and waste materials to biofuels. *Renew. Sust. Energ. Rev.* 82, 1149–1177. doi: 10.1016/j.rser.2017.09.066
- Cavka, A., Wallenius, A., Alriksson, B., Nilvebrant, N.-O., and Jönsson, L. J. (2015). Ozone detoxification of steam-pretreated Norway spruce. *Biotechnol. Biofuels* 8, 196–206. doi: 10.1186/s13068-015-0388-7
- Cesaro, A., and Belgiorno, V. (2013). Sonolysis and ozonation as pretreatment for anaerobic digestion of solid organic waste. *Ultrason. Sonochem.* 20, 931–936. doi: 10.1016/j.ultsonch.2012.10.017
- Chang, C. N., Ma, Y. S., Fang, G.-C., Chao, A. C., Tsai, M.-C., and Sung, H.-F. (2004). Decolorizing of lignin wastewater using the photochemical UV/TiO₂ process. *Chemosphere* 56, 1011–1017. doi: 10.1016/j.chemosphere.2004.04.021
- Cheng, F., Wang, H., and Rogers, R. D. (2014). Oxygen enhances polyoxometalate-based catalytic dissolution and delignification of woody biomass in ionic liquids. *ACS Sustain. Chem. Eng.* 2, 2859–2865. doi: 10.1021/sc500614m
- Chheda, J. N., Huber, G. W., and Dumesic, J. A. (2007). Liquid-phase catalytic processing of biomass-derived oxygenated hydrocarbons to fuels and chemicals. *Angew. Chem. Int. Ed.* 46, 7164–7183. doi: 10.1002/anie.200604274
- Choong, F. X., Bäck, M., Steiner, S. E., Melican, K., Nilsson, N. P. R., Edlund, U., et al. (2017). Nondestructive, real-time, determination and visualization of cellulose, hemicellulose and lignin by luminescent oligothiophenes. *Sci. Rep.* 6:35578. doi: 10.1038/srep35578
- Chum, H. L., Sopher, D. W., and Schroeder, H. A. (1985). “Electrochemistry of lignin materials and derived compounds,” in *Fundamentals of Thermochemical Biomass Conversion*, eds R. P. Overend, T. A. Milne, and L. K. Mudge (Dordrecht: Springer Netherlands), 1103–1113.
- Clark, J. M., Deswarte, F. E. I., and Farmer, T. J. (2009). The integration of green chemistry into future biorefineries. *Biofuels Bioprod. Biorefin.* 3, 72–90. doi: 10.1002/bbb.119
- Colmenares, J. C., Varma, R. S., and Nair, V. (2017). Exploring strategies for selective photocatalysis of lignin-inspired chemicals by integrating hybrid nanocatalysis in microfluidic reactors. *Chem. Soc. Rev.* 46, 6675–6686. doi: 10.1039/C7CS00257B
- Crestini, C., Crucianelli, M., Orlandi, M., and Saladino, R. (2010). Oxidative strategies in lignin chemistry: a new environmental friendly approach for the functionalization of lignin and lignocellulosic fibers. *Catal. Today* 156, 8–22. doi: 10.1016/j.cattod.2010.03.057
- de Almeida, M. N., Falkoski, D. L., Guimarães, V. M., Ramos, H. J. D. O., Visser, E. M., Maitan-Alfenas, G. P., et al. (2013). Characteristics of free endoglucanase and glycosidases multienzyme complex from *Fusarium verticillioides*. *Bioresour. Technol.* 143, 413–422. doi: 10.1016/j.biortech.2013.06.021
- De Bhowmick, G., Sarmah, A. K., and Sen, R. (2017). Lignocellulosic biorefinery as a model for sustainable development of biofuels and value added products. *Bioresour. Technol.* 247, 1144–1154. doi: 10.1016/j.biortech.2017.09.163
- De Gregorio, G. F., Prado, R., Vriamont, C., Erdocia, X., Labidi, J., Hallett, J. P., et al. (2016). Oxidative depolymerization of lignin using a novel polyoxometalate-protic ionic liquid system. *ACS Sustain. Chem. Eng.* 4, 6031–6036. doi: 10.1021/acssuschemeng.6b01339
- Diagne, M., Sharma, V. K., Oturan, N., and Oturan, M. A. (2014). Depollution of indigo dye by anodic oxidation and electro-Fenton using B-doped diamond anode. *Environ. Chem. Lett.* 12, 219–224. doi: 10.1007/s10311-013-0437-z

- Dick, G. R., Frankhouser, A. D., Banerjee, A., and Kanan, M. W. (2017). A scalable carboxylation route to furan-2,5-dicarboxylic acid. *Green Chem.* 19, 2966–2972. doi: 10.1039/C7GC01059A
- Di Marino, D., Stockmann, D., Kriescher, S., Stiefel, S., and Wessling, M. (2016). Electrochemical depolymerisation of lignin in a deep eutectic solvent. *Green Chem.* 18, 6021–6028. doi: 10.1039/C6GC01353H
- Diamantopoulou, L., Papadaki, S., and Karaoglanoğlu, L. (2016). The new era of European biofuels landscape: comparative assessment of socio-environmental sustainability of lignocellulosic feedstocks. *Cell. Chem. Technol.* 50, 507–519. doi: 10.1016/j.envdev.2015.03.006
- Dier, T. K. F., Rauber, D., Durneata, D., Hempelmann, R., and Volmer, D. A. (2017). Sustainable electrochemical depolymerization of lignin in reusable ionic liquids. *Sci. Rep.* 7:5041. doi: 10.1038/s41598-017-05316-x
- Elizabeth, T. A., Julius, K. O., Ekaette, N. D., Sudipta, S. B., Das, S., and Barooah, M. (2016). Influence of different substrates on lignolytic enzyme production in improved strains of wood ear mushroom (*Auricularia* species). *J. Sci. Ind. Res.* 75, 740–746. Available online at: <http://nopr.niscair.res.in/handle/123456789/38166>
- Farag, S., Fu, D., Jessop, P. G., and Chaouki, J. (2014). Detailed compositional analysis and structural investigation of a bio-oil from microwave pyrolysis of kraft lignin. *J. Anal. Appl. Pyrolysis* 109, 249–257. doi: 10.1016/j.jaap.2014.06.005
- Feng, L., and Chen, Z. I. (2008). Research progress on dissolution and functional modification of cellulose in ionic liquids. *J. Mol. Liq.* 142, 1–5. doi: 10.1016/j.molliq.2008.06.007
- Feng, M., Wang, Z., Dionysiou, D. D., and Sharma, V. K. (2017). Metal-mediated oxidation of fluoroquinolone antibiotics in water: a review on kinetics, transformation products, and toxicity assessment. *J. Hazard. Mater.* 344, 1136–1154. doi: 10.1016/j.jhazmat.2017.08.067
- Field, C. B., Campbell, J. E., and Lobell, D. B. (2008). Biomass energy: the scale of the potential resource. *Trends Ecol. Evol.* 23, 65–72. doi: 10.1016/j.tree.2007.12.001
- Fromm, J., Rockel, B., Lautner, S., Windeisen, E., and Wanner, G. (2003). Lignin distribution in wood cell walls determined by TEM and backscattered SEM techniques. *J. Struct. Biol.* 143, 77–84. doi: 10.1016/S1047-8477(03)00119-9
- Frontana-Urbe, B. A., Little, R. D., Ibanez, J. G., Palma, A., and Vasquez-Medrano, R. (2010). Organic electrosynthesis: a promising green methodology in organic chemistry. *Green Chem.* 12, 2099–2119. doi: 10.1039/c0gc00382d
- Fu, D., Farag, S., Chaouki, J., and Jessop, P. G. (2014). Extraction of phenols from lignin microwave-pyrolysis oil using a switchable hydrophilicity solvent. *Bioresour. Technol.* 154, 101–108. doi: 10.1016/j.biortech.2013.11.091
- Gabhane, J., Prince William, S. P. M., Vaidya, A. N., Das, S., and Wate, S. R. (2015). Solar assisted alkali pretreatment of garden biomass: effects on lignocellulose degradation, enzymatic hydrolysis, crystallinity and ultra-structural changes in lignocellulose. *Waste Manag.* 40, 92–99. doi: 10.1016/j.wasman.2015.03.002
- Ganzenko, O., Trellu, C., Papirio, S., Oturan, N., Huguenot, D., van Hullebusch, E. D., et al. (2017). Bioelectro-Fenton: evaluation of a combined biological–advanced oxidation treatment for pharmaceutical wastewater. *Environ. Sci. Pollut. Res.* doi: 10.1007/s11356-017-8450-6. [Epub ahead of print].
- Gao, J., Chen, L., Yan, Z., and Wang, L. (2013). Effect of ionic liquid pretreatment on the composition, structure and biogas production of water hyacinth (*Eichhornia crassipes*). *Bioresour. Technol.* 132, 361–364. doi: 10.1016/j.biortech.2012.10.136
- Garcia-Cubero, M., Gonzalez-Benito, G., Indacoechea, I., Coca, M., and Bolado, S. (2016). Effect of ozonolysis pretreatment on enzymatic digestibility of wheat and rye straw. *Bioresour. Technol.* 100, 1608–1613. doi: 10.1016/j.biortech.2008.09.012
- Gazi, S., Ng, W. K. H., Ganguly, R., Moeljadi, A. M. P., Hirao, H., and Soo, H. S. (2015). Selective photocatalytic C–C bond cleavage under ambient conditions with earth abundant vanadium complexes. *Chem. Sci.* 6, 7130–7142. doi: 10.1039/C5SC02923F
- Gerbrandt, K., Chu, P. L., Simmonds, A., Mullins, K. A., MacLean, H. L., Griffin, W. M., et al. (2016). Life cycle assessment of lignocellulosic ethanol: a review of key factors and methods affecting calculated GHG emissions and energy use. *Curr. Opin. Biotechnol.* 38, 63–70. doi: 10.1016/j.copbio.2015.12.021
- Gnansounou, E., Dauriat, A., Villegas, J., and Panichelli, L. (2009). Life cycle assessment of biofuels: energy and greenhouse gas balances. *Bioresour. Technol.* 100, 4919–4930. doi: 10.1016/j.biortech.2009.05.067
- Gong, J., Imbault, A., and Farnood, R. (2017). The promoting role of bismuth for the enhanced photocatalytic oxidation of lignin on Pt-TiO₂ under solar light illumination. *Appl. Catal. B* 204, 296–303. doi: 10.1016/j.apcatb.2016.11.045
- Haddad, M., Bazinet, L., Savadogo, O., and Paris, J. (2017). A feasibility study of a novel electro-membrane based process to acidify Kraft black liquor and extract lignin. *Proc. Safety Env. Protec.* 106, 68–75. doi: 10.1016/j.psep.2016.10.003
- Hasunuma, T., and Kondo, A. (2012). Consolidated bioprocessing and simultaneous saccharification and fermentation of lignocellulose to ethanol with thermotolerant yeast strains. *Process Biochem.* 47, 1287–1294. doi: 10.1016/j.procbio.2012.05.004
- He, L., Huang, H., Zhang, Z., and Lei, Z. (2016). A Review of hydrothermal pretreatment of lignocellulosic biomass for enhanced biogas production. *Curr. Org. Chem.* 19, 437–446. doi: 10.2174/1385272819666150119223454
- Heinze, T., Schwikal, K., and Barthel, S. (2005). Ionic liquids as reaction medium in cellulose functionalization. *Macromol. Biosci.* 5, 520–525. doi: 10.1002/mabi.200500039
- Hendriks, A. T. W. M., and Zeeman, G. (2009). Pretreatments to enhance the digestibility of lignocellulosic biomass. *Bioresour. Technol.* 100, 10–18. doi: 10.1016/j.biortech.2008.05.027
- Huber, G. W., Iborra, S., and Corma, A. (2006). Synthesis of transportation fuels from biomass: chemistry, catalysts, and engineering. *Chem. Rev.* 106, 4044–4098. doi: 10.1021/cr068360d
- Jain, B., Singh, A. K., and Sharma, V. K. (2017). Degradation of naphthylazo anionic dye by fenton and fenton-like processes: a comparative study with fast sulphon black-F. *Desalin. Water Treat.* 62, 252–256. doi: 10.5004/dwt.2017.1455
- Jung, Y. H., Kim, H. L., Park, H. M., Park, Y.-C., Park, K., Seo, J.-H., et al. (2015). Mimicking the Fenton reaction-induced wood decay by fungi for pretreatment of lignocellulose. *Bioresour. Technol.* 179, 467–472. doi: 10.1016/j.biortech.2014.12.069
- Kato, D. M., Elia, N., Flythe, M., and Lynn, B. C. (2014). Pretreatment of lignocellulosic biomass using fenton chemistry. *Bioresour. Technol.* 162, 273–278. doi: 10.1016/j.biortech.2014.03.151
- Katsoni, A., Mantzavinos, D., and Diamadopoulos, E. (2014). Sequential treatment of diluted olive pomace leachate by digestion in a pilot scale UASB reactor and BDD electrochemical oxidation. *Wat. Res.* 57, 76–86. doi: 10.1016/j.watres.2014.03.010
- Kaur, U., Oberoi, H. S., Bhargav, V. K., Sharma-Shivappa, R., and Dhaliwal, S. S. (2012). Ethanol production from alkali- and ozone-treated cotton stalks using thermo-tolerant *Pichia kudriavzevii* HOP-1. *Ind. Crops Prod.* 37, 219–226. doi: 10.1016/j.indcrop.2011.12.007
- Kavitha, S., Yukesh Kannah, R., Yeom, I. T., Do, K.-U., and Banu, J. R. (2015). Combined thermo-chemo-sonic disintegration of waste activated sludge for biogas production. *Bioresour. Technol.* 197, 383–392. doi: 10.1016/j.biortech.2015.08.131
- Khandelwal, S., Tailor, Y. K., and Kumar, M. (2016). Deep eutectic solvents (DESs) as eco-friendly and sustainable solvent/catalyst systems in organic transformations. *J. Mol. Liq.* 215, 345–386. doi: 10.1016/j.molliq.2015.12.015
- Kim, J., Realf, M. J., Lee, J. H., Whittaker, C., and Furtner, L. (2011). Design of biomass processing network for biofuel production using an MILP model. *Biomass Bioenerg.* 35, 853–871. doi: 10.1016/j.biombioe.2010.11.008
- Kim, J. Y., Lee, J. H., Park, J., Kim, J. K., An, D., Song, I. K., et al. (2015). Catalytic pyrolysis of lignin over HZSM-5 catalysts: effect of various parameters on the production of aromatic hydrocarbon. *J. Anal. Appl. Pyrolysis* 114, 273–280. doi: 10.1016/j.jaap.2015.06.007
- Kirk, T. K., Mozuch, M. D., and Tien, M. (1985). Free hydroxyl radical is not involved in an important reaction of lignin degradation by *Phanerochaete chrysosporium* burds. *Biochem. J.* 226, 455–460. doi: 10.1042/bj2260455
- Koenigs, J. W. (1974). Hydrogen peroxide and iron: a proposed system for decomposition of wood by brown-rot basidiomycetes. *Wood Fiber Sci.* 6, 66–80.
- Kou, J., Wang, J., Sun, W., Lu, C., Xu, Z., and Varma, R. S. (2017). Selective enhancement in heterogeneous photocatalytic transformations. *Chem. Rev.* 117, 1445–1514. doi: 10.1021/acs.chemrev.6b00396
- Kratky, L., and Jirout, T. (2011). Biomass size reduction machines for enhancing biogas production. *Chem. Eng. Technol.* 34, 391–399. doi: 10.1002/ceat.201000357
- Kreetachat, T., Damrongri, M., Punsuwon, V., Vaithanomsat, P., Chiemchaisri, C., and Chomsurin, C. (2007). Effects of ozonation process on lignin-derived

- compounds in pulp and paper mill effluents. *J. Hazard. Mater.* 142, 250–257. doi: 10.1016/j.jhazmat.2006.08.011
- Ksibi, M., Amor, S. B., Cherif, S., Elaloui, E., Houas, A., and Elaloui, M. (2003). Photodegradation of lignin from black liquor using a UV/TiO₂ system. *J. Photochem. Photobiol. A* 154, 211–218. doi: 10.1016/S1010-6030(02)00316-7
- Kumar, P., Barrett, D. M., Delwiche, M. J., and Stroeve, P. (2009). Methods for pretreatment of lignocellulosic biomass for efficient hydrolysis and biofuel production. *Bioresour. Technol.* 162, 273–278. doi: 10.1021/ie801542g
- Kumar, R., and Wyman, C. E. (2009). Effects of cellulase and xylanase enzymes on the deconstruction of solids from pretreatment of poplar by leading technologies. *Biotechnol. Prog.* 25, 302–314. doi: 10.1002/btpr.102
- Kurian, J. K., Nair, G. R., Hussain, A., and Raghavan, G. S. V. (2013). Feedstocks, logistics and pretreatment process for sustainable lignocellulosic biorefineries: a comprehensive review. *Renew. Sustain. Energ. Rev.* 25, 205–219. doi: 10.1016/j.rser.2013.04.019
- Labat, G. A. A., and Gonçalves, A. R. (2008). Oxidation in acidic medium of lignins from agricultural residues. *Appl. Biochem. Biotechnol.* 148, 151–161. doi: 10.1007/s12010-007-8120-0
- Lamers, P., Tan, E. C. D., Searcy, E. M., Scarlata, C. J., Cafferty, K. G., and Jacobson, J. J. (2015). Strategic supply system design – a holistic evaluation of operational and production cost for a biorefinery supply chain. *Biofuels Bioprod. Bioref.* 9, 648–660. doi: 10.1002/bbb.1575
- Laurichesse, S., and Averous, L. (2014). Chemical modification of lignins: towards biobased polymers. *Progr. Polym. Sci.* 39, 1266–1290. doi: 10.1016/j.progpolymsci.2013.11.004
- Lee, H.-J., Ahn, S. J., Seo, Y.-J., and Lee, J.-W. (2013). A feasibility study on the multistage process for the oxalic acid pretreatment of a lignocellulosic biomass using electrodialysis. *Bioresour. Technol.* 130, 211–217. doi: 10.1016/j.biortech.2012.12.061
- Lee, M., Blum, L. C., Schmid, E., Fenner, K., and von Gunten, U. (2017). A computer-based prediction platform for the reaction of ozone with organic compounds in aqueous solution: kinetics and mechanisms. *Environ. Sci. Process Impacts* 19, 465–476. doi: 10.1039/C6EM00584E
- Li, B., Lv, W., Zhang, Q., Wang, T., and Ma, L. (2014). Pyrolysis and catalytic pyrolysis of industrial lignins by TG-FTIR: kinetics and products. *J. Anal. Appl. Pyrolysis* 108, 295–300. doi: 10.1016/j.jaap.2014.04.002
- Li, H., Lei, Z., Liu, C., Zhang, Z., and Lu, B. (2015). Photocatalytic degradation of lignin on synthesized Ag–AgCl/ZnO nanorods under solar light and preliminary trials for methane fermentation. *Bioresour. Technol.* 175, 494–501. doi: 10.1016/j.biortech.2014.10.143
- Li, X., Sun, C., Zhou, B., and He, Y. (2015). Determination of hemicellulose, cellulose and lignin in moso bamboo by near infrared spectroscopy. *Sci. Rep.* 5:17210. doi: 10.1038/srep17210
- Li, X., Zhu, K., Pang, J., Tian, M., Liu, J., Rykov, A. I., et al. (2018). Unique role of Mössbauer spectroscopy in assessing structural features of heterogeneous catalysts. *Appl. Catal. B Environ.* 224, 518–532. doi: 10.1016/j.apcatb.2017.11.004
- Lin, H., Oturan, N., Wu, J., Sharma, V. K., Zhang, H., and Oturan, M. A. (2017). Removal of artificial sweetener aspartame from aqueous media by electrochemical advanced oxidation processes. *Chemosphere* 167, 220–227. doi: 10.1016/j.chemosphere.2016.09.143
- Lin, Q., Chen, G., and Liu, Y. (2012). Scale-up of microwave heating process for the production of bio-oil from sewage sludge. *J. Anal. Appl. Pyrolysis* 94, 114–119. doi: 10.1016/j.jaap.2011.11.014
- Lu, Y., Wei, X.-Y., Wen, Z., Chen, H.-B., Lu, Y.-C., Zong, Z.-M., et al. (2014). Photocatalytic depolymerization of rice husk over TiO₂ with H₂O₂. *Fuel Proc. Technol.* 117, 8–16. doi: 10.1016/j.fuproc.2013.04.001
- Luo, J., Zhang, X., and Zhang, J. (2015). Carbazolic porous organic framework as an efficient, metal-free visible-light photocatalyst for organic synthesis. *ACS Catal.* 5, 2250–2254. doi: 10.1021/acscatal.5b00025
- Luo, J., Zhang, X., Lu, J., and Zhang, J. (2017). Fine tuning the redox potentials of carbazolic porous organic frameworks for visible-light photoredox catalytic degradation of lignin β-O-4 models. *ACS Catal.* 7, 5062–5070. doi: 10.1021/acscatal.7b01010
- Luque, R., and Triantafyllidis, K. (2016). Valorization of lignocellulosic biomass. *ChemCatChem* 8, 1422–1423. doi: 10.1002/cctc.201600226
- Maldhure, A. V., and Ekhe, J. D. (2013). Pyrolysis of purified kraft lignin in the presence of AlCl₃ and ZnCl₂. *J. Environ. Chem. Eng.* 1, 844–849. doi: 10.1016/j.jece.2013.07.026
- Malik, A., Lenzen, M., and Geschke, A. (2016). Triple bottom line study of a lignocellulosic biofuel industry. *GCB Bioenergy* 8, 96–110. doi: 10.1111/gcbb.12240
- Mamleeva, N., Autlov, S. A., Bazarnova, N. G., and Lunin, V. V. (2009). Delignification of softwood by ozonation. *Pure Appl. Chem.* 81, 2081–2091. doi: 10.1351/PAC-CON-08-10-11
- Mancini, G., Papirio, S., Lens, P. N. L., and Esposito, G. (2016). Solvent pretreatments of lignocellulosic materials to enhance biogas production: a review. *Energy Fuels* 30, 1892–1903. doi: 10.1021/acs.energyfuels.5b02711
- McDonough, T. J. (1993). The chemistry of organosolv delignification. *Tappi J.* 76, 186–193.
- Mirahmadi, K., Mohseni Kabir, M., Jeihanipour, A., Karimi, K., and Taherzadeh, M. (2010). Alkaline pretreatment of spruce and birch to improve bioethanol and biogas production. *BioResources* 5, 928–938. doi: 10.15376/biores.5.2.928-938
- Mirmohamadsadeghi, S., Karimi, K., Zamani, A., Amiri, H., and Horvath, I. S. (2014). Enhanced solid-state biogas production from lignocellulosic biomass by organosolv pretreatment. *BioMed. Res. Int.* 2014:350414. doi: 10.1155/2014/350414
- Mirzaei, A., Chen, Z., Haghighat, F., and Yerushalmi, L. (2017). Removal of pharmaceuticals from water by homo/heterogenous Fenton-type processes – a review. *Chemosphere* 174, 665–688. doi: 10.1016/j.chemosphere.2017.02.019
- Monlau, F., Barakat, A., Steyer, J., and Carrere, H. (2012). Comparison of seven types of thermo-chemical pretreatments on the structural features and anaerobic digestion of sunflower stalks. *Bioresour. Technol.* 120, 241–247. doi: 10.1016/j.biortech.2012.06.040
- Morales, M., Quintero, J., Conejeros, R., and Aroca, G. (2015). Life cycle assessment of lignocellulosic bioethanol: environmental impacts and energy balance. *Renew. Sustain. Energ. Rev.* 42, 1349–1361. doi: 10.1016/j.rser.2014.10.097
- Mosier, N., Wyman, C. E., Dale, B. D., Elander, R. T., Lee, Y. Y., Holtzapple, M., et al. (2005). Features of promising technologies for pretreatment of lignocellulosic biomass. *Bioresour. Technol.* 96, 673–686. doi: 10.1016/j.biortech.2004.06.025
- Mulakhadair, A. R., Hanotu, J., and Zimmerman, W. (2017). Exploiting ozonolysis-microbe synergy for biomass processing: application in lignocellulosic biomass pretreatment. *Biomass Bioenergy* 105, 147–154. doi: 10.1016/j.biombioe.2017.06.018
- Nguyen, J. D., Matsuura, B. S., and Stephenson, C. R. J. (2014). A photochemical strategy for lignin degradation at room temperature. *J. Am. Chem. Soc.* 136, 1218–1221. doi: 10.1021/ja4113462
- Nguyen, T. A., Kim, K. R., Han, S. J., Cho, H. Y., Kim, J. W., Park, S. M., et al. (2010). Pretreatment of rice straw with ammonia and ionic liquid for lignocellulose conversion to fermentable sugars. *Bioresour. Technol.* 101, 7432–7438. doi: 10.1016/j.biortech.2010.04.053
- Nieves, D. C., Karimi, K., and Horvath, I. S. (2011). Improvement of biogas production from oil palm empty fruit bunches (OPEFB). *Ind. Crops Prod.* 34, 1097–1101. doi: 10.1016/j.indcrop.2011.03.022
- Ohnishi, H., Matsumura, M., Tsubomura, H., and Iwasaki, M. (1989). Bleaching of lignin solution by a photocatalyzed reaction on semiconductor photocatalysts. *Ind. Eng. Chem. Res.* 28, 719–724. doi: 10.1021/ie00090a012
- Ong, C. B., Ng, L. Y., and Mohammad, A. W. (2018). A review of ZnO nanoparticles as solar photocatalysts: synthesis, mechanisms and applications. *Renew. Sustain. Energ. Rev.* 81, 536–551. doi: 10.1016/j.rser.2017.08.020
- Ouiriemmi, I., Karra, A., Oturan, N., Pazos, M., Rozales, E., Gadri, A., et al. (2017). Heterogeneous electro-Fenton using natural pyrite as solid catalyst for oxidative degradation of vanillic acid. *J. Electroanal. Chem.* 797, 69–77. doi: 10.1016/j.jelechem.2017.05.028
- Ouyang, X., Zhu, G., Huang, X., and Qiu, X. (2015). Microwave assisted liquefaction of wheat straw alkali lignin for the production of monophenolic compounds. *J. Energy Chem.* 24, 72–76. doi: 10.1016/S2095-4956(15)60286-8
- Ozdokur, K. V., Moniruzzaman, M., Yanik, J., and Ono, T. (2016). Synthesis and characterization of a polyoxometalate-based ionic liquid catalyst for delignification of wood biomass. *Wood Sci. Technol.* 50, 1213–1226. doi: 10.1007/s00226-016-0844-y

- Pan, K., Tian, M., Jiang, Z.-H., Kjartansson, B., and Chen, A. (2012). Electrochemical oxidation of lignin at lead dioxide nanoparticles photoelectrodeposited on TiO₂ nanotube arrays. *Electrochim. Acta* 60, 147–153. doi: 10.1016/j.electacta.2011.11.025
- Papathoeofanos, M. G., Billa, E., Koullas, D. P., Monties, B., and Koukios, E. G. (1995). Two-stage acid-catalyzed fractionation of lignocellulosic biomass in aqueous ethanol systems at low temperatures. *Bioresour. Technol.* 54, 305–310. doi: 10.1016/0960-8524(95)00152-2
- Patnaik, S., Sahoo, D. P., and Parida, K. (2018). An overview on Ag modified g-C₃N₄ based nanostructured materials for energy and environmental applications. *Renew. Sustain. Energ. Rev.* 82, 1297–1312. doi: 10.1016/j.rser.2017.09.026
- Pelckmas, M., Renders, T., Vyver, S. V., and Sels, B. F. (2017). Bio-based amines through sustainable heterogeneous catalysis. *Green Chem.* 19, 5303–5321. doi: 10.1039/C7GC02299A
- Perez, A. T. E., Camargo, M., and Rincon, P. C. N. (2017). Key challenges and requirements for sustainable and industrialized biorefinery supply chain design and management: a bibliographic analysis. *Renew. Sustain. Energ. Rev.* 69, 350–359. doi: 10.1016/j.rser.2016.11.084
- Perron, O. M., Colombari, F. M., Rossi, J. S., Moretti, M. M. S., Bordignon, S. M., Nunes, C. C. C., et al. (2016). Ozonolysis combined with ultrasound as a pretreatment of sugarcane bagasse: effect of the enzymatic saccharification and the physical and chemical characteristics of the substrate. *Bioresour. Technol.* 218, 69–76. doi: 10.1016/j.biortech.2016.06.072
- Prasad, A., Sotenko, M., Blenkinsopp, T., and Coles, S. R. (2016). Life cycle assessment of lignocellulosic biomass pretreatment methods in biofuel production. *Int. J. Life Cycle Assess.* 21, 44–50. doi: 10.1007/s11367-015-0985-5
- Qiao, W., Yan, X., Ye, J., Sun, Y., Wang, W., and Zhang, Z. (2011). Evaluation of biogas production from different biomass wastes with/without hydrothermal pretreatment. *Renew. Energy* 36, 3313–3318. doi: 10.1016/j.renene.2011.05.002
- Raman, S., Mohr, A., Helliwell, R., Robeiro, B., Shortall, O., Smith, R., et al. (2015). Integrating social and value dimensions into sustainability assessment of lignocellulosic biofuels. *Biomass Bioenerg.* 82, 49–62. doi: 10.1016/j.biombioe.2015.04.022
- Reichert, J., and Albert, J. (2017). Detailed kinetic investigations on the selective oxidation of biomass to formic acid (OxFA Process) using model substrates and real biomass. *ACS Sustainable Chem. Eng.* 5, 7383–7392. doi: 10.1021/acssuschemeng.7b01723
- Ribeiro, B. E., and Quintanilla, M. A. (2015). Transitions in biofuel technologies: an appraisal of the social impacts of cellulosic ethanol using the Delphi method. *Technol. Forecast. Soc. Change* 92, 53–68. doi: 10.1016/j.techfore.2014.11.006
- Rincón, L. E., Valencia, M. J., Hernández, V., Matallana, L. G., and Cardona, C. A. (2015). Optimization of the Colombian biodiesel supply chain from oil palm crop based on techno-economical and environmental criteria. *Energ. Econ.* 47, 154–167. doi: 10.1016/j.eneco.2014.10.018
- Ringer, M., Putsche, V., and Scabill, J. (2006). *Large-Scale Pyrolysis Oil Production: A Technology Assessment and Economic Analysis*, Vol. NREL/TP-510-37779. Golden, CO: National Renewable Energy Laboratory.
- Romero, A., Cantero, D. A., Nieto-Márquez, A., Martínez, C., Alonso, E., and Cocero, M. J. (2016). Supercritical water hydrolysis of cellulosic biomass as effective pretreatment to catalytic production of hexitols and ethylene glycol over Ru/MCM-48. *Green Chem.* 18, 4051–4062. doi: 10.1039/C6GC00374E
- Sapci, Z. (2013). The effect of microwave pretreatment on biogas production from agricultural straws. *Biores. Technol.* 128, 487–494. doi: 10.1016/j.biortech.2012.09.094
- Sathitsuksanoh, N., Zhu, Z. G., and Zhang, Y. H. P. (2012). Cellulose solvent-based pretreatment for corn stover and Avicel: concentrated phosphoric acid versus ionic liquid [BMIM]Cl. *Cellulose* 19, 1161–1172. doi: 10.1007/s10570-012-9719-z
- Schell, D. J., and Harwood, C. (1994). Milling of lignocellulosic biomass: results of pilots-scale testing. *Appl. Biochem. Biotechnol.* 45–46, 159–168. doi: 10.1007/BF02941795
- Schmitt, D., Regenbrecht, C., Hartmer, M., Stecker, F., and Waldvogel, S. R. (2015). Highly selective generation of vanillin by anodic degradation of lignin: a combined approach of electrochemistry and product isolation by adsorption. *Beilstein J. Org. Chem.* 11, 473–480. doi: 10.3762/bjoc.11.53
- Shadbahr, J., Zhang, Y., and Khan, F. (2015). Life cycle assessment of bioethanol production from woodchips with modifications in the pretreatment process. *Appl. Biochem. Biotechnol.* 175, 1080–1091. doi: 10.1007/s12010-014-1293-4
- Shahriari, H., Warith, M., and Kennedy, K. J. (2012). Anaerobic digestion of organic fraction of municipal solid waste combining two pretreatment modalities, high temperature microwave and hydrogen peroxide. *Waste Manag.* 32, 41–52. doi: 10.1016/j.wasman.2011.08.012
- Shao, D., Liang, J., Cui, X., Xu, H., and Yan, W. (2014). Electrochemical oxidation of lignin by two typical electrodes: Ti/SbSnO₂ and Ti/PbO₂. *Chem. Eng. J.* 244, 288–295. doi: 10.1016/j.cej.2014.01.074
- Sharma, V. K., and Feng, M. (2017). Water depollution using metal-organic frameworks-catalyzed advanced oxidation processes: a review. *J. Hazard. Mater.* doi: 10.1016/j.jhazmat.2017.09.043. [Epub ahead of print].
- Sharma, V. K., and Graham, N. D. (2010). Oxidation of amino acids, peptides, and proteins by ozone. *Ozone: Sci. Eng.* 32, 81–90. doi: 10.1080/01919510903510507
- Shatalov, A. A. (2016). “Homogeneous polyoxometalate catalysis in lignocellulosic biomass conversion,” in *Anonymous Polyoxometalates: Properties, Structure and Synthesis*, ed A. P. Roberts (New York, NY: Nova Scientific Publishers Inc.), 77–114.
- Shimura, K., and Yoshida, H. (2011). Heterogeneous photocatalytic hydrogen production from water and biomass derivatives. *Energy Environ. Sci.* 4, 2467–2481. doi: 10.1039/c1ee01120k
- Silva, J. P. A., Carneiro, L. M., and Roberto, I. C. (2013). Treatment of rice straw hemicellulosic hydrolysate with advanced oxidative processes: a new and promising detoxification method to improve the bioconversion process. *Biotechnol. Biofuel.* 6, 23–36. doi: 10.1186/1754-6834-6-23
- Singh, A., Pant, D., Korres, N. E., Nizami, A.-S., Prasad, S., and Murphy, J. D. (2010). Key issues in life cycle assessment of ethanol production from lignocellulosic biomass: challenges and perspectives. *Bioresour. Technol.* 101, 5003–5012. doi: 10.1016/j.biortech.2009.11.062
- Sires, I., Brillas, E., Oturan, M. A., Rodrigo, M. A., and Panizza, M. (2014). Electrochemical advanced oxidation processes: today and tomorrow. a review. *Environ. Sci. Pollut. Res. Int.* 21, 8336–8367. doi: 10.1007/s11356-014-2783-1
- Song, L.-J., Zhu, N.-W., Yuan, H.-P., Hong, Y., and Ding, J. (2010). Enhancement of waste activated sludge aerobic digestion by electrochemical pre-treatment. *Wat. Res.* 44, 4371–4378. doi: 10.1016/j.watres.2010.05.052
- Song, Z., Yang, G., Guo, Y., and Zhang, T. (2012). Comparison of two chemical pretreatments of rice straw for biogas production by anaerobic digestion. *BioResources* 7, 3223–3236. doi: 10.15376/biores.7.3.3223-3236
- Steter, J. R., Brillas, E., and Sirés, I. (2018). Solar photoelectro-Fenton treatment of a mixture of parabens spiked into secondary treated wastewater effluent at low input current. *Appl. Catal. B Environ.* 224, 410–418. doi: 10.1016/j.apcatb.2017.10.060
- Sun, Y., and Cheng, J. (2002). Hydrolysis of lignocellulosic materials for ethanol production: a review. *Bioresour. Technol.* 83, 1–11. doi: 10.1016/S0960-8524(01)00212-7
- Tabone, M. D., Cregg, J. J., Beckman, E. J., and Landis, A. E. (2010). Sustainability metrics: life cycle assessment and green design in polymers. *Environ. Sci. Technol.* 44, 8264–8269. doi: 10.1021/es101640n
- Tadele, K., Verma, S., Gonzalez, M. A., and Varma, R. S. (2017). A sustainable approach to empower the future: upgrading of biomass via process intensification. *Green Chem.* 19, 1624–1627. doi: 10.1039/C6GC03568J
- Tarkow, H., and Feist, W. C. (1969). A mechanism for improving the digestibility of lignocellulosic materials with dilute alkali and liquid ammonia. *Adv. Chem.* 95, 197–218. doi: 10.1021/ba-1969-0095.ch012
- Tian, M., Wen, J., McDonald, D., Asmussen, R. M., and Chen, A. (2010). A novel approach for lignin modification and degradation. *Electrochem. Commun.* 12, 527–530. doi: 10.1016/j.elecom.2010.01.035
- Tolba, R., Tian, M., Wen, J., Jiang, Z.-H., and Chen, A. (2010). Electrochemical oxidation of lignin at IrO₂-based oxide electrodes. *J. Electroanal. Chem.* 649, 9–15. doi: 10.1016/j.jelechem.2009.12.013
- Travaini, R., Martín-Juarez, J., Lorenzo-Hernando, A., and Bolado-Rodríguez, S. (2016). Ozonolysis: an advantageous pretreatment for lignocellulosic biomass revisited. *Bioresour. Technol.* 199, 2–12. doi: 10.1016/j.biortech.2015.08.143
- Tuck, C. O., Pérez, E., Horváth, I. T., Sheldon, R. A., and Poliakoff, M. (2012). Valorization of biomass: deriving more value from waste. *Science* 337, 695–699. doi: 10.1126/science.1218930

- Tufvesson, L. M., Tufvesson, P., Woodley, J. M., and Börjesson, P. (2013). Life cycle assessment in green chemistry: overview of key parameters and methodological concerns. *Int. J. Life Cycle Assess.* 18, 431–444. doi: 10.1007/s11367-012-0500-1
- Turkulin, H., Holzer, L., and Sell, J. (2005). Application of ESEM technique in wood research: part I. optimization of imaging parameters and working conditions. *Wood Fiber Sci.* 37, 552–564.
- Verma, S., Baig, R. B. N., Nadagouda, M. N., and Varma, R. S. (2016a). Visible light mediated upgrading of biomass to biofuel. *Green Chem.* 18, 1327–1333. doi: 10.1039/C5GC02951A
- Verma, S., Baig, R. B. N., Nadagouda, M. N., and Varma, R. S. (2016b). Sustainable strategy utilizing biomass: visible light-mediated synthesis of γ -valerolactone. *ChemCatChem* 8, 690–693. doi: 10.1002/cctc.201501352
- Verma, S., Baig, R. B. N., Nadagouda, M. N., Len, C., and Varma, R. S. (2017a). Sustainable pathway to furanics from biomass via heterogeneous organo-catalysis. *Green Chem.* 19, 164–168. doi: 10.1039/C6GC02551J
- Verma, S., Nadagouda, M. N., and Varma, R. S. (2017b). Porous nitrogen-enriched carbonaceous material from marine waste: chitosan-derived carbon nitride catalyst for aerial oxidation of 5-hydroxymethylfurfural (HMF) to 2,5-furandicarboxylic acid. *Nat. Sci. Rpts.* 7:13596. doi: 10.1038/s41598-017-14016-5
- von Gunten, U. (2003). Ozonation of drinking water: part I. oxidation kinetics and product formation. *Water Res.* 37, 1443–1467. doi: 10.1016/S0043-1354(02)00457-8
- Wakerley, D. W., Kuehnel, M. F., Orchard, K. L., Ly, K. H., Rosser, T. E., and Reisner, E. (2017). Solar-driven reforming of lignocellulose to H_2 with a CdS/CdO_x photocatalyst. *Nat. Energy* 2:17021. doi: 10.1038/nenergy.2017.21
- Wang, L., Littlewood, J., and Murphy, R. J. (2013). Environmental sustainability of bioethanol production from wheat straw in the UK. *Renew. Sustain. Energy Rev.* 28, 715–725. doi: 10.1016/j.rser.2013.08.031
- Wang, Y., Fan, L., Shan, S., Liu, Y., and Ruan, R. (2016). Review of microwave-assisted lignin conversion for renewable fuels and chemicals. *J. Anal. Appl. Pyrolysis* 119, 104–113. doi: 10.1016/j.jaap.2016.03.011
- Xiong, K., Wan, W., and Chen, J. G. (2016). Reaction pathways of furfural, furfuryl alcohol and 2-methylfuran on Cu(111) and NiCu bimetallic surfaces. *Surf. Sci.* 652, 91–97. doi: 10.1016/j.susc.2016.02.011
- Xiong, K., Yu, W., Vlachos, D. G., and Chen, J. G. (2015). Reaction pathways of biomass-derived oxygenates over metals and carbides: from model surfaces to supported catalysts. *ChemCatChem* 7, 1402–1421. doi: 10.1002/cctc.201403067
- Xu, F., Yu, J., Tesso, T., Dowell, F., and Wang, D. (2013). Qualitative and quantitative analysis of Lignocellulosic biomass using infrared techniques: a mini-review. *Appl. Energy* 104, 801–809. doi: 10.1016/j.apenergy.2012.12.019
- Xu, J., Jiang, J., Hse, C., and Shupe, T. F. (2012). Renewable chemical feedstocks from integrated liquefaction processing of lignocellulosic materials using microwave energy. *Green Chem.* 14, 2821–2830. doi: 10.1039/c2gc35805k
- Xu, Y., Huang, Y., and Zhang, B. (2016). Rational design of semiconductor-based photocatalysts for advanced photocatalytic hydrogen production: the case of cadmium chalcogenides. *Inorg. Chem. Front.* 3, 591–615. doi: 10.1039/C5QI00217F
- Yang, L., Su, J., Carl, S., Lynam, J. G., Yang, X., and Lin, H. (2015). Catalytic conversion of hemicellulosic biomass to lactic acid in pH neutral aqueous phase media. *Appl. Catal. B Environ.* 162, 149–157. doi: 10.1016/j.apcatb.2014.06.025
- Yasuda, M., Miura, A., Yuki, R., Nakamura, Y., Shiragami, T., Ishii, Y., et al. (2011). The effect of TiO_2 -photocatalytic pretreatment on the biological production of ethanol from lignocelluloses. *J. Photochem. Photobiol.* 220, 195–199. doi: 10.1016/j.jphotochem.2011.04.019
- Yong, X., and Schoonen, M. A. A. (2000). The absolute energy positions of conduction and valence bands of selected semiconducting minerals. *Am. Mineral.* 85, 543–556. doi: 10.2138/am-2000-0416
- Ye, C., Yuan, H., Dai, X., Lou, Z., and Zhu, N. (2016). Electrochemical pretreatment of waste activated sludge: effect of process conditions on sludge disintegration degree and methane production. *Env. Technol.* 37, 2935–2944. doi: 10.1080/09593330.2016.1170209
- Zamboni, A., Shah, N., and Bezzo, F. (2009). Spatially explicit static model for the strategic design of future bioethanol production systems. 1. cost minimization. *Energy Fuels* 23, 5121–5133. doi: 10.1021/ef900456w
- Zhang, T., and Zhu, M.-J. (2016). Enhancing enzymolysis and fermentation efficiency of sugarcane bagasse by synergistic pretreatment of Fenton reaction and sodium hydroxide extraction. *Bioresour. Technol.* 214, 769–777. doi: 10.1016/j.biortech.2016.05.032
- Zhang, Y., Zhao, J., Xu, F., and Li, Y. (2014). Pretreatment of lignocellulosic biomass for enhanced biogas production. *Progr. Energy Combust. Sci.* 42, 35–53. doi: 10.1016/j.pecs.2014.01.001

Conflict of Interest Statement: The authors declare that the research was conducted in the absence of any commercial or financial relationships that could be construed as a potential conflict of interest.

The reviewer, AB, and handling Editor declared their shared affiliation.

Copyright © 2018 Den, Sharma, Lee, Nadadur and Varma. This is an open-access article distributed under the terms of the Creative Commons Attribution License (CC BY). The use, distribution or reproduction in other forums is permitted, provided the original author(s) and the copyright owner are credited and that the original publication in this journal is cited, in accordance with accepted academic practice. No use, distribution or reproduction is permitted which does not comply with these terms.



Hydrolysis of Hemicellulose and Derivatives—A Review of Recent Advances in the Production of Furfural

Frederic Delbecq¹, Yantao Wang², Anitha Muralidhara^{2,3,4}, Karim El Ouardi⁵, Guy Marlair³ and Christophe Len^{2,6*}

¹ Ecole Supérieure de Chimie Organique et Minérale, Compiègne, France, ² Sorbonne Universités, Université de Technologie de Compiègne, Compiègne, France, ³ Institut National de l'Environnement Industriel et des Risques, Verneuil-en-Halatte, France, ⁴ Avantium Chemicals, Amsterdam, Netherlands, ⁵ Materials Science and Nano-Engineering Department, Mohammed VI Polytechnic University, Ben Guerir, Morocco, ⁶ Institut de Recherche de Chimie Paris, PSL University, Chimie ParisTech, Paris, France

OPEN ACCESS

Edited by:

Vasile I. Parvulescu,
University of Bucharest, Romania

Reviewed by:

Alina Mariana Balu,
Universidad de Córdoba, Spain
David Kubička,
University of Chemistry and
Technology in Prague, Czechia
Nicoletta Ravasio,
Institute of Molecular Science and
Technologies (CNR), Italy

*Correspondence:

Christophe Len
christophe.len@utc.fr

Specialty section:

This article was submitted to
Green and Sustainable Chemistry,
a section of the journal
Frontiers in Chemistry

Received: 29 January 2018

Accepted: 12 April 2018

Published: 08 May 2018

Citation:

Delbecq F, Wang Y, Muralidhara A, El Ouardi K, Marlair G and Len C (2018) Hydrolysis of Hemicellulose and Derivatives—A Review of Recent Advances in the Production of Furfural. *Front. Chem.* 6:146. doi: 10.3389/fchem.2018.00146

Biobased production of furfural has been known for decades. Nevertheless, bioeconomy and circular economy concepts is much more recent and has motivated a regain of interest of dedicated research to improve production modes and expand potential uses. Accordingly, this review paper aims essentially at outlining recent breakthroughs obtained in the field of furfural production from sugars and polysaccharides feedstocks. The review discusses advances obtained in major production pathways recently explored splitting in the following categories: (i) non-catalytic routes like use of critical solvents or hot water pretreatment, (ii) use of various homogeneous catalysts like mineral or organic acids, metal salts or ionic liquids, (iii) feedstock dehydration making use of various solid acid catalysts; (iv) feedstock dehydration making use of supported catalysts, (v) other heterogeneous catalytic routes. The paper also briefly overviews current understanding of furfural chemical synthesis and its underpinning mechanism as well as safety issues pertaining to the substance. Eventually, some remaining research topics are put in perspective for further optimization of biobased furfural production.

Keywords: furfural, catalysis, green chemistry/safety biorefinery, biomass, dehydration, mechanism

INTRODUCTION

Nowadays, from a global point of view, the need for basic compounds continues to grow day by day. Our planet is confronted to the reduction of fossil resources, majoring the price of fossil-fuel based materials and the increase of greenhouse gas emissions (Harmaajärvi et al., 2004; Kamm et al., 2006; Brown and Brown, 2013) as well as increasing societal demand for industrial ecology aiming at disconnecting growth of production of goods and wealths from environmental impacts of all sorts and associated concepts (Jelinsky et al., 1992; Bourg and Erkmann, 2003). These concerns require the intensive production of biorenewable resources including related residues through intensive processes into identified useful chemicals. The use of plant wastes as recycled feedstocks is one of the alternatives for minimizing the dependence on fossil oil (Hall, 1981; Hacker et al., 2009; Aresta et al., 2012). Chemical companies convert the renewable bioresources into biofuels, in platforms molecules for fine chemicals, agro-chemicals, and specialty chemicals such as bio-lubricants, natural fibers and bio-based solvents (Schieb et al., 2015). Several building blocks derived from

renewable resources such as ethanol, glycerol, lactic acid, succinic acid, levulinic acid, are already in use or considered with potential importance in the near future (Sorensen et al., 2009). Among them, furanic compounds, such as 2-furaldehyde (furfural) and 5-hydroxymethylfurfural (HMF) having various industrial applications (Karinen et al., 2011; Lange et al., 2012) are conventionally produced from plant wastes feedstocks *via* several steps that led to relatively lower overall yield (**Scheme 1**). However, many reports have shown that one-pot and efficient production of furans could be achieved from biomass by well-optimized catalysts, solvents, equipment and process technology upgrades. Generally, furfural was derived from hemicellulose or other pentose rich polysaccharides classified in four main groups: xylans, mannans, xyloglucans, and β -glucans (Ebringerová, 2005). Recent researches have shown that other kinds of carbohydrates as alginate derivatives could also be exploited as feedstocks for furfural production (**Scheme 1**). As a molecule platform chemical, furfural permits to produce a large range of chemicals having different properties and utilities as solvents, plastics, fuel additives (**Scheme 2**). The purpose of the present article is to summarize the state of art in the field of furfural production from sugars and polysaccharides using homogeneous and heterogeneous strategies.

SYNTHESIS OF FURFURAL FROM SUGARS AND POLYSACCHARIDES WITHOUT CATALYSTS

Dehydration in Critical Solvents

Critical solvents are characterized by a critical point which is obtained at specific pressure and temperature (**Figure 1**). When temperature and pressure of a fluid rise higher than relating values defining the critical point of the solvent, this fluid belongs to the family of supercritical solvents. When both: (i) the temperature and/or the pressure are lower than that of the critical point; and (ii) the temperature is higher than that of the boiling point with a pressure higher than 1 bar, subcritical solvent also called hot compressed solvent is obtained. Following physical characteristics: viscosity, density, static dielectric constant and, for the protic ones, ion dissociation constant are deeply modified by heating solvent under pressure, which give them unrivaled properties for some advanced applications in chemistry.

Hydrothermal conversion of D-xylose and hemicelluloses to furfural by simultaneously furfural extraction with supercritical CO₂ (sc-CO₂) in catalyst-free conditions has been studied (Gairola and Smirnova, 2012). Two common reaction models of pentose dehydration (model 1 and model 2) were chosen and compared in terms of their ability to predict the influence of sc-CO₂ extraction on furfural yield (**Scheme 3**). By optimizing the reaction temperature, time, pressure, CO₂ flow rate and D-xylose concentration, a maximum furfural yield of 68% was furnished from 4% D-xylose initial loading at 230°C for 25 min at the pressure of 12 MPa and 3.6 g/min CO₂ flow rate. Kinetics of D-xylose and L-arabinose dehydration demonstrated that the last model is more appropriate than the former one to explain the improvement of furfural yield by simultaneously extraction with

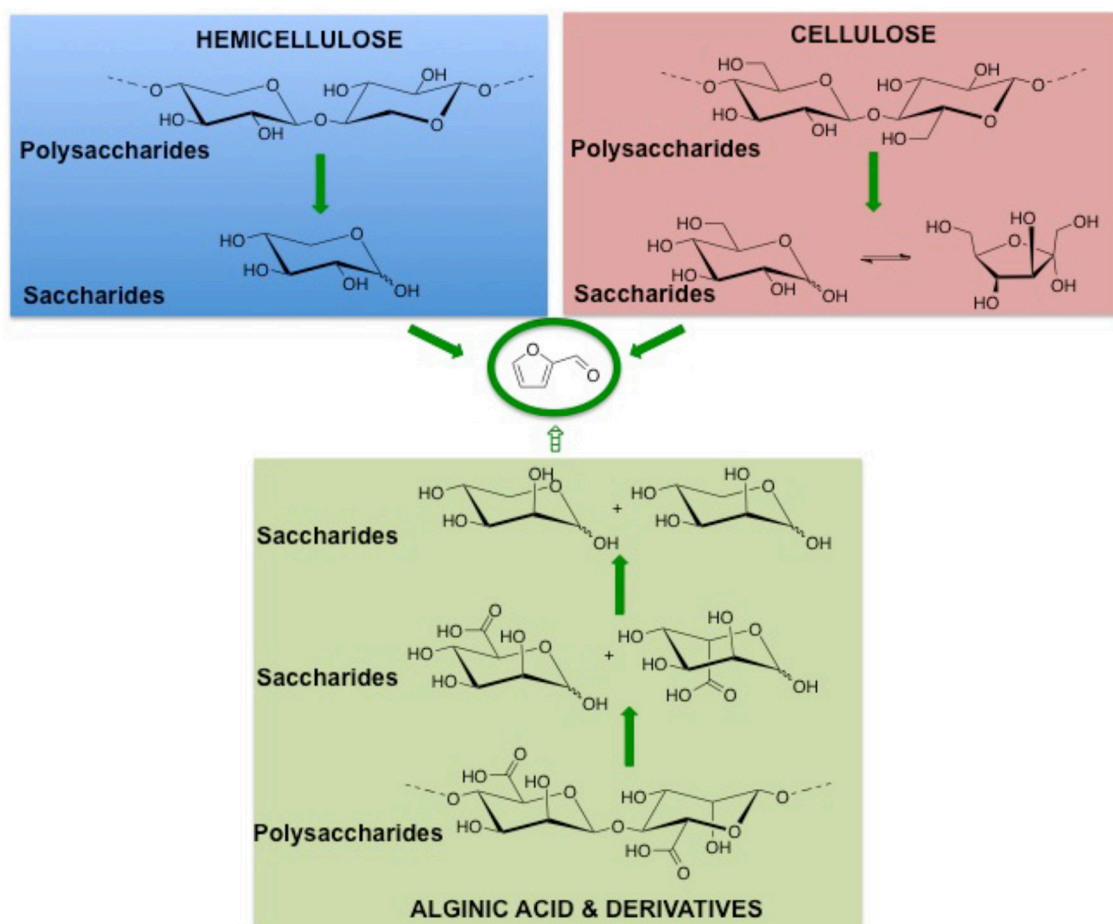
supercritical CO₂ during its formation. Additionally, the method was extended to native biomass as feedstock to produce furfural, it is clear that supercritical extraction improved furfural yield significantly. However, the best result derived from wheat straw furnished furfural in 29% yield, which was far lower than that from pure D-xylose. This result indicated the occurrence of side reactions with other hydrolysate components.

The use of another feedstock: sodium alginate and another solvent in presence or not of a catalyst permitted to have a fast decomposition of alginate at higher temperature (Jeon et al., 2015). However, in catalyst-free sub-critical water (pH = 7), the average molecular weight of products obtained at 250°C was higher than that for products generated under acid and base catalysts. These results suggested that catalyst-assisted hydrothermal treatment is favorable for the depolymerization of sodium alginate. Furthermore, only small amount of furfural formed without catalyst at 200 and 250°C, this phenomenon could be explained by the composition of alginate, which is mainly constituted of two monomeric subunits containing the carboxylic groups. These subunits are respectively D-mannuronic acid and L-guluronic acid, which are both hexuronic acids. Therefore, a decarboxylation processing step is necessary to realize the production of furfural. Obviously, the goal seems to be roughly achieved in subcritical water without catalyst.

Dehydration Using Hot Water Pretreatment

Production furfural assisted by hot water pretreatment does not use in principle acid catalysts (no voluntary addition). Nevertheless some acids can be generated during the process. A lignocellulose liquid hot water pretreatment process was recently developed by direct recycling spent liquor (Lu et al., 2016). During hot water pretreatment, approximately 10.0 g of corn stover and 200 mL of distilled water at 180°C for 30 min furnished 8.0 g/L D-xylose and 0.3 g/L furfural and further increased to 21.3 g/L D-xylose and 4.2 g/L furfural after recycling of the spent liquid. The improvement of furfural yield was attributed to the fact that the formation of by-product acetic acid that will facilitate D-xylose dehydration to furfural, increased from 3.2 to 9.8 g/L as the number of recycling steps increased from 0 to 6. In catalyst-free conditions (without added acid), integration of biomass pretreatment with fast pyrolysis by hot water extraction (HWE) and electron beam (EB) irradiation showed that HWE could be used to reduce the formation of carboxylic acid and ketones whilst improving the yield of target organic compounds (Mante et al., 2014). Besides, EB irradiation has a good potential to increase the formation of useful furanic aldehydes (furfural and HMF) and decrease the yield of hydroxyacetaldehyde by-product.

The reaction kinetics in high-temperature water was studied for the production of furfural from D-xylose as monomer feedstock (Hua et al., 2016). The results indicated that high-temperature water has the potential to substitute solid and liquid acids as a catalyst since it efficiently promotes the transfer of furfural initially formed in the water phase into the organic phase. In this study, ethyl butyrate with its excellent distribution coefficient permitted to furnish furfural in 75% yield at 200°C for 3 h. This yield was superior to that yield obtained without

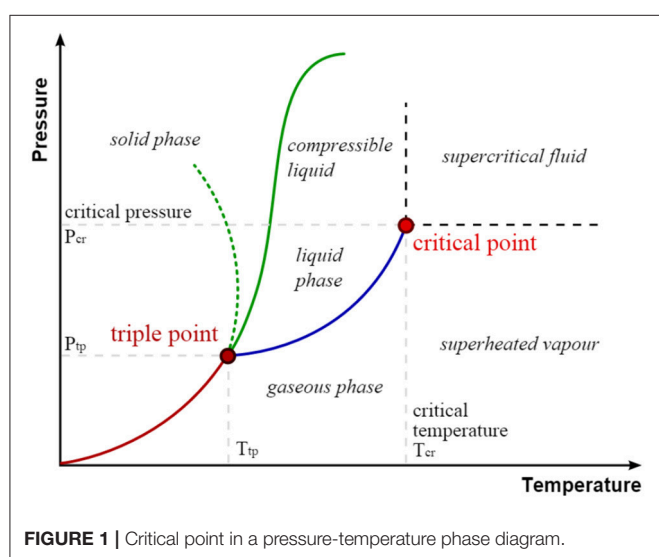
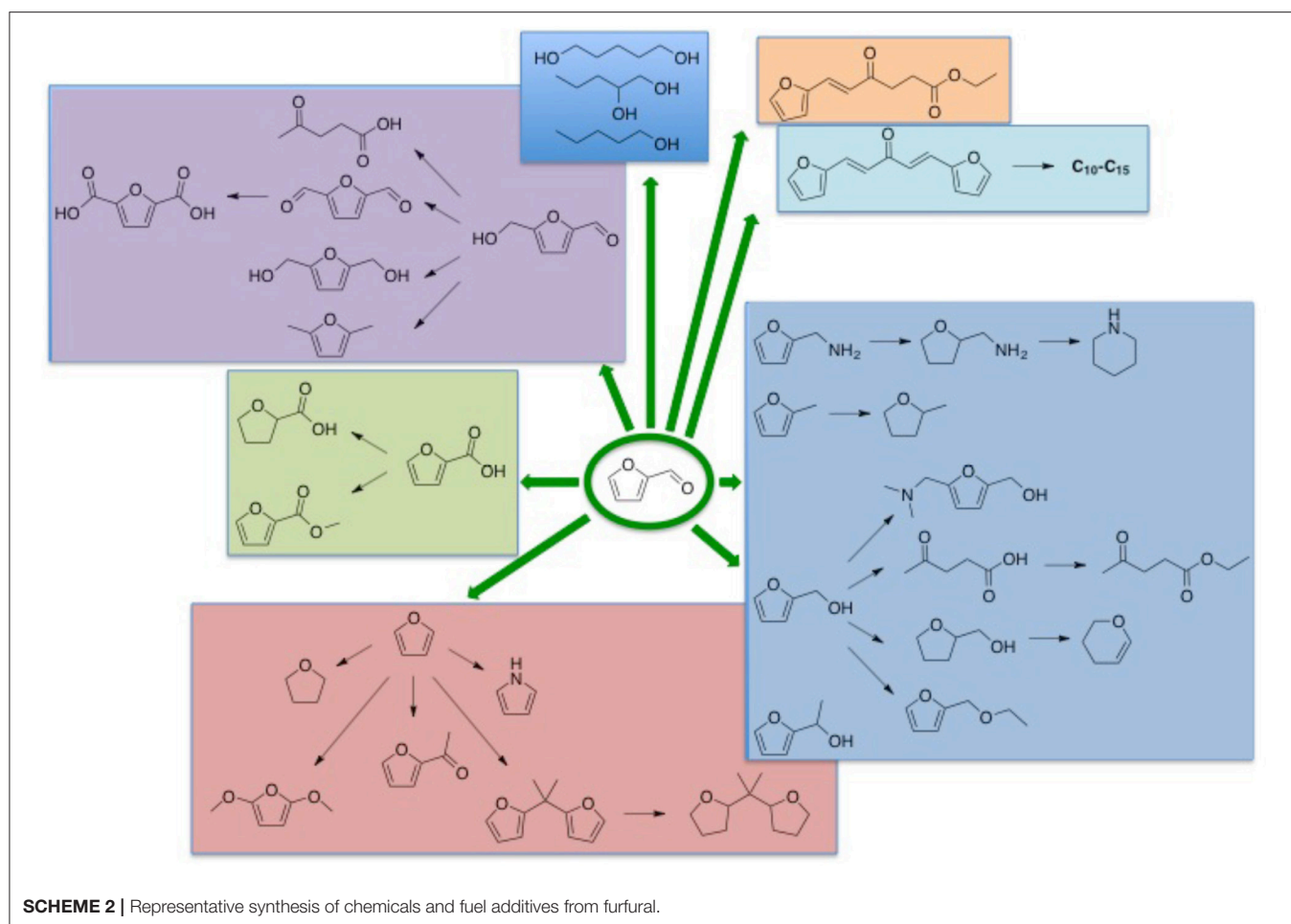


SCHEME 1 | Sources of sugars for the integrated production of furfural.

extraction solvent (75 vs. 50%). In addition, the author also calculated the kinetic order of D-xylose dehydration to furfural in high-temperature water from 160 to 200°C. They found a kinetic order of the reaction of 0.5, associated dehydration rate constant $K_0 = 1.82 \cdot 10^5 \text{ (mol/dm}^3\text{)}^{0.5}/\text{min}$, and an activation energy (E_a) of 68.5 KJ/mol. In order to further investigate the conversion of D-xylose to furfural, furfural formation mechanism from D-xylose and solvent effects on its formation was investigated by density functional theory (DFT) (Wang et al., 2015). Kinetic and thermodynamic analyses proposed that D-xylulose could be the key intermediate that leads to the formation of furfural, and liquid water could stabilize both reactants and transition states with unsaturated C-C bonds, which is favorable to furfural production. This study also indicated a promising way to produce furfural from D-xylose by involving D-xylulose. Isomerization of D-xylose to its corresponding ketose isomer in high yield *via* a simultaneous-isomerization-and-reactive-extraction (SIRE) scheme was previously reported (Li B. et al., 2013). Concentrated and purified D-xylulose by back-extraction (BE) into an acid medium, and then rapidly dehydrated the D-xylulose sugar to furfural at relatively low temperature with no additional catalyst

was studied. Furfural yield of 68% was achieved from D-xylulose at 110°C for 90 min, and was further improved to 90% with methyl isobutyl ketone (MIBK) as extract solvent or 85% in 5 min by replacing partial water with dimethyl sulfoxide (DMSO). The author also pointed out that the mild process conditions resulted in minimal chemical and energy inputs and have significant favorable impact on the overall process economics relative to D-xylose dehydration at 170°C, in spite of the additional unit operations involved. Besides, technical, economic and environmental performances for producing ethanol and furfural from *Pinus patula* bark, on a biorefinery concept was developed (Moncada et al., 2016). Based on different levels of heat integration, three scenarios were evaluated, the results showed that fully integrated plus cogeneration scheme was superior to fully energy integrated and non-integrated scheme from both point view of production costs and environment.

Simultaneous extraction-hydrolysis of lignocellulosic biomass by means of high pressurized CO_2 and H_2O was developed (Morais et al., 2016). In this work, the resulted water-soluble hydrolysate was also exposed to CO_2 at higher pressure and temperature in presence of MIBK as the extractive solvent and



tetrahydrofuran (THF) as co-solvent. At 200°C and 50 bar of CO₂, the residual hemicellulose was decomposed into its pentose sub-units with 81% of overall conversion (**Scheme 4**). The optimized dehydration process required a temperature of

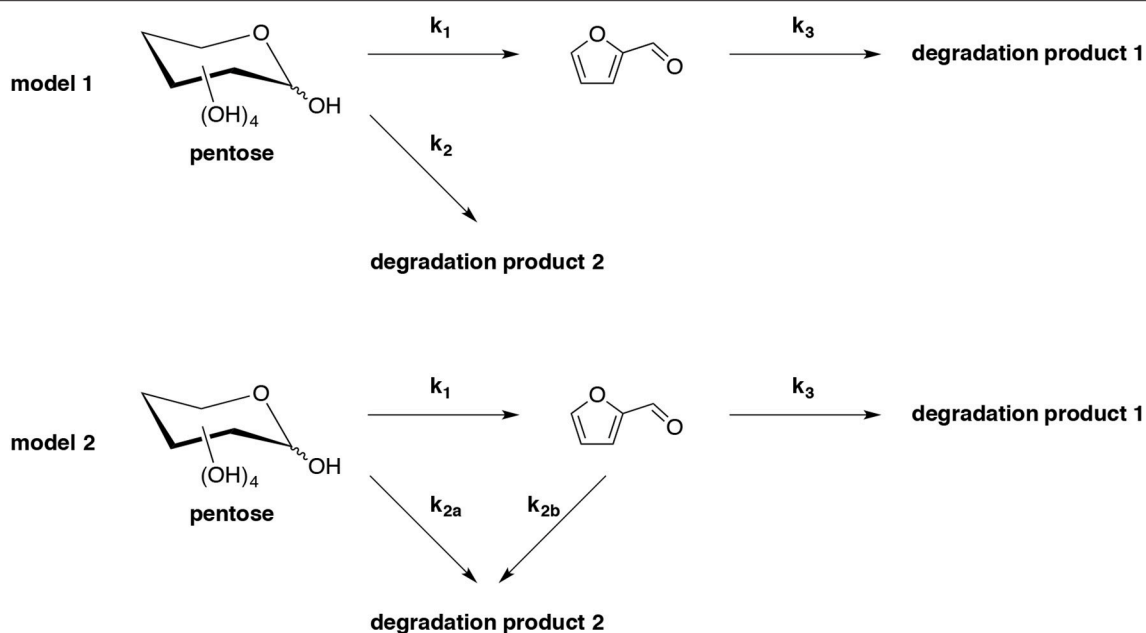
180°C and a residence time of 60 min giving a final furfural selectivity of 63%. In another paper, the same research team reported that they were able to produce furfural directly from D-xylose using a mixture of water and THF (Morais and Bogel-Lukasik, 2016). The dehydration was carried out under higher pressure of CO₂ at 180°C for 1 h. They obtained, respectively 70 and 84% of furfural yield and selectivity.

SYNTHESIS OF FURFURAL FROM SUGARS AND POLYSACCHARIDES USING HOMOGENEOUS CATALYSTS

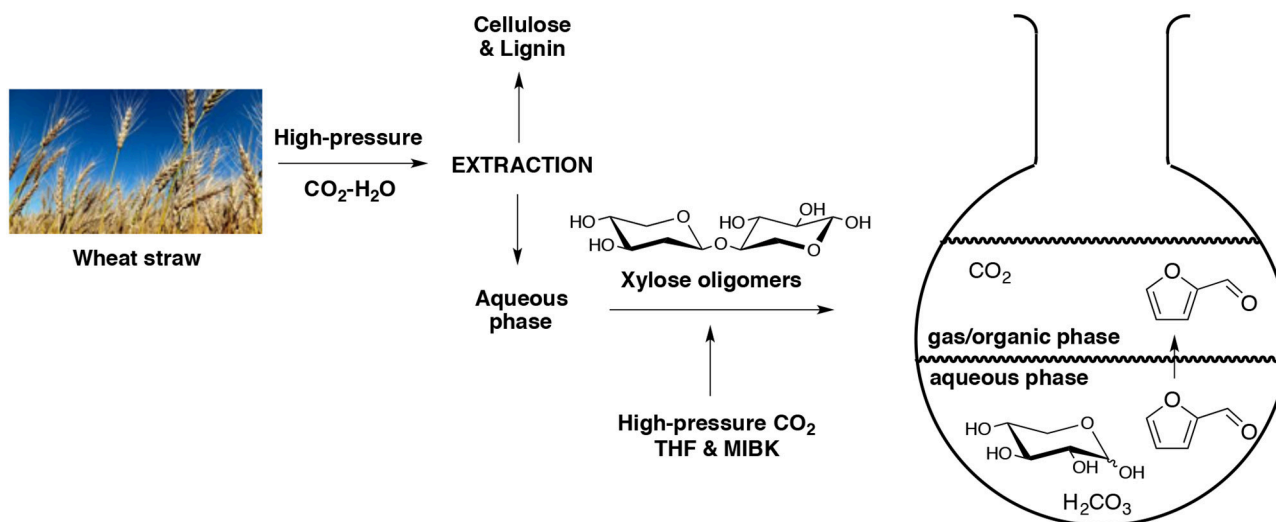
Dehydration of D-xylose and derivatives was studied in presence of either mineral acids (H₂SO₄, HCl, H₃PO₄), organic acid (formic, methanesulfonic acid, maleic acid, succinic acid) or metal salts [FeCl₃, AlCl₃, CrCl₂, CrCl₃, CuCl₂, NaHSO₄, KAl(SO₄)₂, Al₂(SO₄)₃] in water or in aqueous biphasic systems (ABS) using conventional thermal activation or microwave technology.

Dehydration in Presence of Mineral Acids

In many industrial furfural production processes, usual mineral acids, such as sulfuric acid, phosphoric acid, are generally used



SCHEME 3 | Kinetic models (model 1 and model 2) for pentose dehydration into furfural and the associated side-reactions in acidic or hydrothermal environment (Gairola and Smirnova, 2012).



SCHEME 4 | Production of furfural in an aqueous biphasic system using high pressure of CO₂ as catalyst (Morais et al., 2016).

as catalysts. Nevertheless, other mineral acids have been studied in the last decade. A low acid hydrothermal (LAH) fractionation was developed to transform hemicelluloses isolated from *Giant Miscanthus* into D-xylose-rich hydrolyzate which is converted at 180°C in presence of H₂SO₄ into “furfural side-product” with 53% yield (Kim T. H. et al., 2016). Starting from a prehydrolyzate of aspen and maple chips, furfural was produced by use of H₂SO₄ as acid catalyst and heating the mixture in a range of temperature from 160 to 260°C (Mazar et al., 2017). With 3.6 kg/m³ of H₂SO₄, a value of 78% furfural yield was reached at 240°C. The authors

noted that prior lignin removal from the pre-hydrolyzate did not bring any significant enhancement in the yield of furfural generated in this case.

Different additives such as thiourea, NaHSO₄, NaCl were also tested as potential improvers of the dehydration process. For example, the impact of thiourea additive in the furfural production process from corncobs treatment using H₂SO₄ was described (Xu et al., 2017). They reported that thiourea had for effect to improve the furfural yield that reached 61% under a liquid-solid ratio of 2:1 instead 34% with only H₂SO₄. The

transformation needed a temperature of 170°C and an acid concentration of 0.5 M. The authors explained that thiourea as an additive is supposedly acting as a blocking agent of the furfural resinification. In the same period, addition of NaHSO₄ as a catalyst promoter was reported for the direct production of furfural from bagasse (Yazdizadeh et al., 2016). The optimized condition was set up at 160°C under 8 bar. With 23% of NaHSO₄ content, a maximum of 9% furfural yield was reached after 50 min of residence time. NaCl as additive generated Cl[−] ions, which promote the formation of the 1,2-enediol from the acyclic form of D-xylose, and thus enhances the production of furfural in aqueous acidic solution at temperatures between 170 and 200°C (Marcotullio and De Jong, 2010). The addition of NaCl in H₂SO₄ led to good furfural selectivity (90%). Variety of chloride salts as additives were studied and revealed positive effects in terms of reduction of mineral acid needs for the conversion. All of them also showed advantageous effect on furfural yield and selectivity except for FeCl₃; however, they obtained exceptionally high D-xylose reaction rates, which deserved more investigation.

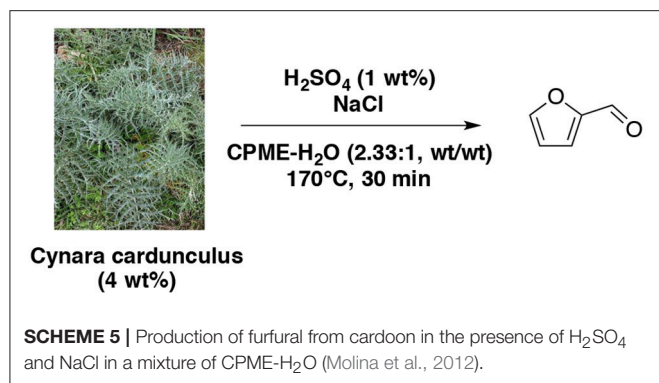
In order to substitute water for the dehydration other eco-friendly solvents such as γ -valerolactone (GVL) were tested and quantification of the effects of polar aprotic organic solvents on the acid-catalyzed conversion of D-xylose into furfural was reported (Mellmer et al., 2014). The use of GVL instead of water decreased the activation energy barrier for D-xylose dehydration from 145 KJ/mol to 114 KJ/mol, whereas the same parameter for furfural degradation increased from 85 KJ/mol to 105 KJ/mol. Accordingly, furfural selectivity from D-xylose of up to 75% could be achieved in GVL using H₂SO₄ as the catalyst, compared to only 50% furfural selectivity from D-xylose in H₂O. The polar aprotic solvents have an influence on the stabilization of the acidic proton relative to the protonated transition states, which resulted in accelerated reaction rates for these acid-catalyzed biomass conversion reactions. The author suggested that the proton of strong solid Brønsted acid catalysts, such as H-beta, become solvated during the liquid-phase catalytic reactions, while the conjugate bases of the associated strong Brønsted acid catalysts have little effect on proton reactivity.

Among the novel alternative technologies developed in chemistry and chemical engineering, microwave heating was applied to produce furfural from D-xylose (Vaz Jr and Donate, 2015). The highest furfural yield of 64% was observed at 200°C for 10 min at aqueous HCl concentration (4 mg/mL), simultaneously with 95% of D-xylose conversion. The conversion of D-xylose and xylan to furfural by microwave-assisted reaction in HCl aqueous media was reported at 180°C for 20 min with a solid-liquid ratio of 1:100 and a pH adjusted to 1.12 with a solution of HCl (0.1 M). This optimized conditions furnished furfural in 38 and 34% yields, respectively from D-xylose and xylan (Yemiş and Mazza, 2011). However, furfural yield obtained from wheat straw, triticale straw and flax shives were 48, 46, and 72%, respectively. Under the optimized conditions, HCl is the most effective catalyst for furfural production from D-xylose and xylan compared to H₂SO₄, HNO₃, H₃PO₄, CH₃COOH and HCOOH. Hydrothermal transformation of giant reed (*Arundo donax* L.) to furfural and levulinic acid was described under microwave irradiation in the presence of diluted HCl (Antonetti

et al., 2015). Furfural and levulinic acid theoretical yield of up to 70 and 90% were achieved under optimized conditions: biomass (0.35 g), water (5 g) with HCl (1.68 wt%) and 210°C for 15 min. It was also demonstrated that microwaves were shown to represent a very efficient alternative to the traditional heating route to give furfural and levulinic acid. However, when water was adopted as reaction medium, condensation by-products named humins was often observed especially at high reaction temperature also under microwave irradiation.

Recently, the additions of organic solvents such as MIBK, THF, toluene, cyclopentyl methyl ether (CPME) which can isolate the furfural formed from aqueous phase and further inhibit the occurrence of side-reactions have been demonstrated as an efficient method to improve furfural yield. Catalytic performance of heteropolyacids (HPAs) in the dehydration of D-xylose to furfural in different solvent system (DMSO, water, water-toluene or water-MIBK) was studied (Dias et al., 2005a). In this work, H₃PW₁₂O₄₀ showed higher selectivity to furfural (64–69%) in comparison with H₄SiW₁₂O₄₀ (52–64%) and H₃PMo₁₂O₄₀ (inferior than 27%) in DMSO. However, H₄SiW₁₂O₄₀ is the most effective one at 140°C for 24 h in water-MIBK biphasic system with furfural yield of 51%. For H₃PW₁₂O₄₀ and H₄SiW₁₂O₄₀ selectivity toward furfural production is higher for toluene-water than for DMSO for conversions up to 80%. In this work, water-MIBK did not seem to be a good solvent system to produce furfural compared to water-toluene or DMSO with tungsten-containing catalytic system.

Using HCl as catalyst, water-MIBK biphasic system by mixing water phase with DMSO and butanol was reported (Chheda et al., 2007). The results showed that furfural yield from D-xylose increased (65 vs. 29%) with a 6-fold improvement in dehydration rate by decreasing pH (1.0 vs. 2.0) in the presence of water-DMSO mixture (5:5, wt/wt) and MIBK-2-butanol (7:3, wt/wt) as an extracting solvent. With xylan as feedstock, 66% of furfural could be achieved at pH = 1.0 in the same conditions. However, in water-DMSO mixture (3:7, wt/wt) and dichloromethane (DCM) as an extracting solvent at 140°C without catalyst, 57 and 76% of furfural yielded from D-xylose and xylan respectively in 3 h. Although the large-scale use of DCM would be restricted due to environmental concerns, this system showed promising conditions to solve the corrosion problem caused by adding mineral acids and effectively deal with insoluble and soluble biomass feedstocks. The evaluation of MIBK efficiency in enhancing furfural yields was also studied (Zhang T. et al., 2013). Using maple wood solid particles (5 wt%) in aqueous sulfuric acid (0.1 M) and water-MIBK mixture (1:1, wt/wt), furfural yield can reach 85% at 170°C for 50 min, which is better compared to the result achieving less than 65% of furfural yield in absence of MIBK extraction and just over 67% with hydrochloric acid catalysis for 60 min. Interestingly, when monosaccharide as D-xylose was chosen as feedstock, HCl revealed more efficient as acid catalyst with about 76% of furfural yield. This result remained superior to the yield of 64% with H₂SO₄ at 170°C for 30 min, simultaneously with MIBK as extraction solvent. In 2017, the production of furfural from 8 wt% pentose-rich corn stover hydrolyzate was reported (Mittal et al., 2017). The optimized procedure employed a diluted aqueous



sulfuric acid solution (0.05 M) and the mixture was heated up at 170°C for 20 min under conventional heating in presence of MIBK. The D-xylose content was entirely converted into furfural with 80% yield. CPME as an efficient eco-friendly co-solvent was used for the selective dehydration of lignocellulosic pentose to furfural (Molina et al., 2012). They have clearly proven that CPME leads to nearly 100% furfural selectivity from lignocellulosic pentose under the following reaction conditions: H_2SO_4 (1 wt%), biomass (4 wt%) referred to aqueous solution at 170°C for 30 min, CPME/aqueous phase mass ratio equal to 2.33, and NaCl/aqueous solution mass ratio of 0.4 (**Scheme 5**). Like other organic co-solvents, CPME not only favors high furfural selectivity, but also prevents furfural degradation by keeping it in organic phase. In this study, NaCl addition was proved to play the role of accelerating furfural formation rate and shortening the reaction times.

In water-toluene biphasic system, the dehydration of D-xylose to furfural with H_2SO_4 as catalyst in association with an inorganic salt such as NaCl or FeCl_3 as promoter was described (Rong et al., 2012). The maximum yield of furfural (83%) could be achieved in their work when NaCl (2.4 g) was added to water-toluene mixture (10:150, v/v) with D-xylose (10%) and H_2SO_4 (10%), while heating the mixture at the boiling temperature for 5 h. As a promoter, FeCl_3 revealed better than NaCl. Aromatic solvent such as alkylphenol derivatives permitted the conversion of hemicellulose to furfural and levulinic acid using biphasic reactors with alkylphenol solvents that selectively partitioned furanic compounds from acidic aqueous solutions (Gürbüz et al., 2012). Then, 2-sec-butylphenol was identified as a new extracting solvent for the effective extraction of levulinic acid from acidic aqueous solution, and also for extracting furfural from aqueous phase with an exceptionally high partition coefficient when aqueous phase is saturated with NaCl. Some results of furfural production from D-xylose and corn stover from reported studies are summarized in **Table 1**.

Alginate could yield furan compounds after acidic treatment at elevated temperature. In this regard, alginic acid direct catalytic conversion to furfural using 12-tungstophosphoric acid (HPA) and H_2SO_4 as catalyst was investigated (Park et al., 2016). HPA exhibited higher catalytic activity than H_2SO_4 , and gave the highest furfural yield (34%) at 180°C for 30 min. THF was found more suitable than water as reaction solvent, and the addition of

a certain amount of water induced a synergistic effect, enhancing the production of furfural.

Microwave irradiation as an alternative technology was studied in the presence of HCl in the water-MIBK mixture together with the delivery of a kinetic model for the dehydration of D-xylose to furfural in a biphasic batch reactor (Weingarten et al., 2010). It was demonstrated that the organic phase, here MIBK, only acted as “storage” for the extracted furfural improving the furfural yield. However, the biphasic system does not alter the fundamental kinetics compared to the current monophasic system. Moreover, microwave heating does not change the kinetics compared to conventional heating technique. Under optimal reaction conditions: D-xylose (10 wt%) and aqueous HCl (0.1 M) at 170°C for ~ 70 min in a water-MIBK solution (1:1, wt/wt) as a biphasic system, furfural yield can reach 85%, which is more than two-fold of that obtained in monophasic system (30%) under the same conditions.

The role of molecular structure on pentose dehydration to furfural has been examined using HCl as a Brønsted acid catalyst in a single phase aqueous media (Choudhary et al., 2012). It appears that the dehydration of D-xylose in the presence of Brønsted acid follows a direct path (**Scheme 6**).

When combined Lewis acid with Brønsted acid, D-xylose could isomerize to D-xylulose and D-lyxose by Lewis acid and subsequently dehydrates to furfural (**Table 2**). With this combined catalyst functionalities, a much higher yield (76%) to furfural can be obtained in a biphasic system at low temperatures and with short times.

An interesting study compared the furfural yields obtained respectively from the dehydration of D-xylulose and D-xylose in presence of H_2SO_4 under microwave heating in a range of temperature found between 180 and 220°C (Ershova et al., 2015). According their kinetic model, one conclusion is that the D-xylose isomerisation in these conditions is not a crucial step in the pentose dehydration process.

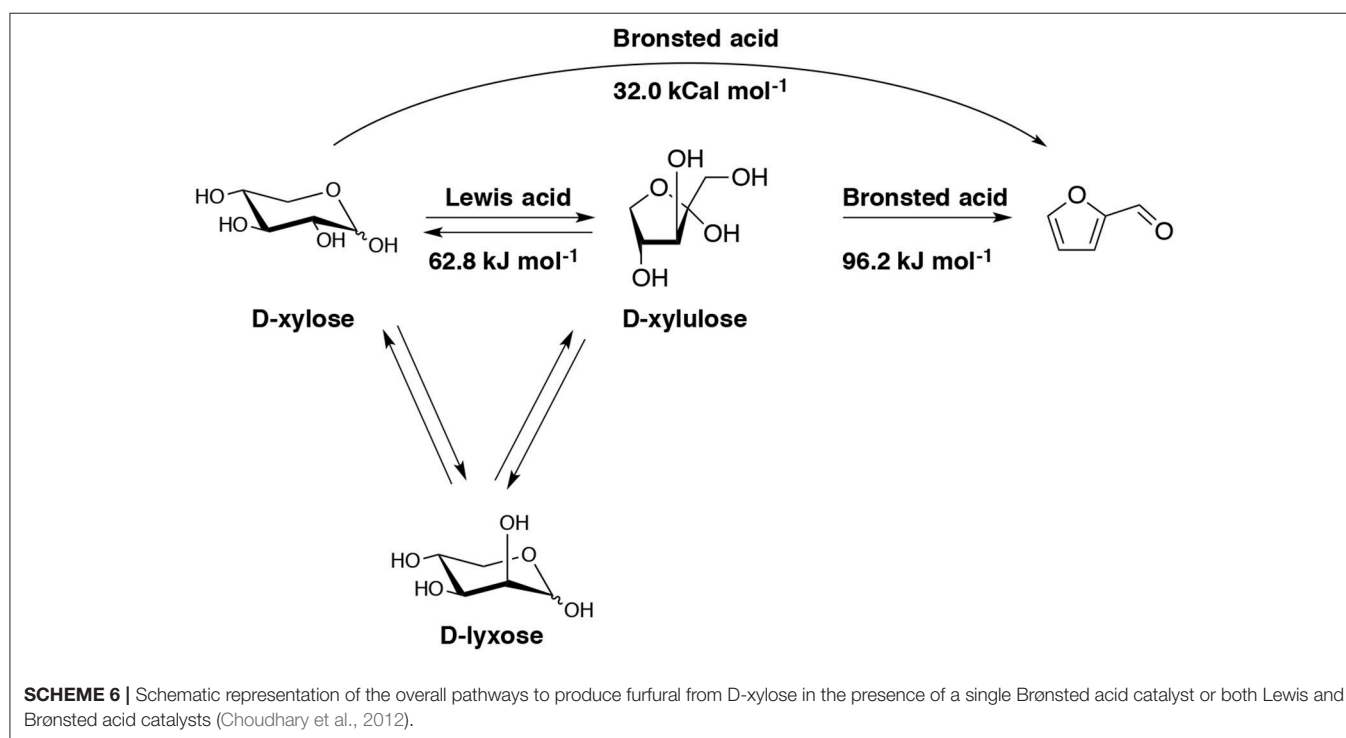
Dehydration in Presence of Organic Acids

Although mineral acids are widely used organic acids are suitable catalyst candidates toward minimization of corrosion issues. The mostly used organic acids for the production of furfural are formic acid and methanesulfonic acid. The comparison of the catalytic action of acids such as formic acid, sulfuric acid and phosphoric acid for the dehydration of D-xylose to furfural at temperature range from 135 to 200°C was reported (Yang W. et al., 2012). Formic acid performed the best furfural yield of 70% at 180°C against 62 and 65% for H_2SO_4 and H_3PO_4 respectively, both set at 160°C . Response surface methodology was applied to optimize furfural yield and selectivity with formic acid as the catalyst, and the best furfural yield reached 74% with D-xylose (40 g/L) and formic acid (10 g/L) initial concentrations, at 180°C . The effect of Kraft-lignin on acid-catalyzed D-xylose to furfural in formic and sulfuric acid using D-optimal design showed that lignin has an acid-neutralizing capacity and a negative effect on furfural formation from D-xylose (Lamminpää et al., 2015). It has been shown that at lower temperature, the yield of furfural is a bit better in the presence of lignin than without lignin in formic acid. Furthermore, the

TABLE 1 | Conditions and results for the D-xylose dehydration with HCl as catalyst in an aqueous NaCl and 2-sec-butylphenol mixture (Gürbüz et al., 2012).

Entry ^a	D-xylose (wt%)	HCl (M)	t (min)	Conv. (%)	Sel. (%)	Yield (%)
1	1.5	0.1	20	98	80	78
2	1.1 (from corn stover)	0.1	30	95	74	70
		0.25	15	92	82	75
3	5	0.1	15	92	77	71
4	2.1 (2 cycles from corn stover)	0.25	15	95	75	71

^aReaction conditions: HCl (0.1–0.25 M), saturated aqueous NaCl-2-sec-butylphenol mixture (6.67:1, wt/wt), 170°C.



effects were greater in H_2SO_4 than in formic acid. The same group also investigated the kinetics of formic acid-catalyzed D-xylose dehydration into furfural and furfural decomposition, using batch experiments within a temperature range of 130–200°C (Lamminpää et al., 2012). By comparing three kinetic models, it is clear that the prediction model must consider other reactions besides furfural formation in overall D-xylose acid-catalyzed conversion. Moreover, the reactions between D-xylose intermediates and furfural play only a minor role. The study also showed that the pH of the reactant solutions has more effect on the reaction rate of furfural decomposition when temperature rises, thus, the kinetic modeling of the D-xylose and furfural decomposition reactions should be considered in water. AlCl_3 as additive was used to improve the role of formic acid as catalyst. The double effect of a catalytic combination of AlCl_3 with HCOOH on the furfural dehydration was studied (Lopes et al., 2017). Herein, the production of furfural was permitted by D-xylose isomerisation into more reactive D-lyxose in presence of the Lewis acid before the dehydration by the organic acid. The optimized condition involved an aqueous solution of AlCl_3

(0.4 M) mixed with formic acid (55 wt%). The furfural selectivity reached a value of 74% when the reaction was carried out at 130°C.

Furfural was produced with a yield of 36% directly from oil palm fronds using formic acid as catalyst when immersed in ethanol under supercritical conditions (Yong et al., 2016). Higher reaction temperature taken between 240 and 280°C showed a great impact on the furfural yield. The supercritical ethanol had a significant role and the highest yield was obtained for an alcohol-acid ratio of 1:2, 0.4 g of solid loading for a mixture heated at 280°C for 20 min.

The use of another organic acid such as methanesulfonic acid was reported in presence of other additives. Under optimized D-xylose (0.3 M) and methanesulfonic acid (0.25 M) loading, furfural yields reached values of 60% at 160°C for 60 min, 65% at 180°C for 15 min and 63% at 200°C for 8 min, which are similar with the results of 66, 62, and 64%, (respectively for same temperature and duration conditions) with H_2SO_4 (Rackemann et al., 2014). The results indicated that methanesulfonic acid is a promising alternative catalyst to H_2SO_4 for the production

TABLE 2 | Process conditions and results for the dehydration of D-xylose with HCl and CrCl₃, 6H₂O and different solvents (Choudhary et al., 2012)^a.

Entry	Catalyst	Solvent	Time (min)	Conv. (%)	Yield (%)
1	HCl (0.1 M)	Water	300	76	29
2	HCl (0.1 M)	Water	150	75	32
3	CrCl ₃ , 6H ₂ O (2 mM)				
4	HCl (0.1 M)	Water	90	90	38
5	CrCl ₃ , 6 H ₂ O (6 mM)				
6	HCl (0.1 M)	Water	60	96	39
7	CrCl ₃ , 6H ₂ O (13.5 mM)				
8	HCl (0.1 M)	Water	120	96	76
9	CrCl ₃ , 6H ₂ O(6mM) +HCl (0.1 M)	Water + Toluene	120	31	27
10	HCl (0.1 M)	Water + Toluene	120	96	35
11	CrCl ₃ , 6H ₂ O (6 mM)	Water + Toluene	120	96	35

^aReaction conditions: Initial D-xylose 1 wt% (1 mL of aqueous solution for entry 1–4, 2 mL of aqueous solution and 2 mL toluene for 5–7), HCl (0.1 M) and/or CrCl₃, 6H₂O (2–13.5 mM), 145°C.

of furfural from D-xylose. It should be noted that the addition of D-glucose into D-xylose had a significant impact on furfural yield, leading to lower yield values in that case with both designated catalysts. For example, furfural yield catalyzed with methanesulfonic acid decreased (45 vs. 63%) as mentioned above with D-glucose addition (0.1 M), and decreased more (41 vs. 64%) with H₂SO₄. It was considered that D-glucose addition resulted in the promotion of furfural degradation. The same group produced furfural in high yield from exposure of pretreated sugarcane bagasse with methanesulfonic acid but the target furanic compound was obtained in association with larger amount of levulinic acid (Rackermann et al., 2016). The use of ionic liquids (IL) in presence of methanesulfonic acid was reported starting from lignocellulosic biomass (Vanoye et al., 2009). In this work, 25% of furfural yield could be obtained at 100°C for 30 min starting from biomass-miscanthus which consist of 44% cellulose and 24% hemicellulose (0.1 g/cm³) in the presence of 1-ethyl-3-methyl-imidazolium chloride (5 mL), methanesulfonic acid (0.11 mL), water (3 mmol/cm³). It should be noted that recent works described thermal and combustion risk profiles of ILs as well as risks of toxicity (Diallo et al., 2012a,b, 2013; Chancelier et al., 2014; Bado-Nilles et al., 2015) and consequently a study of the stability and fate of the ILs in the process should be studied.

In the optic to have a greener process, different biobased compounds obtained in the biorefinery have been tested as acid catalyst. Biobased maleic acid has been used as an efficient catalyst to convert xylan to D-xylose at high yields in aqueous solution at relatively mild temperature (160°C), and to subsequently dehydrate the resulting D-xylose to furfural (Kim et al., 2012). The kinetics of D-xylose dehydration to furfural using maleic acid predicted maximum furfural yield of 72%, while the observed yield was 67% at 200°C for 28 min with microwave heating. In 15 min, furfural yields ranging in 54 to 61% could be achieved with poplar, switchgrass and corn stover respectively as feedstocks, in comparison to a furfural yield not exceeding 29% from pine. Maleic acid also showed some promising advantages in regard to reusability, although maleic acid is slowly hydrated to malic acid.

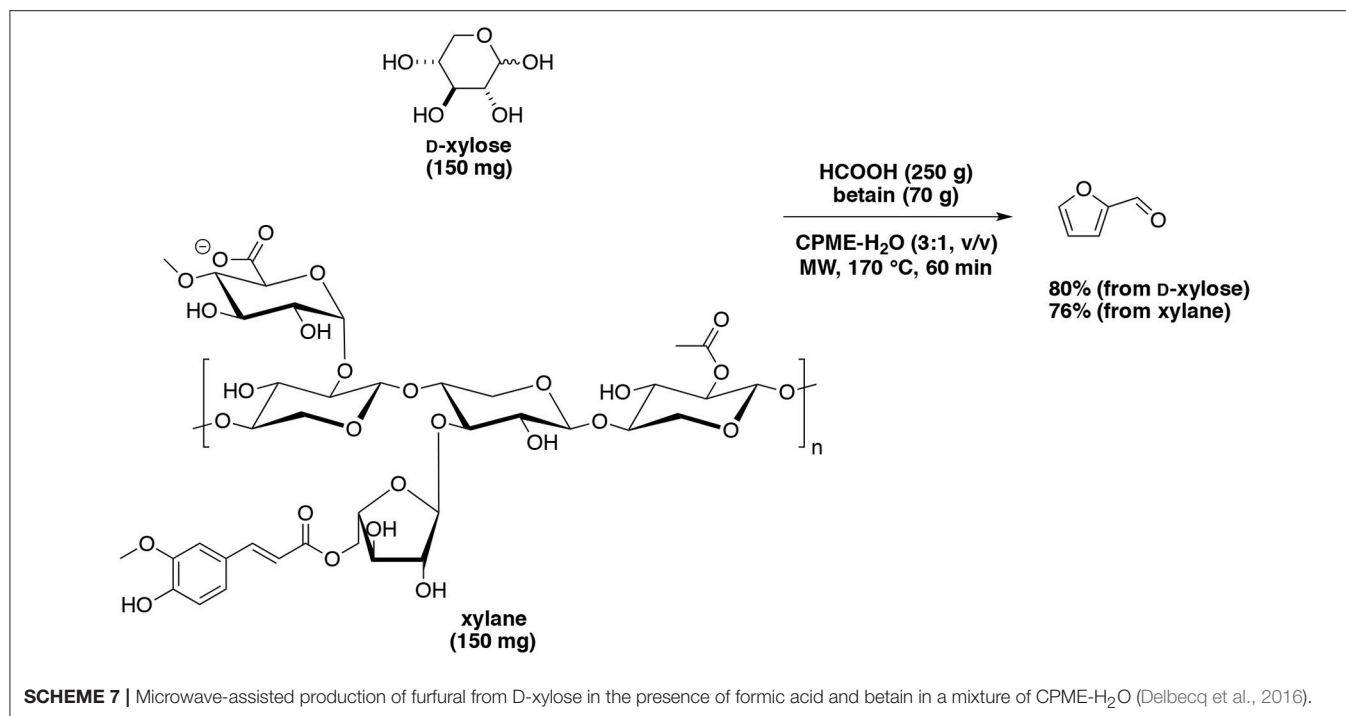
As mentioned above, the addition of organic solvents helps the extraction of furfural. Using organic catalysts, the following process was also studied. o-Nitrotoluene acted as extraction

solvent for furfural production (Yang et al., 2013). The maximum furfural yield of 74% and selectivity of 86% were obtained in 75 min when heated at 190°C starting from D-xylose (80 g/L) and formic acid concentration (20 g/L) with 75% v/v o-nitrotoluene. Additionally, the use of salts (KI, KBr, KCl, and NaCl) was able to enhance the furfural yield and selectivity, whatever their concentration. Len's group demonstrated that formic acid combined with betaine chloride was an efficient and novel homogeneous catalytic system for direct transformation of D-xylose and xylan into furfural (Delbecq et al., 2016). Under optimized conditions at 170°C for 1 h, 80% and 76% of furfural yields were respectively achieved from D-xylose and xylan in a CPME-water biphasic system under microwave-assisted heating (Scheme 7). Other mixtures of solvents such as water-GVL and water-2-methyltetrahydrofuran (MTHF) were used for the dehydration of D-xylose (Xu Z. et al., 2015). Furfural yield (59%) was achieved in the presence of *p*-toluenesulfonic acid for 10 min at 170°C with D-xylose (0.4 g) in a mixture of water-GVL (1.5:15, v/v).

Levulinic acid was explored as a biobased catalyst to produce furfural from pinewood and eucalyptus sawdust in a water or water-MTHF biphasic system (Seemala et al., 2016). Using levulinic acid as the catalyst benefited to both hydrolysis and dehydration processes due to its solubility in the water and MTHF phase. As expected, biphasic system was superior to mono-system. In the presence of feedstock (0.4 g), levulinic acid (0.1 g) and water-MTHF (1:1, wt/wt) loading, eucalyptus isomer revealed to be an easier biomass to convert into furfural than pinewood (565 mg/L at 180°C for 15 min vs. 643 mg/L at 200°C for 60 min), in spite of the fact that eucalyptus gave less C5 sugars which could be due to the different composition of hemicelluloses.

Dehydration in Presence of Metal Salts

Different metal salts have been studied for the production of furfural in a monophasic and biphasic system. Dehydration of xylan and D-xylose to furfural with Cr (II) or Cr (III) as catalysts and *N,N*-dimethylacetamide (DMA) as solvent was reported (Binder et al., 2010). At 100°C, D-xylose was converted into furfural in 30–40% yield in DMA using CrCl₂ and CrCl₃. However, when LiBr was added as an additive, furfural yield catalyzed with CrCl₂ increased up to 56% and 47% if CrCl₂ is



substituted by CrCl₃. Other work on a copper catalyst showed that Cu (II) is the most efficient among various metal cations for alginic acid hydrothermal treatment to produce furfural. In this work, a yield of furfural of 13% was obtained at 200°C for 30 min (Jeon et al., 2016a). In spite of low catalytic performance for degrading alginic acid, Cu (II) ions are favorable for the conversion of alginic acid to furfural. This study implied that algae derivative such as alginic acid could be potentially used as a sustainable alternative feedstock for the production of furfural in the future.

Sodium molybdate as metal salt in presence of HCl as acid co-catalyst permitted the stereospecific conversion of D-xylose and D-lyxose from xylan especially while combined with microwave technology (Hricoviniová, 2013). Simultaneously the homogeneous catalyst leads to higher energy transfer to solution from a microwave source that will improve the yield of furfural. The process involves combined hydrolysis, epimerization and dehydration reactions in a single step and provided higher amounts of furfural (53%) compared to reaction without Mo (VI) ions (42%, 300 W for 5 min of MW heating). Xylan dehydration with conventional heating in the presence of molybdate yielded 36% of furfural that is also higher than the 28% yield obtained without Mo (VI) ions at 150°C for 30 min. It was proposed that chromium, acting as a Lewis acid, catalyzed D-xylose isomerization (Choudhary et al., 2012). In fact, CrCl₃ is an efficient Lewis acid to isomerize D-xylose to D-xylulose and further dehydrated it to furfural (76%) at lower temperature (145°C). When xylan was used as the feedstock, the results implied that depolymerization is the major barrier for chromium-catalyzed furfural production, and less than 25% of furfural was achieved at 140°C with CrCl₂ as catalyst, HCl as co-catalyst in 1-ethyl-3-methylimidazolium chloride.

Focusing only on the use of NaCl as catalyst, a comparison was also made between conventional heating and microwave technology (Xiouras et al., 2016). Higher yields were obtained after 7 min of heating in presence of NaCl (3.5 wt%) at 200°C. The D-xylose conversion was complete giving 76% of furfural yield under microwave heating.

Using metal salts, biphasic systems were developed making use of similar solvents as mentioned above. Isolation of hemicelluloses from *Rubescens* using a water-GVL biphasic system heated at 180°C was studied (Luo et al., 2017). The hemicelluloses rich lignin fraction was then warmed up in presence of NaCl and THF giving a furfural yield of 77%. NaCl was also found responsible of all reactions such as hydrolysis, epimerization and dehydration involved in the processes at the higher temperature of 200°C. A production of furfural was set up in association with bromomethylfurfural (BMF) and HMF from cellulose and lignocellulosic biomass (Yoo et al., 2017). The biphasic system water-DCM (1:3, v/v) involving an organic solvent and a molten lithium bromide hydrate solution was heated for 2 h at 120°C and permitted to obtain furfural in 70% yield. The use of high pressure of CO₂ in a mixture of aqueous isopropanol in the presence of NaCl furnished furfural in 70% yield (Zhao et al., 2017). The high CO₂ concentration reduced the pH of the sugar solution and the optimized condition required a temperature of 200°C for 3 h in a 2:1 ratio of water-alcohol. Different works described the use of iron-catalyzed furfural production in biobased biphasic systems. FeCl₃ was selected as the catalyst, NaCl as additive and MTHF as biomass-derived solvent (Vom Stein et al., 2011). Without NaCl, furfural yield only reached 27% with FeCl₃ as catalyst and a reaction temperature of 140°C, however, the same reaction condition involving NaCl (20 wt%) for 4 h afforded furfural (70%). Furfural formation rate

increased by a factor of more than two. Xylan from beech wood was first hydrolyzed to D-xylose in a concentration of 30 g/L (2.5 mL), then FeCl_3 , $6\text{H}_2\text{O}$ (0.12 M), NaCl (30 wt%), were added together in 2.5 mL of MTHF, and the reaction yielded furfural (37%) at 140°C for 2 h. Furfural yield of 75% was obtained from D-xylose in a water-THF biphasic medium containing AlCl_3 , $6\text{H}_2\text{O}$ and NaCl under microwave heating at 140°C (Yang Y. et al., 2012). It was clear that AlCl_3 could isomerize D-xylose into D-xylulose, followed by the dehydration of the latter to produce furfural, similarly to isomerization catalysts CrCl_3 or NaMoO_4 mentioned above. Moreover, this system was effective in the hydrolysis of xylan and lignocellulosic hemicelluloses to D-xylose, which resulted in fairly good furfural yields in some cases from lignocellulosic biomass (Table 3).

Starting from D-xylose, our team also studied furfural production catalyzed with FeCl_3 and NaCl as additive (Le Guenic et al., 2015). With the aid of microwave irradiation and the eco-friendly mixture: water-CPME (1:3, v/v), the highest furfural yield (74%) was achieved at 170°C for 20 min in the presence of iron chloride (10 mol%) and NaCl 100 (mol%) (Scheme 8). Addition of NaCl was found to increase the catalytic activity of FeCl_3 and allowed to reduce the amounts of FeCl_3 used from 20 mol% to 10 mol%. This system was extended to xylan and afforded furfural yield of 52% at 200°C for 20 min or 170°C for 70 min.

Sulfate derivatives such as NaHSO_4 , $\text{KAl}(\text{SO}_4)_2$ and $\text{Al}_2(\text{SO}_4)_3$ were tested for the production of furfural. Furfural was obtained from various raw lignocellulosic materials in water-THF by using NaHSO_4 as catalyst (Shi et al., 2015). Many reaction parameters were optimized, such as reaction temperature, time, solvent volume ration, feedstock concentration as well as catalyst loading. Under the optimum conditions: 190°C , 90 min, biomass concentration (11.1 wt%), NaHSO_4 (3.31 wt%), H_2O (0.8 mL) and THF (8 mL), 50–60% furfural yields were obtained from diversified lignocellulosic biomass such as corncob, wheat straw, bagasse. Under conventional heating, using $\text{KAl}(\text{SO}_4)_2$ in a water-MIBK biphasic system, furfural was efficiently produced from D-xylose when heated for 6 h at 190°C , since 55% of furfural yield was obtained (Gupta et al., 2017a). The catalytic activity of $\text{Al}_2(\text{SO}_4)_3$ metal salt for the D-xylose dehydration was also reported using a water-GVL biphasic system (Yang et al., 2017). $\text{Al}_2(\text{SO}_4)_3$ decomposes into SO_4^{2-} anions and the hexacoordinated Lewis acidic species $[\text{Al}(\text{OH})_2(\text{HO})_4]$ able to isomerizes D-xylose into D-xylulose, easily converted into furfural. The optimized conditions afforded 88% yield in furfural

Interestingly, a most recent work reported an improvement of the furfural yield from alginic acid also catalyzed by Cu (II) as previously reported in various biphasic system (Wang et al., 2018). With MIBK, the microwave-aided dehydration of the polysaccharide afforded furfural in an overall yield of 31% (hydrolysis, decarboxylation, dehydration) (Scheme 9).

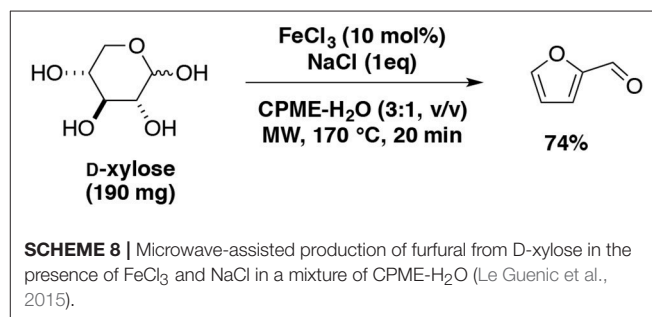
Ionic Liquids (ILs) Applications in Catalysis for Furfural Synthesis

ILs are known as organic salts with melting points below 100°C composed solely of cations and anions, which have many unique properties, such as very low volatility, good dissolving capacity, operational chemical and thermal stability, flame-retardancy

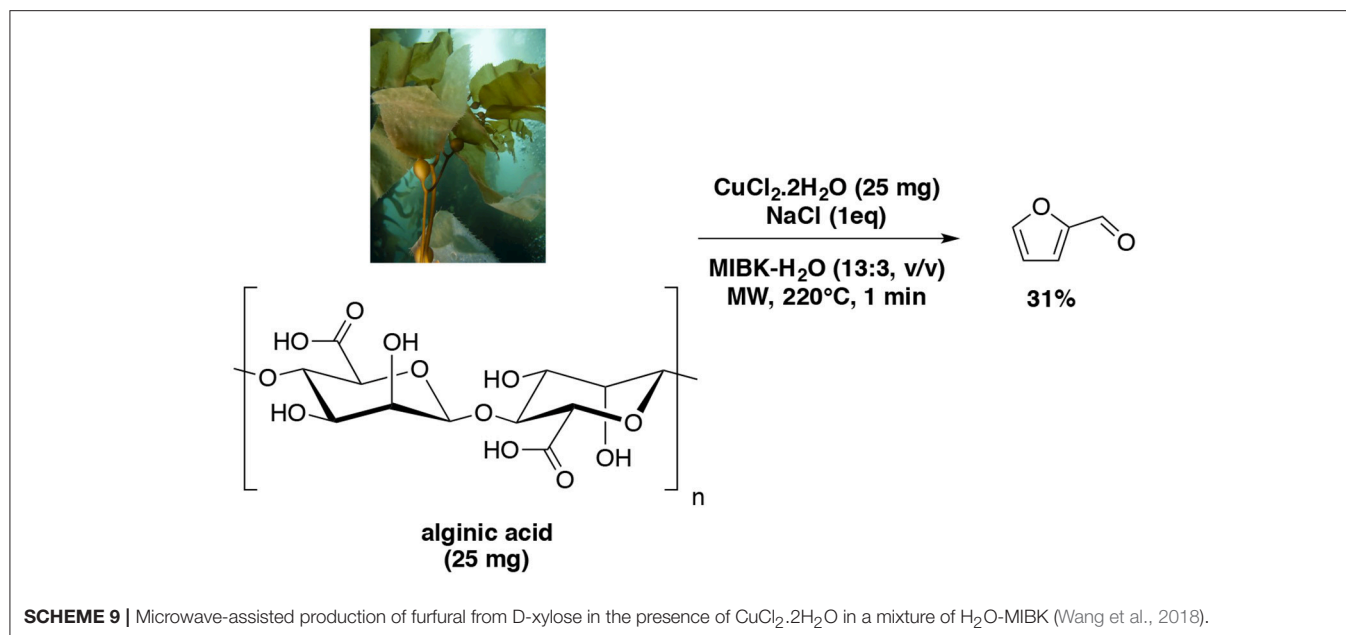
TABLE 3 | Conditions and results for the production of furfural starting from various sources of lignocellulosic biomass in presence of AlCl_3 (Yang Y. et al., 2012).

Entry ^a	Biomass	Temperature ($^\circ\text{C}$)	Time (min)	Yield (%)	
				D-Furfural	D-Xylose
1	Corn stover	140	60	51	2
2	Pinewood			29	12
3	Switchgrass			50	8
4	Poplar			45	6
5	Corn stover	160		55	<1
6	Pinewood			38	<1
7	Switchgrass			56	1
8	Poplar			64	<1
9	Pinewood	180	30	61	<1

^aReaction conditions: Biomass 0.05 g, AlCl_3 , $6\text{H}_2\text{O}$ 0.1 mmol, NaCl 6.0 mmol, water 1 mL, THF 3 mL.



(often leading to qualifying them as “non-flammable” products as resulting from the application of haz-mat regulations. Some are non-toxic, but not all of them and recyclability is more or less easy. ILs are often considered -sometimes too generically- as an example of more sustainable solvents, which contribute to a greener processing of biomass, and are suitable for furfural production (Lima et al., 2011). Some neutral ILs such as 1-butyl-3-methylimidazolium chloride (Sievers et al., 2009; Zhang L. et al., 2013; Peleteiro et al., 2014) has been employed as efficient solvents and 1-ethyl-3-methylimidazolium chloride used as additive (Binder et al., 2010). Generally, acidic ILs were applied as catalysts which performed as reaction mediums (Peleteiro et al., 2016a), such as 1-butyl-3-methylimidazolium hydrogen sulfate (Carvalho et al., 2015; Peleteiro et al., 2015a,b), 1-ethyl-3-methylimidazoliumhydrogen sulfate (Lima et al., 2009), 1-(4-sulfonic acid) butyl-3-methylimidazolium hydrogen sulfate (Tao et al., 2011, 2012). Even though ILs have showed many advantages for the production of furfural, scientists are also facing plenty of challenges to realize their industrial utilization, such as the cost of ILs, deep understanding of their properties, their recovery and recycling problems and also environmental issues. Meanwhile, the recovery of furfural from IL should also become difficult. Moreover, our group reported that ILs could generate fire induced toxicity essentially driven by the presence of hetero-atoms in their structures and induce ecological



disturbance for organism (Diallo et al., 2012a,b, 2013; Chancelier et al., 2014; Bado-Nilles et al., 2015). Thermal stability advantages of ILs need also to be analyzed on a case by case study (Abbott et al., 2018). In order to limit the use of ILs, different groups reported the production of furfural with acid ILs used as reagent and not as solvent (Matsagar et al., 2015; Peleteiro et al., 2016b,c; Liu et al., 2017; Matsagar and Dhepe, 2017; Wang et al., 2017).

SYNTHESIS OF FURFURAL FROM SUGARS AND POLYSACCHARIDES USING SOLID ACID CATALYSTS

Production of furfural starting from pentose derivatives has been reported using carbon acids, clays, ion-exchange resins, oxides, phosphates, silicates and zeolites sometimes assisted by alternative technologies (Bhaumik and Dhepe, 2016).

Dehydration in Presence of Carbon Acids

Carbonaceous materials are frequently used solid acid catalysts in many applications due to their high thermal stability, high chemical activity and low production costs. Therefore, several researchers have considered that they could be an interesting alternative for sugar dehydration in aqueous environment. An activated carbon catalyzed D-xylose dehydration to furfural was compared with an auto-catalytic reactions (Sairanen et al., 2014). The use of Norit as commercially-available activated carbon permitted to have a better control over the unwanted side reactions such as acids and humins formations. It was found that the main isomer with carbon catalyst was D-xylulose and in case of non-catalyzed reaction was D-lyxose. This result demonstrated that activated carbon catalyst could avoid unwanted side reactions by offering acidic sites and could permit isomerization of D-xylose into more reactive keto sugars, these

latter intermediates being more favorable to furfural production. Other carbon sources such as graphene derivatives were studied for the production of furfural to improve the conversion and selectivity. In this regard, four kinds of carbon-based catalysts: graphene, graphene oxide, sulfonated graphene, and sulfonated graphene oxide (SGO) were elaborated and tested (Lam et al., 2012) (Table 4).

SGO was proven to be a rapid and an active catalyst for improving furfural yield from D-xylose aqueous solution even at very low catalyst loadings down to 0.5 wt% vs. D-xylose. Furthermore, SO₃H groups, which are the active acidic sites for dehydration of D-xylose to furfural, have shown good water tolerance and revealed more thermally stable under the reaction conditions than COOH or OH groups. After 12 times repeated tests at 200°C for 30 min, an average furfural yield of 61% was achieved in comparison to 44% for the uncatalyzed system.

Often the carbon-based catalysts are prepared by carbonization of sugar molecules to form sulfonate-functionalized carbon particles. In particular, solvothermal conversion of cassava waste to furfural using a sulfonated carbon-based catalyst was investigated (Daengprasert et al., 2011). Results obtained in presence of H₂SO₄ and without catalyst was compared, the carbon-based catalyst showed its effectiveness for the hydrolysis of xylan to D-xylose and then D-xylose dehydration to furfural. However, in this study, less than 3% of furfural yielded from cassava waste and only 12% from D-xylose and xylan. Sulfonated biochar was prepared successively by carbonization and sulfonation (Deng et al., 2016). The resulted acidic carbonaceous solid was employed for the direct transformation of a pre-hydrolyzed aqueous solution of corncob in a biphasic system involving DCM on the organic layer. When the system was heated at 170°C for 60 min, 83% of furfural selectivity was finally recorded. Len's group employed a sulfonated biochar in a microwave-aided dehydration of

TABLE 4 | Conditions and results for the production of furfural starting from D-xylose and graphene derivatives in water (Lam et al., 2012).

Entry ^a	Catalyst	Conv (%) ^b	Sel. (%) ^b	Yield (%) ^b
1	None	76	58	44
2	Graphene	75	68	51
3	Graphene oxide	80	66	53
4	Sulfonated graphene oxide	83	75	62
5	Sulfonated graphene	86	64	55

^aReaction conditions: D-xylose (2.25 g), catalyst loading 2 wt%, 35 min, 200°C.^bData averaged over 3 runs.

D-xylose and commercial xylan (Wang et al., 2017a). Each substrate was introduced in a water-CPME (1:3, v/v) biphasic system, and warmed up at 190°C for 60 min. Furfural was obtained with 60 and 42% of yield from D-xylose and xylan, respectively (**Scheme 10**).

Another source of carbon catalytic material was prepared (Zhang et al., 2016) by successively carbonization of sucrose and sulfonation, successively. This solid catalyst was able to dehydrate D-xylose and corn stalk into furfural at 170°C for D-xylose and 200°C for the plant waste. The yields obtained were 79 and 61%, respectively, for residence time varying between 30 and 100 min. Recently, a carbonized resorcinol-formaldehyde resin and sulfonated was also tried as a catalyst (Zhu et al., 2017). The material was found efficient for furfural production from D-xylose and corn stover in GVL. When heated at 170°C for 15 min with enough catalyst, the best dehydration conditions afforded furfural in 80% yield with a D-xylose conversion of 100%. In comparison, 69% of furfural yield was achieved from corn stover at 200°C after 100 min of heating with higher amount of the same catalyst. The sulfonation of carbonaceous catalyst SC-CCA prepared by carbonization of sucrose using 4-benzenediazoniumsulfonate as a sulfonating agent produced furfural in 79% yield by use of GVL as unique solvent in a conversion reaction operated at 170°C for 30 min (Zhang et al., 2016). Starting from corn stalk, furfural was obtained in 60% yield for 100 min at 200°C or for 60 min at 210°C. In case of corn stalk, it is noteworthy that addition of water (10 wt%) severely decreased furfural yield. Nevertheless, sulfonated groups grafted onto the C-CCA have been demonstrated to be significantly stable, and SC-CCA could be reused up to 5 runs without the loss of furfural yields. Calcium citrate was used as novel source of biomass for the preparation of sulfonated catalyst (Li et al., 2017). The use of sulfonated carbonaceous residue obtained from the calcination of bio-based calcium citrate in dehydration reaction of raw corn stover in GVL operated at 200°C furnished furfural (93%) in GVL. The authors mentioned that using the same reactions conditions replacing GVL by water was leading to a furfural yield reaching only 51%.

The preparation of a sulfonated graphitic carbon nitride and its application for the dehydration of D-xylose into furfural were reported by Varma and Len's groups (Varma et al., 2017). Starting from D-xylose in presence of sulfonated graphitic carbon nitride in water as sole solvent at 100°C for 30 min, the yield in furfural

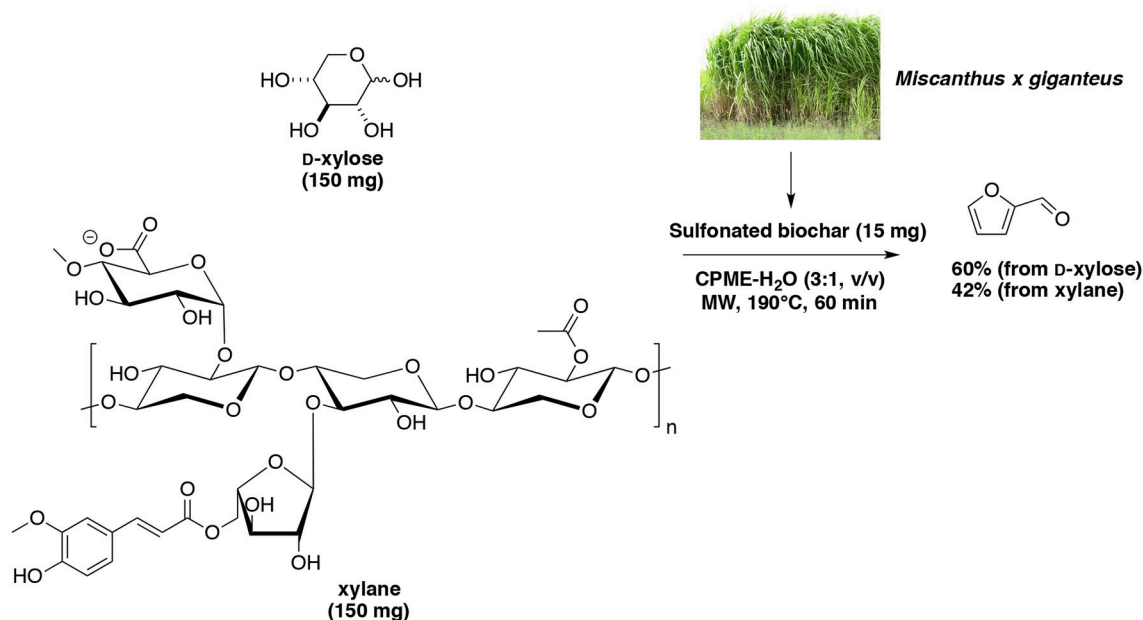
rose to 96% (**Scheme 11**). This process gave one of the best results obtained at the lab scale.

Dehydration in Presence of Clays

Only one report described the use of clays for the dehydration of pentose derivatives into furfural. Four kinds of pillared clays catalysts with different quantities of aluminum and hafnium (labeled as Al-Hf 11-1, Al-Hf 10.5-1.5, Al-Hf 10-2 and Al-Hf8-4) were used and applied into the conversion of D-xylose to furfural (Cortés et al., 2013). The selectivity of furfural in this work reached 53% with Al-Hf 11-1 and increased to 65% with Al-Hf 10.5-1.5 in a reaction operated at 140°C; however, D-xylose conversion were only 45 and 35%, respectively by the way significantly limiting (below 30%) the overall yields in furfural obtained. Increasing reaction temperature to 170°C raised D-xylose conversion, but a loss of selectivity was observed. As a conclusion, an increase of the hafnium content reduced the selectivity for furfural on Al-Hf vermiculites. A maximum Hf content of 2 mmol Hf/g (clay) revealed however to be a promising catalyst for the dehydration of pentose in water as a solvent, producing furfural with an average conversion rate of 78% and a selectivity rate of 50% at 170°C for 4 h in four consecutive reactions.

Dehydration in Presence of Ions-Exchange Resins and Ionomers

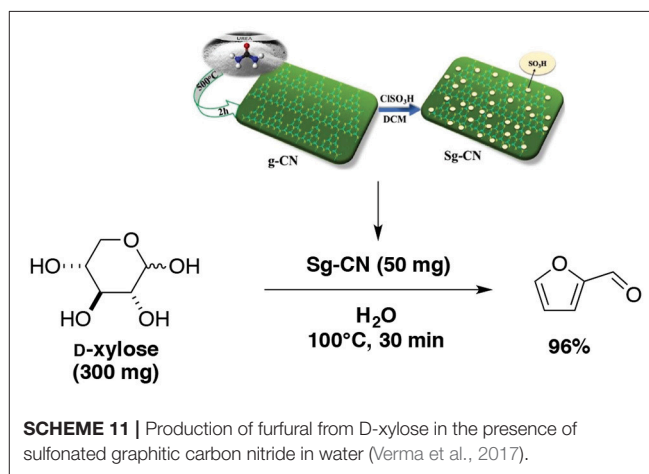
Furfural production catalyzed by an ion-exchange sulfonic resin was extensively studied. The nature and properties of the resins *Amberlyst* and *Nafion*, with different acidities, pore diameters and thermal stabilities, permitted to generate the dehydrated chemicals depending of the process used. The kinetic parameters of furfural production in water and water-toluene biphasic system, with or without catalyst, at different reaction temperatures and time, D-xylose loading and its simultaneous stripping using nitrogen were studied (Agirrezabal-Telleria et al., 2011). In this work, 65% of the stripping furfural was achieved from D-xylose and almost 100% of selectivity in the condensate was observed. Later, the effect of D-glucose addition into D-xylose on furfural production was conducted under different operating configurations (Agirrezabal-Telleria et al., 2012). D-Glucose addition to D-xylose has a negative effect on furfural yield at 175°C, but a positive effect at higher temperature (200°C), which is considered as an “entropy-effect” at high reaction temperature, leading to slower side-reactions. The mixture of D-xylose and D-glucose at similar ratios to the real pentosan-rich biomass led to furfural yields of up to 75% at 200°C, and even 78% with lower D-xylose concentration. The same group showed that *Amberlyst-70* with strong sulfonic acid sites presented a higher furfural selectivity than Nb₂O₅ supported catalyst (Agirrezabal-Telleria et al., 2013a). In all their studies, the strategy of nitrogen stripping showed more industrial feasibility with respect to other biphasic water-solvent systems. Using the same catalyst, *Amberlyst-70*, a research aiming at producing specific humins has been done starting from D-xylose in a mixture of methanol-water (Hu et al., 2012). It was found that high reaction temperature, long residence time, low methanol-water mass ratio, and high catalyst dosage were favorable for



SCHEME 10 | Microwave-assisted production of furfural from D-xylose in the presence of sulfonated biochar (ex *Miscanthus x giganteus*) in a mixture of H₂O-CPME (Wang et al., 2017a).

their formation. Although furfural can be protected to form 2-(dimethoxymethyl)-furan (DOF) in the methanol-rich medium, this did not remarkably suppress polymerization occurrence at high reaction temperature. Additionally, the acid treatment of furfural also produced methyl levulinate in methanol and levulinic acid in water by partial degradation of furfural in those conditions. Later, further study of acid-treatment of C5 and C6 sugar monomers/oligomers with the same catalyst in water or DMSO system was conducted (Hu et al., 2014). Some interaction or cross-polymerization of D-xylose-D-glucose, D-fructose-raffinose, furfural-D-glucose, and furfural-D-fructose occurs. In water, yields of the insoluble polymer from the sugars / (furfural) increase in the order: D-fructose > raffinose > D-glucose > D-xylose > (furfural). In another hand, furfural can be preserved by DMSO and in such a case less insoluble polymer is formed.

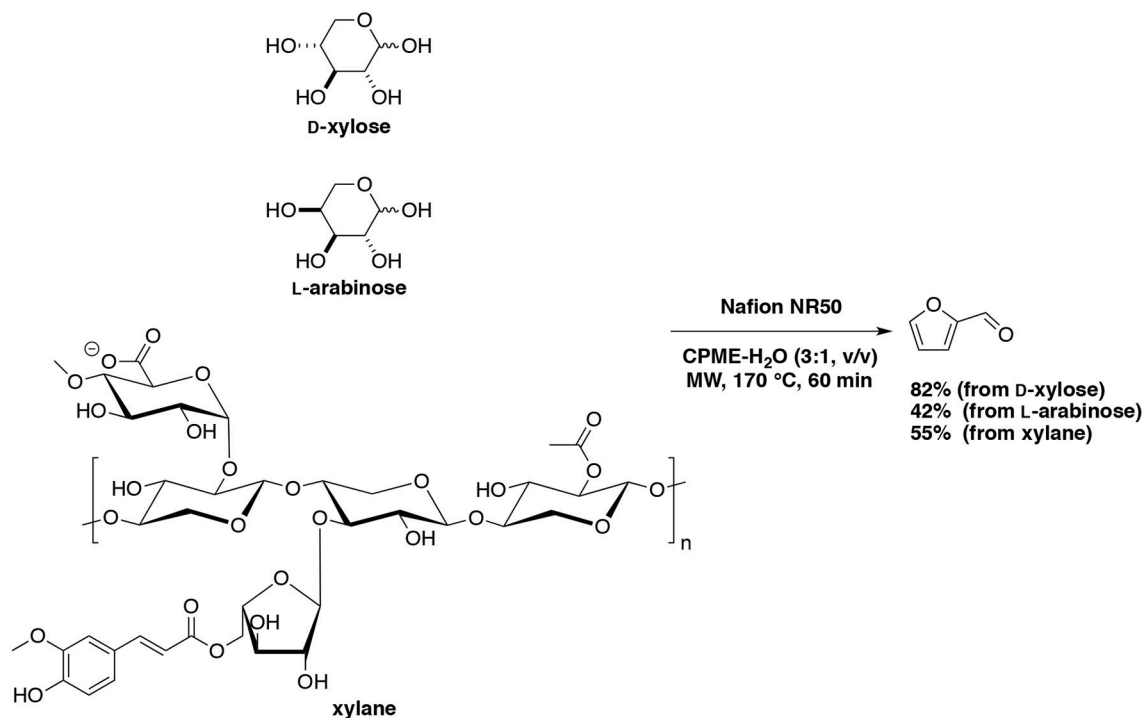
The use of *Amberlyst-15* instead of *Amberlyst-70* has been applied to promote the catalytic hydrothermal reaction of alginic acid toward furfural production (Jeon et al., 2016b). A maximum of 19% furfural yield was obtained at 180°C in 30 min. The catalyst could be recycled 5 times with approximately 30% loss of furfural yield at latest catalyst recycling run. Unfortunately, recovered catalyst could not be regenerated with H₂SO₄ because by-products covering its surface inhibited its regeneration. In water-THF mixture, *Amberlyst-15* led to furfural production in 17% yield at reaction temperature of 170°C maintained for 60 min. The thermal stability of *Amberlyst-15* could explain this result. In comparison with the use of 12-tungstophosphoric acid poorer catalytic efficiency has been observed (Park et al., 2016). Successive dehydration of D-xylose by *Amberlyst-15* and furfural hydrogenation over a hydrophobic Ru/C catalyst in a



SCHEME 11 | Production of furfural from D-xylose in the presence of sulfonated graphitic carbon nitride in water (Verma et al., 2017).

single biphasic reactor have been studied (Ordonsky et al., 2013). Organic solvents butan-1-ol, MTHF and cyclohexane were used. The amounts of the catalysts, solvent, temperature and pressure were optimized in the water-cyclohexane system. The main product tetrahydrofurfuryl alcohol was obtained at 135°C with a selectivity and a conversion ratio of 50 and 32%, respectively. In addition, co-products such as GVL, levulinic acid and pentane diols were also observed with comparable yields.

A more promising heterogeneous catalyst, *Nafion 117* furnished furfural in 58–62% yields in DMSO at 150°C and as a result of 15 consecutive runs with an overall conversion higher than 90% (Lam et al., 2011). Activation energy values for *Nafion 117* at 5 and 20% catalyst weight loading were 86.4 and



SCHEME 12 | Microwave-assisted production of furfural from D-xylose, L-arabinose and lignin in the presence of *Nafion NR50* in a mixture of H_2O -CPME (Le Guenic et al., 2016).

89.3 kJ/mol, respectively which were lower than other solid acid catalysts tested. Our group has tested perfluoroalkane sulfonic resin, *Nafion NR50*, anticipating a good efficiency as a superacid catalyst for the production of furfural (Le Guenic et al., 2016). In a water-CPME biphasic system under microwave irradiation D-xylose, L-arabinose and xylan converted into furfural in the presence of NaCl with maximum yields of 80, 42, and 55%, respectively (**Scheme 12**). It was found that the association of *Nafion NR50* and NaCl generated an unusual stability of the resin, which have synergistic effect in acid catalysis. Unfortunately, gradual deactivation due to humins deposition was also observed after the fourth cycle.

Three kinds of micro-mesoporous sulfonic acid catalysts-silylated MCM-41- SO_3H , coated MCM-41- SO_3H and hybrid- SO_3H have been prepared, characterized, and tested in the dehydration of D-xylose to furfural (Dias et al., 2005b). The hybrid- SO_3H gave a lower furfural selectivity compared to MCM-41- SO_3H materials, which may be due to the hydrophobicity of the surface. This in turn might have enhanced the adsorption of furfural at the surface, and further accelerated its reaction with intermediates on the accessible acid sites. Coated MCM-41- SO_3H yielded slightly higher yield (>75%) than MCM-41- SO_3H (69%) in DMSO or water-toluene biphasic system at 140°C for 24 h. However, silylated MCM-41- SO_3H have a better selectivity than that of coated MCM-41- SO_3H (96 vs. 83%) in water-toluene. The increase of reaction temperature shortened the reaction time, and subsequently benefited to the obtained furfural yield. For example, 70% of furfural yield was achieved

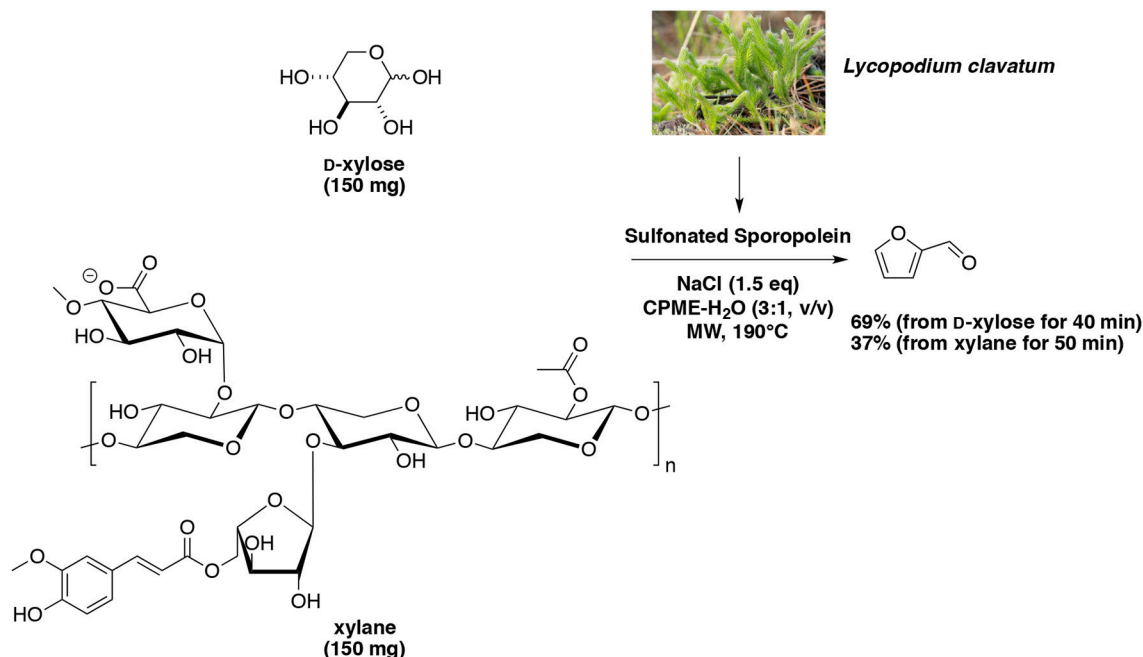
at 170°C for 4 h with coated MCM-41- SO_3H . Unfortunately, apparently catalyst deactivation was observed as soon as and the second catalyst reuse in spite of its regeneration.

Subsequently, a more stable and recyclable biobased catalyst sulfonated sporopollenin was successfully synthesized and tested for the microwave-assisted dehydration of D-xylose and xylan into furfural (Wang et al., 2017b). Under the same methodology developed by Len's group, sulfonated sporopollenin in the presence of NaCl furnished furfural in 69% yield from D-xylose at reaction temperature of 190°C and reaction duration of 40 min (**Scheme 13**). In our hands, when the catalytic system was recharged with carbohydrate and solvent, 10 catalyst recovery steps could be performed without loss of performance. Application to xylane at 190°C for 50 min furnished the aldehyde in 37% yield.

Using the same strategy, a new porous sulfonated triphenylamine was developed to dehydrate pentoses and hexoses in lactone-type organic solvents (Zhang et al., 2017a). When GVL was used as a solvent at reaction temperature of 175°C , furfural was obtained in 74% yield.

Dehydration in Presence of Oxides

Different oxides derivated from Zr, Ti, and Nb have been studied for the production of furfural. Well-ordered mesoporous and super strong acidic sites catalysts $\text{SO}_4^{2-}/\text{ZrO}_2\text{-Al}_2\text{O}_3/\text{SBA-15}$ were tested and the most efficient catalyst $\text{SO}_4^{2-}/12\% \text{ZrO}_2\text{-Al}_2\text{O}_3/\text{SBA-15}$ gave 99% of D-xylose conversion and 53% furfural yield when heating the 160°C during 4 h by Shi et al. (2011).



SCHEME 13 | Microwave-assisted production of furfural from D-xylose in the presence of biobased sulfonated Sporopolenin in a mixture of H₂O-CPME (Wang et al., 2017b).

It was found that the addition of Al to $\text{SO}_4^{2-}/\text{ZrO}_2/\text{SBA-15}$ stabilized the tetragonal ZrO_2 phase and enhanced the activity of the catalyst by increasing the number of acid sites. The reasons for catalyst deactivation and regeneration were examined. In spite of sulfur leaching, catalyst deactivation was related to the accumulation of humins, which might cover the surface of the catalyst, leading to the passivation of the acid site. Furthermore, deactivated catalyst can be completely regenerated with H_2O_2 , but the furfural yield decreased by increasing the number of recycling tests, which was mainly caused by the presence of monoclinic ZrO_2 that decreased the acid strength and acid concentration of the catalyst. Ultraviolet irradiation was tried with a screening of heterogeneous catalysts for the production of furfural from D-xylose (Li H.-L. et al., 2013; Li et al., 2014a), and from corncob (Li et al., 2014b). The optimized photocatalyst $1.0\text{M-SO}_4^{2-}/\text{TiO}_2\text{-ZrO}_2/1.0\text{wt\%-La}^{3+}$ gave 32% of D-xylose conversion and $216.6\ \mu\text{mol/g}$ of furfural yield at 120°C for 4 h under ultraviolet irradiation: this is sharply higher than without catalytic process and absence of ultraviolet irradiation.

Some other scientists studied the simultaneous hydrolysis/dehydration of sugarcane bagasse, rice husk and corncob under hot compressed water in the presence of TiO_2 , ZrO_2 and $\text{TiO}_2\text{-ZrO}_2$ at $200\text{--}400^\circ\text{C}$ (Chareonlimkun et al., 2010). In all cases, TiO_2 showed more efficiency in converting lignocellulosic biomass to furfural than ZrO_2 . It was found that catalysts prepared by (co-)precipitation method gained higher reactivity than those prepared by sol-gel and physical mixing methods. The suitable calcination temperature for TiO_2 and ZrO_2 was formed at 500°C . The use of mixed-oxide $\text{TiO}_2\text{-ZrO}_2$ (Chareonlimkun et al., 2010) offered the highest furfural yield

(10%) from corncob at 300°C with less by-products selectivity when compared with TiO_2 or ZrO_2 at the same conditions. Five-time recycling of this oxides mixture, still ending up with a yield in furfural of 10%, indicated promising operational lifetime of this catalyst. Additionally, this catalyst has the bifunctionality for both acidity and basicity properties, which benefits to hydrolysis, dehydration and also isomerization processes, leading to high furfural production. The suitable calcination temperature for $\text{TiO}_2\text{-ZrO}_2$ was 600°C , which is higher than that for TiO_2 and ZrO_2 .

Note that the introduction of sulfate ion and lanthanum can enhance the photocatalytic performance of metal oxides by increasing the acidic sites (Li et al., 2014b). Subsequently, this kind of catalyst was applied in the hydrothermal pretreatment of corncob into D-xylose and furfural (Li et al., 2014a). After optimizing the reaction parameters, the highest furfural yield (6.18 g of furfural for 100 g of corncob) could be obtained at 180°C for 120 min when the corncob-water ratio of was 10:100. From xylan, a furfural yield of 21% was achieved using $\text{Cr-LaCo}_{0.8}\text{Cu}_{0.2}\text{O}_3$ (1.5%) as catalyst, under 10 h of conventional heating in the 1:600 weight ratio of xylan to water at 160°C (Li H.-L. et al., 2013). It is worth to notice that the amount of chromium in solid catalyst decreased from 1.26 to 0.38% after the first recycling run, which accordingly led to the reduction of furfural yield to 13%. Importantly, there is no effect on pentose formation.

An environmentally-friendly two-step process for furfural production starting from corncob (Deng et al., 2015). Hydrothermal pretreatment was firstly investigated in a temperature range from 160 to 190°C for reaction duration of

0–60 min, and then the resulted hydrolysate was catalyzed with $\text{SO}_4^{2-}/\text{SiO}_2\text{-Al}_2\text{O}_3/\text{La}^{3+}$ as a solid acid catalyst at 150°C for 2.5 h. The maximum yield of furfural achieved was 21% from the hydrolysates (total D-xylose yield 7.01 g/L) obtained at reaction temperature of 190°C for 60 min in the hydrothermal process, and no obvious decrease of furfural yield was detectable after four consecutive runs.

A mesoporous and amorphous niobium oxide was used to dehydrate D-xylose into furfural through a ketone-type intermediate called D-xylulose (Gupta et al., 2017b). Furfural selectivity (48%) was obtained in such environment when the reaction was carried out at 120°C , in sole water; however the yield increased in a water-toluene biphasic system (2:3, v/v) to reach 72% of selectivity. The catalyst activity was also compared to other solid catalyst such as titane oxide (TiO_2).

Dehydration in Presence of Sulfated Oxides

Several bulk and ordered mesoporous silica-supported zirconia catalysts for the dehydration of D-xylose into furfural in a water-toluene solvent mixture at 160°C furnished furfural yields higher than 50% and a conversion higher than 90% (Dias et al., 2007). It should be noted that the initial catalytic activity correlated fairly well with the sulfur content. Unfortunately, sulfur leaching was observed compromising the reusability of the catalyst. The sulfated AZ-MCM-41 (prepared with 3.0 mmol ZrOCl_2 , 8 H_2O and 0.1 mmol $\text{Al}(\text{NO}_3)_3$, 9 H_2O) seems to be the most attractive catalyst for aqueous phase conversion of D-xylose, since it was the one offering the best inhibition to sulfur leaching and that in addition exhibited increasing activity and no significant loss of selectivity to furfural in three recycling runs, regardless of negative effect of Al addition on D-xylose conversion.

Recently, sulfonated carbonaceous materials revealed their potential for furfural production because of their high acidity, water tolerance and metal oxides having Lewis acidic sites. A carbonaceous heterogeneous catalyst, which combined the use of sulfonic acid ($-\text{SO}_3\text{H}$) groups with Lewis acidic TiO_2 in a one-pot synthesis method was prepared (Mazzotta et al., 2014). When testing this sulfated oxide for furfural production from D-xylose, the target chemical was obtained in 51% yield in DMSO as solvent at 140°C for 60 min or in water-MTHF biphasic system at 180°C for 30 min. Maximum furfural yield of 37% was also recorded in 5 min exposure at 180°C in DMA/ LiCl -mediated reaction.

Dehydration in Presence of Niobium-Based Oxides

Few works using niobium-based oxides were related for the dehydration of pentose into furfural. The activities of Lewis acid catalysts namely Nb_2O_5 supported on pyrogenic silica Cabosil (García-Sancho et al., 2014b) and Brønsted acid catalysts as Amberlyst 70 were studied (Agirrezabal-Telleria et al., 2012). Lewis acid sites gave a higher rate in the conversion of D-xylose into furfural than Brønsted acid sites did, because Lewis acid sites could isomerize D-xylose into D-xylulose, while Amberlyst-70 with strong sulfonic acid sites presented a higher furfural selectivity. To improve furfural production, the use of N_2

stripping methodology showed better extraction efficiency than water-toluene biphasic system which benefits to environmental and products separation concerns. Nb_2O_5 catalyst was prepared by a neutral templating route (García-Sancho et al., 2014a). The catalytic behavior was compared with that of a commercial Nb_2O_5 . Higher than 90% of D-xylose conversion and 54% of furfural yield was attained at a temperature of 170°C after 90 min of exposure in presence of a D-xylose-catalyst (3:1, wt/wt). It is noteworthy that 41% of furfural can be achieved at 150°C for the same reaction time. In addition, D-xylose conversion in the non-catalyzed process was practically negligible, and commercial Nb_2O_5 only gave low D-xylose conversion (22%) and very low furfural yield (3%). It was demonstrated that no significant niobium leaching has occurred, the catalytic activity reduced could be attributed to the presence of a large amount of carbonaceous deposits on the catalyst surface. Silica-zirconia supported niobium catalysts were prepared by impregnation (Nb/SZi) or sol-gel (Nb/SZsg) for comparison of their catalytic effect to pure niobic acid (NBO), in the context of D-xylose dehydration in green solvents: water, water-isopropanol, water-GVL, and water-CPME (Molina et al., 2015). In all the solvents, NBO was found more active than the other supported niobium catalysts. All the supported niobium catalysts had got the same activity and showed the highest D-xylose conversion and furfural yield in presence of GVL and CPME. During the recycling and continuous catalytic tests, in spite of the deactivating trend of D-xylose conversion, furfural yield is more stable in such conditions. The niobia supported catalysts promoted furfural production in the range of 45–50% yield and almost 80% selectivity after 7 runs at 180°C for 4 h. These catalysts have lower activity than bulk niobia but higher stability. Note that furfural yield could reach around 60% by increasing reaction time to 4 h at 180°C or reaction temperature to 190°C for more than 2 h catalyzed with NBO.

Dehydration in Presence of Phosphates

Different phosphates associated with Vanadium, Niobium and Tantalum were used as catalysts for the dehydration of pentose derivatives. The orthorhombic vanadyl pyrophosphate ($(\text{VO})_2\text{P}_2\text{O}_7$, prepared by calcination of VOHPO_4 , $0.5\text{H}_2\text{O}$ at 550°C for 2 h, exhibited superior catalytic performance amongst the investigated materials. In this work furfural yield (53%) in consecutive batch runs at 170°C for 4 h was reported (Sádaba et al., 2011). Interestingly, this heterogeneous catalyst actually behaved as a source of very active water-soluble species, which are responsible for the observed catalytic activity. A series of zirconium phosphate catalysts have been synthesized (Cheng et al., 2013). The calcined mesostructural zirconium phosphate ZrP-HT-Am-C exhibited inspiring catalytic performance. At 170°C , D-xylose conversion (96%) and furfural yield (52%) were measured in aqueous-phase after 2 h. The reusability of the catalyst as evaluated from 3 runs seemed fairly good, however conditioned by thermal treatment in air at 500°C for 4 h between runs. Association of niobium and phosphate was done and the corresponding niobium phosphate (NbP) was tested for furfural production (Bernal et al., 2015). Nb^{5+} ions were supported to act as Lewis exposed sites, showing medium strength acidity.

Their previous study showed that NbP recovered catalyst gave furfural in 43% yield and D-xylose conversion in 82% at 160°C for 30 min in water (Bernal et al., 2014). After three consecutive catalytic runs, furfural yield and D-xylose conversion slightly decreased to 36 and 70%, respectively. When corn stover was tried as feedstock, 23% of furfural yield was achieved, only. Eventually, another tentative use of phosphates as heterogeneous catalyst for biomass dehydration was targeting a synergistic effect of tantalum (Li X.-L. et al., 2015). In this regard, different mesoporous tantalum phosphates ($\text{TaOPO}_4\text{-m}$) with various P/Ta molar ratios were prepared and tested for evaluating their respective catalytic activities to convert D-xylose into furfural (Xing et al., 2016). A high Bronsted to Lewis acid site ratio is required to enhance the furfural selectivity. The best candidates afforded a furfural selectivity of 72%.

Dehydration in Presence of Silicates

The main silicates used for the dehydration of biomass into furfural have been mesoporous silicates *MCM-41* and *SBA-15* and derivatives having sulfonated group or metals. They were tried for the dehydration of pentose into furfural. Among the different silicates, *H-MCM-41* gave the highest furfural yield was obtained in the context of unusual C6 sugar levoglucosan treatment at 300°C. Unfortunately, catalysts were deactivated due to coke formation (Käldström et al., 2010). The conversion of D-xylose into furfural with mesoporous molecular sieve *MCM-41* as catalyst in presence of NaCl and butanol as the extraction solvent with treatment at 170°C for 2 h gave a production of furfural in 48% yield (Zhang et al., 2012). In three consecutive runs, its value decreased slightly, which can be due to inefficient removal of by-products adsorbed on the catalyst surface after each run. It was noteworthy that the same process without addition of NaCl gave only the aldehyde in 39% yield.

Metal-containing silicates (Nb, Al) were also tested and compared. In this context, the microporous and mesoporous niobium silicates (*AM-11* and *MCM-41*) as solid acid catalysts were studied for the dehydration of D-xylose in a water-toluene solvent mixture (Dias et al., 2006a). The proton form of *AM-11* (*H-AM-11*) showed a proven reusability and gave the highest furfural yield (50%) and a D-xylose conversion (89%) at 160°C for 6 h after 3 runs. For fresh catalysts, their activities followed the order: *H-AM-11* (46% at 85% conversion) > *ex H-AM-11* (*H-AM-11* after ions-exchange, 39% at 85% conversion) \approx *HY5* (the protonic form of Y-zeolite, with Si/Al = 5, 39% at 94% conversion) \approx *MCM-41* (*Nb50-MCM-41*, *ex Nb50-MCM-41*, *Nb25-MCM-41* and *ex Nb25-MCM-41*, ca. 39% at 92~99% conversion) > *Na,H-AM-11* (31% at 77% conversion) > mordenite (with Si/Al = 6, 28% at 79% conversion). Developing the same idea, the effect of surface acidity on the dehydration of D-xylose was examined using $\text{SiO}_2\text{-Al}_2\text{O}_3$ catalysts with varying alumina contents by You et al. (2014). D-xylose conversion in water as solvent at 140°C for 4 h increased more than 9 fold with the increase of alumina content from 0 to 1. Simultaneously, humins yield reached 45% with Al_2O_3 whereas none was formed with SiO_2 . It was considered that Lewis acid sites significantly affected D-xylose conversion and humins formation. The best furfural yield of ca. 27% was obtained with $\text{SiO}_2\text{-Al}_2\text{O}_3$ (0.6)

while $\text{SiO}_2\text{-Al}_2\text{O}_3$ (0.1) provided the highest furfural selectivity (over 60%). The highest yields of D-lyxose and D-xylulose were attained over $\text{SiO}_2\text{-Al}_2\text{O}_3$ (0.4) and $\text{SiO}_2\text{-Al}_2\text{O}_3$ (0.8).

Silicates with sulfonated groups have been tested for the model reaction. Two kinds of sulfonic *MCM-41* catalysts: the propyl sulfonic acid catalyst (*PrSO}_3\text{H-MCM-41}*) and the methyl propyl sulfonic acid catalyst (*MPrSO}_3\text{H-MCM-41}*) have been prepared (Kaiprommarat et al., 2016). After testing their activities for furfural production from D-xylose in water-toluene biphasic system at 155°C for 2 h, it was found that *PrSO}_3\text{H-MCM-41}* was quite efficient and gave 96% of furfural selectivity and 92% of D-xylose conversion compared to 26% and 99% for *MCM-41*. The authors explained that the preparation of *MPrSO}_3\text{H-MCM-41}* has a significant effect on their acidic densities and pore diameters, which further affect furfural yield and D-xylose conversion. *MPrSO}_3\text{H-MCM-41}* prepared by co-condensation method using dodecyltrimethylammonium bromide as a surfactant template and aged at room temperature gave the smallest pore diameter (3.4 nm). The modification of the catalyst permitted to furnish the highest furfural yield (93%) and selectivity (98%). The reusability of the *MPrSO}_3\text{H-MCM-41}* needs to be challenged as furfural yield rapidly decreased below 50% as soon as recycled for the first time. Mesoporous shell silica bead (*MSHS*) served as support and modified with sulfonic acid (*MSHS-SO}_3\text{H}*) and aluminum (*MSHS-Al*) were prepared (Jeong et al., 2011). Their catalytic performance in the dehydration reaction of D-xylose into furfural under water phase was investigated. *MSHS-Al* gave a higher D-xylose conversion than *MSHS-SO}_3\text{H}* (45 vs. 32%), but showed a lower furfural selectivity (35 vs. 57%). Moreover, *MSHS-Al* isomerized D-xylose to D-lyxose at a concentration of 14%. When compared to general mesoporous catalysts *MCM-41-SO}_3\text{H}* and *HMS-SO}_3\text{H}*, *MSHS-SO}_3\text{H}* is more efficient than *HMS-SO}_3\text{H}* (18 vs. 13% for furfural yield at 170°C for 1 h), but less efficient than *MCM-41-SO}_3\text{H}* (24% in furfural yield) which attribute to its almost three times the number of sulfonic acid groups compared to *MSHS-SO}_3\text{H}*. In addition, *MSHS-SO}_3\text{H}* showed a better hydrothermal stability than *MCM-41-SO}_3\text{H}*.

Dehydration in Presence of Zeolites

Different zeolites have been prepared and tested for the dehydration of carbohydrate derivatives into furfural. Zeolite catalysts [zeolite SM-25, mordenite 13 (Si/Al = 13), mordenite 20, faujasite 13] acidified with H_3PO_4 or H_2SO_4 were tested for D-xylose dehydration to furfural in a continuous two-liquid-phase (water-toluene) plug-flow reactor (Lessard et al., 2010). The optimal conditions were determined: powdered mordenite (H^+) 13 as the catalyst, 12% w/w D-xylose solution, a reactor temperature of 260°C, a pressure of 55 atm, a toluene/D-xylose aqueous solution volumic ratio of 2, and a residence time of 3 min. For the first cycle, the furfural molar yield reached 98% with a conversion rate of 99%, and the second pass gave a furfural yield of 90% associated with the same conversion rate. This indicated that the regeneration of the mordenite cannot recover its original activity.

A series of solid catalysts were tested for selectively converting hemicellulose from crop waste into C5 sugars and furfural (Sahu

and Dhepe, 2012). The *HUSY* (Si/Al = 15) catalyst showed the highest activity to convert hemicellulose (>90% conversion) at 170°C within 3 h in the presence of water, followed by *H-Beta* zeolite (Si/Al = 19), *HMOR* zeolite (Si/Al = 10), and K10 clay. However, herein, less than 12% of furfural formed. Other catalysts: γ -Al₂O₃, Nb₂O₅, and Al-containing mesoporous silica exhibit less activity. The application of a biphasic solvent mixture furnished higher furfural yield. For example, 54–56% of furfural yield was obtained in water-toluene or water-MIBK or water-xylene biphasic system catalyzed with *HUSY* (Si/Al = 15) at 170°C for 6 h. Zeolites seemed to be hydrolytically stable in the reaction mixture and mineral impurities such as Na and K in biomass may be responsible for the reduction in the activity of the catalysts. *ZSM-5* zeolite catalyzed the furfural production from aqueous hemicelluloses solution [which contains D-xylose (164 g/L), D-glucose (11 g/L) and arabinose (4.5 g/L)] (Gao et al., 2014). The effects of reaction temperature, time, catalyst loading, organic solvents and inorganic salts or metal oxides addition were thoroughly investigated. The maximum furfural yield of 82% and the D-xylose conversion of 97% were achieved at 190°C in the presence of *ZSM-5* (1.0 g), NaCl (1.05 g) and organic solvent-to-aqueous phase ratio of 30:15 (v/v) for 3 h. Applying these conditions for conversion of pure D-xylose solution decreased the yield of furfural (51%) which was attributed to easier occurrence of excessive hydrolysis of D-xylose and condensation reactions. Besides, *ZSM-5* has a relative stability and can be reused at least five times with the furfural yield remaining over 67%.

HZSM-5 zeolite was used to improve the production of monoaromatic hydrocarbons, such as benzene, toluene, xylene and ethylbenzene. In fact, usually there is only little amount of furfural formed with this catalyst (less than 0.59 wt% with respect to dry basis sugar maple) (Mante et al., 2014). The same catalyst *HZSM-5* helped however to produce furfural from steam explosion liquor of rice straw (which contains mainly D-xylose oligomers 2.27 kg/m³ in 3.61 kg/m³ total sugar) (Chen et al., 2015). The maximum furfural yield was 310 g/kg under the optimum conditions: *HZSM-5* addition 60 g/kg sugar, reaction temperature 160°C, extraction steam flow rate 2.5 cm³/min and total sugar concentration 61.4 kg/m³. It was worth noting that polymerization inhibitor 4-methoxyphenol and tert-butylcatechol were added into the reaction system to improve furfural yield. It was found that 4-methoxyphenol was more efficient than tert-butylcatechol at the same additive amount, especially with 15 g/kg 4-methoxyphenol addition increased furfural yield to 375 g/kg, which increase by 21% compared with that without polymerization inhibitor. *HZSM-5* catalysts could be reused for 3 runs and the catalytic activity recovered 88% after regeneration through calcinations.

D-Xylose dehydration activity of arenesulfonic *SBA-15* catalysts synthesized at high aging-temperature (180°C) revealed that the catalyst was more selective and hydrothermally stable (Agirrezabal-Telleria et al., 2014a). For example, *SBA-15* modified with 0.2 mole ratio of 2-(4-chlorosulfonylphenyl) ethyltrimethoxysilane (A180-0.2) gave furfural in 82% yield with a conversion of 98% at 160°C in water-toluene biphasic system for 20 h. Modification of the catalyst with 0.3 organosiloxane

molar loading led to furfural in 86% yield with a conversion of 99%. Amberlyst-70 was compared with arenesulfonic *SBA-15* catalysts, which presented obviously lower furfural selectivity. Moreover, regenerated A180-0.2 by using a thermal treatment at 290°C gave furfural in 75% yield and a conversion of 88% after three consecutive runs. The catalysts aged at lower temperature showed important deactivation rates.

Microporous silico aluminophosphates *SAPO-5*, *SAPO-11* and *SAPO-40* were tested as solid acid catalysts for the dehydration of D-xylose into furfural under water-toluene biphasic system at 170°C (Lima et al., 2010). Furfural yields in 4 h using *SAPO-11* (34–38%) are comparable with that for *HMOR* zeolite with Si/Al*6 (34%). under similar reaction conditions, while *SAPO-5* and *SAPO-40* gave less than 25% of furfural yield. Complete D-xylose conversion is reached within 16–24 h, with furfural yields in these conditions of up to 65%. No decrease of Si, P, or Al contents and furfural yield were observed in all catalysts for three consecutive runs. In another work, *SAPO-44* revealed superior efficiency to *SAPO-5*, *SAPO-11*, and *SAPO-46* for one-pot conversion of hemicellulose into furfural since it had higher acid amount and surface area (Bhaumik and Dhepe, 2013). With respect to *HMOR* (Si/Al = 10), even if it has an equal total acid amount of 1.2 mmol/g and a higher surface area than *SAPO-44*, an inferior activity was observed because of its weaker hydrophilic nature. *SAPO-44* could give a furfural yield of 63% with 88% of mass balance at 170°C within 8 h and no loss of catalytic activity was observed after 8 cycles. Later, more hemicellulose type of feedstocks were tested (Bhaumik and Dhepe, 2014), and extraordinarily high yields of furfural through catalysis making use of *SAPO-44* were obtained (about 86–93% from bagasse, rice husk and wheat straw) when these biomasses were treated at 170°C in a water-toluene biphasic system. IN this context of use, *SAPO-44* could also keep consistent activity. Subsequently, adequate engineering of *SAPO-44* catalysts for efficient synthesis of furfural from xylan was investigated (Bhaumik and Dhepe, 2015). It was found that *SAPO-44* having 1.0 mole of Si content is the best catalyst for the xylan-D-xylose conversion to furfural. The use of a biphasic ratio of 1:2 (v/v) showed the highest amount of furfural (82%) production from xylan when processed at 170°C for 10 h of reaction time. Other kinds of catalysts such as *H β* (Si/Al = 19), *HMOR* (Si/Al = 10), *HUSY* (Si/Al = 15), were also compared with *SAPO-44*. Recently, small pore zeolites *SAPO-34* and *SAPO-56* were considered and tested for furfural production from D-xylose and switchgrass in water-GVL monophasic system (Bruce et al., 2016). *ZSM-5*, *Amberlyst-70* and H₂SO₄ led to a better furfural yields (70, 63, 67% from D-xylose respectively), but leaching studies indicated that these good results were attributed to homogeneous catalysis by the acid sites that leached from the catalysts. The commercial *SAPO-34* catalyst gave a moderate furfural yield of 40% from D-xylose and 31% from switchgrass, and showed a good recyclability. At the light of their emerging use, these small pore zeolites may be rationally designed to increase the yield from biomass reactions.

The use of a chabazite-type zeolite prepared from the chemical transformation of a faujasite-type natural one was studied

(Yoshida et al., 2017). The hemicellulose contained in ball-milled pretreated bamboo powder was directly transferred into furfural when it was stirred in a water-toluene biphasic system under conventional heating. From this hemicellulose processed in this biphasic system at 170°C for 10 h, furfural was finally produced in 55% yield.

A special zeolite displaying iron, tin and zirconium sites was synthesized from H- β type material by means of an ion-exchange procedure (Zhang et al., 2017b). The catalyst prepared in this way holds both Brønsted and Lewis acid sites. Surprisingly, by using the more effective Sn-beta, D-glucose became the substrate to produce furfural when heated at 180°C. In a water-GVL biphasic system, furfural was obtained in 69% yield.

SYNTHESIS OF FURFURAL FROM SUGARS AND POLYSACCHARIDES USING SUPPORTED CATALYSTS

Mesoporous silica-supported 12-tungstophosphoric acid (PW) catalysts showed a significant effect on the catalytic performances in biomass conversion to furfural relating to several variables, such as the catalyst preparation method, type of support, PW loading, and the reaction conditions (Dias et al., 2006b). In water-toluene biphasic system, catalysts prepared in 1-butanol reveal better reusability through recycling runs than when prepared in water. Besides, higher PW loadings and temperatures both led to higher furfural yield. The furfural yields and catalyst activity resilience were higher in DMSO than in water-toluene. Furfural was produced at 140°C for 4 h in DMSO in 52% yield when the catalyst was prepared in 1-butanol with 34 wt% of PW supported on medium-pore micelle-templated silica. However, the best catalytic stability performance versus use was obtained in DMSO using either the 15 wt% PW inorganic composites, or PW immobilized in aminopropyl-functionalized silicas. Generally, the catalyst deactivation was due to PW leaching and catalyst surface passivation.

Later, they fixed cesium salts of 12-tungstophosphoric acid on medium-pore MCM-41 (3.7 nm) or large-pore (9.6 nm) micelle-templated silicas and investigated their catalytic performance for D-xylose dehydration to furfural in water-toluene and DMSO solvent systems (Dias et al., 2006c). In this work, similar conclusions have been observed. The initial catalytic activities decreased in the order silica-supported CsPW > Cs_{2.5}PW > Cs_{2.0}PW > HPW. Increasing the CsPW loading from 15 to 34 wt% or using a support with a larger pore diameter, nearly doubled furfural yields.

A series of MCM-41-supported niobium-oxide catalysts were also tested. In general, the catalytic activity of this family of catalysts is related to the presence of niobium species over the silica support. The catalytic activity improves with the increase in the niobium-oxide content (García-Sancho et al., 2013). However, the catalyst with 16% of Nb₂O₅ loading (MCM-Nb16) reveals more efficient than that with 33% of Nb₂O₅ loading which resulted in closure of the pores and partial destruction of the mesoporous framework. MCM-Nb16 has a remarkable ability, including reusability for furfural selectivity, whatever the

increase in conversion efficiency or the reaction temperature. Moreover, in addition of 0.5 g NaCl/g aqueous solution, furfural yield significantly increased from 36 to 60% at 170°C for 180 min in water-toluene biphasic system. Indeed, three consecutive runs did not reveal any drop in catalytic activity with the recovered catalyst. Subsequently, the study of niobium oxide incorporated on different supports indicated that the textural properties of the supports and the total acidity both played significant roles in D-xylose dehydration and furfural selectivity (García-Sancho et al., 2014b). γ -Al₂O₃ showed the highest D-xylose dehydration activity but by contrast low furfural selectivity. This was analyzed as a consequence of its higher than Brønsted Lewis acidity, which might favor side reactions on the catalyst surface. Commercial fumed silica supported catalyst presented larger pore sizes, favoring the diffusivity of D-xylose and consequently the dehydration activity. Whereas SBA-15 and MCM-41 showed higher acid site densities, their intermediate micro-mesoporous structure could provide higher D-xylose dehydration rates to furfural. SBA-15 with 12 wt% niobium oxides loading showed the highest amount of acid sites than catalyst variants containing 4 wt% and 20 wt% niobium oxides loadings. This catalyst gave a D-xylose conversion of 85% and furfural selectivity of 93% in reported process conditions (160°C for 24 h in water-toluene mixture). Moreover, the regenerated catalyst showed similar furfural selectivity with 4% of D-xylose conversion decrease.

Hydrothermal pretreatment of corncob with microwave-assisted irradiation has been systematically studied. Their subsequent hydrolysates with the maximum D-xylose content (160°C, 90 min), the maximum xylobiose content (180°C, 15 min), and the maximum total D-xylose content in monosaccharide and oligosaccharides (DP \leq 6) (160°C, 60 min) were further processed to produce furfural using tin-loaded montmorillonite (Sn-MMT) as the catalyst in the 2-sec-butylphenol/NaCl-DMSO system, respectively (Li H. et al., 2015). The highest furfural yield (58%) was obtained from the hydrolysates with the maximum D-xylose content, whilst the lowest furfural yield (less than 10%) was issued from processing the hydrolysate with the maximum xylobiose content. This result indicated that the production of furfural has a direct connection with the monomeric pentose. Controlled experiments with pure D-xylose solution showed lower furfural yield than that from the hydrolysates with the same total D-xylose amount in monosaccharide and oligosaccharides, which may be related to the slow release of pentose monomers from the oligomers that can impede the formation of humins.

A silica supported poly(styrene sulfonic acid) was prepared in another recent study. The silica particles were first functionalized by means of aminopropyltriethylsilane and showed primary amine moieties on its surface to attach the polymer through electrostatic interactions (Campo-Molina et al., 2017). The catalysts were tested for their capacity to dehydrate D-xylose in the organic solvents. The best performance was obtained using a 10 wt% D-xylose aqueous solution in water-CPME biphasic system. When the medium was heated at 180°C for 60 min, the furfural yield eventually reached a value of 57%.

A series of functional IL supported silica nanoparticles with different acidity (ILs/SiO₂) have been prepared by covalent

bonds using non-toxic ethanol as solvent (Xu H. et al., 2015). With respect to furfural production from D-xylose, the catalytic performance followed the order: IL/SiO₂ < IL-SO₃H/SiO₂ < IL-HSO₄/SiO₂ < IL-SO₃H-HSO₄/SiO₂, and furfural yield increased from 31% to 50% at similar D-xylose conversion efficiency of about 94–96%. In the catalyst IL-SO₃H-HSO₄/SiO₂, the strong acid sites from SO₃H and HSO₄[−] have played the roles of active centers. As for IL/SiO₂, 31% of furfural yield was attributed to positive effect of chlorine anion from the IL.

SYNTHESIS OF FURFURAL FROM SUGARS AND POLYSACCHARIDES USING OTHER CATALYSTS

Other catalysts were tested in that context for their activity regarding the production of furfural. Vanadium (10 wt%) contained *H-MCM-41* catalysts showed the highest catalytic activity for the production of furanic compounds (e.g., the most abundant furanic compound was furfural) during the ex situ catalytic pyrolysis of cellulose, levoglucosan and xylan (Kim B.-S. et al., 2016). It was found that furanic compounds were mainly derived from levoglucosan over weak acid sites of vanadium contained H-MCM-41.

The catalytic activity of functionalized partially hydroxylated MgF₂ catalysts for D-xylose dehydration into furfural was reported (Agirrezabal-Telleria et al., 2013b). Partially hydroxylated MgF₂ which contains Lewis and Brønsted sites, was further modified with perfluorosulfonic or methanefluorosulfonic acids. The former sulfonic precursor showed higher selectivity for furfural than the latter, primarily due to a lower sulfur atom incorporation and also as a consequence of the reduction in furfural resinification reaction rates. Well-optimized Lewis/Brønsted ratios catalyst synthesized by one-step grafting technique could give a maximum furfural selectivity of 90% at 160°C in a water-toluene biphasic system. Another part of their research investigated D-xylose conversion to furfural with partially hydroxylated MgF₂ catalysts synthesized using different HF concentrations (Agirrezabal-Telleria et al., 2014b). MgF₂-71 (synthesized with 71 wt% HF) gave 86% of furfural selectivity with 94% of D-xylose conversion in water-toluene and subsequently, a furfural selectivity of 87% could be achieved using N₂-stripping. The catalyst MgF₂-40, which is rich in Lewis acid-sites promoted the D-xylose conversion rather than furfural selectivity, and MgF₂-87, which has lower Lewis acid-sites content gave opposite trends. It was found that the addition of D-glucose as a co-carbohydrate decreased furfural selectivity in all case. The change of reaction mechanism depended on the catalysts containing different Lewis/Brønsted ratios.

Furfural production using solid acid catalysts in GVL was studied in the presence of γ-Al₂O₃, *Sn-SBA-15* and *Sn-beta*, which contain only Lewis acid-sites (Gürbüz et al., 2013). In their work, furfural was obtained in low yields (<40%). Sulfonic acid functionalized catalysts *Amberlyst-70*, *Nafion SAC-13*, sulfonated carbon, and propylsulfonic acid functionalized *SBA-15*, zeolites (*H-ZSM-5*, *H-mordenite*, and *H-beta*), sulfated inorganic metal

oxides (sulfated zirconia), and even mineral acid H₂SO₄ have been tested. The effect of water content in GVL was investigated since it is known water has significant influence on furfural degradation reactions. Under the best conditions, 81% furfural and 4% formic acid were obtained in GVL with 10% water using *H-mordenite* as catalyst, and no decrease in furfural yield after five cycles, which is more stable than *Amberlyst-70* and propylsulfonic acid functionalized *SBA-15*. Interestingly, the main product of D-glucose conversion using zeolite catalysts and GVL as the solvent is furfural with a yield superior to 30%

A mechano-catalytic strategy aiming to simultaneously release hemicelluloses from the corncob cells and depolymerize the polysaccharide into its pentose subunits in presence of a solid acid catalyst (SO₄^{2−}/SiO₂-Al₂O₃/La³⁺) was published (Li et al., 2016). Herein, ball-milling treatment played an important role in the decomposition of the crop material. During the sonication step, the acid catalyst activated the conversion of the hemicelluloses content into furfural. Finally, furfural yield of 83% was obtained at 190°C for 30 min from the pretreated waste material.

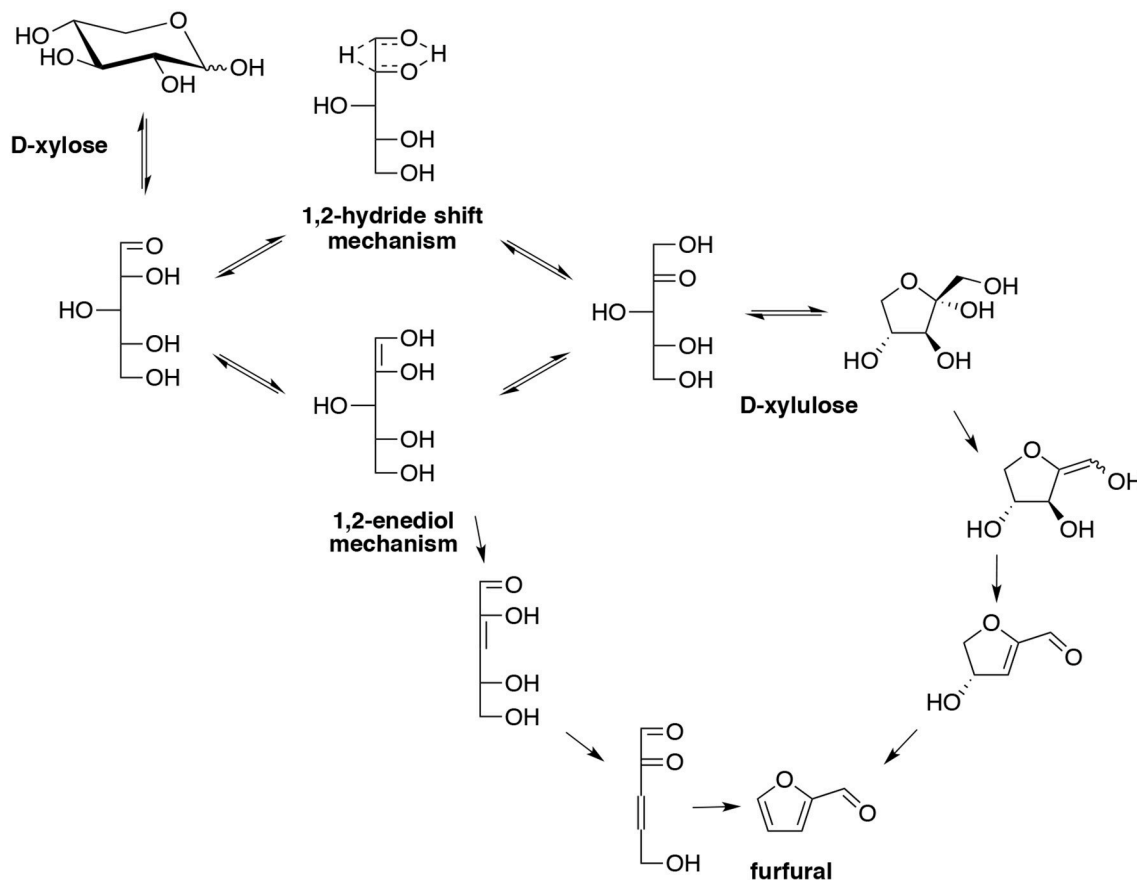
Currently metal organic frameworks (MOFs) are emerging as promising new materials according to their catalytic properties favoring various reactions. A good example is the use of Zn₂(Bim)₄ as an organic filter embedded in polymethylphenylsiloxane (PMPS) (Jin et al., 2016). Both are components of a porous composite membrane potent for the vapor permeation and isolation of produced furfural. After recovery of the product, 41% yield in furfural was obtained when operated at 140°C in aqueous solution.

MECHANISM FOR THE SYNTHESIS OF FURFURAL

Different mechanisms of the formation of furfural from D-xylose have been identified and described in various researches reported in the literature. Among them, different keys steps have been explored using cyclic or acyclic pathways: 1,2-enolization, β-elimination, isomerization *via* 1,2-hydrate shift. A plausible mechanism was proposed based on mechanistic and kinetic aspects in aqueous media employing homogeneous catalysis (Danon et al., 2014). Starting from acyclic D-xylose, the isomerization *via* 1,2-hydrate shift or 1,2-enediol mechanism afforded the corresponding ketose, which was the key intermediate for assuming the cyclic pathway in the mechanism. By contrast, the 1,2-enediol derivative could supply the 2,3-unsaturated aldehyde as a key intermediate if the assumption of the acyclic pathway is made (**Scheme 14**). Such uncertainties are reflected in the contradictory kinetic models exploited and kinetic data presented in the literature, which still prevent scientists today from a common and coherent interpretation.

SAFETY CONSIDERATIONS

Furfural is likely to be the first bio-based industrial chemical ever produced, by Quaker Oats Company since 1920. Furfural has been identified as one of the 30 building block chemicals



SCHEME 14 | Plausible mechanism of D-xylose reaction to furfural in acidic media (Danon et al., 2014).

by the US Department of Energy, as this is one of the widely studied chemicals since nineteenth century and has been referred by many well recognized handbooks and data sheets (Werpy and Petersen, 2004; Peleteiro et al., 2016a). Owing to its physico-chemical properties, production methodologies and its vast industrial applications, it is important to consider potential risks of furfural during its entire life cycle (feedstock storage, production, transportation, furfural storage, end user application, and disposal). Industrial production of furfural is generally dealt with homogeneous or heterogeneous catalytic conversions as described in detail in this review. Homogeneous catalysts can lead to serious operational, safety and environmental issues during the production of furfural in several ways. It is very difficult to separate the mineral acids for recycling, which may lead to some product contamination. These acid catalysts are highly corrosive and might lead to equipment damage and process breakdown and they are toxic and may cause problems during disposal. Heterogeneous catalysis on the other hand may also trigger some hazards during use or recycling (Lamminpää et al., 2012; Melero et al., 2012; Ventura et al., 2016). In the case of solid acid catalysts, depending on the hydrophilic or hydrophobic properties of the chosen (solid acid) catalyst, there is a tendency of severe poisoning of acid sites by water, which loses the catalytic activities in aqueous solutions (Okuhara, 2002).

Based on its physical or chemical properties, furfural is qualified as a dangerous substance and listed under various internationally derived hazardous-material classifications such as UN's GHS [CLP in the EU (Regulation (EC) N° 1907/2006 and 453/2010)] (United Nations, 2015), TDG Regulations based on the UN's "Orange Book" etc. GHS labeling categorizes furfural as toxic by various routes (United Nations, 2009, 2015). Whereas, according to US NFPA 704 Hazard ranking "Standard System for the Identification of the Hazards of Material for Emergency Response," furfural is qualified as instable (hazard rating level 1), flammable (hazard rating level 2) and toxic (hazard rating level 3) (CAMEO Chemicals, 2016¹).

[6] Furfural (flash point (FP) 60°C) clearly has flammability properties and forms air/vapor mixtures above 60°C and these vapor-air mixtures are explosive within known flammable limits (2.1–19.3%) (Urban and Pitt, 2007). Prior to the amendment in CLP regulations, i.e., according to the Regulation (EC) n0 440/2008, furfural with FP 60°C was considered as non-flammable (as a flash point of 55°C was the recognized upper limit of flammable liquids). Due to the modifications in CLP regulations with new (expanded) FP limits (the new upper

¹CAMEO Chemicals. Chemical Datasheet n.d. <https://m.cameochemicals.noaa.gov/chemical/3522> (Accessed September 27, 2016).

limit designing “flammable substances” is by now related to $FP \leq 60^\circ\text{C}$), furfural should have fallen into 3rd category of flammable substances due to most quoted value of furfural flash point (60°C), while it has not been the case in practice, since the risk evaluation by ECHA has retained a flash point of 61.7°C just over the new flammability limit of category 3 of CLP flammable liquids (Chemical Substances Bureau, 2008²). It is noteworthy that, actual physico-chemical properties (particularly the flammability hazard) and its associated risks remain the same irrespective of any classification change.

Early research quotes that furfural has a tendency to impart extreme corrosiveness toward carbon steel equipment (Scarth, 1947). Therefore, in spite of its property of selective absorption of unsaturated hydrocarbons, furfural may not be a suitable solvent in extractive distillation process. Laboratory tests quote that, the rate of corrosion of furfural on carbon steel is over 1.0 mm/year which can cause serious corrosion (Sandvik Material Technology, 2016). In many aspects, corrosion management keeps a complex issue, since the degree of corrosion may also depend on the types of materials and chemicals associated with it, and the type of application.

On the other hand, furfural (as an organic compound) by contrast tends to get adsorbed on the metal-solution interface, which in turn tends to reduce corrosion of metal surface. Some electrochemical tests have outlined some corrosion inhibition effect on low carbon steel when furfural is in ethanol solutions, with an effective concentration of 0.1 mM of furfural (Goncalves and de Olivera, 1992). Moreover, some investigations proved that aliphatic furfural hydrazine derivatives act as corrosion inhibitors of iron in nitric acid (Mohamed et al., 1989). Results from the study conducted confirmed a corrosion inhibition effect of furfural in the presence of HRWR (high range water reducer) superplasticizers (Al-Hubboubi et al., 2012).

Dealing with hazards to health, furfural is qualified as a CMR carcinogen (cat.2, H351) in CLP (Regulation (EC) No 790/2009) and has found to impart toxic effects of human body through inhalation (cat.3, H301), oral consumption (cat.3, H331), dermal absorption (cat.4, H312) and eye irritant (cat.2, H319). In the recent amendment of CLP, furfural is additionally recognized as a skin irritant (cat.2, H315). Although a few animal toxicity tests (with an emphasis on genotoxic, mutagenic and carcinogenic properties) have confirmed some conventional toxicity rating, apparently, no significant threat to human health has actually been recognized from medical observations so far as reported in the literature. As the effect of human exposure of furfural is still under debate, any extrapolation of available animal test results to humans will be highly questionable (Scientific Committee on Consumer Safety, 2012; Abbott, 2016).

Chemical accidents involving furfural may not only occur during manufacture and use, but also during handling, transportation, storage and disposal stages. Although there are no major furfural accidents reported in the recent years, some case studies summarized hereafter demand vigilance while handling this chemical. Several cases of spontaneous ignition were observed when the fine coke particles (containing furfuryl

alcohol derived resin) were exposed to air after their removal from the filter strainers in a petroleum refinery furfural extraction unit. In a regenerative furfural distillation while distilling furfural under nitrogen, furfural residues agglomerated in the boiler. Despite tentative inserting, fire broke due to air entering the boiler from bottom valve due to scrapping of walls because of too long operation, unidentified substances in the solvent forming peroxides, poor waste acceptance procedure etc. Seal of the connection at receiving end broke in a petroleum refining unit due to the corrosion of metal joints resulting in furfural splash on the employees. Rejection of 15 ton of furfural solvent (via cooling water) from a petroleum refinery due to a leak in the heat exchanger of a unit separating aromatics distillate led to the pollution of the Tancarville channel covering around 2 km, resulting in 400 kg of dead fish. A crash between 2 trucks during the transportation of furfural and acetic acid resulted in immediate ignition of trucks and the death of truck drivers. A leak from undetermined number of drums containing furfural led to emergency management difficulties due to lack of available containment equipment to handle flammable liquids; inspecting staff with inadequate knowledge thus leading to wrong methods of handling flammable liquids (ARIA, 2016). Reported case studies clearly depict issues relating to flammability, oxidative, toxic and chemical incompatibility properties of furfural showing some limitation pertaining to conventional hazardous-materials rating systems, and apprehend the need to develop adequate safety and emergency response procedures. In that regard, furfural is no exception.

CONCLUSION

In conclusion, this review tries to summarize all catalytic processes for bio-based synthesis of furfural under the guiding criteria of the various kinds of catalysts that have been considered in reported scientific pertinent works. With respect to homogenous catalysis, mineral and organic acid catalysts mainly consisting of Brønsted acids are facing the need to get over a high activation barrier for furfural production. From this point of view, their combination with Lewis acid salts which benefit to D-xylose isomerization to D-xylulose, a more reactive intermediate, seems to be more promising option, since lower energy is required and higher furfural yield and selectivity could be obtained. However, the corrosive, environmental and handling problems should be taken into appropriate consideration with this kind of catalysts. As for ILs, even if extraordinary results are obtained, a major drawback pertains to their separation difficulty from the chemicals formed when used in biorefining, which still act today as a genuine barrier for their industrial applications. The limitations of solid catalysts basically lie in their complicated and therefore relatively costly synthesis processes, and easier tendency to activation inhibition after reaction. Despite of these drawbacks, some of them do have inherent properties that might deserve valuable applications, such as sulfonated carbonaceous materials (SGO), zeolites (ZSM-5, SAPO-44, H-M) and partially hydroxylated MgF_2 among others. The crucial application of a catalyst would be comprehensively evaluated

²Chemical Substances Bureau. EU Risk assessment - Furfural. 2008.

by its efficiency, cost, chemical/thermal stability, reusability and so on. Additionally, the overall performance of a given catalyst may rely on adequate reactor engineering further improving catalytic furfural production as well as from smart furfural extraction downstream processing (e.g., making use of organic solvents, N₂ stripping or permeation membrane) for consolidating economically-viable furfural production routes at industrial scale (meaning overpassing critical yields of furfural).

Keeping in mind the global hazardous-materials classification of furfural quoted in various regulatory frameworks, it becomes important to perform a complete process safety and end-use assessment that contributes to sustainable production and use the chemical in diverse industrial applications. These aspects must also be given prior importance like a number of furan-based compounds that have proven to entail adverse effects on the health and environment (e.g., dibenzofurans) whereas not produced on a voluntary basis. Clearly, regulations are set by pure conventions and physico-chemical properties of the chemical will persist irrespective of its official hazard classification. Though there are very limited safety concerns observed during the production of furfural from both homogeneous and heterogeneous catalytic point of view, care must be taken during the post-production phase in terms of classification, labeling and packaging of furfural and potential derivatives to

avoid possible chemical accidents. Beyond conventions, risks associated with a chemical merely depend on the type of application and the surrounding environment. In this respect, examining furfural beyond its boundaries of conventional hazard classification would give a better understanding on the reactivity profile at various targeted applications, to avoid misleading conclusions and manage potential associated risks.

AUTHOR CONTRIBUTIONS

FD, YW, AM, and KE analyzed the bibliography; FD, AM, GM, and CL wrote the paper.

ACKNOWLEDGMENTS

This work has been partially funded by the European Commission as part of a H2020 MSCA project named HUGS under the grant agreement # 675325. YW would like to thank the China Scholarship Council (CSC) for the financial support. This work was performed, in partnership with the COST Action FP 1306 Valorization of ligno-cellulosic biomass streams for sustainable production of chemicals, materials and fuels using low environmental impact technologies.

REFERENCES

- Abbott, P. J. (2016). *Who Food Additives Series 46: Furfuryl Alcohol and Related Substances*. Available online at: <http://www.inchem.org/documents/jecfa/jecmono/v46je08.htm>.
- Abbott, P. J., Aldous, L., Borisenko, N., Coles, S., Fontaine, O., Garcia, J. D. G., et al. (2018). Electrochemistry: general discussion. *Faraday Discuss.* 206, 405–426. doi: 10.1039/C7FD90093G
- Agirrezabal-Telleria, I., Garcia-Sancho, C., Maireles-Torres, P., and Arias, P. L. (2013a). Dehydration of xylose to furfural using a Lewis or Brønsted acid catalyst and N₂ stripping. *Chin. J. Catal.* 34, 1402–1406. doi: 10.1016/S1872-2067(12)60599-3
- Agirrezabal-Telleria, I., Guo, Y., Hemmann, F., Arias, P. L., and Kemnitz, E. (2014b). Dehydration of xylose and glucose to furan derivatives using bifunctional partially hydroxylated MgF₂ catalysts and N₂-stripping. *Catal. Sci. Technol.* 4, 1357–1368. doi: 10.1039/C4CY00129J
- Agirrezabal-Telleria, I., Hemmann, F., Jäger, C., Arias, P. L., and Kemnitz, E. (2013b). Functionalized partially hydroxylated MgF₂ as catalysts for the dehydration of D-xylose to furfural. *J. Catal.* 305, 81–91. doi: 10.1016/j.jcat.2013.05.005
- Agirrezabal-Telleria, I., Larreategui, A., Requies, J., Guemez, M. B., and Arias, P. L. (2011). Furfural production from xylose using sulfonic ion-exchange resins (Amberlyst) and simultaneous stripping with nitrogen. *Bioresour. Technol.* 102, 7478–7485. doi: 10.1016/j.biortech.2011.05.015
- Agirrezabal-Telleria, I., Requies, J., Güemez, M. B., and Arias, P. L. (2012). Furfural production from xylose + glucose feedings and simultaneous N₂-stripping. *Green Chem.* 14, 3132–3140. doi: 10.1039/c2gc36092f
- Agirrezabal-Telleria, I., Requies, J., Güemez, M. B., and Arias, P. L. (2014a). Dehydration of D-xylose to furfural using selective and hydrothermally stable arenesulfonic SBA-15 catalysts. *Appl. Catal. B Environ.* 145, 34–42. doi: 10.1016/j.apcatb.2012.11.010
- Al-Hubboubi, S. K., Raouf, Z., Al-A., and Abbood, R. H. (2012). Corrosion-resistance characteristics of concrete containing furfural. *J. Eng.* 18, 472–484.
- Antonetti, C., Bonari, E., Licursi, D., Nassi, O., Di Nasso, N., and Ruspolti Galletti, A. M. (2015). Hydrothermal conversion of giant reed to furfural and levulinic acid: optimization of the process under microwave irradiation and investigation of distinctive agronomic parameters. *Molecules* 20, 21232–21253. doi: 10.3390/molecules201219760
- Aresta, M., Dibenedetto, A., and Dumeignil, F. (2012). *Biorefinery: from Biomass to Chemicals and Fuels*. Berlin; Boston, MA: Walter de Gruyter & Co.
- ARIA (2016). *Furfural Accident Database*. Available online at: <http://www.aria.developpement-durable.gouv.fr/search-result-accident/?lang=en> (Accessed: November 10, 2016).
- Bado-Nilles, A., Diallo, A. O., Marlair, G., Pandard, P., Chabot, L., Geffard, A., et al. (2015). Coupling of OECD standardized test and immunomarkers to select the most environmentally benign ionic liquid option – Towards an innovative “safety by design” approach. *J. Hazard. Mater.* 283, 202–210. doi: 10.1016/j.jhazmat.2014.09.023
- Bernal, H. G., Bernazzani, L., and Galletti, A. M. R. (2014). Furfural from corn stover hemicelluloses. A mineral acid-free approach. *Green Chem.* 16, 3734–3740. doi: 10.1039/C4GC00450G
- Bernal, H. G., Galletti, A. M. R., Garbarino, G., Busca, G., and Finocchio, E. (2015). NbP catalyst for furfural production: FT-IR studies of surface properties. *Appl. Catal. A General* 502, 388–398. doi: 10.1016/j.apcata.2015.06.031
- Bhaumik, P., and Dhepe, P. L. (2013). Efficient, stable, and reusable silicoaluminophosphate for the one-pot production of furfural from hemicellulose. *ACS Catal.* 3, 2299–2303. doi: 10.1021/cs400495j
- Bhaumik, P., and Dhepe, P. L. (2014). Exceptionally high yields of furfural from assorted raw biomass over solid acids. *RSC Adv.* 4, 26215–26221. doi: 10.1039/C4RA04119D
- Bhaumik, P., and Dhepe, P. L. (2015). Effects of careful designing of SAPO-44 catalysts on the efficient synthesis of furfural. *Catal. Today* 251, 66–72. doi: 10.1016/j.cattod.2014.10.042
- Bhaumik, P., and Dhepe, P. L. (2016). Solid acid catalyzed synthesis of furans from carbohydrates. *Catal. Rev.* 58, 36–112. doi: 10.1080/01614940.2015.1099894
- Binder, J. B., Blank, J. J., Cefali, A. V., and Raines, R. T. (2010). Synthesis of furfural from xylose and xylan. *ChemSusChem* 3, 1268–1272. doi: 10.1002/cssc.201000181
- Bourg, D., and Erkman, S. (2003). *Perspectives on Industrial Ecology*. Sheffield: Greenleaf Publishing.
- Brown, R. C., and Brown, T. R. (2013). *Biorenewable Resources: Engineering New Products from Agriculture*. Weinheim: Wiley Blackwell.

- Bruce, S. M., Zong, Z., Chatzidimitriou, A., Avci, L. E., Bond, J. Q., Carreon, M. A., et al. (2016). Small pore zeolite catalysts for furfural synthesis from xylose and switchgrass in a γ -valerolactone/water solvent. *J. Mol. Catal. A Chem.* 422, 18–22. doi: 10.1016/j.molcata.2016.02.025d
- Campo-Molina, M. J., Corral Pérez, J. J., Mariscal, R., and Lopéz-Granados, M. (2017). Silica-poly(styrene sulphonic acid)nanocomposites as promising acid catalysts. *Catal. Today* 279, 155–163. doi: 10.1016/j.cattod.2016.06.042
- Carvalho, A. V., da Costa Lopes, A. M., and Bogel-Lukasik, R. (2015). Relevance of the acidic 1-butyl-3-methylimidazolium hydrogen sulphate ionic liquid in the selective catalysis of the biomass hemicellulose fraction. *RSC Adv.* 5, 47153–47164. doi: 10.1039/c5ra07159c
- Chancelier, L., Diallo, A. O., Santini, C. C., Marlair, G., Gutel, T., Mailley, S., et al. (2014). Targeting adequate thermal stability and fire safety in selecting ionic liquid-based electrolytes for energy storage. *Phys. Chem. Chem. Phys.* 16, 1967–1976. doi: 10.1039/c3cp54225d
- Chareonlimkun, A., Champreda, V., Shotipruk, A., and Laosiripojana, N. (2010). Catalytic conversion of sugarcane bagasse, rice husk and corncob in the presence of TiO_2 , ZrO_2 and mixed-oxide TiO_2 - ZrO_2 under hot compressed water (HCW) condition. *Bioresour. Technol.* 101, 4179–4186. doi: 10.1016/j.biortech.2010.01.037
- Chen, H., Qin, L., and Yu, B. (2015). Furfural production from steam explosion liquor of rice straw by solid acid catalysts (HZSM-5). *Biomass Bioenergy* 73, 77–83. doi: 10.1016/j.biombioe.2014.12.013
- Cheng, L., Guo, X., Song, C., Yu, G., Cui, Y., Xue, N., et al. (2013). High performance mesoporous zirconium phosphate for dehydration of xylose to furfural in aqueous-phase. *RSC Adv.* 3, 23228–23235. doi: 10.1039/C3RA43413C
- Chhedha, J. N., Román-Leshkov, Y., and Dumesic, J. A. (2007). Production of 5-hydroxymethylfurfural and furfural by dehydration of biomass-derived mono- and poly-saccharides. *Green Chem.* 9, 342–350. doi: 10.1039/B611568C
- Choudhary, V., Sandler, S. I., and Vlachos, D. G. (2012). Conversion of xylose to furfural using Lewis and Brønsted acid catalysts in aqueous media. *ACS Catal.* 2, 2022–2028. doi: 10.1021/cs300265d
- Cortés, W., Pineros-Castro, Y., and Rosario, C. (2013). Conversion of D-xylose into furfural with aluminum and hafnium pillared clays as catalyst. *Dyna* 80, 105–112.
- Daengprasert, W., Boonnoun, P., Laosiripojana, N., Goto, M., and Shotipruk, A. (2011). Application of sulfonated carbon-based catalyst for solvothermal conversion of cassava waste to hydroxymethylfurfural and furfural. *Ind. Eng. Chem. Res.* 50, 7903–7910. doi: 10.1021/ie102487w
- Danon, B., Marcotullio, G., and de Jong, W. (2014). Mechanistic and kinetic aspects of pentose dehydration towards furfural in aqueous media employing homogeneous catalysis. *Green Chem.* 16, 39–54. doi: 10.1039/C3GC41351A
- Delbecq, F., Wang, Y., and Len, C. (2016). Conversion of xylose, xylan and rice husk into furfural via betaine and formic acid mixture as novel homogeneous catalyst in biphasic system by microwave-assisted dehydration. *J. Mol. Catal. A* 423, 520–525. doi: 10.1016/j.molcata.2016.07.003
- Deng, A., Liu, Q., Yan, Y., Li, H., Ren, J., Liu, C., et al. (2016). A feasible process for furfural production from the pre-hydrolysis liquor of corncob via biochar catalysts in a new biphasic system. *Bioresour. Technol.* 216, 754–760. doi: 10.1016/j.biortech.2016.06.002
- Deng, A., Ren, J., Li, H., Peng, F., and Sun, R. (2015). Corncob lignocellulose for the production of furfural by hydrothermal pretreatment and heterogeneous catalytic process. *RSC Adv.* 5, 60264–60272. doi: 10.1039/C5RA10472F
- Diallo, A. O., Fayet, G., Len, C., and Marlair, G. (2012a). Evaluation of heats of combustion of ionic liquids through use of existing and purpose built models. *Ind. Eng. Chem. Res.* 51, 3149–3156. doi: 10.1021/ie2023788
- Diallo, A. O., Len, C., Morgan, A. B., and Marlair, G. (2012b). Revisiting phys.-chem. Related safety issues of ionic liquids. *Sep. Purif. Technol.* 97, 228–234. doi: 10.1016/j.seppur.2012.02.016
- Diallo, A. O., Morgan, A. B., Len, C., and Marlair, G. (2013). An innovative experimental approach aiming to understand and quantify the actual fire hazards of ionic liquids. *Energy Environ. Sci.* 6, 699–710. doi: 10.1039/c2ee23926d
- Dias, A. S., Lima, S., Brandão, P., Pillinger, M., Rocha, J., and Finocchio, E. (2006a). Liquid-phase dehydration of D-xylose over microporous and mesoporous niobium silicates. *Catal. Lett.* 108, 179–186. doi: 10.1007/s10562-006-0046-6
- Dias, A. S., Lima, S., Pillinger, M., and Valente, A. A. (2006c). Acidic cesium salts of 12-tungstophosphoric acid as catalysts for the dehydration of xylose into furfural. *Carbohydr. Res.* 341, 2946–2953. doi: 10.1016/j.carres.2006.10.013
- Dias, A. S., Lima, S., Pillinger, M., and Valente, A. A. (2007). Modified versions of sulfated zirconia as catalysts for the conversion of xylose to furfural. *Catal. Lett.* 114, 151–160. doi: 10.1007/s10562-007-9052-6
- Dias, A. S., Pillinger, M., and Valente, A. A. (2005a). Liquid phase dehydration of D-xylose in the presence of Keggin-type heteropolyacids. *Appl. Catal. A* 285, 126–131. doi: 10.1016/j.apcata.2005.02.016
- Dias, A. S., Pillinger, M., and Valente, A. A. (2005b). Dehydration of xylose into furfural over micro-mesoporous sulfonic acid catalysts. *J. Catal.* 229, 414–423. doi: 10.1016/j.jcat.2004.11.016
- Dias, A. S., Pillinger, M., and Valente, A. A. (2006b). Mesoporous silica-supported 12-tungstophosphoric acid catalysts for the liquid phase dehydration of D-xylose. *Micropor. Mesopor. Mat.* 94, 214–225. doi: 10.1016/j.micromeso.2006.03.035
- Ebringerová, A. (2005). Structural diversity and application potential of hemicelluloses. *Macromol. Symp.* 232, 1–12. doi: 10.1002/masy.200551401
- Ersnova, O., Kanervo, J., Hellsten, S., and Sixtu, H. (2015). The role of xylulose as an intermediate in xylose conversion to furfural: insights via experiments and kinetic modelling. *RSC Adv.* 5, 66727–66757. doi: 10.1039/c5ra10855a
- Gairola, K., and Smirnova, I. (2012). Hydrothermal pentose to furfural conversion and simultaneous extraction with sc-CO_2 -kinetics and application to biomass hydrolysates. *Bioresour. Technol.* 123, 592–598. doi: 10.1016/j.biortech.2012.07.031
- Gao, H., Liu, H., Pang, B., Yu, G., Du, J., Zhang, Y., et al. (2014). Production of furfural from waste aqueous hemicellulose solution of hardwood over ZSM-5 zeolite. *Bioresour. Technol.* 172, 453–456. doi: 10.1016/j.biortech.2014.09.026
- García-Sancho, C., Sádaba, I., Moreno-Tost, R., Merida Robles, J., Santamaria-Gonzales, J., Lopez-Granados, M., et al. (2013). Dehydration of xylose to furfural over MCM-41-supported niobium-oxide catalysts. *ChemSusChem* 6, 635–642. doi: 10.1002/cssc.201200881
- García-Sancho, C., Agirrezabal-Telleria, I., Güemez, M. B., and Maireles-Torres, P. (2014b). Dehydration of D-xylose to furfural using different supported niobia catalysts. *Appl. Catal. B* 152, 1–10. doi: 10.1016/j.apcatb.2014.01.013
- García-Sancho, C., Rubio-Caballero, J. M., Mérida-Robles, J. M., Moreno-Tost, R., Santamaria-gonzales, J., and Maireles-Torres, P. (2014a). Mesoporous Nb_2O_5 as solid acid catalyst for dehydration of D-xylose into furfural. *Catal. Today* 234, 119–124. doi: 10.1016/j.cattod.2014.02.012
- Goncalves, R. S., and de Olivera, W. X. (1992). Electrochemical evidences of the protection efficiency of furfural on the corrosion process of low carbon steel in ethanolic medium. *J. Braz. Chem. Soc.* 3, 92–94.
- Gupta, D., Ahmad, E., Paul, K. K., and Saha, B. (2017a). Efficient utilization of potash alum as a green catalyst for production of furfural, 5-hydroxymethylfurfural and levulinic acid from mono-sugars. *RSC Adv.* 7, 41973–41979. doi: 10.1039/c7ra07147g
- Gupta, N. K., Fukuoka, A., and Nakajima, K. (2017b). Amorphous Nb_2O_5 as a selective and reusable catalyst for furfural production from xylose in biphasic water and toluene. *ACS Catal.* 7, 2430–2436. doi: 10.1021/acscatal.6b03682
- Gürbüz, E. I., Gallo, J. M. R., Alonso, D. M., Wettstein, S. G., Lim, W. Y., and Dumesic, J. A. (2013). Conversion of hemicellulose into furfural using solid acid catalysts in γ -valerolactone. *Angew. Chem. Int. Ed.* 52, 1270–1274. doi: 10.1002/anie.201207334
- Gürbüz, E. I., Wettstein, S. G., and Dumesic, J. A. (2012). Conversion of hemicellulose to furfural and levulinic acid using biphasic reactors with alkylphenol solvents. *ChemSusChem* 5, 383–387. doi: 10.1002/cssc.201100608
- Hacker, M., Burghardt, D., Fletcher, L., Gordon, A., and Peruzzi, W. (2009). *Engineering and Technology*. Clifton Park: Delmar Cengage Learning.
- Hall, C. W. (1981). *Biomass as an Alternative Fuel*. Rockville: Government Institutes.

- Harmaajärvi, I., Heinonen, S., and Lahti, P. (2004). *Urban form, Transportation and Greenhouse Gas Emissions: Experiences in the Nordic Countries*. Copenhagen: Nordic Council of Ministers.
- Hricoviniová, Z. (2013). Xylans are a valuable alternative resource: production of D-xylose, D-lyxose and furfural under microwave irradiation. *Carbohydr. Polym.* 98, 1416–1421. doi: 10.1016/j.carbpol.2013.07.066
- Hu, X., Lievens, C., and Li, C.-Z. (2012). Acid-catalyzed conversion of xylose in methanol-rich medium as part of biorefinery. *ChemSusChem* 5, 1427–1434. doi: 10.1002/cssc.201100745
- Hu, X., Wang, S., Wu, L., Dong, D., Hasan, M. M., and Li, C.-Z. (2014). Acid-treatment of C5 and C6 sugar monomers/oligomers: insight into their interactions. *Fuel Process. Technol.* 126, 315–323. doi: 10.1016/j.fuproc.2014.05.024
- Hua, D. R., Wu, Y. L., Liu, Y. F., Chen, Y., Yang, H.-D., Lu, X.-N., et al. (2016). Preparation of furfural and reaction kinetics of xylose dehydration to furfural in high-temperature water. *Pet. Sci.* 13, 167–172. doi: 10.1007/s12182-015-0069-y
- Jelinsky, L. W., Graedel, T. E., Laudise, R. A., McCall, D. W., and Patel, C. K. (1992). Industrial ecology: concepts and approaches. *Proc. Natl. Acad. Sci. U.S.A.* 89, 793–797. doi: 10.1073/pnas.89.3.793
- Jeon, W., Ban, C., Kim, J. E., Woo, H. C., and Kim, D. H. (2016b). Production of furfural from macroalgae-derived alginic acid over Amberlyst-15. *J. Mol. Catal. A Chem.* 423, 264–269. doi: 10.1016/j.molcata.2016.07.020
- Jeon, W., Ban, C., Park, G., Woo, H. C., and Kim, D. H. (2016a). Hydrothermal conversion of alginic acid to furfural catalyzed by Cu (II) ion. *Catal. Today* 265, 154–162. doi: 10.1016/j.cattod.2015.12.001
- Jeon, W., Ban, C., Park, G., Yu, T.-K., Suh, J.-Y., Woo, H. C., et al. (2015). Catalytic hydrothermal conversion of macroalgae-derived alginate: effect of pH on production of furfural and valuable organic acids under subcritical water conditions. *J. Mol. Catal. A Chem.* 399, 106–113. doi: 10.1016/j.molcata.2015.01.011
- Jeong, G. H., Kim, E. G., Kim, S. B., Park, E. D., and Kim, S. W. (2011). Fabrication of sulfonic acid modified mesoporous silica shells and their catalytic performance with dehydration reaction of D-xylose into furfural. *Micropor. Mesopor. Mat.* 144, 134–139. doi: 10.1016/j.micromeso.2011.04.002
- Jin, M., Liu, X., Ban, Y., Peng, Y., Jiao, W., Wang, P., et al. (2016). Conversion of xylose into furfural in a MOF-based mixed matrix membrane reactor. *Chem. Eng. J.* 305, 12–16. doi: 10.1016/j.cej.2015.10.115
- Kaiprommarat, S., Kongparakul, S., Reubroycharoen, P., Guan, and, G., and Smart, C. (2016). Highly efficient sulfonic MCM-41 catalyst for furfural production: Furan-based biofuel agent. *Fuel* 174, 189–196. doi: 10.1016/j.fuel.2016.02.011
- Käldström, M., Kumar, N., Heikkilä, T., Tittla, M., Salmi, T., and Murzin, D. Y. (2010). Formation of furfural in catalytic transformation of levoglucosan over mesoporous materials. *ChemCatChem* 2, 539–546. doi: 10.1002/cctc.201000024
- Kamm, B., Gruber, P. R., and Kamm, M. (2006). *Biorefineries-Industrial Processes and Products*. Weinheim: Wiley-VCH Verlag GmbH.
- Karinen, R., Vilonen, K., and Niemela, M. (2011). Biorefining: heterogeneously catalyzed reactions of carbohydrates for the production of furfural and hydroxymethylfurfural. *ChemSusChem* 4, 1002–1016. doi: 10.1002/cssc.201000375
- Kim, B.-S., Jeong, C. S., Kim, J. M., Park, S. B., Park, S. H., Jeon, J.-K., et al. (2016). *Ex situ* catalytic upgrading of lignocellulosic biomass components over vanadium contained H-MCM-41 catalysts. *Catal. Today* 265, 184–191. doi: 10.1016/j.cattod.2015.08.031
- Kim, E. S., Liu, S., Abu-Omar, M. M., and Mosier, N. S. (2012). Selective conversion of biomass hemicellulose to furfural using maleic acid with microwave heating. *Energy Fuels* 26, 1298–1304. doi: 10.1021/ef2014106
- Kim, T. H., Ryu, H. J., and Oh, K. K. (2016). Low acid hydrothermal fractionation of Giant Miscanthus for production of xylose-rich hydrolyzate and furfural. *Bioresour. Technol.* 218, 367–372. doi: 10.1016/j.biortech.2016.06.106
- Lam, E., Chong, J. H., Majid, E., Liu, Y., Hrapovic, S., Leung, A. C. W., et al. (2012). Carbocatalytic dehydration of xylose to furfural in water. *Carbon* 50, 1033–1043. doi: 10.1016/j.carbon.2011.10.007
- Lam, E., Majid, E., Leung, A. C. W., Chong, J. M., Mahmoud, K. A., and Luong, J. H. (2011). Synthesis of furfural from xylose by heterogeneous and reusable nafion catalysts. *ChemSusChem* 4, 535–541. doi: 10.1002/cssc.201100023
- Lamminpää, K., Ahola, J., and Tanskanen, J. (2012). Kinetics of xylose dehydration into furfural in formic acid. *Ind. Eng. Chem. Res.* 51, 6297–6303. doi: 10.1021/ie2018367
- Lamminpää, K., Ahola, J., and Tanskanen, J. (2015). Acid-catalysed xylose dehydration into furfural in the presence of kraft lignin. *Bioresour. Technol.* 177, 94–101. doi: 10.1016/j.biortech.2014.11.074
- Lange, J. P., Van Der Heide, E., Van Buijtenen, J., and Price, R. (2012). Furfural – A promising platform for lignocellulosic biofuels. *ChemSusChem* 5, 150–166. doi: 10.1002/cssc.201100648
- Le Guenic, S., Delbecq, F., Ceballos, C., and Len, C. (2015). Microwave-assisted dehydration of D-xylose into furfural by diluted inexpensive inorganic salts solution in a biphasic system. *J. Mol. Catal. A Chem.* 410, 1–7. doi: 10.1016/j.molcata.2015.08.019
- Le Guenic, S., Gergela, D., Delbecq, F., and Len, C. (2016). Furfural production from D-xylose and xylan by using stable Nafion NR50 and NaCl in a microwave-assisted biphasic reaction. *Molecules* 21, 1102–1111. doi: 10.3390/molecules21081102
- Lessard, J., Morin, J. F., Wehrung, J. F., Magnin, D., and Chornet, E. (2010). High yield conversion of residual pentoses into furfural via zeolite catalysis and catalytic hydrogenation of furfural to 2-methylfuran. *Top. Catal.* 53, 1231–1234. doi: 10.1007/s11244-010-9568-7
- Li, B., Varanasi, S., and Relue, P. (2013). High yield aldose-ketose transformation for isolation and facile conversion of biomass sugar to furan. *Green Chem.* 15, 2149–2157. doi: 10.1039/C3GC40795K
- Li, H., Chen, X., Ren, J., Deng, H., Peng, F., and Sun, R. (2015). Functional relationship of furfural yields and the hemicellulose-derived sugars in the hydrolysates from corncob by microwave-assisted hydrothermal pretreatment. *Biotechnol. Biofuels* 8:127. doi: 10.1186/s13068-015-0314-z
- Li, H., Deng, A., Ren, J., Liu, C., Lu, Q., Zhong, L., et al. (2014b). Catalytic hydrothermal pretreatment of corncob into xylose and furfural via solid acid catalyst. *Bioresour. Technol.* 158, 313–320. doi: 10.1016/j.biortech.2014.02.059
- Li, H.-L., Wang, S. Y., Wang, W. J., Ren, J. C., Peng, F., Sun, R. C., et al. (2013). One-step heterogeneous catalytic process for the dehydration of xylan into furfural. *Bioresour. Technol.* 143, 3200–3211. doi: 10.1016/j.biortech.2013.03.021
- Li, H., Wang, W., Ren, J., and Sun, R. (2014a). Preparation and characterization of $\text{SO}_4^{2-}/\text{TiO}_2\text{-ZrO}_2/\text{La}^{3+}$ and their photocatalytic performance for the dehydration of xylose to furfural. *J. Biobased Mater. Bioenergy* 8, 50–58. doi: 10.1166/jbmb.2014.1406
- Li, H., Wang, X., Liu, C., Ren, J., Zhao, X., Sun, R., et al. (2016). An efficient pretreatment for the selectivity hydrothermal conversion of corncob into furfural: The combined mixed ball-milling and ultrasonic pretreatments. *Ind. Crops Prod.* 94, 721–728. doi: 10.1016/j.indcrop.2016.09.052
- Li, W., Zhu, Y., Lu, Y., Liu, Q., Guan, S., Chang, H.-M., et al. (2017). Enhanced furfural production from raw corn stover employing a novel heterogeneous acid catalyst. *Bioresour. Technol.* 245, 258–265. doi: 10.1016/j.biortech.2017.08.077
- Li, X.-L., Pan, T., Deng, J., Fu, Y., and Xu, H.-J. (2015). Catalytic dehydration of D-xylose to furfural over a tantalum catalyst in batch and continuous process. *RSC Adv.* 5, 70139–70145. doi: 10.1039/C5RA11411J
- Lima, S., Antunes, M. M., Pillinger, M., and Valente, A. A. (2011). Ionic liquids as tool for the acid-catalyzed hydrolysis/dehydration of saccharides to furanic aldehydes. *ChemCatChem* 3, 1686–1706. doi: 10.1002/cctc.201100105
- Lima, S., Fernandes, A., Antunes, M. M., Pillinger, M., Riberiro, F., and Valente, A. A. (2010). Dehydration of xylose into furfural in the presence of crystalline microporous silicoaluminophosphates. *Catal. Lett.* 135, 41–47. doi: 10.1007/s10562-010-0259-6
- Lima, S., Neves, P., Antunes, M. M., Pillinger, M., Ignatyev, N., and Lukasik, R. B. (2009). Conversion of mono/di/polysaccharides into furan compounds using 1-alkyl-3-methylimidazolium ionic liquids. *Appl. Catal. A Gen.* 363, 93–99. doi: 10.1016/j.apcata.2009.04.049
- Liu, H., Chen, J., Zhao, Y., and Wang, S. (2017). Conversion of C5 Carbohydrates into Furfural catalyzed by SO_3H -functionalized ionic liquid in renewable γ -valerolactone. *Energy Fuels* 31, 3929–3934. doi: 10.1021/acs.energyfuels.6b01975
- Lopes, M., Dussan, K., and Leahy, J. J. (2017). Enhancing the conversion of D-xylose into furfural at low temperature using chloride salts as co-catalysts;

- Catalytic combination of AlCl_3 and formic acid. *Chem. Eng. J.* 323, 278–286. doi: 10.1016/j.cej.2017.04.114
- Lu, H., Liu, S., Zhang, M., Heng, F., Shi, X., and Yan, L. (2016). Investigation of the strengthening process for liquid hot water pretreatments. *Energy Fuels* 30, 1103–1108. doi: 10.1021/acs.energyfuels.5b02658
- Luo, Y., Li, Z., Zuo, Y., Su, Z., and Hu, C. (2017). A simple two-step method for the selective conversion of hemicellulose in pubescens to furfural. *ACS Sustain. Chem. Eng.* 5, 8137–8147. doi: 10.1021/acssuschemeng.7b01766
- Mante, O. D., Amidon, T. E., Stipanovic, A., and Babu, S. P. (2014). Integration of biomass pretreatment with fast pyrolysis: An evaluation of electron beam (EB) irradiation and hot-water extraction (HWE). *J. Anal. Appl. Pyrolysis* 110, 44–54. doi: 10.1016/S0165-2370(96)00956-4
- Marcotullio, G., and De Jong, W. (2010). Chloride ions enhance furfural formation from D-xylose in dilute aqueous acidic solutions. *Green Chem.* 12, 1739–1746. doi: 10.1039/B927424C
- Matsagar, B. M., and Dhepe, P. L. (2017). Effect of cations, anions and H^+ concentrations of acidic ionic liquids in the valorization of polysaccharide into furfural. *New J. Chem.* 41, 6137–6144. doi: 10.1039/C7NJ00342K
- Matsagar, B. M., Munshi, M. K., Kellar, A. A., and Dhepe, P. L. (2015). Conversion of concentrated sugar solution into 5-hydroxymethylfurfural and furfural using Brønsted acidic ionic liquid. *Catal. Sci. Technol.* 5, 5086–5090. doi: 10.1039/c5cy00858a
- Mazar, A., Jemaa, N., Al Dajani, W. W., Marinova, M., and Perrier, M. (2017). Furfural production from a pre-hydrolyzate generated using aspen and maple chips. *Biomass Bioeng.* 104, 8–16. doi: 10.1016/j.biombioe.2017.05.016
- Mazzotta, M. G., Gupta, D., Saha, B., Patra, A. K., Bhaumik, A., and Abu-Omar, M. M. (2014). Efficient solid acid catalyst containing Lewis and Brønsted acid sites for the production of furfurals. *ChemSusChem* 7, 2342–2350. doi: 10.1002/cssc.201402007
- Melero, J. A., Iglesias, J., and Garcia, A. (2012). Biomass as renewable feedstock in standard refinery units. Feasibility, opportunities and challenges. *Energy Environ. Sci.* 5, 7393–7420. doi: 10.1039/C2EE21231E
- Mellmer, M. A., Sener, C., Gallo, J. M. R., Luterbacher, J. S., Alonso, D. M., and Dumesic, J. A. (2014). Solvent effects in acid-catalyzed biomass conversion reactions. *Angew. Chem. Int. Ed.* 53, 11872–11875. doi: 10.1002/anie.201408359
- Mittal, A., Black, S. K., Vinzart, T. B., O'Brien, M., Tucker, M. P., and Johnson, D. K. (2017). Production of furfural from Process-relevant Biomass-derived Pentoses in a Biphasic Reaction System. *ACS Sustain. Chem. Eng.* 5, 5694–5701. doi: 10.1021/acssuschemeng.7b00215
- Mohamed, A. K., Ibrahim, K. M., and Moussa, M. N. H. (1989). Some Furfural Hydrazone Compounds as Corrosion Inhibitors for Iron in Nitric Acid. *Anti-Corrosion Methods Mater.* 36, 4–7. doi: 10.1108/eb007254
- Molina, M. J. C., Granados, M. L., Gervasini, A., and Carniti, P. (2015). Exploitation of niobium oxide effective acidity for xylose dehydration to furfural. *Catal. Today* 254, 90–98. doi: 10.1016/j.cattod.2015.01.018
- Molina, M. J. C., Mariscal, R., Ojeda, M., and Lopez Granados, M. (2012). Cyclopentyl methyl ether: a green co-solvent for the selective dehydration of lignocellulosic pentoses to furfural. *Bioresour. Technol.* 126, 321–327. doi: 10.1016/j.biortech.2012.09.049
- Moncada, J., Cardona, C. A., Higuera, J. C., Velez, J. J., and Lopez-Suarez, F. E. (2016). Wood residue (*Pinus patula* bark) as an alternative feedstock for producing ethanol and furfural in Colombia: experimental, techno-economic and environmental assessments. *Chem. Eng. Sci.* 140, 309–318. doi: 10.1016/j.ces.2015.10.027
- Morais, A. R. C., and Bogel-Lukasik, R. (2016). Highly efficient and selective CO_2 -adjuncted dehydration of xylose to furfural in aqueous media with THF. *Green Chem.* 18, 2331–2334. doi: 10.1039/C5GC02863A
- Morais, A. R. C., Matuchaki, M. D. D. J., Andreass, J., and Bogel-Lukasik, R. (2016). A green and efficient approach of selective conversion of xylose and biomass hemicelluloses into furfural in aqueous media using high-pressure CO_2 as sustainable catalyst. *Green Chem.* 18, 2985–2994. doi: 10.1039/C6GC00043F
- Okuhara, T. (2002). Water-Tolerant Solid Acid Catalysts. *Chem. Rev.* 102, 3641–3666. doi: 10.1021/CR0103569
- Ordonsky, V. V., Schouten, J. C., Van der Schaaf, J., and Nijhuis, T. A. (2013). Biphasic single-reactor process for dehydration of xylose and hydrogenation of produced furfural. *Appl. Catal. A Gen.* 451, 6–13. doi: 10.1016/j.apcata.2012.11.013
- Park, G., Jeon, W., Ban, C., Woo, H. C., and Kim, D. H. (2016). Direct catalytic conversion of brown seaweed-derived alginic acid to furfural using 12-tungstophosphoric acid catalyst in tetrahydrofuran/water co-solvent. *Energy Convers. Manage.* 118, 135–141. doi: 10.1016/j.enconman.2016.03.091
- Peleteiro, S., da Costa Lopes, A. M., Garrote, G., Lukasik, R. B., and Parajo, J. C. (2015a). Manufacture of furfural in biphasic media made up of an ionic liquid and a co-solvent. *Ind. Crops Prod.* 77, 163–166. doi: 10.1016/j.indcrop.2015.08.048
- Peleteiro, S., da Costa Lopes, A. M., Garrote, G., Parajo, J. C., and Lukasik, R. B. (2015b). Simple and efficient furfural production from xylose in media containing 1-Butyl-3-Methylimidazolium hydrogen sulfate. *Ind. Eng. Chem. Res.* 54, 8368–8373. doi: 10.1021/acs.iecr.5b01771
- Peleteiro, S., Garrote, G., Santos, V., and Parajo, J. C. (2014). Conversion of hexoses and pentoses into furans in an ionic liquid. *Afinidad* 71, 202–206.
- Peleteiro, S., Rivas, S., Alonso, J. L., Santos, V., and Parajo, J. C. (2016a). Furfural production using ionic liquids: a review. *Bioresour. Technol.* 202, 181–191. doi: 10.1016/j.biortech.2015.12.017
- Peleteiro, S., Santos, V., Garrote, G., and Parajo, J. C. (2016b). Furfural production From Eucalyptus wood using an acidic ionic liquid. *Carbohydr. Polym.* 146, 20–25. doi: 10.1016/j.carbpol.2016.03.049
- Peleteiro, S., Santos, V., and Parajo, J. C. (2016c). Furfural production in biphasic media using an acidic ionic liquid as a catalyst. *Carbohydr. Polym.* 153, 421–428. doi: 10.1016/j.carbpol.2016.07.093
- Rackemann, D. W., Bartley, J. P., and Doherty, W. O. S. (2014). Methanesulfonic acid-catalyzed conversion of glucose and xylose mixtures to levulinic acid and furfural. *Ind. Crops Prod.* 52, 46–57. doi: 10.1016/j.indcrop.2013.10.026
- Rackemann, D. W., Bartley, J. P., Harrison, H. D., and Doherty, W. O. S. (2016). The effect of pretreatment on methane sulfonic acid-catalyzed hydrolysis on bagasse to levulinic acid, formic acid and furfural. *RSC Adv.* 6, 74525–74535. doi: 10.1039/C6RA14772K
- Rong, C., Ding, X., Zhu, Y., Li, Y., Wang, L., Qu, Y., et al. (2012). Production of furfural from xylose at atmospheric pressure by dilute sulfuric acid and inorganic salts. *Carbohydr. Res.* 350, 77–80. doi: 10.1016/j.carres.2011.11.023
- Sádaba, I., Lima, S., Valente, A. A., and Granada Lopez, M. (2011). Catalytic dehydration of xylose to furfural: vanadyl pyrophosphate as source of active soluble species. *Carbohydr. Res.* 346, 2785–2791. doi: 10.1016/j.carres.2011.10.001
- Sahu, R., and Dhepe, P. L. (2012). A one-pot method for the selective conversion of hemicellulose from crop waste into C5 sugars and furfural by using solid acid catalysts. *ChemSusChem* 5, 751–761. doi: 10.1002/cssc.201100448
- Sairanen, E., Karinen, R., and Lehtonen, J. (2014). Comparison of solid acid-catalyzed and autocatalyzed C5 and C6 sugar dehydration reactions with water as a solvent. *Catal. Lett.* 144, 1839–1850. doi: 10.1007/s10562-014-1350-1
- Sandvik Material Technology (2016). *Furfural - Sandvik Materials Technology*. Available online at: <http://smt.sandvik.com/en/materials-center/corrosion-tables/furfural/> (Accessed: October 15, 2016).
- Scarth, V. (1947). *Prevention of Corrosion in Furfural Rerun Systems*. U.S. Patent No. 2,416,500. Bartlesville, OK: U.S. Patent Office.
- Schieb, P. A., Lescieux-Katir, H., Thénot, M., and Clément-Larosiere, B. (2015). *Biorefinery 2030: Future Prospects for the Bioeconomy*. Berlin, Heidelberg: Springer-Verlag.
- Scientific Committee on Consumer Safety (2012). *Opinion on Furfural*. Available online at: https://ec.europa.eu/health/scientific_committees/consumer_safety/docs/scscs_o_083.pdf
- Seemala, B., Haritos, V., and Tanksale, A. (2016). Levulinic Acid as a Catalyst for the Production of 5-Hydroxymethylfurfural and Furfural from Lignocellulose Biomass. *ChemCatChem* 8, 640–647. doi: 10.1002/cctc.201501105
- Shi, N., Liu, Q., Wang, T., Wang, T. J., and Cai, C. L. (2015). Production of 5-hydroxymethylfurfural and furfural from lignocellulosic biomass in water-tetrahydrofuran media with sodium bisulfate. *Chin. J. Chem. Phys.* 28, 650–656. doi: 10.1063/1674-0068/28/cjcp1501008
- Shi, X., Wu, Y., Li, P., Yi, H., Yang, M., and Wang, G. (2011). Catalytic conversion of xylose to furfural over the solid acid $\text{ZrO}_2\text{-Al}_2\text{O}_3\text{/SBA-15}$ catalysts. *Carbohydr. Res.* 346, 480–487. doi: 10.1016/j.carres.2011.01.001

- Sievers, C., Musin, I., Marzalletti, T., Olante, M. B., Agrawal, P. K., and Jones, C. W. (2009). Acid-catalyzed conversion of sugars and furfurals in an ionic-liquid phase. *ChemSusChem* 2, 665–671. doi: 10.1002/cssc.200900092
- Sorensen, B., Breeze, P., Storvick, T., Yang, Y.-T., da Rosa, A., Gupta, H., et al. (2009). *Renewable Energy Focus Handbook*. Oxford, UK: Academic Press.
- Tao, F., Song, H., and Chou, L. (2011). Hydrolysis of cellulose in SO₃H-functionalized ionic liquids. *Bioresour. Technol.* 102, 9000–9006. doi: 10.1016/j.biortech.2011.06.067
- Tao, F., Song, H., and Chou, L. (2012). Efficient conversion of cellulose into furans catalyzed by metal ions in ionic liquids. *J. Mol. Catal. A Chem.* 357, 11–18. doi: 10.1016/j.molcata.2012.01.010
- United Nations (2009). *Recommendations on the Transport of Dangerous Goods - Model Regulations*, Volume 1. New York, NY; Geneva: United Nations. Available online at: <https://www.oecd.org/chemicalsafety/risk-assessment/48772773.pdf>.
- United Nations (2015). *Globally Harmonized System of Classification and Labelling of Chemicals (GHS)*. New York, NY; Geneva: United Nations. Available online at: https://www.unece.org/fileadmin/DAM/trans/danger/publi/ghs/ghs_rev06/English/ST-SG-AC10-30-Rev6e.pdf.
- Urban, P. G., and Pitt, M. J. (2007). *Bretherick's Handbook of Reactive Chemical Hazards*. Amsterdam: Elsevier.
- Vanoye, L., Fanselow, M., Holbrey, J. D., Atkins, M. P., and Saddon, K. R. (2009). Kinetic model for the hydrolysis of lignocellulosic biomass in the ionic liquid, 1-ethyl-3-methyl-imidazolium chloride. *Green Chem.* 11, 390–396. doi: 10.1039/b817882h
- Vaz Jr., S., and Donate, P. M. (2015). Microwave-assisted green production of furfural from D-xylose of sugarcane bagasse. *BioRes.* 10, 8168–8180. doi: 10.15376/biores.10.4.8168-8180
- Ventura, S. P. M., de Moraes, P., Coelho, J. A. S., Sintra, T., Coutinho, J. A. P., and Afonso, C. A. M. (2016). Evaluating the toxicity of biomass derived platform chemicals. *Green Chem.* 18, 4733–4742. doi: 10.1039/C6GC01211F
- Verma, S., Baig, N., Nadagouda, M. N., Len, C., and Varma, R. S. (2017). Sustainable pathway to furanics from biomass via heterogeneous organo-catalysis. *Green Chem.* 19, 164–168. doi: 10.1039/c6gc02551j
- Vom Stein, T., Grande, P. M., Leitner, W., and Dominguez de Maria, P. (2011). Iron-catalyzed furfural production in biobased biphasic systems: from pure sugars to direct use of crude xylose effluents as feedstock. *ChemSusChem* 4, 1592–1594. doi: 10.1002/cssc.201100259
- Wang, M., Liu, C., Li, Q., and Zhang, D. (2015). Theoretical insight into the conversion of xylose to furfural in the gas phase and water. *J. Mol. Mod.* 21, 1–10. doi: 10.1007/s00894-015-2843-6
- Wang, S., Zhao, Y., Liu, H., Chen, J., Zhu, L., and Luo, Z. (2017). Conversion of C5 carbohydrates into furfural catalyzed by a Lewis acidic ionic liquid in renewable γ -valerolactone. *Green Chem.* 19, 3969–3879. doi: 10.1039/C7GC01298E
- Wang, Y., Delbecq, F., Kwapinski, W., and Len, C. (2017a). Application of sulfonated carbon-based catalyst for the furfural production from D-xylose and xylan in a microwave assisted biphasic reaction. *Mol. Catal.* 438, 167–172. doi: 10.1016/j.mcat.2017.05.031
- Wang, Y., Len, T., Huang, Y., Taboada, A. D., Boa, A. N., Delbecq, F., et al. (2017b). Sulfonated sporopollenin as an efficient and recyclable heterogeneous catalyst for dehydration of D-xylose and xylan into furfural. *ACS Sustai. Chem. Eng.* 5, 392–398. doi: 10.1021/acsschemeng.6b01780
- Weingarten, R., Cho, J., Conner Jr, W. C., and Huber, G. W. (2010). Kinetics of furfural production by dehydration of xylose in a biphasic reactor with microwave heating. *Green Chem.* 12, 1423–1429. doi: 10.1039/c003459b
- Werpy, T., and Petersen, G. (2004). *Top Value Added Chemicals from Biomass Volume I — Results of Screening for Potential Candidates from Sugars and Synthesis Gas*. Oak Ridge, CA: Pacific Northwest National Laboratory. Available online at: <https://www.nrel.gov/docs/fy04osti/35523.pdf>.
- Xing, Y., Yan, B., Yuan, Z., and Sun, K. (2016). Mesoporous tantalum phosphates: preparation, acidity and catalytic performance for xylose dehydration to produce furfural. *RSC Adv.* 6, 59081–59090. doi: 10.1039/C6RA07830C
- Xiouras, C., Radacsi, N., Sturm, G., and Stefanidis, G. D. (2016). Furfural synthesis from D-xylose in the presence of Sodium Chloride: Microwave versus Conventional Heating. *ChemSusChem* 9, 2159–2166. doi: 10.1002/cssc.201600446
- Xu, H., Zhao, H., Song, H., Miao, Z., Yang, J., Zhao, J., et al. (2015). Functionalized ionic liquids supported on silica as mild and effective heterogeneous catalysts for dehydration of biomass to furan derivatives. *J. Mol. Catal. A Chem.* 410, 235–241. doi: 10.1016/j.molcata.2015.09.020
- Xu, W., Zhang, S., Lu, J., and Cai, Q. (2017). Furfural production from corncobs using thiourea as additive. *Environ. Prog. Sustain. Energy* 36, 690–695. doi: 10.1002/ep.12489
- Xu, Z., Li, W., Du, Z., Wu, H., Jameel, H., Chang, H.-M., et al. (2015). Conversion of corn stalk into furfural using a novel heterogeneous strong acid catalyst in γ -valerolactone. *Bioresour. Technol.* 198, 764–771. doi: 10.1016/j.biortech.2015.09.104
- Yang, T., Zhou, Y. H., Zhu, S. Z., Pan, H., and Huang, Y. B. (2017). Insight into aluminium sulfate catalyzed xylan conversion to furfural in γ -valerolactone/water biphasic solvent under microwave condition. *ChemSusChem* 10, 4066–4079. doi: 10.1002/cssc.201701290
- Yang, W., Li, P., Bo, D., and Chang, H. (2012). The optimization of formic acid hydrolysis of xylose in furfural production. *Carbohydr. Res.* 357, 53–61. doi: 10.1016/j.carres.2012.05.020
- Yang, W., Li, P., Bo, D., Chang, H., Wang, X., and Zhu, T. (2013). Optimization of furfural production from D-xylose with formic acid as catalyst in a reactive extraction system. *Bioresour. Technol.* 133, 361–369. doi: 10.1016/j.biortech.2013.01.127
- Yang, Y., Hu, C. W., and Abu-Omar, M. M. (2012). Synthesis of furfural from xylose, xylan, and biomass using AlCl₃ · 6 H₂O in biphasic media via xylose isomerization to xylulose. *ChemSusChem* 5, 405–410. doi: 10.1002/cssc.201100688
- Yazdizadeh, M., Jafari-Nasr, M. R., and Safekordi, A. (2016). A new catalyst for the production of furfural from bagasse. *RSC Adv.* 6, 55778–55785. doi: 10.1039/C6RA10499A
- Wang, Y., Delbecq, F., Varma, R. S., and Len, C. (2018). Comprehensive study on expeditious conversion of pre-hydrolyzed alginic acid to furfural in Cu(II) biphasic systems using microwave. *Mol. Catal.* 73–79. doi: 10.1016/j.mcat.2017.11.013
- Yemiş, O., and Mazza, G. (2011). Acid-catalyzed conversion of xylose, xylan and straw into furfural by microwave-assisted reaction. *Bioresour. Technol.* 102, 7371–7378. doi: 10.1016/j.biortech.2011.04.050
- Yong, T. L. K., Mohamad, N., and Yusof, N. N. M. (2016). Furfural production from oil palm biomass using a biomass-derived supercritical ethanol solvent and formic acid catalyst. *Proc. Eng.* 148, 392–400. doi: 10.1016/j.proeng.2016.06.495
- Yoo, C. G., Zhang, S., and Pan, X. (2017). Effective conversion of biomass into bromomethyl furfural, furfural and depolymerized lignin in lithium bromide molten salt hydrate of a biphasic system. *RSC Adv.* 7, 300–308. doi: 10.1039/c6ra25025d
- Yoshida, K., Nanao, H., Kiyozumi, Y., Sato, K., Sato, O., Yamaguchi, A., et al. (2017). Furfural production from xylose and bamboo powder over chabazite-type zeolite prepared by interzeolite conversion method. *J. Taiwan Inst. Chem. Eng.* 79, 55–59. doi: 10.1016/j.jtice.2017.05.035
- You, S. J., Kim, Y. T., and Park, E. D. (2014). Liquid-phase dehydration of D-xylose over silica-alumina catalysts with different alumina contents. *React. Kinet. Mech. Cat.* 111, 521–534. doi: 10.1007/s11144-013-0655-1
- Zhang, J., Zhuang, J., Lin, L., Liu, S., and Zhang, Z. (2012). Conversion of D-xylose into furfural with mesoporous molecular sieve MCM-41 as catalyst and butanol as the extraction phase. *Biomass Bioenergy* 39, 73–77. doi: 10.1016/j.biombioe.2010.07.028
- Zhang, L., Xi, G., Chen, Z., Jiang, D., Yu, H., and Wang, X. (2017b). Highly selective conversion of glucose into furfural over modified zeolites. *Chem. Eng. J.* 307, 868–876. doi: 10.1016/j.cej.2016.09.001
- Zhang, L., Xi, G., Zhang, J., Yu, H., and Wang, X. (2017a). Efficient catalytic system for the direct transformation of lignocellulosic biomass to furfural and 5-hydroxymethyl furfural. *Bioresour. Technol.* 244, 656–661. doi: 10.1016/j.biortech.2016.11.097
- Zhang, L., Yu, H., Wang, P., Deng, H., and Peng, X. (2013). Conversion of xylan, D-xylose and lignocellulosic biomass into furfural using AlCl₃ as catalyst in ionic liquid. *Bioresour. Technol.* 130, 110–116. doi: 10.1016/j.biortech.2012.12.018
- Zhang, T., Kumar, R., and Wyman, C. E. (2013). Enhanced yields of furfural and other products by simultaneous solvent extraction during thermochemical treatment of cellulosic biomass. *RSC Adv.* 3, 9809–9819. doi: 10.1039/c3ra41857j

- Zhang, T., Li, W., Xu, Z., Liu, Q., Ma, Q., Jameel, H., et al. (2016). Catalytic conversion of xylose and corn stalk into furfural over carbon solid acid catalyst in γ -valerolactone. *Bioresour. Technol.* 209, 108–114. doi: 10.1016/j.biortech.2016.02.108
- Zhao, Y., Lin, H., and Wang, S. (2017). Enhancement of furfural formation from C5 carbohydrate by NaCl in a green reaction system of CO₂-water-isopropanol. *Energy Sci. Eng.* 5, 208–216. doi: 10.1002/ese3.173
- Zhu, Y., Li, W., Lu, Y., Zhang, T., Jameel, H., Chang, H.-H., et al. (2017). Production of furfural from xylose and corn stover catalyzed by a novel carbon solid acid in γ -valerolactone. *RSC Adv.* 7, 29916–29924. doi: 10.1039/c7ra03995f

Conflict of Interest Statement: The authors declare that the research was conducted in the absence of any commercial or financial relationships that could be construed as a potential conflict of interest.

Copyright © 2018 Delbecq, Wang, Muralidhara, El Ouardi, Marlair and Len. This is an open-access article distributed under the terms of the Creative Commons Attribution License (CC BY). The use, distribution or reproduction in other forums is permitted, provided the original author(s) and the copyright owner are credited and that the original publication in this journal is cited, in accordance with accepted academic practice. No use, distribution or reproduction is permitted which does not comply with these terms.



Mechanocatalytic Depolymerization of Cellulose With Perfluorinated Sulfonic Acid Ionomers

Ayman Karam^{1,2†}, Prince N. Amaniampong^{1†}, José M. García Fernández³, Claudio Oldani⁴, Sinisa Marinkovic⁵, Boris Estrine⁵, Karine De Oliveira Vigier^{1,2} and François Jérôme^{1,2*}

¹ INCREASE (FR Centre National De La Recherche Scientifique 3707), ENSIP, Poitiers, France, ² Institut de Chimie des Milieux et Matériaux de Poitiers, Université de Poitiers, Centre National de la Recherche Scientifique, ENSIP, Poitiers, France,

³ Instituto de Investigaciones Químicas, CSIC—University of Sevilla, Sevilla, Spain, ⁴ Solvay Speciality Polymers, Bollate, Italy,

⁵ ARD-Agro-Industrie Recherches et Développements, Green Chemistry Department, Route de Bazancourt, Pomacle, France

OPEN ACCESS

Edited by:

Konstantinos Triantafyllidis,
Aristotle University of Thessaloniki,
Greece

Reviewed by:

Rafael Luque,
Universidad de Córdoba, Spain
Estelle Metay,
UMR5246 Institut de Chimie et
Biochimie Moléculaires et
Supramoléculaires (ICBMS), France
Yanlong Gu,
Huazhong University of Science and
Technology, China

*Correspondence:

François Jérôme
francois.jerome@univ-poitiers.fr

[†]These authors have contributed
equally to this work.

Specialty section:

This article was submitted to
Green and Sustainable Chemistry,
a section of the journal
Frontiers in Chemistry

Received: 22 December 2017

Accepted: 06 March 2018

Published: 22 March 2018

Citation:

Karam A, Amaniampong PN, García
Fernández JM, Oldani C,
Marinkovic S, Estrine B, De Oliveira
Vigier K and Jérôme F (2018)
Mechanocatalytic Depolymerization of
Cellulose With Perfluorinated Sulfonic
Acid Ionomers. *Front. Chem.* 6:74.
doi: 10.3389/fchem.2018.00074

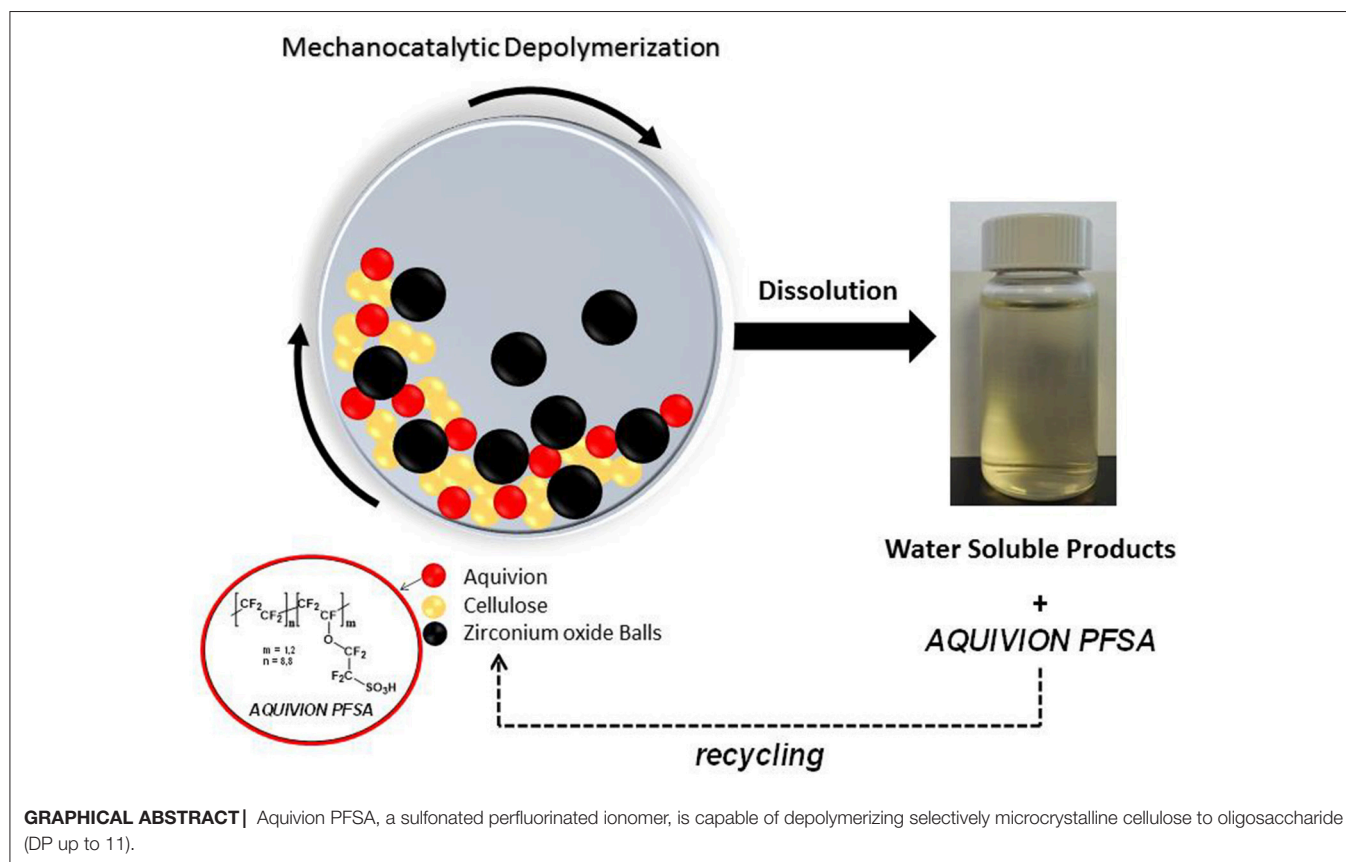
Here, we investigated that the mechanocatalytic depolymerization of cellulose in the presence of Aquivion, a sulfonated perfluorinated ionomer. Under optimized conditions, yields of water soluble sugars of 90–97% were obtained using Aquivion PW98 and PW66, respectively, as a solid acid catalyst. The detailed characterization of the water soluble fraction revealed (i) the selective formation of oligosaccharides with a DP up to 11 and (ii) that depolymerization and reversion reactions concomitantly occurred during the mechanocatalytic process, although the first largely predominated. More importantly, we discussed on the critical role of water contained in Aquivion and cellulose on the efficiency of the mechanocatalytic process.

Keywords: cellulose, depolymerization, mechanocatalysis, Aquivion, biomass

INTRODUCTION

With the transition of our society to a more sustainable development, the manufacture of chemicals, and fuels from renewable feedstocks has become a priority (Huber et al., 2006; Corma et al., 2007; Dhepe and Fukuoka, 2008; Rinaldi and Schüth, 2009a,b; Bozell and Petersen, 2010; Climent et al., 2011; Van de Vyver et al., 2011; Zhou et al., 2011; Gallezot, 2012; Luterbacher et al., 2014; Yabushita et al., 2014; Wang et al., 2015). In this context, due to its low cost, large availability and non-edibility, cellulose, a biopolymer made of β -1,4 linked D-glucose units, represents an attractive raw material. However, cellulose is highly recalcitrant to chemical processing due to the existence of a robust hydrogen bond network, both intrachain between glucose monomers in a single polymer strand and interchain between adjacent polymer chains, van der Waals interaction and electronic effects (Klemm et al., 2005; Shen and Gnanakaran, 2009; Siró and Plackett, 2010; Moon et al., 2011), which protect the glycosidic bond against hydrolysis, a pre-requisite step for the conversion of cellulose to soluble products. Hence, in many cases, the hydrolysis of cellulose requires high temperature or pressure, which leads to the concomitant formation of unwanted byproducts and thus to tedious work-up procedures.

Recently, mechanocatalytic depolymerization of lignocellulosic biomass has emerged as a contemporary frontier in biorefining (Zakrzewska et al., 2010; Groote et al., 2013; Zhang and Jérôme, 2013; Kåldström et al., 2014; Kaufman Rechulski et al., 2015). This technology utterly overcomes the challenges and drawbacks posed by the recalcitrance of lignocellulose, in particular thanks to a synergistic effect between mechanical forces and catalysis (Beyer and Clausen-Schaumann, 2005; Barraud et al., 2008; Carrasquillo-Flores et al., 2013). Although the use of milling for altering the behavior of cellulose has been an old-age practice, as well as the influence



of mechanical grinding on the reactivity of cellulose, the mechanocatalytic depolymerization of cellulose has garnered momentum in recent years (Hick et al., 2010; Meine et al., 2012). Mechanical forces provide energy to alter the crystalline structure and to reduce the particle size of cellulose. More importantly, it also changes the conformation of cellulosic chains and that of the glucose units, thereby lowering the *exo*-anomeric effect responsible to a large extent for the high stability of the β -1,4 glycosidic bond in cellulose (Hick et al., 2010; Carrasquillo-Flores et al., 2013; Loerbroeks et al., 2013; Schmidt et al., 2016). Hence, by combining mechanical forces and an acid catalyst, cellulose was depolymerized in a large extent to water-soluble products that can be further processed into other valuable platform chemicals (Hick et al., 2010; Kaldstrom et al., 2014; Schuth et al., 2014; Kaufman Rechulski et al., 2015). In comparison to the classical depolymerization of cellulose in acidic water, the activation energy barrier associated to the mechanocatalytic depolymerization was reduced by 66%, highlighting the synergistic effect between mechanical forces and catalysis (Kaufman Rechulski et al., 2015). In addition, in contrast to the classical ball-milling of cellulose, the overall energy required for the mechanocatalytic depolymerization of cellulose is much lower thanks to much shorter reaction times (2–6 h, depending on the milling mode, vs. 24–48 h for classical ball-milling).

For an effective mechanocatalytic depolymerization of cellulose, the targeted catalyst must be mechanically robust,

and possesses sites that are physically accessible and chemically active. Planetary mills, shaker mills, attrition mills, and rolling mills are few examples of mills that promote an intimate contact between catalysts and cellulose during mechanocatalysis processes (Schell and Harwood, 1994; Suryanarayana, 2001; Esteban and Carrasco, 2006; Bitra et al., 2009). Recently, Rinaldi and Schuth reported the mechanocatalytic depolymerization of cellulose in the presence of about 10 wt% of sulfuric acid (Schuth et al., 2014). Remarkably, about 90% of cellulose was converted to a water-soluble fraction, which is composed of low molecular weight oligosaccharides with a degree of polymerization in a window 1–7. One drawback associated to this pathway is the removal of sulfuric acid at the end of the mechanocatalytic process, which is a tedious step unless the resulting low molecular weight oligosaccharides are further processed through an acid-catalyzed reaction. Blair and co-workers reported that water-soluble products can be obtained in good yields (~70–80%) upon ball milling of cellulose in the presence of inorganic solid acids, particularly dealuminated kaolinite (Hick et al., 2010). It was observed that kaolinite caused a rapid depolymerization of cellulose thanks to its exfoliation during the milling. However, the selectivity to low molecular weight oligosaccharides was lower than in the case of H_2SO_4 due to the side formation of levoglucosane and brown colored chemicals, presumably humins or furanic derivatives (Hick et al., 2010; Shrotri et al., 2013).

Recently, we reported that cellulose can be depolymerized to low molecular weight oligosaccharides by milling cellulose with Aquivion PW98, a strongly acidic perfluorinated sulfonic acid ionomer ($H_0 = -12$, similar to H_2SO_4) (Karam et al., 2017). It was shown that Aquivion PW98 was chemically and mechanically resistant to the milling, permitting its long term recycling without altering its performances. In this article, we investigate the effect of the proton loading, stirring rate and Aquivion/cellulose mass ratio on the mechanocatalytic process. In particular, we point out the critical effect of water, even in trace amount, on the depolymerization rate of cellulose.

MATERIALS AND METHODS

Reagents

Microcrystalline cellulose (Avicel PH200, FMC Biopolymer) was utilized to investigate the performance of different solid catalysts.

Catalyst Synthesis and Mechanocatalytic Depolymerization of Cellulose

Catalyst Synthesis

SBA-15- SO_3H catalyst was prepared following a reported procedure (Karam et al., 2007). In a typical synthesis process, pluronic (4 g) was dissolved in 125 g of aqueous HCl (1.9 M) and stirred at room temperature. The solution was then heated at 40°C before addition of 7.7 g (0.0369 mol) of TEOS. After stirring for 45 min, MPTMS (0.8 g, 0.0041 mol) and 0.0369 mol of 35% H_2O_2 was added. The solution was then stirred for 24 h at 40°C and aged into a teflon autoclave for an additional 24 h at 100°C. The resulting solid was finally collected by filtration and thoroughly washed with water. The recovered SBA-15- SO_3H was dried in an oven at 50°C for 18 h.

CMK-3- SO_3H was synthesized *via* a reported procedure by Jun et al. (2000). Typically, the calcined SBA-15 was impregnated with aqueous solution of sucrose containing sulfuric acid, 1 g of SBA-15 was added to a solution obtained by dissolving 1.25 g of sucrose and 0.14 g of H_2SO_4 in 5 g of H_2O . The mixture was placed in a drying oven for 6 h at 373 K, and subsequently the oven temperature was increased to 433 K and maintained there for 6 h. The sample turned dark brown or black during the treatment in the oven. The silica sample, containing partially polymerized and carbonized sucrose at the present step, was treated again at 373 and 433 K using the same drying oven after the addition of 0.8 g of sucrose, 0.09 g of H_2SO_4 , and 5 g of H_2O . The carbonization was completed by pyrolysis with heating to typically 1173 K under vacuum. The carbon—silica composite obtained after pyrolysis was washed with 1 M NaOH solution (50 vol % ethanol—50 vol % H_2O) twice at 373 K or 5 wt % hydrofluoric acid at room temperature, to remove the silica template. The template-free carbon product thus obtained was filtered, washed with ethanol, and dried at 393 K. Thereafter, the recovered mesoporous carbon (so-called CMK-3) was suspended in concentrated H_2SO_4 (1 g of solid per 20 mL of acid) and stirred overnight. The CMK-3- SO_3H was washed several times with distilled water and then dried in an oven at 60°C overnight.

Aquivion PW66, PW79, PW87, and PW98 were used without further pretreatment as received from Solvay Specialty Polymers.

Mechanocatalytic Depolymerization of Cellulose

Various amounts of cellulose and catalyst were ground using a planetary ball-mill (Retsch MP100). The mixture of catalyst and cellulose were ground in a 125 mL bowl made of Zirconium Oxide, utilizing 20 of 10 mm balls made of the same material as the milling bowl. The experiments were performed at desired rate for a desired time as described in the main manuscript for each conditions investigated.

Determination of Solubility

After each milling, the milled mixture of cellulose and catalyst was recovered. The determination of solubility involved three parts, dispersion, filtration, and drying. The dispersion is carried out in a 20 mL flacon, weighing 300 mg of the solid mixture and 20 mL distilled water, stirring and leaving it in an ultrasonic bath for 2 h. The mixture is filtered through a 47 mm Millipore Pyrex Filter Holder; the PTFE filter has a pore size of 0.22 μm . The filter containing the solid after filtration is placed in a petri dish in the oven at 60°C overnight. The final mass is measured by the difference between the filter containing the dry solid at ambient temperature and the initial mass of the filter.

RESULTS AND DISCUSSIONS

Aquivion PW98, sulfonated SBA-15 and sulfonated mesoporous carbon (CMK-3- SO_3H) were either synthesized, or purchased, and initially screened as potential solid acid catalysts for the effective depolymerization of cellulose *via* ball-milling. More information on these solid acid catalysts are provided in the supporting information (SI). For starting experiments, 1 g of cellulose was mixed with 0.5 g of solid acid catalyst and stirred at 400 rpm in a planetary ball-mill for 24 h. The influence of experimental parameters such as the cellulose/catalyst mass ratio, stirring rate or reaction time is discussed later. The mechanocatalytic process is described in detail in the supporting information (section Introduction), and a schematic representation is shown in **Scheme 1**.

A < 5% solubility was observed when microcrystalline cellulose (MCC) was ball-milled for 24 h without any catalyst (**Table 1**, entry 1), in line with literature reported investigations (Meine et al., 2012). Treatment of neat MCC in a planetary ball mill in the presence of different solid acid catalysts remarkably improved the dissolution of the resulting product in water, showing the significance of intrinsic acid properties of solid acid catalysts in cleaving the β -1,4 glycosidic bonds in cellulose structures during the milling (**Table 1**). More information on the structure of products formed are provided at the end of the article.

Aquivion PW98 catalyst led to the highest MCC solubility in water (~80%) followed by CMK-3- SO_3H (87%) and SBA- SO_3H (60%) (**Table 1**, entries 2–4). In our planetary ball-mill, kaolinite was found the least performant catalyst, leading to a product with a water solubility of only 50% (**Table 1**, entry 5). A significant difference of performance between the different tested Aquivion catalysts was observed (**Table 1**, entries 2, 6–8). The best result was obtained with Aquivion PW66 (~99%) followed by PW98 (90%), PW87 (80%), and PW 79 (32%). Interestingly, there is

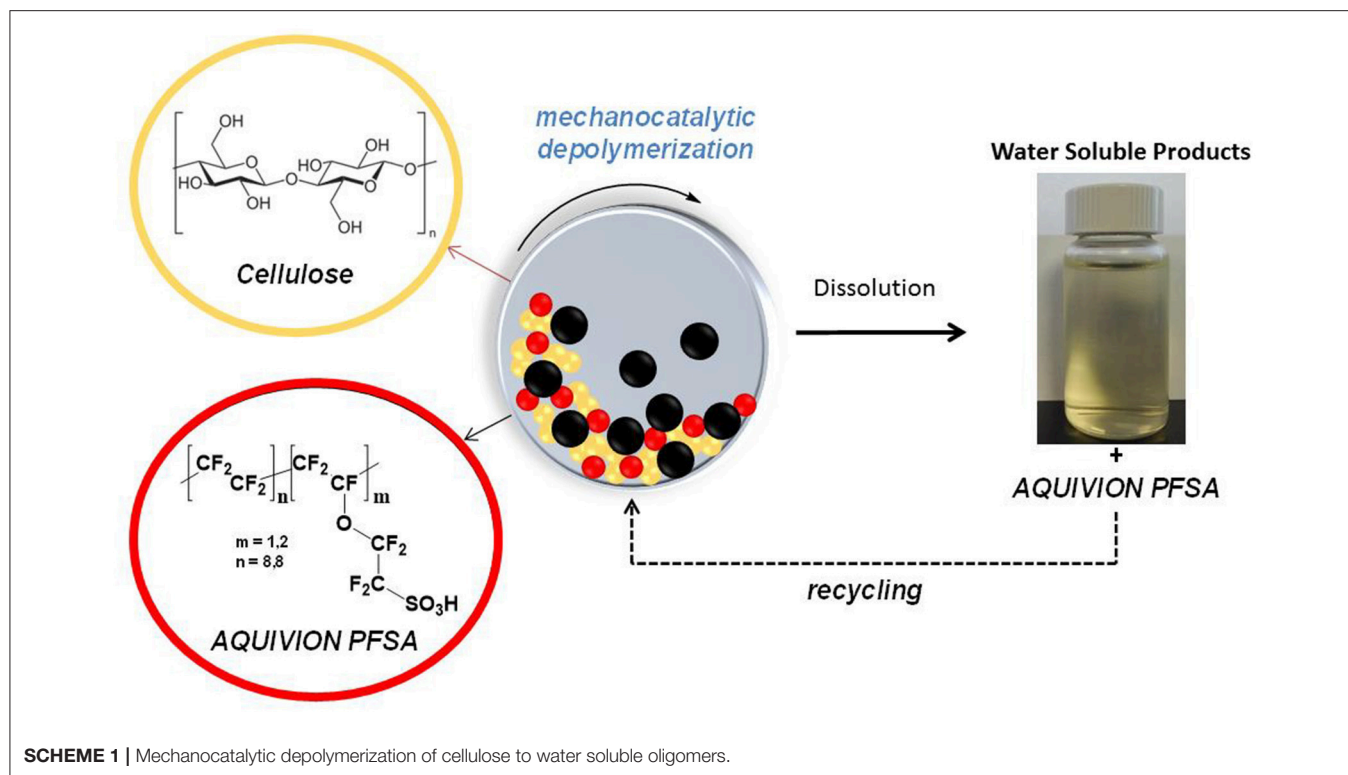


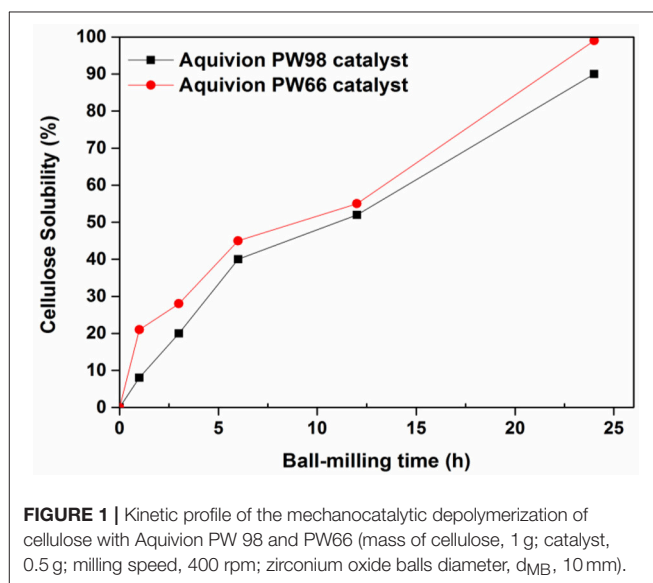
TABLE 1 | Mechanocatalytic depolymerization of cellulose in the presence of different solid acid catalysts^a.

Entry	Catalyst	H ⁺ exchange capacity (mmol/g)	Solubility (%) ^b
1	Blank	—	<5
2	Aquivion PW98	1.0	90
3	SBA-SO ₃ H	0.2	60
4	CMK-3-SO ₃ H	0.7	87
5	Kaolinite (KGa-2)	—	50
6	Aquivion PW66	1.45	99
7	Aquivion PW79	1.26	32
8	Aquivion PW87	1.15	80

^a Reaction conditions: Mass of Cellulose, 1 (g); Mass Catalyst, 0.5 (g); 400 rpm, Ball-milling time, 24 h; 20 Zirconium Oxide-balls $d_{MB} = 10$ mm; ^b $\pm 8\%$.

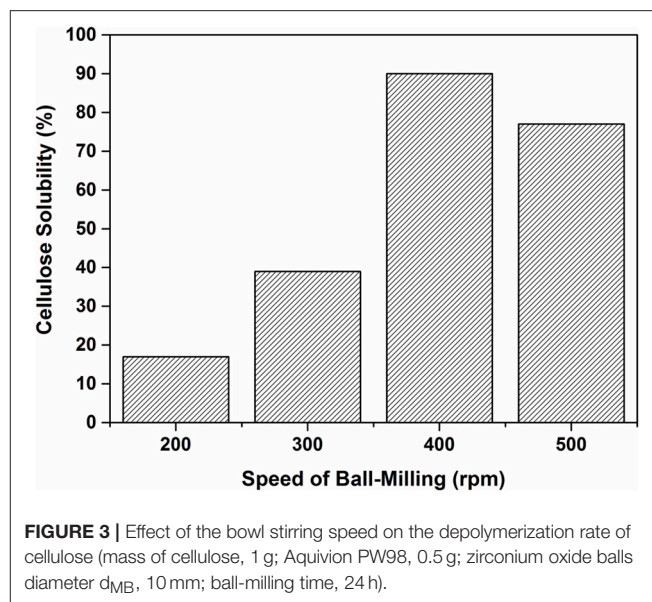
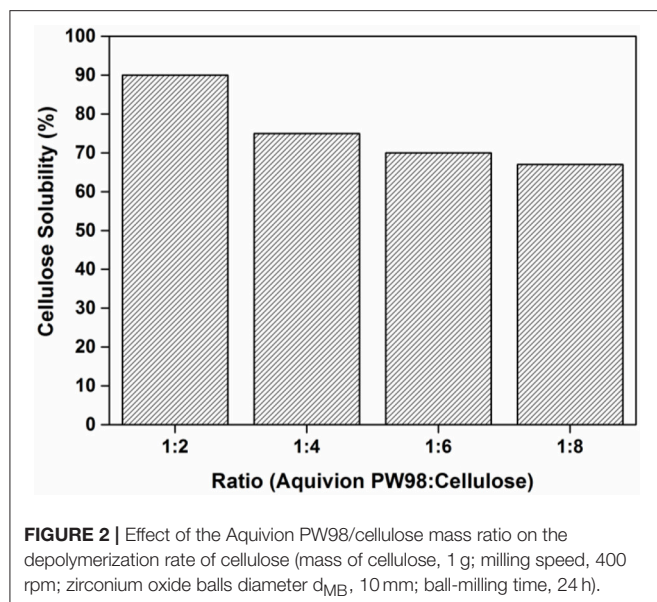
no correlation between the proton loading of Aquivion samples and their efficiencies in the mechanocatalytic depolymerization of cellulose (Table 1, entries 2, 6–8). This result prompted us to investigate the humidity content of all the Aquivion catalysts used in this investigation, which will be discussed later in this manuscript.

Next, the effect of ball-milling time over the most active solid catalysts (Aquivion PW66 and PW98) identified in our preliminary investigations on the production of water soluble products from MCC was investigated. As shown in Figure 1, the solubility of ball-milled MCC increased markedly with ball-milling time, reaching a maximum of 90 and 99% within 24 h with Aquivion PW98 and PW66, respectively. Although both



Aquivion samples have a different proton loading (Table 1), Aquivion PW66 and PW98 exhibited similar kinetic profiles, suggesting that the by—SO₃H groups of Aquivion does not directly govern the kinetic of the reaction.

To support this hypothesis, the amount of cellulose was kept constant (1 g) while varying the amount of Aquivion PW98 (from 500 to 125 mg) during the ball-milling. It corresponds to a variation of the Aquivion PW98/cellulose mass ratio from 1:2 to



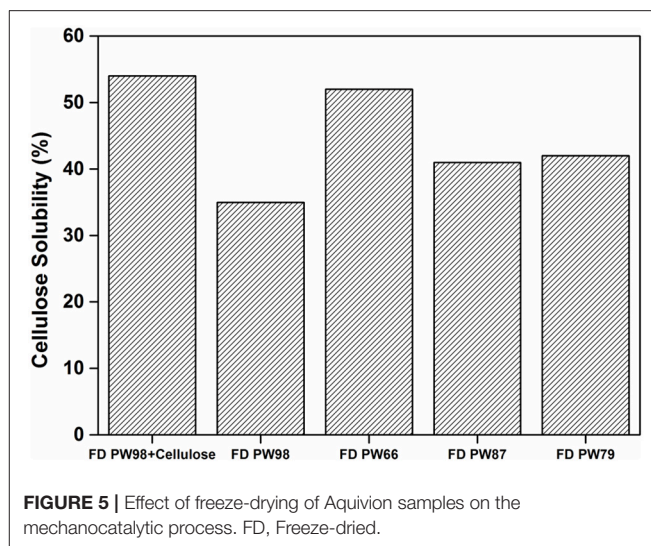
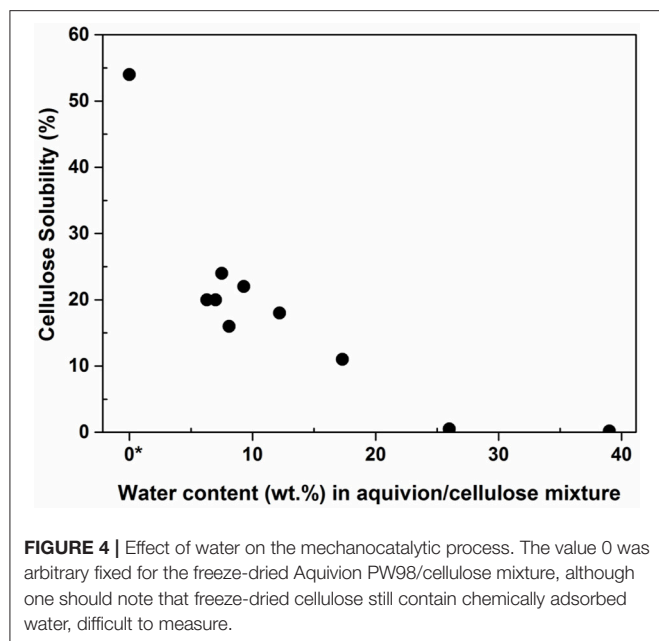
1:8 (**Figure 2**). Interestingly, the water solubility of MCC after the mechanocatalytic reaction did not differ dramatically between both assays, decreasing only from 90 to 70% upon moving from a 1:2 to a 1:8 Aquivion PW98/cellulose mass ratio, after 24 h of ball-milling. Altogether, these results strongly suggest that the depolymerization rate of cellulose under these conditions is not catalytically controlled and that mechanical forces probably play a more important role.

To further substantiate our assumption, the influence of the ball-milling speed in the process was also studied (**Figure 3**). During ball-milling, an increase in rotational speed leads to a subsequent rise in apparent energy due to the effective kinetic energy produced as a result of the frequent collisions of the balls between themselves and also between the balls and walls of the reactor. Working at a milling speed of 200 rpm led to a solubility of ~17% after 24 h, which increased by more than 2-folds (38%) when the milling speed was further switched to 300 rpm (**Figure 3**). At 400 rpm, a striking increase in solubility (90%) was achieved. These results clearly demonstrate that the reaction kinetic is mostly governed by mechanical forces i.e., friction, collisions, shearing, etc. Nonetheless, when the milling speed was further increased to 500 rpm, a reduction of solubility was observed (from 90% at 400 rpm to 77% at 500 rpm). At 500 rpm, colored tar-like insoluble products were formed leading to a decrease in solubility of cellulose after the mechanocatalytic process, due to excessive energy input in this case.

Assuming that mechanical forces have a strong impact on the depolymerization rate of cellulose, it occurred to us that the water content of Aquivion PFSA and cellulose will impact the mechanocatalytic process in a significant way, in particular by buffering the mechanical forces. Previously, it has been well-documented that the presence of a liquid, even in trace amount, dramatically impacts a mechanochemical process, a phenomenon known as liquid-assisted grinding (Käldström

et al., 2014). Aquivion PW98 and cellulose contained 7 and 6 wt% of water, respectively [i.e., 6.3 wt% of water for the Aquivion PW98/cellulose mixture (0.5:1)]. To assess the role of water, the mixture Aquivion PW98/cellulose was next freeze-dried before the mechanocatalytic process. The reaction was stopped after only 3 h of milling to clearly highlight the role of water. Remarkably, an increase in the mechanocatalytic depolymerization rate was observed and 55% of water soluble products were obtained after only 3 h of ball-milling vs. 20% without freeze-drying. An increase of the mechanocatalytic time from 3 to 6 h led to a nearly complete dissolution of cellulose (90%), i.e., a reduction of the mechanocatalytic treatment time by 4 in comparison to non-freeze dried samples (**Figure S1**). Then, water was progressively added in order to monitor its effect on the milling. As shown in **Figure 4**, a sharp drop in the reaction product solubility was observed after 3 h of milling with aliquot amounts of H_2O , further stressing the important role played by water on the mechanocatalytic process.

When only Aquivion PW98 was freeze-dried, a slightly lower solubility of cellulose of 40 % was observed (vs. 54% for the freeze-dried Aquivion PW98/cellulose mixture), indicating that water contained in cellulose was also impacting the mechanocatalytic process to some extent (**Figure 5**; details of water content estimation is provided in SI, section Materials and Methods). Aquivion PFSA PW98, PW66, PW87 have a similar water content of 7% and thus similarly behaved during the mechanocatalytic depolymerization of cellulose. In contrast, Aquivion PFSA PW79 has a water content of 22 wt% and was significantly less active than other Aquivion samples, providing a cellulose depolymerization product with a water solubility of only 32% after 24 h of ball-milling (**Table 1**). However, when Aquivion PW79 was freeze-dried before the mechanocatalytic process, it behaved similarly than the other Aquivion samples (40% of cellulose was solubilized), further demonstrating the important role played by water (**Figure 5**). Here again, once



freeze-dried, no significant difference of performance, in terms of depolymerization rate of cellulose, was observed between all Aquivion samples, although they have different proton loadings. These results confirm that the kinetics of the mechanocatalytic process is not controlled by the catalyst but mainly by mechanical forces, that can be tuned by the rotational stirring rate or the presence of water.

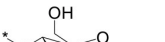
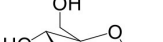
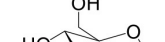
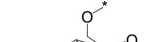
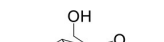
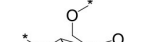
The water soluble products were analyzed in detail by mass spectrometry (MS), gas chromatography (GC) and high performance anionic-exchange chromatography with pulse amperometric detection (HPAEC-PAD). Consistently with previous reports using H_2SO_4 as an acid catalyst, Aquivion catalysts yielded oligosaccharides with a degree of polymerization (DP) up to 11 (MS). Monosaccharides accounted for 13% of the water soluble fraction, formed mainly by free D-glucose (96%) and minor proportions of 1,6-anhydro-D-glucopyranose (levoglucosane, 3%) and 1,5-anhydro-D-glucufuranose (1%) (GC; sample derivatization by sequential oximation-trimethylsilylation reactions as described in the SI). Disaccharides and oligosaccharides with DP 3–11 accounted for 21 and 65% of the water soluble product, respectively (Table 2). No oxidation or degradation product was detected, indicating that the mechanocatalytic process with Aquivion PW98 was fully selective to water soluble oligosaccharides. The disaccharide fraction was analyzed in depth using authentic commercially available standards (GC; sample derivatization by sequential oximation-acetylation reactions as described in the SI). All types of α/β positional regioisomers, namely (1 \rightarrow 1)-, (1 \rightarrow 2)-, (1 \rightarrow 3)-, (1 \rightarrow 4)-, and (1 \rightarrow 6)-linked glucobioses, were detected, with the β -(1 \rightarrow 4) linkage (cellobiose) being dominant (79.5% of the disaccharide fraction). Considering that cellulose exclusively contains β -(1 \rightarrow 4) glycosidic bonds, these results indicate that cellulose depolymerization during the mechanocatalytic process with

Aquivion PW98 proceeds, to some extent, with concomitant self-glycosylation (reversion) reactions, in line with previous reports from Schüth and Beltramini (Meine et al., 2012; Shrotri et al., 2013).

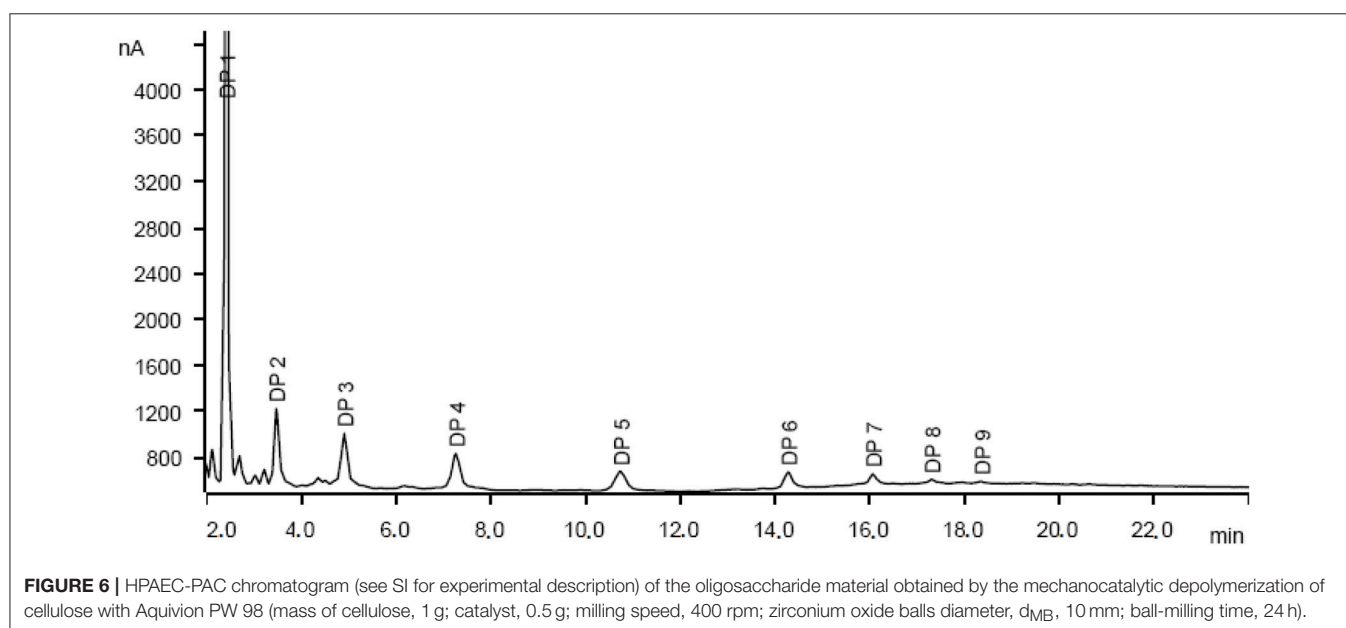
In principle, cross-glycosylation reactions between free glucose and cello-oligosaccharides or between different cello-oligosaccharides could lead to the formation of branched oligosaccharides. To assess the degree of branching, the mixture of oligosaccharides was subjected to a methylation (MeI/NaOH) (Ciucanu and Costello, 2003)—hydrolysis (TFA, 120 °C)—deuteroboration (NaBD_4)—acetylation ($\text{Ac}_2\text{O/TFA}$) sequence (Kim et al., 2006) prior to GC-MS analysis. This protocol affords the corresponding alditols labeled with deuterium at C-1, methylated at non-glycosylated positions and bearing acetyl groups at positions that were glycosylated in the starting oligosaccharide chain, which can be unequivocally assigned from the corresponding fragmentation patterns in MS by comparison with authentic standards (Sasaki et al., 2005). The data indicated that terminal and monoglycosylated residues accounted for more than 96% of the glucosyl units, the majority of the inner chain glucose units were glycosylated at position O-4 as in cellulose (51.8% of total glucose). Only a small proportion (3.8%) of the inner residues are doubly glycosylated at positions O-4 and O-6, supporting that most of the oligosaccharide material keep the (1 \rightarrow 4)-glycosylation pattern of the parent polysaccharide. Cellulose depolymerization is therefore the predominant reaction occurring under these conditions. Indeed, the HPAEC-PAD chromatogram obtained from the crude reaction material showed a profile compatible with the major presence of cello-oligosaccharides of increasing DP. Quantitative analysis indicated that over 93% of the oligosaccharide material is comprised in the DP 2-to-6 fraction (Figure 6).

Noteworthy, the as-obtained oligosaccharides were highly hygroscopic. Water playing an important role in the reaction, the mechanocatalytic process was additionally performed under an argon atmosphere to assess a possible negative effect of

TABLE 2 | Relative composition of oligosaccharides linkages recovered after mechanocatalytic depolymerization of cellulose with Aquivion PW98.

Glycosidic bond (%)						Branching pattern (%)	
							
1→4	1→2	1→3	1→6	1→1'	1→4→6		
79.5	3	3	13	1.5	6		
α	β	α	β	α,α'	α,β'	–	–
6.5 ^a	73 ^b	1.7 ^c	1.3 ^d	2.3 ^e	0.7 ^f	6.5 ^g	6.6 ^h
				1 ⁱ	0.5 ^j		

^amaltose; ^bcellobiose; ^ckojibiose; ^dlaminarabiose; ^enigerose; ^fsoforose; ^gisomaltose; ^hgentiobiose; ⁱtrehalose; ^jneotrehalose.



water coming from the hygroscopicity of oligosaccharides during the milling. No significant change was observed as compared with the mechanocatalytic process conducted under air, however, suggesting that mainly water initially contained in cellulose and Aquivon was responsible for the buffering of mechanical forces. This is an important point as regards industrial perspectives. Indeed, working in air will reduce the complexity of the system leading a more robust and lean process easier to be performed.

CONCLUSIONS

We have demonstrated that Aquivion, a sulfonated perfluorinated ionomer, was capable of promoting the selective depolymerization of cellulose to afford water-soluble oligosaccharides with a DP up to 11. The detailed characterization of the water soluble fraction revealed that depolymerization and reversion reactions concomitantly occurred during the mechanocatalytic process, although the first largely predominated. The kinetic of the reaction is governed by mechanical forces, i.e., friction, collisions, shearing, etc. More

importantly, we discovered that water contained in Aquivion and cellulose lowered the efficiency of the mechanocatalytic process, presumably by buffering mechanical forces. The plasticization effect of water in Aquivion is known although never reported in this frame. A removal of water before the mechanocatalytic process has permitted reducing the milling time. Under optimized conditions, yields of water soluble sugars of up to 90 and 97% were achieved using Aquivion PW98 and PW66, respectively. In comparison to H_2SO_4 which is commonly used in such application, Aquivion is easily separated from soluble sugars (dissolution of sugars in water and filtration of Aquivion), thus opening interesting perspectives to investigate the physicochemical properties of the as-obtained oligosaccharides or to further chemically process these sugars into specialty chemicals.

AUTHOR CONTRIBUTIONS

AK and PA performed the mechanocatalytic depolymerization of cellulose. KD and JG were in charge of the characterization

of water soluble products obtained after the mechanocatalytic process. BE and SM were in charge of the critical role of water. CO was in charge of Aquivion catalysts (preparation, proton loading, water content, etc.). FJ supervised the work.

ACKNOWLEDGMENTS

Authors are grateful to the CNRS, the University of Poitiers, the Ministry of Research and the Région Nouvelle Aquitaine for their financial support. The International Consortium on Eco-conception and Renewable Resources (FR CNRS INCREASE 3707) and the chair TECHNOGREEN are also acknowledged for their funding. Authors are also grateful to the COST Action

FP1306 in supporting interaction between team members and for fruitful discussions on catalysis, processes, and cellulosic waste. JG thank the Spanish Ministerio de Economía y Competitividad (MINECO; Contract No. CTQ2015-64425-C2-1-R) and the Junta de Andalucía (Contract No. FQM2012-1467) for financial support. Co-financing from the European Regional Development Funds (FEDER and FSE) is also acknowledged.

SUPPLEMENTARY MATERIAL

The Supplementary Material for this article can be found online at: <https://www.frontiersin.org/articles/10.3389/fchem.2018.00074/full#supplementary-material>

REFERENCES

- Barraud, E., Bégin-Colin, S., Le Caër, G., Barres, O., and Villieras, F. (2008). Mechanically activated solid-state synthesis of hafnium carbide and hafnium nitride nanoparticles. *J. Alloys Compd.* 456, 224–233. doi: 10.1016/j.jallcom.2007.02.017
- Beyer, M. K., and Clausen-Schaumann, H. (2005). Mechanochemistry: the mechanical activation of covalent bonds. *Chem. Rev.* 105, 2921–2948. doi: 10.1021/cr030697h
- Bitra, V. S., Womac, A. R., Chevanan, N., Miu, P. I., Igathinathane, C., Sokhansanj, S., et al. (2009). Direct mechanical energy measures of hammer mill comminution of switchgrass, wheat straw, and corn stover and analysis of their particle size distributions. *Powder Technol.* 193, 32–45. doi: 10.1016/j.powtec.2009.02.010
- Bozell, J. J., and Petersen, G. R. (2010). Technology development for the production of biobased products from biorefinery carbohydrates—the US department of energy's "Top 10" revisited. *Green Chem.* 12, 539–554. doi: 10.1039/B922014C
- Carrasquillo-Flores, R., Källdström, M., Schüth, F., Dumesic, J. A., and Rinaldi, R. (2013). Mechanocatalytic depolymerization of dry (ligno) cellulose as an entry process for high-yield production of furfurals. *ACS Catal.* 3, 993–997. doi: 10.1021/cs400133z
- Ciucanu, I., and Costello, C. E. (2003). Elimination of oxidative degradation during the per-O-methylation of carbohydrates. *J. Am. Chem. Soc.* 125, 16213–16219. doi: 10.1021/ja035660t
- Climent, M. J., Corma, A., and Iborra, S. (2011). Converting carbohydrates to bulk chemicals and fine chemicals over heterogeneous catalysts. *Green Chem.* 13, 520–540. doi: 10.1039/c0gc00639d
- Corma, A., Iborra, S., and Velty, A. (2007). Chemical routes for the transformation of biomass into chemicals. *Chem. Rev.* 107, 2411–2502. doi: 10.1021/cr050989d
- Dhepe, P. L., and Fukuoka, A. (2008). Cellulose conversion under heterogeneous catalysis. *ChemSusChem* 1, 969–975. doi: 10.1002/cssc.200800129
- Esteban, L. S., and Carrasco, J. E. (2006). Evaluation of different strategies for pulverization of forest biomasses. *Powder Technol.* 166, 139–151. doi: 10.1016/j.powtec.2006.05.018
- Gallezot, P. (2012). Conversion of biomass to selected chemical products. *Chem. Soc. Rev.* 41, 1538–1558. doi: 10.1039/C1CS15147A
- Groote, R., Jakobs, R. T., and Sijbesma, R. P. (2013). Mechanocatalysis: forcing latent catalysts into action. *Polym. Chem.* 4, 4846–4859. doi: 10.1039/c3py00071k
- Hick, S. M., Griebel, C., Restrepo, D. T., Truitt, J. H., Buker, E. J., Bylde, C., et al. (2010). Mechanocatalysis for biomass-derived chemicals and fuels. *Green Chemistry* 12, 468–474. doi: 10.1039/b923079c
- Huber, G. W., Iborra, S., and Corma, A. (2006). Synthesis of transportation fuels from biomass: chemistry, catalysts, and engineering. *Chem. Rev.* 106, 4044–4098. doi: 10.1021/cr068360d
- Jun, S., Joo, S. H., Ryoo, R., Kruk, M., Jaroniec, M., and Liu, Z., (2000). Synthesis of new, nanoporous carbon with hexagonally ordered mesostructure. *J. Am. Chem. Soc.* 122, 10712–10713. doi: 10.1021/ja002261e
- Källdström, M., Meine, N., Farès, C., Schüth, F., and Rinaldi, R. (2014). Correction: deciphering 'water-soluble lignocellulose' obtained by mechanocatalysis: new insights into the chemical processes leading to deep depolymerization. *Green Chem.* 16, 4994–4994. doi: 10.1039/C4GC90048K
- Karam, A., De Oliveira Vigier, K., Marinkovic, S., Estrine, B., Oldani, C., and Jérôme, F. (2017). Conversion of cellulose into amphiphilic Alkyl glycosides catalyzed by aquivion, a perfluorosulfonic acid polymer. *ChemSusChem* 10, 3604–3610. doi: 10.1002/cssc.201700903
- Karam, A., Gu, Y., Jérôme, F., Douliez, J.-P. and Barrault, J. (2007). Significant enhancement on selectivity in silica supported sulfonic acids catalyzed reactions. *Chem. Commun.* 2222–2224. doi: 10.1039/B702997G
- Kaufman Rechulski, M. D., Källdström, M., Richter, U., Schüth, F., and Rinaldi, R. (2015). Mechanocatalytic depolymerization of lignocellulose performed on hectogram and kilogram scales. *Indus. Eng. Chem. Res.* 54, 4581–4592. doi: 10.1021/acs.iecr.5b00224
- Kim, J. S., Reuhs, B. L., Michon, F., Kaiser, R. E., and Arumugham, R. G. (2006). Addition of glycerol for improved methylation linkage analysis of polysaccharides. *Carbohydr. Res.* 341, 1061–1064. doi: 10.1016/j.carres.2006.03.008
- Klemm, D., Heublein, B., Fink, H. P., and Bohn, A. (2005). Cellulose: fascinating biopolymer and sustainable raw material. *Angew. Chem. Int. Ed.* 44, 3358–3393. doi: 10.1002/anie.200460587
- Loerbroks, C., Rinaldi, R., and Thiel, W. (2013). The electronic nature of the 1, 4- β -glycosidic bond and its chemical environment: DFT insights into cellulose chemistry. *Chem. A Eur. J.* 19, 16282–16294. doi: 10.1002/chem.201301366
- Luterbacher, J., Alonso, D. M., and Dumesic, J. (2014). Targeted chemical upgrading of lignocellulosic biomass to platform molecules. *Green Chem.* 16, 4816–4838. doi: 10.1039/C4GC01160K
- Meine, N., Rinaldi, R., and Schüth, F. (2012). Solvent-free catalytic depolymerization of cellulose to water-soluble oligosaccharides. *ChemSusChem* 5, 1449–1454. doi: 10.1002/cssc.201100770
- Moon, R. J., Martini, A., Nairn, J., Simonsen, J., and Youngblood, J. (2011). Cellulose nanomaterials review: structure, properties and nanocomposites. *Chem. Soc. Rev.* 40, 3941–3994. doi: 10.1039/c0cs00108b
- Rinaldi, R., and Schüth, F. (2009a). Acid hydrolysis of cellulose as the entry point into biorefinery schemes. *ChemSusChem* 2, 1096–1107. doi: 10.1002/cssc.200900188
- Rinaldi, R., and Schüth, F. (2009b). Design of solid catalysts for the conversion of biomass. *Ener. Environ. Sci.* 2, 610–626. doi: 10.1039/b902668a
- Sassaki, G. L., Gorin, P. A., Souza, L. M., Czelusniak, P. A., and Iacomini, M. (2005). Rapid synthesis of partially O-methylated alditol acetate standards for GC-MS: some relative activities of hydroxyl groups of methyl glycopyranosides on Purdie methylation. *Carbohydr. Res.* 340, 731–739. doi: 10.1016/j.carres.2005.01.020
- Schell, D. J., and Harwood, C. (1994). Milling of lignocellulosic biomass. *Appl. Biochem. Biotechnol.* 45, 159–168. doi: 10.1007/BF02941795

- Schmidt, R., Fuhrmann, S., Wondraczek, L., and Stolle, A. (2016). Influence of reaction parameters on the depolymerization of H₂SO₄-impregnated cellulose in planetary ball mills. *Powder Technol.* 288, 123–131. doi: 10.1016/j.powtec.2015.11.002
- Schüth, F., Rinaldi, R., Meine, N., Käldestrom, M., Hilgert, J., and Rechulski, M. K. (2014). Mechanocatalytic depolymerization of cellulose and raw biomass and downstream processing of the products. *Cat. Today* 234, 24–30. doi: 10.1016/j.cattod.2014.02.019
- Shen, T., and Gnanakaran, S. (2009). The stability of cellulose: a statistical perspective from a coarse-grained model of hydrogen-bond networks. *Biophys. J.* 96, 3032–3040. doi: 10.1016/j.bpj.2008.12.3953
- Shrotri, A., Lambert, L. K., Tanksale, A., and Beltramini, J. (2013). Mechanical depolymerisation of acidulated cellulose: understanding the solubility of high molecular weight oligomers. *Green Chem.* 15, 2761–2768. doi: 10.1039/c3gc40945g
- Siró, I., and Plackett, D. (2010). Microfibrillated cellulose and new nanocomposite materials: a review. *Cellulose* 17, 459–494. doi: 10.1007/s10570-010-9405-y
- Suryanarayana, C. (2001). Mechanical alloying and milling. *Prog. Mater. Sci.* 46, 1–184. doi: 10.1016/S0079-6425(99)00010-9
- Van de Vyver, S., Geboers, J., Jacobs, P. A., and Sels, B. F. (2011). Recent advances in the catalytic conversion of cellulose. *ChemCatChem* 3, 82–94. doi: 10.1002/cctc.201000302
- Wang, J., Xi, J., and Wang, Y. (2015). Recent advances in the catalytic production of glucose from lignocellulosic biomass. *Green Chem.* 17, 737–751. doi: 10.1039/C4GC02034K
- Yabushita, M., Kobayashi, H., and Fukuoka, A. (2014). Catalytic transformation of cellulose into platform chemicals. *App. Cat. B* 145, 1–9. doi: 10.1016/j.apcatb.2013.01.052
- Zakrzewska, M. E., Bogel-Lukasik, E., and Bogel-Lukasik, R. (2010). Ionic liquid-mediated formation of 5-hydroxymethylfurfural– A promising biomass-derived building block. *Chem. Rev.* 111, 397–417. doi: 10.1021/cr100171a
- Zhang, Q., and Jérôme, F. (2013). Mechanocatalytic deconstruction of cellulose: an emerging entry into biorefinery. *ChemSusChem* 6, 2042–2044. doi: 10.1002/cssc.201300765
- Zhou, C.-H., Xia, X., Lin, C.-X., Tong, D.-S., and Beltramini, J. (2011). Catalytic conversion of lignocellulosic biomass to fine chemicals and fuels. *Chem. Soc. Rev.* 40, 5588–5617. doi: 10.1039/c1cs15124j

Conflict of Interest Statement: The authors declare that the research was conducted in the absence of any commercial or financial relationships that could be construed as a potential conflict of interest.

Copyright © 2018 Karam, Amaniampong, García Fernández, Oldani, Marinkovic, Estrine, De Oliveira Vigier and Jérôme. This is an open-access article distributed under the terms of the Creative Commons Attribution License (CC BY). The use, distribution or reproduction in other forums is permitted, provided the original author(s) and the copyright owner are credited and that the original publication in this journal is cited, in accordance with accepted academic practice. No use, distribution or reproduction is permitted which does not comply with these terms.



Fine-Tuned Enzymatic Hydrolysis of Organosolv Pretreated Forest Materials for the Efficient Production of Cellobiose

Anthi Karnaouri¹, Evangelos Topakas^{1,2}, Leonidas Matsakas¹, Ulrika Rova¹ and Paul Christakopoulos^{1*}

¹ Biochemical Process Engineering, Chemical Engineering, Department of Civil, Environmental and Natural Resources Engineering, Luleå University of Technology, Luleå, Sweden, ² Biotechnology Laboratory, Department of Synthesis and Development of Industrial Processes, School of Chemical Engineering, National Technical University of Athens, Athens, Greece

OPEN ACCESS

Edited by:

Konstantinos Triantafyllidis,
Aristotle University of Thessaloniki,
Greece

Reviewed by:

Antonella Amore,
National Renewable Energy
Laboratory (DOE), United States
Jasmina Nikodinovic-Runic,
University of Belgrade, Serbia

*Correspondence:

Paul Christakopoulos
paul.christakopoulos@ltu.se

Specialty section:

This article was submitted to
Green and Sustainable Chemistry,
a section of the journal
Frontiers in Chemistry

Received: 30 January 2018

Accepted: 04 April 2018

Published: 19 April 2018

Citation:

Karnaouri A, Topakas E, Matsakas L,
Rova U and Christakopoulos P (2018)
Fine-Tuned Enzymatic Hydrolysis of
Organosolv Pretreated Forest
Materials for the Efficient Production
of Cellobiose. *Front. Chem.* 6:128.
doi: 10.3389/fchem.2018.00128

Non-digestible oligosaccharides (NDOs) are likely prebiotic candidates that have been related to the prevention of intestinal infections and other disorders for both humans and animals. Lignocellulosic biomass is the largest carbon source in the biosphere, therefore cello-oligosaccharides (COS), especially cellobiose, are potentially the most widely available choice of NDOs. Production of COS and cellobiose with enzymes offers numerous benefits over acid-catalyzed processes, as it is milder, environmentally friendly and produces fewer by-products. Cellobiohydrolases (CBHs) and a class of endoglucanases (EGs), namely processive EGs, are key enzymes for the production of COS, as they have higher preference toward glycosidic bonds near the end of cellulose chains and are able to release soluble products. In this work, we describe the heterologous expression and characterization of two CBHs from the filamentous fungus *Thermothelomyces thermophila*, as well as their synergism with processive EGs for cellobiose release from organosolv pretreated spruce and birch. The properties, inhibition kinetics and substrate specific activities for each enzyme are described in detail. The results show that a combination of EGs belonging to Glycosyl hydrolase families 5, 6, and 9, with a CBHI and CBHII in appropriate proportions, can enhance the production of COS from forest materials, underpinning the potential of these biocatalysts in the production of NDOs.

Keywords: cellobiohydrolases, hydrolysis, enzymatic cocktail, cellobiose, experimental design, thermostable enzymes, prebiotics

INTRODUCTION

In food and nutraceutical industry, the development of compounds that have the potential to reduce disease risk and thereby enhance human health has attracted much interest. Currently, one of the main targets of research is the gastrointestinal tract and its resident microbiome (Cummings and Macfarlane, 1991). Diet-related modulations of this microflora offers promise for reducing pathogens/mediated gut disorders linked to a variety of chronic diseases, including obesity, type 2 diabetes, and cardiovascular diseases. This has resulted in the development of a prebiotic concept.

Prebiotics are dietary ingredients that are not digested and selectively promote the growth and the activity of the bacteria in the colon (Gibson and Roberfroid, 1995). The level of active prebiotics that can be obtained through the diet is too low to have a significant impact; therefore, a sustainable production of prebiotics with a defined action is to be preferred.

Non-digestible oligosaccharides (NDOs) are oligosaccharides with a degree of polymerization (DP) of 2–9 that are resistant to digestion by human gastric and pancreatic enzymes and seem to be preferred by the gut microbiota. NDOs, especially cellobiose, have attracted much attention since they have low calorific value (Livesey, 1990; Roberfroid et al., 1993), potential prebiotic effect and can add functionality to the food products (e.g., as rheology enhancers, bulking agents, stabilizers; Figueroa-González et al., 2011). The prebiotic potential of cellobiose has been investigated by *in vitro* fermentations in the presence of a human fecal inoculum, where it was shown to increase bifidobacteria, lactobacilli, and short chain fatty acids (SCFA); markers of a potentially beneficial effect in modulating the gut microbiome (van Zanten et al., 2012). Aside from a likely prebiotic candidate, cellobiose has been also used as a sweetener (Kulka and Ungureanu, 2017), a cosmetic additive in its acylated form (Franklin et al., 2002) or a building block in polymers (Berson et al., 2008). Cellobiose and other cello-oligosaccharides (COS) can be obtained by acid-based and enzyme-based hydrolysis of the insoluble cellulose. Enzymatic hydrolysis is considered more attractive due to the relatively mild reaction condition (less by-products) and the easier control of the polysaccharide cleavage breaking (less monomers). A consortium of enzymes is required for the degradation of cellulose, including *endoglucanases* (EG), *cellobiohydrolases* (CBH), and β -*glucosidases* (BGL). In addition, lytic polysaccharide monooxygenases (LPMOs) act in strong synergism with endoglucanases both for the release of neutral and oxidized sugars (Karnaouri et al., 2017). Based on the hydrolysis patterns for each catalytic reaction by cellulases, cellobiose is accumulated when BGL is not present.

CBHs are enzymes of pivotal importance for the cellobiose production, as they catalyze the hydrolysis of the β -1,4 bonds at the ends of the cellulose chains releasing mainly cellobiose. They are characterized as CBH I (glycoside hydrolase family 7; GH7) and CBH II (glycoside hydrolase family 6; GH6) and act on cellulose molecules from reducing and non-reducing ends, respectively. The enzymes belonging to each family possess a high identity degree of their amino acid sequence and common folding domains in their structural conformation. CBHII enzymes act through inversion of the anomeric configuration of the substrate, while CBHI enzymes usually retain the configuration (Schülein, 2000). The typical molecular structure for most fungal CBHs includes a core catalytic domain and a cellulose-binding module (CBM) joined by a flexible peptide linker (van Tilbeurgh et al., 1986; Gilkes et al., 1991) and are often glycosylated, involving both O- and N-linked carbohydrate structures (Maras et al., 1997; Hu et al., 2001). The ability of catalyzing successive cleavage of sugar bonds without detaching from the substrate, called *processivity*, is a common characteristic to CBHs and is considered to boost the catalytic efficiency of the enzyme when acting on substrates with high

crystallinity (Teeri, 1997). Structural studies of CBHs isolated from *Trichoderma reesei* have demonstrated that processivity is associated with the existence of a tunnel-shaped active site, where a single glucan can enter, and the cleavage occurs during its passage (Kurasin and Våljamäe, 2011). An exo–exo synergism between CBHI and CBHII that increases the saccharification yields has been reported (Medve et al., 1994).

EGs are also key enzymes for the production of COS in many ways. Firstly, a class of them, namely *processive*, that have higher preference toward glycosidic bonds near the end of cellulose chains, are able to release soluble COS (mainly C2 and C4) before detaching from the substrate (Wilson and Kostylev, 2012). In addition, individual cellulolytic activity of EGs has been related to rapid and efficient liquefaction of cellulose-rich lignocellulosic materials, such as wheat straw, under high dry matter loadings [19% (w/w) DM], which is of outmost importance in order to achieve high COS yields (Karnaouri et al., 2014). When CBHs act in concert with the EGs, hydrolysis yields increase drastically due to endo–exo synergy between two classes of the enzymes (Henrissat et al., 1985).

In the present work, we used CBHI and CBHII from *Thermothelomyces thermophila* cloned in *Pichia pastoris*, and tested them in optimized enzyme mixtures with the aim to maximize cellulose conversion into cellobiose, using organosolv pretreated spruce and birch. First, the optimal mixture that maximizes cellobiose production was identified by using different combinations of commercially available enzymes, two EGs and two CBHs. The optimal cocktails were identified via statistically-designed experiments based on cellobiose release. Subsequently, *Tt*CBH6 and *Tt*CBH7 were used to replace the CBHs in optimized combinations in order to evaluate the performance of these *in-house* produced enzymes and compare with that of commercially available CBHs.

MATERIALS AND METHODS

Enzymes and Chemicals

For the cloning of the CBHs genes, KOD Hot Start[®] DNA polymerase was purchased from Novagen (USA) and restriction enzymes were from TAKARA (Japan). Nucleospin Gel Clean-up and GeneJET Plasmid Miniprep kits were obtained from Macherey–Nagel (Germany) and Fermentas (USA), respectively. Barley β -glucan, xylooligosaccharides and mannoooligosaccharides were purchased from Megazyme, microcrystalline cellulose Avicel PH-101 was from Merck (Darmstadt, Germany) and D-cellobiose was from Fluka. 4-Nitrophenyl β -D-glucopyranoside, 4-Nitrophenyl β -D-lactopyranoside and 4-methylumbelliferyl β -D-cellobioside were from Sigma–Aldrich. All other chemicals used in this study were of analytical grade. Phosphoric acid swollen cellulose (PASC) was prepared from Avicel, following the protocol initially described by Wood (1988).

For the cellobiose production experiments, endo-1,4- β -D-glucanase (EG7) and cellobiohydrolase I (CBH7) from *Trichoderma longibrachiatum*, endo-1,4- β -D-glucanase (EG5) from *Talaromyces emersonii* and cellobiohydrolase II (CBH6) from microbial source were from Megazyme. Cellulase 6A (EG6)

from *Podospora anserina*, Cellulase 9A (EG9) from *Clostridium thermocellum* and Cellulase 12B (EG12) from *Thermotoga maritima* were purchased from NZytech (NZYTech, Lda., Portugal). Organosolv-pretreated birch (200°C for 30 min, 60% EtOH) and spruce (200°C for 30 min, 52% EtOH) were used as substrates. The composition of birch (w/w) was 67.1% cellulose, 21% hemicellulose and 7.1% lignin and that of spruce was 66% cellulose, 6% hemicellulose, and 14.9% lignin.

Cloning of *cbh6* and *cbh7* Genes From *T. thermophila*

The host-vector system of One Shot® Top10 *Escherichia coli* cells (Invitrogen, USA) and Zero Blunt® PCR Cloning Kit (Invitrogen, USA) was used for the cloning of the both CBH genes from *T. thermophila*. The wild-type strain of *M. thermophila* ATCC 42464 was used. Protein expression was achieved with *P. pastoris* host strain X33 and pPICZαC (Invitrogen, USA). *P. pastoris* was cultivated in shaking flasks at 30°C following the EasySelect™ *Pichia* Expression Kit (Invitrogen, USA) instructions. Genomic DNA was prepared and isolated as previously described (Topakas et al., 2012). The *E. coli*/*P. pastoris* shuttle vector pPICZαC, containing the tightly regulated AOX1 promoter and the *Saccharomyces cerevisiae* α-factor secretion signal (Higgins et al., 1998), was used for the expression of *TtCBH6a* and *TtCBH7a*. The genes coding for the hypothetical proteins *TtCBH6* [MYCTH_66729, GenBank: AEO55787.1] and *TtCBH7* [MYCTH_109566, GenBank: AEO55544.1] were amplified with PCR from genomic DNA using primers EF/ER (Tables S1A, S2A) designed accordingly to the gene sequences (<http://genome.jgi-psf.org/>, DOE Joint Genome Institute, Berka et al., 2011).

A high fidelity KOD Hot Start® DNA polymerase was used for the DNA amplification, which was carried out with 30 cycles of denaturation (20 s at 95°C), annealing (10 s at 58°C for *TtCBH6* and 60°C for *TtCBH7*), and extension (32 s at 70°C), followed by 1 min of further extension at 70°C (Tables S1B, S2B). In order to determine the DNA sequence, the PCR product, containing exons 2–4 and introns was cloned into the pCRBlunt® vector following the protocol described by the Zero Blunt® PCR Cloning Kit. Intron removal was achieved using the molecular technique of overlap extension polymerase chain reaction (OEPCR; Topakas et al., 2012). For the *TtCBH6*, two complementary DNA primers per intron (Ee2F/Ee2R, Ee3F/Ee3R, Ee4F/ER, Table S1A) were used to generate two DNA fragments with overlapping ends following the appropriate PCR amplification process and using the recombinant plasmid pCRBlunt/*cbh6* as template. The primer Ee2F included the sequence of exon 1, as well as the *Clal* restriction enzyme site at 5'-end and was used for the synthesis of the N-terminal part of the protein in order to avoid overlapping PCR (Figure S1). The annealing and extension conditions for each DNA fragment are described in Table S1B. The three PCR products were combined together in a subsequent hybridization reaction. The generated “fusion” fragment was amplified further by overlapping PCR through the utilization of the two external primers, EF end ER, performing an extended annealing step in order to improve

base-pairing between the complementary ends of each fragment. Intron removal of *TtCBH7* was achieved using the plasmid pCRBlunt/*cbh7* as template, with two pairs of complementary DNA primers (EF/Ee1R, Ee2F/ER, Table S2A). The two PCR products harboring overlapping ends were combined together in a subsequent hybridization reaction with EF and ER primers (Table S2A), as described above. The produced *cbh7* and *cbh6* DNA fragments were digested with the enzymes *Clal* and *XbaI*, cloned into the pPICZαC vector and amplified in *E. coli* TOP10F'. The recombinant vectors were confirmed by restriction analysis and DNA sequencing and finally transformed into *P. pastoris* according to the EasySelect™ *Pichia* Expression Kit. The production and purification of recombinant *TtCBH6* and *TtCBH7* enzymes were performed as previously described (Karnaouri et al., 2017).

Characterization of *TtCBH6* and *TtCBH7*

The activity of *TtCBH6* and *TtCBH7* was determined on Avicel 5% (w/v) for 1 h, at 50°C in 0.1 M citrate-phosphate buffer pH 5.0. The concentration of reducing ends was determined using the dinitrosalicylic acid reagent (DNS; Miller, 1959) and glucose for the standard curve. One unit (U) of enzymatic activity was defined as the amount of enzyme that released 1 μmol of sugar (glucose equivalents) per minute. Protein concentration was determined by the bicinchoninic acid (BCA) protein assay microplate procedure (Pierce Chemical Co., Rockford, IL), with bovine serum albumin as standard, according to the manufacturer's instructions (Smith et al., 1985). Substrate specificity of pure *TtCBH6* and *TtCBH7* enzymes was tested against 4-nitrophenyl β-D-cellobioside 5 mM, 4-nitrophenyl β-D-lactopyranoside 5 mM, β-glucan 0.5% w/v, PASC 0.5% w/v and carboxyl-methyl-cellulose (CMC) 1% w/v. Enzyme activity was determined in 0.1 M citrate-phosphate buffer pH 5.0 at 50°C for 15 min. The amount of reducing sugars released from β-glucan, PASC and CMC was estimated using the DNS method, as described above. The formation of 4-nitrophenol was measured at A₄₁₀, after addition of 1 M Na₂CO₃ to the reaction mixtures, using a standard curve under the same conditions.

The determination of optimal temperature of *TtCBH6* and *TtCBH7* was performed using Avicel 5% (w/v) as a substrate, in 0.1 M citrate-phosphate buffer pH 5.0, at temperatures ranging from 30 to 90°C. Temperature stability was determined by measuring the residual activity under the same assay procedure, after incubation of 0.32 and 0.45 mg of purified *TtCBH6* and *TtCBH7*, respectively at various temperatures for different amount of time. pH optimal was estimated at 50°C, over the pH range 3.0–11.0 using either 0.1 M citrate-phosphate buffer pH 3.0–7.0, 0.1 M Tris-HCl pH 7.0–9.0 or 0.1 M glycine-NaOH buffer pH 9.0–11.0. The stability at different pH was determined after incubating the enzymes in the above buffers at 4°C for 24 h and then measuring the activity remaining using the Avicel assay, as described above.

The values of the maximum velocity (V_{max}) and the Michaelis constant (K_m) for *TtCBH6* and *TtCBH7* were determined by incubating the enzymes in 0.1 M sodium acetate buffer pH 5.0 at 45°C for 30 min with 4-methyl-umbelliferyl-β-cellobiose (MUG2) at concentrations ranging from 0.1 to 2 mM

(Boschker and Cappenberg, 1994). The release of methylumbelliferyl was followed by measuring the absorbance at A_{350} . The inhibition of CBHs by specific mono/oligosaccharides was determined by estimating the enzymatic activity on MUG2 in presence of different inhibitor concentrations (5 and 10 mM). Kinetic analysis of inhibition was carried out on xylose (X1), xylobiose (X2), xylotriose (X3), mannose (M1), mannobiose (M2), mannotriose (M3), glucose (G1), cellobiose (G2), and xylosyl-cellobiose (XC). Lineweaver–Burk plots were drawn to determine K_m , V_{max} , and inhibition constant (K_i) values.

Hydrolysis of Organosolv Pretreated Materials

The release of cellobiose from organosolv-pretreated materials (birch and spruce) with different enzyme mixtures was studied. The four major commercial cellulases EG5, EG7, CBH7, and CBH6 were used to set up an experimental design (#1) with the software Design Expert® 7.0.0 (Stat-Ease Inc.), targeting increased % cellobiose yield. The algorithmically built *D-optimal* design was employed to generate 20 experimental conditions (Table 1) where the enzymes varied between specified levels (Table 2). Among these combinations, 5 replicates were included in the design, in order to increase the power of the model and reduce the prediction error. The replicates represented enzyme concentrations that corresponded to the upper and lower limit values. Based on literature data (Billard et al., 2012; Karnaouri et al., 2016) combined with preliminary experimental results, the upper and lower limits of each enzyme and their relative abundance were carefully chosen. In all the experimental combinations, the proportion of each enzyme varied, with the total amount of the enzyme loading to be kept constant and set to be equal to 1 (or 100%). Evaluation of the results and determination of the suitable model that fits the experimental data was done with the same software. The two models applied were either the *quadratic* or the *special cubic* (Karnaouri et al., 2016). The efficiency of the model was evaluated by calculating the *p*-value and R^2 . Optimization of the mixture toward maximal cellobiose yields was also performed by the same software. All reactions were performed at 50°C, with 2.5% initial dry matter content, in 0.1 M phosphate-citrate buffer pH 5.0 with 0.02% NaN_3 , in a final volume of 1 mL. The total enzyme loading was 25 mg/g substrate. Samples were taken at 24 and 48 h, filtered and analyzed for the release of cellobiose and glucose with isocratic ion-exchange chromatography using an Aminex HPX-87P column (Bio-Rad Laboratories, Hercules, CA, USA) and Millipore water as the mobile phase.

After identifying the optimal enzyme combination that maximizes cellobiose production, another experimental design (#2) was set up using different proportions of EG5, CBH7, EG9, and EG6, while the CBH6 and EG7 were kept constant and equal with those values that gave the maximal cellobiose concentration and % yield in design #1. Data analysis, evaluation of the model and optimization of the mixture were performed as described above. The theoretically predicted highest yields in both experimental designs were verified with time-course experiments. *TtCBH6* and *TtCBH7* were finally used to replace

TABLE 1 | Experimental combinations used for the hydrolysis tests generated with *D-optimal* design (Design Expert® 7.0.0, Stat-Ease Inc.).

Component	#1				#2			
	A	B	C	D	A	B	C	D
Run	EG5	EG7	CBH6	CBH7	EG5	EG7	EG9	EG6
1	0.25	0.2	0.05	0.5	0.38	0.55	0.04	0.03
2	0.1	0.05	0.05	0.8	0.20	0.70	0.06	0.05
3	0.1	0.1	0.3	0.5	0.35	0.50	0.10	0.06
4	0.221	0.05	0.193	0.537	0.20	0.69	0.10	0.01
5	0.3	0.055	0.145	0.5	0.27	0.70	0.02	0.01
6	0.182	0.122	0.135	0.56	0.32	0.55	0.06	0.07
7	0.1	0.2	0.2	0.5	0.25	0.63	0.06	0.05
8	0.1	0.2	0.05	0.65	0.45	0.50	0.02	0.03
9	0.1	0.05	0.211	0.639	0.33	0.60	0.06	0.01
10	0.156	0.102	0.05	0.693	0.45	0.50	0.02	0.03
11	0.175	0.05	0.275	0.5	0.20	0.68	0.02	0.10
12	0.179	0.193	0.05	0.578	0.20	0.60	0.10	0.10
13	0.27	0.05	0.05	0.63	0.20	0.60	0.10	0.10
14	0.176	0.051	0.133	0.64	0.20	0.68	0.02	0.10
15	0.27	0.05	0.05	0.63	0.30	0.50	0.10	0.10
16	0.25	0.2	0.05	0.5	0.38	0.50	0.02	0.10
17	0.1	0.05	0.132	0.718	0.27	0.57	0.06	0.10
18	0.1	0.2	0.2	0.5	0.27	0.70	0.02	0.01
19	0.3	0.055	0.145	0.5	0.33	0.60	0.02	0.06
20	0.1	0.05	0.05	0.8	0.20	0.69	0.10	0.01

TABLE 2 | Upper and lower constraints for all variables used for the experimental design #1 and #2.

Variable in model		Lower limit	Upper limit
#1			
EG5	A	0.1	0.2
EG7	B	0.05	0.2
CBH6	C	0.05	0.3
CBH7	D	0.5	0.8
#2			
EG5	A	0.2	0.45
CBH7	B	0.5	0.7
EG9	C	0.02	0.1
EG6	D	0.01	0.1

CBH7 and CBH6 in optimized combinations in order to evaluate the performance of these in-house produced enzymes and compare with that of commercially available cellobiohydrolases.

RESULTS

Heterologous Expression and Characterization of *TtCBH6* and *TtCBH7*

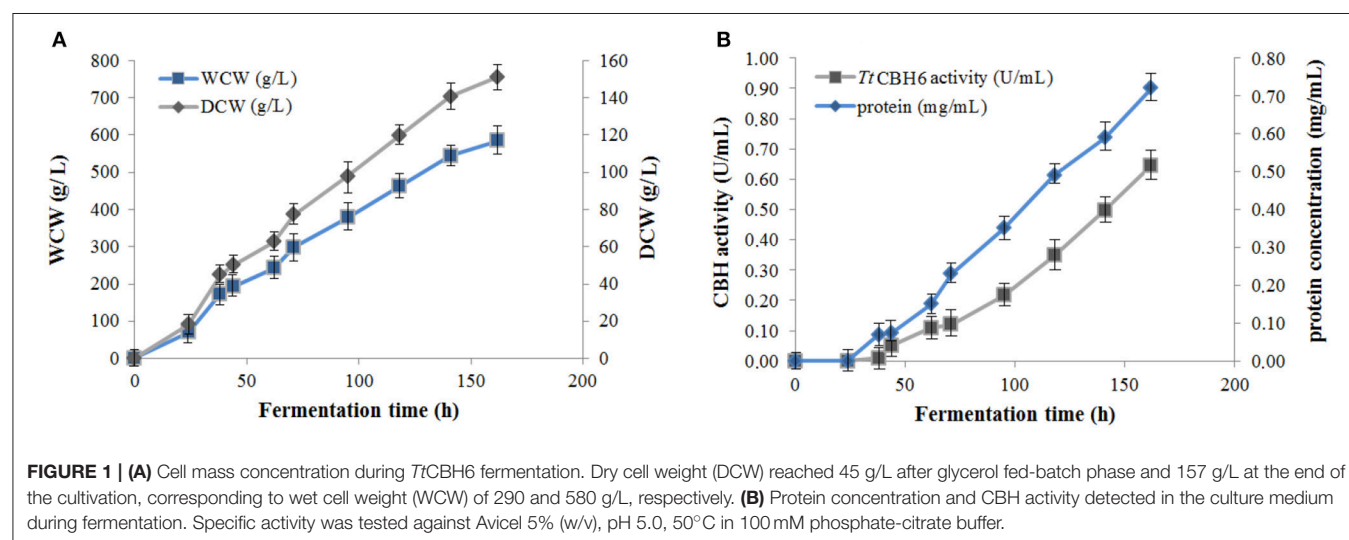
From genome analysis, the translation of *cbh6* and *cbh7* open reading frames (ORF) from the *T. thermophila* genome database show significant primary sequence identity with characterized

CBHs acting on the non-reducing and the reducing end of the carbohydrate molecules, which have been classified to GH families 6 and 7, respectively, on CAZy database (<http://www.cazy.org/>; Cantarel et al., 2009; Terrapon et al., 2017). The putative cellobiohydrolase *TtCBH6* showed high sequence identity (79%) with the CBHII from *Humicola insolens* [PDB ID: 1BVW] and 64% with the CBHII from *Trichoderma viride* [GenBank: AAQ76094.1]. The putative *TtCBH7* showed high sequence identity (67%) with the Cel7d (Cbh58) *Phanerochaete chrysosporium* [PDB: 1GPI] and 61% identity with the CBH I from *Humicola grisea* [GenBank: BAA09785.1]. The hypothetical proteins of 66729 and 109566 were selected as putative CBHs and the corresponding genes, provisionally named *cbh6* and *cbh7*, were cloned and used to transform *P. pastoris* X33, encoding *TtCBH6* and *TtCBH7*, respectively (Table S3). The ORF of *cbh6* encodes a protein of 465 amino acids including a secretion signal peptide of 17 amino acids (MAKKLFITAALAAVLA) based upon the prediction using SignalP v4.0 (<http://www.cbs.dtu.dk/services/SignalP/>). The predicted mass and isoelectric point (pI) of the mature protein is 49.41 kDa and pI 5.28, respectively, by calculations using the ProtParam tool of ExPASy (<http://web.expasy.org/protparam/>). The ORF of *cbh7* encodes a protein of 509 amino acids including a secretion signal peptide of 17 amino acids (MYAKFATLAALVAGAAA), while the predicted mass and isoelectric point (pI) of the mature protein is 54 kDa and pI 4.77.

Protein expression of *TtCBH6* and *TtCBH7* was first evaluated in small scale shake flask cultures, and the clone that exhibited the highest activity against Avicel 5% w/v was chosen for the production of the recombinant enzymes and further characterization studies. *TtCBH6* was subsequently produced in high cell-density cultivation in bioreactor using the basal salts medium supplemented with PTM₁ trace salts, according to Invitrogen, *Pichia* Fermentation Process Guidelines, reaching a maximum level of enzyme expression equal to 0.65 U/mL (activity against Avicel for varying time points shown at **Figure 1**). As methanol was used as carbon source, there was an increase in cell-density during the fed batch phase. At the end of

the fermentation, the dry weight of cells reached 151.5 g/L and the total amount of crude extracellular protein obtained was 0.72 g/L. The production of *TtCBH7* was tested in 1 L shake flasks, in BMGY medium for 18–24 h. After examination of the CBH activity, no efficient yield of recombinant protein was achieved. The major factor causing this problem was primarily the proteolytic degradation of enzymes produced, which hampered the yield. Proteolysis led to low full-length recombinant protein levels and active products that were smaller than the full-length protein. Degraded proteins ran as a “smear” at SDS-PAGE (Figure S2). As a result, in spite of high protein amounts measured at the culture medium, only a small proportion was biologically active. In order to eliminate proteolysis and achieve higher production levels of homogenous and stable enzyme, several strategies were followed, and a series of different parameters were evaluated, such as the reduction of incubation temperature, the influence of initial pH, ammonium sulfate and methanol concentration and agitation. Of all the above parameters, it was found that when the initial concentration of ammonium sulfate in the culture medium was Two-fold higher than the one usually used (10 g/L, as suggested by EasySelect™ *Pichia* Expression Kit protocol), the protein appeared full length sized and homogenous. Activity on Avicel 5% w/v could be first detected in the medium 24 h after inoculation and peaked at 168 h with a titer of 47 U/ml (**Figure 2**).

Purification of the enzymes with immobilized metal ion affinity chromatography (IMAC) and removal of background impurities from the fermentation broth resulted in 294 mg of pure *TtCBH6* and 39.5 mg of pure *TtCBH7* per L of culture supernatant. The molecular weight of *TtCBH6* and *TtCBH7* was estimated to be ca. 75 and 78 kDa, respectively (**Figure 3**), which appears to be significantly higher than the predicted values using the ProtParam tool of ExPASy, even after considering the presence of the myc epitope and the polyhistidine tag. This observation might be explained by the existence of *N*- and *O*-glycosylation post-translational modifications. Indeed, 1 *Asn*-*Xaa*-*Ser*/*Thr* sequon and 44 *Ser*-*Thr* residues were predicted in



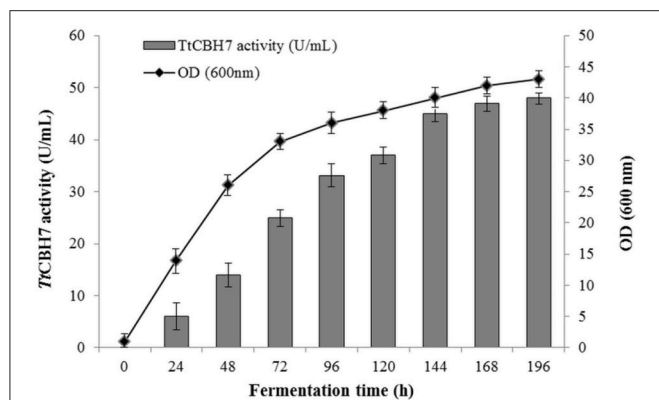


FIGURE 2 | Time course of *TtCBH7* activity (gray bar) and biomass (black circle) production of the recombinant *P. pastoris* harboring the *cbh7* gene. The enzyme was expressed in culture broth by induction with 0.5% v/v methanol and addition of 20 g/L ammonium sulfate and its activity was measured with Avicel as substrate.

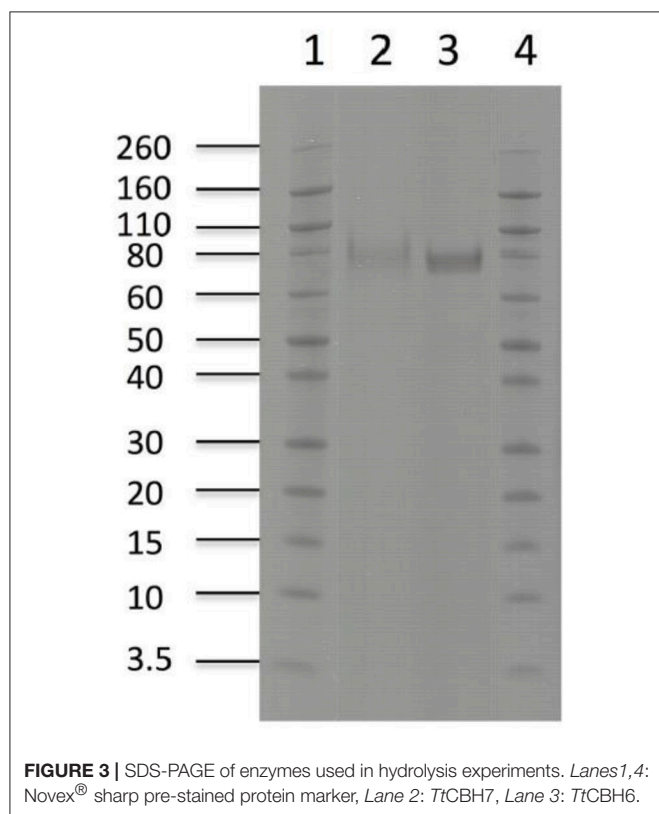


FIGURE 3 | SDS-PAGE of enzymes used in hydrolysis experiments. Lanes 1, 4: Novex® sharp pre-stained protein marker, Lane 2: *TtCBH7*, Lane 3: *TtCBH6*.

TtCBH6 sequence by using the NetNGlyc 1.0 server (<http://www.cbs.dtu.dk/services/NetNGlyc/>) and the NetOGlyc 3.1 server (<http://www.cbs.dtu.dk/services/NetOGlyc/>), while 1 *Asn-Xaa-Ser/Thr* sequon and 23 *Ser-Thr* residues were predicted in *TtCBH7* sequence.

The purified *TtCBH6* and *TtCBH7* were assayed for their activity toward different substrates. *TtCBH6* showed a specific activity of 1.63 ± 0.05 U/mg on Avicel 5% w/v, 1.19 ± 0.12 U/mg on β -glucan 0.1% w/v and 0.25 ± 0.09 U/mg for CMC 1% w/v. No

activity of *TtCBH6* on pNP-substituted substrates was detected, while it had a low activity on PASC (1.10 ± 0.23 U/mg). *TtCBH7* was preferentially active toward PASC 0.5% w/v, exhibiting an activity of 3.21 ± 0.24 U/mg, followed by Avicel 5% w/v (2.81 ± 0.13 U/mg), while on CMC 1% w/v the specific activity was lower and reached 0.21 ± 0.11 U/mg. The activity of *TtCBH7* was also tested on pNP- β -cellobioside 5 mM (0.13 ± 0.08 U/mg) and pNP- β -lactopyranoside 5 mM (2.25 ± 0.05 U/mg). The optimal temperature activity of *TtCBH6* was observed at 60°C, losing rapidly its activity for temperatures over 70°C. The enzyme remained fairly stable up to 55°C after preincubation for 24 h in 0.1 M phosphate-citrate buffer pH 5.0 and exhibited half-life of 16.02 h at 60°C. The optimum temperature activity of *TtCBH7* was also observed at 60°C. The enzyme remained stable up to 50°C, after preincubation for 24 h and exhibited half-life of 18.1 h at 55°C and 9.41 h at 60°C, respectively. Both enzymes presented the highest activity levels at pH 5.0, while the activity dropped rapidly for pH less than 4 or higher than 6. *TtCBH6* and *TtCBH7* were found remarkably stable in the pH range 3–11 after 24 h retaining their initial activity.

Lineweaver–Burk plots of the *TtCBH6* and *TtCBH7* activities at different substrate concentrations of MUG2 in the absence and presence of different concentrations of inhibitors are shown in **Figure 4**. The inhibitory effect of sugars on *TtCBH7*, when observed, indicated a competitive mode of inhibition, based on the intersection of the lines on the Y-axis, while no inhibitory effect on *TtCBH6* was observed for the inhibitors tested in concentrations of 5 and 10 mM (plots not shown). As depicted in **Table 3**, the K_m for MUG2 was 0.90 mM upon the absence of any inhibitor, while the K_m^{app} increased to 1.58 and 6.54 mM in the presence of 10 mM glucose and 10 mM cellobiose, respectively, indicating that cellobiose is a strong inhibitor for *TtCBH7*. The K_m^{app} was 1.17 and 1.04 for 10 mM xylobiose and 10 mM mannobiose, while the respective trioses (xylotriose and manntriose) had a very weak inhibitory effect on the enzyme activity. The K_m^{app} values tend to increase following the inhibitors concentration increase, revealing that the competitive mode of inhibition.

Hydrolysis of Natural Substrates With Commercial Cellulases

Four different commercial enzymes (two CBHs and two EGs) representing the main cellulolytic activities were used for the design of a multi-component mixture and were tested against two organosolv pretreated lignocellulolytic substrates (spruce and birch) for the release of cellobiose. To determine the CBH1:EG5 ratio that gives the maximal % cellobiose yield, preliminary experiments with different combinations of CBH1 and EG5 were conducted, using an enzyme loading of 25 mg/g substrate and incubating the reaction for 48 h. The results, as depicted in **Table 4** showed that a relative abundance of CBH7 to EG5 equal to 60:40–70:30 (for spruce) and 50:50–60:40 (for birch) is required in order to maximize the cellobiose yield, corresponding to 31 and 38% of glucan conversion for spruce and birch, respectively. To evaluate the effect of EG12 on the % cellobiose yield, the enzyme was added at 3% of the total mixture and

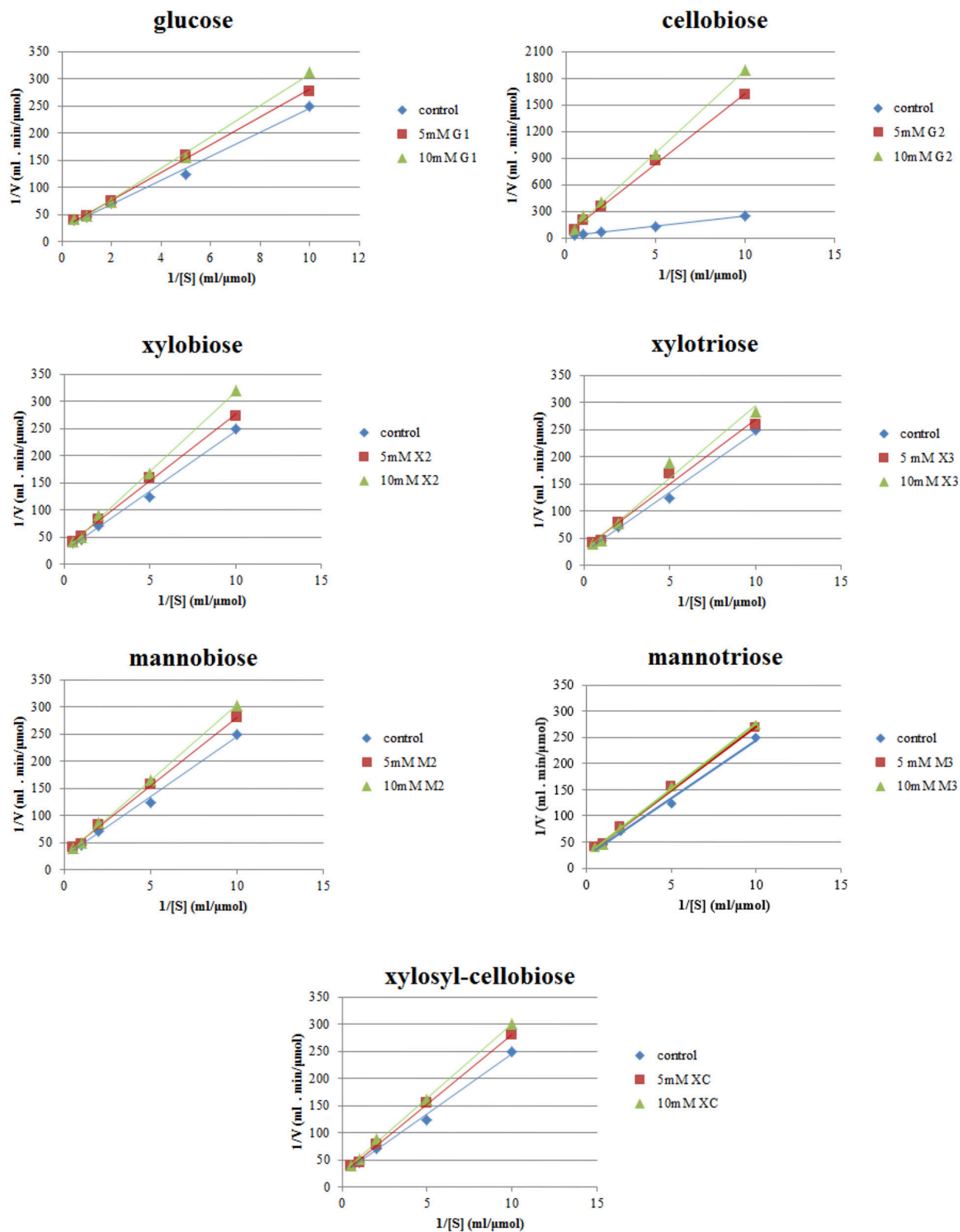


FIGURE 4 | Inhibition studies of *TtCBH7* by glucan, xylan, and mannan mono- and oligo-saccharides. Absorbance at 355 nm was measured after 30 min incubation with MUG2 at concentrations ranging from 0.1 to 2 mM, at 45°C, pH 5.0.

TABLE 3 | Enzyme kinetic parameters for glucan, xylan, and mannan mono- and oligo-saccharide inhibition of TtCBH6 and TtCBH7 using MUG2 as a substrate.

		TtCBH7			TtCBH6	
		V_{max} ($\mu\text{M}/\text{min}$)	K_m/K_m^{app} (μM)	K_i (mM)	V_{max} ($\mu\text{M}/\text{min}$)	K_m/K_m^{app} (μM)
MUG2		41×10^3	0.90		33×10^3	0.42
Cellobiose	5 mM	25×10^3	4.04	1.43	33×10^3	0.40
	10 mM	35×10^3	6.54	1.59	34×10^3	0.45
Glucose	5 mM	39×10^3	1.00		31×10^3	0.39
	10 mM	54×10^3	1.58	13.23	33×10^3	0.41
Xylotriase	5 mM	32×10^3	0.77		32×10^3	0.42
	10 mM	36×10^3	0.95		28×10^3	0.46
Xylobiose	5 mM	33×10^3	0.81		30×10^3	0.44
	10 mM	40×10^3	1.17	33.3	32×10^3	0.41
Mannotriase	5 mM	36×10^3	0.88		30×10^3	0.41
	10 mM	39×10^3	0.98		34×10^3	0.44
Mannobiose	5 mM	36×10^3	0.91		31×10^3	0.38
	10 mM	38×10^3	1.04		29×10^3	0.35
Xylosyl-Cellobiose	5 mM	37×10^3	0.99		30×10^3	0.43
	10 mM	39×10^3	1.01		33×10^3	0.48

There was no inhibition observed for TtCBH6 upon the addition of 5 and 10 mM concentration of different inhibitors. K_m -value was calculated from the reaction in the absence of inhibitors.

TABLE 4 | Preliminary experiments with various CBH7:EG5 ratios.

CBH7:EG5 ratio	Birch		Spruce	
	Cellobiose mg/mL	Cellobiose yield (%) (mg/g glucan)	Cellobiose mg/mL	Cellobiose yield (%) (mg/g glucan)
1:100	2.87 ± 0.12	19.0 (190)	1.96 ± 0.04	13.2 (132)
40:60	5.43 ± 0.89	35.9 (359)	4.19 ± 0.31	28.2 (282)
50:50	5.74 ± 0.67	38.0 (380)	4.57 ± 0.23	30.7 (307)
60:40	5.78 ± 0.51	38.3 (383)	4.62 ± 0.61	31.1 (311)
70:30	5.48 ± 0.55	36.3 (363)	4.65 ± 0.50	31.3 (313)
80:20	5.08 ± 0.46	33.6 (336)	4.51 ± 0.11	30.3 (303)
90:10	4.64 ± 0.21	30.7 (307)	4.41 ± 0.14	29.7 (297)
100:1	3.57 ± 0.39	23.7 (237)	3.82 ± 0.22	25.7 (257)

The reactions were performed with 25 mg total enzyme/g substrate and incubated for 48 h. The results are expressed as a percentage of the conversion of the total glucan content of the substrates. Bold values indicate the enzyme combinations giving the maximal hydrolysis yields.

the results showed an increase of ~7% in the hydrolysis levels, yielding 36.7% conversion rates for spruce and 42.1% for birch. According to these results, the limits of the relative abundances of the enzymes for the experimental design #1 were chosen. Table 5 shows the model prediction and the experimental results for % cellobiose yields using the four commercial enzymes, where cellobiose is expressed as a percentage of the total glucan content of the substrates. The relative proportions of the enzymes were independently optimized for each substrate for 24 and 48 h.

Hydrolysis of Organosolv Pretreated Spruce

The maximum concentration of cellobiose released from the hydrolysis of *spruce* was calculated using the quadratic model ($p = 0.0025$, $R^2 = 0.8655$ for 24 h and $p = 0.0015$, $R^2 = 0.8796$ for 48 h, Figure S3 and Table S7) and reached 3.37 and 5.6

mg/mL after 24 and 48 h incubation, respectively (Table S5). After 24 h, the % cellobiose yield corresponded to $22.7 \pm 1.7\%$ of the initial glucan content of the substrate and was achieved with high levels of CBH7 (66.6%) and EG5 (23.3%; Table 5). The experimental data with the optimal ternary mixture were very close to the predicted ones, resulting in 22.3% hydrolysis. As illustrated in Figure 5A and Figure S4, a decrease in CBH7 proportion resulted in steep drop in cellobiose concentration, even if EG7 and CBH6 levels are high, indicating the key role of this enzyme for the reaction. EG5 is also depicted as an important enzyme for the glucan conversion to cellobiose. With the relative proportion of CBH7 constant and equal with 66.6%, the value that corresponds to that of the optimized mixture, the hydrolysis is mostly dependent on the levels of EG5, as depicted in Figure S4Aii. When being together, CBH7 and EG5 comprise 89.9% of the total enzyme mixture and they can partially compensate each

TABLE 5 | Model prediction values and experimental results of the optimized mixtures and final % cellobiose yields, after 24 and 48 h of reaction for #1 and #2 experimental design.

#1	Substrate	Optimal enzyme proportions (%)				Cellobiose yield (%)	
		CBH7	CBH6	EG5	EG7	Mod. Pr.	Exp. data
24 h	Spruce	66.6	5.0	23.3	5.0	22.7	22.3 ± 1.7
	Birch	58.5	6.5	30.0	5.0	26.4	27.1 ± 2.3
48 h	Spruce	50.0	12.0	27.0	11.0	37.7	36.2 ± 0.5
	Birch	50.0	5.0	30.0	15.0	43.8	40.2 ± 1.2

#2	Substrate	Optimal enzyme proportions (%)				Cellobiose yield (%)	
		CBH7	EG5	EG9	EG6	Mod. Pr.	Exp. data
48 h	Spruce	64.9	21.6	4.3	9.2	42.5	40.0 ± 2.1
	Birch	69.3	20.0	9.7	1.0	41.6	42.7 ± 1.1

In experimental design #2, CBH6 and EG7 were kept constant and equal with those values that gave the maximal cellobiose yield in design #1. The % cellobiose yields have been calculated on the basis of total glucan content of initial substrates.

other, as shown at Figures S4Aiii–iv and has also been verified by the preliminary results mentioned above.

After 48 h of hydrolysis, optimal % cellobiose yield was predicted to be 37.7% with a ternary mixture of 50% CBH7, 12% CBH6, 27% EG5, and 11% EG7. CBH6 and EG7 appear in higher proportions to the composition of the optimal mixture than they did for 24 h hydrolysis. Experimental values showed a slightly decreased yield ($36.2 \pm 0.5\%$) in comparison to the predicted one. From the ternary plot of **Figure 5B** it can be concluded that the contribution of CBH6 and EG7 is more important in this stage of hydrolysis than that at 24 h, as when moving from point **A** to point **B**, CBH6 can compensate for EG7 and maintain high cellobiose yields, while EG5 is constant and equal with the proportion of the optimal cocktail. From **Figure S4Bii** it is also obvious that, when CBH7 comprises 50% of the final mixture and the proportions of EG5 decrease below a certain level, the hydrolysis rate drops. In contrast, as shown in **Figure S4Biii**, CBH7/EG7 together can partially compensate for the low amount of EG5, so the high cellobiose concentration is conserved. In experimental design #2, CBH7 and EG5 comprise ~85% of the optimal mixture of the processive enzymes, resulting to a cellobiose production of 6.3 mg/mL that corresponds to 42.5% substrate conversion (Table S6). The ternary mixture, as calculated by the special cubic model ($p = 0.0111$, $R^2 = 0.9409$; Table S8) was 64.9% CBH7, 21.6% EG5, 4.3% EG9, and 9.2% EG6. Apart from CBH7 and EG5, EG6 also stands necessary for achieving high yields, as depicted in **Figure 6C** and **Figure S6B**.

Hydrolysis of Organosolv Pretreated Birch

After 24 h of reaction, the highest product formation was 3.98 mg/mL which corresponded to 26.37 % of glucan conversion (Table S4) and was achieved with a ternary mixture of 58.5% CBH7, 6.5% CBH6, 30% EG5, and 5% EG7, as determined by the quadratic model ($p < 0.0001$, $R^2 = 0.9484$, **Figure S3** and Table S7). Experimental values were close to the predicted ones (27.1 ± 2.3). The ternary plot of **Figure 7A** and **Figure S5Ai** shows that when the proportion of EG5 is equal to that one of the optimized

cocktail (30%), an increase of CBH7 and decrease of CBH6 or *vice versa*, within the limits of the experimental design, practically has no effect on the hydrolysis rate which remains relatively high, for example when moving from point **A** to **B**. This is indicative of the pivotal importance of EG5 for the cellobiose production from birch, which is also apparent in **Figures S5Aii–iv**. Aside from EG5, the activity of CBH7 has a great impact, as it consists 58.5% of the total enzyme mixture that maximizes the substrate conversion.

The maximum yield of cellobiose released from the 48-h hydrolysis of birch was 6.6 mg/mL and corresponded to 43.8%, according to the quadratic model prediction ($p = 0.0168$, $R^2 = 0.7932$, **Figure S3**). It was achieved with an enzyme combination of 50% CBH7, 5% CBH6, 30% EG5, and 15% EG7. The experimental values were slightly lower ($40.2\% \pm 1.2$) in comparison to the predicted one. The pivotal importance of EG5 and CBH7 for the maximal cellobiose yields, similarly to the results after 24 h of reaction, is shown at **Figure 7B** and **Figures S5Bi–iv**, with the difference that EG7 contributes in higher proportions and can partially compensate for CBH7. From the **Figure S5Bii**, it is profound that when EG5 is in its lower limit proportion, the hydrolysis rate is very low. In experimental design #2, similarly to the results from spruce hydrolysis, CBH7 and EG5 comprise ~90% of the optimal mixture of the processive enzymes, resulting to a cellobiose production of 6.28 mg/mL that corresponds to 41.64% substrate conversion (Table S6). The ternary mixture, as calculated by the special cubic model ($p = 0.0094$, $R^2 = 0.8189$) was 69.3% CBH7, 20% EG5, 9.7% EG9, and 1% EG6 (Table S8). Apart from CBH7 and EG5, the requirement of EG9 to high yields product formation is also highlighted, as shown in **Figures 6A,B** and **Figure S6A**.

Evaluation of *Tt*CBH6 and *Tt*CBH7 in Ternary Mixtures

After identifying the optimal mixture that maximizes cellobiose production using commercial enzymes, *Tt*CBH6 and *Tt*CBH7

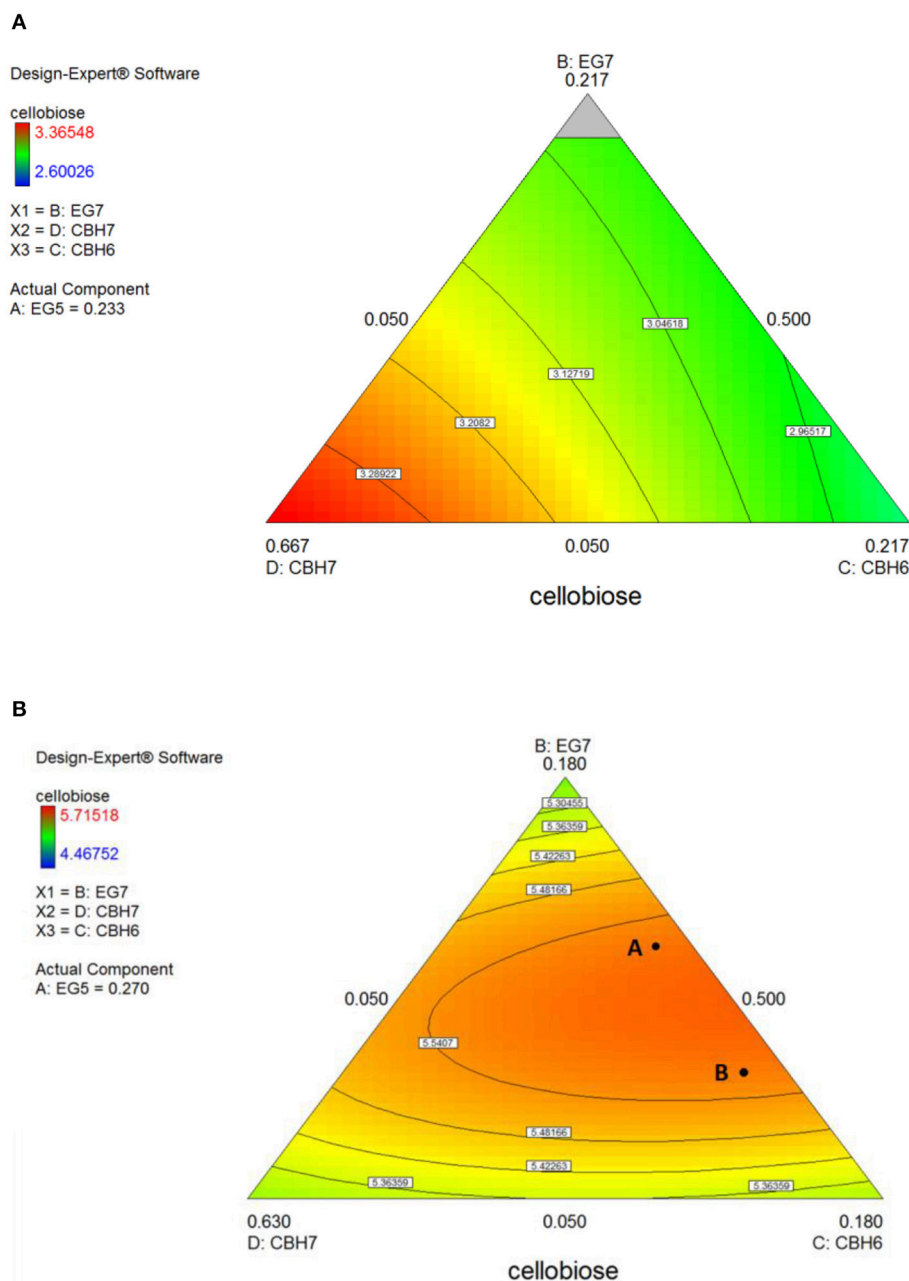


FIGURE 5 | Ternary plots for the experimental design #1, showing predicted final total cellobiose concentration (mg/mL) from spruce hydrolysis for 24 h (A) and 48 h (B), as a function of three out of four enzymes (CBH7, CBH6, EG7) content.

were used to replace CBH6 and CBH7 in optimized combinations in order to evaluate the performance of these *in-house* produced enzymes and compare with that of commercially available CBHs. The results showed that the hydrolysis rates were slightly lower when compared to the optimized mixtures that contain the commercial CBHs, achieving 32 ± 1.1 and $35.2 \pm 1.8\%$ of spruce and birch conversion, respectively, with the #1 enzyme mixture (Table 6). With #2 enzyme mixture, the yields reached $36 \pm 0.9\%$ for spruce and $35.2 \pm 2.1\%$ for birch.

DISCUSSION

Large-scale production of cellobiose and other sugars can occur via enzymatic or acid-catalyzed hydrolysis, or a combination of these processes (Lim and Lee, 2013). Acid-catalyzed processes have been extensively reported throughout the literature, either as an initial pretreatment step to facilitate the subsequent enzymatic saccharification yields, either by using solid acid catalysts in heterogeneous catalysis approaches (Lim and

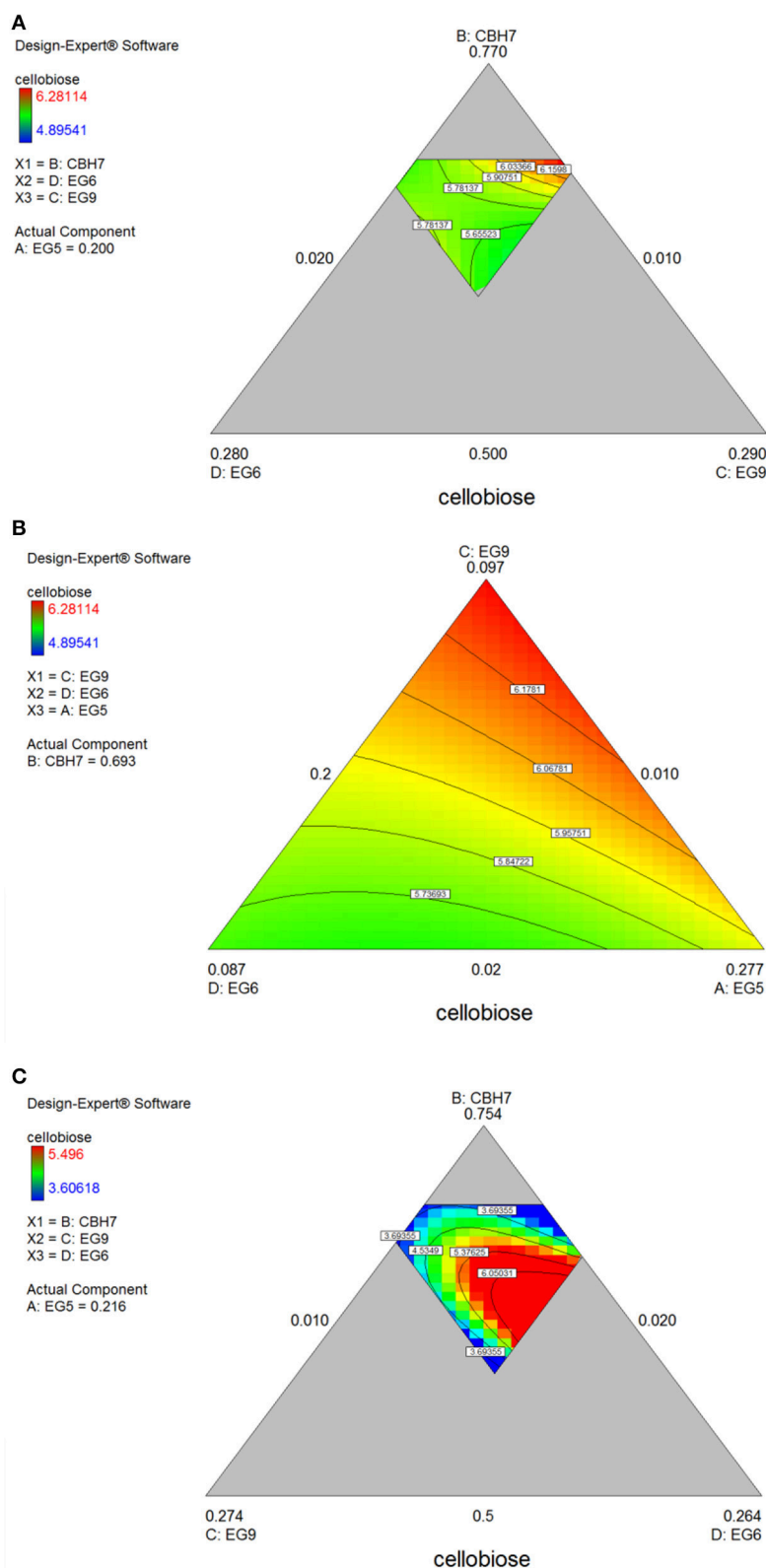


FIGURE 6 | Ternary plots for the experimental design #2 showing predicted final total cellobiose concentration (mg/mL) from *spruce* (A,B) and *birch* (C) hydrolysis, as a function of three out of four enzymes (CBH7, EG6, EG9 or EG9, EG6, EG5) content.

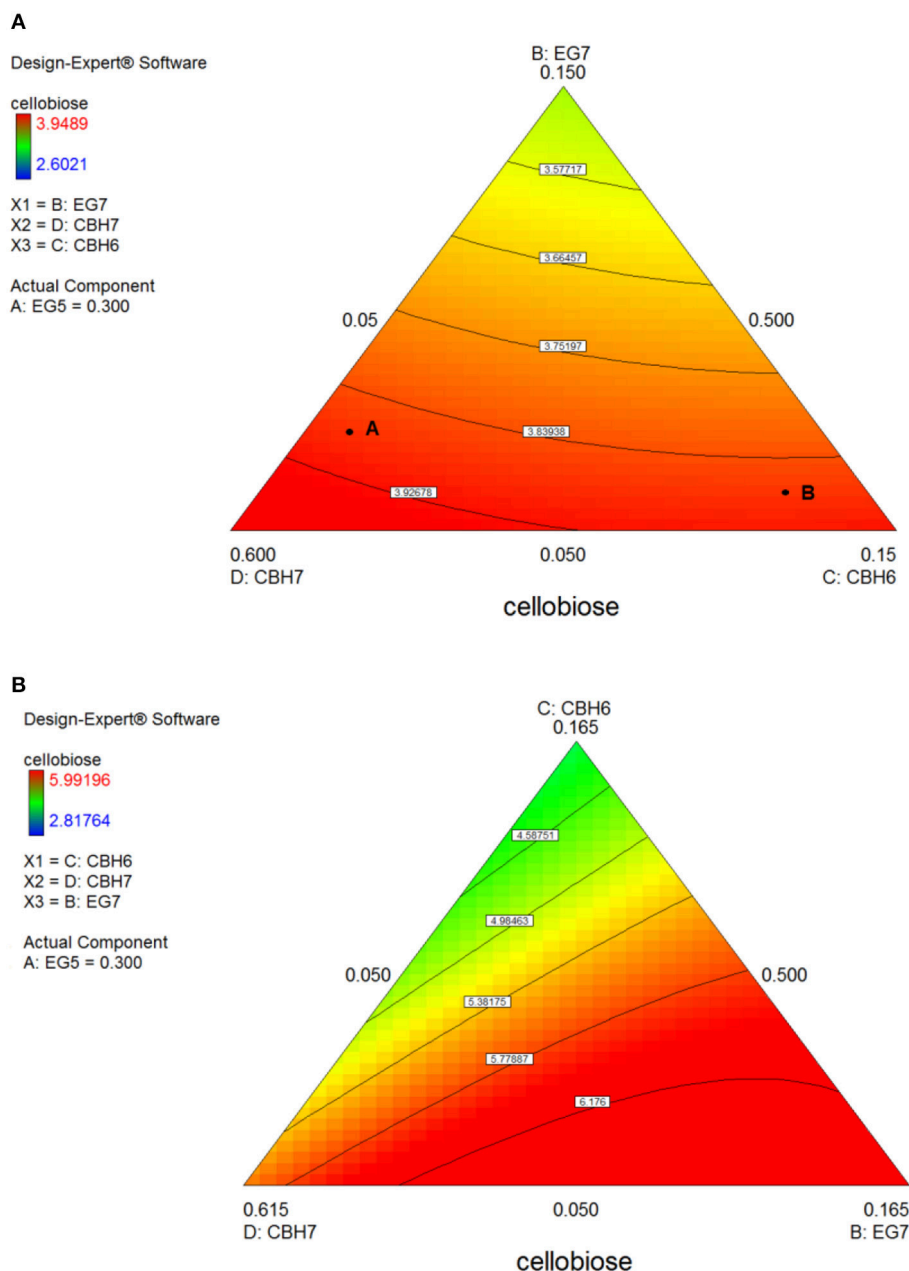


FIGURE 7 | Ternary plots for the experimental design #1, showing predicted final total cellobiose concentration (mg/mL) from *birch* hydrolysis for 24 h (A) and 48 h (B), as a function of three out of four enzymes (CBH7, CBH6, EG7) content.

Lee, 2013; Vilcoq et al., 2014). Apart from the low yield and the formation of toxic by-products, such as furfural and 5-hydroxymethylfurfural (HMF), the use and handling of concentrated acids create additional problems. Enzymatic hydrolysis processes offer numerous benefits, as they are typically milder, environmentally friendly and are carried out under lower pressure and at ambient temperature while producing less by-products. Until now, the major bottleneck that could possibly hamper the wide use of enzymes is the slow conversion rate after the initial hydrolysis stage, which is attributed to

the biomass recalcitrance (Auxenfans et al., 2017), and their high-production cost. As a result, efforts are made to improve the enzyme performance and produce efficient biocatalysts, toward a reduced enzyme consumption and, thus, to increase the overall sustainability of the process. The main enzymes for the cellobiose production are CBHs and processive EGs. The latter enzymes have gained much attention recently, after some microorganisms were reported to be able to degrade cellulose by using only EGs with both endo- and exo-activity that act in processive manner, while they completely lack

TABLE 6 | Experimental values of % cellobiose yields after 24 and 48 h of reaction, using the optimized ternary mixtures identified by #1 and #2 designs, after replacement of commercial CBH6 and CBH7 with *Tt*CBH6 and *Tt*CBH7 that were produced and characterized in the present study.

#1	Substrate	Optimal enzyme proportions (%)				Cellobiose yield (%) (mg/g glucan)
		<i>Tt</i> CBH7	<i>Tt</i> CBH6	EG5	EG7	
24 h	Spruce	66.6	5.0	23.3	5.0	18.4 ± 2.7 (184)
	Birch	58.5	6.5	30.0	5.0	28.1 ± 0.3 (281)
48 h	Spruce	50.0	12.0	27.0	11.0	32.0 ± 1.1 (320)
	Birch	50.0	5.0	30.0	15.0	35.2 ± 1.8 (352)
#2	Substrate	Optimal enzyme proportions (%)				Cellobiose yield (%) (mg/g glucan)
		<i>Tt</i> CBH7	EG5	EG9	EG6	
48 h	Spruce	64.9	21.6	4.3	9.2	36.0 ± 0.9 (360)
	Birch	69.3	20.0	9.7	1.0	35.2 ± 2.1 (352)

The % cellobiose yields have been calculated on the basis of total glucan content of initial substrates.

exoglucanases from their genome (Watson et al., 2009; Zhu et al., 2013). These findings raised the interest and questioned the role of the processive enzymes for the degradation of cellulose and their interactions with CBHs. In this context, we report here the heterologous expression and characterization of two CBHs from *T. thermophila* in the methylotrophic yeast *P. pastoris*. The two enzymes were tested in optimized enzyme mixtures together with processive endoglucanases for their ability to release high amounts of cellobiose. *T. thermophila* is a filamentous ligno-cellulolytic ascomycete with a wide range of synonyms over the history of its classification and distinction of sexual states (previously known as *Sporotrichum thermophilum* and *Myceliophthora thermophila*; Marin-Felix et al., 2015). A repertoire of enzymes, including GHs, oxidoreductases and esterases from this fungus have been widely studied (Topakas et al., 2012; Charavgi et al., 2013; Karnaouri et al., 2014, 2017; Zerva et al., 2016).

Even though numerous studies report the expression of CBHs in the methylotrophic yeast *P. pastoris* and other yeasts (Boer et al., 2000; Igarashi et al., 2012; den Haan et al., 2013; Fang and Xia, 2015; Woon et al., 2017), their use in scale-up processes is hampered due to their weak enzymatic activities together with the low production yields from the host cells. Weak enzymatic activities can be related to the heterogeneity of glycosylation patterns promoted by yeasts cells that, though in several cases increases the thermostability of the enzymes and the resistance to proteolytic attack (Amore et al., 2017), it may interact with the enzyme active site (Cereghino and Cregg, 2000; Mattanovich et al., 2012). Heterogeneity in glycosylation is a result of differences in oligosaccharide-protein populations in terms of the type, length, and identity of the oligosaccharides added, resulting in protein products whose micro-properties, such as the isoelectric point, vary slightly. In our study, the molecular weight of both *Tt*CBH6 and *Tt*CBH7 was significantly higher than the theoretical one, which was attributed to the existence of *N*- and *O*-glycosylation post-translational modifications. Aside

from glycosylation, many processive enzymes, especially CBHs, exhibit *N*-terminal modifications, such as the formation of a pyroglutamate residue, which is necessary for their activity; this modification is lacking in *P. pastoris* and other yeast systems for heterologous expression (Dana et al., 2014). Low production yields from the heterologous expression cells can also occur due to extensive proteolysis.

Proteolytic degradation has been a perpetual problem during the production of recombinant enzymes, especially when yeasts, such as *P. pastoris*, are employed (Gimenez et al., 2000). Proteolysis is susceptible to amplify over the fermentation induction period, following the reduction of the number of viable cells in the culture and is related mainly to the vacuole proteases (van den Hazel et al., 1996). Though several studies have been focused on the proteolytic degradation of the extracellular recombinant proteins, there is no in-depth analysis on the parameters that could promote proteolysis or the type of the proteases implied. Addition of ammonium ions in the form of ammonium sulfate has been recommended in the literature as a possible strategy to reduce proteolysis. Tsujikawa et al. (1996), observed a 10-fold reduction of proteolysis by supplementing medium with ammonium ions. In another study, the addition of 20 g/L (NH₄)₂SO₄ to a culture medium has been reported not only to increase the amount of glucoamylase produced but also for maintaining glucoamylase activity at a high level during the fermentation (Kobayashi and Nakamura, 2003). It was suggested that limited proteolysis can be attributed to the fact that the solubility of the proteases decreases upon the addition of (NH₄)₂SO₄ by sulfate conjugation, leading to decrease of the total proteolytic activity in the culture supernatant. País-Chanfrau et al. (2004) also reported an increased expression of recombinant mini-proinsulin in *P. pastoris* in bioreactors, achieved by, among others, periodical addition of ammonium sulfate. In this study, we describe the successful expression of *Tt*CBH7 in *P. pastoris*, under high osmotic pressure and increased salinity conditions. Two-fold increase of the ammonium sulfate in the culture medium resulted in the production of full-length

product, as shown by the higher protein purity on SDS-PAGE gel.

TtCBH6 and *TtCBH7* were shown to retain 100% of activity after 24 h incubation at 55 and 50°C, respectively, while they both showed activity on β -glucan. *TtCBH7* was active on a wide range of substrates, including crystalline, amorphous, and pNP-substituted substrates, as described above, whereas *TtCBH6* showed selectivity, with no detectable activity on pNP-substrates. However, *TtCBH6* exhibited a higher affinity for MUG2 in comparison to *TtCBH7*, as depicted by the K_m values, which has also been reported in the literature (Badino et al., 2017). It is related to the distinct catalytic properties and active site configuration observed in CBHs belonging to different families, with the GH6 CBHs to present weaker interactions with the cellulose substrate, which leads to higher association-dissociation rates and, consequently, higher catalytic rates. Both CBHs exhibit fairly high thermostability, which supports the potential application of these enzymes in the lignocellulosic materials degradation processes. Though CBHs have a major role to the conversion of the substrate to cellobiose, their activity is usually characterized as slow and susceptible to inhibition. The effect of glucan-, xylan-, and mannan-fragments have been widely studied as one of the main factors limiting the activity of CBHs, with cellobiose being the main compound that causes the enzyme end-product inhibition (Selig et al., 2008; Baumann et al., 2011). Depending on the pretreatment methods used, the type of the substrate and the pretreatment severity factor that is applied, variable amounts and different types of hemicelluloses may remain in the solid fraction of lignocellulosic materials. In hardwoods and agricultural plants, the main hemicellulosic structure is xylan, while softwoods are dominated by glucomannan. After enzymatic hydrolysis which usually takes place by employing a commercially available cellulolytic enzyme mixture which also contains side enzymatic activities acting on xylan and mannan structures, xylo- and manno-oligomers and monomers are released as hydrolysis products. These products, especially when found in increased concentrations, regularly cause inhibition of cellulases, with CBHs to be primarily affected (Qing et al., 2010). The structural similarity of xylobiose, mannobiose, and cellobiose may result in their competitive binding onto the active site of CBH forming a steric hindrance and, preventing the glucan chain to move into the tunnel, thus leading to a sharp decrease in their hydrolytic activity (Baumann et al., 2011). CBHs belonging to family 6 have been reported to be less susceptible to end product inhibition than those belonging to family 7 (Hele Teugjas and Väljamäe, 2013; Badino et al., 2017). In this study, no inhibitory effect of glucose, cellobiose, xylo- and manno-oligomers on *TtCBH6* was observed for inhibitor concentrations up to 10 mM, whereas *TtCBH7* was found to be strongly inhibited, especially by cellobiose.

Several strategies have been proposed with the aim to boost the enzymatic hydrolysis and increase cellobiose yields, including, among others, enzyme recycling by using multi-stage processes (Vanderghem et al., 2010, 2012) or product removal using membrane filtration (Gavilighi et al., 2013). The approach of the current study was to use *tailor-made* enzyme combinations

and test their efficiency in glucan conversion to cellobiose. Commercially available cocktails have been optimized targeting hydrolysis of specific type of substrate. Moreover, when cellobiose production is the main target product, although it is possible to inhibit the β -glucosidase activity upon addition of an inhibitor such as D-gluconolactone (Reese et al., 1971; Dale et al., 1985), these cocktails also contain other hemicellulolytic activities, as mentioned above, resulting in production of oligomers that can act as inhibitors of cellulase activity, especially CBHs. Since different lignocellulosic biomass residues have heterogeneous properties by nature and consequently degradability, tailor-made sets of enzymes are required for conversion of each substrate. CBHs belonging to GH7 family are the major enzymes for the production of cellobiose, but they are susceptible to severe end-product inhibition; supplementation with processive EGs can help alleviating that problem, as the latter have a cleft-like active site with a looser structure than the tunnel-shaped binding region of CBHs which is not easy to be blocked by the inhibitors (Murphy et al., 2009; Watson et al., 2009). This is verified by the preliminary results of this study, where a combination of CBH1 and EG5 in appropriate proportions can achieve up to Two-fold increase of hydrolysis rates when compared to CBH1 or EG5 alone; these results are more profound in case of birch that has higher cellulose and lower lignin content than spruce.

Comparing the theoretical predicted and the experimental values for 24 and 48 h of hydrolysis (Table 4), it is obvious that the reaction rate is higher at the initial conditions but seems to decrease in later stages of the reaction. Numerous factors have been suggested to affect the hydrolysis yields and result in declined hydrolysis rate at the late stage, including high cellulose crystallinity that renders the substrate inaccessible to the enzymes, reduction of enzyme stability and non-specific adsorption of enzymes on the substrate, especially on lignin components (Chundawat et al., 2011). In this study, both lignocellulosic materials have undergone organosolv pretreatment with the use of ethanol as organic catalyst resulting in a high amount of cellulose together with low amount of lignin, thus minimizing the adsorption of cellulases and increasing their catalytic efficiency. *Organosolv* is typically applied as a pretreatment process step of lignocellulosic residues within the biorefinery and enables their fractionation through solubilization of hemicellulose and lignin fractions into the cooking liquor and production of a cellulose-rich solid stream highly susceptible to enzymatic hydrolysis (Sannigrahi et al., 2010; Nitsos et al., 2018). The hydrolysis rates were slightly higher when birch was used as a substrate, which could be possible attributed to the lower lignin content of birch (7.1%) compared to spruce (14.9%). It has been observed that the carbohydrate-acting enzymes and, more specifically, cellulases possessing a CBM module can be adsorbed non-selectively onto lignin compounds of the substrate; this interaction possibly hampers their activity and leads to lower production yields.

The composition of optimal ternary mixtures for design #1 show that CBH7 and EG5 together consist the main component of the reaction mixture producing the highest cellobiose yields;

with CBH7 to be the prevailing component. As the incubation time increases from 24 to 48 h, the participation of EG7 and CBH6 becomes more profound for both spruce and birch. Possible factors that could explain this is either the end-product inhibition of CBH7 or the limited number of active sites as EG5 and CBH7 compete for the same sites and there is a depletion, so EG7, as an enzyme with a true endo-action, creates new chain ends for CBHs and EG5. *Exo-endo synergy* between CBHs and non-processive EGs, like EG7 is usually attributed to the ability of the latter to act on the middle-chain of cellulose molecule, thus creating two new chain ends, while the enzymes with a processive mode of action prefer to complex with the ends of the glucan chain (Jalak et al., 2012). Regarding the role of CBH6, this enzyme exhibits a greater impact during the later stages of hydrolysis, as shown by the results after 48 h of incubation. Although CBH II enzymes are regularly known to participate in the deconstruction of the crystalline cellulose areas, it has been proved that they can act in concert with EGs by removing amorphous cellulose and polishing the crystalline substrate regions so as to enable the attack of CBHI (Ganner et al., 2012), which is crucial in order to create new sites for the action of CBHI. Up to now, enzymes belonging to GH6 family are the only ones known that present an inverting catalytical mechanism and attack from the non-reducing end of cellulose chain (Cantarel et al., 2009). CBHI and CBHII enzymes exhibit *exo/exo synergy*, acting on the opposite ends of the glucan chain and using complementary modes of catalytical activity.

In experimental design #2, where all processive enzymes were used together with CBH6 and EG7, the conversion rate was lower than design #1, where only the four “core” enzymes (CBH7, CBH6, EG5, EG7) were used. In these reactions, CBH6 and EG7 proportions were kept constant and equal with those values that gave the maximal cellobiose yield in design #1. The ternary mixtures revealed that CBH7 stands as the most important enzyme among the processive activities, comprising 65–70% of the total cocktail of processive enzymes, for both spruce and birch, while the proportion of EG5 is 20%. The experimental values for hydrolysis rates after 48 h of reaction appear relatively close, but slightly higher than those determined in #1, despite the addition of processive enzymes from different GH families that would theoretically increase the cellobiose yields. This can be possibly attributed to the competition for the same binding sites or a phenomenon known as “traffic jam” which has been proposed to obstruct the activity of the CBHI enzymes (Igarashi et al., 2011). Replacement of commercial CBH6 and CBH7 in optimal ternary mixtures of design #1 and #2 with *TtCBH6* and *TtCBH7* produced in this study, led to relatively lower hydrolysis rates, but still a 35% of substrate conversion was achieved, which is rather high. This offers new perspectives for the use of *in-house* produced enzymes with specified and distinct activities to replace and/or supplement the commercial enzyme mixtures.

CONCLUSION

The efficient cellobiose production from lignocellulosic materials requires enzymes that act on the reducing and non-reducing cellulose chains. *TtCBH6* and *TtCBH7* from *T. thermophila* are two CBHs that were heterologously produced in *P. pastoris* and fully characterized with the aim to be tested in optimized enzyme mixtures for cellobiose production from organosolv pretreated spruce and birch. The impact of a changing cocktail composition on the cellobiose yields was evaluated, leading to the development of tailor-made mixtures, customized for each substrate. Determination of the distinct role of the individual enzymes and their synergistic interactions revealed that CBH7 and EG5 are the key enzymes for the production of cellobiose at the early stage of the reaction, but other enzymes acting on the amorphous areas, such as EG7 and CBH6, are needed as the reaction proceeds. These enzymes contribute to the generation of new chain ends to promote the action of the processive enzymes. Replacement of commercial CBHs with *TtCBH6* and *TtCBH7* resulted in yields that, although slightly lower, could still compete with the #1 and #2 optimized mixture performances, reaching 35% of substrate conversion to cellobiose. Processive EGs coupled with CBHs could alleviate the adverse effects of end-product inhibition of CBHs and, thus present a new perspective for the cellobiose production from lignocellulosic materials.

AUTHOR CONTRIBUTIONS

AK: Carried out the experiments and wrote the manuscript; ET: Contributed in the molecular cloning and heterologous expression of the enzymes; LM: Performed the pretreatment and the compositional analysis of the forest materials; UR and PC: Participated in study conception, data interpretation and corrected the manuscript. All authors have read and approved the final manuscript.

ACKNOWLEDGMENTS

This work was partially funded by Vinnova, BioInnovation Program Food-grade prebiotic oligosaccharide production, merging marine, and forest resources for moving up the cellulose value-chain (ForceUpValue). Sveaskog is greatly acknowledged for providing the forest materials. AK, UR, and PC thank the COST Action FP1306. Bio4Energy, a strategic research environment appointed by the Swedish government, is also acknowledged for supporting this work.

SUPPLEMENTARY MATERIAL

The Supplementary Material for this article can be found online at: <https://www.frontiersin.org/articles/10.3389/fchem.2018.00128/full#supplementary-material>

REFERENCES

- Amore, A., Knott, B. C., Supekar, N. T., Shajahan, A., Azadi, P., Zhao, P., et al. (2017). Distinct roles of N- and O-glycans in cellulase activity and stability. *Proc. Natl. Acad. Sci. U.S.A.* 114, 13667–13672. doi: 10.1073/pnas.1714249114
- Auxenfans, T., Terryn, C., and Paës, G. (2017). Seeing biomass recalcitrance through fluorescence. *Sci. Rep.* 7:8838. doi: 10.1038/s41598-017-08740-1
- Badino, S. F., Kari, J., Christensen, S. J., Borch, K., and Westh, P. (2017). Direct kinetic comparison of the two cellobiohydrolases Cel6A and Cel7A from *Hypocrea jecorina*. *Biochim. Biophys. Acta* 1865, 1739–1745. doi: 10.1016/j.bbapap.2017.08.013
- Baumann, M. J., Borch, K., and Westh, P. (2011). Xylan oligosaccharides and cellobiohydrolase I (TrCel7A) interaction and effect on activity. *Biotechnol. Biofuels* 4:45. doi: 10.1186/1754-6834-4-45
- Berka, R. M., Grigoriev, I. V., Otilar, R., Salamov, A., Grimwood, J., Reid, I., et al. (2011). Comparative genomic analysis of the thermophilic biomass-degrading fungi *Myceliophthora thermophila* and *Thielavia terrestris*. *Nat. Biotechnol.* 29, 922–927. doi: 10.1038/nbt.1976
- Berson, S., Viet, D., Halila, S., Driguez, H., Etienne Fleury, E., and Hamaide, T. (2008). Synthesis of new cellobiose-based glycopolysiloxanes and their use as polymer stabilizers in miniemulsion polymerization. *Macromol. Chem. Phys.* 209, 1814–1825. doi: 10.1002/macp.200800194
- Billard, H., Faraj, A., Lopes-Ferreira, N., Menir, S., and Heiss-Blanquet, S. (2012). Optimization of a synthetic mixture composed of major *Trichoderma reesei* enzymes for the hydrolysis of steam-exploded wheat straw. *Biotechnol. Biofuels* 5:9. doi: 10.1186/1754-6834-5-9
- Boer, H., Teeri, T. T., and Koivula, A. (2000). Characterization of *Trichoderma reesei* cellobiohydrolase Cel7A secreted from *Pichia pastoris* using two different promoters. *Biotechnol. Bioeng.* 69, 486–494. doi: 10.1002/1097-0290(20000905)69:5<486::AID-BIT3>3.0.CO;2-N
- Boschker, H. T. S., and Cappenberg, T. E. (1994). A sensitive method using 4-methylumbelliferyl- β -cellobiose as a substrate to measure (1,4)- β -glucanase activity in sediments. *Appl. Environ. Microbiol.* 60, 3592–3596.
- Cantarel, B. L., Coutinho, P. M., Rancurel, C., Bernard, T., Lombard, V., and Henrissat, B. (2009). The carbohydrate-active EnZymes database (CAZy): an expert resource for glycogenomics. *Nucleic Acids Res.* 37, D233–D238. doi: 10.1093/nar/gkn663
- Cereghino, J. L., and Cregg, J. M. (2000). Heterologous protein expression in the methylotrophic yeast *Pichia pastoris*. *FEMS Microbiol. Rev.* 24, 45–66. doi: 10.1111/j.1574-6976.2000.tb00532.x
- Charavgi, M. D., Dimarogona, M., Topakas, E., Christakopoulos, P., and Chrysina, E. D. (2013). The structure of a novel glucuronoyl esterase from *Myceliophthora thermophila* gives new insights into its role as a potential biocatalyst. *Acta Crystallogr. D Biol. Crystallogr.* 69(Pt 1), 63–73. doi: 10.1107/S0907444912042400
- Chundawat, S. P., Beckham, G. T., Himmel, M. E., and Dale, B. E. (2011). Deconstruction of lignocellulosic biomass to fuels and chemicals. *Annu. Rev. Chem. Biomol. Eng.* 2, 121–145. doi: 10.1146/annurev-chembioeng-061010-114205
- Cummings, J. H., and Macfarlane, G. T. (1991). The control and consequences of bacterial fermentation in the human colon. *J. Appl. Bacteriol.* 70, 443–459. doi: 10.1111/j.1365-2672.1991.tb02739.x
- Dale, M. P., Ensley, H. E., Kern, K., Sastry, K. A., and Byers, L. D. (1985). Reversible inhibitors of beta-glucosidase. *Biochemistry*. 24, 3530–3539. doi: 10.1021/bi00335a022
- Dana, C. M., Dotson-Fagerstrom, A., Roche, C. M., Kal, S. M., Chokhawala, H. A., Blanch, H. W., et al. (2014). The importance of pyroglutamate in cellulase Cel7A. *Biotechnol. Bioeng.* 111, 842–847. doi: 10.1002/bit.25178
- den Haan, R., Kroukamp, H., van Zyl, J. H. D., and van Zyl, W. H. (2013). Cellobiohydrolase secretion by yeast: current state and prospects for improvement. *Process Biochem.* 48, 1–12. doi: 10.1016/j.procbio.2012.11.015
- Fang, H., and Xia, L. (2015). Heterologous expression and production of *Trichoderma reesei* cellobiohydrolase II in *Pichia pastoris* and the application in the enzymatic hydrolysis of corn stover and rice straw. *Biomass Bioenergy* 78, 99–109. doi: 10.1016/j.biombioe.2015.04.014
- Figuerola-González, I., Quijano, G., Ramírez, G., and Cruz-Guerrero, A. (2011). Probiotics and prebiotics—perspectives and challenges. *J. Sci. Food Agric.* 91, 1341–1348. doi: 10.1002/jsfa.4367
- Franklin, K. R., Hopkinson, A., Webb, N., and White, M. S. (2002). *Acylated Cellobiose Compounds*. WO/2002/032914. PEARCE, Timothy; Unilever Plc, Patent Department, Bedford. International Application No.: PCT/EP2001/010869.
- Ganner, T., Bubner, P., Eibinger, M., Mayrhofer, C., Plank, H., and Nidetzky, B. (2012). Dissecting and reconstructing synergism: *in situ* visualization of cooperativity among cellulases. *J. Biol. Chem.* 287, 43215–43222. doi: 10.1074/jbc.M112.419952
- Gavilighi, H. A., Meyer, A. S., and Mikkelsen, J. D. (2013). Enhanced enzymatic cellulose degradation by cellobiohydrolases via product removal. *Biotechnol. Lett.* 35, 205–212. doi: 10.1007/s10529-012-1067-4
- Gibson, G. R., and Roberfroid, M. B. (1995). Dietary modulation of the human colonic microbiota: introducing the concept of prebiotics. *J. Nutr.* 125, 1401–1412.
- Gilkes, N. R., Henrissat, B., Kilburn, D. G., Miller, R. C., and Warren, R. A. J. (1991). Domains in microbial β -1,4-glycanases—sequence conservation, function, and enzyme families. *Microbiol. Rev.* 55, 303–315.
- Gimenez, J. A., Monkovic, D. D., and Dekleva, M. L. (2000). Identification and monitoring of protease activity in recombinant *Saccharomyces cerevisiae*. *Biotechnol. Bioeng.* 67, 245–251. doi: 10.1002/(SICI)1097-0290(20000120)67:2<245::AID-BIT15>3.0.CO;2-7
- Hele Teugjas, H., and Väljamäe, P. (2013). Product inhibition of cellulases studied with 14C-labeled cellulose substrates. *Biotechnol. Biofuels* 6:104. doi: 10.1186/1754-6834-6-104
- Henrissat, B., Driguez, H., Viet, C., and Schulein, M. (1985). Synergism of cellulose from *Trichoderma reesei* in degradation of cellulose. *Biotechnology* 3, 722–726. doi: 10.1038/nbt0885-722
- Higgins, D. R., Busser, K., Comiskey, J., Whittier, P. S., Purcell, T. J., and Hoeffler, J. P. (1998). “Small vectors for expression based on dominant drug resistance with direct multicopy selection,” in *Methods in Molecular Biology: Pichia Protocols*, eds D. R. Higgins and J. M. Cregg (Totowa, NJ: Humana), 28–41.
- Hu, J. P. M., Lanthier, P., White, T. C., McHugh, S. G., Yaguchi, M., Roy, R., et al. (2001). Characterization of cellobiohydrolase I (Cel7A) glycoforms from extracts of *Trichoderma reesei* using capillary isoelectric focusing and electrospray mass spectrometry. *J. Chromatogr. B* 752, 349–368. doi: 10.1016/S0378-4347(00)00373-X
- Igarashi, K., Maruyama, M., Nakamura, A., Ishida, T., Wada, M., and Samejima, M. (2012). Degradation of crystalline celluloses by *Phanerochaete chrysosporium* cellobiohydrolase II (Cel6A) heterologously expressed in methylotrophic yeast *Pichia pastoris*. *J. Appl. Glycosci.* 59, 105–110. doi: 10.5458/jag.jag.JAG-2011_029
- Igarashi, K., Uchihashi, T., Koivula, A., Wada, M., Kimura, S., Okamoto, T., et al. (2011). Traffic jams reduce hydrolytic efficiency of cellulase on cellulose surface. *Science* 333, 1279–1282. doi: 10.1126/science.1208386
- Jalak, J., Kurašin, M., Teugjas, H., and Väljamäe, P. (2012). Endo-exo synergism in cellulose hydrolysis revisited. *J. Biol. Chem.* 287, 28802–28815. doi: 10.1074/jbc.M112.381624
- Karnaouri, A. C., Topakas, E., and Christakopoulos, P. (2014). Cloning, expression, and characterization of a thermostable GH7 endoglucanase from *Myceliophthora thermophila* capable of high-consistency enzymatic liquefaction. *Appl. Microbiol. Biotechnol.* 98, 231–242. doi: 10.1007/s00253-013-4895-9
- Karnaouri, A., Matsakas, L., Topakas, E., Rova, U., and Christakopoulos, P. (2016). Development of thermophilic tailor-made enzyme mixtures for the bioconversion of agricultural and forest residues. *Front. Microbiol.* 7:177. doi: 10.3389/fmicb.2016.00177
- Karnaouri, A., Muraleedharan, M. N., Dimarogona, M., Topakas, E., Rova, U., Sandgren, M., et al. (2017). Recombinant expression of thermostable processive MtEG5 endoglucanase and its synergism with MtLPMO from *Myceliophthora thermophila* during the hydrolysis of lignocellulosic substrates. *Biotechnol. Biofuels* 10:126. doi: 10.1186/s13068-017-0813-1
- Kobayashi, F., and Nakamura, Y. (2003). Efficient production by *Escherichia coli* of recombinant protein using salting-out effect protecting against proteolytic degradation. *Biotechnol. Lett.* 25, 779–782. doi: 10.1023/A:1023524520023
- Kulka, H., and Ungureanu, I. M. (2017). *Sweetness Enhancement*. WO/2017/068034. MCSTE, John; Chemin de la Parfumerie 5 1214 Vernier (CH), International Application No.: PCT/EP2016/075210.

- Kurasin, M., and Våljamäe, P. (2011). Processivity of cellobiohydrolases is limited by the substrate. *J. Biol. Chem.* 286, 169–177. doi: 10.1074/jbc.M110.161059
- Lim, W. S., and Lee, J. W. (2013). Influence of pretreatment condition on the fermentable sugar production and enzymatic hydrolysis of dilute acid-pretreated mixed softwood. *Bioresour. Technol.* 140, 306–311. doi: 10.1016/j.biortech.2013.04.103
- Livesey, G. (1990). Energy values of unavailable carbohydrates and diets: an inquiry and analysis. *Am. J. Clin. Nutr.* 51, 617–637. doi: 10.1093/ajcn/51.4.617
- Maras, M., De Bruyn, A., Schraml, J., Herdewijn, P., Claeysens, M., Fiers, W., et al. (1997). Structural characterization of N-linked oligosaccharides from cellobiohydrolase I secreted by the filamentous fungus *Trichoderma reesei* RUTC 30. *Eur. J. Biochem.* 245, 617–625. doi: 10.1111/j.1432-1033.1997.00617.x
- Marin-Felix, Y., Stchigel, A. M., Miller, A. N., Guarro, J., and Cano-Lira, J. F. (2015). A re-evaluation of the genus *Myceliophthora* (Sordariales, Ascomycota): its segregation into four genera and description of *Corynascus fumimontanus* sp. nov. *Mycologia*. 107, 619–632. doi: 10.3852/14-228
- Mattanovich, D., Branduardi, P., Dato, L., Gasser, B., Sauer, M., and Porro, D. (2012). Recombinant protein production in yeasts. *Methods Mol. Biol.* 824, 329–358. doi: 10.1007/978-1-61779-433-9_17
- Medve, J., Stahlberg, J., and Tjerneld, F. (1994). Adsorption and synergism of cellobiohydrolase I and II of *Trichoderma reesei* during hydrolysis of microcrystalline cellulose. *Biotechnol. Bioeng.* 44, 1064–1073. doi: 10.1002/bit.260440907
- Miller, G. L. (1959). Use of dinitrosalicylic acid reagent for determination of reducing sugars. *Anal. Chem.* 31, 426–428. doi: 10.1021/ac60147a030
- Murphy, L., Bohlin, C., Baumann, M. J., Olsen, S. N., Sørensen, T. H., Anderson, L., et al. (2009). Product inhibition of five *Hypocrea jecorina* cellulases. *Enzyme Microb. Technol.* 52, 163–169. doi: 10.1016/j.enzmictec.2013.01.002
- Nitsos, C., Rova, U., and Christakopoulos, P. (2018). Organosolv fractionation of softwood biomass for biofuel and biorefinery applications. *Energies* 11:50. doi: 10.3390/en11010050
- Pais-Chanfrau, J. M., García, Y., Licor, L., Besada, V., Castellanos-Serra, L., Cabello, C. I., et al. (2004). Improving the expression of mini-proinsulin in *Pichia pastoris*. *Biotechnol. Lett.* 26, 1269–1272. doi: 10.1023/B:BILE.0000044871.80632.f9
- Qing, Q., Yang, B., and Wyman, C. E. (2010). Xylooligomers are strong inhibitors of cellulose hydrolysis by enzymes. *Bioresour. Technol.* 101, 9624–9630. doi: 10.1016/j.biortech.2010.06.137
- Reese, E. T., Parrish, F. W., and Ettlinger, M. (1971). Nojirimycin and D-glucono-1,5-lactone as inhibitors of carbohydrases. *Carbohydr. Res.* 18, 381–388. doi: 10.1016/S0008-6215(00)80274-8
- Roberfroid, M., Gibson, G. R., and Delzenne, N. (1993). The biochemistry of oligofructose, a non-digestible fiber: an approach to calculate its caloric value. *Nutr. Rev.* 51, 137–146. doi: 10.1111/j.1753-4887.1993.tb03090.x
- Sannigrahi, P., Miller, S. J., and Ragauskas, A. J. (2010). Effects of organosolv pretreatment and enzymatic hydrolysis on cellulose structure and crystallinity in Loblolly pine. *Carbohydr. Res.* 345, 965–970. doi: 10.1016/j.carres.2010.02.010
- Schülein, M. (2000). Protein engineering of cellulases. *Biochim. Biophys. Acta* 1543, 239–252. doi: 10.1016/S0167-4838(00)00247-8
- Selig, M. J., Knoshaug, E. P., Adney, W. S., Himmel, M. E., and Decker, S. R. (2008). Synergistic enhancement of cellobiohydrolase performance on pretreated corn stover by addition of xylanase and esterase activities. *Bioresour. Technol.* 99, 4997–5005. doi: 10.1016/j.biortech.2007.09.064
- Smith, P. K., Krohn, R. I., Hermanson, G. T., Mallia, A. K., Gartner, F. H., Provenzano, M. D., et al. (1985). Measurement of protein using bicinchoninic acid. *Anal. Biochem.* 150, 76–85.
- Teeri, T. T. (1997). Crystalline cellulose degradation: new insight into the function of cellobiohydrolases. *Trends Biotechnol.* 15, 160–167. doi: 10.1016/0003-2697(85)90442-7
- Terrapon, N., Lombard, V., Drula, E., Coutinho, P. M., and Henrissat, B. (2017). “The CAZy database/the carbohydrate-active enzyme (CAZy) database: principles and usage guidelines,” in *A Practical Guide to Using Glycomics Databases*, ed K. Aoki-Kinoshita (Tokyo: Springer), 117–131.
- Topakas, E., Moukoulis, M., Dimarogona, M., and Christakopoulos, P. (2012). Expression, characterization and structural modelling of a feruloyl esterase from the thermophilic fungus *Myceliophthora thermophila*. *Appl. Microbiol. Biotechnol.* 94, 399–411. doi: 10.1007/s00253-011-3612-9
- Tsujikawa, M., Okabayashi, K., Morita, M., and Tanabe, T. (1996). Secretion of a variant of human single-chain urokinase-type plasminogen activator without an N-glycosylation site in the methylotrophic yeast, *Pichia pastoris* and characterization of the secreted product. *Yeast* 12, 541–553. doi: 10.1002/(SICI)1097-0061(199605)12:6<541::AID-YEA935>3.0.CO;2-A
- van den Hazel, H. B., Kielland-Brandt, M. C., and Winther, J. R. (1996). Review: biosynthesis and function of yeast vacuolar proteases. *Yeast* 12, 1–16. doi: 10.1002/(SICI)1097-0061(199601)12:1<1::AID-YEA902>3.0.CO;2-N
- Vanderghem, C., Boquel, P., Blecker, C., and Paquot, M. (2010). A multistage process to enhance cellobiose production from cellulosic materials. *Appl. Biochem. Biotechnol.* 160, 2300–2307. doi: 10.1007/s12010-009-8724-7
- Vanderghem, C., Jacquet, N., Danthine, S., Blecker, C., and Paquot, M. (2012). Effect of physicochemical characteristics of cellulosic substrates on enzymatic hydrolysis by means of a multi-stage process for cellobiose production. *Appl. Biochem. Biotechnol.* 166, 1423–1432. doi: 10.1007/s12010-011-9535-1
- van Tilbeurgh, H., Tomme, P., Claeysens, M., Bhikhabhai, R., and Pettersson, G. (1986). Limited proteolysis of the cellobiohydrolase I from *Trichoderma reesei*. Separation of the functional domains. *FEBS Lett.* 204, 223–227. doi: 10.1016/0014-5793(86)80816-X
- van Zanten, G. C., Knudsen, A., Røytö, H., Forssten, S., Lawther, M., Blennow, A., et al. (2012). The effect of selected synbiotics on microbial composition and short-chain fatty acid production in a model system of the human colon. *PLoS ONE* 7:e47212. doi: 10.1371/journal.pone.0047212
- Vilcoco, L., Castilho, P. C., Carvalheiro, F., and Duarte, L. C. (2014). Hydrolysis of oligosaccharides over solid acid catalysts: a review. *ChemSusChem*. 7, 1010–1019. doi: 10.1002/cssc.201300720
- Watson, B. J., Zhang, H., Longmire, A. G., Moon, Y. H., and Hutcheson, S. W. (2009). Processive endoglucanases mediate degradation of cellulose by *Saccharophagus degradans*. *J. Bacteriol.* 191, 5697–5705. doi: 10.1128/JB.00481-09
- Wilson, D. B., and Kostylev, M. (2012). Cellulase processivity. *Methods Mol. Biol.* 908, 93–99. doi: 10.1007/978-1-61779-956-3_9
- Wood, T. M. (1988). Preparation of crystalline, amorphous, and dyed cellulose substrates. *Method. Enzymol.* 160, 19–25. doi: 10.1016/0076-6879(88)60103-0
- Woon, J. S., Mackeen, M. M., Illias, R. M., Mahadi, N. M., Broughton, W. J., Murad, A. M. A., et al. (2017). Cellobiohydrolase B of *Aspergillus niger* over-expressed in *Pichia pastoris* stimulates hydrolysis of oil palm empty fruit bunches. *PeerJ*. 5:e3909. doi: 10.7287/peerj.preprints.3044v1
- Zerva, A., Manos, N., Vouyiouka, S., Christakopoulos, P., and Topakas, E. (2016). Bioconversion of biomass-derived phenols catalyzed by *Myceliophthora thermophila* laccase. *Molecules* 21:550. doi: 10.3390/molecules21050550
- Zhu, Y., Zhou, H., Bi, Y., Zhang, W., Chen, G., and Liu, W. (2013). Characterization of a family 5 glycoside hydrolase isolated from the outer membrane of cellulolytic *Cytophaga hutchinsonii*. *Appl. Microbiol. Biotechnol.* 97, 3925–3937. doi: 10.1007/s00253-012-4259-x

Conflict of Interest Statement: The authors declare that the research was conducted in the absence of any commercial or financial relationships that could be construed as a potential conflict of interest.

Copyright © 2018 Karnaouri, Topakas, Matsakas, Rova and Christakopoulos. This is an open-access article distributed under the terms of the Creative Commons Attribution License (CC BY). The use, distribution or reproduction in other forums is permitted, provided the original author(s) and the copyright owner are credited and that the original publication in this journal is cited, in accordance with accepted academic practice. No use, distribution or reproduction is permitted which does not comply with these terms.



Silylated Zeolites With Enhanced Hydrothermal Stability for the Aqueous-Phase Hydrogenation of Levulinic Acid to γ -Valerolactone

Hue-Tong Vu, Florian M. Harth and Nicole Wilde*

Institute of Chemical Technology, Universität Leipzig, Leipzig, Germany

OPEN ACCESS

Edited by:

Konstantinos Triantafyllidis,
Aristotle University of Thessaloniki,
Greece

Reviewed by:

Jimmy Alexander Faria,
University of Twente, Netherlands
Tamer S. Saleh,
National Research Centre (Egypt),
Egypt
Oleg Kikhtyanin,
University of Chemistry and
Technology in Prague, Czechia

*Correspondence:

Nicole Wilde
nicole.wilde@uni-leipzig.de

Specialty section:

This article was submitted to
Green and Sustainable Chemistry,
a section of the journal
Frontiers in Chemistry

Received: 02 February 2018

Accepted: 12 April 2018

Published: 16 May 2018

Citation:

Vu H-T, Harth FM and Wilde N (2018)
Silylated Zeolites With Enhanced
Hydrothermal Stability for the
Aqueous-Phase Hydrogenation of
Levulinic Acid to γ -Valerolactone.
Front. Chem. 6:143.
doi: 10.3389/fchem.2018.00143

A systematic silylation approach using mono-, di-, and trichlorosilanes with different alkyl chain lengths was employed to enhance the hydrothermal stability of zeolite Y. DRIFT spectra of the silylated zeolites indicate that the attachment of the silanes takes place at surface silanol groups. Regarding hydrothermal stability under aqueous-phase processing (APP) conditions, i.e., pH \approx 2, 473 K and autogenous pressure, the selective silylation of the zeolite surface using monochlorosilanes has no considerable influence. By using trichlorosilanes, the hydrothermal stability of zeolite Y can be improved significantly as proven by a stability test in an aqueous solution of 0.2 M levulinic acid (LA) and 0.6 M formic acid (FA) at 473 K. However, the silylation with trichlorosilanes results in a significant loss of total specific pore volume and total specific surface area, e.g., 0.35 cm³ g⁻¹ and 507 m² g⁻¹ for the silylated zeolite Y functionalized with n-octadecyltrichlorosilane compared to 0.51 cm³ g⁻¹ and 788 m² g⁻¹ for the parent zeolite Y. The hydrogenation of LA to γ -valerolactone (GVL) was conducted over 3 wt.-% Pt on zeolite Y (3PtY) silylated with either n-octadecyltrichlorosilane or methyltrichlorosilane using different reducing agents, e.g., FA or H₂. While in the stability test an enhanced hydrothermal stability was found for zeolite Y silylated with n-octadecyltrichlorosilane, its stability in the hydrogenation of LA was far less pronounced. Only by applying an excess amount of methyltrichlorosilane, i.e., 10 mmol per 1 g of zeolite Y, presumably resulting in a high degree of polymerization among the silanes, a recognizable improvement of the stability of the 3 PtY catalyst could be achieved. Nonetheless, the pore blockage found for zeolite Y silylated with an excess amount of methyltrichlorosilane was reflected in a drastically lower GVL yield at 493 K using FA as reducing agent, i.e., 12 vs. 34% for 3PtY after 24 h.

Keywords: hydrothermal stability, biomass, hydrogenation, levulinic acid, formic acid, γ -valerolactone, silylation, zeolite Y

INTRODUCTION

Today's global economies heavily rely on the utilization of fossil resources. The most predominant side effect of this dependence is the emission of greenhouse gases resulting in global warming and climate changes. Additionally, the uncertain supply of crude oil also drives the accelerated search for sustainable substitutes in order to reduce the strong reliance on fossil resources. In this regard, biomass has been extensively studied as a renewable resource for the production of chemicals and fuels due to its ubiquity (Alonso et al., 2010).

Lignocellulose, i.e., non-edible plant biomass, is the most abundant class of biomass and is commonly produced as a waste by-product in the agricultural and forestry industry. Aqueous-phase processing (APP) is a selective and comparatively mild approach to utilize lignocellulosic biomass via hydrolysis and subsequent heterogeneously catalyzed upgrading. In this respect, the highly oxygenated macromolecules as present in lignocellulosic biomass are depolymerized and converted to a number of platform chemicals, including hydroxymethylfurfural (HMF), levulinic acid (LA), 2-methyltetrahydrofuran (Alonso et al., 2013), levulinate esters (Sun and Cheng, 2002), δ -aminolevulinic acid (Chheda et al., 2007), or γ -valerolactone (GVL) (Cortright et al., 2002; Huber et al., 2004; Gallezot, 2012). Of these, GVL has attracted high interest as a potential fuel additive, a “green solvent,” an intermediate for the manufacture of chemicals (Alonso et al., 2013) and a new class of biofuels named “valeric biofuels” (Lange et al., 2010). The production of GVL entails the hydrogenation of LA. LA can be selectively produced via acid hydrolysis of lignocellulosic biomass, which results in a high-water content mixture containing formic acid (FA) as by-product with an equimolar amount (Kamm et al., 2005). Therefore, the use of the as-synthesized aqueous mixture of LA and FA allows economically efficient production of GVL since no subsequent separation is required for further upgrading. In most studies, molecular hydrogen is used as a reducing agent for hydrogenation of LA (Mehdi et al., 2008; Deng et al., 2009, 2010; Geilen et al., 2010; Li et al., 2012; Wright and Palkovits, 2012; Delhomme et al., 2013; Luo et al., 2013; Abdelrahman et al., 2015; Huang et al., 2015). However, the direct utilization of FA is a promising approach to avoid the application of external hydrogen supply. Possible reaction pathways proposed for the hydrogenation of LA toward GVL involve two steps, hydrogenation and acid-catalyzed dehydration (Abdelrahman et al., 2014). Hence, bifunctional catalysts, containing both acid sites, e.g., zeolites, $\text{SiO}_2\text{-Al}_2\text{O}_3$, and metal sites, e.g., Pt, Pd, Ru, to catalyze dehydration and hydrogenation reactions, respectively, are required (Scheme S.1). In this regard, zeolites appear to be the promising materials for the preparation of the bifunctional catalyst due to the adjustable acidic properties, i.e., strength and density of both Brønsted and Lewis acid sites (Li et al., 2012; Ennaert et al., 2016). Owing to the comparatively large specific surface area, zeolites can also act as support materials for well dispersed metal particles.

Even though zeolites and especially ultra-stable zeolite Y (USY) are known for their tolerance to steam, their stability in aqueous-phase processes employing hot liquid water is less pronounced (Galadima and Muraza, 2017). Under this severe environment, zeolites suffer framework collapse, which was shown to be facilitated by the presence of silanol defects (Ravenelle et al., 2010; Ennaert et al., 2015). Zhang et al. (2015) demonstrated the vital role of the density of Si-OH groups in determining the stability of zeolites in hot liquid water at 473 K. Additionally, the silylation with ethyltrichlorosilane was found to significantly improve the stability of USY. This method both decreases the surface silanol density and increases the surface hydrophobicity, which prevents attack by water. Based on a similar concept, Proding et al. (2016) demonstrated

the stability-enhancing effect of the selective silylation using chlorotrimethylsilane on retaining the framework of BEA zeolites after 48 h at 433 K in hot liquid water. However, systematic studies on the stability of zeolites and stabilization strategies via silylation have not been reported in acidic aqueous solutions, typically at $\text{pH} \approx 2$, under APP conditions, i.e., 473 K.

Thus, in the present study, a systematic silylation approach using mono-, di-, and trichlorosilanes with different alkyl chain lengths, i.e., C1, C3, and C18, was employed to enhance the hydrothermal stability of zeolite Y. The hydrothermal stability of the resulting silylated zeolites was investigated in an aqueous acidic solution containing 0.2 M LA and 0.6 M FA under APP conditions. For Pt catalysts on selected silylated zeolites the activity and selectivity toward GVL were assessed in the aqueous-phase *in-situ* hydrogenation of LA using different reducing agents, i.e., FA or H_2 .

MATERIALS AND METHODS

Materials

Zeolite Y (CBV 720, H^+ form, $n_{\text{Si}}/n_{\text{Al}} = 15$) was supplied by Zeolyst. Levulinic acid (LA) ($\geq 98\%$) was provided by Merck Schuchardt OHG. Formic acid (FA) (99–100%) and GVL (99%) were obtained from Sigma–Aldrich. Toluene (100%) and ethanol (99.8%) were purchased from VWR International S.A.S. Tetraammine platinum (II) nitrate [$\text{Pt}(\text{NH}_3)_4(\text{NO}_3)_2$, 99.99%] was purchased from Alfa Aesar. The silylating agents are listed in Table S.1. All chemicals were used as received without further purification.

Catalyst Preparation

Surface Modification via Silylation Using Organosilanes

The silylated zeolites were prepared via a procedure developed by Zapata et al. (2013). Accordingly, 2 g of zeolite Y was dried in static air at 373 K overnight and subsequently dispersed in 40 cm^3 toluene using an ultrasonic bath. The silylating agent (0.5 mmol organosilane per 1 g of zeolite, unless noted) was dissolved in 50 cm^3 toluene and added to the zeolite suspension. The mixture was stirred for 24 h at room temperature before the zeolite was collected, washed with ethanol and dried overnight at 373 K in static air. A variety of organosilanes comprising mono-, di-, trichlorosilanes with different alkyl chain lengths were applied (cf. Table S.1). The obtained zeolites were labeled as $x\text{Cl}_y\text{C}_z$ with x being the number of chlorine atoms in the respective silane molecule ($x = 1, 2, 3$), y being the number of carbon atoms in the alkylsilyl group ($y = 1, 3, 8, 18$), and z being the organosilane/zeolite ratio ($z = 0.5, 10$ mmol per 1 g of zeolite) (cf. Table S.1).

Silylation of Pt/Zeolite Y Catalyst

In the first step, Pt/zeolite Y catalyst was prepared via incipient wetness impregnation. In a typical experiment, to obtain an aimed loading of 3 wt.-% of Pt, a solution of 0.061 g of tetraammine platinum (II) nitrate in 0.75 cm^3 of deionized water was added dropwise to 1 g of parent zeolite Y. The resulting solid was then dried in static air at 373 K for 12 h and subsequently

calcined for 4 h at 723 K with a heating rate of 5 K min⁻¹ in static air. The calcined catalyst (600 mg) was reduced at 673 K under a flow of H₂ (2.0 cm³ min⁻¹) in N₂ (8.0 cm³ min⁻¹) for 4 h.

Subsequent silylation of the Pt/zeolite Y catalyst using n-octadecyltrichlorosilane and methyltrichlorosilane with the ratio of organosilanes to zeolite being 0.5 and 10 mmol g⁻¹ respectively yielded the modified catalysts (cf. section Surface Modification via Silylation Using Organosilanes). Prior to the catalytic experiment, a second reduction for these silylated catalysts was conducted at 473 K under a flow of H₂ (2.0 cm³ min⁻¹) in N₂ (8.0 cm³ min⁻¹) for 4 h.

Characterization

The parent zeolite Y and silylated zeolite Y, as well as Pt/Y (3PtY) and silylated Pt/Y (3PtYxClyCz) were characterized by diffuse reflectance infrared Fourier transform spectroscopy (DRIFTS), N₂ physisorption, elemental analysis via optical emission spectroscopy with inductively coupled plasma (ICP-OES), and powder X-ray diffraction (XRD).

DRIFTS was carried out in a Bruker Vector 22 FTIR solid phase spectrometer equipped with a heated DRIFTS cell with a ZnSe window. Prior to the measurement, the samples were dried at 473 K for 30 min and the spectra were taken at 373 K in a N₂ flow rate of 100 cm³ min⁻¹. Spectra were recorded under a N₂ atmosphere at 373 K, in the range of 800–4,000 cm⁻¹, by addition of 100 scans and with a nominal resolution of 4 cm⁻¹.

A micromeritics ASAP2010—physisorption analyzer was used to record N₂ physisorption isotherms. The samples were evacuated at 523 K under vacuum pressure of 3 × 10⁻¹¹ MPa for 6 h prior to the measurements. The isotherms were taken at 77 K. The total specific surface area (A_{BET}) was determined by the Brunauer-Emmett-Teller (BET) model. The total specific pore volume (V_{total}) was estimated from the N₂ uptake at a relative pressure (p/p₀) of 0.99. The specific micropore surface area and specific micropore volume were calculated using the t-plot model.

The Pt content was determined by optical emission spectroscopy with inductively coupled plasma (ICP-OES) using a PerkinElmer Optima 8000. Prior to the analysis, the samples were dissolved in 2.0 cm³ HF, 3.0 cm³ HNO₃, and 3.0 cm³ HCl and diluted to obtain aqueous solutions which also contained 12.0 cm³ H₃BO₄ for complexation of excessive HF.

Powder XRD patterns were recorded at room temperature using a Siemens, D5000 diffractometer. The diffracted intensity of Cu-Kα radiation (λ = 0.154 nm) was measured in the range of 2θ between 4° and 90°, with a step size of 0.005° and a counting time of 0.2 second for phase identification.

Stability Test

Stability tests were conducted with zeolite Y and silylated zeolite Y. The reactant solution used in the stability test was the same used for the catalytic experiments (see below), which was a 5 wt.-% aqueous solution of LA (0.2 M) and FA (0.6 M). In a stainless steel autoclave with a 60 cm³ polytetrafluoroethylene (PTFE) liner, 1 g of the zeolite sample, dried at 373 K for 12 h prior to the experiment, was added to 40 cm³ of the reactant solution. The sealed autoclave was kept in the oven at 473 K

for 24 h. Afterwards, the parent zeolite Y was separated via centrifugation, and subsequently washed three times with 30 cm³ of deionized water. Silylated samples were separated by filtration, and subsequently washed three times with 30 cm³ of ethanol. Finally, the samples were dried overnight at 373 K in static air.

Aqueous-Phase Hydrogenation of Levulinic Acid

Reactions were carried out in a 300 cm³ stainless steel batch reactor (Model # 4560, Parr Instruments Company) with a head stirrer, a heater, as well as an external monitor (Model # 4848, Parr Instruments Company) for temperature, pressure and stirring speed. For each catalytic experiment, 0.50 g of the pre-reduced catalyst and 125 cm³ of an aqueous solution containing LA (0.2 M) were loaded into the reactor. The reactor was sealed, purged with a flow of N₂ (4.0 MPa) for 15 min, heated up to 393 or 493 K and kept at that temperature for 24 h while stirring at 700 min⁻¹. Either FA or H₂ was applied as the reducing agent. In the first case, FA was added directly to the starting reactant solution, giving a 5 wt.-% aqueous solution of LA (0.2 M) and FA (0.6 M) and the reaction ran at autogenous pressure. In the latter case, an excess amount of gaseous H₂ (2.5 MPa) was applied to the reactor when the desired temperature was reached, typically after 30 min.

Liquid samples were withdrawn at the start (when the desired temperature was reached, typically after 30 min) and after 24 h. The withdrawn samples were filtered and diluted by a volume factor of 5 in triple deionized water. A high-performance liquid chromatography (HPLC) system (Prominence-HPLC, Shimadzu, Kyoto, Japan) equipped with a photo-diode array detector and a Macherey-Nagel Nucleodur PolarTec column (4.6 × 250 mm) was used for the quantification of FA, LA, and GVL. An aqueous solution of 5 M H₂SO₄ was used as the mobile phase at a flow rate of 0.8 cm³ min⁻¹ and the column was operated at 313 K. The substances were quantified using chromatograms at the wavelength of 210 nm. Retention times for FA, LA, and GVL were determined using commercial FA, LA, and GVL.

The conversion of FA (X_{FA}), LA (X_{LA}), and the yield of GVL (Y_{GVL}) were calculated from the concentration of the compounds determined via external calibration of the respective integrated peak area.

$$X_{FA} = \frac{C_{0,FA} - C_{t,FA}}{C_{0,FA}} \times 100 \% \quad (1)$$

$$X_{LA} = \frac{C_{0,LA} - C_{t,LA}}{C_{0,LA}} \times 100 \% \quad (2)$$

$$Y_{GVL} = \frac{C_{t,GVL}}{C_{theoretical,GVL}} \times 100 \% \quad (3)$$

C_{0,FA,LA}: initial FA, LA concentration, C_{t,FA,LA,GVL}: FA, LA, GVL concentration at specific reaction time and C_{theoretical,GVL} represents the stoichiometric calculated yield of GVL.

After the reaction, the reactor was cooled to room temperature, and the catalyst was removed from the reaction mixture by centrifugation, washed three times with 30 cm³ deionized water and dried at 373 K for 12 h.

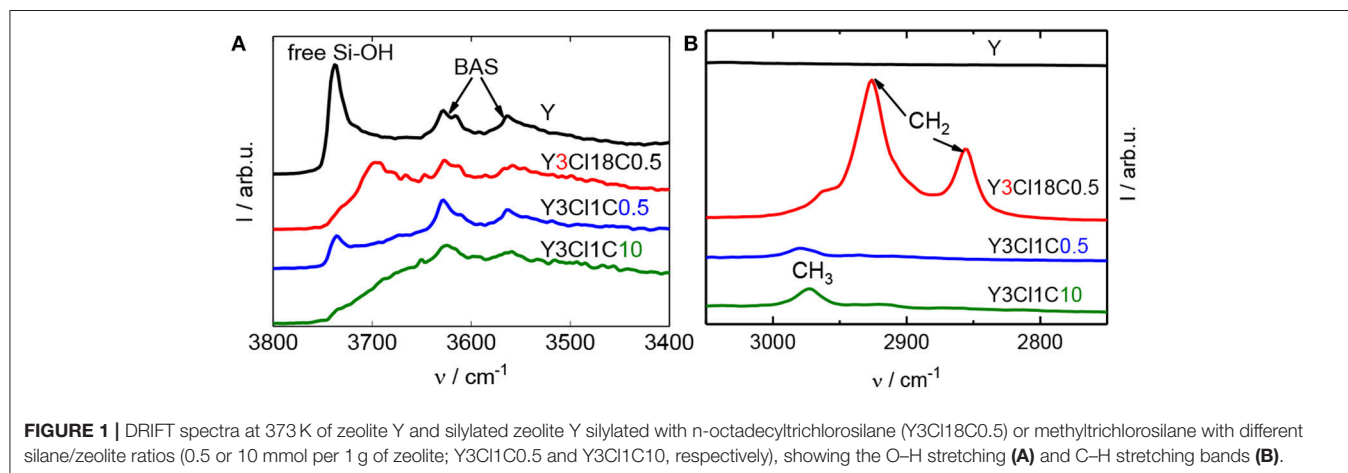
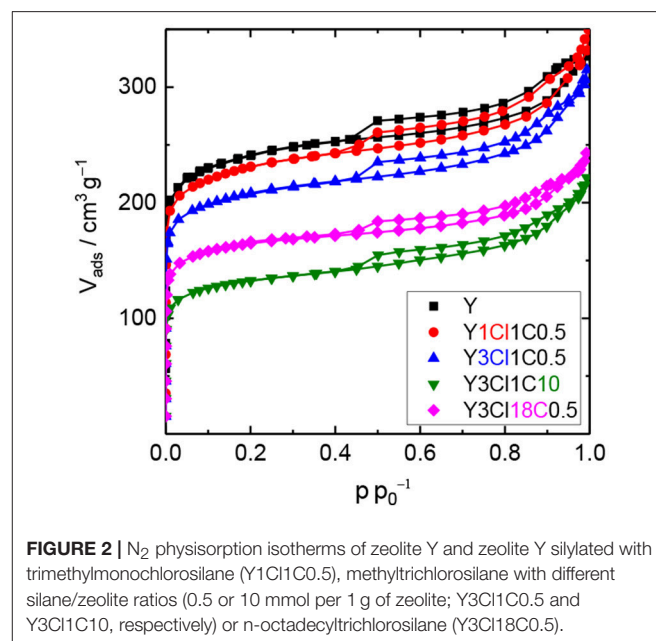
RESULTS AND DISCUSSION

Impact of Attached Organosilanes on Textural and Structural Properties of Zeolite Y

The silylation of zeolite Y was conducted using different organosilanes including mono-, di-, trichlorosilanes as well as with different aimed silanes loadings. **Figure 1** shows DRIFT spectra for zeolite Y and selected silylated samples with different alkyl chain lengths, e.g., Y3Cl1C0.5 and Y3Cl18C0.5. In the O–H stretching vibration region (**Figure 1A**), the parent zeolite Y displayed a dominant band at $3,738\text{ cm}^{-1}$, which can be assigned to the free silanol groups, and two other bands characteristic of Brønsted acid sites (BAS) located in the supercages ($3,627\text{ cm}^{-1}$) and the sodalite cages ($3,562\text{ cm}^{-1}$) of the zeolite framework (Weitkamp, 2000). The band for free silanol groups was present with significantly lower intensity for silylated zeolites using monochlorosilanes (cf. Figure S.1). In these cases, the silylation is found to be selective toward the free surface silanol groups. Interestingly, this band at $3,738\text{ cm}^{-1}$ is remained at the same frequency for Y3Cl1C0.5 with a lower intensity. However, it is slightly shifted to $3,700\text{ cm}^{-1}$ for the silylated zeolite using n-octadecyltrichlorosilane (**Figure 1A**). This shift of the band indicates the presence of unreacted silanol groups due to the fact that this bulky silylating agent might experience difficulty to reach all free silanol groups. The shift in the frequency was claimed to result from the interaction between the unreacted Si–OH and the attached alkylsilyl groups (Zapata et al., 2012). Changing the amount of methyltrichlorosilane applied in the silylation from 0.5 to 10 mmol g^{-1} , i.e., Y3Cl1C10, the band representative of the free silanol groups was no longer found. Therefore, it can be assumed that all accessible Si–OH groups were grafted. The two above-mentioned O–H vibration bands associated with BAS remain present for all silylated samples, which indicates that these internal sites remained unaffected during the silylation. In coherence with the results of Zapata et al. (2012), characteristic bands were found for the silylated zeolites in the C–H vibration range, as depicted in **Figure 1B**. The band centered at $2,974\text{ cm}^{-1}$ is corresponding to the C–H stretching

vibration of methyl (CH_3) groups and is shifted to $2,964\text{ cm}^{-1}$ for Y3Cl18C0.5. For silanes with long alkyl chains this spectral region is dominated by bands at $2,928$ and $2,856\text{ cm}^{-1}$ assigned to the methylene (CH_2) groups. As expected, all these bands are absent in the spectrum of the parent zeolite. These observations in the O–H and C–H vibration range for silylated zeolites can be taken as an indication of the attachment of the alkylsilyl groups to the silanol groups of the external zeolite surface (Zapata et al., 2012).

N_2 physisorption experiments were conducted with the silylated materials to investigate the effect of the introduced organosilanes on the textural properties. **Figure 2** shows the N_2 physisorption isotherms for the parent zeolite Y and four silylated samples. Similar to zeolite Y, silylated samples exhibit combined type I and type II isotherms with a steep rise in



the adsorbed N_2 volume at $p/p_0^{-1} < 0.01$, an uptake at a relative pressure above 0.7 as well as a type H4 hysteresis loop. Silylation with monochlorosilanes especially does not have a strong influence on the textural properties of the zeolite (cf. Table 1). The specific volume of the mesopores was found virtually unaffected remaining $\sim 0.23 \text{ cm}^3 \text{ g}^{-1}$. On the other hand, the specific micropore volume was reduced from 0.28 to $0.20 \text{ cm}^3 \text{ g}^{-1}$ for Y1Cl18C0.5. The loss of microporosity is also correlated to the loss of the specific surface area to a large extent. The highest decrease in the specific surface area of up to 25% was found for Y1Cl18C0.5. This might be explained by pore blockage as a result of organosilane introduction.

The decrease in the microporosity after silylation is more intense when changing from mono- to the corresponding trichlorosilanes (cf. Figure S.2). Significant losses of 37% in the specific micropore surface area and 32% in the specific micropore volume were evident for Y3Cl18C0.5. In addition, the mesoporosity was also affected, which contributed to the loss of 36% in the total specific surface area and 31% in the total specific pore volume of this material. Most probably the drastic loss in both micro- and mesopore volume can be explained by the formation of a polymeric layer due to the condensation of trichlorosilanes during silylation making the pores inaccessible for N_2 (Yoshida et al., 2001). Noticeably, this effect is most pronounced for the sample Y3Cl1C10, silylated with an excess amount of $(\text{CH}_3)_3\text{SiCl}_3$.

In addition, XRD patterns of silylated zeolites showed major reflections at $2\theta = 6.3, 10.3$, and 15.9° corresponding to the (111), (220), and (331) lattice planes of the faujasite framework

topology. This observation indicated no considerable change in structural property of the zeolites after silylation (cf. Figure 3).

Hydrothermal Stability of Silylated Zeolite Y in an Acidic Aqueous Solution

In the stability test, zeolite Y and silylated zeolite Y were exposed to the reactant solution containing 0.2 M LA and 0.6 M FA at 473 K for 24 h. After the stability test, the characteristic reflections for Y-type zeolite framework can no longer be found in the XRD patterns for both zeolite Y and zeolite Y silylated with monochlorosilanes, e.g., Y1Cl18C0.5 (cf. Figure 3, Figure S.4). A broad background typical for amorphous material is visible, which indicates the destruction of the crystalline zeolite framework. By increasing the number of Cl atom of the organosilanes applied in the silylation, the materials, e.g., Y2Cl18C0.5 and Y3Cl18C0.5, obtained after the stability test still exhibited the characteristic reflections of the faujasite framework topology. However the characteristic reflections possess a lower intensity emerging from a broad background. This indicates a partial retention of the zeolite framework. Y3Cl18C0.5 appeared to retain the crystalline zeolite structure to a much higher degree after the stability test than the parent zeolite Y. However, the broad underlying background representative of the amorphous, non-microporous solid typically formed via

TABLE 1 | Textural properties, i.e., specific surface area (A_{BET}), specific micropore surface area (A_{micro}), total specific pore volume (V_{total}), specific micropore volume (V_{micro}), specific mesopore volume (V_{meso}), and difference in A_{BET} , V_{total} compared to parent zeolite Y (ΔA_{BET} , ΔV_{total}) of zeolite Y before and after silylation.

Sample	A_{BET}^a / $\text{m}^2 \text{ g}^{-1}$	ΔA_{BET}^a /%	A_{micro}^b / $\text{m}^2 \text{ g}^{-1}$	V_{total}^c / $\text{cm}^3 \text{ g}^{-1}$	$\Delta V_{\text{total}}^c$ /%	V_{micro}^b / $\text{cm}^3 \text{ g}^{-1}$	V_{meso}^d / $\text{cm}^3 \text{ g}^{-1}$
Y	788	0	574	0.51	0	0.28	0.23
Y1Cl1C0.5	715	9	506	0.49	4	0.27	0.22
Y1Cl1C1.5	725	8	430	0.47	8	0.22	0.25
Y1Cl3C0.5	633	20	431	0.47	8	0.23	0.24
Y1Cl8C0.5	565	28	387	0.44	14	0.20	0.24
Y1Cl18C0.5	564	28	415	0.38	25	0.20	0.18
Y1Cl18C1	589	25	430	0.40	22	0.21	0.19
Y2Cl18C0.5	436	45	297	0.35	31	0.16	0.19
Y3Cl1C0.5	644	18	450	0.49	4	0.24	0.25
Y3Cl1C10	411	48	285	0.34	33	0.15	0.19
Y3Cl18C0.5	507	36	359	0.35	31	0.19	0.16

^avia BET.

^bvia t-plot.

^cvia Single point.

^d $V_{\text{meso}} = V_{\text{total}} - V_{\text{micro}}$.

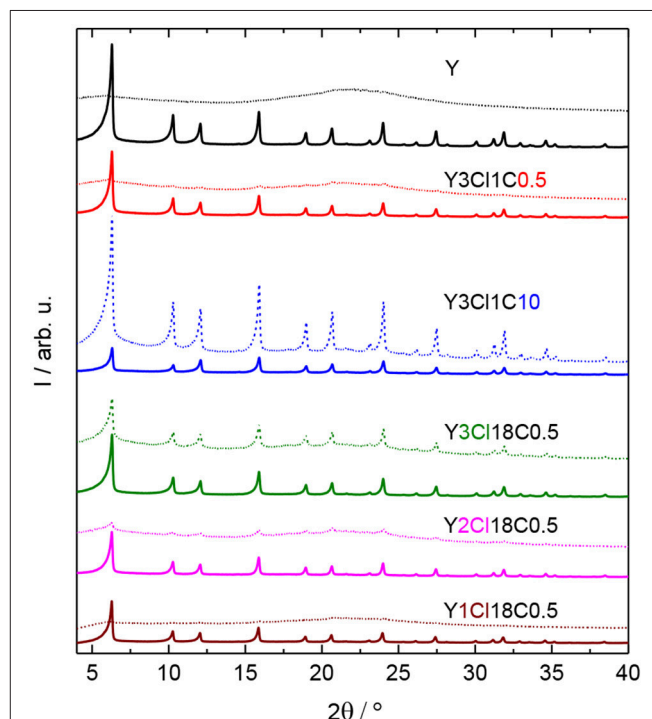


FIGURE 3 | XRD patterns of zeolite Y and zeolite Y silylated with n-octadecyltrichlorosilane (Y3Cl18C0.5) or methyltrichlorosilane with different silane/zeolite ratios (0.5 or 10 mmol per 1 g of zeolite; Y3Cl1C0.5 and Y3Cl1C10, respectively) before (solid lines) and after (dashed lines) the stability test in the aqueous solution of 0.2 M LA and 0.6 M FA at 473 K, autogenous pressure for 24 h.

framework destruction is still evident. In contrast, Y3Cl1C10 showed the highest relative degree of crystallinity among the samples, indicating that the high-loading silylation of zeolite Y with $(\text{CH}_3)_3\text{SiCl}_3$ seems to successfully result in a comparatively stable material.

The observations from XRD are in agreement with the N_2 physisorption data shown in **Figure 4**. From the isotherm of the zeolite Y after the stability test, the absence of the steep increase in adsorbed N_2 volume at $p/p_0^{-1} < 0.01$ is indicative of the total loss of microporosity. In addition, the observation of a H3 type hysteresis loop might indicate the formation of macropores in the spent zeolite Y (Thommes et al., 2015). Accordingly, significant losses of about 86% in the total specific surface area and 31% in total specific pore volume were found. Therefore, it can be concluded that the parent zeolite Y is hydrothermally unstable undergoing complete framework destruction when exposed to the acidic aqueous conditions in the stability test. However, the silylation has a positive effect on the hydrothermal stability of zeolite Y. The N_2 physisorption isotherm for Y3Cl18C0.5 after the stability test displayed a lower uptake of adsorbed nitrogen at $p/p_0^{-1} < 0.01$ and a larger hysteresis loop indicative of larger mesopores compared to the fresh counterpart (cf. **Figure 2**). Additionally, application of t-plot model evidently confirmed a decrease in the specific micropore surface area by $251 \text{ m}^2 \text{ g}^{-1}$ and a slight increase in the specific mesopore volume by $0.07 \text{ cm}^3 \text{ g}^{-1}$ compared to the fresh Y3Cl18C0.5 (**Table 2**). The deterioration in the textural structure of Y3Cl18C0.5 after the stability test is probably caused by the partial hydrothermal deconstruction of the zeolite framework to a large extent. By silylation using trichloromethylsilane (Y3Cl1C0.5) a complete loss of $0.24 \text{ cm}^3 \text{ g}^{-1}$ in microporosity could not be prevented. As confirmed

by XRD (cf. **Figure 3**) this loss can be mainly attributed to framework destruction. However, silylation using 3Cl1C with an excess amount, i.e., 10 mmol per 1 g of zeolite (Y3Cl1C10) resulted in an almost complete retention of the zeolite structure after the stability test as indicated by the obtained similarity in the shape of the corresponding N_2 physisorption isotherm when compared to the fresh sample. Interestingly, the specific mesopore volume was found to be the same ($0.19 \text{ cm}^3 \text{ g}^{-1}$) for Y3Cl1C10 before and after stability test with a slight decrease of $0.03 \text{ cm}^3 \text{ g}^{-1}$ in the specific micropore volume. In comparison, for Y3Cl18C0.5 the corresponding loss was more pronounced with $0.13 \text{ cm}^3 \text{ g}^{-1}$ which is in coherence with the observation from XRD pattern proving that Y3Cl1C10 is more stable than Y3Cl18C0.5. Most probably the more pronounced framework destruction is due to the availability of the unreacted silanol groups in Y3Cl18C0.5 caused by the bulky shape of the n-octadecylsilyl groups inhibiting complete silylation of silanol groups as mentioned before in section Impact of Attached Organosilanes on Textural and Structural Properties of Zeolite Y. Among the silylated zeolites, Y3Cl18C0.5 and Y3Cl1C10 are the most stable materials under these APP related conditions. Hence, to investigate in the impact of the silylation on the catalytic activity, these two silylating agents were applied over 3wt.-% Pt supported on zeolite Y.

Catalytic Activity of Silylated Pt on Zeolite Y Catalysts in the Hydrogenation of LA

To study the impact of silylation on the catalytic activity of silylated catalysts, 3PtY and 3PtY3Cl18C0.5, 3PtY3Cl1C10 were used in the aqueous-phase hydrogenation of LA. The LA conversion, the GVL yield and the selectivity toward GVL after 24 h are displayed in **Table 3** and **Figure 5**. Notably, no other product besides GVL was found in the aqueous product solution after the catalytic experiments as confirmed by the HPLC, ^1H NMR, and ^{13}C NMR (cf. Figures S.7, S.8). However, non-soluble

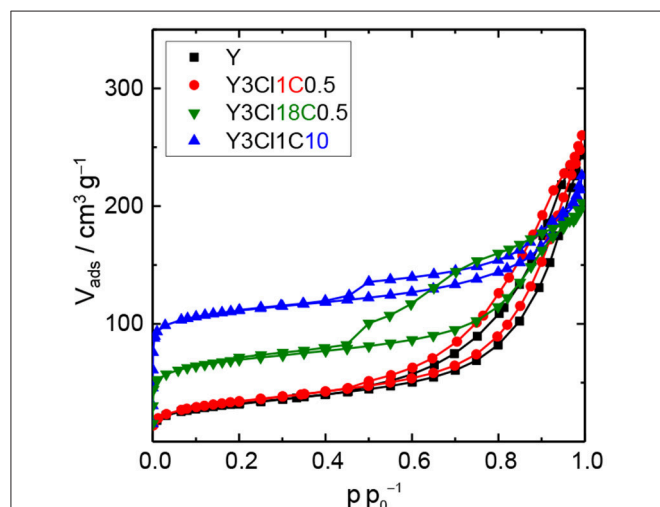


FIGURE 4 | N_2 physisorption isotherms of zeolite Y and zeolite Y silylated with n-octadecyltrichlorosilane (Y3Cl18C0.5) or methyltrichlorosilane with different silane/zeolite ratios (0.5 or 10 mmol per 1 g of zeolite; Y3Cl1C0.5 and Y3Cl1C10, respectively) after the stability test in the aqueous solution of 0.2 M LA and 0.6 M FA at 473 K, autogenous pressure for 24 h.

TABLE 2 | Textural properties, i.e., specific surface area (A_{BET}), specific micropore surface area (A_{micro}), total specific pore volume (V_{total}), specific micropore volume (V_{micro}), specific mesopore volume (V_{meso}), and difference in A_{BET} , V_{total} compared to fresh counterpart (ΔA_{BET} , ΔV_{total}), of zeolite Y and silylated zeolite Y after the stability test at 473 K and autogenous pressure for 24 h.

Sample	A_{BET}^a / $\text{m}^2 \text{ g}^{-1}$	ΔA_{BET}^a /%	A_{micro}^b / $\text{m}^2 \text{ g}^{-1}$	V_{total}^c / $\text{cm}^3 \text{ g}^{-1}$	$\Delta V_{\text{total}}^c$ /%	V_{micro}^b / $\text{cm}^3 \text{ g}^{-1}$	V_{meso}^d / $\text{cm}^3 \text{ g}^{-1}$
Y	113	86	0	0.35	31	0	0.35
Y1Cl1C1.5	143	80	0	0.38	19	0	0.38
Y1Cl18C1	87	85	0	0.32	20	0	0.32
Y2Cl18C0.5	144	67	0	0.28	20	0	0.28
Y3Cl1C0.5	120	81	0	0.35	29	0	0.35
Y3Cl1C10	346	16	235	0.31	9	0.12	0.19
Y3Cl18C0.5	223	56	108	0.29	17	0.06	0.23

^avia BET.

^bvia t-plot.

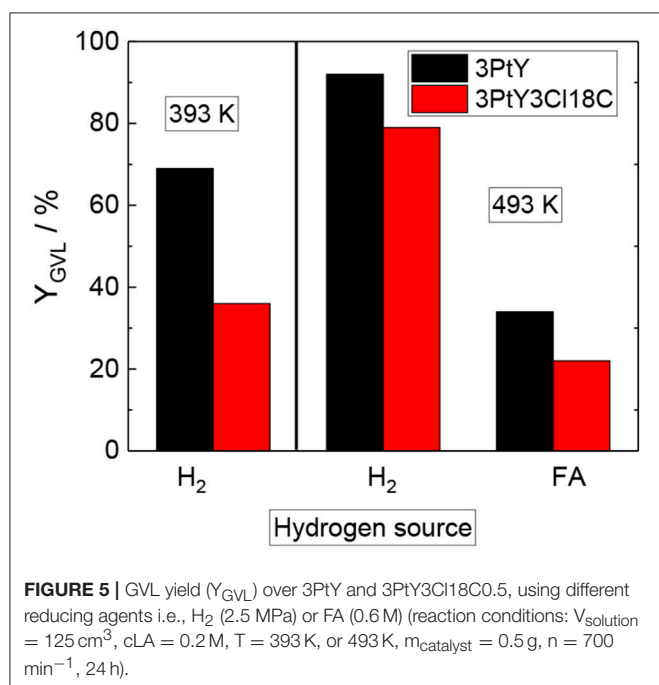
^cvia Single point.

^d $V_{\text{meso}} = V_{\text{total}} - V_{\text{micro}}$.

TABLE 3 | LA conversion (X_{LA}), GVL yield (Y_{GVL}), and selectivity toward GVL (S_{GVL}) in the hydrogenation of LA using different reducing agents, i.e., FA or H_2 , over 3PtY and 3PtY silylated with n-octadecyltrichlorosilane (3PtY3Cl18C0.5) or methyltrichlorosilane with different silane/zeolite ratios (0.5 or 10 mmol per 1 g of 3PtY; 3PtY3Cl1C0.5 and 3PtY3Cl1C10, respectively).

Catalysts	Pt loading* /wt.-%	Reducing agent	T /K	X_{LA} /%	Y_{GVL} /%	S_{GVL} /%
Y	n.d.	FA	493	n.d.	13	n.d.
3PtY	2.7	FA	493	42	34	80
		H_2	493	100	92	92
		H_2	393	95	69	73
3PtY3Cl18C0.5	2.5	FA	493	42	22	52
		H_2	493	97	79	81
		H_2	393	60	36	60
3PtY3Cl1C10	2.4	FA	493	38	12	32

Reaction conditions: reducing agent H_2 (2.5 MPa) or FA (0.6 M), $V_{solution} = 125\text{ cm}^3$, $c_{LA} = 0.2\text{ M}$, $m_{catalyst} = 0.5\text{ g}$, $n = 700\text{ min}^{-1}$, 24 h, n.d., not determined, *via ICP-OES.



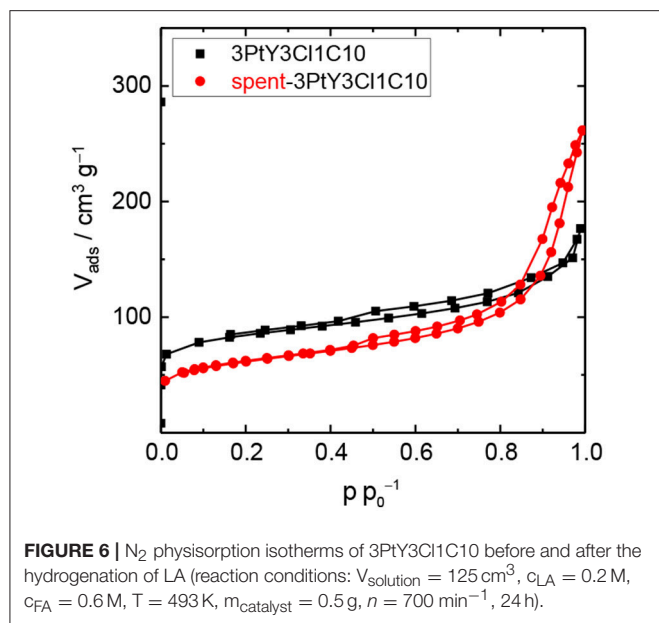
carbonaceous deposits were obtained after hydrogenation of LA over all catalysts tested. These non-soluble carbonaceous deposits, presumably humins, are most likely the side products leading to the difference between LA conversion and GVL yield.

The hydrogenation of LA over 3PtY was conducted using different reducing agents, i.e., FA and H_2 . In the presence of FA, the GVL yield was found to be much lower compared to that obtained when H_2 was used as the reducing agent, i.e., 34 vs. 92%, respectively. The significantly decreased GVL yield in hydrogenation of LA using FA as the reducing agent was also reported over Pd, Pt, Ru based catalysts on carbon by Ruppert et al. (2015). They suggested that CO formed during the decomposition of FA poisons the Pt catalyst (Du

et al., 2011). Another important factor might be the competitive adsorption of FA and LA on the active sites of the catalyst surface. In comparison to unsilylated catalysts, the silylated counterparts exhibited lower catalytic performance, e.g., a GVL yield of 22% was observed over 3PtY3Cl18C0.5 after 24 h of reaction at 493 K using FA as a reducing agent. Under the same reaction conditions, 12% of GVL yield could be achieved over 3PtY3Cl1C10. This drastically lower activity of silylated catalysts is caused by a combination of silylation-induced changes in the catalyst's properties. Firstly, 3PtY3Cl1C10 displayed a much lower specific surface area ($483\text{ m}^2\text{ g}^{-1}$) compared to 3PtY ($775\text{ m}^2\text{ g}^{-1}$) due to the blockage of micropores as described above (cf. section Impact of Attached Organosilanes on Textural and Structural Properties of Zeolite Y). Secondly, the attachment of organosilanes on the surface might also reduce the accessibility of active Pt sites. Thirdly, after silylation a decrease in the Pt loading of 16%, probably due to the additionally attached organosilanes, was obtained via ICP-OES for 3PtY3Cl18C0.5 in comparison to 3PtY. This decrease in the Pt loading might partly explain the drastically lower hydrogenation activity. Furthermore, silylation changes the wettability of the materials. The apparently hydrophobic catalysts obtained after silylation, therefore, impose a hydrophobic barrier which may negatively influence the catalytic activity.

The presence of FA was found to considerably impede the aqueous-phase hydrogenation of LA. Therefore, in later catalytic experiments H_2 was used as the reducing agent in the absence of FA under similar reaction conditions, i.e., 125 cm^3 of LA 0.2 M, at 493 K with 2.5 MPa H_2 for 24 h (cf. Table 3 and Figure 5). In contrast to the LA conversion achieved using FA as reducing agent, after 24 h over both 3PtY as well as 3PtY3Cl18C0.5 an almost complete LA conversion is observed when using H_2 . However, over the silylated catalyst 3PtY3Cl18C0.5 a lower GVL yield of 79% was observed compared to 92% of GVL yield obtained over 3PtY. Interestingly, if the hydrogenation using H_2 is conducted at 393 K, over 3PtY the LA conversion remains almost unchanged at a considerably lower GVL yield of 69%. Over 3PtY3Cl18C0.5 at 393 K both the LA conversion as well as GVL yield are largely impact amounting to 60 and 36%, respectively.

To investigate the hydrothermal stability of these catalysts after catalytic experiments, spent catalysts were collected and characterized via N_2 physisorption (cf. Figure 6, Figure S.5) and XRD (cf. Figure S.5). N_2 physisorption results revealed that the silylated catalyst using 3Cl18C as silylating agent was not stable at 493 K, under autogenous pressure after 24 h in the presence of FA. Similar to 3PtY, a decrease of 91% in the total specific surface area ($44\text{ vs. }483\text{ m}^2\text{ g}^{-1}$) and 70% in total specific pore volume ($0.11\text{ vs. }0.37\text{ cm}^3\text{ g}^{-1}$) were found for 3PtY3Cl18C0.5 (cf. Table S.2). The severe degradation of the faujasite framework is further confirmed by the absence of the characteristic reflections in the XRD patterns of these samples (cf. Figure S.5). When using only H_2 as the reducing agent for the hydrogenation of LA at the same reaction temperature of 493 K or even in the case of lower temperature, i.e., 393 K, the absence of the characteristic reflections in the XRD indicative for the faujasite framework topology is also observed for



3PtY3Cl18C0.5 (cf. Figure S.5). Moreover, the total specific surface area decreased from 483 to 91 m² g⁻¹ at 493 K and to 76 m² g⁻¹ at 393 K, which is consistent with the loss in the total specific pore volume from 0.37 to 0.25 cm³ g⁻¹ at 493 K and to 0.31 cm³ g⁻¹ at 393 K as a result of the structural collapse as confirmed by XRD. On the other hand, as can be seen in the N₂ isotherm for 3PtY3Cl1C10 a plateau was observed after a slight increase in the adsorbed N₂ volume at $p/p_0 < 0.01$, which is indicative of a partial retention of microporosity compared to 3PtY3Cl18C0.5 (Figure 6). Application of t-plot model evidenced the preservation of 50% of specific micropore volume for 3PtY3Cl1C10 after hydrogenation of LA in the presence of FA at 493 K under autogenous pressure for 24 h. In spite of the presence of the characteristic reflections of faujasite framework in the XRD pattern for this material, the shape of the baseline indicates that the crystalline zeolite phase was partly converted into an amorphous solid. However, the silylation using 3Cl1C with an excess amount could considerably enhance the hydrothermal stability of zeolite Y compared to 3PtY3Cl18C0.5.

CONCLUSIONS

We demonstrated that selective silylation of the free silanol groups on the external surface is evident by DRIFTS for zeolite Y silylated with monochlorosilanes. Nonetheless, zeolite Y silylated with monochlorosilanes were still prone to the degradation within 24 h under APP related conditions in the stability test, i.e., in an aqueous solution of 0.2 M LA and 0.6 M FA at

REFERENCES

- Abdelrahman, O. A., Heyden, A., and Bond, J. Q. (2014). Analysis of kinetics and reaction pathways in the aqueous-phase hydrogenation of levulinic acid to form γ -valerolactone over Ru/C. *ACS Catal.* 4, 1171–1181. doi: 10.1021/cs401177p
- 473 K under autogenous pressure. In contrast, by silylation with trichlorosilanes the hydrothermal stability of zeolite Y can be improved significantly. For zeolite Y functionalized with n-octadecyltrichlorosilane the destruction of the zeolite structure was found to be considerably retarded probably due to the partial polymerization of the attached organosilanes, which is feasible with more than one chlorine atom per silane. Noticeably, zeolite Y modified with methyltrichlorosilane in an excess amount, e.g., 10 mmol per gram of zeolite, was found to be the most stable material under APP conditions in the stability test.
- In the hydrogenation of LA to GVL over 3 wt.-% Pt on zeolite Y silylated either with n-octadecyltrichlorosilane or methyltrichlorosilane using different reducing agents, e.g., FA or H₂, the stabilizing effect of the silylation is far less pronounced. Only by applying an excess amount of methyltrichlorosilane, i.e., 10 mmol per 1 g of zeolite (3PtY3Cl1C10), a recognizable improvement of the stability of the 3PtY catalyst could be achieved in the LA hydrogenation using FA as reducing agent at 493 K. However, at a comparable LA conversion of 38 and 42%, the GVL yield observed over 3PtY3Cl1C10 is much lower than for 3PtY, i.e., 12 vs. 34% after 24 h. Since no further products could be evidenced by HPLC, ¹H as well as ¹³C NMR in the liquid product solution after 24 h of reaction it is most likely that insoluble humins are formed leading to the discrepancy in conversion and yield. In addition, 3PtY3Cl1C10 still suffers from partial damage of the zeolite framework.
- These results show, that silylation of zeolite Y using an excess amount of methyltrichlorosilane can improve its hydrothermal stability in aqueous acidic solutions, and, moreover, that 3 wt.-% Pt on zeolite Y silylated in this manner is active in the *in-situ* hydrogenation of LA using FA as reducing agent.

AUTHOR CONTRIBUTIONS

All authors listed have made a substantial, direct and intellectual contribution to the work, and approved it for publication.

ACKNOWLEDGMENTS

The author, H-TV, would like to thank the Vietnam Ministry of Education and Training (MOET) for the support of this work via Project 911. COST Action FP1306 is further gratefully acknowledged.

SUPPLEMENTARY MATERIAL

The Supplementary Material for this article can be found online at: <https://www.frontiersin.org/articles/10.3389/fchem.2018.00143/full#supplementary-material>

- Abdelrahman, O. A., Luo, H. Y., Heyden, A., Román-Leshkov, Y., and Bond, J. Q. (2015). Towards rational design of stable, supported metal catalysts for aqueous phase processing: insights from the hydrogenation of levulinic acid. *J. Catal.* 329, 10–21. doi: 10.1016/j.jcat.2015.04.026

- Alonso, D. M., Bond, J. Q., and Dumesic, J. A. (2010). Catalytic conversion of biomass to biofuels. *Green Chem.* 12, 1493–1513. doi: 10.1039/c004654j
- Alonso, D. M., Wettstein, S. G., and Dumesic, J. A. (2013). Gamma-valerolactone, a sustainable platform molecule derived from lignocellulosic biomass. *Green Chem.* 15, 584–595. doi: 10.1039/c3gc37065h
- Chhedha, J. N., Huber, G. W., and Dumesic, J. A. (2007). Liquid-phase catalytic processing of biomass-derived oxygenated hydrocarbons to fuels and chemicals. *Angew. Chem. Int. Ed. Engl.* 46, 7164–7183. doi: 10.1002/anie.200604274
- Cortright, R. D., Davda, R. R., and Dumesic, J. A. (2002). Hydrogen from catalytic reforming of biomass-derived hydrocarbons in liquid water. *Nature* 418, 964–967. doi: 10.1038/nature01009
- Delhomme, C., Schaper, L.-A., Zhang-Preße, M., Raudaschl-Sieber, G., Weuster-Botz, D., Kühn, F. E. (2013). Catalytic hydrogenation of levulinic acid in aqueous phase. *J. Organomet. Chem.* 724, 297–299. doi: 10.1016/j.jorganchem.2012.10.030
- Deng, L., Li, J., Lai, D.-M., Fu, Y., and Guo, Q.-X. (2009). Catalytic conversion of biomass-derived carbohydrates into gamma-valerolactone without using an external H₂ supply. *Angew. Chem. Int. Ed. Engl.* 48, 6529–6532. doi: 10.1002/anie.200902281
- Deng, L., Zhao, Y., Li, J., Fu, Y., Liao, B., and Guo, Q.-X. (2010). Conversion of levulinic acid and formic acid into γ -Valerolactone over heterogeneous catalysts. *ChemSusChem* 3, 1172–1175. doi: 10.1002/cssc.201000163
- Du, X.-L., He, L., Zhao, S., Liu, Y.-M., Cao, Y., He, H.-Y., et al. (2011). Hydrogen-independent reductive transformation of carbohydrate biomass into γ -valerolactone and pyrrolidone derivatives with supported gold catalysts. *Angew. Chem. Int. Ed. Engl.* 50, 7815–7819. doi: 10.1002/anie.201100102
- Ennaert, T., Geboers, J., Gobechiya, E., Courtin, C. M., Kurttepli, M., et al. (2015). Conceptual frame rationalizing the self-stabilization of H-USY zeolites in hot liquid water. *ACS Catal.* 5, 754–768. doi: 10.1021/cs501559s
- Ennaert, T., Van Aelst, J., Dijkmans, J., de Clercq, R., Schutyser, W., Dusselier, M., et al. (2016). Potential and challenges of zeolite chemistry in the catalytic conversion of biomass. *Chem. Soc. Rev.* 45, 584–611. doi: 10.1039/C5CS00859J
- Galadima, A., and Muraza, O. (2017). Stability improvement of zeolite catalysts under hydrothermal conditions for their potential applications in biomass valorization and crude oil upgrading. *Microporous Mesoporous Mater.* 249, 42–54.
- Gallezot, P. (2012). Conversion of biomass to selected chemical products. *Chem. Soc. Rev.* 41, 1538–1558. doi: 10.1039/C1CS15147A
- Geilen, F. M. A., Engendahl, B., Harwardt, A., Marquardt, W., Klankermayer, J., and Leitner, W. (2010). Selective and flexible transformation of biomass-derived platform chemicals by a multifunctional catalytic system. *Angew. Chem.* 122, 5642–5646. doi: 10.1002/ange.201002060
- Huang, B. T., Leveneur, S., Zamar, T., Mikkola, J. P., and Taouk, B. (2015). Towards Production of γ -valerolactone via hydrogenation of aqueous levulinic acid. *Int. J. Chem. React. Eng.* 13, 119–127. doi: 10.1515/ijcre-2014-0077
- Huber, G. W., Cortright, R. D., and Dumesic, J. A. (2004). Renewable alkanes by aqueous-phase reforming of biomass-derived oxygenates. *Angew. Chem. Int. Ed. Engl.* 43, 1549–1551. doi: 10.1002/anie.200353050
- Kamm, B., Gruber, P. R., and Kamm, M. (eds.) (2005). *Biorefineries-Industrial Processes and Products: Status Quo and Future Directions*. Weinheim: Wiley-VCH.
- Lange, J.-P., Price, R., Ayoub, P. M., Louis, J., Petrus, L., Clarke, L., et al. (2010). Valeric biofuels: a platform of cellulosic transportation fuels. *Angew. Chem. Int. Ed. Engl.* 49, 4479–4483. doi: 10.1002/anie.201000655
- Li, W., Xie, J.-H., Lin, H., and Zhou, Q.-L. (2012). Highly efficient hydrogenation of biomass-derived levulinic acid to γ -valerolactone catalyzed by iridium pincer complexes. *Green Chem.* 14, 2388–2390. doi: 10.1039/C2GC35650C
- Luo, W., Deka, U., Beale, A. M., van Eck, E. R., Bruijninx, P. C., Weckhuysen, B. M., (2013). Ruthenium-catalyzed hydrogenation of levulinic acid: influence of the support and solvent on catalyst selectivity and stability. *J. Catal.* 301, 175–186. doi: 10.1016/j.jcat.2013.02.003
- Mehdi, H., Fábos, V., Tuba, R., Bodor, A., Mika, L. T., and Horváth, I. T. (2008). Integration of homogeneous and heterogeneous catalytic processes for a multi-step conversion of biomass: From sucrose to levulinic acid, γ -valerolactone, 1,4-pentanediol, 2-methyl-tetrahydrofuran, and alkanes. *Top Catal.* 48, 49–54. doi: 10.1007/s11244-008-9047-6
- Prodinger, S., Derewinski, M. A., Vjunov, A., Burton, S. D., Arslan, I., and Lercher, J. A. (2016). Improving stability of zeolites in aqueous phase via selective removal of structural defects. *J. Am. Chem. Soc.* 138, 4408–4415. doi: 10.1021/jacs.5b12785
- Ravenelle, R. M., Schüßler, F., D'Amico, A., Danilina, N., van Bokhoven, J. A., Lercher, J. A., et al. (2010). Stability of zeolites in hot liquid water. *J. Phys. Chem. C* 114, 19582–19595. doi: 10.1021/jp104639e
- Ruppert, A. M., Grams, J., Jedrzejczyk, M., Matras-Michalska, J., Keller, N., Ostojka, K., et al. (2015). Titania-supported catalysts for levulinic acid hydrogenation: influence of support and its impact on γ -valerolactone yield. *ChemSusChem* 8, 1538–1547. doi: 10.1002/cssc.201403332
- Sun, Y., and Cheng, J. (2002). Hydrolysis of lignocellulosic materials for ethanol production: a review. *Bioresour. Technol.* 83, 1–11. doi: 10.1016/S0960-8524(01)00212-7
- Thommes, M., Kaneko, K., Neimark, A. V., Olivier, J. P., Rodriguez-Reinoso, F., Rouquerol, J., et al. (2015). Physisorption of gases, with special reference to the evaluation of surface area and pore size distribution (IUPAC Technical Report). *Pure Appl. Chem.* 87, 1051–1069. doi: 10.1515/pac-2014-1117
- Weitkamp, J. (2000). Zeolites and catalysis. *Solid State Ionics* 131, 175–188. doi: 10.1016/S0167-2738(00)00632-9
- Wright, W. R. H., and Palkovits, R. (2012). Development of heterogeneous catalysts for the conversion of levulinic acid to γ -valerolactone. *ChemSusChem* 5, 1657–1667. doi: 10.1002/cssc.201200111
- Yoshida, W., Castro, R. P., Jou, J.-D., and Cohen, Y. (2001). Multilayer alkoxysilane silylation of oxide surfaces. *Langmuir* 17, 5882–5888. doi: 10.1021/la001780s
- Zapata, P. A., Huang, Y., Gonzalez-Borja, M. A., Resasco, D. E. (2013). Silylated hydrophobic zeolites with enhanced tolerance to hot liquid water. *J. Catal.* 308, 82–97. doi: 10.1016/j.jcat.2013.05.024
- Zapata, P. A., Faria, J., Ruiz, M. P., Jentoft, R. E., and Resasco, D. E. (2012). Hydrophobic zeolites for biofuel upgrading reactions at the liquid-liquid interface in water/oil emulsions. *J. Am. Chem. Soc.* 134, 8570–8578. doi: 10.1021/ja3015082
- Zhang, L., Chen, K., Chen, B., White, J. L., and Resasco, D. E. (2015). Factors that determine zeolite stability in hot liquid water. *J. Am. Chem. Soc.* 137, 11810–11819. doi: 10.1021/jacs.5b07398

Conflict of Interest Statement: The authors declare that the research was conducted in the absence of any commercial or financial relationships that could be construed as a potential conflict of interest.

Copyright © 2018 Vu, Harth and Wilde. This is an open-access article distributed under the terms of the Creative Commons Attribution License (CC BY). The use, distribution or reproduction in other forums is permitted, provided the original author(s) and the copyright owner are credited and that the original publication in this journal is cited, in accordance with accepted academic practice. No use, distribution or reproduction is permitted which does not comply with these terms.



Vapor-Phase Hydrogenation of Levulinic Acid to γ -Valerolactone Over Bi-Functional Ni/HZSM-5 Catalyst

Margarita Popova¹, Petar Djinoić², Alenka Ristić², Hristina Lazarova¹, Goran Dražić², Albin Pintar², Alina M. Balu³ and Nataša Novak Tušar^{2,4*}

¹ Institute of Organic Chemistry with Centre of Phytochemistry, Bulgarian Academy of Sciences, Sofia, Bulgaria, ² National Institute of Chemistry, Ljubljana, Slovenia, ³ Departamento de Química Orgánica, Universidad de Córdoba, Córdoba, Spain, ⁴ University of Nova Gorica, Nova Gorica, Slovenia

OPEN ACCESS

Edited by:

Konstantinos Triantafyllidis,
Aristotle University of Thessaloniki,
Greece

Reviewed by:

Miguel Angel Centeno,
Consejo Superior de Investigaciones
Científicas (CSIC), Spain
Renaud Cousin,
Université du Littoral Côte d'Opale,
France

*Correspondence:

Nataša Novak Tušar
natasa.novak.tusar@ki.si

Specialty section:

This article was submitted to
Green and Sustainable Chemistry,
a section of the journal
Frontiers in Chemistry

Received: 02 March 2018

Accepted: 25 June 2018

Published: 17 July 2018

Citation:

Popova M, Djinoić P, Ristić A,
Lazarova H, Dražić G, Pintar A,
Balu AM and Novak Tušar N (2018)
Vapor-Phase Hydrogenation of
Levulinic Acid to γ -Valerolactone Over
Bi-Functional Ni/HZSM-5 Catalyst.
Front. Chem. 6:285.
doi: 10.3389/fchem.2018.00285

The hydrogenation of levulinic acid (LA) to γ -valerolactone (GVL) in vapor-phase is economically more viable route if compared to reaction in liquid-phase. To improve the GVL yield in the vapor-phase reaction, the optimization of nickel modified zeolite as bi-functional catalyst (Ni/HZSM-5) was studied. Ni/HZSM-5 materials with fixed Al/Si molar ratio of 0.04 and different nominal Ni/Si molar ratios (from 0.01 to 0.05) were synthesized without the use of organic template and with the most affordable sources of silica and alumina. Materials were characterized by X-ray powder diffraction, SEM-EDX, TEM-EDX, pyridine TPD and DRIFTS, H₂-TPR, N₂ physisorption and isoelectric point. In the synthesized materials, 61–83% of nickel is present as bulk NiO and increases with nickel content. Additionally, in all catalysts, a small fraction of Ni²⁺ which strongly interacts with the zeolite support was detected (10–18%), as well as Ni²⁺ acting as charge compensating cations for Brønsted acid sites (7–21%). Increasing the nickel content in the catalysts leads to a progressive decrease of Brønsted acid sites (BAS) and concomitant increase of Lewis acid sites (LAS). When BAS/LAS is approaching to 1 and at the same time the amount of NiO reducible active sites is around 80%, the bi-functional Ni/HZSM-5-3 catalyst (Ni/Al = 0.59) leads to 99% conversion of LA and 100% selectivity to GVL at 320°C. This catalyst also shows stable levulinic acid hydrogenation to GVL in 3 reaction cycles conducted at 320°C. The concerted action of the following active sites in the catalyst is a key element for its optimized performance: (1) Ni metallic active sites with hydrogenation effect, (2) Lewis acid sites with dehydration effect, and (3) nickel aluminate sites with synergetic and stabilizing effects of all active sites in the catalyst.

Keywords: Ni/HZSM-5, Ni/Al molar ratio acidity regulation, vapor-phase hydrogenation, levulinic acid conversion, γ -valerolactone selectivity, biomass valorization

INTRODUCTION

The decrease in fossil fuel reserves and the high price of petrochemicals have focused the attention to the renewable energy resources (Corma et al., 2007; Hayes, 2009; Bond et al., 2010; Climent et al., 2014; Mika et al., 2018). Lignocellulosic biomass is a promising inexpensive renewable material that could satisfy society's requirements for chemicals and fuels (Corma et al., 2007; Chang, 2011; Climent et al., 2014; Li et al., 2016). Lignocellulosic biomass can be hydrolyzed into a mixture of cellulose, hemicellulose and lignin. Further hydrolysis of the hemicellulose and cellulose leads to the formation of C5 and C6 monosaccharides. Levulinic acid (LA) can be derived from lignocellulosics via acid-catalyzed hydrolysis processes (Wettstein et al., 2012; Wright and Palkovits, 2012) and can be utilized as a platform molecule for the production of valuable products including biofuels precursors such as γ -valerolactone (GVL) (Son et al., 2014). GVL can be used as a solvent, fuel additive, and intermediate in the production of diverse value-added chemicals (Horváth et al., 2008; Heeres et al., 2009; Serrano-Ruiz and Dumesic, 2011; Kumar et al., 2015; Long et al., 2015; Li et al., 2016; Jiang et al., 2016; Song et al., 2017).

GVL has been produced from LA via catalytic hydrogenation to hydroxyvaleric acid followed by ring closing and dehydration to GVL (Ruiz et al., 2010). In recent years, a lot of research has been done on the catalytic hydrogenation of LA to GVL using homogeneous, as well as heterogeneous catalysts (Shu et al., 1995; Hengne et al., 2012; Yan and Chen, 2014; Abdelrahman et al., 2014; Nadgeri et al., 2014; Song et al., 2017; Sun et al., 2017). However, heterogeneous catalytic processes are more economical as they offer advantages such as easy recovery and recycling. Typically GVL could be produced by liquid-phase hydrogenation of LA using heterogeneous catalytic processes over supported noble metal (Ru, Ir, and Pd), or non-noble metal catalysts such as Co, Cu, and Ni (Shu et al., 1995; Hengne et al., 2012; Nadgeri et al., 2014; Yan and Chen, 2014; Song et al., 2017; Sun et al., 2017). In spite of the excellent performance, unfortunately, some drawbacks including high cost of noble metals, and metal leaching in harsh conditions limit their applications for large-scale LA production. Additionally, the liquid phase conversion of LA to GVL has a number of disadvantages, such as the requirement for high pressure, purification after the reaction process, as well as safety and waste emission. Vapor-phase hydrogenation of levulinic acid gives the opportunity to overcome these disadvantages.

To the best of our knowledge, only limited studies were performed from 2015 to 2018 in vapor-phase hydrogenation in which Cu, Co and Ni supported catalysts were studied (Kumar et al., 2015, 2016; Sun et al., 2017; Yoshida et al., 2017; Lomate et al., 2018). The optimization of reaction parameters (temperature, pressure, space velocity, reaction time) and type of used catalysts are key factors for development of technology for preparation of GVL by hydrogenation of levulinic acid (Galletti et al., 2012; Zhou et al., 2014). Another important task is related to the increase of the levulinic acid conversion by the addition of stable solid acid co-catalysts as supports (i.e., zeolites) to conventional catalysts.

Zeolites are well known and widely employed industrial acid catalysts (Ertl et al., 2008). The introduction of low-cost transition metals supported on zeolite is a promising way for industrial applications requiring bi-functional catalysts (metallic and acidic function) to achieve the desired chemical conversions. Zeolites are acidic microporous crystalline aluminosilicates. Among many different zeolite structure types, the MFI (ZSM-5) has been widely reported for its use in the catalytic treatment of hydrocarbons. Recent studies report that sitting and distribution of Al sites in zeolites (Brønsted acid sites) is not statistical, but depends on the zeolite hydrothermal synthesis conditions (Perea et al., 2015). The acidity and textural properties of zeolites can be modified by the addition of transition metal oxides, obtaining bi-functional catalysts. Acidity regulation of bi-functional catalyst balances its hydrocarbon cracking function and can slow down the coke formation, thus contributing to a longer catalyst lifetime. On the basis of our previous experience (Szegedi et al., 2007), nickel metallic species exhibit higher intrinsic activity for toluene hydrogenation reaction and they are generally regarded as the active sites in traditional hydrogenation catalysts. Recently, Ni/HZSM-5 with excellent stability for the cascade transformation of LA to GVL with 100% yield was developed, where acidity was regulated by potassium (Al/Si = 0.026, 10 wt. % Ni and 0.5% K) (Sun et al., 2016).

In the present study, we describe the application of Ni functionalized HZSM-5 catalyst for vapor-phase hydrogenation of levulinic acid to γ -valerolactone with 100% yield, where the catalytic properties of the catalysts are regulated by Ni/Al molar ratio. In this way, the requirement for additional metal to attenuate the acidity of the catalyst was avoided, which makes the synthesis of the catalysts simpler and more economic. A template-free ZSM-5 zeolite was synthesized, which is considered as a green and sustainable process, avoiding the use of any organic structure-directing agents (templates). The synthesis process was developed in collaboration between the National Institute of Chemistry and a local zeolite producer in Slovenia, SILKEM (Fakin et al., 2015). The structural, acidic and catalytic properties of ZSM-5 support with different Al/Si molar ratio were described in our previous study. The ZSM-5 support with optimal Al/Si molar ratio 0.04 was chosen for this study (Ojeda et al., accepted).

MATERIALS AND METHODS

Materials

Sodium aluminate, sodium aqueous glass NaVS3M, sulphuric acid, ammonium sulfate and nickel (II) nitrate hexahydrate ($\text{Ni}(\text{NO}_3)_2 \cdot 6\text{H}_2\text{O}$) were provided by Sigma Aldrich. Sodium hydroxide was provided by Merck. ZSM-5 crystallization seeds were provided from Zeolyst (CBU2314, $\text{SiO}_2/\text{Al}_2\text{O}_3 = 23$).

Synthesis

ZSM-5 was prepared by seed-assisted synthesis following a procedure previously reported (Fakin et al., 2015). ZSM-5 crystallization seeds (CBU2314, Zeolyst, $\text{SiO}_2/\text{Al}_2\text{O}_3 = 23$) were dissolved in distilled water (solution A). Sodium aqueous glass (NaVS3M, Silkem, $\text{Na}_2\text{O} = 8.62\%$, $\text{SiO}_2 = 27.83\%$) was added to solution A during stirring at room temperature with the aqueous

solution of sodium aluminate (Silkem, $\gamma(\text{Na}_2\text{O}) = 170.19 \text{ g/L}$, $\gamma(\text{Al}_2\text{O}_3) = 148.46$)—solution B. Aqueous solution of sulphuric acid (Sigma Aldrich, 96%) was slowly added to the solution B and stirred for 10 min in order to regulate the pH value at 11. Hydrogel was aged for 30 min and then transferred to 1 L reactor (Parr) for crystallization at 180°C for 24 h during continuous stirring. The obtained product was filtered, washed with water, and dried at 60°C overnight. Acidic zeolites were prepared by NH_4^+ exchange. Ammonium sulfate ($(\text{NH}_4)_2\text{SO}_4$, Sigma Aldrich, $\geq 99.0\%$), distilled water and zeolite (ZSM-5) were used as the main components in the molar ratio of 1:1:20 and mixed at 30°C for 2 h. The exchanged product was filtered, washed with distilled water, dried overnight at 105°C and calcined in air at 500°C for 2 h. The Ni containing HZSM-5 catalysts were obtained by incipient wetness impregnation method using $(\text{Ni}(\text{NO}_3)_2 \cdot 6\text{H}_2\text{O})$, Sigma Aldrich, purity = 99.999%) with the theoretical molar ratios of Ni/Si = 0.01, 0.03, and 0.05. Finally, the products were calcined in air at 500°C for 2 h, to obtain the corresponding metal oxide (Szegeedi et al., 2007). The products were denoted: Ni/HZSM-5-1 (Ni/Si = 0.01), NiHZSM-5-3 (Ni/Si = 0.03), NiHZSM-5-5 (Ni/Si = 0.05).

Characterization

The prepared catalysts were characterized by different techniques in order to determine their physicochemical properties. The crystal structure of the prepared and spent catalysts was analyzed by X-ray diffraction (XRD) using a PANalytical X'Pert PRO MPD X-ray diffractometer ($\text{CuK}\alpha_1 = 0.15406 \text{ nm}$) with an accelerating voltage of 45 kV and an emission current of 40 mA. XRD patterns were obtained at room temperature from 2θ from 5 to 70° with a step of 0.034° and time of 16 h.

Scanning electron microscopy (SEM) was used to determine the morphology and particle size of the catalysts using a Zeiss Supra TM 3VP electron microscopy. The elemental analysis was performed by energy-dispersive X-ray spectroscopy (EDXS), using a Zeiss Supra TM 3VP scanning electron microscope with an INCA Energy system attached.

The surface area and pore volume of the samples were determined from N_2 physisorption isotherms collected at -196°C using a Tristar 3000 analyzer (Micromeritics). The specific surface area was determined using the Brunauer-Emmett-Teller (BET) method. Before N_2 adsorption, the samples were outgassed under vacuum for 2 h at 200°C in the apparatus. The micropore surface area and micropore volume were determined using the t-plot method.

Isoelectric point, defined as the pH value at which the surface charge is zero, was determined using Zetasizer nano ZS (Malvern) based on electrophoretic scattering of light in the pH range from 2 to 10. The pH value was controlled by a 0.1 M NaOH and 0.1 M HCl solutions. The pH value of each suspension was measured using a digital pH meter.

Thermogravimetric method of pyridine adsorption was used for quantification of acid sites on investigated materials using Pyris 1 TGA apparatus from Perkin Elmer. Prior to analysis, the samples were degassed *in-situ* in N_2 stream (30 mL/min) at 500°C for 1 h. Afterwards, the samples were cooled to 125°C and saturated with pyridine vapors by passing the N_2 stream through

a saturator filled with liquid pyridine. Saturation was followed by desorption of weakly bound pyridine by degassing the sample in N_2 at 125°C for additional 2 h until achieving a stable sample weight. Total number of acid sites was calculated based on the weight difference before and after sample saturation. Strength of the acid sites was estimated using temperature programmed desorption based on the assumption that stronger acid sites desorb pyridine at higher temperatures. The sample was heated in N_2 stream (30 mL/min) until 500°C and mass change was continuously monitored.

Differentiation between Brønsted (BAS) and Lewis (LAS) acid sites was done for pure HZSM-5 and Ni/HZSM-5 materials by DRIFTS analysis using Frontier IR spectrometer (Perkin Elmer), DiffusIR[®] accessory from Pike Scientific and pyridine as the probe molecule. The powdered samples ($\sim 10 \text{ mg}$) were positioned in the ceramic sample cup and pretreated in N_2 (50 mL/min) at 500°C for 30 min. After cooling to 125°C , the samples were saturated with pyridine vapors (nitrogen (50 mL/min) was bubbled through a saturator filled with liquid pyridine) for 10 min, followed by degassing in vacuum ($1 \times 10^{-5} \text{ mbar}$) for 1 h. Spectra were recorded with 8 accumulations and spectral resolution of 4 cm^{-1} between 800 and $4,000 \text{ cm}^{-1}$. For characterization of LAS and BAS, adsorption bands at 1,445 and $1,545 \text{ cm}^{-1}$ were considered. The first originates from pyridine adsorbed on LAS, while the second from pyridinium ion coordinatively bound to BAS. The BAS/LAS ratio was calculated as follows:

$$\text{BAS/LAS} = 1.73/1.23 \times I_{\text{BAS}}/I_{\text{LAS}}$$

In this equation, I_{BAS} and I_{LAS} represent intensity of absorption bands at 1,545 and $1,445 \text{ cm}^{-1}$, 1.73 and 1.23 are extinction coefficients, as reported by Tamura et al. (2012).

Temperature programmed reduction with hydrogen (H_2 -TPR) was used to characterize the interaction between the HZSM-5 support and the supported reducible nickel containing species. The AutoChem II 2920 apparatus from Micromeritics was used. During the experiment, 100 mg of a sample was positioned inside the quartz reactor and pretreated in 20% O_2/N_2 at 300°C for 5 min. After sample cooling to 10°C , it was degassed in Ar for 10 min. TPR analysis was performed between 10 and 750°C , 25 mL/min of 5% H_2/Ar flow and a heating rate of $10^\circ\text{C}/\text{min}$. The recorded TPR curves were deconvoluted with Peakfit software using symmetrical Gaussian peaks to quantitatively evaluate the contribution of NiO, nickel phyllosilicates and Ni^{2+} charge compensating cations.

UV-Vis DR spectra were recorded on a Perkin Elmer Lambda 35 apparatus equipped with a Praying Mantis accessory. Background was recorded with Spectralon[®] reference. Samples were scanned in the spectral range between 200 and 900 nm, with slit set to 2 nm and scanning speed of 240 nm/min.

Ni/HZSM-5 materials were studied by probe Cs corrected scanning transmission electron microscope Jeol ARM 200 CF with cold-FEG cathode, equipped with dual-EELS (Electron Energy Loss Spectroscopy) system Quantum ER from Gatan and Centurio EDXS system (Energy dispersive X-ray spectroscopy) with 100 mm^2 SDD detector (Silicon drifted detector). In

scanning transmission mode (STEM) two observation techniques were used: high-angle annular dark-field (HAADF) imaging and bright-field (BF) imaging.

Catalytic Activity Measurements

Prior to the catalytic tests, samples were pretreated for 1 h in N₂ flow at 400°C.

Levulinic acid hydrogenation was studied at atmospheric pressure using a fixed-bed flow reactor with hydrogen as carrier gas (30 mL/min). In the reaction, 50 mg sample (particle size 0.2–0.8 mm) was tested, diluted with 50 mg of glass beads of the same diameter, which were previously checked to be inactive. The reactor itself was a quartz tube of 15 mm inner diameter, with the catalyst bed at the middle. A thermocouple was positioned in the catalyst bed for accurate temperature measurements. All gas lines of the apparatus were heated continuously to 150°C in order to minimize condensation of reactants and products on the tube walls. The hydrogen stream passed through a saturator filled with levulinic acid equilibrated at 0°C. The reactants were fed into the reactor with a flow rate of 30 mL/min and catalytic tests were carried out in the temperature range of 250–350°C. The reaction steady state was established after 30 min at each temperature. On-line analysis of the reaction products was performed using HP-GC with a 30 m HP-5MS capillary column. The reusability of the most active sample was studied in 3 reaction cycles and the catalyst was regenerated in air at 500°C, reduced in hydrogen at 400°C, and studied in the catalytic reaction in every reaction cycle.

RESULTS AND DISCUSSION

Physico-Chemical Characterization

The X-Ray patterns of the catalysts before the reaction (prepared catalysts) and after the reaction (spent catalysts) are shown in **Figures 1A,B**, respectively. All the prepared catalysts present the typical XRD patterns corresponding to a single crystalline phase with MFI structure. The crystalline structure of HZSM-5 is not affected by deposition of nickel, however, broad diffraction peaks belonging to NiO are detected (**Figure 1A**), indicating on the formation of nanosized particles, located on the surface of zeolite crystals. The crystallite sizes of NiO are calculated using Scherrer's equation based on the selected diffraction peaks of the corresponding XRD pattern and it was found to be 21, 12, and 10 nm for Ni/HZSM-5-5, Ni/HZSM-5-3, and Ni/HZSM-5-1, respectively. No other crystalline phases are detected in the prepared catalysts. XRD patterns (**Figure 1B**) of the spent catalysts show the preservation of the ZSM-5 structure and the presence of the metallic Ni crystallites, having from 36 (Ni/HZSM-5-3) to 44 nm (Ni/HZSM-5-1 and Ni/HZSM-5-5) in size.

SEM photos revealed the presence of nicely formed crystals in all samples. The crystals were about 3–5 μm in size with a typical shape of hexagonal prisms for ZSM-5 (**Figure 2**).

The data from the EDXS elemental analysis of Ni/HZSM-5 materials are summarized in **Table 1**. The measured amount of aluminum in the catalysts corresponds closely to the nominal value for all analyzed materials. The measured amount of

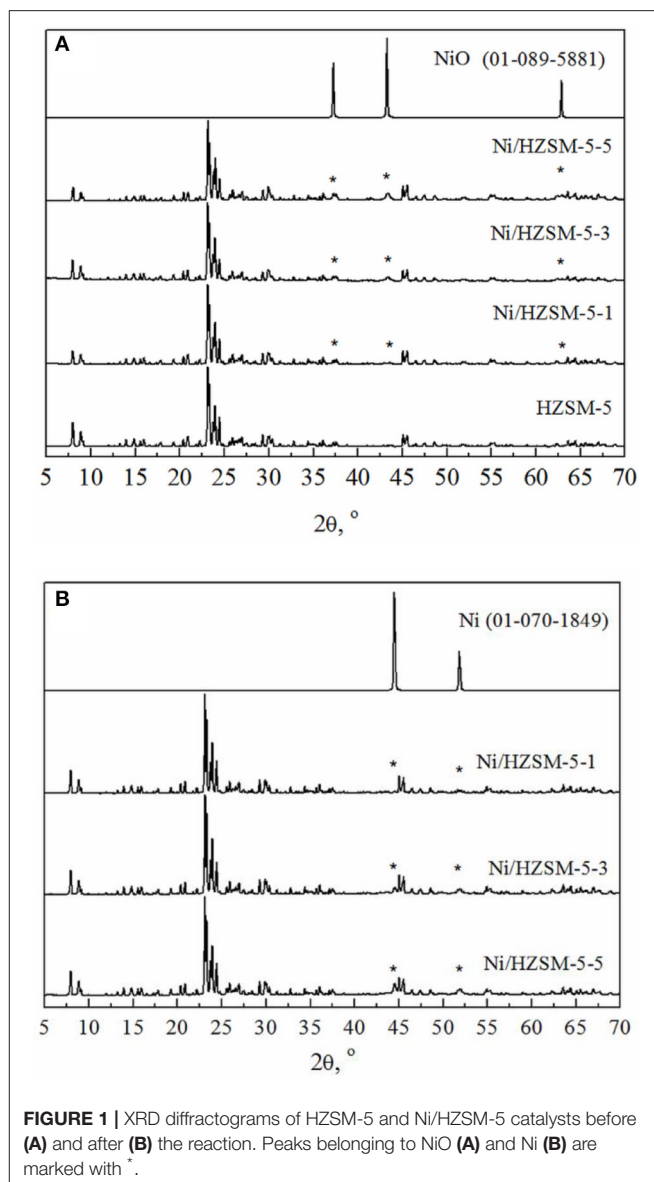


FIGURE 1 | XRD diffractograms of HZSM-5 and Ni/HZSM-5 catalysts before (A) and after (B) the reaction. Peaks belonging to NiO (A) and Ni (B) are marked with *.

nickel present in the Ni/HZSM-5-1 and Ni/HZSM-5-3 materials corresponds approximately to the nominal values, whereas it is significantly lower in the Ni/HZSM-5-5 sample.

The modification of HZSM-5 by nickel causes the specific surface area of the catalysts to decrease progressively with the increase of nickel content (**Table 2**). This is most likely due to the deposition of NiO crystallites on the surface of zeolite crystals, which is in agreement with XRD results. Micropore surface area decreased due to Ni²⁺ exchanged Brønsted acid sites in micropores (Ma et al., 2016).

The redox properties of the catalysts and interaction between nickel containing reducible phases and HZSM-5 support were analyzed with H₂-TPR. The reduction profiles of examined Ni/ZSM-5 catalysts (**Figure 3**) are composed of several overlapping peaks indicating presence of different reducible nickel containing phases. The main envelope of peaks between

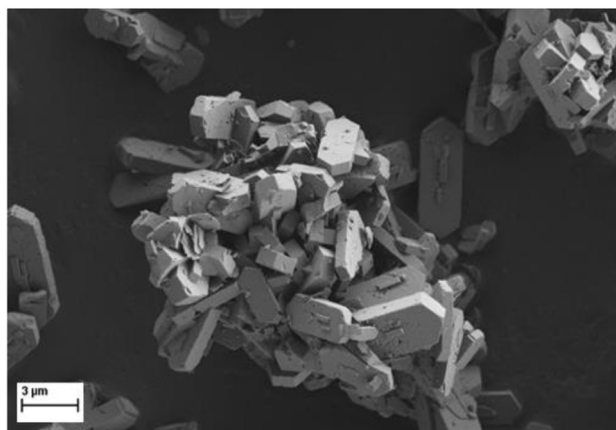


FIGURE 2 | SEM micrograph of Ni/HZSM-5-3 catalyst sample (2.2 wt. % Ni).

TABLE 1 | Elemental analysis of the Ni/HZSM-5 materials, measured with EDXS technique.

Catalyst	Molar ratio (theoretical)		Metal content (EDXS)		Molar ratio (practical)	
	Ni/Si	Al/Si	Ni (wt. %)	Al (wt. %)	Ni/Si	Al/Si
Ni/HZSM-5-1	0.01	0.04	1.18	1.71	0.013	0.042
Ni/HZSM-5-3	0.03	0.04	2.22	1.73	0.025	0.042
Ni/HZSM-5-5	0.05	0.04	2.71	1.71	0.031	0.042

TABLE 2 | Structural properties of fresh Ni/HZSM-5 catalysts containing different nickel amounts.

Catalyst	Specific surface area (m ² /g)	Micropore volume (cm ³ /g)	Micropore surface area S _{mp} (m ² /g)	External surface area S _{ext} (m ² /g)
Ni/HZSM-5-1	400	0.125	313	87
Ni/HZSM-5-3	381	0.119	298	83
Ni/HZSM-5-5	345	0.109	270	75

300 and 400°C shows a progressive shift to higher temperatures (apex shifts from 306 to 362°C) when the nominal Ni/Si content is increased from 0.01 to 0.05. These peaks can be assigned to reduction of polydisperse bulk NiO having weak or no interaction with the zeolite support (Louis et al., 1993; Yuan et al., 2006; Maia et al., 2010). The NiO crystallites measuring from 8 to 30 nm have been identified performing TEM analysis on all catalysts. The second peak (above 400°C) increases in intensity and its apex shifts toward higher temperatures (from 427 to 477°C) when increasing NiO loading. This is a consequence of increasing amount of Ni²⁺ strongly interacting with the zeolite support. A broad shoulder above 550°C which extends up to 700°C belongs to reduction of Ni²⁺ species, which are distributed over the surface of catalysts as charge compensating cations for Brønsted acid sites (nickel aluminate phase). The H₂ quantity, consumed during the TPR analyses was sufficient for total reduction of Ni²⁺ to metallic nickel.

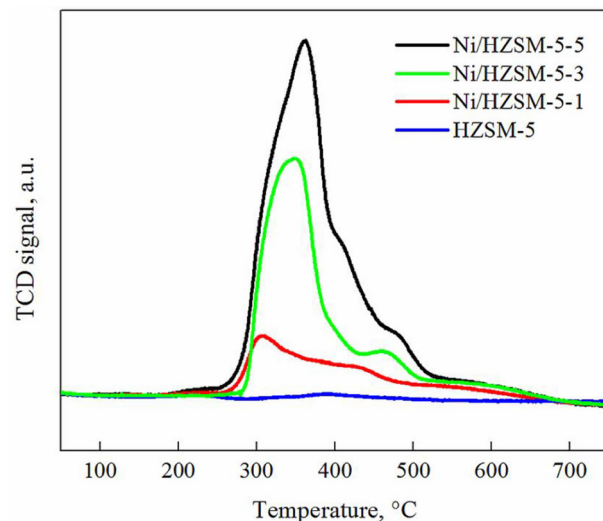


FIGURE 3 | H₂-TPR profiles of HZSM-5 and Ni/HZSM-5 catalysts containing 1, 2, and 3 weight % of nickel (Ni/HZSM-5-1, Ni/HZSM-5-3, Ni/HZSM-5-5).

TABLE 3 | Total H₂ consumed during TPR analysis and qualitative distribution of different nickel containing species for Ni/HZSM-5 catalysts.

Sample	Total H ₂ consumed, mmol/g _{cat}	NiO, %	Ni ²⁺ strongly interacting with the zeolite support, %	Ni ²⁺ as charge compensating cations, %
Ni/HZSM-5-1	0.25	61	18	21 (0.042) ^a
Ni/HZSM-5-3	0.57	77	12	11 (0.062)
Ni/HZSM-5-5	0.92	83	10	7 (0.064)

^aValues in parentheses represent the amount of Ni²⁺ (mmol/g_{cat}) acting as charge compensating cations for Brønsted acid sites.

The TPR curves were further deconvoluted into several contributions (bulk NiO, Ni²⁺ strongly interacting with the zeolite support and charge compensating Ni²⁺ cations), according to the temperature range where they occur, in order to estimate their contribution to the overall amount of H₂ consumed. It was found that the bulk NiO is the predominant phase in all analyzed materials, accounting for 61–83% of all nickel. With increasing nickel loading, the fraction of bulk NiO increases due to progressive segregation of this phase on the surface of the zeolite crystals (confirmed by TEM analysis). The Ni²⁺ strongly interacting with the zeolite support accounts for 10–18% of all nickel. The remaining are Ni²⁺ charge compensating cations for the Brønsted acid sites (nickel aluminate phase). Their amount (Table 3) is about an order of magnitude lower compared to the measured total number of Brønsted acid sites in the parent HZSM-5 zeolite (i.e., 0.70 mmol/g_{cat}), indicating that nickel addition only slightly decreases their abundance.

Gravimetric chemisorption of pyridine, followed by TPD was used to evaluate the total number and strength of acid sites present in the catalysts. Based on the amount of chemisorbed pyridine, total acidity changed very little when nickel was

deposited to the HZSM-5 support (**Table 4**). The measured value for the pure HZSM-5 ($0.70 \text{ mmol/g}_{\text{cat}}$) corresponds closely to the theoretical calculation ($0.64 \text{ mmol/g}_{\text{cat}}$), which assumed all Al^{3+} as tetrahedrally coordinated and located in the zeolite framework.

Strength of acid sites was evaluated using temperature programmed desorption of the chemisorbed pyridine. It can be seen in **Figure 4** that as nickel content increases, the acid site strength decrease. This is due to the fact that the newly formed Lewis acid sites (LAS - coordinatively unsaturated Ni^{2+}), exhibit intrinsically weaker electrophilic character and consequently lower acid site strength compared to Brønsted acid sites. The sharp pyridine desorption peak recorded over Ni/HZSM-5-3 and Ni/HZSM-5-5 catalysts between 470 and 550°C could only tentatively be ascribed to pyridine desorption from the LAS due to the most abundant NiO phase present in these materials. Due to the fact that all samples were pretreated at 500°C (to avoid excessive sintering of nickel containing phases), catalyst dehydroxylation above this temperature (represented by shaded area in **Figure 4**) could also occur and result in mass loss, which could be erroneously assigned to pyridine desorption.

Nature of acid sites was analyzed using pyridine as the probe molecule. Pure HZSM-5 contains predominantly Brønsted acid sites (BAS), with BAS/LAS ratio equaling 13.1 (**Figure 5A**). This confirms the large majority (93 %) of aluminum is present in tetrahedral framework coordination. Addition of increasing nickel amounts leads to a progressive decrease of BAS and concomitant increase of LAS (**Table 4**), resulting in a BAS/LAS ratio of ~ 1 . The observed changes in the nature of acid sites are due to Ni^{2+} cations replacing H^+ - nickel aluminate phase (observed also indirectly through the occurrence of high temperature reduction peak during H_2 -TPR analysis, **Figure 3**). Also, hardly reducible Ni^{2+} species strongly interacting with the zeolite support act as newly generated Lewis acidic sites.

Changes in the nature of acid sites in the Ni/HZSM-5 catalysts after the catalytic hydrogenation reaction show the same trend, regardless of the nickel content (comparison of **Figures 5A,B** and **Table 4**). The BAS/LAS ratio increases slightly due to a more notable drop in LAS compared to BAS.

The isoelectric point of the pure HZSM-5 is around 2.5 (**Figure 6**). With the impregnation of nickel, the isoelectric point

of Ni/HZSM-5 samples does not change substantially, since the acidity of their surface is related to the number of BAS which are governed by the amount of framework aluminum. However, the displacement of the isoelectric points for Ni/HZSM-5-1 and Ni/HZSM-5-3 below 2.5 (isoelectric point for HZSM-5, **Figure 6**) and below 3.5-4 (isoelectric point for NiO, Hernandez et al., 2005) is observed (**Figure 5**). This means that the Ni and Al interactions in samples with a molar ratio of $\text{Ni/Si} = 0.01$ and 0.03 ($\text{Ni/Al} < 0.5$) can have a higher synergistic effect in reactions than in the sample with a molar ratio of $\text{Ni/Si} = 0.05$ ($\text{Ni/Al} > 0.5$) due to so called spinel like effect (Kosmulski, 2009; Yung et al., 2016). This is confirmed with the fact that the spinel structure is not tolerant concerning the change of Ni/Al molar ratio > 0.5 .

UV-Vis DRS analysis was performed to probe the electronic transitions and gain more insight into the phases present in the synthesized catalysts. **Figure 7** shows that all Ni/HZSM-5 samples absorb light strongly in the UV range ($\lambda < 350 \text{ nm}$), which is associated with $\text{O}^{2-} \rightarrow \text{Ni}^{2+}$ ligand to metal charge transfer (LMCT) transition (Pawelec et al., 2004). The bands

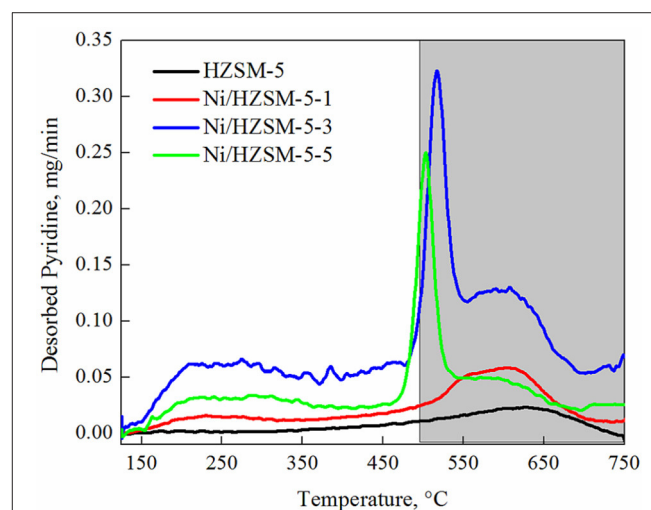


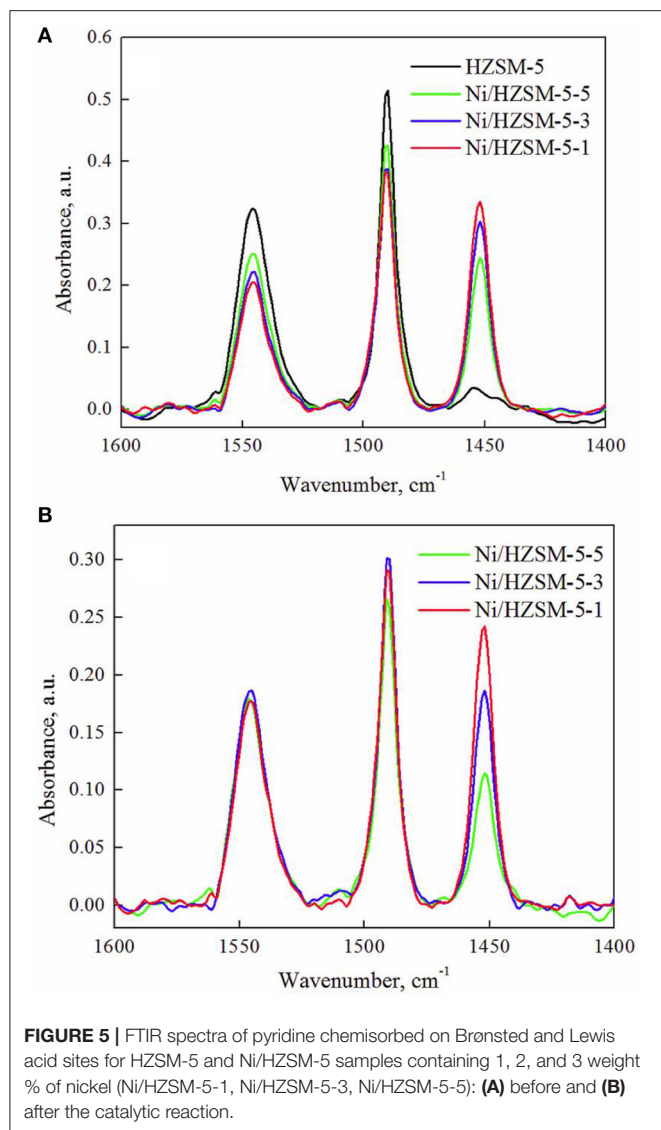
FIGURE 4 | Desorption of pyridine as a function of temperature for Ni/HZSM-5 samples containing 1, 2, and 3 weight % of nickel (Ni/HZSM-5-1, Ni/HZSM-5-3, Ni/HZSM-5-5).

TABLE 4 | Total acidity for HZSM-5 and Ni/ZSM-5 samples containing different amounts of nickel and BAS/LAS ratio for the same materials before and after the catalytic reaction.

Sample	Total acidity, $\text{mmol/g}_{\text{cat}}$	Before reaction BAS/LAS, /	Normalized BAS amount, /*	Normalized LAS amount, /*	After reaction BAS/LAS, /	BAS remaining after reaction, %**	LAS remaining after reaction, %**
HZSM-5	0.70	13.1	1	0.10	N.D.	N.D.	N.D.
Ni/HZSM-5-1	0.68	1.44	0.78	0.73	2.20	71	48
Ni/HZSM-5-3	0.72	1.03	0.68	0.90	1.41	85	63
Ni/HZSM-5-5	0.75	0.86	0.63	1	1.03	86	73

* In catalysts before the catalytic reaction.

** Calculated as a ratio of characteristic IR peak intensity ($1,545 \text{ cm}^{-1}$ for BAS and $1,450 \text{ cm}^{-1}$ for LAS) after and before reaction.



at 380, 420, and 715 nm are characteristic for octahedrally coordinated Ni^{2+} in NiO lattice (López-Fonseca et al., 2012; Anjaneyulu et al., 2016). It can be seen that all catalysts contain bulk NiO, its contribution is strongest in catalysts containing the highest nickel content, namely Ni/HZSM-5-3 and Ni/HZSM-5-5. Bands at 580 nm and between 600 and 645 nm are related to the tetrahedrally coordinated Ni^{2+} species in the nickel aluminate phase (Kim et al., 2004). It can be seen that for samples Ni/HZSM-5-1 and Ni/HZSM-5-3 the contribution of nickel aluminate phase is the highest. This is in agreement with the results of H_2 -TPR and isoelectric point measurements.

In Figure 8 STEM-BF micrographs of samples Ni/HZSM-5-1 (Figure 8A), Ni/HZSM-5-3 (Figure 8B) and Ni/HZSM-5-5 (Figures 8C,D) are shown. Regularly shaped NiO particles with nicely expressed crystal planes are distributed uniformly in Ni/HZSM-5-3, and non-uniformly in Ni/HZSM-5-1. In Ni/HZSM-5-5 sample, a specific chain-like network of NiO crystals becomes apparent. The latter suggest presence of NiO

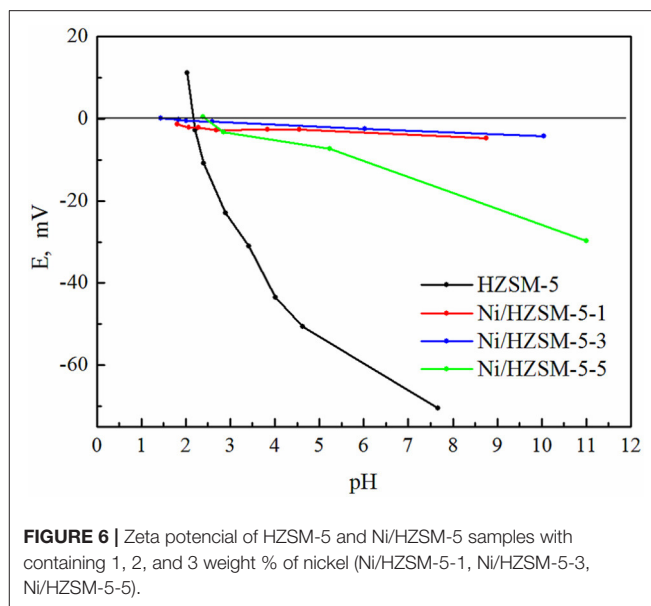


FIGURE 6 | Zeta potential of HZSM-5 and Ni/HZSM-5 samples with containing 1, 2, and 3 weight % of nickel (Ni/HZSM-5-1, Ni/HZSM-5-3, Ni/HZSM-5-5).

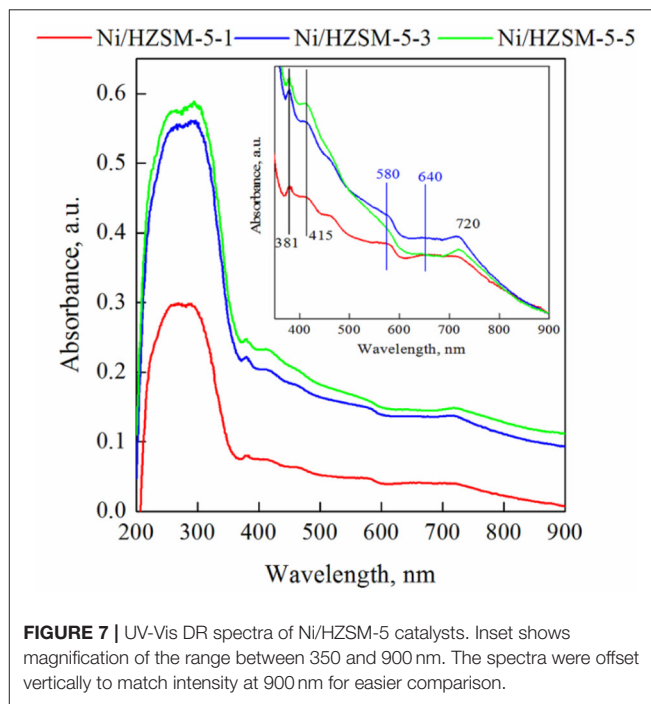
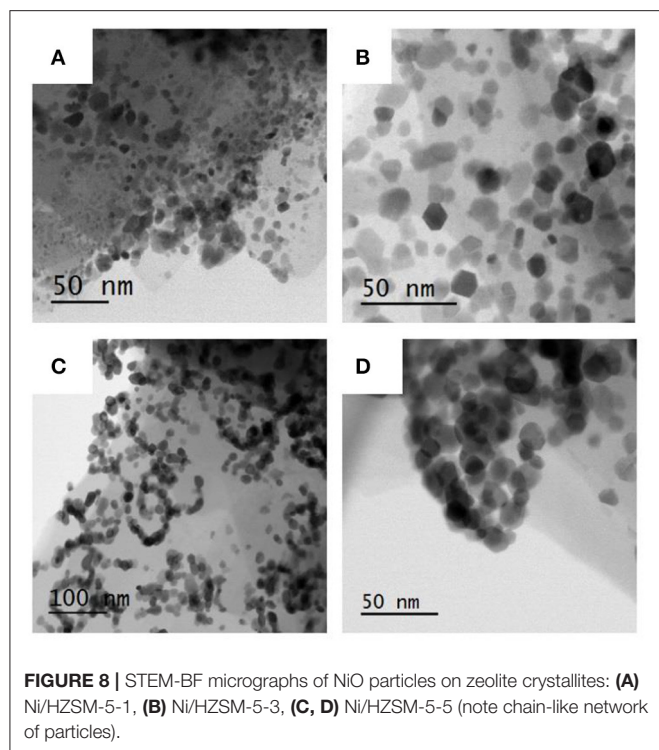


FIGURE 7 | UV-Vis DR spectra of Ni/HZSM-5 catalysts. Inset shows magnification of the range between 350 and 900 nm. The spectra were offset vertically to match intensity at 900 nm for easier comparison.

phase without direct contact with the HZSM-5 support when the nickel content reaches 2.7 wt. %. The size of the NiO particles in all three samples was between 8 and 30 nm.

Additional information on distribution of Ni and Al inside the Ni/HZSM-5 catalysts was obtained with TEM-EDXS elemental mapping (Figure 9). Nickel is highly dispersed over the support, in addition to nickel concentrated in NiO particles. This corroborates presence of different nickel containing species, as suggested indirectly by H_2 -TPR and UV-Vis DRS analyses. Aluminum elemental map shows its homogeneous dispersion in the catalyst. This is in agreement with pyridine IR analysis,



which suggested that 93% of Al^{3+} is tetrahedrally coordinated and integrated in the zeolite framework.

Catalytic Performance

Catalytic results of the Ni/HZSM-5 catalysts in levulinic acid conversion to GVL are compiled in **Table 5**. The only reaction products formed in measurable quantities are γ -hydroxyvaleric acid, α -angelica lactone and GVL. GVL can be produced by two independent reaction pathways, which both involve hydrogenation (H) and dehydration (D) reactions (**Scheme 1**). The order in which reactions (H) and (D) occur is diametrically different in both pathways and depends on the availability and reactivity of active catalytic sites present on the catalysts (acid and metal sites), as well as reaction conditions.

At 250°C levulinic acid conversions between 53 and 82% were achieved and γ -hydroxyvaleric acid, α -angelica lactone and γ -valerolactone were registered products on all the studied samples. The highest levulinic acid conversion was registered for the Ni/HZSM-5-3 sample (82%). The α -angelica lactone was the predominant product with yields between 22 and 46%, indicating that the dominant reaction is dehydration of levulinic acid over acid sites present at lower reaction temperature. The yield of γ -hydroxyvaleric acid was between 12 and 23% and increased with nickel content. This directly shows that the hydrogenation of levulinic acid becomes increasingly prominent as the hydrogenation function (nickel content) of the catalyst increases. GVL yields were relatively low, between 9 and 19%.

The increase of reaction temperature to 300°C led to a drastic rise in levulinic acid conversion (51–96%) and change in product distribution: GVL became the most abundant reaction product

with yields between 31 and 93%. The Ni/HZSM-5 catalyzed the reaction cascade all the way to the ultimate and desired reaction product: GVL. The yields of γ -hydroxyvaleric and α -angelica lactone were below 4%, except for γ -hydroxyvaleric acid on Ni/HZSM-5-1, which remained relatively high at 16%.

No drastic changes in catalysis were observed at 320°C: The Ni/HZSM-5-3 catalyst showed the highest levulinic acid conversion (99%) and 100% GVL yield, α -angelica lactone was produced in yields below 2% on all catalysts. The catalytic activity of Ni/HZSM-5-1 catalyst was markedly lower compared to Ni/HZSM-5-3 and Ni/HZSM-5-5 and γ -hydroxyvaleric acid yield remained relatively high at 19%.

The following paragraphs discuss the role of metallic nickel sites as well as LAS and BAS in the catalytic conversion of levulinic acid to GVL. Metallic catalytic function provided by nickel crystallites is crucial to produce GVL, as it enables hydrogenation of levulinic acid to γ -hydroxyvaleric acid and α -angelica lactone to GVL (**Scheme 1**). In the synthesized Ni/HZSM-5 catalysts, a notable fraction of nickel (17, 23, and 39% for Ni/HZSM-5-5, Ni/HZSM-5-3 and Ni/HZSM-5-1, respectively, **Table 3**) exists as poorly reducible Ni^{2+} cations and BAS compensating Ni^{2+} cations (nickel aluminate phase). They are converted to metallic nickel at temperatures (>500°C) much higher compared to reaction temperatures employed here, and are thus very likely present in ionic form with negligible hydrogenation ability. As a result, only a limited amount of nickel remains “free” to form the metallic domains upon reduction. This is most notable in the Ni/HZSM-5-1 sample and as a result of the lagging hydrogenation ability of this catalyst, much lower levulinic acid conversions and GVL yields are achieved compared to Ni/HZSM-5-3 and Ni/HZSM-5-5 catalysts.

The exact discrimination between the individual roles of LAS (electron acceptor) and BAS (proton donor) in the dehydration reactions (γ -hydroxyvaleric acid to GVL and levulinic acid to α -angelica lactone, **Scheme 1**) is difficult on the tested group of catalysts since they are both present in comparable amounts. Values in **Table 4** show that with increasing Ni^{2+} content, the BAS number decreases and LAS number increases. The intrinsic acid strength of LAS is weaker compared to BAS, which was confirmed also with thermogravimetric pyridine desorption tests (**Figure 4**). The structure of strong BAS in the synthesized HZSM-5 based catalysts is well known from the literature: protons that act as charge compensating ions for the Al^{3+} cations which are tetrahedrally coordinated in the zeolite framework.

The LAS can originate from extra framework Al^{3+} that forms an ill-defined separate AlO_x phase (7% of Al^{3+} in pure HZSM-5 was identified as extra framework by pyridine FTIR analysis, **Figure 5A** and **Table 4**), which is expected to be present also in Ni/HZSM-5 materials. In addition, ionic Ni^{2+} which are not reduced under reaction conditions, exhibit electrophilic character and consequently Lewis acidity.

The yield of α -angelica lactone at 250°C (primary reaction product formed on acid sites) correlates with total acidity of the catalysts (Ni/HZSM-5-5 > Ni/HZSM-5-3 > Ni/HZSM-5-1) and more specifically, increasing fraction of LAS. As a result, we can conclude that Lewis acid sites are the

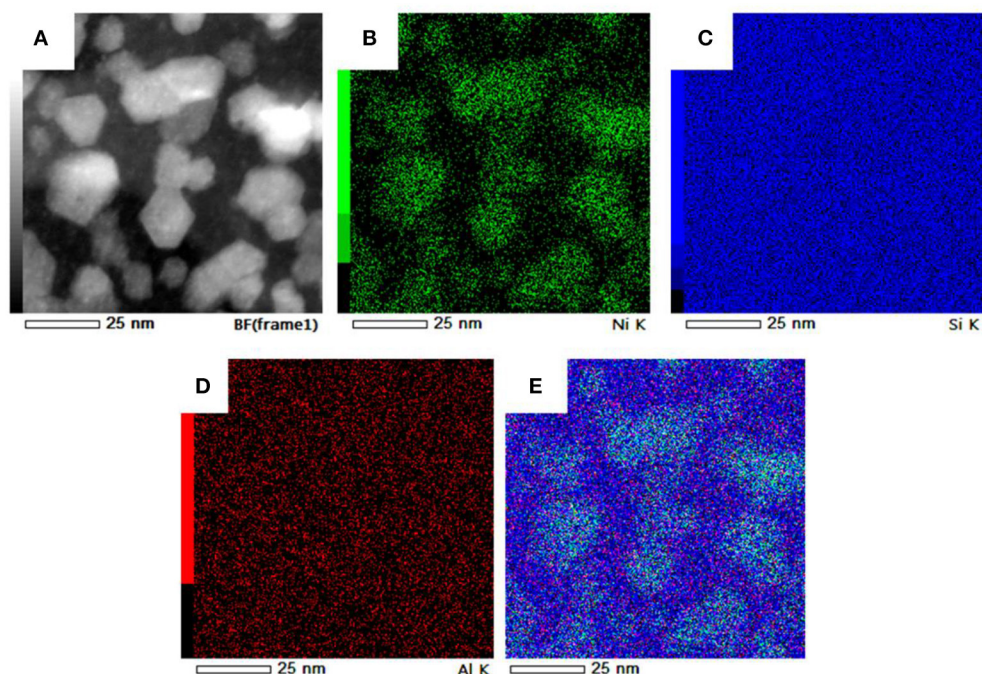


FIGURE 9 | EDXS mapping of support particle in sample Ni/HZSM-5-3 with up to 20 nm sized NiO based particles: **(A)** HAADF micrograph, **(B)** elemental distribution of Ni, **(C)** distribution of Si, **(D)** elemental distribution of Al, **(E)** composite image.

TABLE 5 | Catalytic activity and product yields at different reaction temperatures for the studied samples.

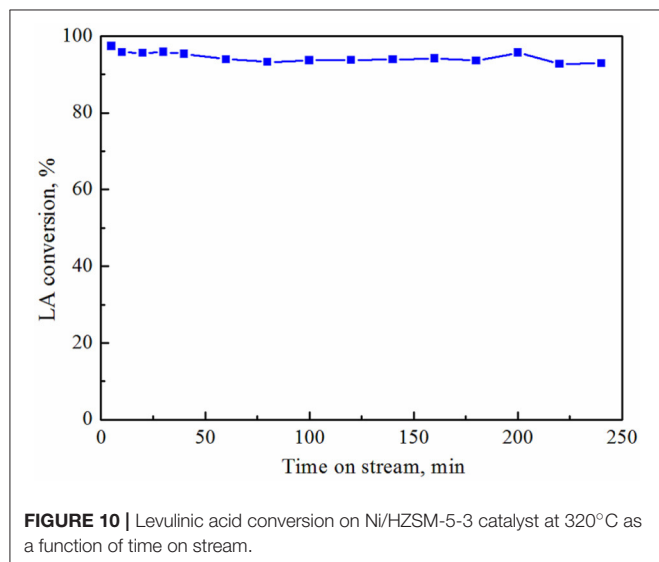
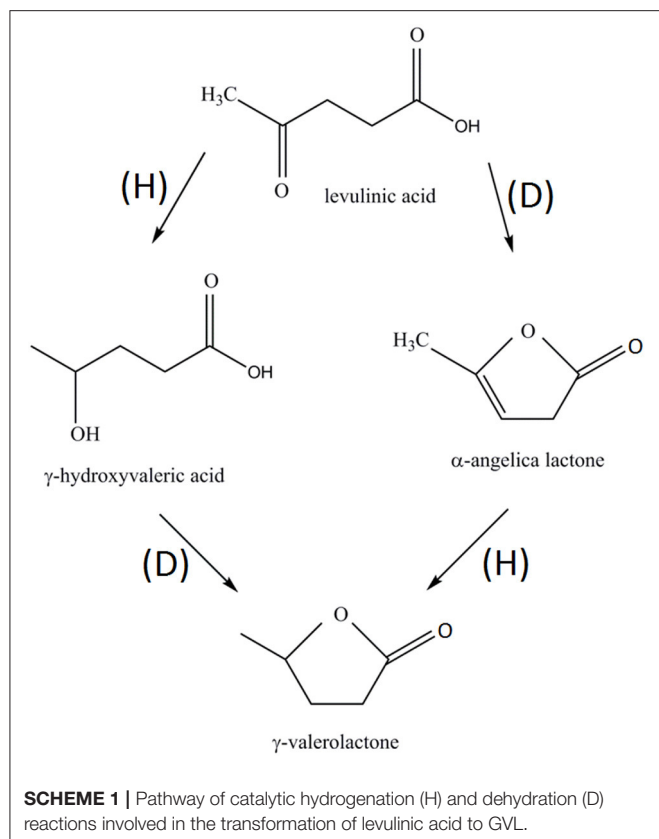
T, °C	Catalyst	Yield of GVL, wt. %	Yield of γ -hydroxyvaleric acid, wt. %	Yield of α -angelica lactone, wt.%	Conversion, %
250	ZSM-5-1Ni	18.8	11.7	22.5	52.9
	ZSM-5-3Ni	12.4	21.7	38.0	82.2
	ZSM-5-5Ni	9.0	23.4	45.6	77.9
300	ZSM-5-1Ni	31.4	16.5	3.3	51.2
	ZSM-5-3Ni	92.8	3.5	0	96.3
	ZSM-5-5Ni	90.2	3.2	1.3	94.7
320	ZSM-5-1Ni	57.5	19.3	1.5	78.3
	ZSM-5-3Ni	98.6	0	0	98.6
	ZSM-5-5Ni	95.3	1.4	0	96.7

dominant active sites performing the dehydration function in the cascade of reactions shown in **Scheme 1** over Ni/HZSM-5 catalysts. Kumar et al. (2016) came to similar conclusions, stating that a metal site (Ni) in close proximity to a Lewis acid site is active for the selective conversion of LA to GVL.

From above discussion we come to the conclusion that the Brønsted acid sites (nickel aluminate phase) create the synergetic and stabilizing effects of all active sites in the catalyst, when BAS/LAS is approaching to 1 and at the same time the amount of Ni easy reducible active sites is 80% (Ni/HZSM-5-3, **Table 4**).

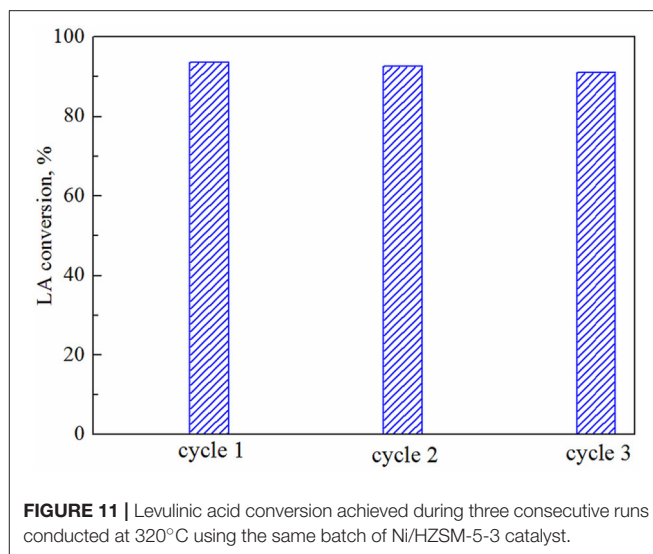
The stability of the Ni/HZSM-5-3 catalyst was studied at 320°C (**Figure 10**). A negligible decrease in the conversion of levulinic acid was observed during the 240 min of reaction:

from 97 to 93.6%. GVL is the only registered product in the studied reaction time in all reaction cycles. After the steady-state stability test, the same catalyst sample was regenerated in air at 500°C, reduced in hydrogen at 400°C, and reexamined in three consecutive reaction cycles at 320°C. During these cycles, only a marginal drop in levulinic acid conversion from 93.6 to 91% was observed (**Figure 11**). The stability test was performed also at 250°C for 12 h and the small decrease in the activity from 82.2 to 80.5% was registered (not shown). The stable catalytic activity and selectivity to GVL could be explained by sufficient stability of the metallic and acidic functionalities in the synthesized catalysts (under the employed steady state reaction conditions, as well as redox cycling), which makes them a potential candidate for industrial applications.



CONCLUSIONS

HZSM-5 zeolite was synthesized with Al/Si molar ratio of 0.04 (1.7 wt. %) without any organic template and was modified with different Ni content (approx. from 1 to 3 wt. %) by incipient wetness impregnation. TEM-EDX, UV-Vis DRS and H₂-TPR analyses showed presence of different reducible nickel containing



species in the catalysts: (i) bulk crystalline NiO which is the predominant phase in all materials, (ii) Ni²⁺ strongly interacting with the zeolite support and (iii) Ni²⁺ charge compensating cations on Brønsted sites in zeolite. The TPD of pyridine shows that the total amount of acid sites (Lewis and Brønsted) changes very little when Ni content is increased (Ni/HZSM-5-1 < HZSM-5 < Ni/ZSM-5-3 < Ni/HZSM-5-5) and their strength decreases with increasing nickel content: HZSM-5 > Ni/HZSM-5-1 > Ni/HZSM-5-3 > Ni/HZSM-5-5. The latter is due to formation of Lewis acid sites, associated with electrophilic poorly reducible Ni²⁺ species. The fraction of these nickel species is not negligible (17, 23, and 39% for Ni/HZSM-5-5, Ni/HZSM-5-3, and Ni/HZSM-5-1, respectively). They are converted to metallic nickel at temperatures much higher compared to reaction temperatures employed in the present study, and are thus very likely present in ionic form with negligible hydrogenation ability.

Catalytic tests of LA conversion to GVL revealed that the Ni/HZSM-5-3 (Ni/Si = 0.03) catalyst was the most active, and reached 99% conversion of levulinic acid and 100% selectivity to GVL at 320°C. Further increase of Ni content in Ni/HZSM-5-5 (Ni/Si = 0.05) does not lead to improved catalytic activity or selectivity. Ni/HZSM-5-3 catalyst shows also stable levulinic hydrogenation to GVL in 3 reaction cycles carried out at 320°C. The highest catalytic activity and stability of the Ni/HZSM-5-3 catalyst is achieved due to: (1) the metallic hydrogenation function and acidic dehydration have to be present simultaneously in the form of nickel metallic clusters and Lewis acid sites (2) nickel aluminate phase on Brønsted acid sites having synergetic and stability effects on all active sites in the catalysts.

AUTHOR CONTRIBUTIONS

Synthesis and standard characterization of the catalysts were performed and discussed by AR. Characterization of the catalysts by acidity tests, UV-VIS and IR were performed and discussed by

PD and AP. GD performed and discussed TEM characterization. Catalytic tests were performed and discussed by MP, HL, and AB. NT gave the research idea, coordinated the work and led the discussion on the results. All authors listed have made a substantial, direct and intellectual contribution to the work, and approved it for publication.

FUNDING

This work was supported by NSF of Bulgaria (Grant ДКОСТ 01/21, 09.2016), Slovenian Research Agency (ARRS) (Programs P1-0021 and P2-0150) and EU COST action FP 1306.

REFERENCES

- Abdelrahman, O. A., Heyden, A., and Bond, J. Q. (2014). Analysis of kinetics and reaction pathways in the aqueous-phase hydrogenation of levulinic acid to form γ -valerolactone over Ru/C. *ACS Catal.* 4, 1171–1181. doi: 10.1021/cs401177p
- Anjaneyulu, Ch., Naresh, G., Vijay Kumar, V., Padmasri, A. H., Tardio, J., Bhargava, S. K., et al. (2016). Ni/H-ZSM-5 as a stable and promising catalyst for CO₂ free H₂ production by CH₄ decomposition. *RSC Adv.* 6, 34600–34607. doi: 10.1039/C6RA03857C
- Bond, J. Q., Alonso, D. M., Wang, D., West, R. M., and Dumesic, J. A. (2010). Integrated catalytic conversion of γ -valerolactone to liquid alkenes for transportation fuels. *Science* 327, 1110–1114. doi: 10.1126/science.1184362
- Chang, J. (2011). Direct hydrocyclization of biomass-derived levulinic acid to 2-methyltetrahydrofuran over nanocomposite copper/silica catalysts. *ChemSusChem* 4, 1749–1752. doi: 10.1002/cssc.201100380
- Climent, M. J., Corma, A., and Iborra, S. (2014). Conversion of biomass platform molecules into fuel additives and liquid hydrocarbon fuels. *Green Chem.* 16, 516–547. doi: 10.1039/c3gc41492b
- Corma A., Iborra, S., and Velt, A. (2007). Chemical routes for the transformation of biomass into chemicals. *Chem. Rev.* 107, 2411–2502. doi: 10.1021/cr050989d
- Ertl, G., Knözinger, H., Schüth, F., and Weitkamp, J. (2008). *Handbook of Heterogeneous Catalysis (Editors), 2nd Edn.* Weinheim: WILEY-VCH Verlag.
- Fakin, T., Ristić, A., Mavrodinova, V., and Zabukovec Logar, N. (2015). Highly crystalline binder-free ZSM-5 granules preparation. *Micropor. Mesopor. Mater.* 213, 108–117. doi: 10.1016/j.micromeso.2015.04.010
- Galletti, A. M. R., Antonetti, C., De Luise, V., and Martinelli, M. (2012). A sustainable process for the production of γ -valerolactone by hydrogenation of biomass-derived levulinic acid. *Green Chem.* 14, 688–694. doi: 10.1039/c2gc15872h
- Hayes, D. J. (2009). An examination of biorefining processes, catalysts and challenges. *Catal. Today* 145, 138–151. doi: 10.1016/j.cattod.2008.04.017
- Heeres, H., Handana, R., Chunai, D., Borromeus Rasrendra, C., Girisuta, B., and Jan Heeres, H. (2009). Combined dehydration/(transfer)-hydrogenation of C6-sugars (D-glucose and D-fructose) to γ -valerolactone using ruthenium catalysts. *Green Chem.* 11, 1247–1255. doi: 10.1039/b904693c
- Hengne, A. M., Biradar, S., and Rode, C. V. (2012). Role of supported Ru catalyst for hydrogenation of bio-derived methyl levulinate to γ -valerolactone. *Catal. Lett.* 142, 779–787. doi: 10.1007/s10562-012-0822-4
- Hernández, N., Moreno, R., Sánchez-Herencia, A. J., and Fierro, J. L. (2005). Surface behavior of nickel powders in aqueous suspensions. *J. Phys. Chem. B* 109, 4470–4474. doi: 10.1021/jp0448954
- Horváth, I. T., Mehdi, H., Fábos, V., Boda, L., and Mika, L. T. (2008). γ -Valerolactone—a sustainable liquid for energy and carbon-based chemicals. *Green Chem.* 10, 238–242. doi: 10.1039/B712863K
- Jiang, K., Sheng, D., Zhang, Z., Fu, J., Hou, Z., and Lu, X. (2016). Hydrogenation of levulinic acid to γ -valerolactone in dioxane over mixed MgO–Al₂O₃ supported Ni catalyst. *Catal. Today* 274, 55–59. doi: 10.1016/j.cattod.2016.01.056
- Kim, P., Kim, Y., Kim, H., Song, I. K., and Yi, J. (2004). Synthesis and characterization of mesoporous alumina with nickel incorporated for use in the partial oxidation of methane into synthesis gas. *Appl. Catal. A* 272, 157–166. doi: 10.1016/j.apcata.2004.05.055
- Kosmulski, M. (2009). pH-dependent surface charging and points of zero charge. IV. Update and new approach. *J. Colloid Interface Sci.* 337, 439–448. doi: 10.1016/j.jcis.2009.04.072
- Kumar, V. V., Naresh, G., Sudhakar, M., Anjaneyulu, Ch., Bhargava, S. K., Tardio, J., et al. (2016). An investigation on the influence of support type for Ni catalysed vapour phase hydrogenation of aqueous levulinic acid to γ -valerolactone. *RSC Adv.* 12, 9872–9879. doi: 10.1039/C5RA24199E
- Kumar, V. V., Naresh, G., Sudhakar, M., Tardio, J., Bhargava, S. K., and Venugopal, A. (2015). Role of Bronsted and Lewis acid sites on Ni/TiO₂ catalyst for vapour phase hydrogenation of levulinic acid: kinetic and mechanistic study. *Appl. Catal. A* 505, 217–223. doi: 10.1016/j.apcata.2015.07.031
- Li, H., Fang, Z. h., Smith, R. L. Jr., and Yang, S. (2016). Efficient valorization of biomass to biofuels with bifunctional solid catalytic materials. *Prog. Energy Combust. Sci.* 55, 98–194. doi: 10.1016/j.pecs.2016.04.004
- Lomate, S., Sultana, A., and Fujitani, T. (2018). Vapor phase catalytic transfer hydrogenation (CTH) of levulinic acid to γ -valerolactone over copper supported catalysts using formic acid as hydrogen source. *Catal. Lett.* 148, 348–358. doi: 10.1007/s10562-017-2241-z
- Long, X., Sun, P., Li, Z., Lang, R., Xia, Ch., and Li, F. (2015). Magnetic Co/Al₂O₃ catalyst derived from hydrotalcite for hydrogenation of levulinic acid to γ -valerolactone. *Chin. J. Catal.* 36, 1512–1518. doi: 10.1016/S1872-2067(15)60934-2
- López-Fonseca, R., Jiménez-González, C., de Rivas, B., and Gutiérrez-Ortiz, J. I. (2012). Partial oxidation of methane to syngas on bulk NiAl₂O₄ catalyst. Comparison with alumina supported nickel, platinum and rhodium catalysts. *Appl. Catal. A* 437, 53–62. doi: 10.1016/j.apcata.2012.06.014
- Louis, C., Xing Cheng, Z., and Che, M. (1993). Characterization of nickel/silica catalysts during impregnation and further thermal activation treatment leading to metal particles. *J. Phys. Chem.* 97, 5703–5712. doi: 10.1021/j100123a040
- Maia, A. J., Louis, B., Lam, Y. L., and Pereira, M. M. (2010). Ni-ZSM-5 catalysts: detailed characterization of metal sites for proper catalyst design. *J. Catal.* 269, 103–109. doi: 10.1016/j.jcat.2009.10.021
- Ma, B., Yi, X., Chen, L., Zheng, A., and Zhao, C. (2016). Interconnected hierarchical HUSY zeolite-loaded Ni nano-particles probed for hydrodeoxygenation of fatty acids, fatty esters, and palm oil. *J. Mater. Chem. A* 4, 11330–11341.
- Mika, L. T., Cséfalvay, E., and Németh á. (2018). Catalytic conversion of carbohydrates to initial platform chemicals: chemistry and sustainability. *Chem. Rev.* 118, 505–613. doi: 10.1021/acs.chemrev.7b00395
- Nadgeri, J. M., Hiyoshi, N., Yamaguchi, A., Sato, O., and Shirai, M. (2014). Liquid phase hydrogenation of methyl levulinate over the mixture of supported ruthenium catalyst and zeolite in water. *Appl. Catal. A* 470, 215–220. doi: 10.1016/j.apcata.2013.10.059
- Pawelec, B., Mariscal, R., Navarro, R. M., Campos-Martin, J. M., and Fierro, J. L. G. (2004). Simultaneous 1-pentene hydroisomerisation and thiophene hydrodesulphurization over sulphided Nu/FAU and Ni/ZSM-5 catalysts. *Appl. Catal. A* 262, 155–166. doi: 10.1016/j.apcata.2003.11.037

ACKNOWLEDGMENTS

We thank Mrs. Mojca Opresnik from the National Institute of Chemistry, Slovenia, for the dedicated work on measuring nitrogen physisorption isotherms and Mr. Edi Kranjc for XRD measurements.

- Perea, E. D., Arslan, I., Liu, J., Ristanović, Z., Kovarik, L., Arey, B. W., et al. (2015). Determining the location and nearest neighbours of aluminium in zeolites with atom probe tomography. *Nat. Comm.* 6:7589. doi: 10.1038/ncomms8589
- Ruiz, J. C., West, R. M., and Dumesic, J. A. (2010). Catalytic conversion of renewable biomass resources to fuels and chemicals. *Annu. Rev. Chem. Biomol. Eng.* 1, 79–100. doi: 10.1146/annurev-chembioeng-073009-100935
- Serrano-Ruiz, J. C., and Dumesic, J. A. (2011). Catalytic routes for the conversion of biomass into liquid hydrocarbon transportation fuels. *Energy Environ. Sci.* 4, 83–99. doi: 10.1039/C0EE00436G
- Shu, C. K., Lawrence, B. M., and Agric, J. (1995). Formation of 4-alkoxy- γ -valerolactones from levulinic acid and alcohols during storage at room temperature. *Food Chem.* 43, 782–784. doi: 10.1021/jf00051a041
- Son, P. A., Nishimura, S., and Ebitani, K. (2014). Production of γ -valerolactone from biomass-derived compounds using formic acid as a hydrogen source over supported metal catalysts in water solvent. *RSC Adv.* 4, 10525–10530. doi: 10.1039/c3ra47580h
- Song, S., Yao, S., Cao, J., Di, L., Wu, G., Guan, N., et al. (2017). Heterostructured Ni/NiO composite as a robust catalyst for the hydrogenation of levulinic acid to γ -valerolactone. *Appl. Catal. B* 217, 115–124. doi: 10.1016/j.apcatb.2017.05.073
- Sun, D., Ohkubo, A., Asami, K., Katori, T., Yamada, Y., and Sato, S. (2017). Vapor-phase hydrogenation of levulinic acid and methyl levulinate to γ -valerolactone over non-noble metal-based catalysts. *Mol. Catal.* 437, 105–113. doi: 10.1016/j.mcat.2017.05.009
- Sun, P., Gao, G., Zhao, Z., Xia, C., and Li, F. (2016). Acidity-regulation for enhancing the stability of Ni/HZSM-5 catalyst for valeric biofuel production. *Appl. Catal. B* 189, 19–25. doi: 10.1016/j.apcatb.2016.02.026
- Szegedi, A., Popova, M., Mavrodinova, V., Urban, M., Kiricsi, I., and Minchev, Ch. (2007). Synthesis and characterization of Ni-MCM-41 materials with spherical morphology and their catalytic activity in toluene hydrogenation. *Micropor. Mesopor. Mater.* 99, 149–158. doi: 10.1016/j.micromeso.2006.07.040
- Tamura, M., Shimizu, K., and Satsuma, A. (2012). Comprehensive IR study on acid/base properties of metal oxides. *Appl. Catal. A* 433, 135–145. doi: 10.1016/j.apcata.2012.05.008
- Wettstein, S. G., Alonso, D. M., Chong, Y., and Dumesic, J. A. (2012). Production of levulinic acid and gamma-valerolactone (GVL) from cellulose using GVL as a solvent in biphasic systems. *Energy Environ. Sci.* 5, 8199–8203. doi: 10.1039/c2ee22111j
- Wright, W. R. H., and Palkovits, R. (2012). Development of heterogeneous catalysts for the conversion of levulinic acid to γ -valerolactone. *ChemSusChem* 5, 1657–1667. doi: 10.1002/cssc.201200111
- Yan, K., and Chen, A. (2014). Selective hydrogenation of furfural and levulinic acid to biofuels on the ecofriendly Cu-Fe catalyst. *Fuel* 115, 101–108. doi: 10.1016/j.fuel.2013.06.042
- Yoshida, R., Sun, D., Yamada, Y., Sato, S., and Hutchings, G. J. (2017). Vapour-phase hydrogenation of levulinic acid to γ -Valerolactone over Cu bimetallic catalysts. *Catal. Commun.* 97, 79–82. doi: 10.1016/j.catcom.2017.04.018
- Yuan, H. X., Xia, Q. H., Zhan, H. J., Lu, X. H., and Su, K. X. (2006). Catalytic oxidation of cyclohexane to cyclohexanone and cyclohexanol by oxygen in a solvent-free system over metal-containing ZSM-5 catalysts. *Appl. Catal. A* 304, 178–184. doi: 10.1016/j.apcata.2006.02.037
- Yung, M. M., Starace, A. K., Mukarakate, C., Crow, A. M., Leshnov, M. A., and Magrini, K. A. (2016). Biomass catalytic pyrolysis on Ni/ZSM-5: effects of nickel pretreatment and loading. *Energy Fuels* 30, 5259–5268. doi: 10.1021/acs.energyfuels.6b00239
- Zhou, H., Song, J., Fan, H., Zhang, B., Yang, Y., Hu, J., et al. (2014). Cobalt catalysts: very efficient for hydrogenation of biomass-derived ethyl levulinate to gamma-valerolactone under mild conditions. *Green Chem.* 16, 3870–3875. doi: 10.1039/C4GC00482E

Conflict of Interest Statement: The authors declare that the research was conducted in the absence of any commercial or financial relationships that could be construed as a potential conflict of interest.

Copyright © 2018 Popova, Djinović, Ristić, Lazarova, Dražić, Pintar, Balu and Novak Tušar. This is an open-access article distributed under the terms of the Creative Commons Attribution License (CC BY). The use, distribution or reproduction in other forums is permitted, provided the original author(s) and the copyright owner(s) are credited and that the original publication in this journal is cited, in accordance with accepted academic practice. No use, distribution or reproduction is permitted which does not comply with these terms.



Physico-Chemical Properties of MgGa Mixed Oxides and Reconstructed Layered Double Hydroxides and Their Performance in Aldol Condensation of Furfural and Acetone

Oleg Kikhtyanin^{1,2}, Libor Čapek³, Zdeněk Tišler¹, Romana Velvarská¹, Adriana Panasewicz³, Petra Diblíková⁴ and David Kubička^{2*}

OPEN ACCESS

Edited by:

Konstantinos Triantafyllidis,
Aristotle University of Thessaloniki,
Greece

Reviewed by:

Jozef Mikulec,
VÚRUP (Slovakia), Slovakia
Miguel Angel Centeno,
Consejo Superior de Investigaciones
Científicas (CSIC), Spain
Ioannis N. Lykakis,
Aristotle University of Thessaloniki,
Greece

*Correspondence:

David Kubička
kubickad@vscht.cz

Specialty section:

This article was submitted to
Green and Sustainable Chemistry,
a section of the journal
Frontiers in Chemistry

Received: 30 January 2018

Accepted: 03 May 2018

Published: 24 May 2018

Citation:

Kikhtyanin O, Čapek L, Tišler Z,
Velvarská R, Panasewicz A,
Diblíková P and Kubička D (2018)
Physico-Chemical Properties of MgGa
Mixed Oxides and Reconstructed
Layered Double Hydroxides and Their
Performance in Aldol Condensation of
Furfural and Acetone.
Front. Chem. 6:176.
doi: 10.3389/fchem.2018.00176

MgGa layered double hydroxides (Mg/Ga = 2–4) were synthesized and used for the preparation of MgGa mixed oxides and reconstructed hydrotalcites. The properties of the prepared materials were examined by physico-chemical methods (XRD, TGA, NH₃-TPD, CO₂-TPD, SEM, and DRIFT) and tested in aldol condensation of furfural and acetone. The as-prepared phase-pure MgGa samples possessed hydrotalcite structure, and their calcination resulted in mixed oxides with MgO structure with a small admixture phase characterized by a reflection at $2\theta \approx 36.0^\circ$. The interaction of MgGa mixed oxides with pure water resulted in reconstruction of the HTC structure already after 15 s of the rehydration with maximum crystallinity achieved after 60 s. TGA-MS experiments proved a substantial decrease in carbonates in all rehydrated samples compared with their as-prepared counterparts. This allowed suggesting presence of interlayer hydroxyls in the samples. Acido-basic properties of MgGa mixed oxides determined by TPD technique did not correlate with Mg/Ga ratio which was explained by the specific distribution of Ga atoms on the external surface of the samples. CO₂-TPD method was also used to evaluate the basic properties of the reconstructed MgGa samples. In these experiments, an intensive peak at $T = 450^\circ\text{C}$ on CO₂-TPD curve was attributed to the decomposition of carbonates newly formed by CO₂ interaction with interlayer carbonates rather than to CO₂ desorption from basic sites. Accordingly, CO₂-TPD method quantitatively characterized the interlayer hydroxyls only indirectly. Furfural conversion on reconstructed MgGa materials was much larger compared with MgGa mixed oxides confirming that Brønsted basic sites in MgGa catalysts, like MgAl catalysts, were active in the reaction. Mg/Ga ratio in mixed oxides influenced product selectivity which was explained by the difference in textural properties of the samples. In contrast, Mg/Ga ratio in reconstructed catalysts had practically no effect on the composition of

reaction products suggesting that the basic sites in these catalysts acted similarly in aldol condensation of acetone with furfural. It was concluded that the properties of MgGa samples resembled in a great extent those of MgAl hydrotalcite-based materials and demonstrated their potential as catalysts for base-catalyzed reactions.

Keywords: MgGa layered double hydroxides, mixed oxides, reconstructed hydrotalcites, aldol condensation, acido-basic properties

INTRODUCTION

A common feature of the Layered Double Hydroxides (LDH) or Hydrotalcite-like (HTC) family, both natural and synthesized, is that they all have a structure closely related to that of the mineral hydrotalcite, that is, rhombohedral $\text{Mg}_6\text{Al}_2(\text{OH})_{16}\text{CO}_3 \cdot 4\text{H}_2\text{O}$. All these materials are composed of two-dimensional layers of positively charged double hydroxides together with water molecules and exchangeable charge-compensating anions which located in interlayer (Cavani et al., 1991; Sels et al., 2001; Debecker et al., 2009; Takehira, 2017). The general formula of LDHs can be described as $[\text{M}_{1-x}^{2+}\text{M}_x^{3+}(\text{OH})_2]^{x+}[\text{A}_{x/n}]^{n-} \cdot m\text{H}_2\text{O}$, where M^{2+} is a divalent cation, M^{3+} is a trivalent cation and A is a charge-compensating anion. Mg-Al hydrotalcites, most known and well-studied among the total family, are derived from brucite $\text{Mg}(\text{OH})_2$ as a general crystallographic structure. These brucite layers are stacked on top of each other and held together by weak interactions through hydrogen atoms (Cavani et al., 1991; Debecker et al., 2009). In the brucite layers a part of Mg^{2+} cations are substituted with Al^{3+} cations thus creating a positive charge in the layers. In synthetic MgAl HTCs, the substitution degree of $\text{Mg} \rightarrow \text{Al}$ may be different but lies in the range of $x = 0.1\text{--}0.5$ (Cavani et al., 1991). A charge resulting from this substitution is compensated by interlayer anions (CO_3^{2-} , NO_3^- , Cl^- , etc). Additionally, water molecules are in the interlayer in amounts dependent on the temperature, on the water vapor pressure and the nature of the anions present (Cavani et al., 1991; Debecker et al., 2009). The chemical composition of LDHs is not limited to Mg and Al cations, and at the present the family of these compounds consists of a large variety of synthetic materials which are composed of Mg^{2+} , Zn^{2+} , Co^{2+} , Cu^{2+} , etc., as divalent cations, and Al^{3+} , Fe^{3+} , Cr^{3+} , La^{3+} , etc., as trivalent cations (Cavani et al., 1991; Choudary et al., 2001; Sels et al., 2001; Motokura et al., 2006; Pérez-Ramírez et al., 2007a; Debecker et al., 2009; Takehira, 2017).

The most popular method of synthesizing LDHs is based on the co-precipitation of aqueous solutions of the corresponding salts (usually nitrates) with alkaline solutions (Na or K hydroxide and carbonate) at low supersaturating conditions and fixed pH values. As a consequence, carbonate groups are present as charge-compensation anions in as-prepared LDHs. The as-prepared materials exhibit low activity in catalytic applications and therefore have to be activated. Heat treatment is the main and the simple way to activate the as-prepared LDHs which results in the removal of water, the dehydroxylation of brucite-like layers and the decomposition of interlayer carbonates. Mixed oxides

formed by the thermal decomposition of as-prepared LDHs exhibit much better basic properties than the starting as-prepared LDHs. The mixed oxides possess Lewis basic sites and are widely used in base-catalyzed reactions such as transesterification (Zeng et al., 2008), condensations (Kustrowski et al., 2006; Perez et al., 2009), alkylation (Cavani et al., 2005), and Michael addition (Prescott et al., 2005).

A distinctive feature of HTC-like materials is so-called “memory effect” described for the first time by Miyata (1980), i.e., the recovery of original lamellar structure by hydration of mixed oxide. Thus, the interaction of MgAl mixed oxide either with water vapor or by immersion in decarbonated water leads to the formation of meixnerite $[\text{Mg}_6\text{Al}_2(\text{OH})_{18} \cdot 4\text{H}_2\text{O}]$ which is a hydrotalcite analog with OH^- groups as compensating anions in the interlayer instead of the original carbonates (Climent et al., 2002b; Tichit and Coq, 2003; Abelló et al., 2005; Pérez-Ramírez et al., 2007b; Kikhtyanin et al., 2017b). The interlayer hydroxyls are Brønsted basic sites and, therefore, the reconstructed materials are widely used in a number of base-catalyzed-reactions which require Brønsted basicity, such as self- and cross-aldol condensation of aldehydes and ketones (Tichit et al., 1998, 2002; Climent et al., 2002a; Abelló et al., 2005), Michael additions (Choudary et al., 1999), Knoevenagel and Claisen-Schmidt condensation (Cavani et al., 1991; Climent et al., 1995; Guida et al., 1997; Di Cosimo et al., 1998), etc.

In a zeolite family, the substitution of aluminum atoms by gallium in a silicate matrix leads to the formation of gallium silicates of various structural types whose specific physicochemical properties are successfully used in a number of acid-catalyzed reactions (Fricke et al., 2000; Chao and Liu, 2005; Wu et al., 2010). It is therefore not surprising that a possibility to replace Al atoms by Ga atoms is also assumed in other classes of inorganic compounds. Indeed, the synthesis and the study of the physico-chemical properties of MgGa LDHs have been reported repeatedly (Rebours et al., 1994; López-Salinas et al., 1996, 1997; Aramendía et al., 1999a,b, 2000; Thomas and Vishnu Kamath, 2005; Grand et al., 2010). Similar to other LDHs, the synthesis of MgGa is performed starting from Mg and Ga salt solutions mixed with sodium hydroxide and carbonate solutions; the heat treatment of the as-prepared materials results in MgGa mixed oxides. Nevertheless, in most cases, the studies on the properties of the prepared MgGa LDHs and mixed oxides are limited to their synthesis and characterization by different physico-chemical methods, such as XRD, TGA, DRIFT, MAS, NMR. More rarely, studies on the basic properties of MgGa mixed oxides have also been documented (López-Salinas et al., 1997; Prinetto et al., 2000). In addition, the “memory effect”

has been demonstrated for this type of materials. Indeed, MgGa mixed oxides restored LDH structure (i) by exposure to a water-saturated atmosphere for 18 h followed by CO₂ picked up from the ambient for this reconstruction (Thomas and Vishnu Kamath, 2005), (ii) by the dispersion of MgGa mixed oxide under vigorous magnetic stirring during 1 h into the decarbonated water at 298 K and 1×10^5 Pa (Prinetto et al., 2000), or (iii) by the treatment of MgGa mixed oxide with a carbonate-containing aqueous solution (López-Salinas et al., 1996). Despite the growing interest to Ga-containing catalysts in different applications, there is a lack of available information which reports about their catalytic performance in base-catalyzed reactions. Concerning Ga-containing MgGa LDHs, Prinetto et al. (2000) demonstrated that the substitution of Al³⁺ with Ga³⁺ slightly increased the density of the basic sites in the Mg-containing mixed oxides and slightly increased their catalytic activity in acetone self-condensation. Tabanellia et al. (2018) used MgGa mixed oxide for the gas-phase methylation of phenol to 2,4,6-trimethylphenol and attributed the outstanding performance of the catalyst to its high activity in methanol dehydrogenation to formaldehyde as well as to the moderate acidic features due to Ga sites, which enhanced the intramolecular rearrangement of O-alkylated compounds. Rousselot et al. (1999) investigated the catalytic performance of both as-prepared and calcined MgGa LDHs in Knoevenagel condensation of benzaldehyde with ethyl cyanoacetate. They explained the obtained results by a rehydration process of the calcined samples during the catalytic reaction.

Nevertheless, there is a great lack in information about the performance of catalysts based on reconstructed MgGa LDHs. Moreover, in contrast to MgAl materials (Pérez-Ramírez et al., 2007b; Kikhtyanin et al., 2017b), the effect of reconstruction time on the physico-chemical properties of MgGa LDHs and the catalytic performance of the reconstructed materials has not been reported yet.

Aldol condensation of furfural and acetone (**Scheme 1**) is an attractive object for an investigation from several points of view. First of all, this reaction has a great practical potential as it allows increasing the carbon atom chain length starting from the relatively simple ones which can be produced by

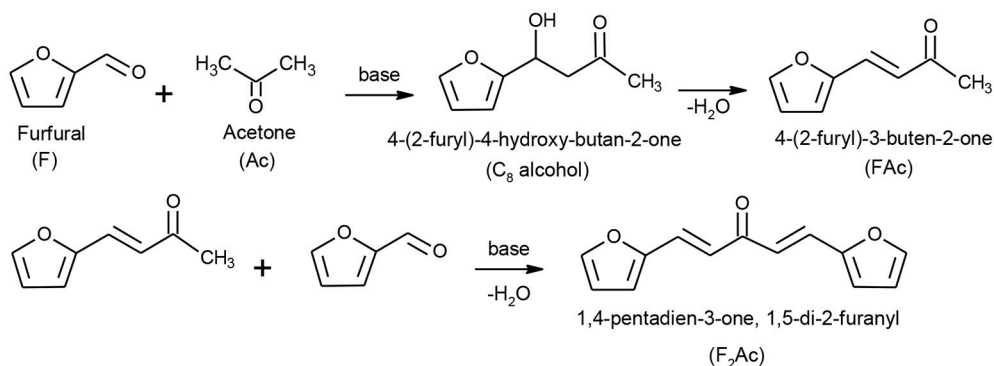
biomass processing (Gámez et al., 2006; Mäki-Arvela et al., 2011). The obtained condensation products can be further hydrogenated/deoxygenated to afford hydro-carbons, namely C₈ and C₁₃ alkanes (Zapata et al., 2012; Ramos et al., 2016). On the other hand, aldol condensation of furfural and acetone attracts also a scientific interest, because this reaction makes it possible to probe both the acid (Kikhtyanin et al., 2014, 2015) and basic sites (Sádaba et al., 2011; Faba et al., 2012; Thanh et al., 2016) of heterogeneous catalysts. Regularities found in preceding studies help to evaluate and understand the catalytic performance of following catalytic materials.

The purpose of this paper is to correlate the physicochemical characteristics of samples derived from MgGa LDHs varied by Mg/Ga ratio with their catalytic performance. A special attention is paid to the reconstructed MgGa materials, namely, a possibility to recover HTC structure by the interaction of MgGa mixed oxide with pure water. For this purpose, the effect of rehydration duration of MgGa mixed oxides on the properties of the obtained samples was studied in detail and the catalytic performance of both MgGa mixed oxides and reconstructed LDHs were compared in aldol condensation of furfural and acetone.

MATERIALS AND METHODS

Preparation of MgGa Mixed Oxides

MgGa layered double hydroxides varied in Mg:Ga molar ratio in reactive mixture in the range of (2–4):1 were prepared based on a method described in Hora et al. (2015). For these syntheses Ga nitrate was prepared by the dissolution of powder metallic Ga (Unimagnet) in concentrated nitric acid followed by the evaporation of the excessive acid by using vacuum evaporator. The composition of obtained salt was determined by ICP. MgGa LDHs with Mg:Ga molar ratio from 2:1 to 4:1 were synthesized by co-precipitation method at constant pH value (pH = 9.5) and constant temperature (T = 60°C). The preparation procedure involves mixing of aqueous solutions of nitrates consisting of Gallium nitrate Ga(NO₃)₂·6H₂O prepared as described above and magnesium nitrate Mg(NO₃)₂·6H₂O (Lach-ner, p.a. purity) (C_{Mg+Ga} = 1 mol/dm³), and a basic solution containing potassium carbonate K₂CO₃ (Penta, p.a.



SCHEME 1 | Reaction scheme of aldol condensation between furfural and acetone.

purity) and potassium hydroxide KOH (Lach-ner, p.a. purity) ($c_{\text{KOH}} = 2 \text{ mol/dm}^3 + c_{\text{K}_2\text{CO}_3} = 0.2 \text{ mol/dm}^3$). After precipitation the solids were isolated by press-filtration using paper filter plate S15N (Hobra); the filter cake was washed by demineralized water to neutral pH and dried in oven overnight at 65°C .

The MgGa mixed oxides were prepared by calcination of the dried as-prepared LDHs at 450°C for 3 h (heating rate $5^\circ\text{C}\cdot\text{min}^{-1}$). The rehydration of the mixed oxides with deionized water was performed at room temperature and rehydrate on time in the range of 0–40 min. All samples chosen for physico-chemical characterization and catalytic runs were dried for 40 min. Other details in the preparation of the rehydrated samples are available in Kikhtyanin et al. (2017b). After preparation (rehydration+drying steps), all materials were kept in a desiccator under inert atmosphere to prevent contact of the samples with CO_2 from air during their storage. The samples were taken away from the desiccator only before performing experiments on their characterization. Further in the text, the as-prepared MgGa LDHs are denoted as MgGa-xA, calcined MgGa mixed oxides are denoted as MgGa-xC and rehydrated samples are denoted as MgGa-xR-y, where x stands for Mg/Ga molar ratio and y stands for rehydration time.

Physico-Chemical Characterization

Chemical composition was determined by ICP-OES. The phase composition of the prepared samples was determined by X-ray powder diffraction using a Philips MPD 1880 instrument with Cu K_α irradiation ($\lambda = 0.154 \text{ nm}$) in the 2θ range of $5\text{--}70^\circ$ at the 2θ scanning rate of $2.4^\circ\cdot\text{min}^{-1}$. In each group of prepared catalysts, i.e., as-prepared LDHs, MgGa mixed oxides and reconstructed LDHs, the sample with the highest crystallinity was assigned relative crystallinity 100%. Textural properties were determined from N_2 physisorption isotherms at 77 K obtained by using a Quantachrome AUTOSORB unit. Prior to the analyses, the samples were outgassed at 250°C for 3 h in flowing N_2 . BET equation was used to calculate the specific surface area of the samples. Thermogravimetric analysis (TGA/DTG) of the dried as-prepared LDHs, MgGa mixed oxides and rehydrated samples was performed using a TA Instruments TGA Discovery series equipment operating with a heating ramp of $10^\circ\text{C}\cdot\text{min}^{-1}$ from room temperature to 900°C in N_2 flow. TGA-MS experiments were performed using the same TGA unit equipped with a mass-spectrometer OmniStar GSD 320 (Pfeiffer-Vacuum) with a MID (Multiple Ion Detection) measurement mode, a SEM (Secondary Electron Multiplier) detector, and a quadrupole mass-analyzer. DRIFT spectra were recorded on a Nicolet IS 10 FTIR spectrometer equipped with a DTGS detector and KBr beam splitter. All spectra were collected over the range of $4,000\text{--}400 \text{ cm}^{-1}$ at a spectral resolution of 4 cm^{-1} and number of scans 128 (both for the background and the sample spectra).

Samples for Scanning Electron Microscopy (SEM) observations were mounted on a holder and sputter-coated (Q150R ES, Quorum Technologies Ltd., United Kingdom) by 10 nm of gold to neutralize charging-effects and to increase an SE yield at final micrographs. Further, the images of coated samples were acquired using field emission scanning electron microscope (Lyra3 GMU, Tescan Orsay Holding a.s., Czech

Republic) at an accelerating voltage of 12 kV and absorbed current ranging from 200 to 300 pA. For imaging, the SE detection was used to investigate the morphology of samples. The temperature-programmed desorption of carbon dioxide (CO_2 -TPD) or ammonia (NH_3 -TPD) was used to evaluate basic and acidic properties of MgGa mixed oxides and reconstructed LDHs. The details of the methods are presented in Kikhtyanin et al. (2017a). Maximum temperature in TPD experiments was chosen as 450°C which is temperature used for the preparation of MgGa mixed oxides.

Catalytic Test

Furfural (Sigma-Aldrich) and acetone (LachNer, Czech Republic) used for catalytic experiments were pre-dried with a molecular sieve 3A to exclude the effect of moisture originating from the chemicals.

For catalytic experiments with MgGa mixed oxides, 0.5 g of freshly calcined HTC was used. For catalytic experiments with reconstructed MgGa LDHs, 0.5 g of freshly calcined HT was pre-rehydrated according to the method described above.

Aldol condensation of furfural with acetone was carried out in a 100-ml stirred batch reactor (a glass flask reactor) at temperature of 50°C in the case of mixed oxides or 25°C in the case of reconstructed LDHs. Prior to the catalytic tests, the mixture of 19.7 g of acetone and 6.5 g of furfural (acetone to furfural molar ratio 5/1) was stirred at 200 RPM and kept at the predetermined reaction temperature. After that, a studied catalyst (grain of 0.25–0.5 mm) was added and the reaction was carried out at predetermined temperature for 120 min at 200 RPM. It was previously established that the reaction is limited neither by external nor internal mass transfer under the chosen reaction conditions (in tests with changing stirring rate and catalyst particle size; Hora et al., 2015). Samples of liquid products were periodically withdrawn from the reactor during the experiment, filtered and analyzed by Agilent 7890A GC unit equipped with a flame ionization detector (FID), using a HP-5 capillary column (30 m/0.32 mm ID/0.25 μm). Catalytic results of aldol condensation of furfural and acetone were described by conversion and selectivity parameters that were calculated as follows:

$$\text{reactant conversion (t) (mol\%)} = 100 \times (\text{reactant}_{t=0} - \text{reactant}_t) / \text{reactant}_{t=0};$$

$$\text{selectivity to product i} = (\text{mole of reactant converted to product i}) / (\text{total moles of reactant converted}).$$

Carbon balance was monitored in all experiments as the total number of carbon atoms detected in each organic compound with C_n atoms (where $n = 3, 5, 8, \dots$, etc.) divided by the initial number of carbon atoms in F+Ac feed:

$$\text{C balance (\%)} = (3 \text{ molC}_3 + 5 \text{ molC}_5 + \dots \text{ nmolC}_n) / (3 \text{ molC}_{3(t=0)} + 5 \text{ molC}_{5(t=0)}).$$

RESULTS AND DISCUSSION

Chemical, Structural, and Textural Properties of As-Prepared LDHs and Mixed Oxides

ICP data showed that gallium content in the prepared samples was higher than the values calculated based on the composition of the chemical mixture used for the synthesis. Similar deviation from the theoretical composition was observed for MgGa LDHs repeatedly (López-Salinas et al., 1996; Aramendía et al., 1999a,b) what was explained by the considerable solubility of intermediate $\text{Ga}(\text{OH})_3$ species in a basic solution (López-Salinas et al., 1996).

The XRD data confirmed that Ga was highly efficiently incorporated into the brucite-like layers of MgGa LDHs in a wide range of Mg/Ga molar ratios. XRD patterns of the as-prepared MgGa LDHs varying by gallium content (Figure 1) show the intensive symmetric lines of a pure hydrotalcite phase (similar to JCPDS Card No. 22-0700). The reflections at $2\theta \approx 11.2^\circ$, 22.8° , 36° , and 60° are characteristic for the brucite-like layers (Di Cosimo et al., 1998; Abelló et al., 2005; Kikhtyanin et al., 2017a). The absence of additional lines in the diffractograms suggests that no other crystalline phases are present in the samples thus proving the high phase purity of the as-prepared MgGa LDHs materials. The preparation of phase-pure MgGa LDHs has also been reported in other studies (Rebours et al., 1994; Aramendía et al., 1999b; Thomas and Vishnu Kamath, 2005). MgGa-3A possesses the highest crystallinity; the other two samples show crystallinity of 93–95% relative to MgGa-3A.

The diffraction peaks assigned to (003) and (110) reflections (i.e., at 11.2° and 60°) were used to calculate the basal spacing between the layers (d) and unit cell dimension a (as $a = 2d_{110}$), respectively. Both the d and a values increase with the increasing Mg/Ga molar ratio (Table 1), which is an usual trend observed for MgAl hydrotalcites with different Al content (Yun and Pinnavaia, 1995; Di Cosimo et al., 1998; Kikhtyanin et al., 2017a). The increase in the spacing between layers in LDH structure is unequivocally ascribed to differences in the ionic

radii of Ga^{3+} and Mg^{2+} being 0.62 and 0.72 Å, respectively¹, proving the isomorphous substitution of Mg^{2+} by Ga^{3+} atoms within the brucite-like layers. The calcination of the as-prepared materials at $T = 450^\circ\text{C}$ results in total destruction of the LDH structure as evidenced by the disappearance of diffraction lines corresponding to the HTC structure. Two intensive diffraction lines observed in XRD patterns of all MgGa mixed oxides at $2\theta \approx 43.0^\circ$ and 62.5° and a smaller diffraction peak at $2\theta \approx 37.0^\circ$ are typical for MgO periclase-type structure (JCPDS card No. 45-0946). Similar XRD patterns were observed also after heat treatment of MgAl hydrotalcites (Yun and Pinnavaia, 1995; Di Cosimo et al., 1998; Kikhtyanin et al., 2017a). The relative crystallinity of the MgO phase decreased dramatically with the decline in the Mg/Ga ratio of the mixed oxides (Table 1) suggesting the presence of amorphous phase at high Ga content. The decrease in the MgO basal spacing, $d(200)$, from 2.112 to 2.105 Å with the increasing Ga content (Table 1) indicates that Ga replaced partially Mg in the MgO crystalline framework. Besides, an additional reflection is present in XRD patterns of MgGa mixed oxides at $2\theta \approx 36.0^\circ$. It becomes more intensive with the increasing Ga content suggesting that it is originated from a Ga-containing compound. The appearance of an additional line in XRD patterns of MgGa mixed oxides after the calcination of MgGa LDHs at moderate temperatures was reported earlier in several studies (Rebours et al., 1994; Aramendía et al., 1999b; Grand et al., 2010). Rebours et al. (1994) suggested that the reflection at $2\theta \approx 36.0^\circ$ was either due to the presence of magnesium gallate, MgGa_2O_4 , or due to the presence of Ga cations in the tetrahedral sites in magnesia lattice.

As-prepared MgGa LDHs possess BET surface area in the range of $68\text{--}82\text{ m}^2\text{g}^{-1}$, but the values of BET surface area for MgGa mixed oxides increases to $123\text{--}140\text{ m}^2\text{g}^{-1}$ (Table 1) what is a consequence of the collapse of lamellar HTC structure.

DRIFT spectra of the as-prepared MgGa LDH samples are presented in Figure 2. They agree with those published elsewhere

¹Database of Ionic Radii. Available online at: <http://abulafia.mt.ic.ac.uk/shannon/ptable.php>

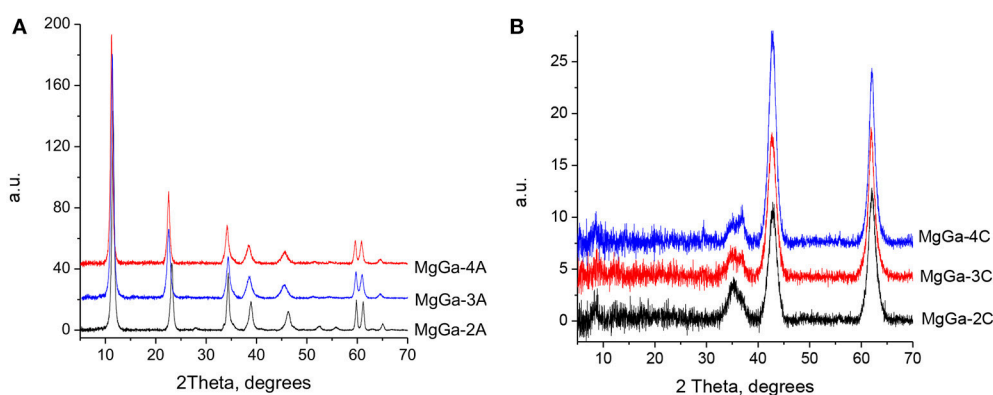
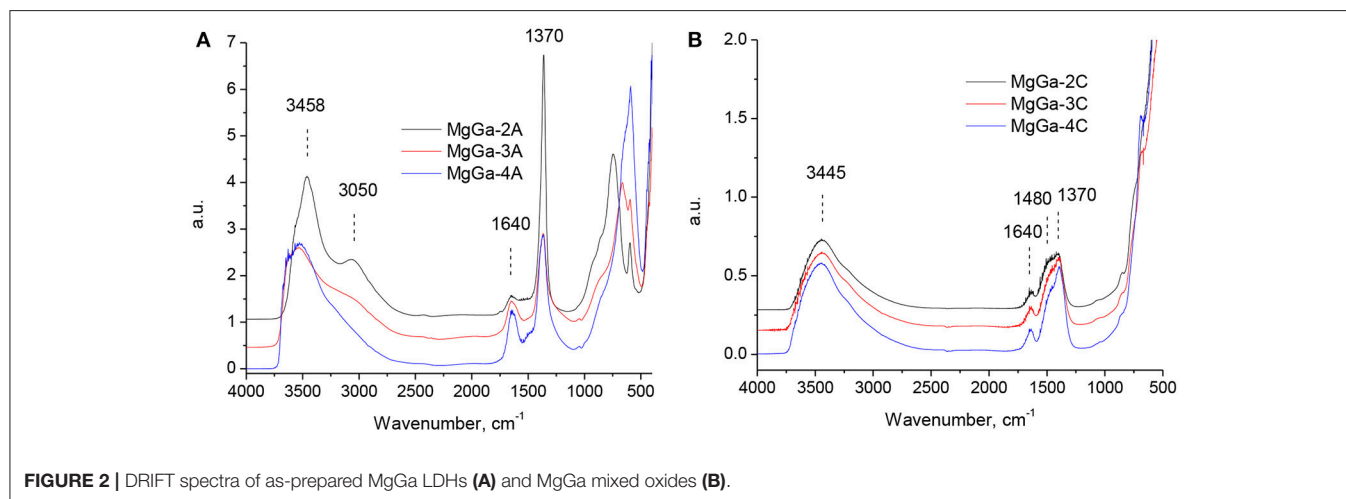


FIGURE 1 | XRD patterns of as-prepared MgGa LDHs (A) and mixed oxides (B).

TABLE 1 | Phase composition and BET surface area of the as-prepared hydrotalcites.

Sample	Mg/Ga ratio	Phase composition	HTC/MgO crystallinity, %	HTC basal spacing <i>d</i> , Å	HTC unit cell <i>a</i> , Å	MgO <i>d</i> (200), Å	BET surface, m ² ·g ⁻¹
MgGa-2A	2.75	HTC	93	7.69	3.090	—	77
MgGa-3A	4.11	HTC	100	7.78	3.091	—	68
MgGa-4A	5.24	HTC	95	7.90	3.102	—	82
MgGa-2C		MgO	56	—	—	2.105	123
MgGa-3C		MgO	67	—	—	2.111	127
MgGa-4C		MgO	100	—	—	2.112	140
MgGa-2R10		HTC	83	7.86	n.d.	—	5.5
MgGa-3R10		HTC	100	7.88	n.d.	—	5.7
MgGa-4R10		HTC	91	7.96	n.d.	—	3.0



for MgAl (Di Cosimo et al., 1998; Abelló et al., 2005; Kikhtyanin et al., 2017b) and MgGa hydrotalcites (López-Salinas et al., 1996; Aramendía et al., 1999a,b; Thomas and Vishnu Kamath, 2005).

The broad band in the range of 2,700–3,700 cm⁻¹ with the maximum at about 3,450–3,550 cm⁻¹ is usually attributed to the stretching vibrations of structural hydroxyl groups in the brucite-like layer (Roy et al., 1953) and the twisting vibrations of physisorbed water (Allegra and Ronca, 1978). The shoulder at 3,050 cm⁻¹ is assigned to the hydrogen bonding between water molecules and interlayer carbonate anions (López-Salinas et al., 1996). **Figure 2** shows that the intensity of this shoulder increases with increase in Ga content. It may be considered as an additional proof that Ga atoms in the composition of brucite-like layers are compensated by interlayer carbonates. The band corresponding to the vibration mode δ_{HOH} at 1,630–1,645 cm⁻¹ indicates the presence of interlayer water molecules and the band at 1,370 cm⁻¹ arises from the ν_3 mode of interlayer CO₃²⁻ (chelating or bridging bidentate) anions (Abelló et al., 2005). The low intensive band at 1,515 cm⁻¹ is ascribed to the reduction in the symmetry caused by the presence of monodentate carbonates ($\nu_{\text{asym O-C-O}}$) interacting with Mg²⁺ (Di Cosimo et al., 1998; Abelló et al., 2005). In low frequency region the band at 870 cm⁻¹ is characteristic for the out-of-plane deformation of carbonate,

whereas the in-plane bending is located at 680 cm⁻¹ (Abelló et al., 2005). In Mg-Al hydrotalcites, a band at about 560 cm⁻¹ corresponds to the translation modes of hydroxyl groups influenced by Al³⁺ cations (Abelló et al., 2005; Pérez-Ramírez et al., 2007b). Accordingly, the band at 590 cm⁻¹ observed in DRIFT spectra of MgGa samples could be attributed to the translation modes of hydroxyl groups influenced by Ga³⁺ cations. Indeed, López-Salinas et al. (1996) proposed that the appearance of this band may be related with Mg-O-Mg or Mg-O-Ga vibrations.

Calcination of the as-prepared MgGa hydrotalcites resulted in a collapse of the lamellar structure accompanied by H₂O and CO₂ removal. Correspondingly, DRIFT spectra of the resulting mixed oxides changed significantly (**Figure 2B**). The intensity of the bands in the range of 2,700–3,700 cm⁻¹ substantially decreased due to dehydroxylation. Water removal can be evidenced also by the disappearance of the band at around 1,640 cm⁻¹ (water bending vibrations) and of the shoulder at 3,000 cm⁻¹ (H₂O–CO₃²⁻ interaction in the interlayer). Decomposition of the interlayer carbonates resulted in a decrease in the intensity of the band at 1,370 cm⁻¹. A new broad band in the range of 1,400–1,500 cm⁻¹ arisen from the interaction of non-interlayer carbonates with Mg²⁺ cations on the surface of mixed oxides

(Abelló et al., 2005). Additionally, the DRIFT spectra of mixed oxides show that reversible adsorption of water from air can take place during experiments as evidenced by the existence of a small band at around $1,640\text{ cm}^{-1}$ and re-appearance of a broad band with the maximum at $3,450\text{ cm}^{-1}$.

Thermal Treatment of the As-Prepared MgGa LDHs to Mixed Oxides

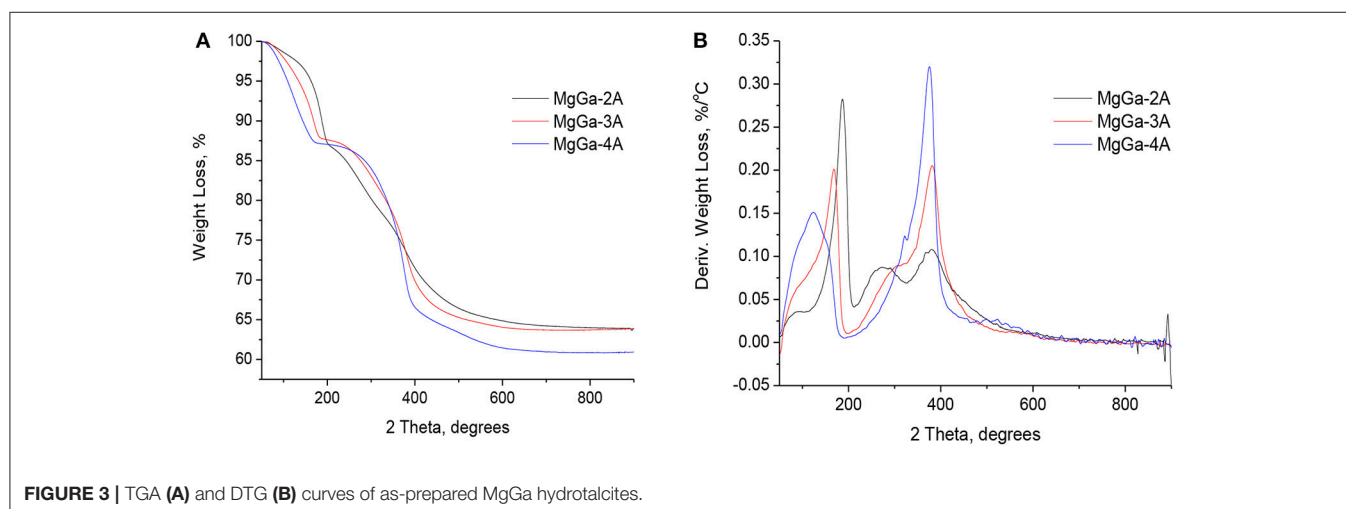
Figure 3 depicts the TGA (A) and DTG (B) profiles of the as-prepared MgGa hydrotalcites affording the corresponding MgGa mixed oxides. The total weight loss of the samples is in the range of 36.1–39.1 wt.% (**Table 2**) and it corresponds well with the data reported earlier for similar materials (López-Salinas et al., 1996; Aramendía et al., 1999a; Thomas and Vishnu Kamath, 2005). The weight loss is 12.2–12.8 wt.% in the temperature range of 50–200°C (**Table 2**) and it corresponds to the removal of both physically adsorbed and interlayer water molecules. **Figure 3B** depicts that with increasing Ga content in the as-prepared MgGa LDHs the amount of physisorbed water ($T_{\text{max.}} = 100\text{--}120^\circ\text{C}$) constantly decreases while the amount of interlayer water ($T_{\text{max.}} = 170\text{--}185^\circ\text{C}$) correspondingly increases. The second weight loss of 21.0–22.6 wt.% is observed in the temperature range of 200–500°C and it originates from dehydroxylation of the brucite-like layers and decomposition of carbonates in the interlayer with the corresponding evolution of water and CO_2 , respectively. **Figure 3B** evidences that the shape of DTG curve in this temperature range depends on Ga content in the samples. MgGa-3A and MgGa-4A have only one predominant signal at $T \approx 380^\circ\text{C}$, while the DTG curve of MgGa-2A has an additional signal at $T = 270^\circ\text{C}$. Earlier, the presence of more than one kind of OH-groups which differ in properties was suggested in MgAl hydrotalcites with low Mg/Al ratio (Kikhtyanin et al., 2017a). Similarly, the presence of the low-temperature signal in DTG curve of MgGa-2A can be attributed either to the dehydroxylation of defective Ga atoms in the composition of layered structure or to the dehydroxylation of XRD invisible Ga hydroxide phase.

Above 500°C , the DTG curve evidences the small additional weight loss of 2.8–4.3 wt.%. Aramendía et al. (1999a) suggested that the final weight loss involves the sustained release of water which results from the residual dehydroxylation of the species with results in Ga_2O_3 phase. Nevertheless, without carrying out additional TGA-MS experiments, it is impossible to uniquely assign this signal to a certain species.

MS curves from the TGA-MS experiments (**Figure 4**) demonstrate that the dehydroxylation of brucite-like layers and decomposition of charge-compensating carbonates in MgGa hydrotalcites occurs simultaneously in similar temperature range. Nevertheless, the removal of water due to dehydroxylation takes place in a broader range compared to decarbonation (**Figure 4**) and it ends at temperatures of $550\text{--}600^\circ\text{C}$. It is also seen (**Figure 4**) that the dehydroxylation of samples with high Ga content occurs in two steps which are characterized by the presence of two peaks at $T \approx 290$ and $T \approx 370^\circ\text{C}$. It allows suggesting that these samples possess two kinds of hydroxyl groups in their composition. Additionally, a slight increase in the TGA-MS- H_2O profile at temperatures up to 800°C suggests dehydroxylation of the residual OH groups in MgGa mixed oxides, while a small peak at 590°C in TGA-MS- CO_2 profile can be attributed to the decomposition of residual carbonates. A ratio between areas under TGA-MS- H_2O and

TABLE 2 | The results of thermal analysis for the studied MgGa hydrotalcites.

Sample	Weight loss (%)				Ratio between signals TGA-MS _{H2O} /TGA- MS _{CO2} in the range of T = 200–500°C
	20–200°C	200–500°C	>500°C	Total	
MgGa-2A	12.8	21.0	4.3	36.1	4.3
MgGa-3A	12.2	21.3	2.8	36.3	4.8
MgGa-4A	12.8	22.6	3.8	39.2	5.0
MgGa-2R10				53.2	16.4
MgGa-3R10				56.8	21.2
MgGa-4R10				51.3	31.6



TGA-MS- CO_2 curves in the temperature range from 200 to 500°C can serve as a measure of the ratio of removed H_2O and CO_2 molecules by dehydroxylation and decarbonation, respectively. This ratio increases from 4.3 to 5.0 with an increase in Mg/Ga ratio from 2 to 4 (Table 2) and it reflects the decrease in carbonate groups in the as-prepared samples. It seems to be logical since the theoretical $\text{Ga}^{3+}/\text{CO}_3^{2-}$ ratio in the as-prepared hydrotalcites is constant and equal to 0.5, while the content of structural hydroxyls is independent on Mg/Ga ratio, so less carbonate groups are present in low-gallium samples.

Reconstructed MgGa LDH Materials

Figure 5A depicts XRD patterns of MgGa-3R0.25 to MgGa-3R40 samples prepared by rehydration of MgGa-3C using decarbonized water under vigorous stirring for different time ranging from 0.25 to 40 min. All prepared samples represent well-crystalline materials with hydrotalcite structure and, therefore, evidence that the prepared MgGa mixed oxides demonstrate a “memory effect” firstly described for MgAl mixed oxides (Miyata, 1980). **Figure 5B** shows the effect of the duration of the rehydration of MgGa mixed oxide on the crystallinity of the resulting reconstructed LDH. Two main conclusions can be drawn from the observed dependence. Firstly, the crystallinity

exceeds 50% already after 0.25 min of rehydration and is close to 100% after 1 min without a visible change with further increase in treatment time. Secondly, **Figure 5A** shows that the intensity of the XRD reflexes at low 2θ values ($<25^\circ$) are higher whereas those at higher 2θ values ($>25^\circ$) are lower in comparison with the XRD patterns of the as-prepared MgGa LDHs. This difference may be due to a change in the textural characteristics of the reconstructed materials, which will be discussed further when considering SEM results.

The results suggest that the transformation of MgGa mixed oxide occurs very rapidly upon contact with water, similar to the behavior of MgAl mixed oxides (Kikhtyanin et al., 2017b). Only a few minutes of rehydration are enough to get reconstructed MgGa LDHs with maximal crystallinity. In addition, the peak at $2\theta \approx 36^\circ$, which was present in the XRD patterns of MgGa mixed oxides (attributed either to the presence of magnesium gallate, MgGa_2O_4 , or to the presence of Ga cations in tetrahedral sites in the magnesia lattice), is not observed in the XRD patterns of the reconstructed materials. The disappearance of this line designates either the reverse transformation of such a specific MgGa compound into the HTC structure or, at least, these species become XRD-invisible because of a decrease in their size, concentration, or crystallinity during the rehydration treatment.

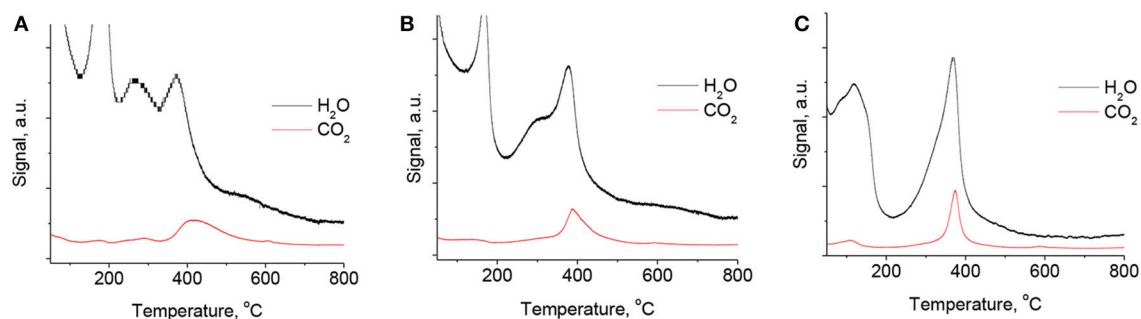


FIGURE 4 | TGA-MS spectra of evolved H_2O and CO_2 molecules for MgGa-2A (A), MgGa-3A (B), and MgGa-4A (C) samples.

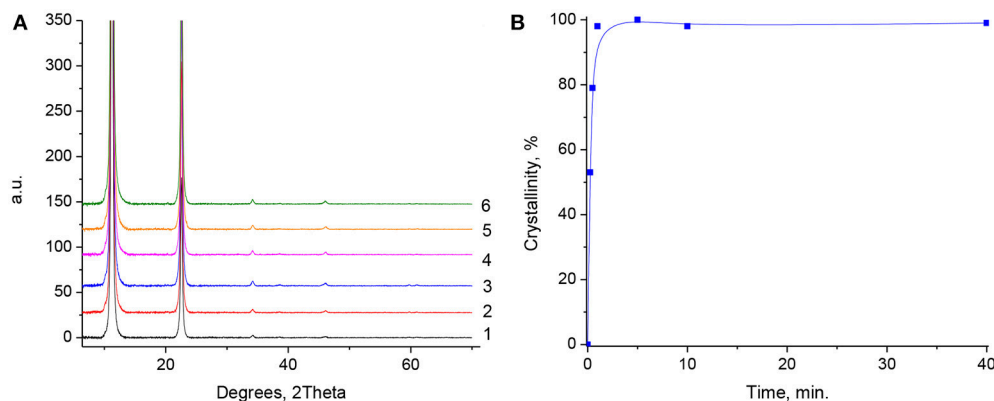


FIGURE 5 | (A) XRD patterns of reconstructed MgGa hydrotalcites at different rehydration times. 1-MgGa-3R0.25; 2-MgGa-3R0.5; 3-MgGa-3R1; 4-MgGa-3R5; 5-MgGa-3R-10; 6-MgGa-3R40. (B) The dependence of MgGa-3R crystallinity on the duration of MgGa mixed oxides rehydration.

The basal spacing between the layers (d) can be calculated from the position of the peak assigned to (003) reflection, however, the calculation of unit cell dimension (a) for the reconstructed samples not possible because of the very low intensity of (110) reflection. **Table 1** evidences that the d -value calculated for MgGa-2R10, MgGa-3R10, and MgGa-4R10 (**Table 1**) is less than that for the as-prepared samples. The basal spacing (d) can be considered as an indicator for the number of heteroatoms (Ga in this study) in “brucite-like” layers. Therefore, the increase in this value observed for the reconstructed samples allows suggesting that not all Ga atoms are recovered to the crystallographic sites of HTC framework after the rehydration of MgGa mixed oxide. Plausibly they are part of an amorphous phase.

DRIFT study (**Figure 6**) provides an additional proof for the existence of the “memory effect” for MgGa samples: DRIFT spectra of the reconstructed materials are very similar to those of the as-prepared materials. Moreover, the spectra do not show any dependence on the rehydration time of MgGa mixed oxides, so **Figure 6** depicts only the results for the reconstructed samples prepared by rehydration for 10 min. The recovery of the structural hydroxyl groups in the brucite-like layer is evidenced by an increase in the intensity of the wide band in the range of 2,500–3,600 cm^{-1} . The shoulder signal at 3,050 cm^{-1} and the band at 1,670 cm^{-1} re-appear in the spectra, indicating the presence of physisorbed and interlayer water in the prepared samples. The high intensity of the band at 1,370 cm^{-1} suggests the presence of a large number of interlayer compensating anions. As mentioned earlier, this band is attributed to interlayer carbonates in the case of the as-prepared samples. Abelló et al. (2005) noted that this band in the reconstructed MgAl hydrotalcites may also indicate the presence of carbonate groups in the prepared samples due to their contamination with CO_2 during the rehydration step. However, based on TGA-MS results we proposed that the band at 1,370 cm^{-1} can characterize not only carbonate, but also hydroxyl groups in the interlayer (Kikhtyanin et al., 2017b). Accordingly, we believe that the band at 1,370 cm^{-1} present in the spectra of MgGa reconstructed materials is mostly due to hydroxyl groups rather than carbonate groups. In the analysis, we considered the differences in the signals from H_2O and CO_2 in TGA-MS spectra (see below).

According to TGA results, the total weight loss of the reconstructed MgGa samples is in the range of 51–57% (**Table 2**), which is larger than expected based on the composition of these samples. As shown in Kikhtyanin et al. (2017b), this can be explained by the presence of excessive physisorbed water in the reconstructed samples, which is not removed during the drying of the samples after rehydration. In this case, the TGA method gives only general information about the increase in weight of the obtained samples. More useful information can be obtained by using the TGA-MS method, which allows estimating the relative amount of released H_2O and CO_2 molecules and, consequently, the relative content of hydroxyl and carbonate groups in the reconstructed MgGa LDHs.

There were observed approximately similar intensities of TGA-MS- H_2O and TGA-MS- CO_2 signals of reconstructed samples with different Mg/Ga molar ratios. Also, the

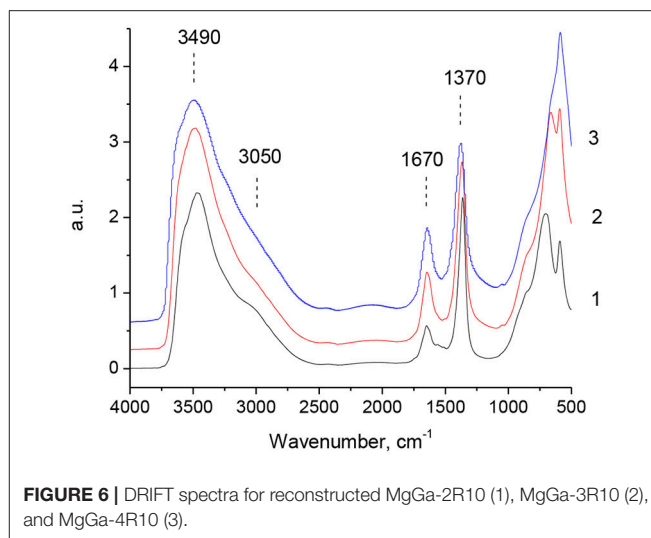


FIGURE 6 | DRIFT spectra for reconstructed MgGa-2R10 (1), MgGa-3R10 (2), and MgGa-4R10 (3).

TGA-MS- H_2O and TGA-MS- CO_2 profiles did not show a significant dependence on the rehydration duration. Therefore, **Figure 7** depicts the selected characteristic TGA-MS profiles of reconstructed samples with different Mg/Ga ratios and the same rehydration time (10 min) of the corresponding mixed oxides. **Figure 7** evidences that the intensity of the signal in TGA-MS- CO_2 profiles is substantially lower for all the rehydrated samples compared with their as-prepared MgGa LDHs counterparts (**Figure 4**).

Table 2 shows the range of ratios calculated from the areas under the TGA-MS signals of H_2O and CO_2 evolution in the range of 200–500°C. This ratio continuously increases from 16.4 to 31.6 with growing Mg/Ga ratio in the reconstructed MgGa samples. In an ideal case, carbonate groups should be completely absent in the reconstructed MgGa LDHs. In the prepared reconstructed MgGa samples, the presence of carbonates can have two causes. Firstly, MgGa mixed oxides may contain a certain amount of residual carbonates that have not been decomposed during the thermal treatment of the corresponding MgGa LDHs. Indeed, TGA-MS spectra (**Figure 4**) evidence residual CO_2 evolution at temperatures above 450°C, which is calcination temperature for the as-prepared materials. Secondly, the reconstructed LDHs can be accidentally exposed to CO_2 from air during the rehydration/drying processes involved in their preparation and/or during the TGA experiment. In any case, it is practically impossible to avoid completely the presence of carbonates in the reconstructed MgGa materials.

SEM

SEM images were recorded to investigate the morphology of MgGa materials with different Mg/Ga ratio. The micrographs of the as-synthesized LDHs with Mg/Ga molar ratio in the range of 2–4 (**Figure 8**) show a well-developed layered structure which is typical for hydrotalcite-like materials.

MgGa-3A with the highest crystallinity was formed by well-developed large platelet aggregates with the size in the range

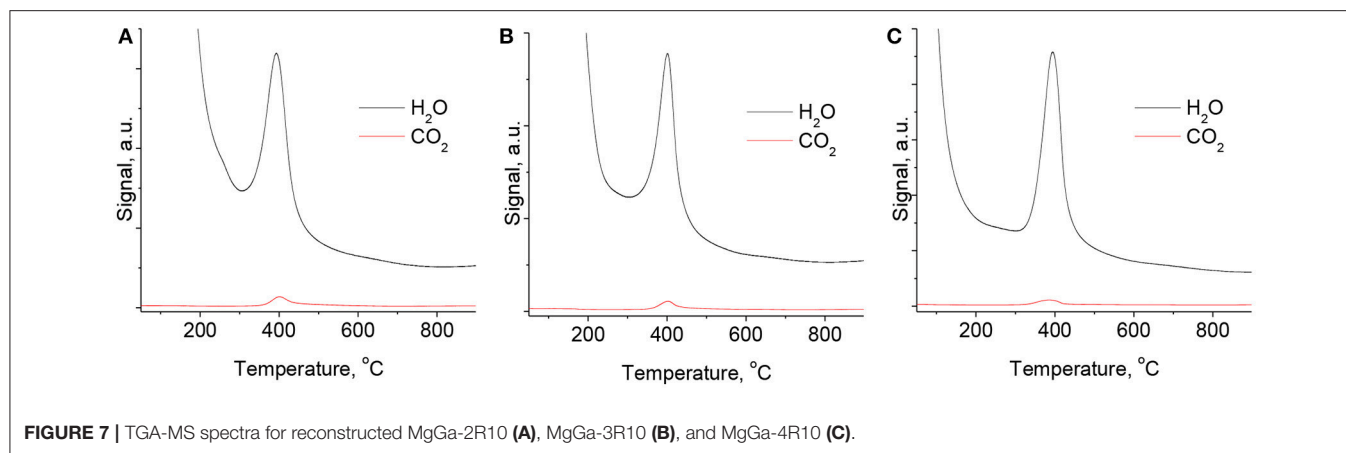


FIGURE 7 | TGA-MS spectra for reconstructed MgGa-2R10 (A), MgGa-3R10 (B), and MgGa-4R10 (C).

of 5–10 μm consisting of thin, hexagonal, plate-like crystals of 1.5–2.5 μm in length (**Figure 8A1**). MgGa-2A with higher Ga content was formed by smaller aggregates of $\leq 5 \mu\text{m}$ in size (**Figure 8B1**). They were composed of plate-like crystals which were smaller in size (0.7–1.5 μm) and significantly thinner than those in Mg/Ga = 3. This tendency was observed previously also for MgAl LDHs (Kikhtyanin et al., 2017a). MgGa-4A with lower Ga content was built of large massive agglomerates where the plate-like crystals had the size of 1.7–3.5 μm (**Figure 8C1**). The SEM images of the as-prepared MgGa LDHs also evidence that MgGa-3A has the largest size of individual platelets.

MgGa mixed oxides obtained upon calcination at 450°C maintained a lamellar structure (**Figures 8A2–C2**). Moreover, the morphology and the size of plate-like crystals and agglomerates were very similar to that of the corresponding as-prepared samples. Nevertheless, the morphology of the crystals of the reconstructed MgGa LDHs was significantly different from the as-prepared materials and mixed oxides. **Figures 8A3–C3** depict the SEM images of the reconstructed MgGa materials prepared by rehydration of the corresponding MgGa mixed oxides for 10 min. First of all, separate plate-like crystals became stacked together and created large unshaped agglomerates with the size $\geq 20 \mu\text{m}$ in MgGa-3R10 and $\geq 10 \mu\text{m}$ in MgGa-2R10 and MgGa-4R10. The size of the individual platelets in the crystals of the reconstructed MgGa LDHs was noticeably smaller, but the thickness of the platelets slightly increased in comparison with the as-prepared materials and mixed oxides. The shape of these platelets became irregular and more defective after rehydration. Finally, **Figure 8B3** evidences that the surface of the platelets was cracked. It is obvious that rehydration of mixed oxides had a significant effect on the morphology of the resulting crystals of rehydrated LDHs even though their layered character was preserved. Because of these transformations, the intensity of reflexes in XRD patterns of the reconstructed MgGa LDHs also changed in comparison with the as-prepared materials.

Acid-Base Properties

Figure 9A depicts the NH_3 -TPD profiles of MgGa mixed oxides with different Mg/Ga ratio while **Table 3** reports the total

concentration of acid sites determined from the total amount of desorbed NH_3 from MgGa mixed oxides.

MgGa-3C possesses the largest concentration of acid sites, 190 $\mu\text{mol}\cdot\text{g}^{-1}$, while MgGa-2C and MgGa-4C have similar concentration of acid sites, 96 $\mu\text{mol}\cdot\text{g}^{-1}$. A comparison in the shapes of the obtained curves allows suggesting that the mixed oxides contain acid sites varied in their strength. Indeed, two peaks with maximums at about 160 and 250°C can be identified in the TPD profiles (**Figure 9A**). However, there is no clear dependence of the intensity of individual peaks on Mg/Ga molar ratio. Assuming that the acidity of MgGa mixed oxides should originate from Ga oxidic species, the obtained result is rather curious. Nevertheless, it allows suggesting that the acidity of mixed oxides is not only a consequence of their composition, but other factors, such as presence of admixtures, the distribution of heteroatoms throughout the crystalline framework, etc., should be considered. This implies using broader characterization methods than those used in the present study.

Figure 9B shows the CO_2 -TPD profiles of MgGa mixed oxides. **Table 3** gives the total concentration of basic sites derived from the total amount of evolved CO_2 . The TPD curves obtained for all three MgGa mixed oxides have a pronounced maximum between 100 and 120°C. As mentioned previously (López-Salinas et al., 1997; Aramendía et al., 1999a), the peak in the low-temperature region of CO_2 -TPD curve may be assigned to weak basic sites (OH groups). In our previous work, we reported for MgAl mixed oxides that this peak also could reflect the part of medium basic sites (Mg-Al pairs) (Smoláková et al., 2017). Additionally, López-Salinas et al. (1997) observed the second peak on the CO_2 -TPD curve for MgGa mixed oxides, which was present at 200–250°C as a shoulder partially overlapped with the first peak, and a small third peak present as a shoulder above 400°C. The authors ascribed these additional peaks to the appearance of medium and very strong basic sites present in MgGa mixed oxides, respectively (López-Salinas et al., 1997). Taking into account the shape of CO_2 -TPD profiles obtained in the present study, we do not dare to discriminate with certainty between different peaks in the curve and, consequently, we do not provide quantitative contribution of basic sites varied by their strengths to the total basicity of MgGa mixed oxides. Similarly,

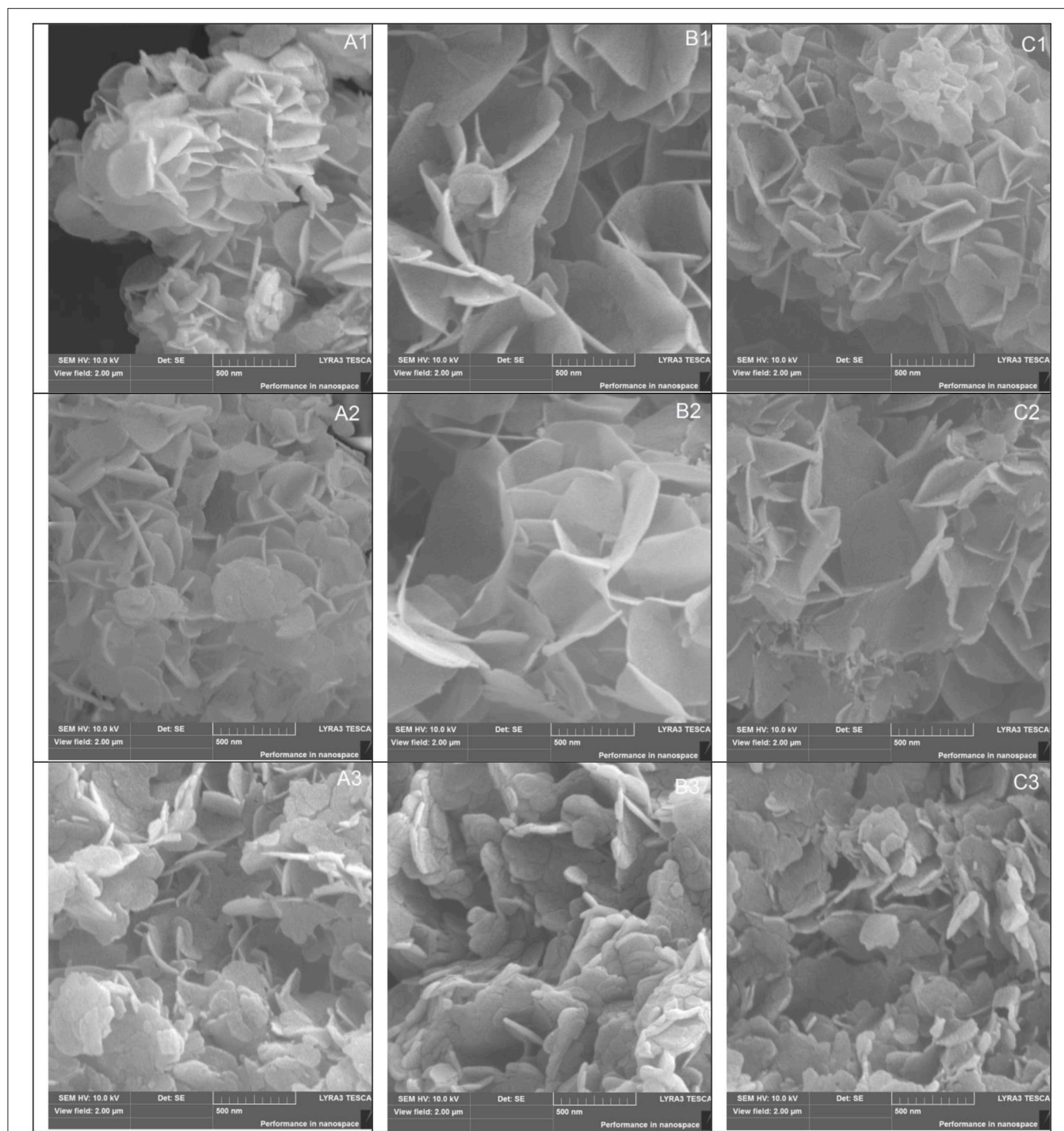


FIGURE 8 | SEM images of MgGa as-prepared materials (A1–C1), mixed oxides (A2–C2), and reconstructed LDHs rehydrated during 10 min (A3–C3). A, Mg/Ga = 2; B, Mg/Ga = 3; C, Mg/Ga = 4.

Aramendia et al. (1999a) reported it was difficult to express the strength of basic sites on an absolute scale and to quantify the number of the sites.

The total concentration of basic sites in the MgGa mixed oxides is 149 and 178 $\mu\text{mol}\cdot\text{g}^{-1}$ for MgGa-2C and MgGa-3C,

respectively, but it noticeably decreases to 90 $\mu\text{mol}\cdot\text{g}^{-1}$ for MgGa-4C. MgGa-3C mixed oxide possesses both the highest amount of acid and basic sites. The dependence of the number of basic sites on Mg/Ga molar ratio follows a general trend between a chemical composition and the total basicity that was earlier

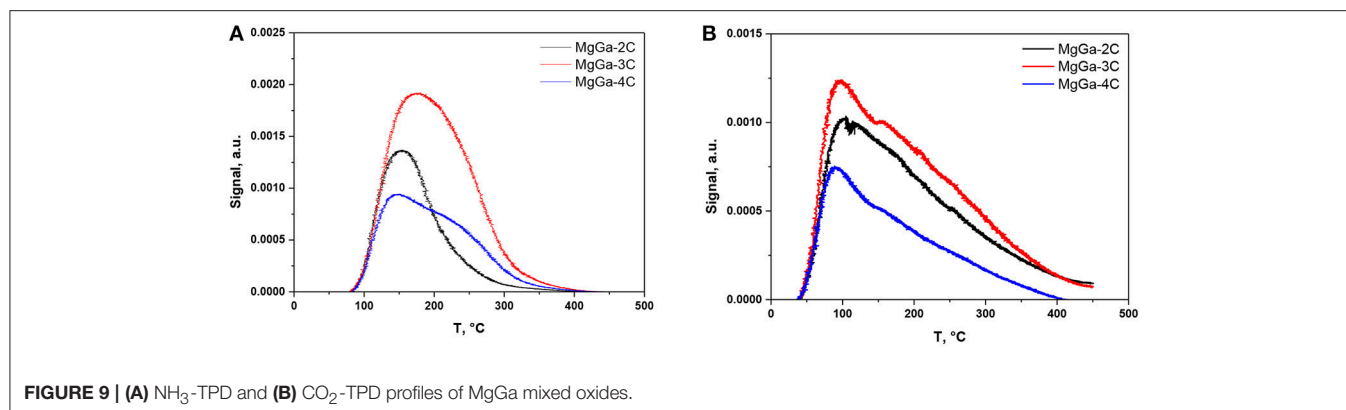


FIGURE 9 | (A) NH_3 -TPD and **(B)** CO_2 -TPD profiles of MgGa mixed oxides.

TABLE 3 | Concentration of acid and basic sites in MgGa mixed oxides determined by TPD of adsorbed NH_3 and CO_2 , correspondingly.

Sample	Amount of desorbed NH_3 , $\mu\text{mol}\cdot\text{g}^{-1}$	Amount of desorbed CO_2 , $\mu\text{mol}\cdot\text{g}^{-1}$			Evaluated concentration of interlayer hydroxyls, $\mu\text{mol}\cdot\text{g}^{-1}$	Theoretical concentration of interlayer hydroxyls, $\mu\text{mol}\cdot\text{g}^{-1}$	Recovery of Ga atoms by reconstruction process, %
		Total	L.T.	H.T.			
MgGa-2C	96	149	64	784	1,568	3,784	41
MgGa-3C	190	178	113	770	1,540	3,016	51
MgGa-4C	96	90	88	886	1,772	2,565	69
MgGa-2R10	–	848					
MgGa-3R10	–	883					
MgGa-4R10	–	974					

observed for MgAl mixed oxides (Kikhtyanin et al., 2017a). Earlier, Di Cosimo et al. (1998) explained the decrease in the basicity observed for MgAl mixed oxides with low Al content by a significant Al surface enrichment. In line with this explanation, it can be assumed that the loss of the total basicity observed for MgGa-4C compared to materials with larger Ga content can also be explained by the specific distribution of Ga atoms on the external surface of the mixed oxides.

CO_2 -TPD is usually used to characterize the basic properties (in terms of both the concentration of basic sites and their distribution by strength) of mixed oxides prepared by heat treatment of LDH materials (López-Salinas et al., 1997; Aramendía et al., 1999a; Di Cosimo et al., 2000; Aramenda et al., 2003; Kikhtyanin et al., 2017a). In contrast, the basic properties of reconstructed hydrotalcites are characterized less often. Abelló et al. (2005) performed an investigation of reconstructed MgAl hydrotalcites by using CO_2 -TPD and identified two peaks in their TPD profile, at around 400–420°C and at $\approx 550^\circ\text{C}$. They attributed the observed peaks to two types of basic sites in the rehydrated MgAl mixed oxides. The authors considered the first peak as the contribution of mainly bidentate carbonates, together with bicarbonate species, on the catalyst surface, whereas the second smaller peak was ascribed to monodentate species, similar to those observed in mixed oxides after CO_2 adsorption.

Figure 10 depicts CO_2 -TPD profiles observed after the interaction of CO_2 with three reconstructed MgGa materials, MgGa-2R10, MgGa-3R10, and MgGa-4R10. A strong intensive peak with a maximum at around 400°C was observed in the

CO_2 -TPD profiles of all the samples. Additionally several smaller peaks can be distinguished between 50 and 230°C. The obtained profiles inevitably indicate the presence of different basic sites in the reconstructed MgGa LDHs.

Table 3 gives the amount of CO_2 desorbed up to 230°C and between 230 and 450°C. The amount of CO_2 that desorbed up to 230°C is between 64 and 113 $\mu\text{mol}\cdot\text{g}^{-1}$. That amount of CO_2 is lower compared to the amount of CO_2 desorbed from the corresponding MgGa mixed oxides (90–178 $\mu\text{mol}\cdot\text{g}^{-1}$). However, it has to be mentioned that the absolute amount of CO_2 desorbed from MgGa mixed oxides and reconstructed MgGa LDHs cannot be directly compared due to the higher amount of water present in the reconstructed materials. The highest amount of desorbed CO_2 in the range of $T \leq 230^\circ\text{C}$ is observed for the reconstructed MgGa-3R10 material being prepared from mixed oxide MgGa-3C having the highest number of acid and basic sites. Nonetheless, most CO_2 (between 770 and 886 $\mu\text{mol}\cdot\text{g}^{-1}$) desorbed from the reconstructed MgGa materials between 230 and 450°C. This is considerably more than for CO_2 desorbed from MgGa mixed oxides (90–178 $\mu\text{mol}\cdot\text{g}^{-1}$, **Table 3**).

To explain the origin of the desorption peak between 230 and 450°C in TPD profiles of reconstructed MgGa materials, we did the same experiment as in the case of TPD- CO_2 , but without any adsorption of CO_2 . In that case, only a marginal amount of CO_2 desorbed from MgGa-3R10 up to 230°C, but 1,186 $\mu\text{mol}\cdot\text{g}^{-1}$ of CO_2 desorbed between 230 and 450°C. The desorbed CO_2 can be either from an external or an internal source. It is worth noting that water used for rehydration can be excluded as a source of carbonates.

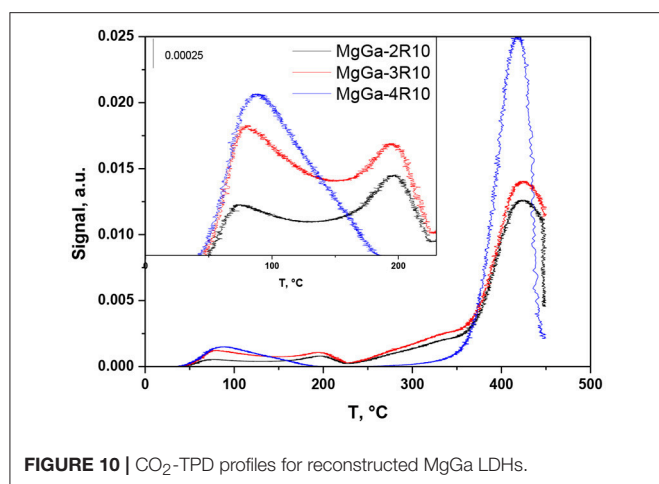


FIGURE 10 | CO₂-TPD profiles for reconstructed MgGa LDHs.

The external origin could be attributed to a dramatic increase in the number of basic sites in the reconstructed MgGa materials compared to MgGa mixed oxides, followed by the rapid interaction of interlayer hydroxyls in freshly prepared reconstructed materials with CO₂ from air during the preparations for TPD measurements.

The internal origin could be explained by redistribution of CO₂ from carbonate species that were not decomposed, i.e., that require >450°C to decompose thermally. In a special experiment we checked the amount of residual carbonate species in MgGa-3C mixed oxide and found that the amount of CO₂ desorbed during a thermal treatment of MgGa-3C from 450 to 900°C is 155 μmol·g⁻¹ (not shown). Consequently, the amount of residual carbonates is too low to explain the CO₂ desorbed from the rehydrated materials between 230 and 450°C. Based on this experiment, the internal origin of carbonates in reconstructed materials can be excluded.

Accordingly, we may conclude that interlayer hydroxyl groups (i.e., charge-compensating anions) in the reconstructed materials readily interact with CO₂ from air forming interlayer carbonates similar to those present in as-prepared materials. It is evident that the interaction of hydroxyl groups with CO₂ from air is fast as TPD-CO₂ experiment with reconstructed MgGa-3R10 material without CO₂ adsorption followed the rehydration process (the contact of the sample with air could not be excluded). It seems more probable that the intensive peak at around 400°C in the CO₂-TPD profile of reconstructed MgGa LDHs originates from the decomposition of the newly-formed interlayer carbonates rather than from the decomposition of different species (bidentate or monodentate) on the surface of reconstructed MgGa LDHs, as proposed in Abelló et al. (2005).

If so, the amount of desorbed CO₂ molecules desorbed between 230 and 450°C in CO₂-TPD experiments may be considered as a quantitative characteristic of interlayer hydroxyls, which exist in freshly reconstructed LDHs after rehydration treatment. Such assumption can be valid provided that (i) MgGa mixed oxide used for rehydration treatment is substantially free from residual carbonates; and (ii) each CO₂ molecule during CO₂-TPD experiments with reconstructed LDHs interacts with

two interlayer hydroxyls forming carbonate and water. Based on these assumptions, the concentration of interlayer hydroxyls should be two times larger than the concentration of desorbed CO₂, i.e., 1,540–1,772 μmol·g⁻¹ (Table 3).

The maximum possible concentration of interlayer hydroxyls in reconstructed MgGa LDHs can be calculated from the theoretical composition of the corresponding samples, provided that all Ga are in the crystallographic sites of HTC structure (it is lower as evidenced by XRD data for the reconstructed materials). Table 3 shows that the concentration of interlayer hydroxyls estimated from the amount of desorbed CO₂ in the range of 230–450°C is lower than the theoretically expected values. Moreover, the increasing Ga content in MgGa LDH should increase the concentration of interlayer hydroxyls. Nevertheless, the obtained results suggest a reverse trend: the evaluated concentration of hydroxyls decreases with the growth of Ga content. It should be however noted that the amount of interlayer hydroxyls in reconstructed materials may be underestimated because not all such hydroxyls in interlayer can be probed by CO₂, but those located at the edges of the platelets, as proposed by Abelló et al. (2005). Additionally, it should be considered that TPD experiments with the rehydrated materials were terminated at T = 450°C, and this can also contribute to the underestimation of evolved CO₂, i.e., of interlayer hydroxyls. In any case, the performed CO₂-TPD experiments give, albeit indirectly, a possibility to evaluate the amount of Brønsted basic sites in reconstructed MgGa materials.

Catalysis

Before discussing the catalytic results obtained for MgGa catalysts, several related aspects need to be considered. Firstly, on the interaction of reaction mixture with a basic catalyst, both aldol condensation of furfural and acetone self-condensation take place simultaneously. However, in the performed experiments it was found that acetone conversion by self-condensation route did not exceed 2% and therefore it was excluded from further consideration. Secondly, partial dissolution of a catalyst in a reaction mixture may occur under liquid phase conditions which could enable homogeneous reactions. To test this possibility, MgGa-3C was separated from the reaction mixture after 20 min (in a dedicated experiment) and the remaining reaction mixture was stirred for 2 h. The composition of the reaction mixture after 20 min and after the additional 2 h of the experiment was virtually unchanged and catalyst leaching could therefore be excluded. Thirdly, furfural conversion in the presence of the as-prepared MgGa materials was below 0.5% proving that aldol condensation of furfural and acetone required basic sites formed by calcination (MgGa mixed oxides) or calcination followed by rehydration (reconstructed MgGa LDHs) of the as-prepared MgGa LDHs.

Figure 11A depicts furfural conversion as a function of reaction time in presence of MgGa mixed oxides with different Mg/Ga ratio at T = 50°C.

Among all studied catalysts, MgGa-2C demonstrated the largest furfural conversion of 6.7% after 120 min of the reaction at T = 50°C (Figure 11A). The increase of Mg/Ga ratio in the MgGa mixed oxides resulted in a consistent decline of furfural conversion. The observed trend in the furfural

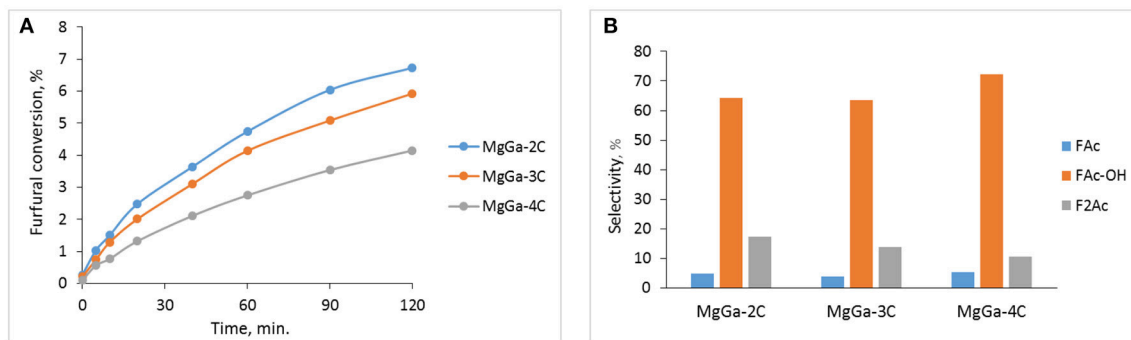


FIGURE 11 | Catalytic properties of MgGa mixed oxides. **(A)** Furfural conversion, **(B)** Selectivity to reaction products at furfural conversion $\approx 4\%$. $T = 50^\circ\text{C}$, molar ratio $\text{Ac}/\text{F} = 5$.

conversion (**Figure 11A**) does not show a direct correlation with the concentration of neither acid nor basic sites present in these catalysts (**Table 3**), and it contrasts with what was usually observed for HTC-derived MgAl mixed oxides (Di Cosimo et al., 1998; Kustrowski et al., 2006; Kikhtyanin et al., 2017a). Therefore, other characteristics of the catalysts should be also considered. For instance, not only the number of active sites, but also their accessibility plays a key role in the observed catalyst activity. **Figure 8A2** evidences that the size of the individual platelets of MgGa-2C is lower than that of MgGa-3C. The smaller platelets of MgGa-2C could facilitate the access of reactant molecules to active sites and the removal of reaction products, thus contributing to the increase in furfural conversion. Similarly, Abelló et al. (2005) also discussed the accessibility of active sites in the reconstructed MgAl materials differing in both the size of the platelets and porosity.

Figure 11B shows the product selectivity at furfural conversion $\approx 4\%$ observed for MgGa mixed oxides with different Mg/Ga ratio. For all catalysts, the selectivity toward FAc is similar (3.9–5.2%), but the selectivity to F_2Ac obviously increased with the increasing gallium content in the catalysts. In view of the smaller platelets in MgGa-2C, the favorable formation of the second (larger) condensation product seems to be reasonable.

Figure 12A demonstrates the dependence of furfural conversion on the duration of catalytic experiment at $T = 25^\circ\text{C}$ observed for reconstructed MgGa-3R materials varied by the rehydration time. The furfural conversion is significantly higher compared to the corresponding MgGa mixed oxides (**Figure 11A**). The observed change in the furfural conversion is in agreement with results obtained earlier for MgAl-derived materials (Kikhtyanin et al., 2017b) thus suggesting that, independently on the chemical composition of LDHs, Brønsted rather Lewis basic sites are favorable for aldol condensation of furfural and acetone. **Figure 12A** also evidences that the increase in rehydration time resulted in an increased furfural conversion. Such behavior was earlier reported for reconstructed MgAl hydrotalcites (Kikhtyanin et al., 2017b). Taken together, the catalytic performance of both MgAl and MgGa reconstructed LDHs is enabled by rehydration of the corresponding mixed

oxides. Regardless of rehydration duration, all reconstructed MgGa LDHs exhibit same product distribution in dependence on furfural conversion (**Figure 12B**) with selectivity to FAc, FAc-OH, and F_2Ac being in the range of 8.7–9.8, 76.7–79.2, and 7.8–9.2%, respectively at furfural conversion $\approx 30\%$. The similarity in the composition of reaction products regardless the rehydration time allows suggesting that the acid-base characteristics of the catalysts are identical. Consequently, the incomplete reconstruction of HTC framework has no impact on the selectivity but affects the catalytic behavior of the catalysts.

Figure 12C depicts the dependence of furfural conversion on Mg/Ga ratio of reconstructed MgGa materials. The reconstructed MgGa materials with Mg/Ga ratio in the range of 2–4 exhibit the high furfural conversion of 56.6–59.7% after 120 min of the reaction at 25°C . Nevertheless, despite the observed similarity at the end of experiment, the furfural conversion over MgGa-2R10 is lower than that over the other two catalysts, particularly at the beginning of the experiment indicating a lower activity of MgGa-2R10. The observed tendency does not correlate totally with the CO_2 -TPD results for the reconstructed MgGa materials (**Figure 10** and **Table 3**). Indeed, provided that the amount of CO_2 removed from the samples in CO_2 -TPD experiments in the range of 230 – 450°C characterizes the amount of interlayer hydroxyls which are Brønsted basic sites, i.e., the active sites of the reaction, the furfural conversion for the reconstructed MgGa LDHs in the reaction should increase in the following order: $\text{MgGa-3R10} \approx \text{MgGa-2R10} < \text{MgGa-4R10}$. Actually, furfural conversion observed on MgGa-2R10 and MgGa-3R10 differs. As with MgGa mixed oxides, also in the case of reconstructed MgGa LDHs the accessibility of active sites could play a crucial role. In this case a difference in the size of CO_2 and organic molecules which is responsible for their diffusion to Brønsted basic sites should be taken into account.

A change in Mg/Ga ratio had practically no effect on the composition of reaction products obtained on the reconstructed MgGa LDHs. At furfural conversion of about 30% MgGa-2R10 all reconstructed materials have FAc-OH selectivity of 71–73.5%, FAc selectivity of 8.1–9.3% and F_2Ac selectivity of 12.1–12.9% (**Figure 12D**). The obtained results show that, independently on chemical composition, the basic sites in the reconstructed

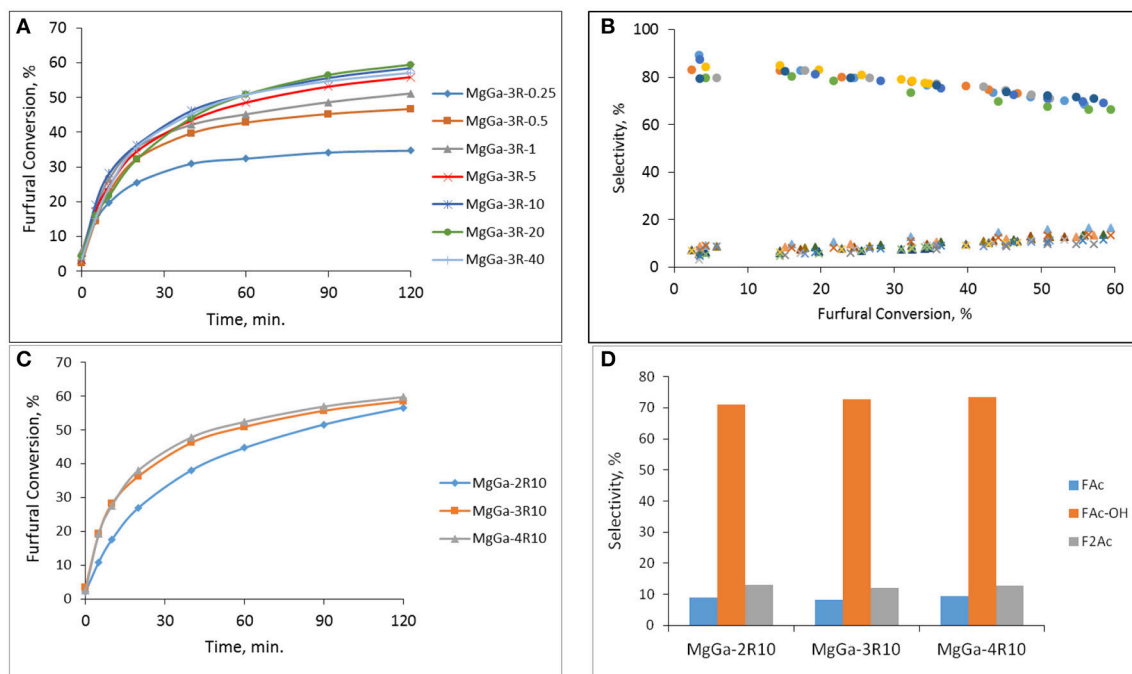


FIGURE 12 | (A) The change in furfural conversion in the course of experiment observed on MgGa-3R samples prepared by different rehydration time. (B) The dependence of product selectivity on furfural conversion observed on MgGa-3R-X catalysts (● – FAC-OH, Δ – FAC, x – F₂Ac). (C) Influence of Mg/Ga in reconstructed MgGaXR-10 samples on furfural conversion. (D) Influence of Mg/Ga in reconstructed MgGaXR-10 samples on product selectivity at furfural conversion ≈30%. T = 25°C, molar ratio Ac/F = 5.

MgGa LDHs act similarly in aldol condensation of acetone with furfural (Scheme 1). Thus, the prepared reconstructed MgGa LDHs exhibit similar trends in catalytic performance in aldol condensation reaction that have been previously observed for MgAl hydrotalcite-derived materials, i.e., the enhanced activity compared to corresponding mixed oxides and the dependence of reaction product composition on the acid-base and textural characteristics of the catalysts. Nevertheless, a direct comparison of the physico-chemical properties and the catalytic performance of MgAl and MgGa mixed oxides and reconstructed LDHs could be considered as the subject of a separate study.

CONCLUSION

The results obtained in this paper demonstrate that the synthesis and the characterization approaches developed earlier for Mg-Al LDH-derived materials can be successfully applied in the case of MgGa samples. The heat treatment of as-prepared MgGa LDHs leads to the destruction of HTC structure and the formation of MgGa mixed oxides. These oxidic materials have both acidic and basic sites and they demonstrate an intersiting values of furfural conversion in the aldol condensation of furfural and acetone. The contact of freshly calcined MgGa mixed oxides with pure water results in the fast recovery of HTC structure of MgGa materials, as it is evidenced by XRD, TGA, and DRIFT. The XRD study of the reconstructed MgGa LDHs suggests that after the rehydration process only part of Ga atoms

occupy the crystallographic sites of the HTC crystal framework. Nevertheless, the reconstructed MgGa LDHs have significantly higher values of furfural conversion in the aldol condensation of furfural and acetone compared to the corresponding MgGa mixed oxides. Being catalyzed by Brønsted basic sites more effectively, the reaction proves presence of interlayer hydroxyls in the reconstructed MgGa LDHs. Nevertheless, the basic properties of the reconstructed materials cannot be properly characterized by such routine method as CO₂-TPD because during the experiment CO₂ as a probe molecule reacts with the interlayer hydroxyls forming interlayer carbonates rather than adsorbed CO₂ species on basic sites. By the combination of physico-chemical properties and catalytic performance, MgGa mixed oxides and reconstructed MgGa LDHs are analogous to the corresponding Mg-Al counterparts. However, a difference in the nature of the M³⁺ element, Al vs. Ga, which are present in HTC structure should have a significant effect in other applications of these materials, which can be identified in forthcoming studies.

AUTHOR CONTRIBUTIONS

OK performed and evaluated catalytic experiments and participated in preparing the manuscript. LC evaluated TPD data and participated in preparing the manuscript. ZT prepared MgGa samples and collected the data of physico-chemical characterization. RV carried out and evaluated TGA (TGA-MS)

experiments. AP carried out and evaluated TPD experiments. PD carried out and evaluated SEM. DK focused on interpretation of data and participated in preparing manuscript.

ACKNOWLEDGMENTS

The publication is a result of the project reg. No. GA15-21817S which was financially supported by the Czech Science

Foundation of the Czech Republic. AP, from Maria Curie-Skłodowska University (Lublin, Poland), thanks the ERASMUS + program for funding her internship at the University of Pardubice. The work was inspired by the discussions within the COST Action FP1306 Valorization of lignocellulosic biomass streams for sustainable production of chemicals, materials and fuels using low environmental impact technologies.

REFERENCES

- Abelló, S., Medina, F., Tichit, D., Pérez-Ramírez, J., Groen, J. C., Sueiras, J. E., et al. (2005). Aldol condensations over reconstructed Mg–Al hydrotalcites: structure-activity relationships related to the rehydration method. *Chem. Eur. J.* 11, 728–739. doi: 10.1002/chem.200400409
- Allegre, G., and Ronca, G. (1978). Crystal powder statistics. II. Line profiles in diffraction spectra of identical crystals and of Gaussian samples. Crystal size distributions. *Acta Crystallogr. Sect. A* 34, 1006–1013. doi: 10.1107/S0567739478002053
- Aramendia, M. A., Borau, V., Jiménez, C., Marinas, J. M., Ruiz, J. R., and Urbano, F. J. (2003). Catalytic hydrogen transfer from 2-propanol to cyclohexanone over basic Mg–Al oxides. *Appl. Catal. A Gen.* 255, 301–308. doi: 10.1016/S0926-860X(03)00569-6
- Aramendia, M. A., Avilés, Y., Benítez, J. A., Borau, V., Jiménez, C., Marinas, J. M., et al. (1999a). Comparative study of Mg/Al and Mg/Ga layered double hydroxides. *Micropor. Mesopor. Mater.* 29, 319–328. doi: 10.1016/S1387-1811(98)00345-X
- Aramendia, M. A., Avilés, Y., Borau, V., Luque, J. M., Marinas, J. M., Ruiz, J. R., et al. (1999b). Thermal decomposition of Mg/Al and Mg/Ga layered-double hydroxides: a spectroscopic study. *J. Mater. Chem.* 9, 1603–1607. doi: 10.1039/a900535h
- Aramendia, M. A., Borau, V., Jiménez, C., Marinas, J. M., Ruiz, J. R., and Urbano, F. J. (2000). XRD and ^1H MAS NMR spectroscopic study of mixed oxides obtained by calcination of layered-double hydroxides. *Mater. Lett.* 46, 309–314. doi: 10.1016/S0167-577X(00)00193-2
- Cavani, F., Maselli, L., Scagliarini, D., Flego, C., and Perego, C. (2005). How basic properties of MgO-based mixed oxides affect the catalytic performance in gas-phase and liquid-phase methylation of m-cresol. *Stud. Surf. Sci. Catal.* 155, 167–177. doi: 10.1016/S0167-2991(05)80146-6
- Cavani, F., Trifirò, F., and Vaccari, A. (1991). Hydrotalcite-type anionic clays: preparation, properties and applications. *Catal. Today* 11, 173–301. doi: 10.1016/0920-5861(91)80068-K
- Chao, K.-J., and Liu, P.-H. (2005). Gallium-containing zeolites: characterization of catalytic role of gallium species in converting light paraffins to aromatics. *Catal. Surveys Asia* 9, 11–15. doi: 10.1007/s10563-005-3332-1
- Choudary, B. M., Kantam, M. L., Rahman, A., Reddy, C. V., and Rao, K. K. (2001). The first example of activation of molecular oxygen by nickel in Ni–Al hydrotalcite: a novel protocol for the selective oxidation of alcohols. *Angew. Chem.* 113, 785–788. doi: 10.1002/1521-3773(20010216)40:4<763::AID-ANIE7630>3.0.CO;2-T
- Choudary, B. M., Kantam, M. L., Reddy, C. R. V., Rao, K. K., and Figueras, F. (1999). The first example of Michael addition catalysed by modified Mg–Al hydrotalcite. *J. Mol. Catal. A Chem.* 146, 279–284. doi: 10.1016/S1381-1169(99)00099-0
- Climent, M. J., Corma, A., Fornés, V., Guil-Lopez, R., and Iborra, S. (2002a). Aldol condensations on solid catalysts: a cooperative effect between weak acid and base sites. *Adv. Synth. Catal.* 344, 1090–1096. doi: 10.1002/1615-4169(200212)344:10<1090::AID-ADSC1090>3.0.CO;2-X
- Climent, M. J., Corma, A., Iborra, S., and Primo, J. (1995). Base catalysis for fine chemicals production: Claisen-Schmidt condensation on zeolites and hydrotalcites for the production of chalcones and flavanones of pharmaceutical interest. *J. Catal.* 151, 60–66. doi: 10.1006/jcat.1995.1008
- Climent, M. J., Corma, A., Iborra, S., and Velly, A. (2002b). Synthesis of methylpseudoionones by activated hydrotalcites as solid base catalysts. *Green Chem.* 4, 474–480. doi: 10.1039/b205532p
- Debecker, D. P., Gaigneaux, E. M., and Busca, G. (2009). Exploring, tuning, and exploiting the basicity of hydrotalcites for applications in heterogeneous catalysis. *Chem. Eur. J.* 15, 3920–3935. doi: 10.1002/chem.200900060
- Di Cosimo, J. I., Apestegua, C. R., Gines, M. J. L., and Iglesia, E. (2000). Structural requirements and reaction pathways in condensation reactions of alcohols on Mg_xAlO_x catalysts. *J. Catal.* 190, 261–275. doi: 10.1006/jcat.1999.2734
- Di Cosimo, J. I., Díez, V. K., Xu, M., Iglesia, E., and Apestegua, C. R. (1998). Structure and surface and catalytic properties of Mg–Al basic oxides. *J. Catal.* 178, 499–510. doi: 10.1006/jcat.1998.2161
- Faba, L., Díaz, E., and Ordóñez, S. (2012). Aqueous-phase furfural-acetone aldol condensation over basic mixed oxides. *Appl. Catal. B Environ.* 113–114, 201–211. doi: 10.1016/j.apcatb.2011.11.039
- Fricke, R., Kosslick, H., Lischke, G., and Richter, M. (2000). Incorporation of gallium into zeolites: syntheses, properties and catalytic application. *Chem. Rev.* 100, 2303–2406. doi: 10.1021/cr9411637
- Gámez, S., González-Cabral, J. J., Ramírez, J. A., Garrote, G., and Vázquez, M. (2006). Study of the hydrolysis of sugar cane bagasse using phosphoric acid. *J. Food Eng.* 74, 78–88. doi: 10.1016/j.jfoodeng.2005.02.005
- Grand, L.-M., Palmer, S. J., and Frost, R. L. (2010). Synthesis and thermal stability of hydrotalcites based upon gallium. *J. Therm. Anal. Calorim.* 101, 195–198. doi: 10.1007/s10973-009-0456-y
- Guida, A., Lhouty, M. H., Tichit, D., Figueras, F., and Geneste, P. (1997). Hydrotalcites as base catalysts. Kinetics of Claisen-Schmidt condensation, intramolecular condensation of acetylacetone and synthesis of chalcone. *Appl. Catal. A Gen.* 164, 251–264. doi: 10.1016/S0926-860X(97)00175-0
- Hora, L., Kikhtyanin, O., Čapek, L., Bortnovskiy, O., and Kubička, D. (2015). Comparative study of physico-chemical properties of laboratory and industrially prepared layered double hydroxides and their behavior in aldol condensation of furfural and acetone. *Catal. Today* 241, 221–230. doi: 10.1016/j.cattod.2014.03.010
- Kikhtyanin, O., Chlubná, P., Jindrová, T., and Kubička, D. (2014). Peculiar behavior of MWW materials in aldol condensation of furfural and acetone. *Dalton Trans.* 43, 10628–10641. doi: 10.1039/c4dt00184b
- Kikhtyanin, O., Kubička, D., and Cejka, J. (2015). Toward understanding of the role of Lewis acidity in aldol condensation of acetone and furfural using MOF and zeolite catalysts. *Catal. Today* 243, 158–162. doi: 10.1016/j.cattod.2014.08.016
- Kikhtyanin, O., Čapek, L., Smoláková, L., Tišler, Z., Kadlec, D., Lhotka, M., et al. (2017a). Influence of Mg–Al mixed oxide compositions on their properties and performance in aldol condensation. *Ind. Eng. Chem. Res.* 56, 13411–13422. doi: 10.1021/acs.iecr.7b03367
- Kikhtyanin, O., Tišler, Z., Velvarská, R., and Kubička, D. (2017b). Reconstructed Mg–Al hydrotalcites prepared by using different rehydration and drying time: physico-chemical properties and catalytic performance in aldol condensation. *Appl. Catal. A Gen.* 536, 85–96. doi: 10.1016/j.apcata.2017.02.020
- Kustrowski, P., Sulkowska, D., Chmielarz, L., and Dziembaj, R. (2006). Aldol condensation of citral and acetone over mesoporous catalysts obtained by thermal and chemical activation of magnesium-aluminum hydrotalcite-like precursors. *Appl. Catal. A Gen.* 302, 317–324. doi: 10.1016/j.apcata.2006.02.003
- López-Salinas, E., García-Sánchez, M., Ramon-García, M., L., and Schiffer, I. (1996). New gallium-substituted hydrotalcites:

- [Mg_{1-x}Ga_x(OH)₂](CO₃)_{x/2}·mH₂O. *J. Porous Mater.* 3, 169–174. doi: 10.1007/BF01134028
- López-Salinas, E., García-Sánchez, M., Llanos-Serrano, Ma, E., and Navarrete-Bolaños J (1997). Formation of base sites on calcined Mg-Ga hydrotalcite-like [Mg_{1-x}Ga_x(OH)₂](CO₃)_{x/2}·mH₂O. *J. Phys. Chem. B* 101, 5112–5117. doi: 10.1021/jp9702558
- Mäki-Arvela, P., Salmi, T., Holmbom, B., Willfor, S., and Murzin, D. Y. (2011). Synthesis of sugars by hydrolysis of hemicelluloses - a review. *Chem. Rev.* 111, 5638–5666. doi: 10.1021/cr2000042
- Miyata, S. (1980). Physico-chemical properties of synthetic hydrotalcites in relation to composition. *Clay Clay Miner.* 28, 50–56. doi: 10.1346/CCMN.1980.0280107
- Motokura, K., Fujita, N., Mori, K., Mizugaki, T., Ebitani, K., Htsukawa, K., et al. (2006). Environmentally friendly one-pot synthesis of α -alkylated nitriles using hydrotalcite-supported metal species as multifunctional solid catalysts. *Chem. Eur. J.* 12, 8228–8239. doi: 10.1002/chem.200600317
- Perez, C. N., Monteiro, J. L. F., Nieto, J. M. L., and Henriques, C. A. (2009). Influence of basic properties of Mg,Al-mixed oxides on their catalytic activity in Knoevenagel condensation between benzaldehyde and phenylsulfonylacetonitrile. *Quim. Nova* 32, 2341–2346. doi: 10.1590/S0100-40422009000900020
- Pérez-Ramírez, J., Abelló, S., and van der Pers, N. M. (2007a). Influence of the divalent cation on the thermal activation and reconstruction of hydrotalcite-like compounds. *J. Phys. Chem. C* 111, 3642–3650. doi: 10.1021/jp064972q
- Pérez-Ramírez, J., Abelló, S., and van der Pers, N. M. (2007b). Memory effect of activated Mg-Al hydrotalcite: *in situ* XRD studies during decomposition and gas-phase reconstruction. *Chem. Eur. J.* 13, 870–878. doi: 10.1002/chem.200600767
- Prescott, H. A., Li, Z. J., Kemnitz, E., Trunschke, A., Deutsch, J., Lieske, H., et al. (2005). Application of calcined Mg-Al hydrotalcites for Michael additions: an investigation of catalytic activity and acid-base properties. *J. Catal.* 234, 119–130. doi: 10.1016/j.jcat.2005.06.004
- Prinotto, F., Tichit, D., Teissier, R., and Coq, B. (2000). Mg- and Ni-containing layered double hydroxides as soda substitutes in the aldol condensation of acetone. *Catal. Today* 55, 103–116. doi: 10.1016/S0920-5861(99)00230-8
- Ramos, R., Tišler, Z., Kikhtyanin, O., and Kubička, D. (2016). Towards understanding the hydrodeoxygenation pathways of furfural-acetone aldol condensation products over supported Pt catalysts. *Catal. Sci. Technol.* 6, 1829–1841. doi: 10.1039/C5CY01422K
- Rebours, B., d'Espinose de la Caillerie, J.-B., and Clause, O. (1994). Decoration of nickel and magnesium oxide crystallites with spinel-type phases. *J. Am. Chem. Soc.* 116, 1707–1717. doi: 10.1021/ja00084a011
- Rousselot, I., Taviot-Gueho, C., and Besse, J. P. (1999). Synthesis and characterization of mixed Ga/Al-containing layered double hydroxides: study of their basic properties through the Knoevenagel condensation of benzaldehyde and ethyl cyanoacetate, and comparison to other LDHs. *Int. J. Inorg. Mater.* 1, 165–174. doi: 10.1016/S1466-6049(99)00025-2
- Roy, D., Roy, R., and Osborn, E. (1953). The system MgO-Al₂O₃-H₂O and influence of carbonate and nitrate ions on the phase equilibria. *Am. J. Sci.* 251, 337–361. doi: 10.2475/ajs.251.5.337
- Sádaba, I., Ojeda, M., Mariscal, R., Richards, R., and López Granados, M. (2011). Mg-Zr mixed oxides for aqueous aldol condensation of furfural with acetone: effect of preparation method and activation temperature. *Catal. Today* 167, 77–83. doi: 10.1016/j.cattod.2010.11.059
- Sels, B. F., De Vos, D. E., and Jacobs, P. A. (2001). Hydrotalcite-like anionic clays in catalytic organic reactions. *Catal. Rev. Sci. Eng.* 43, 443–488. doi: 10.1081/CR-120001809
- Smoláková, L., Frolich, K., Kocik, J., Kikhtyanin, O., and Čapek, L. (2017). Influence of acido-basic properties of Zn(Mg)Al mixed oxides on its catalytic activity in aldol condensation of furfural with acetone. *Ind. Eng. Chem. Res.* 56, 4638–4648. doi: 10.1021/acs.iecr.6b04927
- Tabanellia, T., Cocchi, S., Gumina, B., Izzo, L., Mella, M., Passeri, S., et al. (2018). Mg/Ga mixed-oxide catalysts for phenol methylation: outstanding performance in 2,4,6-trimethylphenol synthesis with co-feeding of water. *Appl. Catal. A Gen.* 552, 86–97. doi: 10.1016/j.apcata.2018.01.001
- Takehira, K. (2017). Recent development of layered double hydroxide-derived catalysts – Rehydration, reconstitution, and supporting, aiming at commercial application. *Appl. Clay Sci.* 136, 112–141. doi: 10.1016/j.clay.2016.11.012
- Thanh, D. N., Kikhtyanin, O., Ramos, R., Kothari, M., Ulbrich, P., Munshi, T., et al. (2016). Nanosized TiO₂ - A promising catalyst for the aldol condensation of furfural with acetone in biomass upgrading. *Catal. Today* 277, 97–107. doi: 10.1016/j.cattod.2015.11.027
- Thomas, G. S., and Vishnu Kamath, P. (2005). Reversible thermal behavior of the layered double hydroxides (LDHs) of Mg with Ga and In. *Mater. Res. Bull.* 40, 671–681. doi: 10.1016/j.materresbull.2004.12.011
- Tichit, D., Bennani, M. N., Figueras, F., Tessier, R., and Kervennal, J. (1998). Aldol condensation of acetone over layered double hydroxides of the meixnerite type. *Appl. Clay Sci.* 13, 401–415. doi: 10.1016/S0169-1317(98)00035-0
- Tichit, D., and Coq, B. (2003). Catalysis by hydrotalcites and related materials. *Cat. Tech.* 7, 206–217. doi: 10.1023/B:CATT.0000007166.65577.34
- Tichit, D., Coq, B., Cerneaux, S., and Durand, R. (2002). Condensation of aldehydes for environmentally friendly synthesis of 2-methyl-3-phenyl-propanal by heterogeneous catalysis. *Catal. Today* 75, 197–202. doi: 10.1016/S0920-5861(02)00069-X
- Wu, W., Wu, W., Kikhtyanin, O. V., Li, L., Toktarev, A. V., Ayupov, A. B., et al. (2010). Methylation of naphthalene on MTW-type zeolites. Influence of template origin and substitution of Al by Ga. *Appl. Catal. A Gen.* 375, 279–288. doi: 10.1016/j.apcata.2010.01.003
- Yun, S. K., and Pinnavaia, T. J. (1995). Water-content and particle texture of synthetic hydrotalcite-like layered double hydroxides. *Chem. Mater.* 7, 348–354. doi: 10.1021/cm00050a017
- Zapata, A., Faria, J., Pilar Ruiz, M., and Resasco, D. E. (2012). Condensation/hydrogenation of biomass-derived oxygenates in water/oil emulsions stabilized by nanohybrid catalysts. *Top. Catal.* 55, 38–52. doi: 10.1007/s11244-012-9768-4
- Zeng, H. Y., Feng, Z., Deng, X., and Li, Y. Q. (2008). Activation of Mg-Al hydrotalcite catalysts for transesterification of rape oil. *Fuel* 87, 3071–3076. doi: 10.1016/j.fuel.2008.04.001

Conflict of Interest Statement: The authors declare that the research was conducted in the absence of any commercial or financial relationships that could be construed as a potential conflict of interest.

The reviewer, IL, and handling Editor declared their shared affiliation.

Copyright © 2018 Kikhtyanin, Čapek, Tišler, Velvarská, Panasewicz, Diblíková and Kubička. This is an open-access article distributed under the terms of the Creative Commons Attribution License (CC BY). The use, distribution or reproduction in other forums is permitted, provided the original author(s) and the copyright owner are credited and that the original publication in this journal is cited, in accordance with accepted academic practice. No use, distribution or reproduction is permitted which does not comply with these terms.



Temperature Dependence of Single Step Hydrodeoxygenation of Liquid Phase Pyrolysis Oil

Klara Treusch^{1,2*}, Nikolaus Schwaiger^{1,2}, Klaus Schlackl², Roland Nagl², Peter Pucher¹ and Matthäus Siebenhofer²

¹ BDI – BioEnergy International GmbH, Research and Development, Raaba-Grambach, Austria, ² Institute of Chemical Engineering and Environmental Technology, Graz University of Technology, Graz, Austria

OPEN ACCESS

Edited by:

Christophe Len,
University of Technology of
Compiègne, France

Reviewed by:

Benjaram M. Reddy,
Indian Institute of Chemical
Technology (CSIR), India
Pavel Nikulshin,
Samara State University, Russia
Rafael Luque,
Universidad de Córdoba, Spain

*Correspondence:

Klara Treusch
klara.treusch@bdi-bioenergy.com

Specialty section:

This article was submitted to
Green and Sustainable Chemistry,
a section of the journal
Frontiers in Chemistry

Received: 15 December 2017

Accepted: 26 June 2018

Published: 19 July 2018

Citation:

Treusch K, Schwaiger N, Schlackl K,
Nagl R, Pucher P and Siebenhofer M
(2018) Temperature Dependence of
Single Step Hydrodeoxygenation of
Liquid Phase Pyrolysis Oil.
Front. Chem. 6:297.
doi: 10.3389/fchem.2018.00297

In this paper, continuous hydrodeoxygenation (HDO) of liquid phase pyrolysis (LPP) oil in lab-scale is discussed. Pyrolysis oil is derived from the bioCRACK pilot plant from BDI - BioEnergy International GmbH at the OMV refinery in Vienna/Schwechat. Three hydrodeoxygenation temperature set points at 350, 375, and 400°C were investigated. Liquid hourly space velocity (LHSV) was 0.5 h⁻¹. Hydrodeoxygenation was performed with an *in situ* sulfided metal oxide catalyst. During HDO, three product phases were collected. A gaseous phase, an aqueous phase and a hydrocarbon phase. Experiment duration was 36 h at 350 and 375°C and 27.5 h at 400°C in steady state operation mode. Water content of the hydrocarbon phase was reduced to below 0.05 wt.%. The water content of the aqueous phase was between 96.9 and 99.9 wt.%, indicating effective hydrodeoxygenation. The most promising results, concerning the rate of hydrodeoxygenation, were achieved at 400°C. After 36/27.5 h of experiment, catalyst deactivation was observed.

Keywords: hydrodeoxygenation, liquid phase pyrolysis, pyrolysis oil, temperature variation, 2nd generation biofuels

INTRODUCTION

Biomass pyrolysis is a suitable pathway for the production of second generation biofuels (Demirbas, 2011). During pyrolysis, one of the major products is pyrolysis oil. Due to its high water content, high corrosivity and other negative properties, according to **Table 1**, pyrolysis oil needs intensive upgrading prior to usage as fuel for combustion engines. To achieve fuel quality standards, an upgrading step is necessary. Hydrodeoxygenation (HDO) is a high potential upgrading technology (Pucher et al., 2015). In literature, mainly experiments with fast pyrolysis oil are reported.

One of the biggest issues during HDO of pyrolysis oil in general is catalyst deactivation caused by coke formation. Especially the single-step HDO above 300°C is seen as troublesome, as it leads to coking and plugging (Elliott and Bager, 1989). Therefore, a two-step process is proposed in literature (Elliott, 2007; Elliott et al., 2009; Carpenter et al., 2016; Meyer et al., 2016; Olarte et al., 2016, 2017). In a first step, pyrolysis oil is stabilized (Pucher et al., 2014) through mild hydrotreatment at low temperature. In a second step, the final hydrodeoxygenation, or hydrocracking, takes place. Hydrotreatment temperatures are between 140 and 375°C, at liquid hourly space velocities between 0.28 and 0.5 h⁻¹. The hydrocracking step is performed at temperatures of about 400°C and liquid hourly space velocities of 0.1–0.4 h⁻¹ (Elliott et al., 2009; Olarte et al., 2016).

Contrary to these results, in this paper LPP oil is processed continuously in a single-step HDO reactor at 350–400°C. The LHSV was set on the limits of HDO of fast pyrolysis oil with 0.5 h⁻¹ (Volume LPP oil/ Volume of empty tube and hour).

LIQUID PHASE PYROLYSIS

In liquid phase pyrolysis, biomass is pyrolyzed in a liquid heat carrier (Schwaiger et al., 2011, 2012). During this conversion, a part of the biomass dissolves in the heat carrier, while a second liquid phase, a polar water containing hydrocarbon phase, is generated (Schwaiger et al., 2015). In the bioCRACK process (Ritzberger et al., 2014; Treusch et al., 2017), LPP was operated with the heat carrier vacuum gas oil to enable integration in an oil refinery. From 2012 to 2014 a pilot plant was operated by BDI – BioEnergy International GmbH at the OMV refinery in Vienna/Schwechat.

MATERIALS AND METHODS

Experiments were carried out in a plug flow reactor with an inner diameter of 3/8 inches and a heated zone of about 30 cm, made by Parr Instrument Company. It was designed for a maximum pressure of 220 bar and a maximum temperature of 550°C. The temperature was detected by an inner thermowell with a thermocouple with three probe points. Heat was provided by a single zone external electric heater. In the temperature range between 350 and 400°C, three operation points were tested: 350, 375, and 400°C. Hydrogen pressure was kept constant at 121.5 bar for all experiments.

Materials

The LPP oil was derived from the bioCRACK pilot plant. It was produced by LPP of spruce wood. The composition of LPP oil is shown in **Table 1**.

HDO was performed with a sulfided CoMo/Al₂O₃ catalyst, details are shown in **Table 2**. It was obtained as extrudates with a length of 2–3 mm. The catalyst was chosen as it is cheaper than noble metal catalysts and not susceptible for catalyst poisoning through sulfur, in contrary it gets more active by adding sulfur. For sulfidation, 35 wt.% di-tert-butyl disulfide (DTBDS) in decane was used. To provide enough sulfur during HDO, 150 ppm of sulfur as DTBDS were added to the LPP oil. Hydrogen 5.0 was provided in a 300 bar gas cylinder from AIR LIQUIDE AUSTRIA GmbH.

Analytical Methods

The ultimate analysis of all streams was done by a vario MACRO CHN-analyser from Elementar Analysensysteme GmbH. The oxygen was determined by difference. The water content of the aqueous product phase was determined by a gas-phase chromatograph, type Agilent 7890A, with a TCD-detector and a HP-INNOWAX column, 30 m*0.530 mm*1 µm. For determination of the water content, the GC was calibrated with high-purity water (type I) in THF in the range of 1–8 wt.% water. The boiling range of the hydrocarbon product phase was determined by a gas-phase chromatograph, type

TABLE 1 | Properties and composition of LPP oil.

Property	Unit	LPP oil
Water content	[wt.%]	57.0
Lower heating value	[MJ/kg]	7.4
Density	[kg/m ³]	1092
Viscosity	[mPa·s]	3.5
Carbon content	[wt.%]	22.3
Hydrogen content	[wt.%]	9.4
Oxygen content (balance)	[wt.%]	67.8
Nitrogen content	[wt.%]	<1

TABLE 2 | Catalyst details (CoMo/Al₂O₃).

Supplier	Alfa Aesar
Cobalt oxide [wt.%]	4.4
Molybdenum oxide [wt.%]	11.9
Surface area [m ² /g]	279
Stock number	45579

Agilent 7890A, with a FID-detector and a Restek-column MXT-2887, 10 m *0.530 mm *2.65 µm, according to ASTM Method D2887. The water content of the oil fraction was determined by Karl-Fischer-titration with a Schott Titro Line KF-Titrator and a Hydranal titration reagent. Density and viscosity were measured by a digital viscosimeter, SVM 3000, of Anton Paar GmbH. The composition of the hydrocarbon product phase was determined by gas chromatography-MS with a quadrupole mass spectrometer (GC-MS), type Shimadzu GCMS QP 2010 Plus, with a VF-1701 MS column, 60 m *0.25 mm *0.25 µm. The GC-MS was calibrated with a multi-component standard, consisting of: pentane, 2-methyl-pentane, hexane, methyl-cyclohexane, ethyl-cyclopentane, octane, toluene, ethyl-cyclohexane, propyl-cyclohexane and decane in THF, in the range of 100–3,000 ppmw each. Additionally, flouranthene was used as internal standard. The gas phase composition was determined by a micro gas-phase chromatograph (micro-GC), type Agilent 3000A, with a TCD-detector, a molecular sieve column and a plot u column. The micro-GC was calibrated with oxygen, nitrogen, hydrogen, methane, ethane, acetylene and carbon dioxide.

Catalyst Preparation

To increase the specific surface area, the catalyst was milled in a centrifugal mill with trapezoidal perforations of 1 mm diameter. The ground material was sieved in a sieving tower of Retsch to obtain the target particle size of 200–600 µm. The reactor was then filled upside down with catalyst. On bottom and top a few cm of catalyst extrudates were applied. The heated zone of the reactor (30 cm) was filled with particles of 200–600 µm size. The catalyst was held in the reactor with a sieve at the bottom.

For each experiment, the reactor was filled with fresh CoMo/Al₂O₃ catalyst of Alfa Aesar and inertised with nitrogen. Afterwards the reactor was flushed with hydrogen. Then a hydrogen flow rate of 0.5 l/h was adjusted.

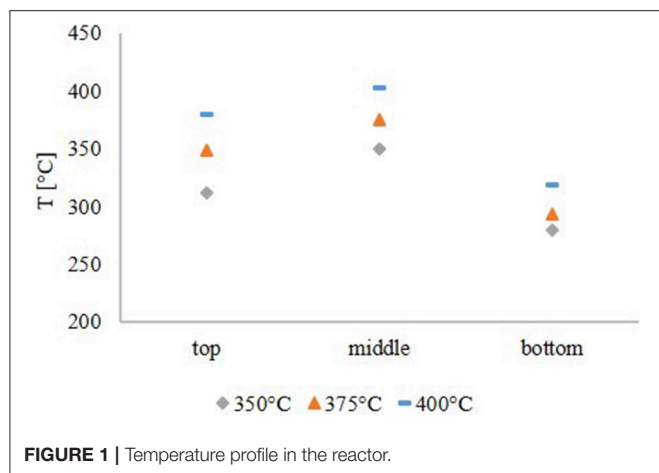


FIGURE 1 | Temperature profile in the reactor.

For the activation of the catalyst, a sulfidation step preceded the HDO experiments. Thus, 35 wt.% di-tert-butyl disulfide (DTBDS) in decane was pumped through the reactor during heating up. Sulfidation was continued for five hours at 400°C. After sulfidation, the temperature was reduced to the requested temperature of HDO procedure.

Experimental Procedure

After sulfidation, 5 h of HDO of LPP oil were performed in the unsteady state operation mode. Afterwards, 36 h of HDO were performed, with liquid product sampling every 12 h for experiments at 350 and 375°C. At 400°C, experiment duration was 27.5 h and sampling periods were 8, 7.5, and 12 h. The gas phase composition was monitored every 4 h. After 36/27.5 h of steady state operation, the reactor was shut down and the catalyst bed was washed with acetone for catalyst analysis. Plugging was not observed.

RESULTS

In this chapter, observations during experiments, mass balance and product characterization are given. Possible pathways of biomass constituents to components in the final product, derived from GC-MS analysis, are discussed.

Temperature Profile in the Reactor

The temperature profile, shown in **Figure 1**, was similar for all experiments. Due to the fact, that the pyrolysis oil was not pre-heated, the feed temperature was lower than the temperature in the middle of the reactor. The temperature maximum was obtained in the middle of the reactor. This temperature was the set point temperature for all HDO experiments. At the exit of the reactor, the temperature dropped significantly due to external cooling effects. From the temperature profile it was concluded, that the exothermal HDO reaction was completed after about 2/3 of the reactor.

TABLE 3 | Mass balance based on LPP oil and H₂ feed.

Temperature	350°C	375°C	400°C
LPP oil [wt.%]	79.13	79.32	80.47
H ₂ [wt.%]	20.87	20.68	19.53
Aqueous [wt.%]	59.96	58.94	58.62
Hydrocarbon [wt.%]	7.68	7.76	7.79
Gaseous [wt.%]	26.82	27.55	28.37
Coke [wt.%]	1.34	1.35	1.36

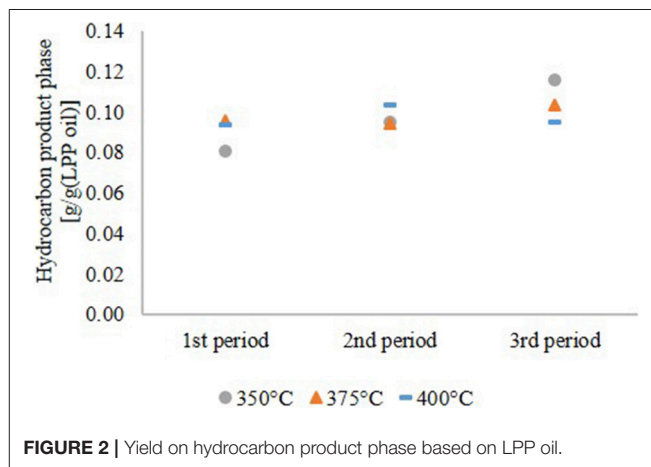


FIGURE 2 | Yield on hydrocarbon product phase based on LPP oil.

Mass Balance and Coke Formation

During HDO, three product phases were formed. A hydrocarbon phase, the target product, an aqueous phase and a gaseous phase. In general, the difference concerning the product distribution between hydrocarbon product and aqueous phase is not depending on temperature in the range of 350–400°C. The differences are more recognizable in the stream compositions. **Table 3** shows that the yield of aqueous phase decreased with temperature, whereas the gas yield increased.

The yield of the hydrocarbon product phase based on the LPP oil in the feed is shown in **Figure 2**. At 350 and 375°C it increased continuously until the end of experiment. The increasing production rate of organic phase at 350 and 375°C is not caused by a higher conversion of LPP oil to fuel, it is rather a consequence of incomplete HDO. This indicates faster catalyst deactivation at lower temperatures. However, at 400°C the hydrocarbon product yield was constant.

Rate of HDO

As shown in **Table 1**, LPP oil contains a high amount of water. Yield, based on the LPP oil feed, was therefore low too. Referring to the carbon content of LPP oil, a carbon transfer into the hydrocarbon product phase, given in **Figure 3**, of up to 45 wt.% was obtained. The rest merged into the gas phase. Scattered carbon transfer was observed at 350°C HDO temperature. After 12 h of operation, it was only about 30 wt.% and increased to 45 wt.% after 36 h. This observation goes along with the

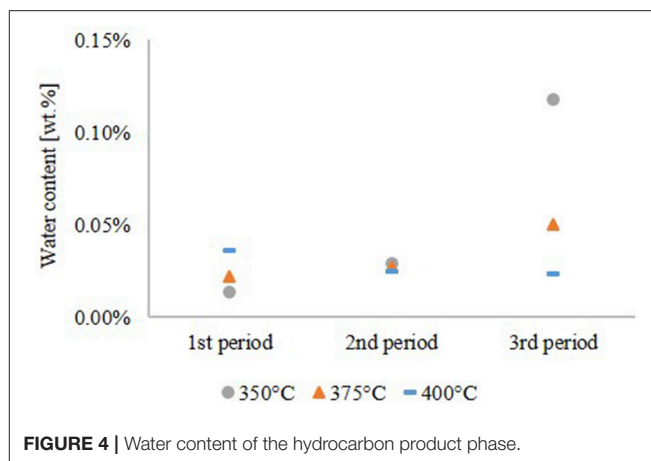
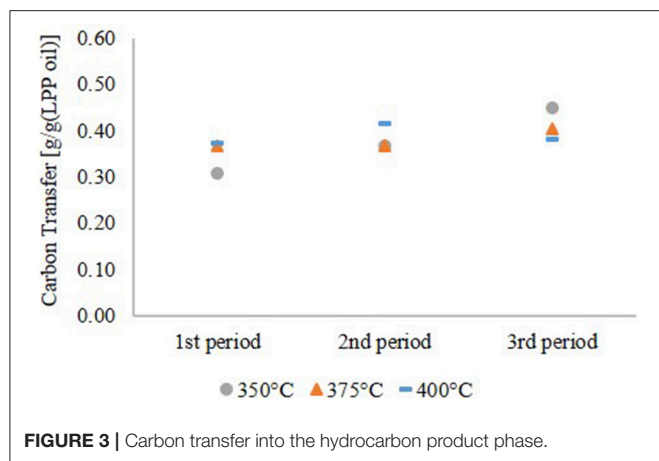


TABLE 4 | Oxygen content of the organic product phase (determined by balance of the ultimate analysis).

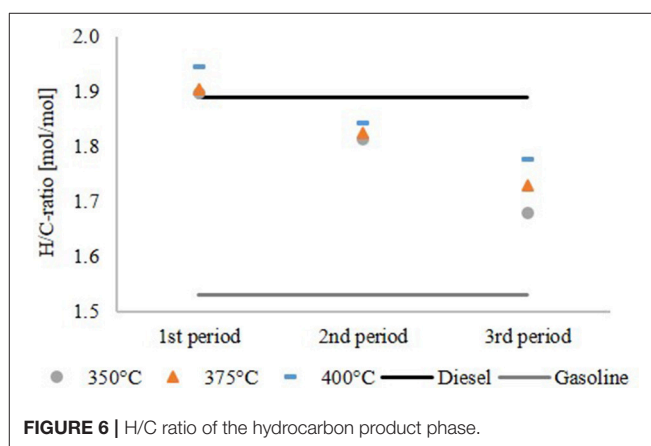
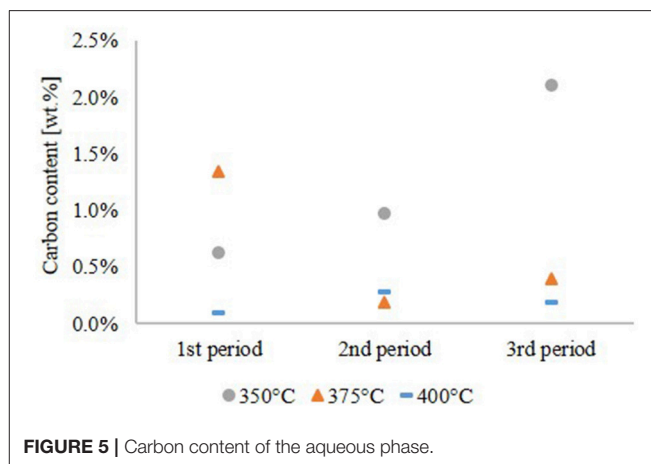
Oxygen [wt.%]	1 st Period	2 nd Period	3 rd Period
350°C	0.00	0.00	1.11
375°C	0.00	0.00	0.00
400°C	0.00	0.00	0.00

yield of hydrocarbon products and is partly caused by a higher oxygen content. This leads to the conclusion, that more polar compounds are dissolved in the hydrocarbon product phase. Due to the lower gas yield one can also assume, that less cracking reactions occurred due to deactivation of the catalyst at low temperature. The carbon transfer increased slightly at 375°C and was nearly constant at 400°C, indicating stable catalyst performance.

The H/C ratio, is a very significant indicator for characterizing the degree of hydrogenation. In combination with the oxygen content, it quantifies the degree of HDO. The oxygen content was derived from the balance of the ultimate analysis. According to **Table 4**, the oxygen content was zero for all experiments over the whole time range except for the experiment at 350°C after 36 h of operation. It is obvious that at this temperature the activity of the catalyst depleted during the experiment. Therefore, the H/C ratio can be considered as main quality criterion for the degree of HDO for all other data points.

As shown in **Figure 4**, the water content of the hydrocarbon product phase correlates with the oxygen content. Except the experiment at 350°C, the water content of the hydrocarbon product phase was 0.02–0.05 wt.%.

The carbon content of the aqueous phase, given in **Figure 5**, is a complementary quality parameter for the HDO performance. A high carbon content of the aqueous phase correlates with a high oxygen content of the hydrocarbon product phase due to incomplete hydrophobation of LPP oil. At 350°C, the carbon content of the aqueous phase increased during the experiment with a maximum of about 2.1 wt.%. The opposite



happened at 375°C, where the carbon content was highest in the first period of the experiment. At 400°C the carbon content, indicating carbon loss into the aqueous phase, was below 0.5 wt.% over the whole experiment and didn't show a trend.

The water content of the aqueous phase was between 96.9 and 99.9 wt.% in all cases, as shown in **Table 5**. This result confirms

TABLE 5 | Water content of the aqueous phase.

Water [wt.%]	1 st Period	2 nd Period	3 rd Period
350°C	99.9	99.7	97.8
375°C	97.0	97.6	96.9
400°C	98.5	97.6	98.1

the low carbon loss into the aqueous phase and high effectiveness of HDO.

Figure 6 shows the H/C ratio of the hydrocarbon product phase compared to diesel and gasoline. For comparison, the H/C ratio of diesel with hydrotreated vegetable oil (HVO) additives and gasoline without biogenic additives were used. The H/C ratio decreased over the time span of the experiment and increased with the temperature. The highest H/C ratio was observed at 400°C in the first period of the experiment. Afterwards deactivation of the catalyst became detectable, although the H/C ratio was still in the range of diesel and gasoline. The results of the experiment at 350°C again confirmed a significant oxygen content, indicating insufficient HDO.

Product Characterization

In **Table 6**, the properties of the hydrocarbon product phase, depending on the HDO temperature, are summarized and compared to diesel and gasoline. Water content, lower heating value, density, viscosity and boiling range are between the values for diesel and gasoline, indicating that the product is a mixture of diesel and gasoline and that these fractions can be obtained by distillation. Through the high grade of HDO a high heating value of about 42.7 wt.% was achieved.

The ultimate analysis is compared with gasoline without biogenic additives and diesel with HVO additives. The lower heating value was calculated with the algorithm of Boie (Grote and Feldhusen, 2007 Equation 1).

$$\text{LHV} = 35 \cdot c + 94,3 \cdot h - 10,8 \cdot o + 10,4 \cdot s + 6,3 \cdot n - 2,44 \cdot w \quad (1)$$

with, *c*, *h*, *o*, *s*, *n* and *w* representing the amount of carbon, hydrogen, oxygen, sulfur, nitrogen and water in wt.%, respectively.

Water content, density, viscosity and boiling cut points of diesel and gasoline are derived from the standard of diesel (EN 590, 2004) and gasoline (EN 228, 2004).

By GC-MS analysis, the components in the HDO product phases were determined. The 10 most frequent components are shown in **Figure 7**. Nine of them are alkanes and cycloalkanes, only one of them is an aromatic hydrocarbon, toluene. The components amount between 6.5 and 10 wt.% Together with the high H/C ratio this implies a high grade of saturation in the organic product. In general, the amount of saturated molecules increased with the HDO temperature. This means, that HDO is more effective at higher temperature in the range of 350–400°C. Through the composition of LPP oil, one can assume a few transfer routes from the biomass constituents

cellulose, hemicellulose and lignin to the final product after HDO. In LPP oil, the main components were: levoglucosan, 1-(4-hydroxy-3-methoxyphenyl)-2-propanone, 2-hydroxy-3-methyl-2-cyclopentenone, 1-hydroxy-2-butanone, 1-hydroxypropanone, acetic acid and methyl acetate. After fractionation of lignin during pyrolysis, the phenol-alcohols are possibly transformed into cyclohexanes during HDO. This might explain the presence of propyl cyclohexane, as it could be derived from 1-(4-hydroxy-3-methoxyphenyl)-2-propanone, and cyclohexane from guaiacol. Hexane can both be derived from lignin derivatives, such as 2-hydroxy-3-methyl-2-cyclopentenone or levoglucosan, or the cellulose derivative glucose. Pentane is a characteristic hemicellulose fragment, referring to the high amount of pentoses present in hemicellulose (Collard and Blin, 2014).

These suggested pathways are supplemented by many other routes, such as the fractionation from higher molecular structures and formation of C-C bonds, occurring during the pyrolysis of lignocellulosic biomass.

Gas Phase Composition

The main components of the product gas phase, given in **Figure 8**, were alkanes as methane and ethane. No oxygen or nitrogen was detected. Acetylene was measured but only detected in the first few hours of experiments as a startup effect. The rest of the gas phase was assumed to be “C₃ and higher,” describing all alkanes and alkenes with 3 or more carbon atoms. Due to the high excess, the gas phase consisted to about 95 mol% of hydrogen and only to about 5 mol% of product gas. Although little differences are visible, no temperature dependency was detected. Cracking reactions start at elevated temperature and are not observable in large amounts at those process conditions.

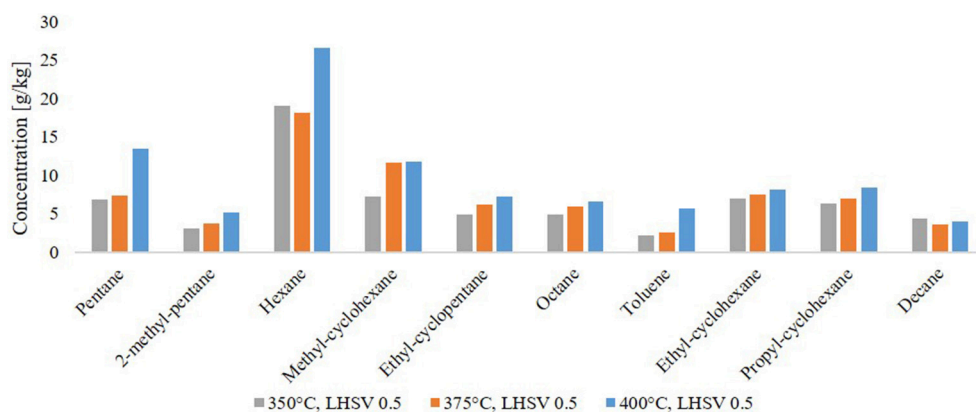
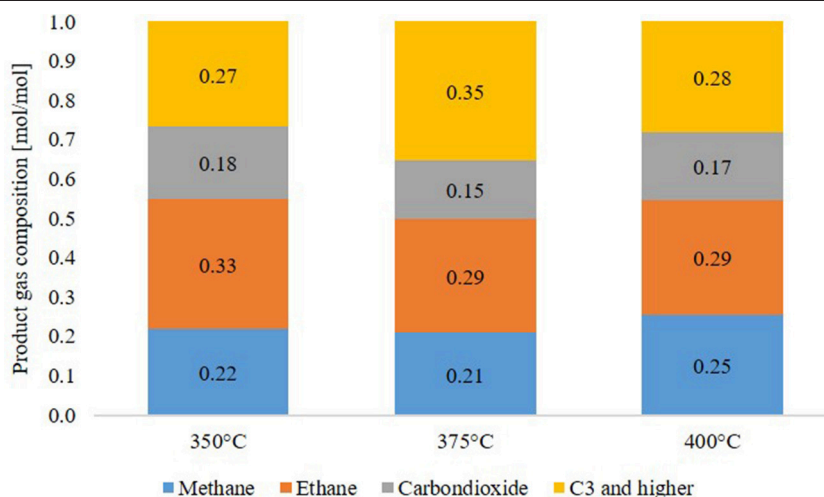
DISCUSSION

HDO has been performed successfully in a single-step process. The water content of LPP oil could be decreased to below 0.05 wt.%. The carbon loss into the aqueous product phase was very low, with carbon contents of 0.5 wt.% at 400°C. Nine of the 10 most frequent components were alkanes and cycloalkanes, as determined by GC-MS analysis. Decreasing HDO rate at 350°C indicates deactivation of the catalyst. The carbon transfer from LPP oil into the hydrocarbon product phase was highest at 400°C. Also the H/C ratio, an indicator for the degree and effectiveness of HDO, was highest at this temperature. The decreasing H/C ratio even at 400°C indicates catalyst activation loss. This can be caused by coke formation, another potential reason might be sulfur depletion during HDO. Ongoing tests indicate a more stable operation if 1000 ppm of sulfur are added to LPP oil (Treusch et al., 2018).

Coke formation at HDO of LPP oil was very low with about 1.35 wt.% based on LPP oil and H₂ feed and didn't depend on the temperature at the conditions mentioned above. Assuming that the mass growth at the catalyst was 100 wt.% carbon, this still results in a comparable very low carbon transfer from LPP oil to coke of 7.5 wt.%, despite the high LHSV. In comparison, Kim G. et al. proposed a two-step process at an overall LHSV of 0.4 h⁻¹, obtaining 1–17 g coke per g pyrolysis oil in the first step

TABLE 6 | Hydrocarbon product characterization of the 2nd period of experiment compared to diesel and gasoline.

Compound	Unit	HDO 350°C	HDO 375°C	HDO 400°C	Diesel	Gasoline
Water content	[wt.%]	0.03	0.03	0.03	<0.02 EN 590, 2004	n.a.
Lower heating value (Boie; Grote and Feldhusen, 2007)	[MJ/kg]	42.68	42.73	42.72	43.2	41.8
Density	[kg/m ³]	829	823	805	820–845 EN 590, 2004	720–775 EN 228, 2004
Viscosity	[mPa·s]	1.56	1.45	1.07	2.0–4.5 EN 590, 2004	n.a.
Boiling at 150°C	[V.%]	32.6	31.0	20.7	n.a.	≥75 EN 228, 2004
Boiling at 350°C	[V.%]	96.6	97.2	98.5	≥85 EN 590, 2004	n.a.
Carbon transfer	[%]	36.7	36.6	41.5	–	–
Carbon content	[wt.%]	86.37	86.35	86.03	86.3	88.7
Hydrogen content	[wt.%]	13.17	13.24	13.33	13.7	11.4
Balance (oxygen content)	[wt.%]	0.00	0.00	0.00	0.0	0.0
Nitrogen content	[wt.%]	<1	<1	<1	<1	<1

**FIGURE 7** | Molecules found in the hydrocarbon product phase by GC-MS analysis.**FIGURE 8** | Product gas composition after 12 h of experiment.

at 100–190°C and 1–23 g coke per g pyrolysis oil in the second step at 300–390°C (Kim G. et al., 2017). These results are most

likely to be effected by the pyrolysis oil itself. Plugs are typically polymerized bio-oil and inorganic constituents (Olarte et al.,

2016). Additionally, organic condensation products of partially upgraded pyrolysis oil components lead to fouling of the catalyst, inhibiting educts to bind to the catalyst and get hydrogenated, which leads to more coking (De Miguel Mercader et al., 2011; Weber et al., 2015). Another point is coke, that is already contained in pyrolysis oil. Fast pyrolysis oils usually contain between 0.3 and 3 wt.% particles (Bridgwater and Peacocke, 2000). In LPP oil, no particles were detected as they are retained by the heat carrier oil during the liquid phase pyrolysis step. Furthermore, through the high dilution by water, heat of reaction is buffered and coke formation, caused by overheating of the catalyst surface, is lowered. At the relatively high LHSV of 0.5 h^{-1} , the temperature profile in the reactor shows a lower temperature at the top due to the high heat capacity of water. This results in a short preheating zone and might explain the low coke formation, as high heating ramps promote coking (De Miguel Mercader et al., 2011). Water is also described as stabilization agent for instable charged molecules in pyrolysis oil, reducing the activation energy of ketonisation and increasing the driving force for forming ketones, that are afterwards hydrodeoxygenated (De Miguel Mercader et al., 2011). These reactions usually occur at the front end of the reactor, where coke formation is highest (Elliott et al., 2009).

Compared to LPP oil, the water content of fast pyrolysis oils is much lower. HDO reactions are highly exothermic. Therefore, a two-step process is necessary, where the first step acts as a stabilizing step. It reduces the reactivity of functional groups such as aldehydes, ketones and double C-C bonds (Laurent et al., 1992). Routray et al. described the goal of the first, mild HDO step to be the reduction of some more active compounds like alkenes, aromatics and carbonyl groups, as they are most likely responsible for coke formation. They proposed a two-step process with mild hydrotreatment taking place at 130°C using a Ru/C catalyst and deep HDO taking place at $300\text{--}400^\circ\text{C}$ using a Pt/ZrP catalyst. Both steps were performed at 140–150 bar. Although they managed to produce a hydrocarbon phase with primarily cyclic alkanes, after 55 h time on stream (TOS), more than 25 wt.% of the carbon contained in the feed pyrolysis oil was transformed into coke. Plugging by coke formation occurred in all experiments after 55–72 h TOS. (Routray et al., 2017) Elliott et al. described coking in single step processes at 340°C after 30–40 h TOS (Elliott et al., 2009). Olarte et al. observed

plugging of the reactor in a single-step reference experiment using fast pyrolysis oil after 48 h TOS at a space velocity of $0.1 \text{ h}^{-1} (\text{ml}_{\text{oil}}/\text{ml}_{\text{catalyst}})$ (Olarte et al., 2016). Kim I. et al. investigated a preceding extraction step to remove particles and most likely lignin components, which are partly responsible for coking. Although experiments were performed at high liquid hourly space velocities of up to 2.3 h^{-1} , they observed rapidly decreasing product quality, beginning at about 3 h TOS, resulting in a product with 6.1 wt.% oxygen after 13.1 h TOS. Due to plugging, experiments had to be stopped after 5.7–14.2 h TOS (Kim I. et al., 2017).

The low coke formation during HDO is significant for LPP oil and distinguishes LPP oil from fast pyrolysis oils. Therefore, a two-step process is not obligatory.

AUTHOR CONTRIBUTIONS

KT was responsible for laboratory experiments, analytics, data analysis and drafted the manuscript. NS was head of this project at Graz, University of Technology, coordinated the study, was responsible for laboratory experiments and was involved in the conception of the laboratory setup. KS and RN participated in laboratory experiments, analytics and data analysis. PP was head of this project on the site of BDI—BioEnergy International GmbH and coordinated the study. MS is the director of the Institute of Chemical Engineering and Environmental Technology and helped draft the manuscript. All authors gave final approval for publication.

FUNDING

This work has been funded by the Austrian Research and Promotion Agency (FFG) under the scope of the Climate and Energy Fund. Grant number: 853577.

ACKNOWLEDGMENTS

The authors want to acknowledge Andrea Rollett, Michael Schädler, Thomas Pichler, Manuel Tandl, Anna Mauerhofer, Manuel Menapace and Dominik Heinrich for their outstanding work in our labs as well as the contribution of COST Action FP1306 in supporting interaction and collaboration.

REFERENCES

- Bridgwater, A. V., and Peacocke, G. V. C. (2000). Fast pyrolysis processes for biomass. *Renew. Sustain. Energy Rev.* 4, 1–73. doi: 10.1016/S1364-0321(99)00007-6
- Carpenter, D., Westover, T., Howe, D., Deutch, S., Starace, A., Emerson, R., et al. (2016). Catalytic hydroprocessing of fast pyrolysis oils: impact of biomass feedstock on process efficiency. *Biomass Bioenergy* 96, 142–151. doi: 10.1016/j.biombioe.2016.09.012
- Collard, F. X., and Blin, J. (2014). A review on pyrolysis of biomass constituents: mechanisms and composition of the products obtained from the conversion of cellulose, hemicelluloses and lignin. *Renew. Sustain. Energy Rev.* 38, 594–608. doi: 10.1016/j.rser.2014.06.013
- Demirbas, A. (2011). Competitive liquid biofuels from biomass. *Appl. Energy* 88, 17–28. doi: 10.1016/j.apenergy.2010.07.016
- De Miguel Mercader, F., Koehorst, P. J. J., Heeres, H. J., Kersten, S. R. A., and Hogendoorn, J. A. (2011). Competition between hydrotreating and polymerization reactions during pyrolysis oil hydrodeoxygenation. *AIChE J.* 57, 3160–3170. doi: 10.1002/aic.12503
- Elliott, D. C. (2007). Historical developments in hydroprocessing bio-oils. *Energy Fuels* 21: 1792–1815. doi: 10.1021/ef070044u
- Elliott, D. C., and Bager, E. C. (1989). *Process for Upgrading Biomass Pyrolyzates*. 4,795,841, issued 1989. Richland, WA.
- Elliott, D. C., Hart, T. R., Neuenschwander, G. G., Rotness, L. J., and Zacher, A. H. (2009). Catalytic hydroprocessing of biomass fast pyrolysis bio-oil to

- produce hydrocarbon products. *Environ. Prog Sustainable Energy* 28, 441–449. doi: 10.1002/ep.10384
- EN 228 (2004). *DIN EN 228:204-03, Automotive Fuels – Unleaded Petrol – Requirements and Test Methods*. German version EN228:2004.
- EN 590 (2004). *DIN EN 590:2004-03, Automotive Fuels – Diesel – Requirements and Test Methods*. German version EN 590:2004.
- Grote, K. H., and Feldhusen, J. (2007). *Dubbel Taschenbuch Für Maschinenbau*. 22nd Edn. Berlin: Springer.
- Kim, G., Seo, J., Choi, W. J., Jae, J., Ha, J. M., Suh, D. J., et al. (2017). Two-step continuous upgrading of sawdust pyrolysis oil to deoxygenated hydrocarbons using hydrotreating and hydrodeoxygenating catalysts. *Catal. Today* 303, 130–135. doi: 10.1016/j.cattod.2017.09.027
- Kim, I., Dwiatioko, A. A., Choi, J. W., Suh, D. J., Jae, J., Ha, J. M., et al. (2017). Upgrading of sawdust pyrolysis oil to hydrocarbon fuels using tungstate-zirconia-supported Cu catalysts with less formation of cokes. *J. Industr. Eng. Chem.* 56, 74–81. doi: 10.1016/j.jiec.2017.06.013
- Laurent, E., Pierret, C., Grange, P., and Delmon, B. (1992). “Control of the deoxygenation of pyrolytic oils by hydrotreatment,” in *Proceedings of the 6th Conference on Biomass for Energy, Industry and Environment*. Vol. 6. (Athens: ECC).
- Meyer, P. A., Snowden-Swan, L. J., Rappé, K. G., Jones, S. B., Westover, T. L., and Cafferty, K. G. (2016). Field-to-fuel performance testing of lignocellulosic feedstocks for fast pyrolysis and upgrading: techno-economic analysis and greenhouse gas life cycle analysis. *Energy Fuels* 30, 9427–9439. doi: 10.1021/acs.energyfuels.6b01643
- Olarte, M. V., Padmaperuma, A. B., Ferrell, J. R., Christensen, E. D., Hallen, R. T., Lucke, R. B., et al. (2017). characterization of upgraded fast pyrolysis oak oil distillate fractions from sulfided and non-sulfided catalytic hydrotreating. *Fuel. Elsevier Ltd.* 202, 620–630. doi: 10.1016/j.fuel.2017.03.051
- Olarte, M. V., Zacher, A. H., Padmaperuma, A. B., Burton, S. D., and Job, H. M., Lemmon, T. L., et al. (2016). Stabilization of softwood-derived pyrolysis oils for continuous bio-oil hydroprocessing. *Topics Catal.* 59, 55–64. doi: 10.1007/s11244-015-0505-7
- Ritzberger, J., Pucher, P., and Schwaiger, N. (2014). The BioCRACK Process - a refinery integrated biomass-to-liquid concept to produce diesel from biogenic feedstock. *Chem. Eng. Trans.* 39, 1189–94. doi: 10.3303/CET1439199
- Pucher, H., Schwaiger, N., Feiner, R., Ellmaier, L., Pucher, P., Chernev, B. S. et al. (2015). Biofuels from liquid phase pyrolysis oil: a two-step hydrodeoxygenation (HDO) process. *J. Green Chem.* 17, 1291–1298. doi: 10.1039/c4gc01741b
- Pucher, H., Schwaiger, N., Feiner, R., Pucher, P., Ellmaier, L., and Siebenhofer, M. (2014). Catalytic hydrodeoxygenation of dehydrated liquid phase pyrolysis oil. *Energy Res.* 31:3205. doi: 10.1002/er.3205
- Routray, K., Barnett, K. J., and Huber, G. W. (2017). Hydrodeoxygenation of pyrolysis oils. *Energy Technol.* 5, 80–93. doi: 10.1002/ente.201600084
- Schwaiger, N., Feiner, R., Pucher, H., and Ellmaier, L. (2015). BiomassPyrolysisRefinery – Herstellung von Nachhaltigen Treibstoffen *Chemie Ingenieur Technik* 87, 1–8. doi: 10.1002/cite.201400099
- Schwaiger, N., Feiner, R., Zahel, K., Pieber, A., Witek, V., Pucher, P., et al. (2011). Liquid and solid products from liquid-phase pyrolysis of softwood. *Bioenergy Res.* 4, 294–302. doi: 10.1007/s12155-011-9132-8
- Schwaiger, N., Witek, V., Feiner, R., Pucher, H., Zahel, K., Pieber, A., et al. (2012). Formation of liquid and solid products from liquid phase pyrolysis. *Bioresour. Technol.* 124. Elsevier Ltd: 90–94. doi: 10.1016/j.biortech.2012.07.115
- Treusch, K., Schwaiger, N., Schlackl, K., Nagl, R., Rollett, A., Schadler, M., et al. (2018). High-throughput continuous hydrodeoxygenation of liquid phase pyrolysis oil. *Reaction Chem. Eng. R. Soc. Chem.* 3, 258–266. doi: 10.1039/C8RE00016F
- Treusch, K., Ritzberger, J., Schwaiger, N., Pucher, P., and Siebenhofer, M. (2017). Diesel production from lignocellulosic feed : the bioCRACK process. *R. Soc. Open Sci.* 4:171122. doi: 10.1098/rsos.171122
- Weber, R. S., Mariefel, V. O., and Huamin, W. (2015). Modeling the kinetics of deactivation of catalysts during the upgrading of bio-oil. *Energy Fuels* 29, 273–277. doi: 10.1021/ef502483t

Conflict of Interest Statement: The authors declare that the research was conducted in the absence of any commercial or financial relationships that could be construed as a potential conflict of interest.

Copyright © 2018 Treusch, Schwaiger, Schlackl, Nagl, Pucher and Siebenhofer. This is an open-access article distributed under the terms of the Creative Commons Attribution License (CC BY). The use, distribution or reproduction in other forums is permitted, provided the original author(s) and the copyright owner(s) are credited and that the original publication in this journal is cited, in accordance with accepted academic practice. No use, distribution or reproduction is permitted which does not comply with these terms.



Catalytic Fast Pyrolysis of Kraft Lignin With Conventional, Mesoporous and Nanosized ZSM-5 Zeolite for the Production of Alkyl-Phenols and Aromatics

Polykarpos A. Lazaridis¹, Apostolos P. Fotopoulos¹, Stamatia A. Karakoulia² and Konstantinos S. Triantafyllidis^{1,2*}

¹ Department of Chemistry, Aristotle University of Thessaloniki, Thessaloniki, Greece, ² Chemical Process and Energy Resources Institute, Centre for Research and Technology Hellas, Thessaloniki, Greece

OPEN ACCESS

Edited by:

Jirí Cejka,
J. Heyrovsky Institute of Physical
Chemistry (ASCR), Czechia

Reviewed by:

Roger Gläser,
Leipzig University, Germany
Patricia Pizarro,
Universidad Rey Juan Carlos, Spain

*Correspondence:

Konstantinos S. Triantafyllidis
ktrianta@chem.auth.gr

Specialty section:

This article was submitted to
Green and Sustainable Chemistry,
a section of the journal
Frontiers in Chemistry

Received: 13 February 2018

Accepted: 26 June 2018

Published: 18 July 2018

Citation:

Lazaridis PA, Fotopoulos AP,
Karakoulia SA and Triantafyllidis KS
(2018) Catalytic Fast Pyrolysis of Kraft
Lignin With Conventional,
Mesoporous and Nanosized ZSM-5
Zeolite for the Production of
Alkyl-Phenols and Aromatics.
Front. Chem. 6:295.
doi: 10.3389/fchem.2018.00295

The valorization of lignin that derives as by product in various biomass conversion processes has become a major research and technological objective. The potential of the production of valuable mono-aromatics (BTX and others) and (alkyl)phenols by catalytic fast pyrolysis of lignin is investigated in this work by the use of ZSM-5 zeolites with different acidic and porosity characteristics. More specifically, conventional microporous ZSM-5 (Si/Al = 11.5, 25, 40), nano-sized (≤ 20 nm, by direct synthesis) and mesoporous (9 nm, by mild alkaline treatment) ZSM-5 zeolites were tested in the fast pyrolysis of a softwood kraft lignin at 400–600°C on a Py/GC-MS system and a fixed-bed reactor unit. The composition of lignin (FT-IR, 2D HSQC NMR) was correlated with the composition of the thermal (non-catalytic) pyrolysis oil, while the effect of pyrolysis temperature and catalyst-to-lignin (C/L) ratio, as well as of the Si/Al ratio, acidity, micro/mesoporosity and nano-size of ZSM-5, on bio-oil composition was thoroughly investigated. It was shown that the conventional microporous ZSM-5 zeolites are more selective toward mono-aromatics while the nano-sized and mesoporous ZSM-5 exhibited also high selectivity for (alkyl)phenols. However, the nano-sized ZSM-5 zeolite exhibited the lowest yield of organic bio-oil and highest production of water, coke and non-condensable gases compared to the conventional microporous and mesoporous ZSM-5 zeolites.

Keywords: kraft softwood lignin, fast pyrolysis, bio-oil, ZSM-5 zeolite, mesoporosity, alkyl-phenols, aromatics, hierarchical MFI

INTRODUCTION

Lignocellulosic biomass is considered as an alternative source of fuels/energy, chemicals and products, with the potential to replace, at least partially, the fossil raw materials, i.e., petroleum oil and coal (Huber et al., 2006; Triantafyllidis, 2013). Biomass consists mainly of two carbohydrate polymers (polysaccharides), i.e., cellulose (30–50%) and hemicellulose (15–30%) and the phenolic polymer lignin (10–30%) (Mosier et al., 2005; Azadi et al., 2013; Isikgor and Becer, 2015). Lignin is nature's most abundant aromatic and water insoluble polymer, consisting of three primary phenylpropane units, i.e., syringyl (S), guaiacyl (G), and p-hydroxyphenyl (H) units which

correspond to three monolignols, i.e., sinapyl, coniferyl and p-coumaryl alcohols, all three joined by ether and C–C linkages to form the 3-dimensional macromolecule of lignin (Zakzeski et al., 2010; Azadi et al., 2013; Li et al., 2015; Rinaldi et al., 2016). The most common linkages in lignin structure are ether linkages, such as the β -O-4 which predominates (40–50%) and α -O-4, as well as the 5-5, β -5, β -1, dibenzodioxocin, spirodienone and β - β linkages (Chakar and Ragauskas, 2004; Zakzeski et al., 2010; Rinaldi et al., 2016). The content of lignin depends on the type of raw biomass, i.e., 20–30 wt.% in softwoods (i.e., spruce, pine, fir, yew), 15–25 wt.% in hardwoods (i.e., beech, aspen, birch, oak, poplar) and 10–20 wt.% in grasses, straw and stover. The structure and composition of lignin is also related to the type of plant species, i.e., softwood lignins contain mainly guaiacyl (coniferyl alcohol) units with one methoxy group attached to the aromatic ring, hardwood lignins contain both guaiacyl and syringyl (sinapyl alcohol) units, the latter having two methoxy groups, while grass lignins contain also p-hydroxyphenyl (p-coumaryl alcohol) units in addition to the G- and S-units (Azadi et al., 2013; Li et al., 2015).

In traditional wood valorization industry (i.e., pulping/Kraft process) or more recently developed biorefining processes, lignin has been considered as a low-value byproduct that can be burnt to generate heat and power. However, over the last two decades, this low-cost raw material has found increased valorization potential in various sectors, such as polymers/resins, binders, foams, cement, carbon fibers and activated carbons, vanillin, etc. (Setua et al., 2000; Lora and Glasser, 2002; Suhas et al., 2007; Silva et al., 2009; Pandey and Kim, 2011; Strassberger et al., 2014). Nowadays, intensive research is being conducted on the development of efficient processes for the thermo-catalytic and bio-catalytic conversion of this aromatic/phenolic natural polymer toward high value chemicals and fuels (Ragauskas et al., 2014; Xu et al., 2014; Li et al., 2015; Beckham et al., 2016). Most studied depolymerization-valorization processes of kraft and other types of lignin (i.e., hydrolysis, organosolv) are hydrogenolysis and fast pyrolysis. The hydrogenolysis of lignin usually requires moderate reaction temperature (ca. 150–350°C), high hydrogen pressure (ca. 20–90 bar) and/or hydrogen-donor solvents (catalytic transfer hydrogenation) in neutral/acidic/basic medium, using supported metal catalysts such as Pt, Ni, Pd, Cr, Cu etc. on carbon, carbides, zeolites and various oxides, targeting to cleavage of the C–O bonds (ca. β -O-4 ether bond) and C–C bonds in order to produce low molecular weight fragments or monomeric phenolic/aromatic/alkanes compounds (Zakzeski et al., 2010; Sergeev and Hartwig, 2011; Xu et al., 2012; Barta et al., 2014; Onwudili and Williams, 2014; Liu et al., 2016; Molinari et al., 2016; Opris et al., 2017).

Fast pyrolysis is a relatively intense, in terms of temperature (400–700°C), thermochemical process which is capable to break-down lignin into smaller fragments in the absence of oxygen, toward the production of bio-oil which consists mainly of alkoxy-phenols and oxygenated aromatics (e.g., guaiacol, methyl guaiacol, syringol, methyl syringol, vanillin, syringaldehyde, vinyl syringol, vinyl guaiacol, 1,2,3-trimethoxy-benzene), as well as some gaseous products (mainly CO₂ and CO) and char (Fox and McDonald, 2010; Jiang et al., 2010; Pandey and

Kim, 2011; Patwardhan et al., 2011; Li et al., 2015). The lignin-derived pyrolysis oil is more homogeneous compared to the bio-oil that derives from the parent lignocellulosic biomass, the latter consisting, in addition to the phenolic compounds, of various ketones, aldehydes, acids, furans, esters, ethers, alcohols, sugars and few aromatics and aliphatics (Azeez et al., 2010; Stephanidis et al., 2011). Such a phenolic bio-oil, derived from lignin, has greater potential of being utilized in the production of phenol-based resins substituting the petroleum derived phenol (Vithanage et al., 2017). Alternatively, the lignin-derived bio-oil can be upgraded via down-stream catalytic hydrodeoxygenation (HDO) to produce hydrocarbons, mainly aromatics and (cyclo)alkanes. The HDO process requires moderate reaction temperatures (ca. 150–300°C), ambient to high hydrogen pressures (ca. up to 50 bars) and/or hydrogen-donor solvents in neutral/acidic medium in the case of liquid phase processing, using various supported catalytic systems, such as typical petroleum hydrotreating catalysts, i.e., bimetallic catalyst sulfided CoMo, NiMo/ γ -Al₂O₃ (Laurent and Delmon, 1994; Ryymin et al., 2010), unsupported and alumina-supported MoS₂ and CoMoS catalysts (Bui et al., 2011), Mo₂C catalysts (Lee et al., 2014), combined systems of a hydrogenating and an acidic catalyst, i.e., Pd/C and H-ZSM-5 (Zhao and Lercher, 2012), and various Ni, Pd, Pt, Ru, etc. catalysts supported on carbon, SiO₂, Al₂O₃, TiO₂, ZrO₂, CeO₂, zeolites, etc. (Mortensen et al., 2013; Jin et al., 2014; de Souza et al., 2017; Kordouli et al., 2017).

The bio-oil can also be *in situ* deoxygenated, i.e., during the biomass fast pyrolysis process by the use of an appropriate, usually acidic catalyst. In the catalytic fast pyrolysis (CFP) of biomass the initially formed (via thermal pyrolysis) vapors of oxygenated oligomers and monomers (i.e., ketones, aldehydes, furans, acids, alkoxy-phenols, etc.) undergo deoxygenation (dehydration, decarbonylation, decarboxylation), cracking, isomerization, aromatization, condensation and oligomerization reactions on the catalyst surface. The use of catalysts with strong Brønsted acidity, such as zeolites and especially ZSM-5 zeolite, induce deep-deoxygenation of the produced bio-oil which consist mainly of mono-aromatics (i.e., benzene, toluene, xylenes, etc.) and naphthalenes, as well as alkyl-phenols. Inevitably, more water, gases and coke-on-catalyst are being produced at the expense of the organic phase of bio-oil (Iliopoulou et al., 2007, 2017; Jae et al., 2011; Mihalcik et al., 2011; Wang et al., 2014; Thommes et al., 2015). In the case of lignin CFP, the same concept, catalysts and reaction mechanisms apply (Mullen and Boateng, 2010; Ma et al., 2012; Ben and Ragauskas, 2013). Most studies have investigated the performance of different microporous zeolitic catalysts (i.e., ZSM-5 with various Si/Al ratio, Beta, Mordenite, Ferrierite, USY) (Jackson et al., 2009; Mihalcik et al., 2011; Li et al., 2012; Ma et al., 2012; Ben and Ragauskas, 2013; Zhang et al., 2014). As with biomass CFP, H-ZSM-5 zeolite has been identified as the most suitable for the production of aromatics, due to its unique micropore structure and Brønsted acidity strength. Still, USY zeolite with larger micropores than those of ZSM-5, has been also proposed as very efficient for the production of hydrocarbons in the CFP of kraft lignin, exhibiting also

relatively lower degree of tar formation (Ma et al., 2012). More recently, the use of high surface area ordered mesoporous Al- or Zr-substituted silicas, with average pore width in the range of ca. 3–10 nm, has been also investigated (Custodis et al., 2016; Elfadly et al., 2016). Custodis et al. studied the effect of acidity and porosity of Al-MCM-41, Al-SBA-15, and Al-MSU-J on product yields and bio-oil composition in the CFP of alkali softwood lignin, showing that a nano-sized Al-MCM-41 catalyst may exhibit similar deoxygenation and aromatization activity as a strongly acidic microporous ZSM-5 zeolite (Custodis et al., 2016).

The development of mesoporous zeolites or “hierarchical” zeolites (i.e., comprising of micro-, meso- and macro-porous structures) has attracted the interest for the cracking/pyrolysis of heavy oil fractions (Choi et al., 2006; Park et al., 2009) as well as lignocellulosic biomass (Park et al., 2010; Kelkar et al., 2014; Li et al., 2014; Zheng et al., 2014; Gamliel et al., 2016), aiming to combine the beneficial diffusion characteristics of mesoporous materials with the strong acidity and stability of zeolites. Mesoporous MFI (ZSM-5) zeolites, having in some cases moderate/tuned acidity or even acid-base properties (Kelkar et al., 2014; Feroso et al., 2016), have been the main type of hierarchical zeolites studied for biomass pyrolysis. With regard to lignin CFP, very few studies have been reported yet on the use hierarchical zeolites. Lee et al. tested a meso-Y zeolite (prepared from commercial USY) in the CFP of kraft lignin and showed that the production of mono-aromatics and polycyclic aromatic hydrocarbons (PAHs) was significantly enhanced compared to Al-MCM-41 which produced mostly phenolics (Lee et al., 2013). In addition Kim et al. showed that the main products in lignin pyrolysis with mesoporous MFI zeolite were alkyl-phenols and mono-aromatics (benzene, toluene, ethylbenzene, and xylene) owing to the strong Brønsted acidity of the zeolite in comparison to mesoporous Al-SBA-15 (Kim et al., 2014). Li et al. also showed that in the CFP of lignin by alkaline-treated mesoporous ZSM-5 zeolite the aromatics and phenols were increased while char/coke was decreased compared to the parent microporous zeolite (Li et al., 2014).

In the present work, we studied the catalytic fast pyrolysis of kraft lignin (spruce, softwood) using a series of conventional microporous ZSM-5 zeolites (with different Si/Al ratio), a nanosized crystalline ZSM-5 with high textural porosity/external area and a mesoporous ZSM-5 zeolite with intracrystal mesoporosity prepared by mild alkaline treatment of a commercial ZSM-5 zeolite. The non-catalytic and catalytic tests of lignin pyrolysis were conducted on a Pyrolyzer/Gas Chromatography-Mass Spectrometry (Py/GC-MS) instrument at different temperatures (400–600°C) and catalyst to lignin ratios (1–4), in order to study the effect of the various ZSM-5 catalysts on the composition of bio-oil. Furthermore, a fixed bed fast pyrolysis unit was also used, in order to determine the product yields (bio-oil, gases, char/coke). The catalytic results have been rationalized on the basis of the catalysts’ acidic, porous and morphology characteristics and reaction mechanisms for the deoxygenation of the initially formed alkoxy-phenols toward alkyl-phenols and aromatics have been proposed.

MATERIALS AND METHODS

Catalyst Preparation

Three commercial ZSM-5 zeolites with different Si/Al ratio (provided by Zeolyst) were tested: CBV 2314 (Si/Al = 11.5), CBV 5524G (Si/Al = 25), CBV 8014 (Si/Al = 40). All the commercial samples were received in ammonium form and were converted to proton form via calcination at 500°C for 3 h in air flow prior to use and were denoted as ZSM-5 (11.5), ZSM-5 (25), and ZSM-5 (40) respectively. A mesoporous ZSM-5 sample, denoted as Meso-ZSM-5 (9nm), was prepared by mild alkaline treatment of the commercial H-CBV8014 (Si/Al = 40) zeolite with 0.2 M NaOH aq. solution, followed by treatment with 0.1 N HCl aq. solution (the detailed procedure is described in Supplementary Material). The nanosized zeolite (Nano-ZSM-5) was synthesized based on typical template hydrothermal methods applied for ZSM-5 zeolite, using tetraethylorthosilicate (TEOS, 98%, Sigma-Aldrich) and aluminum-tri-sec-butoxide (97%, Sigma-Aldrich) as Si and Al sources, and 1.0 M-Tetrapropylammonium hydroxide (TPAOH, Sigma-Aldrich) solution as the structure-directing agent for MFI-type zeolite. In brief, TEOS and Al-tri-sec-butoxide were initially mixed under stirring followed by addition of the TPAOH solution (mixture molar ratio: 1 SiO₂: 0.01 Al₂O₃: 0.37 TPAOH: 16.4 H₂O) and further stirring for 1 h at room temperature. The hydrothermal aging of the resulting suspension was conducted at 100°C for 4 days, followed by filtration of the resulting solids, washing (with plenty of water), drying (100°C overnight) and calcination (600°C, 6 h, in air). All zeolite powders were pelletized, crushed and sieved to a particle size range of 180–500 μm before use in the fixed bed lignin pyrolysis experiments.

Characterization of Kraft Lignin

The kraft lignin (from spruce, softwood) used in this study was provided by Sigma-Aldrich. The elemental analysis of dried kraft lignin sample was performed by a Carbon/Hydrogen/Nitrogen/Sulfur elemental analyzer (LECO 628 and LECO 932, USA). Oxygen content was calculated by difference. Thermogravimetric analysis (TGA, NETZSCH STA 449 F5 Jupiter) of the dried kraft lignin sample was carried out using N₂ as carrier gas (purity >99.99 vol %) at a flow rate of 50 mL/min. The samples were heated from room temperature to 850°C at heating rate of 10°C/min. FTIR spectra were obtained on a Perkin-Elmer FTIR spectrometer, model SPECTRUM 1000, using the KBr method (KBr was previously oven-dried to avoid interferences due to the presence of water). Measurements were carried out using thin disks prepared in a hydraulic press and spectra recorded over the range from 4,000 to 400 cm⁻¹ at a resolution of 2 cm⁻¹ while 64 scans were averaged to reduce noise. The spectra presented were baseline-corrected and converted to the absorbance mode.

The molecular weight distribution (MWD) and the average molecular weight of kraft lignin were determined by Gel Permeation Chromatography (GPC). The instrument used was from Polymer Laboratories, model PL-GPC 50 Plus, and comprised of an isocratic pump, a differential refractive index detector, and three PLgel 5l MIXED-C columns in series.

Approximately 5 mg of lignin were suspended in 1 mL glacial acetic acid/acetyl bromide (9:1 v/v) for ~2 h (Asikkala et al., 2012). Afterwards the solvent was fully removed in vacuum evaporator, and the residue sample was dissolved in THF at a constant concentration of 1 mg/mL and sonicated overnight. After filtration with PTFE-L 0.45 μ m, 200 μ L of sample was injected into the chromatograph. The elution solvent was THF (HPLC grade) at a constant flow rate of 1 mL/min, and the entire system was kept at a constant temperature of 30°C. Calibration of GPC was carried out with standard polystyrene samples (Polymer Laboratories).

The 2D HSQC NMR spectrum was obtained on a Varian (Agilent) 500 MHz spectrometer. 200 mg of Kraft lignin were dissolved in 0.45 mL DMSO- d_6 and stirred overnight before the analysis and chemical shifts were referenced to the solvent signal (2.500/39.520 ppm). The interscan relaxation delay was set to 5 s that has been found to be sufficient time for full relaxation of the signals (Heikkinen et al., 2003). The spectral widths were from 13 to -1 ppm and from 160 to 0 ppm for the ^1H and ^{13}C dimensions, respectively. In the ^{13}C dimension the number of transients was 16 and the increments were set at 300. The spectrum was processed using MestReNova software. Prior to Fourier transformation, FIDs were apodized with a $\pi/2$ sine square bell function in both dimensions and zero-filled up to 1,024 points in the ^{13}C dimension and 2,048 points in the ^1H -dimension. A semi-quantitative analysis of the heteronuclear single quantum coherence (HSQC) spectra was performed by integration of cross-peaks in the different regions of the spectra with MestReNova. In the HSQC spectrum, the signal of the G2 (C2-H) aromatic units was used as internal standard. More specifically, the area obtained from the integration of the G2 unit was set as 100 aromatic units and the amount of each linkage type (expressed as a number per 100 Ar) was calculated by the equation:

$$X = \frac{\int X}{\int G2} \times 100$$

Characterization of Catalytic Materials

The chemical composition (wt. % of Al and Na) of the zeolitic catalysts was determined by inductive coupled plasma—atomic emission spectroscopy (ICP-AES) using a Plasma 400 (Perkin Elmer) spectrometer, equipped with Cetac6000AT+ ultrasonic nebulizer.

Nitrogen adsorption/desorption experiments at -196°C were performed on an Automatic Volumetric Sorption Analyzer (Autosorb-1MP, Quantachrome). The samples were previously outgassed at 350°C for 16 h under 5×10^{-9} Torr vacuum. The BET area (i.e., total surface area) of the catalysts was determined by the multi-point BET method, the mesopore width distribution by the BJH analysis of the adsorption data, and the micropore volume and area by the t-plot method. Argon (Ar) physisorption measurements at -186°C were also performed, using the multi-point BET method for total surface area determination and the t-plot method for determination of the microporous characteristics. The NLDFT adsorption model

was applied for the pore width distribution analysis. The BJH analysis was also used in the mesopore range for comparison.

Transmission electron microscopy (TEM and HRTEM) experiments were carried out in a JEOL 2011 high resolution transmission electron microscope operating at 200 kV, with a point resolution of 0.23 nm and Cs = 1.0 mm.

Powder X-ray diffraction (XRD) was applied for the determination of the crystallinity of zeolites using a Rigaku Rotaflex 200B diffractometer equipped with Cu K α X-ray radiation and a curved crystal graphite monochromator operating at 45 kV and 100 mA; counts were accumulated in the range of 5–75° 2 θ every 0.02° (2 θ) with counting time 2 sec per step.

The determination of the amount and relative strength of Brønsted and Lewis acid sites of the catalysts was performed by Fourier transform—infrared (FT-IR) spectroscopy combined with *in situ* adsorption of pyridine. The FT-IR spectra were recorded on a Nicolet 5700 FTIR spectrometer (resolution 4 cm^{-1}) using the OMNIC software and a specially designed heated, high-vacuum IR cell with CaF $_2$ windows. All samples were finely ground in a mortar and pressed in self-supported wafers (15 mg/ cm^2). The wafers were outgassed *in situ* at 450°C for 1 h under high vacuum (10–6 mbar) and a background spectrum was recorded at 150°C. Adsorption/equilibrium with pyridine vapors was then conducted at 150°C, by adding pulses of pyridine for 1 h at a total cell pressure of 1 mbar. Spectra were recorded at 150°C, after equilibration with pyridine at that temperature and after outgassing for 30 min at higher temperatures, i.e., 250, 350, and 450°C, in order to evaluate the strength of the acid sites. The bands at 1,545 cm^{-1} (pyridinium ions) and 1,450 cm^{-1} (coordinated pyridine) were used to identify and quantify the Brønsted and Lewis acid sites, respectively, by adopting the molar extinction coefficients provided by Emeis (Emeis, 1993).

Pyrolysis Experiments Using Py/GC-MS System

The thermal and catalytic fast pyrolysis experiments of kraft lignin were performed on a Multi-Shot Micro-Pyrolyzer (EGA/PY-3030D, Frontier Laboratories, Japan) connected to a gas chromatographer – mass spectrometer system (GCMS-QP2010, Shimadzu). Detailed description of the experimental set-up and procedure is provided in Supplementary Material (Figure S1). In brief, for the thermal (non-catalytic) pyrolysis tests, a dried (80°C under vacuum for 6 h) mixture of 1 mg lignin and 2 mg silica sand (as inert heat carrier material) was loaded in a stainless steel cup which was instantaneously dropped in the hot reactor/furnace and pyrolysis was conducted at the preset temperatures of ca. 400, 500, and 600°C, for 12 s. In the catalytic fast pyrolysis (CFP) experiments, mixtures of 1 mg of dried lignin with 1–4 mg of the various zeolites were used (catalyst to lignin ratio range: 1–4). Identification of mass spectra peaks was achieved by the use of the scientific library NIST11s. The derived compounds were classified and categorized in the following 16 groups-families: mono-aromatics (AR), aliphatics (ALI), phenols (PH), acids (AC), esters (EST), alcohols (AL), ethers

(ETH), aldehydes (ALD), ketones (KET), polycyclic aromatic hydrocarbons (PAH's), sugars (SUG) nitrogen compounds (NIT), sulfur compounds (SUL), oxygenated aromatics (OxyAR), oxygenated phenols (OxyPH) and unidentified compounds (UN). At least three experiments were performed for each catalyst/condition and the reported data are the mean values with a standard deviation being below 10% in all cases.

Pyrolysis Experiments on Fixed Bed Reactor

The thermal and catalytic pyrolysis tests were performed on a bench-scale fixed bed tubular reactor, made of stainless steel 316 and heated by a 3-zone furnace. A specially designed piston system was used to introduce lignin into the reactor. The amount of lignin (dried at 80°C under vacuum for 6 h) used in all experiments was 0.5 g and the amount of silica sand (thermal pyrolysis experiments, non-catalytic) or catalyst (in the catalytic experiments) was also 0.5 g. In a typical pyrolysis experiment, the solid lignin was inserted from the top of the reactor and was pushed down instantaneously with the aid of the piston in the hot reactor zone, where it was vaporized at 600°C. The produced pyrolysis vapors were then driven downwards through the catalyst's bed with the aid of a constant N₂ flow (100 cm³/min) for 20 min. The pyrolysis product vapors were condensed in pre-weighted spiral glass receivers placed in a cooling bath (dry ice). Afterwards, the obtained bio-oil was collected with absolute ethanol and analyzed by GC-MS (GCMS-QP2010, Shimadzu). For the identification of the produced bio-oil vapors, the NIST11s mass spectral library was used and the derived compounds were classified and categorized in the 16 groups-families, as in the case of Py/GC-MS experiments. The water content of bio-oil was determined by Karl-Fischer titration (ASTM E203-08), while the elemental analysis (C/H/N/S) of the organic fraction of the bio-oil was determined by LECO 628 and LECO 932 analyzers (USA); O was determined by difference.

The amount of solids, which comprised of char in the non-catalytic pyrolysis experiment and char plus coke-on-catalyst in the catalytic pyrolysis experiments, was determined by direct weighing. An indirect estimation of the coke formed on the catalyst, as wt.% on initial lignin, was performed by subtracting the measured char content of the non-catalytic experiment from the char+coke content of the catalytic experiments (char formation is not affected by the presence of the catalysts, as lignin and catalysts do not come in contact, see Supplementary Materials, Figure S2). Furthermore, the decomposition profile of the collected char and coke (on the spent catalysts) was studied by thermogravimetric analysis (TGA, NETZSCH STA 449 F5 Jupiter) using dry air as carrier gas, at a flow rate of 50 mL/min. The samples were heated from room temperature to 850°C at heating rate of 10°C/min. Non-condensable gases (NGC's) were measured by the liquid displacement method and were analyzed by GC equipped with TCD and FID (HP5890 Series II). More details on the experimental set-up and analytic procedures are provided in Supplementary Material (Figure S2). The standard deviation of the product yield values reported is in all cases below 5%.

RESULTS AND DISCUSSION

Physicochemical Characteristics of Kraft Lignin

The elemental analysis of the lignin used as feedstock is given in **Table 1**. The C/H/O content was typical for such type of lignins, while ~ 1.5% S was also measured owing to the kraft pulping process. The molecular weight of lignin was also in the range of previously reported values for similar lignins (Vishtal and Kraslawski, 2011; Li et al., 2012).

The thermal decomposition profile of lignin, both as TG (weight %) and DTG (%/min) curves, is shown in **Figure 1**. A small initial weight loss of 3–4% up to ca. 150°C was observed due to evaporation of humidity, followed by a steep decrease of weight (~55% loss, DTG peak maximum at 375°C) initiating at about 170–200°C and ending at about 600°C which corresponds to the decomposition of lignin. A further progressive limited decrease of weight was observed up to 900°C which is probably attributed to the slow pyrolysis/gasification of the initially formed carbonaceous material. The high residual char at 800°C (37.6% minus 2.04% ash: 35.5%) is indicative of the high thermal stability of the complex cross-linked aromatic polymer of lignin (Yang et al., 2006).

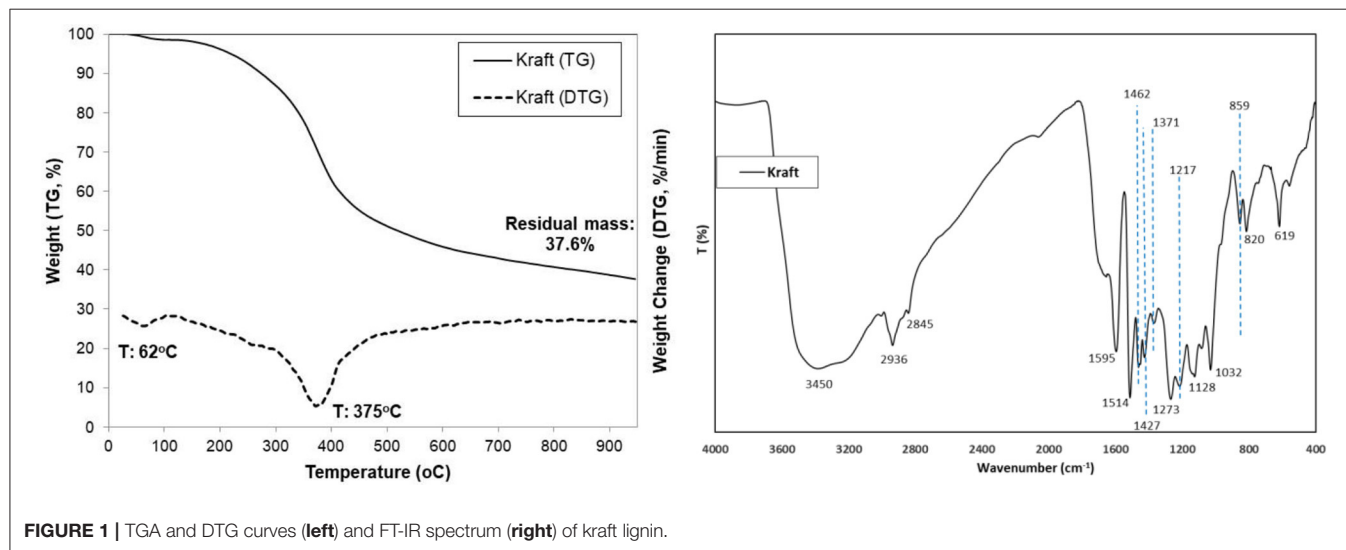
The FTIR spectrum of lignin is also presented in **Figure 1**. Assignment of representative peaks was based on previous reported work (Kang et al., 2012; Minu et al., 2012; Yang et al., 2016). A strong absorbance at 3,450 cm⁻¹ assigned to -OH stretching vibrations was induced by the presence of alcoholic and phenolic hydroxyl groups involved in hydrogen bonds. Peaks at 2,936 and 2,845 cm⁻¹ are assigned to C-H asymmetric and symmetrical vibrations of alkyls in side-chains (Zhang et al., 2012). Absorption bands located at around 1,595, 1,514, 1,462, and 1,427 cm⁻¹ were assigned to vibrations of aromatic rings, suggesting they were left intact and that the aromatic structure of lignin was not changed appreciably during the pulping process (Chen et al., 2016; Yang et al., 2016). The peaks at 1,217 and 1,273 cm⁻¹ were assigned to the vibrations of guaiacyl rings (Minu et al., 2012). The strong band at 1,032 cm⁻¹ corresponds to the aromatic C-H in-plane deformation (G>S units). The band at 859 cm⁻¹ represented the deformation vibrations of C-H bonds in the aromatic rings of p-hydroxyphenylpropane (Yang et al., 2016). The band at 820 cm⁻¹ is attributed to aromatic C-H out of plane vibrations. The absorption band at 620 cm⁻¹ indicate probably the presence of sulfonic groups (S-C) that remained after the kraft pulping process (Domínguez-Robles et al., 2016).

In order to study the structural characteristics of kraft lignin, the 2D HSQC NMR technique was applied. More specifically, the types of side-chain linkages and of aromatic units contained in the lignin were identified. The side-chain (δ C/ δ H 50–95/2.5–6.0) and the aromatic (δ C/ δ H 100–135/6–8) region of the HSQC spectrum of the kraft lignin sample is shown in **Figure 2**. Using literature data, the HSQC cross-peaks of the spectrum were assigned to specific types of aromatic rings and linkages (Table S1, Supplementary Material) (del Río et al., 2009; Ralph et al., 2009; Sette et al., 2011; Kang et al., 2012; Constant et al., 2016; Yang et al., 2016; Crestini et al., 2017). The main signals in the aromatic region of the HSQC spectrum are attributed to the

TABLE 1 | Physicochemical characteristics of kraft lignin (dry basis).

Lignin	C (wt.%)	H (wt.%)	S (wt.%)	N (wt.%)	O* (wt.%)	Ash (wt.%)	Mn (g/mol)	Mw (g/mol)	PD
Kraft (spruce)	61.84	5.62	1.50	0.80	30.24	2.04	1,350	6,140	4.54

*Calculated by difference.



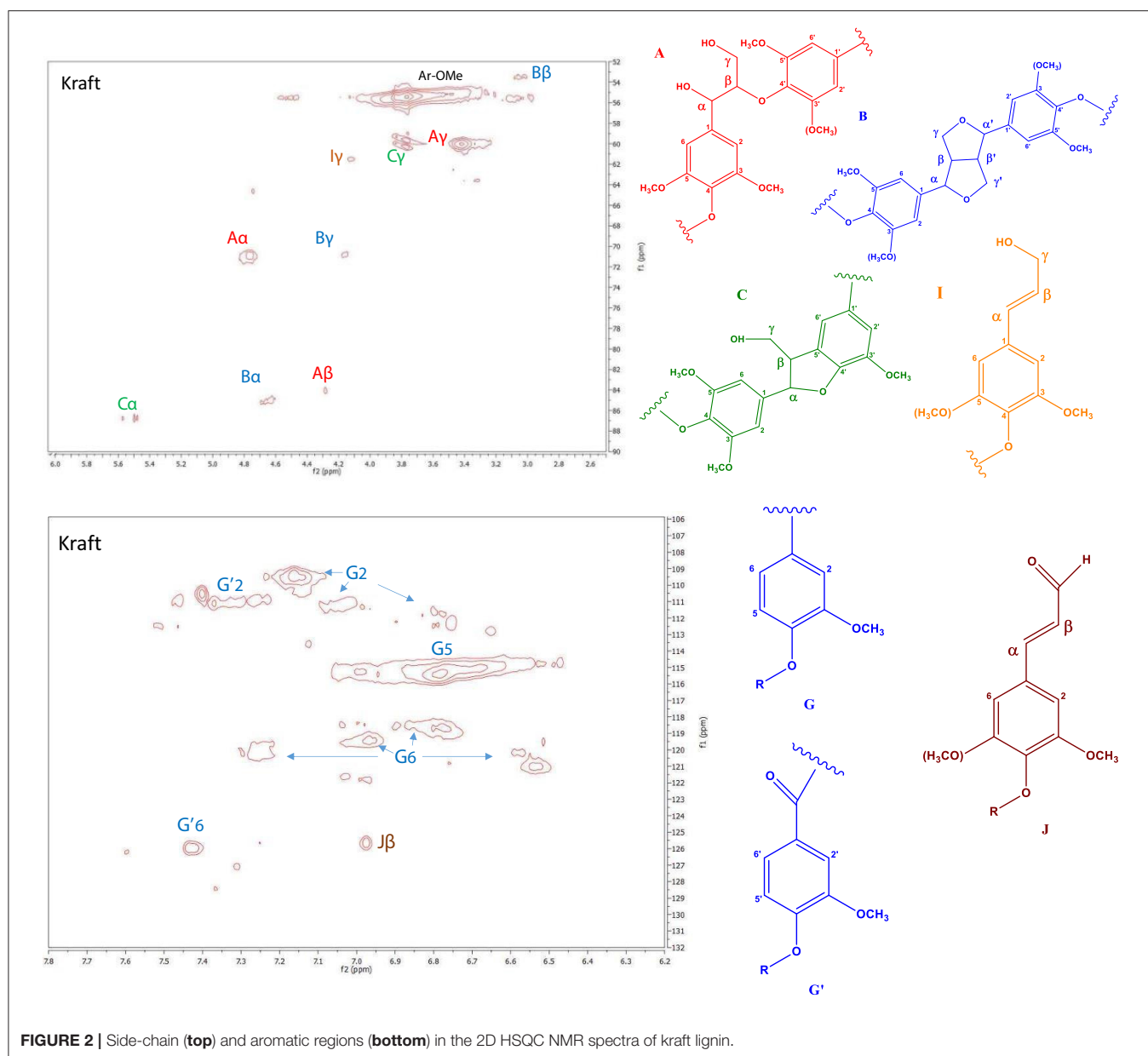
substituted aromatic rings of the kraft lignin units. The spectrum is predominated by the strong signals of guaiacyl (G) units at C2–H2 ($\delta\text{C}/\delta\text{H}$ 109.5–112.8/6.7–7.2 ppm), C5–H5 ($\delta\text{C}/\delta\text{H}$ 115.3/6.8 ppm), and C6–H6 ($\delta\text{C}/\delta\text{H}$ 118.7–121.8/6.5–7.3 ppm). The kraft lignin of the present study was originated by a softwood (spruce), which is known to contain mainly coniferyl (guaiacyl, G units) alcohol units as lignin precursor (Azadi et al., 2013). A smaller signal related to cinnamaldehyde (J β , 125.6/7 ppm) was also observed, and maybe due to aldehydes produced during the kraft pulping, in low amounts (Crestini et al., 2017).

The main signals in the part of the spectrum with the inter-unit linkages correspond to the common structures of β -O-4' aryl ethers, resinol substructures β - β' , and the phenylcoumaran substructures β -5' linkages (Table S1). These linkages represent the major internal connections, which construct the three-dimensional structure of lignin. More specifically, the α -, β - and strong signal at γ -position of β -O-4' (type A) linkages are shown at $\delta\text{C}/\delta\text{H}$ 71/4.8, 84.1/4.3, and 60.0/3.4 ppm, respectively. In addition, the signals of α , β and γ C atoms of resinol structures (β - β' linkages, type B) are observed in the spectrum at $\delta\text{C}/\delta\text{H}$ 84.9/4.6, 53.5/3.1, and 70.9/4.16 ppm respectively. The phenylcoumaran (β -5', type C) units are also identified on the spectrum, and the signals of α and γ carbon atoms are observed at $\delta\text{C}/\delta\text{H}$ 86.8/5.5 and 60–60.3/3.8 ppm, respectively. Moreover, a small peak that correspond to cinnamyl alcohol end groups (I) are also observed by their C γ -H γ correlations at $\delta\text{C}/\delta\text{H}$ 61.5/4.1 ppm. For the calculation of the ratio of the different types of inter-unit linkages, the cross-peaks that correspond to the α atoms of each type of linkage were integrated, except for the peaks of J and I structures for whom the peaks of β and

γ C atoms were used, respectively. The resulting ratio of A, B, C, J, I structures was 25.4/2.4/1.2/6.4/1.2 respectively, based on the area of G2 units that was set as 100 Ar. Apart from the cross-peaks that correspond to α , β , γ C atoms of A, B, C types of interunit linkages, there is also the above mentioned cross-peak at 125.6/7.0 that some studies (Yuan et al., 2011; Wen et al., 2013; Crestini et al., 2017) assigned to the β atom of the cinnamaldehyde (J structure) and some other (for example Constant et al., 2016) to the α , β C atoms of the stilbene structure. These two structures are similar and both have a double bond in conjunction with the aromatic ring. The existence of this peak implies that such double bond exists in our kraft lignin sample in addition to the A, B, C types of inter-unit linkages. The existence of J structure is also evidenced from the presence of the cross-peak at 61.5/4.1 on the linkage part of the spectrum that is assigned to the γ atom of cinnamyl alcohol (I) which is the reduced form of the J structure and exists in a smaller extent.

Physicochemical Characteristics of the ZSM-5 Catalysts

The XRD patterns of the ZSM-5 zeolite catalysts used are shown in Figure 3. The patterns of all the samples (commercial microporous, meso- and nano-ZSM-5 zeolites) showed the characteristic diffraction peaks of the MFI crystalline structure. However, a slight decrease of the peak intensity in the range of ca. 20–25° 2 θ was observed for the nano-sized and mesoporous ZSM-5 samples, as well as a very broad and low intensity bump in the pattern of the mesoporous ZSM-5 prepared by alkaline



treatment, due probably to the presence of small amounts of amorphous silica phases.

The N_2 adsorption-desorption isotherms and the BJH pore width distribution curves of the ZSM-5 zeolite catalysts are shown in **Figure 3**. The conventional microporous ZSM-5 zeolites with different Si/Al ratio exhibit the type I(a) adsorption isotherm according to the updated IUPAC classification (Thommes et al., 2015), with a plateau at higher relative pressures and no distinct hysteresis loop, typical for microporous zeolitic materials without significant mesoporosity. The BET area of the conventional microporous ZSM-5 zeolites ranged between 425 and 455 m^2/g with about 330–350 m^2/g being attributed to microporous area (t-plot method) (**Table 2**). The absence of any intra-crystal defects or voids which may induce increased

meso/macroporosity was evidenced by the well-formed crystals observed in their TEM images. A representative image of ZSM-5(40) is shown in **Figure 4** where relatively large “plate”-like crystals of parallelepiped shape typical for the MFI zeolites can be seen.

The N_2 adsorption isotherm of the nano-sized ZSM-5 were also of type I(a) with an additional feature at high relative pressures ($P/P_0 \geq 0.9$) where a steep increase of adsorbed nitrogen was observed, indicating high macroporous/external surface area due to the very small crystallites/particles of this zeolite. This was confirmed by the TEM image (**Figure 4**) of nano-ZSM-5 which revealed the presence of aggregated primary nanocrystals of less than 20 nm in size, generating inter-crystal (textural) porosity and high macroporous/external

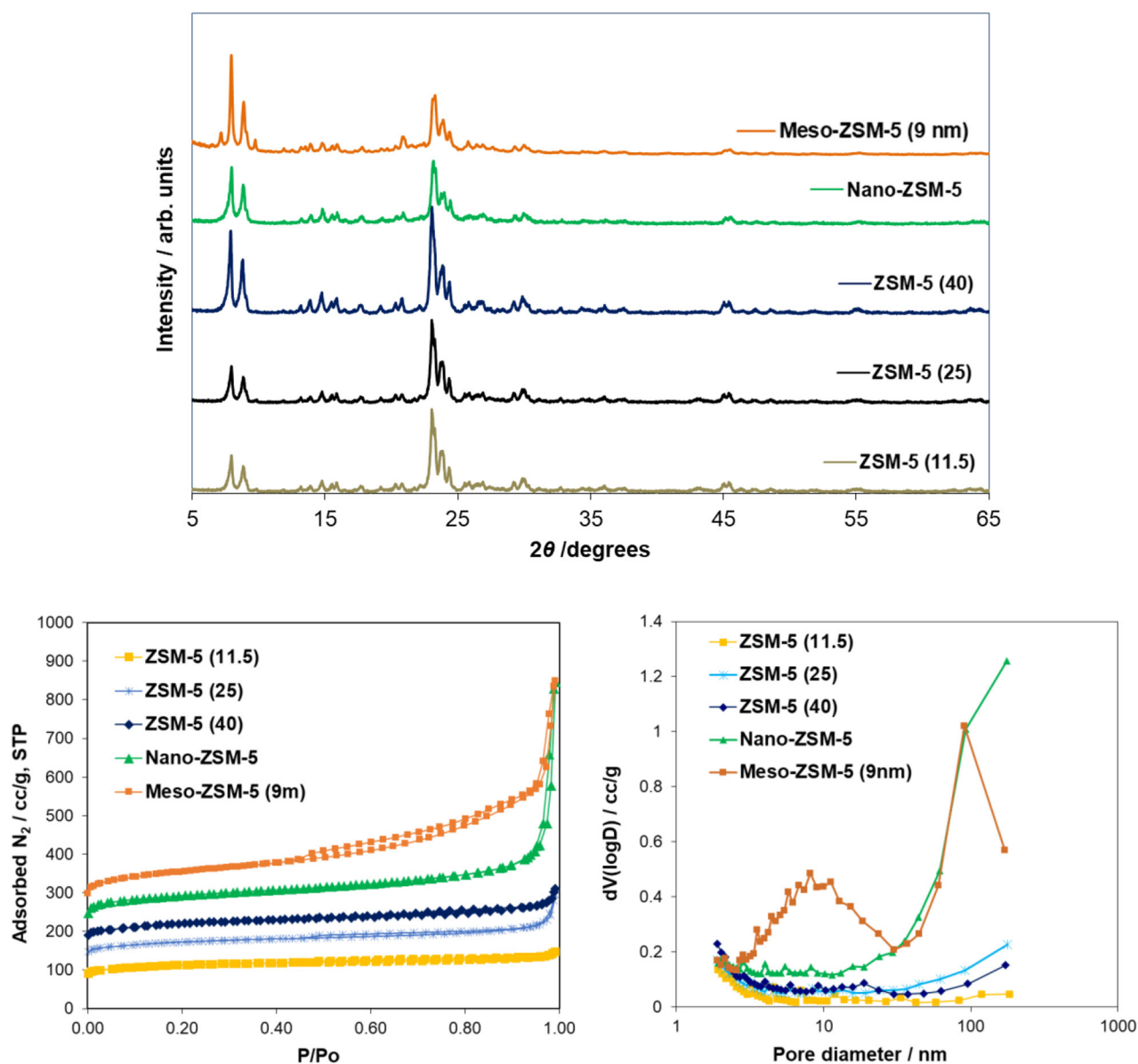


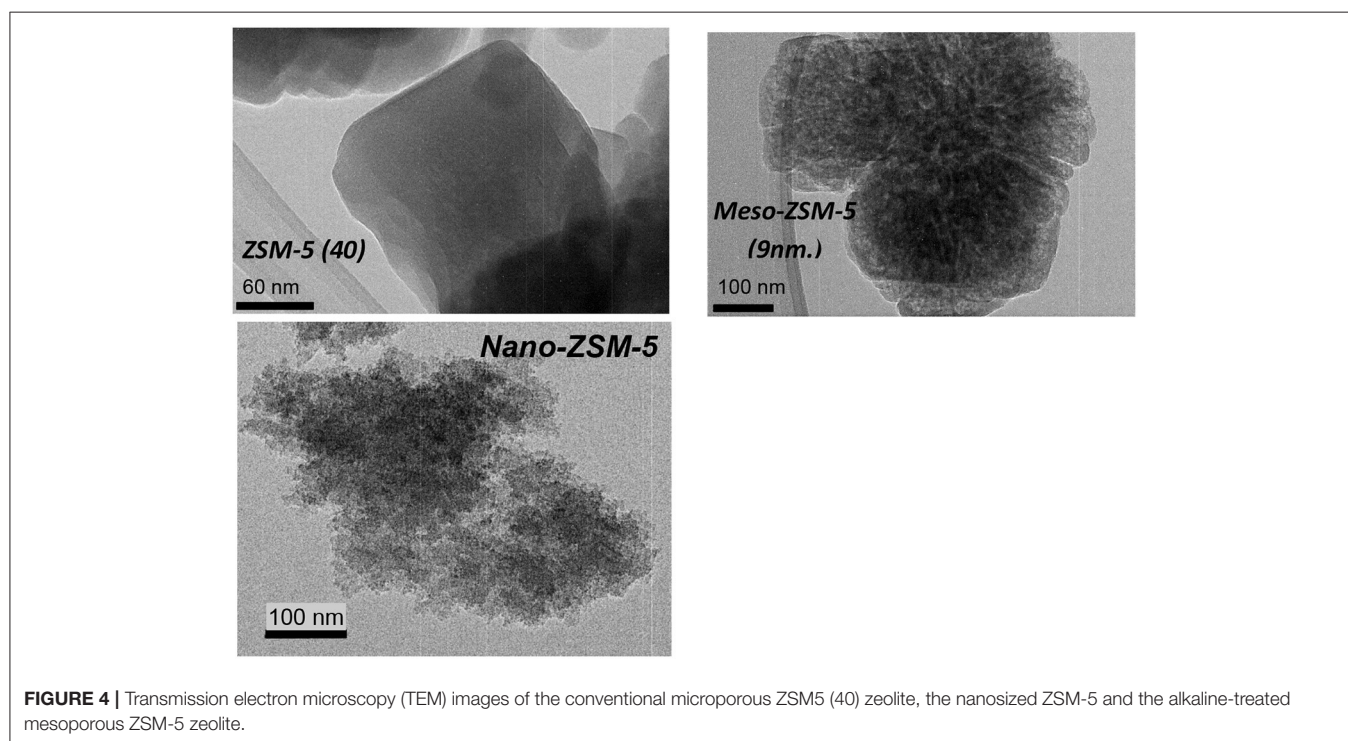
FIGURE 3 | X-ray diffraction patterns (XRD) and N_2 adsorption-desorption isotherms of the conventional microporous ZSM-5 (Si/Al = 11.5, 25, 40) zeolites, the nanosized ZSM-5 zeolite synthesized under controlled/mild template hydrothermal synthesis, and the mesoporous ZSM-5 (9nm) zeolite prepared by mild alkaline treatment of the conventional ZSM-5(40) zeolite.

surface area. As a result, the nano-ZSM-5 zeolite possesses equally high micropore area with the conventional microporous zeolites and additional increased macropore/external surface area (Table 2). In the case of meso-ZSM-5 (9 nm) prepared by mild alkaline treatment followed by treatment with dilute acid aqueous solution, the N_2 adsorption isotherm was of combined type I(a) and II, indicating the presence of both micropores and mesopores with very broad width distribution. Indeed, as can be seen in the BJH curves of Figure 3, the pore width distribution of meso-ZSM-5 exceeds from ca. 2.5 to 30 nm, with a maximum at about 9 nm. Such broad distribution of the size

of intra-crystal mesopores is typical for meso-ZSM-5 zeolites prepared by mild alkaline treatment, compared to ZSM-5 zeolites synthesized by the use of a meso-structure directing agent (Choi et al., 2006; Groen et al., 2006; Park et al., 2009; Gamliel et al., 2016). The significant increase of the meso/macroporous and external area is also accompanied by a substantial decrease of the microporous area (Table 1). This effect is often observed in mesoporous ZSM-5 zeolites with intra-crystal mesoporosity (Park et al., 2009; Gamliel et al., 2016) and can be attributed to partial disordering of the mesopore walls, not contributing to zeolitic microporosity, as well as to the presence of small amounts

TABLE 2 | Porosity, chemical composition and acidity data of the various ZSM-5 zeolite catalysts.

Catalyst	BET area ^a (m ² /g)	Micro- pore area ^b (m ² /g)	Meso/ macro pore & external area ^c (m ² /g)	Average mesopore diameter ^e (nm)	Chemical composition ^f		Acidity ^g		
					Al (wt.%)	Na (wt.%)	FT-IR/pyridine (μmol Pyr/g)		
							Brønsted	Lewis	B/L
ZSM-5(11.5)	424	349	75	–	3.20	0.06	430	123	3.5
ZSM-5(25)	456	350	106	–	1.50	0.03	216	46	4.7
ZSM-5(40)	437	332	105	–	0.91	0.03	190	26	7.3
Meso-ZSM-5 (9nm)	560	259	301	9.0	0.82	0.05	192	21	9.1
Nano-ZSM-5	524	343	181 ^d	–	0.86	0.08	100	53	1.9

^aBET area from N₂ sorption at –196°C, Multi-point BET method.^bt-plot method.^cDifference of BET area minus micropore area.^dAttributed mainly to macropores and external surface area.^eBJH analysis using adsorption data; ^fICP-AES chemical analysis data.^gDetermination of the amount of Brønsted and Lewis acid sites performed by Fourier transform – infrared (FT-IR) spectroscopy combined with in situ adsorption of pyridine.**FIGURE 4** | Transmission electron microscopy (TEM) images of the conventional microporous ZSM5 (40) zeolite, the nanosized ZSM-5 and the alkaline-treated mesoporous ZSM-5 zeolite.

of amorphous silica-alumina impurities. The partial dissolution of the zeolitic silicate framework, the consequent removal of Al atoms and the “healing” of the Si-OH nests lead to the formation of “secondary” cavities and pores in the crystal, as can be seen in the representative TEM image of meso-ZSM-5(9 nm) in **Figure 4**.

Representative Ar physisorption data are shown in Figure S3 and Table S2 in Supplementary Material. Small differences (<10%) in the BET (total) and micropore areas derived from the two probes (N₂ and Ar) were observed. On the other hand, a noticeable difference was found in the determination of the average mesopore width of the mesoporous ZSM-5 zeolite when

applying different analysis methods (~9nm from N₂ and Ar—BJH, ~6.5 from N₂ NLDFT and ~5.7 nm from Ar NLDFT). Still, the formation of intra-crystal mesoporosity, with relative broad width distribution, in the meso-ZSM-5 zeolite prepared by mild alkaline treated was clearly shown.

The acidic properties of zeolite catalysts are of high importance when they are intended for use in biomass or petroleum cracking/pyrolysis. ZSM-5 zeolite is considered as a relatively strongly acidic zeolite containing mainly Brønsted acid sites, if no extra-framework amorphous phases are present (Triantafyllidis et al., 2001; Triantafyllidis et al., 2004; Komvokis et al., 2012). As shown in **Table 2**, the number of Brønsted

acid sites decreases with increasing Si/Al of the commercial microporous ZSM-5 zeolites; however, the content of Lewis acid sites follows the reverse trend and increases with increasing Al content, i.e., lower Si/Al ratio. This is attributed to the easier framework dealumination of Al-rich zeolites during the calcination procedures that are subjected to, i.e., for removing the organic template after synthesis and for converting the NH_4^+ -form to H^+ -form. Overall, the ratio of Brønsted to Lewis acid sites increases with Si/Al ratio. Furthermore, as can be seen in Figure S4 (Supplementary Material), the Brønsted acid sites of ZSM-5(11.5) are of lower relative strength compared to those of ZSM-5(25) and ZSM-5(40). In the case of meso-ZSM-5 (9 nm) prepared by mild alkaline treatment followed by treatment with the dilute HCl aqueous solution, the content of Brønsted sites and the B/L ratio remain high, thus showing that the acidic properties of ZSM-5 are not sacrificed by this methodology. The relatively low content of Lewis acid sites is attributed to the “cleaning” of the alkaline-treated sample from the extra-framework aluminum phases by the use of the dilute HCl solution. The nano-ZSM-5 zeolite, despite having similar Al content with the ZSM-5(40) zeolite (Table 2), contained almost half of its Brønsted sites, possibly due to the relatively lower degree of crystallinity and inadequate organization of the zeolitic framework. The relatively higher content of Lewis acid sites may further confirm this hypothesis.

Non-catalytic and Catalytic Fast Pyrolysis of Kraft Lignin (Py/GC-MS)

Thermal Pyrolysis of Kraft Lignin at Various Temperatures (Py/GC-MS System)

Non-catalytic fast pyrolysis tests using silica sand as inert heat carrier were conducted on the Py/GC-MS system at 400, 500, and 600°C. Representative chromatograms at 400 and 600°C are presented in Figure 5, while detailed list of the identified compounds at all three temperatures is given in Table S3 (Supplementary Material). The lignin pyrolysis vapors comprised mainly of alkoxy-phenols with single alkoxy group, i.e., of the guaiacol (G) type, such as guaiacol (2-methoxy phenol), creosol, 2-methoxy-4-vinylphenol, 4-ethyl-2-methoxy phenol, vanillin and trans-isoeugenol. This clearly indicates that the predominant G units identified by 2D HSQC NMR in the structure of lignin were “transferred” to the produced bio-oil vapors. At 400°C, trace amounts of oxy-aromatics, ketones, furans and alkyl-phenols (not oxygenated) were also produced in addition to the alkoxy-phenols.

It has been previously shown that the increase of the pyrolysis temperature promotes the decomposition of high molecular weight phenolic oligomers to smaller compounds via depolymerisation and cracking of C-C bonds (Jiang et al., 2010; Wang et al., 2014). In the present work, this effect was only slightly identified as by increasing the pyrolysis temperature from 400 to 500, and 600°C the concentration of alkoxy-phenols decreased by ca. 5% giving rise to more alkyl-phenols (increase by 6–7%). Unidentified compounds, usually being high molecular weight fragments, were also decreased. Thermal pyrolysis of lignin is also known to produce relatively

high amounts of solid carbonaceous material (char), due to recondensation/repolymerization of primary pyrolysis oligomers as well as condensation and coupling reactions of guaiacol and other small alkoxy-phenols (Gayubo et al., 2004; Wang et al., 2009, 2014; Stefanidis et al., 2014; Custodis et al., 2016). The char produced by pyrolysis of kraft lignin at 400°C was 54.5 wt.% and decreased to 43.3 wt.% at 500°C and 34.5 wt.% at 600°C (Table S3), thus indicating that higher temperatures, at least in the range of 400–600°C, favor the formation of low molecular weight species instead of polymerized products and char.

Catalytic Fast Pyrolysis of Lignin With ZSM-5 Zeolite: Effect of Temperature and C/L Ratio (Py/GC-MS System)

The catalytic fast pyrolysis (CFP) tests in the Py/GC-MS system were performed with the different ZSM-5 zeolites described in the previous section. The effect of pyrolysis temperature and catalyst-to-lignin (C/L) ratio was initially investigated by the use of the conventional microporous zeolite ZSM-5(40). As a general observation, the use of the ZSM-5 zeolite induced the substantial conversion of alkoxy-phenols toward mono-aromatics (BTX, such as benzene, toluene, p-xylene, o-xylene, 1,3-dimethyl-benzene, etc.), PAHs (mainly naphthalenes) and alkyl-phenols, such as phenol, 2-methyl-phenol, 2,3-dimethyl-phenol, etc. (Figure 6 and Table S2), in accordance with previous related works on the use of zeolites and especially ZSM-5 in lignin pyrolysis (Jackson et al., 2009; Li et al., 2012; Ben and Ragauskas, 2013; Custodis et al., 2016). By increasing the pyrolysis temperature from 500 to 600°C, this effect was more pronounced favoring mostly the mono-aromatics and the naphthalenes (Figure 6). The higher C/L ratio had also a beneficial effect on the conversion of alkoxy-phenols toward mono-aromatics and PAHs, both at 500°C (Figure 6) as well as at 600°C (Figure 7). At the more intense conditions, i.e., C/L = 4 and temperature of 600°C, a highly deoxygenated bio-oil can be produced which contains mainly aromatics as well as some alkyl-phenols. The concentration of alkyl-phenols appears to be less depended on the pyrolysis temperature and the C/L ratio, exhibiting a nearly constant value for all C/L and temperatures tested.

In addition to the char formed in thermal (non-catalytic) pyrolysis of lignin, in the case of CFP coke is also formed via condensation/polymerization reactions on the acid sites of the zeolites. It has been suggested that thermally resistant lignin oligomers and the low reactivity of phenolics over zeolitic catalysts may be the reasons for enhanced formation of char/coke, in addition to the more classical polymerization of aromatics and PAHs (Wang et al., 2014). The char/coke obtained with zeolite ZSM-5(40) as catalyst, at 500°C and C/L = 2 ratio, was 44.6 wt.% and was slightly higher compared to thermal (non-catalytic) char at 500°C (43.3 wt.%), as can be seen in Table S4 (Supplementary Material). The same trend was observed at 600°C, at C/L = 2, when the thermal char and catalytic char/coke were compared. However, at both temperatures, when the amount of zeolite catalyst was increased

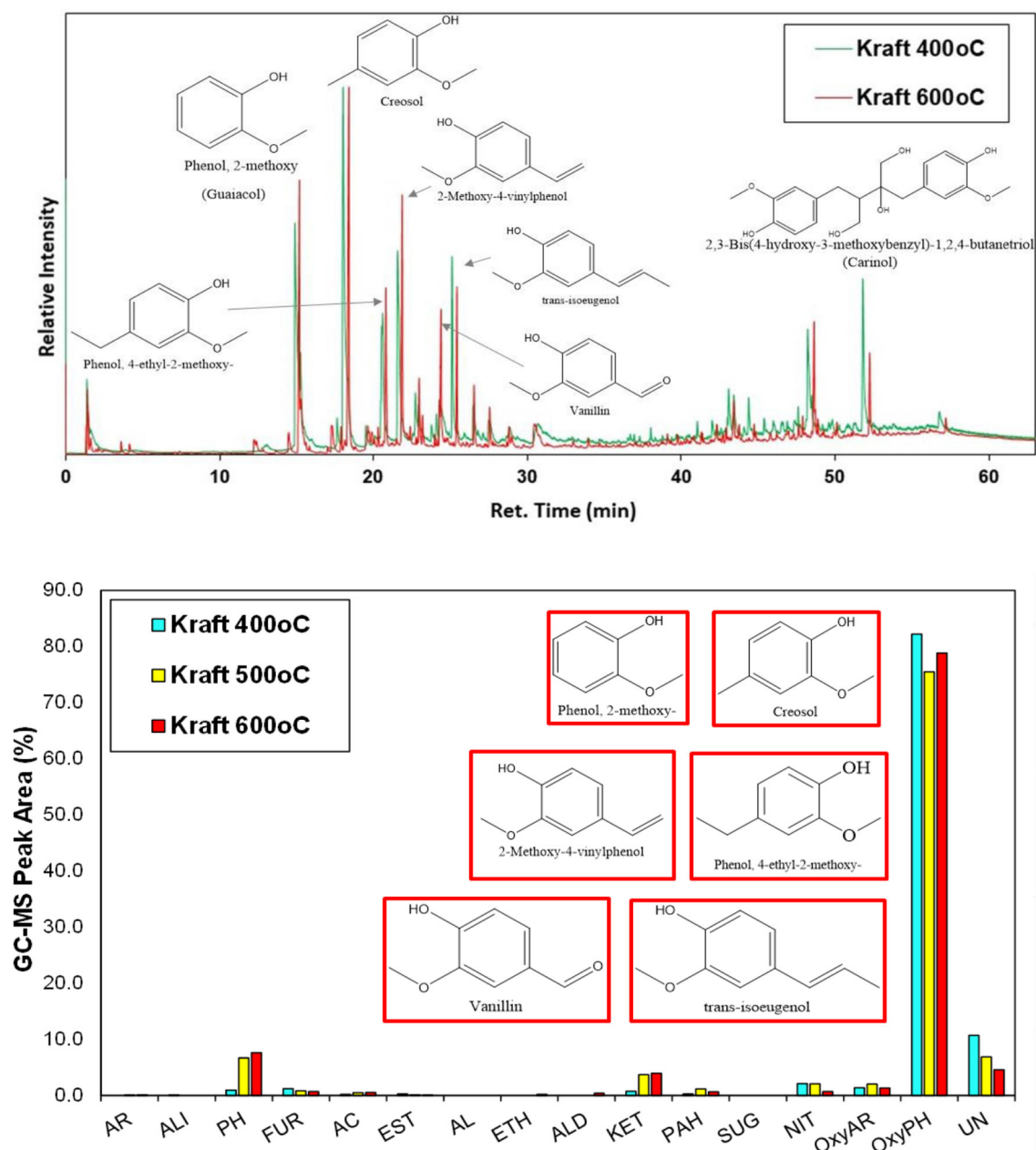


FIGURE 5 | Representative Py/GC-MS spectra of non-catalytic (thermal) fast pyrolysis of kraft (spruce) lignin (up), and relative concentration of the various groups of compounds in the bio-oil (down); indicated compounds in the graph are for the experiment at 600°C.

(C/L = 4), the amount of char/coke was markedly lower in the catalytic tests compared to the non-catalytic thermal pyrolysis, i.e., from 43.3 and 34.5% to 39.9% and 28.1% at 500 and 600°C, respectively (Table S4). This can be attributed to the increased conversion of intermediate lignin oligomers toward aromatics and alkyl-phenols on the active acid sites of ZSM-5 and the balanced/suppressed formation of reaction coke via polymerization. Similar results were reported previously by the use of ZSM-5 and USY catalysts in alkali lignin pyrolysis (Ma et al., 2012; Custodis et al., 2016).

Catalytic Fast Pyrolysis of Lignin With ZSM-5 Zeolite: Effect of Si/Al (Py/GC-MS System)

The acidity of the zeolitic catalysts, mainly the Brønsted acid sites, are responsible for the deoxygenation of the bio-oil via dehydration, decarbonylation and decarboxylation reactions, as well as for the enhanced formation of aromatics either via deoxygenation of the phenolics or via aromatization of the small alkenes C2= and C3= formed initially via thermal or catalytic cracking (Mullen and Boateng, 2010; Ma et al., 2012; Ben and Ragauskas, 2013; Wang et al., 2014). The amount and strength of

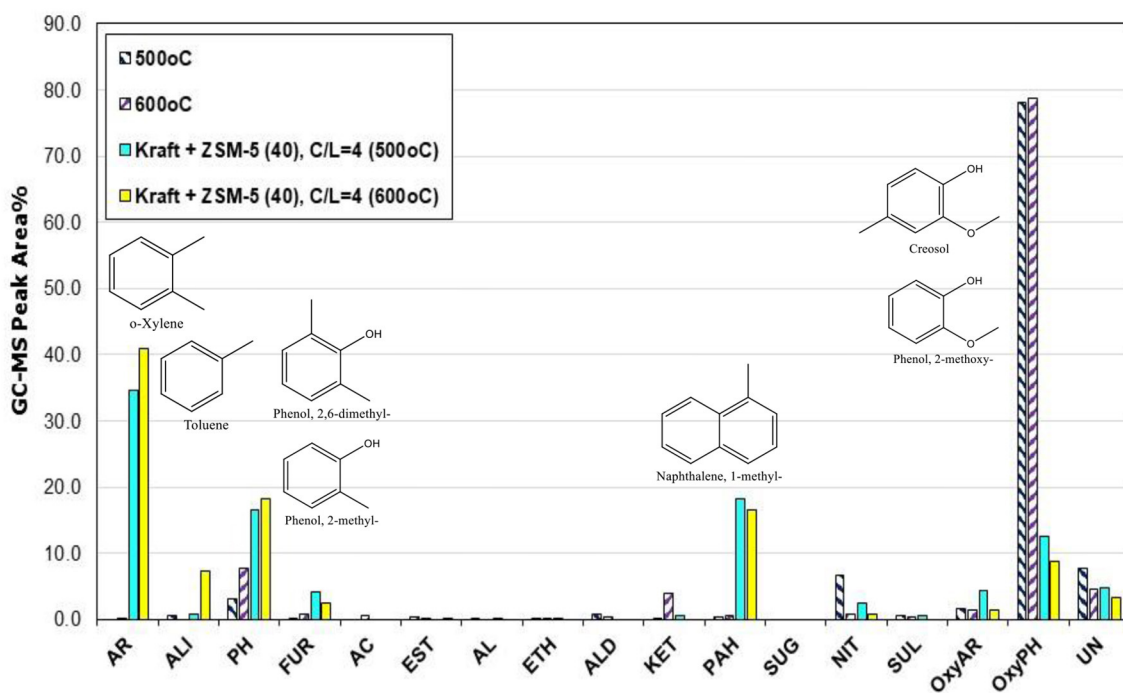


FIGURE 6 | Relative concentration of the various groups of compounds in the bio-oils derived by catalytic fast pyrolysis (CFP) of kraft lignin with ZSM-5(40) zeolite at two temperatures (500 and 600°C) and catalyst-to-lignin (C/L) ratio of 4; indicated compounds in the graph refer to the experiment at 600°C.

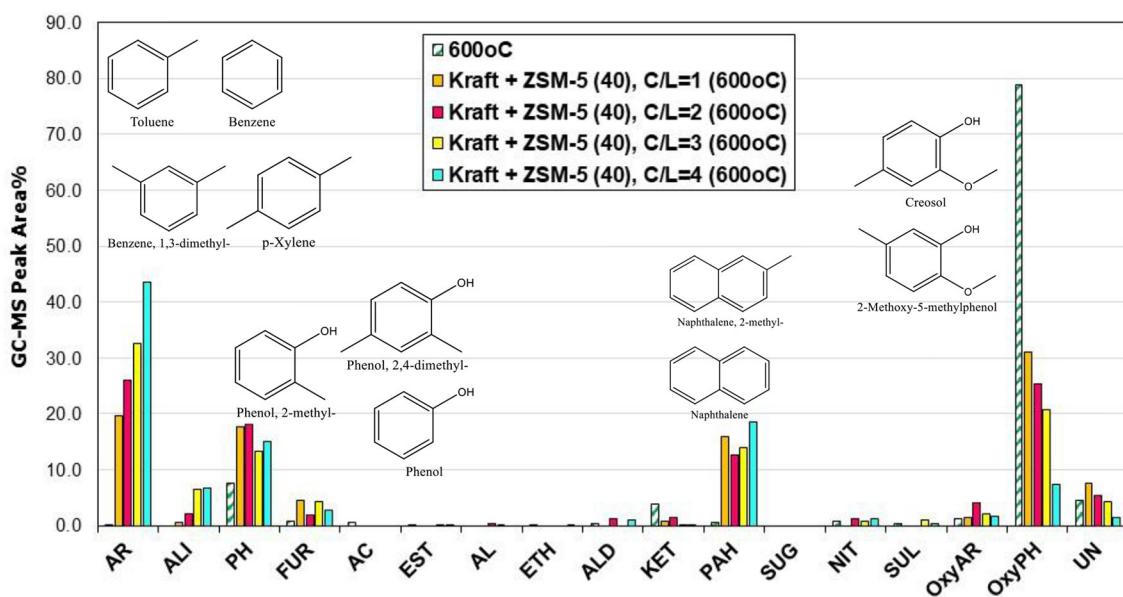


FIGURE 7 | Relative concentration of the various groups of compounds in the bio-oils derived by catalytic fast pyrolysis (CFP) of kraft lignin with ZSM-5(40) zeolite at 600°C and at different catalyst-to-lignin (C/L) ratios of 1, 2, 3, and 4; indicated compounds in the graph refer to the experiment at C/B = 4.

acid sites, in combination with the specific micropore framework structure of each zeolite type, have a pronounced effect on the reactions that occur during the pyrolysis process and the final product yields and bio-oil composition. For this reason,

we investigated the effect of Si/Al ratio (11.5, 25, and 40) of ZSM-5 zeolite on the composition of bio-oil via the Py/GC-MS lignin pyrolysis tests. Many studies suggested that when the Si/Al ratios of ZSM-5 decreased and the amount of acid sites

was increased (due to higher aluminum content), the yields of phenolics and other oxygenates progressively declined, while the yields of aromatics increased substantially (Li et al., 2012; Ma et al., 2012; Yu et al., 2012). In the present work, we examined the effect of Si/Al ratio of ZSM-5 at 600°C and at two C/L ratios, i.e., 2 and 4. The relative concentration of the various groups of compounds produced is shown in **Figure 8**. At C/L = 2 all three ZSM-5 zeolites induced a similar conversion/decrease of alkoxy-phenols, while the ZSM-5(11.5) sample with the higher content of Brønsted acid sites (**Table 2**) exhibited an enhanced formation of aromatics and some aliphatics (mainly azulene) compared to the other two ZSM-5's, in accordance with the previous works. However, when using higher amount of catalyst (C/L = 4), the ZSM-5(25) and especially the ZSM-5(40) zeolite were more reactive in converting the alkoxy-phenols toward mono-aromatics as well as alkyl-phenols compared to ZSM-5(11.5). This indicates the beneficial effect of using higher amount of Brønsted acid sites of higher strength, since ZSM-5(40) possessed fewer but relatively stronger acid sites compared to ZSM-5(11.5), as can be revealed by the FT-IR/sorbed pyridine measurements at increasing pyridine equilibration temperature, i.e., 150–450°C (data shown in Figure S4, Supplementary Material). Thus, it can be suggested that the bio-oil can be enriched in mono-aromatics and alkyl-phenols when higher amount of ZSM-5 zeolite (higher C/L ratio) with relatively high Si/Al ratio (ca. 40) and fewer but stronger acid sites is used. The effect of Si/Al ratio of ZSM-5 on the most important groups of compounds in bio-oil is more clearly presented in **Figure 9**.

Catalytic Fast Pyrolysis of Lignin With Conventional Microporous, Nano-Sized and Mesoporous ZSM-5 Zeolites (Py/GC-MS System)

The effect of porous characteristics and crystal/particle size of ZSM-5 zeolite on the composition of bio-oil was investigated by using the most reactive (based on the above comparisons) conventional microporous ZSM-5(40) zeolite, a synthesized nano-sized ZSM-5, and a mesoporous ZSM-5 prepared via alkaline treatment of the ZSM-5(40) zeolite. The aluminum content (and Si/Al ratio) of all three zeolites was similar (**Table 2**); however, they differed in the amount of acid sites as the nano-sized zeolite contained almost half Brønsted acid sites compared to the other two zeolites. Considering also its relatively higher amount of Lewis acid sites, this can be attributed to incomplete crystallization of this zeolite, despite the clear and strong reflections shown in its XRD pattern (**Figure 3**). The Py/GC-MS lignin pyrolysis results (at 600°C and C/L = 4) with the three zeolites are shown in **Figure 10**. All catalysts were very reactive in converting the alkoxy-phenols toward mono-aromatics, naphthalenes (PAHs) and alkyl-phenols. Interestingly, the nano-sized ZSM-5, despite its significantly lower amount of Brønsted acid sites, exhibited similar reactivity/performance compared to the other two zeolites, thus proving the beneficial effect of the higher accessibility of this zeolite due to its small crystal/particle size and the high textural/interparticle porosity (**Table 2**, **Figures 3, 4**). However, the char/coke production by the nano-sized zeolite was higher (about 33.4 wt.%) compared to that by the microporous ZSM-5(40) zeolite (28.1 wt.%) (data

shown in Table S4), thus indicating that condensation and polymerization reactions of mono-aromatics or phenolics are facilitated on the acid sites located in the intra-particle voids (high textural porosity of nano-sized ZSM-5). Similar trends of increased char/coke production by the use of nano-sized ZSM-5 with ca. <100 nm crystal size, have been observed in catalytic pyrolysis of lignocellulosic biomass (Zheng et al., 2014; Gamliel et al., 2016).

The mesoporous ZSM-5 (9 nm) zeolite prepared by mild alkaline treatment, possessed similar acidic properties with the parent ZSM-5(40) zeolite (**Table 2**) and its performance in the pyrolysis of lignin was very promising. More specifically, as can be seen in **Figure 10**, it exhibited the highest reactivity in converting the alkoxy-phenols, the highest concentration of alkyl-phenols (phenol, 2-methyl-phenol, 3-methyl-phenol, 2,5-dimethyl-phenol, etc.), slightly less mono-aromatics (benzene, toluene, 1,3-dimethyl-benzene, 1,2,4-trimethyl-benzene, etc.), as well as fewer PAHs (1-methyl-naphthalene, 2,6-dimethylnaphthalene, etc.). A possible reason for the lower formation of aromatics could be the reduction of its microporosity (with parallel increase of the mesoporosity) compared to the parent ZSM-5(40) zeolite, thus not promoting the aromatization reactions that take place on the Brønsted sites within the tubular micropores of ZSM-5. Interestingly, the char/coke produced by the mesoporous ZSM-5 (9 nm) zeolite (30.3%) was less compared to that with the nano-sized ZSM-5 (33.4%) and closer to that with the parent microporous ZSM-5(40) (28.1%) (Table S3). Previous works on biomass or lignin fast pyrolysis have reported either increased (Park et al., 2010; Foster et al., 2012) or decreased (Kelkar et al., 2014; Li et al., 2014; Gamliel et al., 2016) char/coke formation by the use of mesoporous ZSM-5 zeolites compared to conventional microporous ZSM-5. However, a general trend is difficult to be established as coking depends on pyrolysis temperature, mesopore width and acidic properties, catalyst to biomass/lignin ratio, type of feedstock and type of experimental set-up (micro-pyrolyzer vs. bench scale fixed bed units, etc.), as discussed also below.

Non-catalytic and Catalytic Fast Pyrolysis of Kraft Lignin (Fixed-Bed Unit)

The three ZSM-5 zeolites, i.e., the conventional microporous ZSM-5(40), the nano-sized ZSM-5 and the mesoporous ZSM-5(9nm), were also evaluated in the fixed bed unit described in the experimental section and in Supplementary Material. The total liquids (bio-oil) yield in the non-catalytic test was 36.6 wt.% (6.1 wt.% being water and the remaining 30.6 wt.% comprising of organics), the non-condensable gases 14 wt.% and the solids (char) 42.4 wt.% (**Figure 11** and Table S5 in Supplementary Material). By the use of conventional microporous ZSM-5(40) zeolite, the total liquids yield decreased to 25.6 wt.%, due to significant decrease of the organic fraction (16.2 from 30.6 wt.% in the thermal bio-oil). The non-condensable gases and the solids (char plus coke on catalyst in this case) increased to 22.0 and 47.9 wt.%, respectively. The corresponding changes in yield values were slightly enhanced by the use of mesoporous ZSM-5(9 nm), while in the case of nano-sized ZSM-5, the total liquids were

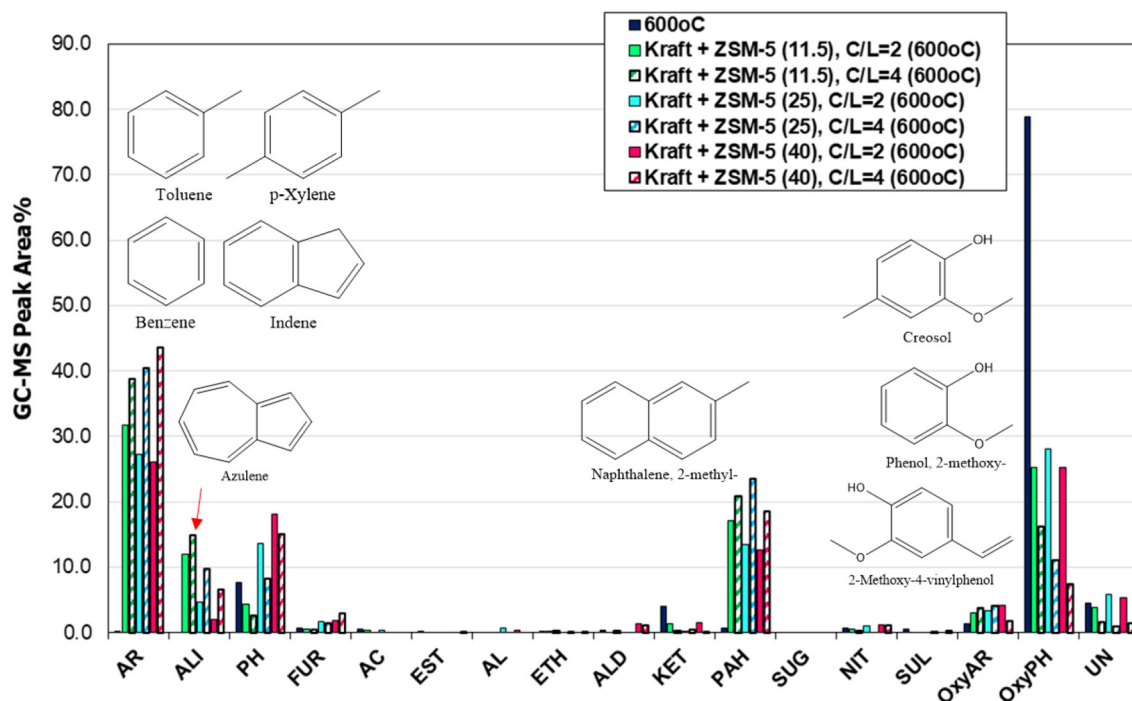


FIGURE 8 | Relative concentration of the various groups of compounds in the bio-oils derived by catalytic fast pyrolysis (CFP) of kraft lignin with ZSM-5 zeolites having different Si/Al ratio (11.5, 25, and 40) at 600°C and at different catalyst-to-lignin (C/L) ratios (2 and 4); indicated compounds in the graph are for ZSM-5 (11.5) at C/L = 4.

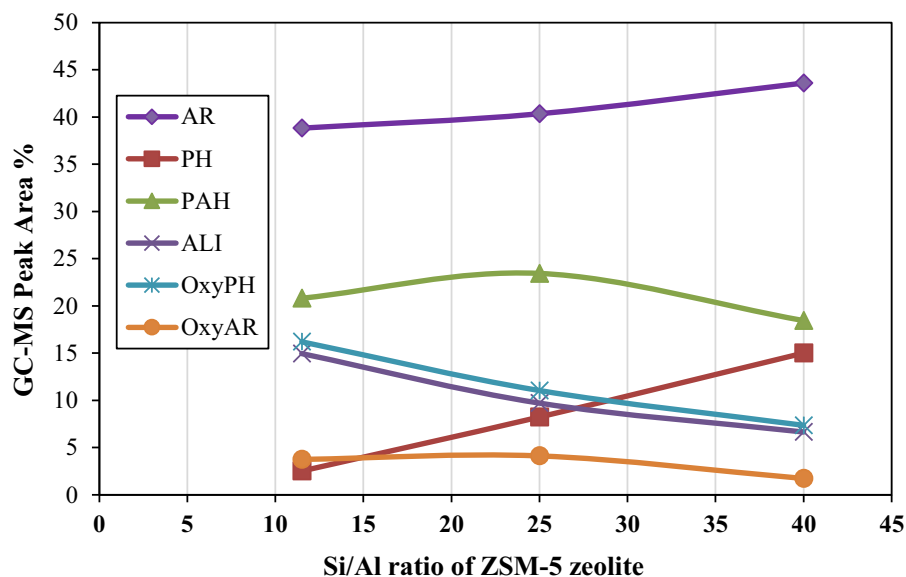


FIGURE 9 | Correlation between the Si/Al ratio of ZSM-5 zeolite with the relative concentration of the most representative groups of compounds in the bio-oil derived by catalytic fast pyrolysis (CFP) of kraft lignin at 600°C and C/L = 4 (AR, mono-aromatics; PH, phenol and alkyl-phenols; PAHs, polycyclic aromatic hydrocarbons; ALI, aliphatic hydrocarbons, OxyPH, oxygenated phenolics; OxyAR, oxygenated aromatics).

further reduced to 20.3 wt.% (the organic fraction dropped to 7.6 wt.%) and the gases and solids were even higher (26.4 and 49.9 wt.%, respectively). Similar changes in the product yields have

been previously reported by the use of conventional microporous or mesoporous ZSM-5 zeolites in biomass or lignin pyrolysis using fixed bed units where the initially formed biomass pyrolysis

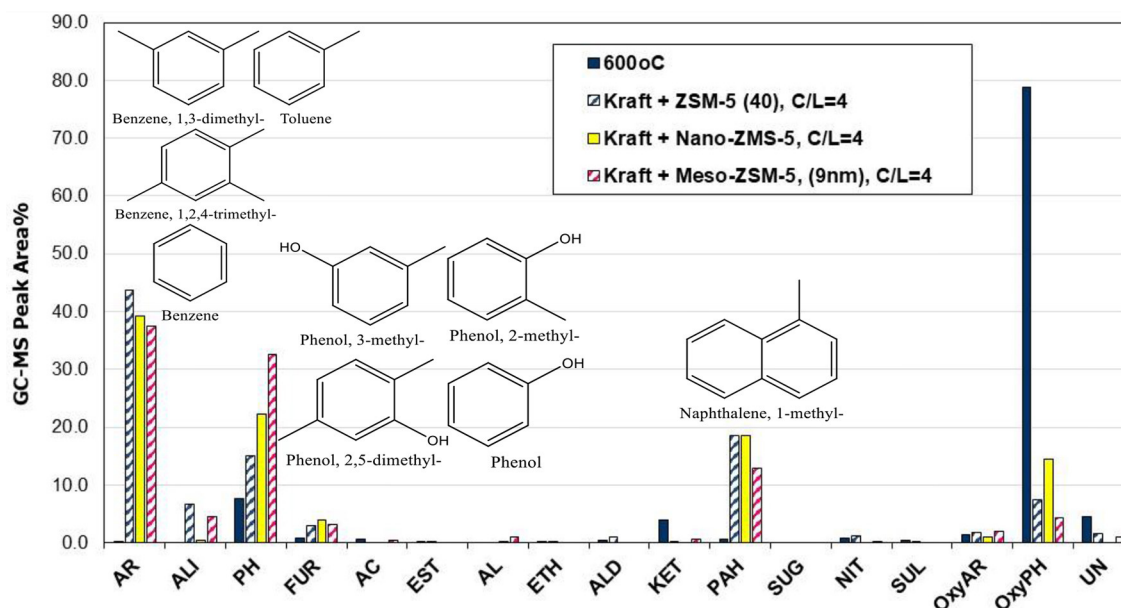


FIGURE 10 | Relative concentration of the various groups of compounds in the bio-oils derived by catalytic fast pyrolysis (CFP) of kraft lignin with conventional microporous, nano-sized and mesoporous ZSM-5 zeolites at 600°C and at catalyst-to-lignin C/L = 4; indicated compounds in the graph are for the mesoporous ZSM-5 (9 nm).

vapors reacted subsequently over the catalyst bed in the same reactor (Park et al., 2010; Stephanidis et al., 2011; Kalogiannis et al., 2015). On the other hand, in several studies based on micro-pyrolyzer systems either with tube (Ma et al., 2012; Custodis et al., 2016) or bucket (Mihalcik et al., 2011; Wang et al., 2014) form, the presence of the zeolite resulted in decrease of the solids (char plus coke) and in some cases increase of the bio-oil yield compared to the non-catalytic pyrolysis. In the present work, the Py/GC-MS experiments discussed in the previous section showed also a decrease of the solids formation upon use of either of the three ZSM-5 zeolites compared to the non-catalytic thermal pyrolysis (Table S4), in contrast to the results obtained from the fixed bed unit (Figure 11 and Table S5). However, the observed trend with regard to the effect of the type of ZSM-5 zeolite was the same for both experimental set-ups, i.e., the microporous ZSM-5(40) produced the lowest char plus coke and the nano-sized ZSM-5 the highest.

The increase of solids in the catalytic pyrolysis experiments is solely attributed to the coke formed on the catalysts, due to the design of the fixed bed reactor as described in the experimental section and in Supplementary Material. The data in Table S5 show that the formation of coke on the nano-ZSM-5 zeolite (7.7 wt.% on lignin) is clearly more pronounced compared to the conventional microporous ZSM-5 and the meso-ZSM-5(9 nm) (5.7 and 5.8 wt.% on lignin, respectively). The char derived from the thermal pyrolysis of lignin (as collected from the upper zone of the fixed bed reactor, Figure S2) and the coked catalysts (lower bed of the reactor, Figure S2), were further studied by thermogravimetric analysis (TGA); representative data are depicted in Figure S5 (Supplementary Material). It can

be clearly seen that the thermal char decomposes under oxidative (air) atmosphere at lower temperature (DTG peak maximum at ~465°C) compared to the reaction coke formed on the zeolitic catalysts (DTG peak maximum at ~560–570°C), indicating different structure/composition of these two, and possibly the more condensed/carbonaceous nature of the coke on catalyst. However, more detailed characterization of the char and coke on catalyst are necessary in order to better understand their nature and associated mechanisms of formation.

The analysis of non-condensable gases is presented in Figure 11. The use of all three ZSM-5 zeolite catalysts induced the production of ethane, ethylene, propane and propylene which were not produced by the non-catalytic pyrolysis. The production of these gases is indicative of enhanced cracking and dealkylation reactions catalyzed by ZSM-5 in accordance with its performance in biomass fast pyrolysis (Mullen and Boateng, 2010; Stephanidis et al., 2011; Wang et al., 2014; Margeriat et al., 2018). As discussed below, ethylene and propylene serve as precursors for the production of aromatics in the channels of ZSM-5. The more abundant gases both in non-catalytic and catalytic lignin pyrolysis are methane, CO and CO₂. With the use of the ZSM-5 zeolite catalysts both CO and CO₂ were significantly increased due to decarbonylation and decarboxylation reactions, with CO being affected/increased to a higher extent. This is also typically observed in biomass CFP where ZSM-5 favors the formation of CO instead of CO₂, as well as the formation of water via dehydration reactions (Stephanidis et al., 2011; Stefanidis et al., 2016).

The effect of the zeolite catalysts on bio-oil composition (Figure 12) was similar to that observed in the Py/GC-MS

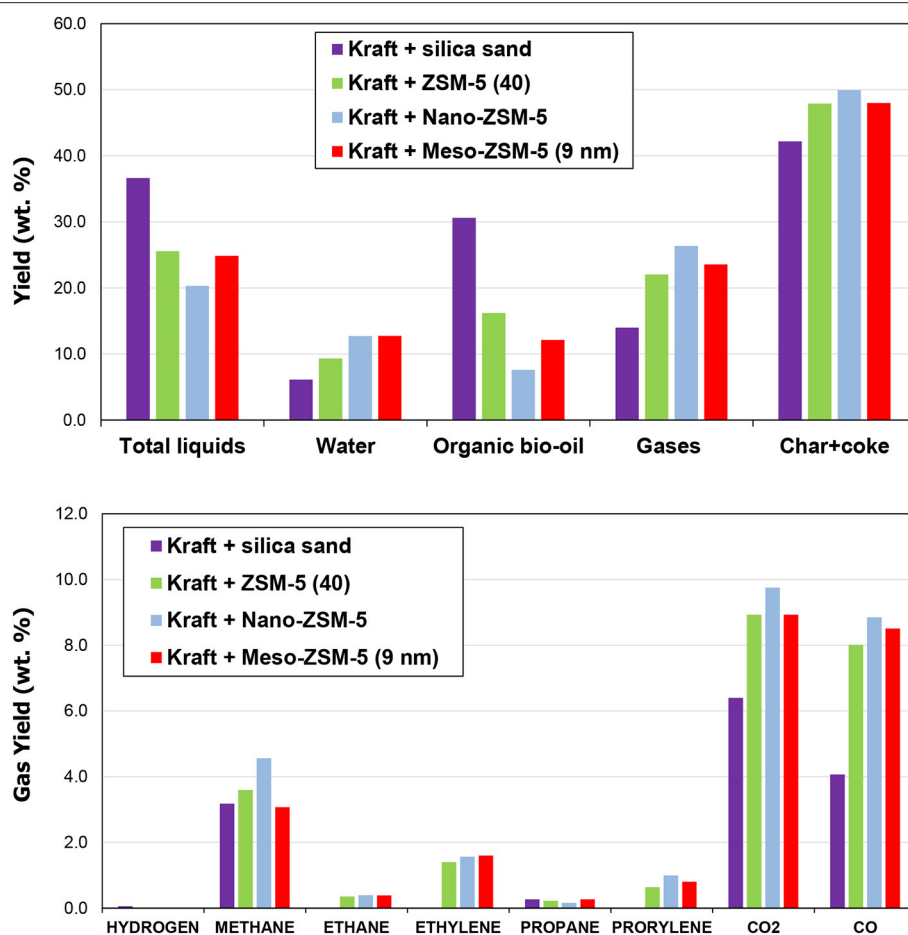


FIGURE 11 | Product yield distribution and gas analysis from the thermal and catalytic fast pyrolysis of kraft lignin (results from the fixed bed unit).

experiments (see results in previous section), although in the case of the fixed bed reactor the relative abundance between mono-aromatics and alkyl-phenols was in favor of the latter. More specifically, the conventional microporous ZSM-5(40) zeolite exhibited the highest selectivity toward aromatics formation, while the nano-sized ZSM-5 and especially the mesoporous ZSM-5(9nm) was more selective toward alkyl-phenols. These results are in line with the deoxygenation degree of the organic phase of bio-oil, as determined by elemental analysis, which was more pronounced by the use of the conventional ZSM-5 compared to the meso- and nano-ZSM-5 (Table S5, Supplementary Material). Nonetheless, all three ZSM-5 variants were quite effective in deoxygenating the bio-oil, inducing 50–60% reduction of oxygen compared to the oxygen of the thermal (non-catalytic) pyrolysis oil. However, it should be noted that the GC-MS analysis is capable of identifying only low molecular weight compounds and not bulkier oligomers usually present in thermal, non-catalytic bio-oils of biomass or lignin pyrolysis. Applying more advanced analytical techniques, such as 2DGC-ToFMS analysis, quantitative analysis of about 45% of the organic phase of lignin pyrolysis oil could be achieved, reaching as high as ~100%

for the bio-oil obtained by the use of ZSM-5 zeolite catalyst (Kalogiannis et al., 2015).

Both the thermal and catalytic bio-oils contained also small amounts of sulfur, i.e., <0.1 wt.% on lignin, thus indicating that most of the S of the parent kraft lignin (1.5 wt.%) has been “trapped” in the solids. Indeed, the elemental analysis of the thermal char and the coked catalysts showed the presence of about 0.3–0.6 wt.% S (Tables S5 and S6, Supplementary Material). Furthermore, sulfur in the gases (i.e., as H₂S) was only scarcely identified at very low concentrations.

Reaction Mechanism and Effect of ZSM-5 Characteristics

Based on the analysis of the 2D HSQC NMR spectra (discussed above), as well as previous works on lignin characterization, the β -O-4 ether bond is the main linkage between lignin units isolated from softwood lignocellulosic biomass (i.e., spruce) (Sette et al., 2011; Chu et al., 2013; Du et al., 2013; Liu et al., 2015; Constant et al., 2016; Rinaldi et al., 2016). The relatively intense pyrolysis conditions, i.e., 600°C, provide the necessary energy for the thermal cleavage of the β -O-4 and α -O-4 ether bonds, thus providing the smaller oligomers and monomers that

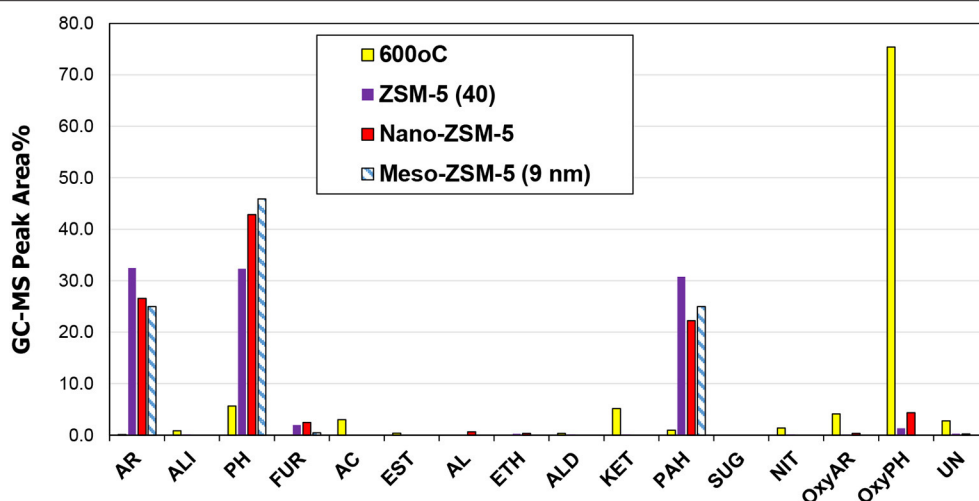


FIGURE 12 | Relative concentration of the various groups of compounds in the bio-oils derived by non catalytic and catalytic fast pyrolysis (CFP) of kraft lignin with conventional microporous, nano-sized and mesoporous ZSM-5 zeolites (fixed bed unit, 600°C, C/L = 1).

may react further on the acid sites of the zeolites (Figure 13). The non-catalytic Py/GC-MS results of the present work at different temperatures (400–600°C) revealed the formation of alkoxy-phenols with additional C2-C3 alkyl side chains as well as larger oligomers such as carinol (Figure 5 and Table S2). Thermal pyrolysis at higher temperatures, i.e., 600°C favored the formation of smaller alkoxy-phenols such as guaiacol, vanillin and creosol, as indicated in the mechanism of Figure 13. As suggested above and in accordance with previous studies, the alkoxy-phenols can re-polymerize toward char (thermal coke) but in the presence of the relatively strong Brønsted acidity of ZSM-5 zeolite they can undergo dehydration, decarbonylation, decarboxylation, dealkoxylation and cracking (C-C breaking) reactions, followed by enhanced formation of aromatics either via deoxygenation of the produced mono-phenolics or via aromatization of the small alkenes C2= and C3= formed initially via thermal or catalytic cracking or via dehydration of small intermediate alcohols (Mullen and Boateng, 2010; Ma et al., 2012; Yu et al., 2012; Ben and Ragauskas, 2013; Chu et al., 2013; Wang et al., 2014). All the above suggested pathways are depicted in the overall reaction mechanism shown in Figure 13.

The formation of ethylene and propylene has been verified in the present work by the use of ZSM-5 (Figure 11 and Table S4), thus supporting further the pathway of their aromatization toward mono-aromatics (Figure 13). These small alkenes may form via cracking of the C2/C3 side chains of the intermediate phenolics or via dehydration of intermediate small alcohols derived from the cleavage of the β -O-4 ether bonds (Ben and Ragauskas, 2013). The reactivity of ZSM-5 zeolite in the dealkoxylation of the primary produced alkoxy-phenols toward alkyl-phenols (as well as phenol via additional demethylation) was clearly shown by the results of the present work, both in the Py/GC-MS and in the fixed-bed reactor experiments. Interestingly, an inter-balance between aromatics and alkyl-phenols was observed, with the microporous ZSM-5(40) zeolite

shifting the balance toward aromatics while the nano-sized and mainly the mesoporous ZSM-5 favoring the alkyl-phenols. Preliminary tests on the catalytic pyrolysis of model compounds (i.e., guaiacol and vanillin) has shown that they are mainly converted to alkyl-phenols (especially with the mesoporous ZSM-5) with few aromatics being also formed. It can thus be suggested that the prevailing route for aromatics formation is that via aromatization of small alkenes. Furthermore, it is also evident that the conventional microporous ZSM-5(40) zeolite with a crystal size of $\sim 0.3\text{--}1\ \mu\text{m}$ exhibit higher aromatization activity compared to the nano-sized and mesoporous ZSM-5 zeolites, thus proving the beneficial combination of strong Brønsted acidity with the appropriate space confinement offered by the $\sim 5.5\text{ Å}$ channels of the MFI structure. On the other hand, the high textural porosity of the nano-sized ZSM-5 zeolite favors the subsequent polymerization of the initially formed mono-aromatics, thus resulting in higher coke yields and slightly reduced aromatics. The mesoporous ZSM-5 zeolite with an average mesopore width of $\sim 9\text{ nm}$ prepared by mild alkaline treatment, exhibits less polymerization and coking activity compared to nano-sized ZSM-5, being closer to the performance of conventional ZSM-5. The benefit however that is provided by the mesoporous ZSM-5 is the parallel high selectivity toward mono-aromatics and alkyl-phenols which can be attributed to the high mesopore volume and surface area that enhances the dealkoxylation of the relatively large alkoxy-phenols formed initially via thermal pyrolysis (Figure 13).

CONCLUSIONS

The thermal (non-catalytic) and catalytic fast pyrolysis (CFP) of lignin has been studied with emphasis on the effect of process parameters and type of ZSM-5 zeolite catalyst on the selectivity of phenolics and aromatics in the bio-oil. By combining the detailed characterization of the softwood kraft lignin used by



with regard to their effect on bio-oil composition while it further showed that the total liquids (bio-oil), gas and coke yields by the mesoporous ZSM-5 were similar to those of the microporous ZSM-5. However, water production was higher with the meso-ZSM-5, thus leading to lower yield of organic bio-oil. On the other hand, the nano-sized ZSM-5 produced less total liquids with substantially less organic phase and significantly higher non-condensable gases and coke on catalyst. The observed differences in the performance of the microporous, mesoporous and nano-sized ZSM-5 zeolites were attributed to reaction pathways that may occur during lignin pyrolysis, comprising of initial thermal depolymerization reactions (C-O cleavage of the ether bonds in lignin), cracking of the side chains and dealkylation of the intermediate larger alkoxy-phenols toward the production of small (C₂, C₃) alkenes that may then be converted to mono-aromatics on the strong Brønsted acid sites of ZSM-5 zeolite channels, dealkoxylation (C-O cleavage) of the all the initially formed alkoxy-phenols toward the corresponding alkyl-phenols and phenol, and the less favored dehydrogenation/dehydration (C-O cleavage of the phenyl-OH bond) toward (alkyl)benzenes. The overall reaction mechanism scheme is complemented by polymerization/condensation reactions, either thermally or catalyzed by the acid sites of ZSM-5, of mono-aromatics and PAHs to reaction coke as well as of alkoxy-phenols to thermal char.

REFERENCES

- Asikkala, J., Tamminen, T., and Argyropoulos, D. S. (2012). Accurate and reproducible determination of lignin molar mass by acetobromination. *J. Agric. Food Chem.* 60, 8968–8973. doi: 10.1021/jf303003d
- Azadi, P., Inderwildi, O. R., Farnood, R., and King, D. A. (2013). Liquid fuels, hydrogen and chemicals from lignin: a critical review. *Renew. Sustain. Energ. Rev.* 21, 506–523. doi: 10.1016/j.rser.2012.12.022
- Azeez, A. M., Meier, D., Odermatt, J., and Willner, T. (2010). Fast pyrolysis of African and European lignocellulosic biomasses using Py-GC/MS and fluidized bed reactor. *Energ. Fuels* 24, 2078–2085. doi: 10.1021/ef9012856
- Barta, K., Warner, G. R., Beach, E. S., and Anastas, P. T. (2014). Depolymerization of organosolv lignin to aromatic compounds over Cu-doped porous metal oxides. *Green Chem.* 16, 191–196. doi: 10.1039/C3GC41184B
- Beckham, G. T., Johnson, C. W., Karp, E. M., Salvachúa, D., and Vardon, D. R. (2016). Opportunities and challenges in biological lignin valorization. *Curr. Opin. Biotechnol.* 42, 40–53. doi: 10.1016/j.copbio.2016.02.030
- Ben, H., and Ragauskas, A. J. (2013). Influence of Si/Al Ratio of ZSM-5 zeolite on the properties of lignin pyrolysis products. *ACS Sustain. Chem. Eng.* 1, 316–324. doi: 10.1021/sc300074n
- Bui, V. N., Laurenti, D., Afanasiev, P., and Geantet, C. (2011). Hydrodeoxygenation of guaiacol with CoMo catalysts. Part I: promoting effect of cobalt on HDO selectivity and activity. *Appl. Catal. B Environ.* 101, 239–245. doi: 10.1016/j.apcatb.2010.10.025
- Chakar, F. S., and Ragauskas, A. J. (2004). Review of current and future softwood kraft lignin process chemistry. *Ind. Crops Prod.* 20, 131–141. doi: 10.1016/j.indcrop.2004.04.016
- Chen, J., Liu, C., Wu, S., Liang, J., and Lei, M. (2016). Enhancing the quality of bio-oil from catalytic pyrolysis of kraft black liquor lignin. *RSC Adv.* 6, 107970–107976. doi: 10.1039/C6RA18923G
- Choi, M., Cho, H. S., Srivastava, R., Venkatesan, C., Choi, D.-H., and Ryoo, R. (2006). Amphiphilic organosilane-directed synthesis of crystalline zeolite with tunable mesoporosity. *Nat. Mater.* 5:718. doi: 10.1038/nmat1705
- Chu, S., Subrahmanyam, A. V., and Huber, G. W. (2013). The pyrolysis chemistry of a [small beta]-O-4 type oligomeric lignin model compound. *Green Chem.* 15, 125–136. doi: 10.1039/C2GC36332A
- Constant, S., Wienk, H. L. J., Frissen, A. E., Peinder, P., Boelens, R., van Es, D. S., et al. (2016). New insights into the structure and composition of technical lignins: a comparative characterisation study. *Green Chem.* 18, 2651–2665. doi: 10.1039/C5GC03043A
- Crestini, C., Lange, H., Sette, M., and Argyropoulos, D. S. (2017). On the structure of softwood kraft lignin. *Green Chem.* 19, 4104–4121. doi: 10.1039/C7GC01812F
- Custodis, V. B. F., Karakoulia, S. A., Triantafyllidis, K. S., and van Bokhoven, J. A. (2016). Catalytic fast pyrolysis of lignin over high-surface-area mesoporous aluminosilicates: effect of porosity and acidity. *ChemSusChem* 9, 1134–1145. doi: 10.1002/cssc.201600105
- de Souza, P. M., Rabelo-Neto, R. C., Borges, L. E. P., Jacobs, G., Davis, B. H., Resasco, D. E., et al. (2017). Hydrodeoxygenation of Phenol over Pd Catalysts. Effect of support on reaction mechanism and catalyst deactivation. *ACS Catal.* 7, 2058–2073. doi: 10.1021/acscatal.6b02022
- del Río, J. C., Rencoret, J., Marques, G., Li, J., Gellerstedt, G., Jiménez-Barbero, J., et al. (2009). Structural characterization of the lignin from jute (*Corchorus capsularis*) fibers. *J. Agric. Food Chem.* 57, 10271–10281. doi: 10.1021/jf900815x
- Dominguez-Robles, J., Espinosa, E., Savy, D., Rosal, A., and Rodriguez, A. (2016). Biorefinery process combining specel® process and selective lignin precipitation using mineral acids. *BioRes.* 11, 7061–7077. doi: 10.15376/biores.11.3.7061-7077
- Du, L., Wang, Z., Li, S., Song, W., and Lin, W. (2013). A comparison of monomeric phenols produced from lignin by fast pyrolysis and hydrothermal conversions. *Int. J. Chem. React. Eng.* 11, 135–145. doi: 10.1515/ijcre-2012-0085
- Elfadly, A. M., Zeid, I. F., Yehia, F. Z., Rabie, A. M., aboualala, M. M., and Park, S. E. (2016). Highly selective BTX from catalytic fast pyrolysis of lignin over supported mesoporous silica. *Int. J. Biol. Macromol.* 91, 278–293. doi: 10.1016/j.ijbiomac.2016.05.053

AUTHOR CONTRIBUTIONS

PL conducted the experimental work (catalyst preparation and characterization, lignin characterization, pyrolysis tests, analysis of results) and drafted the manuscript. AF contributed in lignin analysis by NMR and in manuscript proof reading. SK contributed in catalysts preparation and characterization. KT organized and coordinated the research and experimental work and reviewed the final version of the manuscript.

ACKNOWLEDGMENTS

This research has been co-financed by the European Union (European Social Fund) and Greek national funds through the Operational Program Education and Lifelong Learning of the National Strategic Reference Framework (NSRF)—Action: Aristeia II (project 4778). The authors would also like to acknowledge the contribution of COST Action FP1306 for supporting the dissemination of the results and for promoting collaboration with other European groups working in this topic.

SUPPLEMENTARY MATERIAL

The Supplementary Material for this article can be found online at: <https://www.frontiersin.org/articles/10.3389/fchem.2018.00295/full#supplementary-material>

- Emeis, C. A. (1993). Determination of integrated molar extinction coefficients for infrared absorption bands of pyridine adsorbed on solid acid catalysts. *J. Catal.* 141, 347–354. doi: 10.1006/jcat.1993.1145
- Fermoso, J., Hernando, H., Jana, P., Moreno, I., Prech, J., Ochoa-Hernández, C., et al. (2016). Lamellar and pillared ZSM-5 zeolites modified with MgO and ZnO for catalytic fast-pyrolysis of eucalyptus woodchips. *Catal. Today* 277, 171–181. doi: 10.1016/j.cattod.2015.12.009
- Foster, A. J., Jae, J., Cheng, Y.-T., Huber, G. W., and Lobo, R. F. (2012). Optimizing the aromatic yield and distribution from catalytic fast pyrolysis of biomass over ZSM-5. *Appl. Catal. A Gen.* 423–424, 154–161. doi: 10.1016/j.apcata.2012.02.030
- Fox, S. C., and McDonald, A. G. (2010). Chemical and thermal characterization of three industrial lignins and their corresponding lignin esters. *Biores.* 5, 990–1009.
- Gamliel, D. P., Cho, H. J., Fan, W., and Valla, J. A. (2016). On the effectiveness of tailored mesoporous MFI zeolites for biomass catalytic fast pyrolysis. *Appl. Catal. A Gen.* 522, 109–119. doi: 10.1016/j.apcata.2016.04.026
- Gayubo, A. G., Aguayo, A. T., Atutxa, A., Aguado, R., and Bilbao, J. (2004). Transformation of oxygenate components of biomass pyrolysis oil on a HZSM-5 zeolite. I. Alcohols and Phenols. *Indust. Eng. Chem. Res.* 43, 2610–2618. doi: 10.1021/ie030791o
- Groen, J. C., Moulijn, J. A., and Perez-Ramirez, J. (2006). Desilication: on the controlled generation of mesoporosity in MFI zeolites. *J. Mater. Chem.* 16, 2121–2131. doi: 10.1039/B517510K
- Heikkinen, S., Toikka, M. M., Karhunen, P. T., and Kilpeläinen, I. A. (2003). Quantitative 2D HSQC (Q-HSQC) via suppression of j -dependence of polarization transfer in NMR spectroscopy: application to wood lignin. *J. Am. Chem. Soc.* 125, 4362–4367. doi: 10.1021/ja029035k
- Huber, G. W., Iborra, S., and Corma, A. (2006). Synthesis of transportation fuels from biomass: chemistry, catalysts, and engineering. *Chem. Rev.* 106, 4044–4098. doi: 10.1021/cr068360d
- Iliopoulou, E. F., Antonakou, E. V., Karakoulia, S. A., Vasalos, I. A., Lappas, A. A., and Triantafyllidis, K. S. (2007). Catalytic conversion of biomass pyrolysis products by mesoporous materials: effect of steam stability and acidity of Al-MCM-41 catalysts. *Chem. Eng. J.* 134, 51–57. doi: 10.1016/j.cej.2007.03.066
- Iliopoulou, E. F., Lazaridis, P. A., and Triantafyllidis, K. S. (2017). “Nanocatalysis in the fast pyrolysis of lignocellulosic biomass,” in *Nanotechnology in Catalysis*, ed M. Van de Voorde (Weinheim: Wiley-VCH Verlag GmbH & Co. KGaA), 655–714.
- Isikgor, F. H., and Becer, C. R. (2015). Lignocellulosic biomass: a sustainable platform for the production of bio-based chemicals and polymers. *Polym. Chem.* 6, 4497–4559. doi: 10.1039/C5PY00263J
- Jackson, M. A., Compton, D. L., and Boateng, A. A. (2009). Screening heterogeneous catalysts for the pyrolysis of lignin. *J. Anal. Appl. Pyrolysis* 85, 226–230. doi: 10.1016/j.jaap.2008.09.016
- Jae, J., Tompsett, G. A., Foster, A. J., Hammond, K. D., Auerbach, S. M., Lobo, R. F., et al. (2011). Investigation into the shape selectivity of zeolite catalysts for biomass conversion. *J. Catal.* 279, 257–268. doi: 10.1016/j.jcat.2011.01.019
- Jiang, G., Nowakowski, D. J., and Bridgwater, A. V. (2010). Effect of the temperature on the composition of lignin pyrolysis products. *Energ. Fuels* 24, 4470–4475. doi: 10.1021/ef100363c
- Jin, S., Xiao, Z., Li, C., Chen, X., Wang, L., Xing, J., et al. (2014). Catalytic hydrodeoxygenation of anisole as lignin model compound over supported nickel catalysts. *Catal. Today* 234, 125–132. doi: 10.1016/j.cattod.2014.02.014
- Kalogiannis, K. G., Stefanidis, S. D., Michailof, C. M., Lappas, A. A., and Sjöholm, E. (2015). Pyrolysis of lignin with 2DGC quantification of lignin oil: effect of lignin type, process temperature and ZSM-5 *in situ* upgrading. *J. Anal. Appl. Pyrolysis* 115, 410–418. doi: 10.1016/j.jaap.2015.08.021
- Kang, S., Xiao, L., Meng, L., Zhang, X., and Sun, R. (2012). Isolation and structural characterization of lignin from cotton stalk treated in an ammonia hydrothermal system. *Int. J. Mol. Sci.* 13, 15209–15226. doi: 10.3390/ijms131115209
- Kelkar, S., Saffron, C. M., Li, Z., Kim, S.-S., Pinnavaia, T. J., Miller, D. J., et al. (2014). Aromatics from biomass pyrolysis vapour using a bifunctional mesoporous catalyst. *Green Chem.* 16, 803–812. doi: 10.1039/C3GC41350K
- Kim, S.-S., Lee, H. W., Ryoo, R., Kim, W., Park, S. H., Jeon, J.-K., et al. (2014). Conversion of kraft lignin over hierarchical MFI zeolite. *J. Nanosci. Nanotechnol.* 14, 2414–2418. doi: 10.1166/jnn.2014.8545
- Komvokis, V. G., Karakoulia, S., Iliopoulou, E. F., Papapetrou, M. C., Vasalos, I. A., Lappas, A. A., et al. (2012). Upgrading of Fischer–Tropsch synthesis bio-waxes via catalytic cracking: effect of acidity, porosity and metal modification of zeolitic and mesoporous aluminosilicate catalysts. *Catal. Today* 196, 42–55. doi: 10.1016/j.cattod.2012.06.029
- Kordouli, E., Kordulis, C., Lycourghiotis, A., Cole, R., Vasudevan, P. T., Pawelec, B., et al. (2017). HDO activity of carbon-supported Rh, Ni and Mo–Ni catalysts. *Mol. Catal.* 441, 209–220. doi: 10.1016/j.mcat.2017.08.013
- Laurent, E., and Delmon, B. (1994). Study of the hydrodeoxygenation of carbonyl, carboxylic and guaiacyl groups over sulfided CoMo/ γ -Al₂O₃ and NiMo/ γ -Al₂O₃ catalyst. *Appl. Catal. A Gen.* 109, 97–115. doi: 10.1016/0926-860X(94)85005-4
- Lee, H. W., Kim, T. H., Park, S. H., Jeon, J. K., Suh, D. J., and Park, Y. K. (2013). Catalytic fast pyrolysis of lignin over mesoporous Y zeolite using Py-GC/MS. *J. Nanosci. Nanotechnol.* 13, 2640–2646. doi: 10.1166/jnn.2013.7421
- Lee, W.-S., Wang, Z., Wu, R. J., and Bhan, A. (2014). Selective vapor-phase hydrodeoxygenation of anisole to benzene on molybdenum carbide catalysts. *J. Catal.* 319, 44–53. doi: 10.1016/j.jcat.2014.07.025
- Li, C., Zhao, X., Wang, A., Huber, G. W., and Zhang, T. (2015). Catalytic transformation of lignin for the production of chemicals and fuels. *Chem. Rev.* 115, 11559–11624. doi: 10.1021/acs.chemrev.5b00155
- Li, J., Li, X., Zhou, G., Wang, W., Wang, C., Komarneni, S., et al. (2014). Catalytic fast pyrolysis of biomass with mesoporous ZSM-5 zeolites prepared by desilication with NaOH solutions. *Appl. Catal. A Gen.* 470, 115–122. doi: 10.1016/j.apcata.2013.10.040
- Li, X., Su, L., Wang, Y., Yu, Y., Wang, C., Li, X., et al. (2012). Catalytic fast pyrolysis of Kraft lignin with HZSM-5 zeolite for producing aromatic hydrocarbons. *Front. Environ. Sci. Eng.* 6, 295–303. doi: 10.1007/s11783-012-0410-2
- Liu, F., Liu, Q., Wang, A., and Zhang, T. (2016). Direct catalytic hydrogenolysis of kraft lignin to phenols in choline-derived ionic liquids. *ACS Sustain. Chem. Eng.* 4, 3850–3856. doi: 10.1021/acssuschemeng.6b00620
- Liu, W.-J., Jiang, H., and Yu, H.-Q. (2015). Thermochemical conversion of lignin to functional materials: a review and future directions. *Green Chem.* 17, 4888–4907. doi: 10.1039/C5GC01054C
- Lora, J. H., and Glasser, W. G. (2002). Recent industrial applications of lignin: a sustainable alternative to nonrenewable materials. *J. Polym. Environ.* 10, 39–48. doi: 10.1023/a:1021070006895
- Ma, Z., Troussard, E., and van Bokhoven, J. A. (2012). Controlling the selectivity to chemicals from lignin via catalytic fast pyrolysis. *Appl. Catal. A Gen.* 423, 130–136. doi: 10.1016/j.apcata.2012.02.027
- Margeri, A., Bouzeggane, A., Lorentz, C., Laurenti, D., Guilhaume, N., Mirodatos, C., et al. (2018). Catalytic conversion of beech wood pyrolytic vapors. *J. Anal. Appl. Pyrolysis* 130, 149–158. doi: 10.1016/j.jaap.2018.01.015
- Mihalcik, D. J., Mullen, C. A., and Boateng, A. A. (2011). Screening acidic zeolites for catalytic fast pyrolysis of biomass and its components. *J. Anal. Appl. Pyrolysis* 92, 224–232. doi: 10.1016/j.jaap.2011.06.001
- Minu, K., Jiby, K. K., and Kishore, V. V. N. (2012). Isolation and purification of lignin and silica from the black liquor generated during the production of bioethanol from rice straw. *Biomass Bioenerg.* 39, 210–217. doi: 10.1016/j.biombioe.2012.01.007
- Molinari, V., Clavel, G., Graglia, M., Antonietti, M., and Esposito, D. (2016). Mild continuous hydrogenolysis of kraft lignin over titanium nitride–nickel catalyst. *ACS Catal.* 6, 1663–1670. doi: 10.1021/acscatal.5b01926
- Mortensen, P. M., Grunwaldt, J.-D., Jensen, P. A., and Jensen, A. D. (2013). Screening of catalysts for hydrodeoxygenation of phenol as a model compound for bio-oil. *ACS Catal.* 3, 1774–1785. doi: 10.1021/cs400266e
- Mosier, N., Wyman, C., Dale, B., Elander, R., Lee, Y. Y., Holtzapfel, M., et al. (2005). Features of promising technologies for pretreatment of lignocellulosic biomass. *Bioresour. Technol.* 96, 673–686. doi: 10.1016/j.biortech.2004.06.025
- Mullen, C. A., and Boateng, A. A. (2010). Catalytic pyrolysis-GC/MS of lignin from several sources. *Fuel Process. Technol.* 91, 1446–1458. doi: 10.1016/j.fuproc.2010.05.022
- Onwudili, J. A., and Williams, P. T. (2014). Catalytic depolymerization of alkali lignin in subcritical water: influence of formic acid and Pd/C catalyst on the yields of liquid monomeric aromatic products. *Green Chem.* 16, 4740–4748. doi: 10.1039/C4GC00854E
- Opris, C., Cojocaru, B., Gheorghe, N., Tudorache, M., Coman, S. M., Parvulescu, V. I., et al. (2017). Lignin fragmentation onto multifunctional Fe₃O₄@Nb₂O₅@Co@Re catalysts: the role of the composition and deposition route of rhenium. *ACS Catal.* 7, 3257–3267. doi: 10.1021/acscatal.6b02915

- Pandey, M. P., and Kim, C. S. (2011). Lignin depolymerization and conversion: a review of thermochemical methods. *Chem. Eng. Technol.* 34, 29–41. doi: 10.1002/ceat.201000270
- Park, D. H., Kim, S. S., Wang, H., Pinnavaia, T. J., Papapetrou, M. C., Lappas, A. A., et al. (2009). Selective petroleum refining over a zeolite catalyst with small intracrystal mesopores. *Angewandte Chemie Int. Edition* 48, 7645–7648. doi: 10.1002/anie.200901551
- Park, H. J., Heo, H. S., Jeon, J.-K., Kim, J., Ryoo, R., Jeong, K.-E., et al. (2010). Highly valuable chemicals production from catalytic upgrading of radiata pine sawdust-derived pyrolytic vapors over mesoporous MFI zeolites. *Appl. Catal. B Environ.* 95, 365–373. doi: 10.1016/j.apcatb.2010.01.015
- Patwardhan, P. R., Brown, R. C., and Shanks, B. H. (2011). Understanding the Fast Pyrolysis of Lignin. *ChemSusChem* 4, 1629–1636. doi: 10.1002/cssc.201100133
- Ragauskas, A. J., Beckham, G. T., Biddy, M. J., Chandra, R., Chen, F., Davis, M. F., et al. (2014). Lignin valorization: improving lignin processing in the biorefinery. *Science* 344:1246843. doi: 10.1126/science.1246843
- Ralph, S. A., Ralph, J., and Larry, L. L. (2009). NMR database of lignin and cell wall model compounds. Available online at: www.glbrc.org/databases_and_software/nmrdatabase/
- Rinaldi, R., Jastrzebski, R., Clough, M. T., Ralph, J., Kennema, M., Bruijninx, P. C. A., et al. (2016). Paving the way for lignin valorisation: recent advances in bioengineering, biorefining and catalysis. *Angewandte Chemie Int. Edition* 55, 8164–8215. doi: 10.1002/anie.201510351
- Ryymin, E.-M., Honkela, M. L., Viljava, T.-R., and Krause, A. O. I. (2010). Competitive reactions and mechanisms in the simultaneous HDO of phenol and methyl heptanoate over sulphided NiMo/ γ -Al₂O₃. *Appl. Catal. A Gen.* 389, 114–121. doi: 10.1016/j.apcata.2010.09.010
- Sergeev, A. G., and Hartwig, J. F. (2011). Selective, nickel-catalyzed hydrogenolysis of aryl ethers. *Science* 332, 439–443. doi: 10.1126/science.1200437
- Sette, M., Wechselberger, R., and Crestini, C. (2011). Elucidation of lignin structure by quantitative 2D NMR. *Chem. A Eur. J.* 17, 9529–9535. doi: 10.1002/chem.201003045
- Setua, D. K., Shukla, M. K., Nigam, V., Singh, H., and Mathur, G. N. (2000). Lignin reinforced rubber composites. *Polymer Comp.* 21, 988–995. doi: 10.1002/pc.10252
- Silva, E. A. B. d., Zabkova, M., Araújo, J. D., Cateto, C. A., Barreiro, M. F., Belgacem, M. N., et al. (2009). An integrated process to produce vanillin and lignin-based polyurethanes from Kraft lignin. *Chem. Eng. Res. Des.* 87, 1276–1292. doi: 10.1016/j.cherd.2009.05.008
- Stefanidis, S. D., Kalogiannis, K. G., Iliopoulou, E. F., Michailof, C. M., Pilavachi, P. A., and Lappas, A. A. (2014). A study of lignocellulosic biomass pyrolysis via the pyrolysis of cellulose, hemicellulose and lignin. *J. Anal. Appl. Pyrolysis* 105, 143–150. doi: 10.1016/j.jaap.2013.10.013
- Stefanidis, S. D., Karakoulia, S. A., Kalogiannis, K. G., Iliopoulou, E. F., Delimitis, A., Yiannoulakis, H., et al. (2016). Natural magnesium oxide (MgO) catalysts: a cost-effective sustainable alternative to acid zeolites for the *in situ* upgrading of biomass fast pyrolysis oil. *Appl. Catal. B Environ.* 196, 155–173. doi: 10.1016/j.apcatb.2016.05.031
- Stephanidis, S., Nitsos, C., Kalogiannis, K., Iliopoulou, E. F., Lappas, A. A., and Triantafyllidis, K. S. (2011). Catalytic upgrading of lignocellulosic biomass pyrolysis vapours: effect of hydrothermal pre-treatment of biomass. *Catal. Today* 167, 37–45. doi: 10.1016/j.cattod.2010.12.049
- Strassberger, Z., Tanase, S., and Rothenberg, G. (2014). The pros and cons of lignin valorisation in an integrated biorefinery. *RSC Adv.* 4, 25310–25318. doi: 10.1039/C4RA04747H
- Suhas, Carrott, P. J. and Ribeiro Carrott, M. M. (2007). Lignin – from natural adsorbent to activated carbon: a review. *Bioresour. Technol.* 98, 2301–2312. doi: 10.1016/j.biortech.2006.08.008
- Thommes, M., Kaneko, K., Neimark Alexander, V., Olivier James, P., Rodriguez-Reinoso, F., Rouquerol, J., et al. (2015). Physisorption of gases, with special reference to the evaluation of surface area and pore size distribution (IUPAC Technical Report). *Pure Appl. Chem.* 87, 1051–1069. doi: 10.1515/pac-2014-1117
- Triantafyllidis, C. S., Vlessidis, A. G., Nalbandian, L., and Evmiridis, N. P. (2001). Effect of the degree and type of the dealumination method on the structural, compositional and acidic characteristics of H-ZSM-5 zeolites. *Micro. Mesopor. Mater.* 47, 369–388. doi: 10.1016/S1387-1811(01)00399-7
- Triantafyllidis, K. S., Lappas, A. A., and Stöcker, M. (eds.). (2013). *The Role of Catalysis for the Sustainable Production of Bio-fuels and Bio-chemicals*. Amsterdam: Elsevier B.V.
- Triantafyllidis, K. S., Nalbandian, L., Trikalitis, P. N., Ladavos, A. K., Mavromoustakos, T., and Nicolaides, C. P. (2004). Structural, compositional and acidic characteristics of nanosized amorphous or partially crystalline ZSM-5 zeolite-based materials. *Micro. Mesopor. Mater.* 75, 89–100. doi: 10.1016/j.micromeso.2004.07.016
- Vishtal, A. G., and Kraslawski, A. (2011). Challenges in industrial applications of technical lignins. *Bioresour. Technol.* 6, 3547–3568.
- Vithanage, A. E., Chowdhury, E., Alejo, L. D., Pomeroy, P. C., DeSisto, W. J., Frederick, B. G., et al. (2017). Renewably sourced phenolic resins from lignin bio-oil. *J. Appl. Polymer Sci.* 134:44827. doi: 10.1002/app.44827
- Wang, K., Kim, K. H., and Brown, R. C. (2014). Catalytic pyrolysis of individual components of lignocellulosic biomass. *Green Chem.* 16, 727–735. doi: 10.1039/C3GC41288A
- Wang, S., Wang, K., Liu, Q., Gu, Y., Luo, Z., Cen, K., et al. (2009). Comparison of the pyrolysis behavior of lignins from different tree species. *Biotechnol. Adv.* 27, 562–567. doi: 10.1016/j.biotechadv.2009.04.010
- Wen, J.-L., Sun, S.-L., Xue, B.-L., and Sun, R.-C. (2013). Recent Advances in Characterization of Lignin Polymer by Solution-State Nuclear Magnetic Resonance (NMR) Methodology. *Materials* 6, 359–391. doi: 10.3390/ma6010359
- Xu, C., Arancon, R. A. D., Labidi, J., and Luque, R. (2014). Lignin depolymerisation strategies: towards valuable chemicals and fuels. *Chem. Soc. Rev.* 43, 7485–7500. doi: 10.1039/C4CS00235K
- Xu, W., Miller, S. J., Agrawal, P. K., and Jones, C. W. (2012). Depolymerization and hydrodeoxygenation of switchgrass lignin with formic acid. *ChemSusChem* 5, 667–675. doi: 10.1002/cssc.201100695
- Yang, H., Xie, Y., Zheng, X., Pu, Y., Huang, F., Meng, X., et al. (2016). Comparative study of lignin characteristics from wheat straw obtained by soda-AQ and kraft pretreatment and effect on the following enzymatic hydrolysis process. *Bioresour. Technol.* 207, 361–369. doi: 10.1016/j.biortech.2016.01.123
- Yang, H., Yan, R., Chen, H., Zheng, C., Lee, D. H., and Liang, D. T. (2006). In-depth investigation of biomass pyrolysis based on three major components: hemicellulose, cellulose and lignin. *Energ. Fuels* 20, 388–393. doi: 10.1021/ef0580117
- Yu, Y., Li, X., Su, L., Zhang, Y., Wang, Y., and Zhang, H. (2012). The role of shape selectivity in catalytic fast pyrolysis of lignin with zeolite catalysts. *Appl. Catal. A Gen.* 447(Suppl. C), 115–123. doi: 10.1016/j.apcata.2012.09.012
- Yuan, T.-Q., Sun, S.-N., Xu, F., and Sun, R.-C. (2011). Characterization of lignin structures and Lignin–Carbohydrate Complex (LCC) linkages by quantitative ¹³C and 2D HSQC NMR Spectroscopy. *J. Agric. Food Chem.* 59, 10604–10614. doi: 10.1021/jf2031549
- Zakzeski, J., Bruijninx, P. C. A., Jongerius, A. L., and Weckhuysen, B. M. (2010). The catalytic valorization of lignin for the production of renewable chemicals. *Chem. Rev.* 110, 3552–3599. doi: 10.1021/cr900354u
- Zhang, M., Resende, F. L. P., and Moutsoglou, A. (2014). Catalytic fast pyrolysis of aspen lignin via Py-GC/MS. *Fuel* 116, 358–369. doi: 10.1016/j.fuel.2013.07.128
- Zhang, M., Resende, F. L. P., Moutsoglou, A., and Rainey, D. E. (2012). Pyrolysis of lignin extracted from prairie cordgrass, aspen, and Kraft lignin by Py-GC/MS and TGA/FTIR. *J. Anal. Appl. Pyrol.* 98, 65–71. doi: 10.1016/j.jaap.2012.05.009
- Zhao, C., and Lercher, J. A. (2012). Selective hydrodeoxygenation of lignin-derived phenolic monomers and dimers to cycloalkanes on Pd/C and HZSM-5 catalysts. *ChemCatChem* 4, 64–68. doi: 10.1002/cctc.201100273
- Zheng, A., Zhao, Z., Chang, S., Huang, Z., Wu, H., Wang, X., et al. (2014). Effect of crystal size of ZSM-5 on the aromatic yield and selectivity from catalytic fast pyrolysis of biomass. *J. Mol. Catal. A Chem.* 383, 23–30. doi: 10.1016/j.molcata.2013.11.005

Conflict of Interest Statement: The authors declare that the research was conducted in the absence of any commercial or financial relationships that could be construed as a potential conflict of interest.

Copyright © 2018 Lazaridis, Fotopoulos, Karakoulia and Triantafyllidis. This is an open-access article distributed under the terms of the Creative Commons Attribution License (CC BY). The use, distribution or reproduction in other forums is permitted, provided the original author(s) and the copyright owner(s) are credited and that the original publication in this journal is cited, in accordance with accepted academic practice. No use, distribution or reproduction is permitted which does not comply with these terms.



One-Pot Enzymatic Production of Lignin-Composites

Sabina Ion¹, Cristina Opris¹, Bogdan Cojocaru¹, Madalina Tudorache^{1*}, Irina Zgura², Aurelian C. Galca³, Adina M. Bodescu⁴, Madalin Enache⁵, Gabriel-Mihai Maria⁵ and Vasile I. Parvulescu^{1*}

¹ Department of Organic Chemistry, Biochemistry and Catalysis, Faculty of Chemistry, University of Bucharest, Bucharest, Romania, ² Laboratory of Optical Processes in Nanostructured Materials, National Institute of Materials Physics, Magurele, Romania, ³ Laboratory of Multifunctional Materials and Structures, National Institute of Materials Physics, Magurele, Romania, ⁴ Faculty of Food Engineering, Tourism and Environmental Protection, Research Center in Technical and Natural Sciences, "Aurel Vlaicu" University, Arad, Romania, ⁵ Institute of Biology Bucharest of the Romanian Academy, Bucharest, Romania

OPEN ACCESS

Edited by:

Rafael Luque,
Universidad de Córdoba, Spain

Reviewed by:

Regina De Fatima Peralta Muniz
Moreira,
Universidade Federal de Santa
Catarina, Brazil
Evangelos Topakas,
National Technical University of
Athens, Greece

*Correspondence:

Madalina Tudorache
madalina.sandulescu@g.unibuc.ro
Vasile I. Parvulescu
vasile.parvulescu@g.unibuc.ro

Specialty section:

This article was submitted to
Green and Sustainable Chemistry,
a section of the journal
Frontiers in Chemistry

Received: 14 December 2017

Accepted: 03 April 2018

Published: 20 April 2018

Citation:

Ion S, Opris C, Cojocaru B,
Tudorache M, Zgura I, Galca AC,
Bodescu AM, Enache M, Maria G-M
and Parvulescu VI (2018) One-Pot
Enzymatic Production of
Lignin-Composites.
Front. Chem. 6:124.
doi: 10.3389/fchem.2018.00124

A novel and efficient one-pot system for green production of artificial lignin bio-composites has been developed. Monolignols such as sinapyl (SA) and coniferyl (CA) alcohols were linked together with caffeic acid (CafAc) affording a polymeric network similar with natural lignin. The interaction of the dissolved SA/CA with CafAc already bound on a solid support (SC₂/SC₆-CafAc) allowed the attachment of the polymeric product direct on the support surface (SC₂/SC₆-CafAc-L₁ and SC₂/SC₆-CafAc-L₂, from CA and SA, respectively). Accordingly, this procedure offers the advantage of a simultaneous polymer production and deposition. Chemically, oxi-copolymerization of phenolic derivatives (SA/CA and CafAc) was performed with H₂O₂ as oxidation reagent using peroxidase enzyme (2-1B mutant of versatile peroxidase from *Pleurotus eryngii*) as catalyst. The system performance reached a maximum of conversion for SA and CA of 71.1 and 49.8%, respectively. The conversion is affected by the system polarity as resulted from the addition of a co-solvent (e.g., MeOH, EtOH, or THF). The chemical structure, morphology, and properties of the bio-composites surface were investigated using different techniques, e.g., FTIR, TPD-NH₃, TGA, contact angle, and SEM. Thus, it was demonstrated that the SA monolignol favored bio-composites with a dense polymeric surface, high acidity, and low hydrophobicity, while CA allowed the production of thinner polymeric layers with high hydrophobicity.

Keywords: bio-composites, oxi-copolymerization, monolignols, peroxidase enzyme, lignin

INTRODUCTION

Together with cellulose and hemicellulose, lignin is one of the most abundant natural polymers (Zakzeski et al., 2010). As an effect of the excessive valorization of the natural resources, the pulp-paper and bio-refining industries are important providers of lignins (Lora and Glasser, 2002). However, the papermaking industry produces annually over 50 million tons of lignin wastes that are mainly used as an energy source (by direct combustion). Today, only 2 wt% of it is used for the polymeric industry (e.g., production of phenolic resins, polyurethane foams, bio-dispersants, or epoxy resins) (Gosselink et al., 2004b). Additionally, the wastes of the paper-pulp industry generate serious environmental pollution concerns. So that, an improvement of the market competitiveness of bio-refining industry is necessary. Accordingly, new perspectives for the valorization of the lignin are required.

The general perception on the lignin is that of a “renewable chemical resource” formed from the assembling of functionalized aromatic entities with phenolic hydroxyl, alcoholic hydroxyl, carboxyl, or methoxy groups (Xiong et al., 2015; Aro and Fatehi, 2017). It presents an amorphous polymeric structure assumed to derive from up to three monolignols, e.g., coniferyl alcohol (CA), synapyl alcohol (SA), and coumaryl alcohol. These monolignols are incorporated in phenylpropanoid units expressed in varied modes such as guaiacyl, syringyl, and *p*-hydroxyphenyl connected by ether and carbon-carbon bonds in a complex three dimensional polymeric network (Nair et al., 2014). Thus, what is named lignin corresponds to a material with a large variety of chemical structures in which the above mentioned entities exist in various proportions. The differences are the direct consequence of its origin (type of the plant species, climate, geographical location) and the extraction process (Gosselink et al., 2004a).

As a bio-polymer, there are many potential value-added applications of lignin with significant impact on industry (Lee and Wendisch, 2017). Derivatization of lignin is often chosen as alternative leading to functionalized bio-polymers with role of the dispersant for cement, pesticide, coal-water slurry, rubber-based material, component of animal feed, surfactants, additive in oil drilling, stabilizers in colloidal suspensions, etc (Xiong et al., 2015; Aro and Fatehi, 2017). The lignin derivatives may also acquire antioxidant, antiviral, antibiotic, and/or anticarcinogenic activities (Yamamoto et al., 1997; Vinardell et al., 2008; Nair et al., 2014). Lignin has been used as alternative to phenol in phenolic resins and also in the composition of thermoplastic polyesters, polyurethanes, active carbons, and carbon fibers (Stewart, 2008; Thanh Binh et al., 2009; Nair et al., 2014). Additionally, lignin-based composites appeared as another low cost eco-friendly reinforcement attractive alternative (Morandim-Giannetti et al., 2012; Pupure et al., 2013; Qian et al., 2014; Thakur et al., 2014). They confirmed as important ingredients for composites with various properties like thermoplastic polymers (Pucciariello et al., 2004; Barzegari et al., 2013), thermosetting polymers (Yin et al., 2012; Stanzione et al., 2013), rubbers (Setua et al., 2000; Kramárová et al., 2007), or foam-based materials (Del Saz-Orozco et al., 2012; Luo et al., 2013). For this purpose, lignin and its derivatives were incorporated in bio-composites using both chemical or/and physical methods leading to homogeneous lignin particles (Nair et al., 2014) or colloidal spheres produced through self-assembly of acetylated lignin (Qian et al., 2014). However, such a valorization of lignin is still restricted due to two main reasons: its relative low reactivity and high heterogeneity of the polymeric mixture (Qu et al., 2015). Therefore, in the last years several chemical methods have been reported to enhance lignin reactivity, e.g., methylation, demethylation, acetylation, etc (Hu et al., 2011). Additionally, the lignin modification has been achieved *via* catalytic and solvent-free methods (e.g., graft copolymerization of lactides to lignin catalyzed by triazabicyclodecenes) (Chung et al., 2013). However, the heterogeneity of the polymeric mixture of lignin is still a challenge today.

In this study, we investigated the production of lignin-composites (bio-composites) using monolignol fractions (e.g., SA

or CA) with the aim to find another route for the valorization of lignin. There are evidences that lignin can be efficiently disrupted into a cocktail of monomers and oligomers (Lee et al., 2013; Opris et al., 2016, 2017). The produced fragments can be re-combined leading to an artificial lignin structure with enhanced homogeneity compared to the original lignin (Opris et al., 2018). In this study, particles functionalized with CafAc were used as solid supports allowing the synthesis of bio-composites. Therefore, monolignols can be directly oxipolymerized on the particles surface involving the CafAc as comonomer. Accordingly, the coverage process was called oxicopolymerization. The use of monolignols instead of whole lignin molecule ensures a better control of the composition of the polymeric layer providing to a good structural homogeneity of the polymeric material.

Usually, the functionalization of the particles surface (e.g. silica particles) by either physical or chemical methods requires a prior modification before covering with the polymeric layer. Most of the modifiers are derived from the fossil resources increasing the cost of these materials but also the toxicity (Zou et al., 2008). In this study, the particles surface (methacrylate) was functionalized with a natural modifier, i.e., CafAc (CafAc occurs frequently in fruits, grains, *Salvia* species) (Hao et al., 2015). Also, the polymeric layer (artificial lignin) covering the surface is bio-derived, mimicking the original lignin. In accordance to its characteristic structure and properties, the lignin-based polymer may afford the required modification of the particles for further bio-applications (e.g., carrier/support for enzymes). Additionally, the lignin bio-composites can provide an important example of a high value utilization of lignin residues.

The oxicopolymerization of monolignols reported in this study for the synthesis of bio-composites was designed as a biocatalytic process where a peroxidase enzyme assisted the oxidation of both monolignols (SA or CA) and CafAc by means of H₂O₂. The developed system acts based on an one-pot approach combining the oxicopolymerization of SA/CA with CafAc, and the attachment of the resulted polymer on the support surface. From our best knowledge, it is the first time when a lignin-composite (bio-composite) with controlled and reproducible composition is prepared based on one-pot approach. Additionally, the influence of a co-solvent (e.g., MeOH, EtOH, THF) on the oxicopolymerization process has also been investigated. The production of the bio-composites was monitored using spectrophotometric as well as Folin-Ciocalteu analysis. Also, detailed characterization of the lignin-composites was performed using different techniques, e.g., FTIR, TPD-NH₃, TGA, contact angle, and SEM.

EXPERIMENTAL

Chemicals and Solutions

The oxicopolymerization process was performed with 2-1B mutant of versatile peroxidase original from *Pleurotus eryngii*, expressed in *Saccharomyces cerevisiae* (12.95 U mL⁻¹ enzyme activity) (Garcia-Ruiz et al., 2012; Molina-Espeja et al., 2014, 2015). 2-1B mutant was provided by Dr. Miguel Alcalde (Institute of Catalysis, CSIC, Madrid, Spain). The solid support

of bio-composites (SC_2 -amino C2 methacrylate, ECR8309F and SC_6 -amino C6 methacrylate, ECR8409F) was kindly offered by the Purolite Life Sciences Company. Both supports were constituted from the beads (150–300 μm of diameter) originally functionalized with $-\text{NH}_2$ groups using methacrylate cross-linkers.

Ten milli molar of PBS (phosphate buffer saline) solution ($\text{pH} = 7.4$) was used as aqueous buffer solution. Its composition consisted of: 8 g NaCl, 0.2 g KCl, 1.43 g $\text{Na}_2\text{HPO}_4 \times 2\text{H}_2\text{O}$ and 0.34 g KH_2PO_4 in 1 L distilled water. 10 mM MES (2-(N-morpholino)ethanesulfonic acid) buffer ($\text{pH} = 4.7$) was prepared by dissolving a corresponding MES mass in distilled water followed of NaOH addition for adjusting the pH value of the solution.

CA, SA, CafAc, 1-ethyl-3-(3-dimethylaminopropyl) carbodiimide (ECD), 30 wt% solution of hydrogen peroxide (H_2O_2), methanol (MeOH), ethanol (EtOH), and tetrahydrofuran (THF) were of analytic purity and purchased from Sigma-Aldrich. Stock solutions of monolignols (e.g., CA and SA) with concentration of 10 mg mL^{-1} were prepared in MeOH.

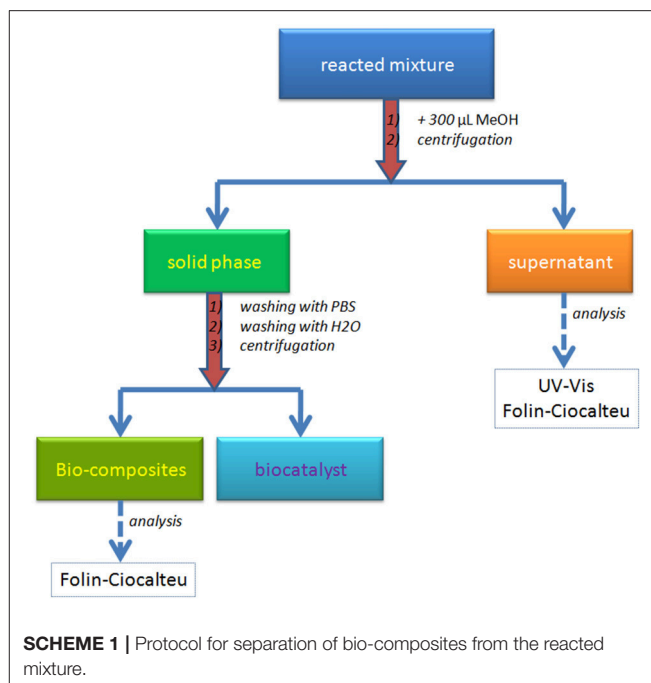
SC_2/SC_6 Functionalization

For the attachment of the lignin polymer, the solid supports SC_2 and SC_6 were functionalized with CafAc in order to ensure the phenolic structures on the particles surface. 0.2 g of SC_2/SC_6 support were dispersed in 10 mL solution containing 10 mg mL^{-1} CafAc in MES (10 mM, $\text{pH} = 4.7$). 0.96 g of EDC was added in the suspension under continuous shaking for activating the $-\text{COOH}$ groups of CafAc in order to interact with $-\text{NH}_2$ groups on the support. Coupling of CafAc on support surface was performed over the night, at room temperature under gentle agitation. Then, the functionalized particles (SC_2 -CafAc and SC_6 -CafAc) were separated by centrifugation and washed several times with MES buffer and distilled water.

Bio-Composites Preparation

The bio-composites construction was performed in one-pot system by enzyme oxi-copolymerization of monolignols (e.g., CA or SA) directly on the surface of the previously prepared supports (SC_2/SC_6 functionalized with CafAc, section SC_2/SC_6 functionalization). One hundred microliters of monolignol stock solution (10 mg mL^{-1} SA/CA in MeOH) were diluted with 300 μL PBS (10 mM, $\text{pH} 7.4$). 10 mg of functionalized support (SC_2 -CafAc or SC_6 -CafAc) were added in the solution followed by the addition of 10 μL H_2O_2 (30%) and 50 μL 2-1B peroxidase mutant (H_2O_2 :enzyme molar ratio of 1760:1). The reaction mixture was incubated at 40°C in a thermo-shaker (100 rpm) over night. For comparison, the monolignols polymerization was also performed in the absence of the functionalized support (homogeneous system).

The separation of the bio-composite was performed using a set up protocol detailed in **Scheme 1**. The reacted mixture was treated with 300 μL MeOH for biocatalyst precipitation and solubilization of unattached oligomers. The centrifugation of the new mixture allowed the separation of the two phases: the liquid phase (supernatant) with unreacted monolignols and/or



oligolignols, and the solid phase containing the bio-composites and precipitated biocatalyst. The supernatant was analyzed using UV-Vis and Folin-Ciocalteu methods. While the UV-Vis analysis allowed the determination of the aromatic content, the Folin-Ciocalteu method permeated the detection of the phenolic $-\text{OH}$ groups. The solid phase was washed consecutively with PBS and distilled water in order to remove the precipitated enzyme (biocatalyst) from the bio-composites surface. The centrifugation step allowed the separation of the bio-composites and the recovery of the enzyme as a PBS solution. Bio-composite surface was investigated based on Folin-Ciocalteu approach.

Analysis of Reacted Mixture

UV-Vis method was used for the determination of mono-/oligolignols (phenolic derivatives) in the liquid phase (**Scheme 1**). The sample absorbance was read at 280 nm with a Specord 250 (Analytik Jena). The conversion of monolignols based on the oxi-copolymerization process was calculated using the absorbance of the solutions before and after the reaction. Folin-Ciocalteu analysis was performed for the determination of free $-\text{OH}$ groups on the aromatic ring (Singleton et al., 1999). The protocol was adapted for the investigation of the bio-composites and the liquid phase (**Scheme 1**). Twenty microliters of sample solution (supernatant or 10 mg/mL bio-composites in MeOH) were dispersed in 1.5 mL of distilled water and the resulted mixture was enriched with 100 μL Folin-Ciocalteu reagent and 300 μL saturated solution of sodium carbonate as supporting medium (adjusting the pH of solution to a basic value). After 2 h incubation time, the mixture was centrifuged and the supernatant absorbance was read at 765 nm.

GPC analysis was performed for the determination of the average molecular weight of the polymers produced in the

absence of the functionalized support. The analysis approach was detailed in our previous report (Opris et al., 2018). Thus, the GPC analysis was carried out using an Agilent Technologies instrument (Model 1260) equipped with two columns (Zorbax PSM 60-S, 6.5×250 mm, $5 \mu\text{m}$, and Polargel-M, 300×7.5 mm) and a multidetection unit (Refractive Index, Light Scattering, and Viscosity detectors). Experimental conditions were set up at 1 mL min^{-1} THF as mobile phase, $100 \mu\text{L}$ injection volume of sample, and temperature of the detectors and columns of 35°C . The calibration of the GPC system was performed using polystyrene standards in the range of $162\text{--}10,000 \text{ g mol}^{-1}$. The Agilent GPC/SEC Software (Version 1.1, Agilent Technologies) was utilized for the determination of the average molecular weight (MW).

The Characterization of the Bio-Composites

FTIR spectra of bio-composites and simple/functionalized supports were recorded using Vertex 70 (Bruker, Ettlingen, Germany) spectrophotometer equipped with the Total Attenuated Reflectance cell in the range of $600\text{--}2000 \text{ cm}^{-1}$. Sixteen scans were collected with a resolution of 4 cm^{-1} in the range of $600\text{--}4000 \text{ cm}^{-1}$.

The total acidity was evaluated by temperature-programmed desorption of ammonia (TPD- NH_3) using a Micromeritics Chemisorb 2750 instrument. Before NH_3 desorption, the samples were heated to 80°C ($20^\circ\text{C min}^{-1}$) in 30 mL high pure Helium flow. Subsequently, the samples were cooled down to room temperature in helium flow. NH_3 adsorption was performed under ambient conditions and saturation for about 60 min in a flow of 10% ammonia in Helium (30 mL min^{-1}). Then, the samples were purged in a Helium flow until a constant baseline level was attained. The desorption of NH_3 was carried out with the linear heating rate ($10^\circ\text{C min}^{-1}$) in a flow of Helium until 300°C .

The thermo-gravimetric analysis (TGA) was performed with a Shimadzu instrument (SDT Q600) in order to determine the thermo stability of the bio-composite according to the original/functionalized support. Maximum 10 mg of sample were used. The analysis was carried out at increasing temperature with a rate of $10^\circ\text{C min}^{-1}$ in the range of $30\text{--}600^\circ\text{C}$ under N_2 atmosphere.

Static contact angle of bio-composites was measured with a Drop Shape Analysis System, model DSA100 (Kruss GmbH). The sample was placed on a horizontal stage, under the tip of a water-dispensing disposable blunt-end stainless steel needle with an outer diameter of 0.5 mm . The water droplet ($1 \mu\text{L}$) was delivered on the sample surface by the needle attached to a syringe pump controlled with a PC (through DSA3[®] software supplied with the instrument). The viewing camera for taking the picture was positioned to observe the droplet under an angle of about $2\text{--}3^\circ$ with respect to the plane of the sample surface supporting the droplet. The tests were carried out at room temperature. The contact angle was measured by fitting a polynomial equation of second degree or a circle equation to the shape of the sessile drop. Then, the slope of the tangent to the drop at the liquid-solid vapor

interface line was calculated. (Zgura et al., 2010, 2013; Popescu et al., 2011; Duta et al., 2012; Preda et al., 2013).

For scanning electron microscopy (SEM) analysis, freeze, and dried particles (e.g., bio-composites and original/functionalized supports) were examined using a Jeol instrument (JSM-6610LV). The pretreatment of the samples followed the dispersion of the particles in EtOH solution (30%) and deposition of $10 \mu\text{L}$ suspension on the microscopic blade covered with gold layer. After EtOH evaporation at room temperature, prepared blades were dried in vacuum followed by metal coating using a sputter coater (Jeol auto fine coater, JFC-1300). SEM investigations were performed under high vacuum conditions.

RESULTS AND DISCUSSION

Co-polymerization of Monolignols for the Construction of Bio-Composites

The concept of the one-pot synthesis of bio-composites has been described above. The oxi-copolymerization of monolignols (e.g., CA or SA) was directly performed on the supports (SC_2 and SC_6) surface functionalized with CafAc ($\text{SC}_2\text{-CafAc}$ and $\text{SC}_6\text{-CafAc}$) in the presence of the 2-1B mutant of versatile peroxidase as catalyst using an adapted procedure (Opris et al., 2018). In this study CafAc used as a co-monomer afforded the oxi-copolymerization of monolignols. CA allowed the production of $\text{SC}_2/\text{SC}_6\text{-CafAc-L}_1$ bio-composite, while the oxi-copolymerization of SA led to $\text{SC}_2/\text{SC}_6\text{-CafAc-L}_2$.

Under the investigated homogeneous conditions, the oxi-copolymerization of monolignols (SA/CA) and CafAc led to the results presented in **Table 1**. A higher conversion was achieved for SA compared to CA (65.3 vs. 21.1%) leading to polymers with different molecular weights (3500 and 856 Da for SA and CA, respectively). The affinity of the biocatalyst for the monolignols can be a reasonable explanation of the system behavior. These results are in accordance with the previous report (Opris et al., 2018).

Under heterogeneous conditions, i.e., with SA/CA dissolved in liquid phase, and CafAc attached on the particles ($\text{SC}_2/\text{SC}_6\text{-CafAc}$), the monolignols and immobilized CafAc were linked together in a polymeric structure miming the natural lignin directly attached on the particles surface (**Table 1**). This heterogeneous design allowed to improve the conversion of

TABLE 1 | Efficiency of the oxi-copolymerization process.

Solid support	SA		CA	
	C (%)	MW (Da)	C (%)	MW (Da)
–	65.3	3500	21.1	856
$\text{SC}_2\text{-CafAc}$	71.1	–	49.8	–
$\text{SC}_6\text{-CafAc}$	65.7	–	36.3	–

Experimental conditions: 2 mg/mL monolignol (SA/CA), 1.295 U mL^{-1} 2-1B peroxidase mutant, 0.6% H_2O_2 , and 20 mg/mL functionalized support for heterogeneous co-polymerization in PBS (10 mM , $\text{pH} = 7.4$); 40°C , 24 h and 100 rpm . C, conversion of the oxi-copolymerization process. MW, average molecular weight of copolymer.

monolignols compared to homogeneous system keeping the same advantage of SA vs. CA. Different conversions were also determined as a function of the functionalized support (SC₂-CafAc and SC₆-CafAc) demonstrating that the solid support influenced the co-polymerization process (Table 1).

Important parameters of this process are the loading of the polymeric products on the solid surface and the percent of the oligomers in the residual phase (supernatant, see Scheme 1). To determine these, both the supernatants and bio-composites were analyzed using spectrophotometric (UV-Vis) and Folin-Ciocalteu approaches (F-C) (Scheme 1). Moreover, the results were converted in the concentration of recovered monolignols (i.e., the ratio between the concentration of monolignol in/on residues/bio-composite and initial concentration of monolignol) (Table 2). The relative low difference between the F-C and UV-Vis results can be an indicative for the insignificant content of the oligolignols in the supernatant. Moreover, the UV-Vis results should be interpreted with caution because of the production of quinone derivatives as secondary products of co-oxipolymerization process. For bio-composites, the same measurements evidenced the presence of small concentration of free OH groups (around 10 times lower than in the supernatant). The participation of the OH groups into the formation of the etheric bonds of the synthetic lignin is a plausible explanation.

TABLE 2 | Evaluation of supernatant content in monolignols and oligolignols using spectrophotometric (UV-Vis) and Folin-Ciocalteu (F-C) methods (recovered concentration, %).

Solid support		SA		CA	
		UV-Vis	F-C	UV-Vis	F-C
SC ₂ -CafAc	Supernatant	28.90	24.70	58.37	52.64
	Bio-composite	–	2.78	–	5.51
SC ₆ -CafAc	Supernatant	34.30	24.41	74.07	65.41
	Bio-composite	–	2.89	–	3.70

The effect of the co-solvent (e.g., MeOH, EtOH, THF) has also been evaluated showing a different influence depending on the monolignol type (Figure 1). For SA, the use of MeOH as co-solvent led to better results affording a higher conversion for SC₆-CafAc support compared to SC₂-CafAc. For CA, the presence of the co-solvent doubled the conversion of monolignols. However, the reproducibility was low, and high standard deviation has been determined for co-solvent (e.g., MeOH, EtOH, THF). In conclusion, poor reproducibility for the bio-composite production using a co-solvent enforces the use of H₂O despite of smaller conversions.

Characterization of the Bio-Composite

FTIR analysis confirmed the attachment of the artificial lignin on the support surface during the oxi-copolymerization (Figures S1–S3). Table 3 presents the differences between the spectra collected for SC₂-CafAc-L₁/L₂ and SC₆-CafAc-L₁/L₂, and those of the original/functionalized supports (SC₂, SC₆, SC₂-CafAc and SC₆-CafAc). The attachment of the CafAc on the solid support led to a consistent modification of the spectrum (Figure S1). The intensity of the OH band stretching at 3370 cm^{−1} on the particles surface (SC₂/SC₆) (Poletto and Zattera, 2013) decreased for SC₂/SC₆-CafAc. Additionally, new bands occurred at 1041 cm^{−1} and 1563–1564 cm^{−1} due to the presence of C–O bonds on the aromatic ring and the formation of amide bonds (CO–NH) by the attachment of CafAc on the support surface. Both functionalized supports (SC₂-CafAc and SC₆-CafAc) have similar FTIR spectra (Figure S1).

SC₂-CafAc-L₁/L₂ and SC₆-CafAc-L₁/L₂ presented modified spectra in the regions of 3700–3000 cm^{−1} and 1200–700 cm^{−1} compared with SC₂-CafAc and SC₆-CafAc, respectively (Figure S2). The differences are summarized in Table 3. The shoulder at around 3600 cm^{−1} is attributed to an aliphatic OH group of the monolignol structure (Poletto and Zattera, 2013), while the new bands at 2952/2953 and 2942/2943 cm^{−1} were to the C–H stretching vibration of the methyl and methylene groups introduced by the SA and CA monolignols (Xiong et al., 2015). The presence of the aromatic ring has been confirmed

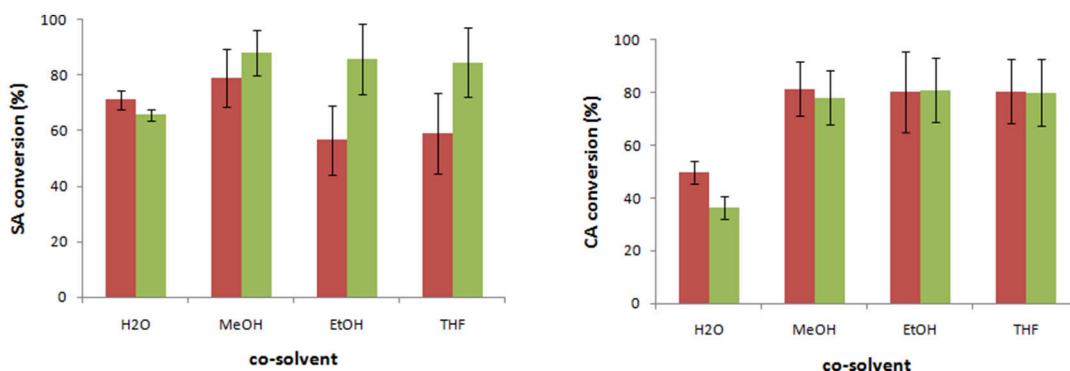


FIGURE 1 | Preparation of the bio-composite in the presence of organic solvent. Experimental conditions: 2 mg/mL monolignol (SA/CA), 1.295 U mL^{−1} 2-1B peroxidase mutant, 0.6% H₂O₂ 20 mg/mL functionalized support for heterogeneous co-polymerization, and 6% added solvent (H₂O, MeOH, EtOH, THF) in PBS (10 mM, pH = 7.4); 40°C, 24 h and 100 rpm. (Triplicates analysis were performed).

TABLE 3 | Summary of the specific bands observed for bio-composites, original, and functionalized supports.

Assignment	Band position (cm ⁻¹)						
	S _{C2} /C ₆	S _{C2} -CafAc	S _{C6} -CafAc	S _{C2} -CafAc-L1	S _{C6} -CafAc-L1	S _{C2} -CafAc-L2	S _{C6} -CafAc-L2
O-H stretching	3370	3361	3368	3385	3378	3392	3364
Aromatic methyl and methylene groups	—	—	—	2953	2942	2952	2943
	—	2724	2721	—	—	—	—
-CO-NH-	—	1563	1564	—	—	—	—
C-C in aromatic skeleton	—	—	—	1544	1538	1546	1540
Syringyl units	—	—	—	—	—	1120	1120
C-O deformation of aromatic ethers	—	—	—	1080	1080	1076	1076
C-O on the aromatic skeleton	—	1041	1041	—	—	—	—
C-H out of plane for guaiacyl units	—	—	—	859	859	858	859

by the bands in the range 1538–1546 cm⁻¹. The new band at 1120 cm⁻¹ observed for S_{C2}/S_{C6}-CafAc-L₂ represents an evidence of the presence of the syringyl units detected in the polymeric layer of the bio-composites. Guaiacyl units were also detected at low intensity at 858 and 859 cm⁻¹ (Poletto and Zattera, 2013). However, the band at 1264 cm⁻¹ typical for guaiacyl (Poletto and Zattera, 2013; Fitigău et al., 2015) is not visible for S_{C2}/S_{C6}-CafAc-L₁ due to a superposition with an already existing band at 1257 cm⁻¹. Poor covering of the support with polymers from CA (Table 1) can represent another reason for the absence of this band. All bio-composites showed also absorbance bands at 1076 and 1080 cm⁻¹ attributed to etheric groups (C-O-C) connecting the aromatic rings (Qu et al., 2015; Xiong et al., 2015). This is also an evidence for the production of the artificial lignin onto the bio-composite surface.

FTIR spectra of bio-composites prepared in the presence of co-solvent showed differences between MeOH and EtOH, on one side, and THF, on the other side (Figure S3). Thus, the presence of MeOH or EtOH led to structures for which the bands at 1076 and 1078 cm⁻¹ were not present anymore while those at 973/949 and 858 cm⁻¹ presented a dramatic decrease in the intensity. These results confirm that MeOH and EtOH inhibit the formation of the artificial lignin structures, and especially of the guaiacyl units. So, the increased conversion for the oxi-copolymerization in the presence of an organic solvent does not correspond to the formation of lignolic structures (i.e., guaiacyl units).

The acidity of the bio-composites has been evaluated from TPD-NH₃ measurements (Table 4). The bio-composites incorporating CA have similar acidic properties with the functionalized support confirming the conservation of the phenolic OH group (NH₃ desorption peaks at 197°C). However, the number of acidic centers has been doubled for the bio-composite showing an enrichment of phenolic OH owing of the synthetic lignin structure. CA and SA led to bio-composites with two different acidity centers (NH₃ desorption peaks at 197 and 210°C) that were assigned to phenolic and aliphatic OH groups. Also, the total number of the acid centers was higher for SA polymer than for the corresponding CA-based bio-composite. These results fit the values of the conversion calculated for the oxi-copolymerization of the monolignols (Table 1).

TABLE 4 | Acidity of bio-composites compared to the CafAc-functionalized support based on TPD-NH₃.

Bio-composite	Acidity (μmol/g)	
	Phenolic OH	Aliphatic OH
S _{C6} -CafAc	26	—
S _{C6} -CafAc-L ₁	52	—
S _{C6} -CafAc-L ₂	37	44

The thermo-stability of produced lignin bio-composites (S_{C2}-CafAc-L₁/L₂ and S_{C6}-CafAc-L₁/L₂) compared to the original/functionalized supports (S_{C2}, S_{C6}, S_{C2}-CafAc, S_{C6}-CafAc) has been evaluated in the temperature range of 30–600°C (Figure 2). TGA profiles of bio-composites were quit similar. The mass loss up to 230°C is mainly due to the removal of water (<8 wt%). The differences in the shape of the profiles for the functionalized support and corresponding bio-composite may account the degradation of propanoid chain of the polymer (Strzemieska et al., 2016). Further heating (230–430°C) corresponded to a larger mass loss (about 45%). This is related to the decomposition of polymeric material linked to the support surface (L₁/L₂). The heterogeneity of the bio-composite surface (artificial lignin) is confirmed by the different losses in this temperature range. However, an important information provided by these results is the increased thermo-stability as effect of the covering the support with synthetic lignin. This is confirmed by the shift of the thermal effects to higher temperatures in accordance to literature data (Brebu et al., 2013; Brostow et al., 2016; Strzemieska et al., 2016).

The investigation of surface hydrophobicity was performed using contact angle measurements of distilled water onto CafAc-functionalized silica chips (S-CafAc) and corresponding bio-composites (S-CafAc-L₁/L₂) (Figure 3). The contact angle of the chip (S) was of 29°, while for the bio-composites increased to 63° for CA-based polymer or decreased to 18° for the SA-based polymer. These results indicate an enhancement of the hydrophobicity for the chip surface covered by CA monolignol reported also in the previous literature for natural lignin (Xiong et al., 2015; Salanti et al., 2016). Moreover, the artificial lignin

prepared by oxi-copolymerization is more hydrophobic than some natural lignins (e.g., soda lignin from *Triticum* sp and *Saccharum officinarum* with a 35° contact angle) (Buono et al., 2016). SA led to a hydrophilic polymer than the support as an effect of the ratio between phenolic and alkyl OH groups. For L₁, the hydrophobicity of the aromatic ring was enforced due to the relative low density of OH confirmed by the TPD-NH₃ measurements (Table 4). The hydrophilicity of the L₂ surface is also according to TPD-NH₃ results (Table 4). The hydrophobicity/hydrophilicity property of bio-composites represents an important characteristics for their

further application as support/carrier of biomolecules (e.g., immobilization of lipase enzyme on hydrophobic surface turn on the enzyme in active form; Thomas et al., 2005).

SEM images of bio-composites and original/functionalized supports are presented in Figure 4. The parent particles (SC₂ and SC₆) presented a smooth surface, while the functionalized particles (SC₂/SC₆-CafAc) showed roughened morphology. Differences in the morphologies of the bio-composites (SC₂/SC₆-CafAc-L₁/L₂) were also induced by the monolignol oxi-copolymerization (the polymeric layer looks more dense for L₂ than L₁).

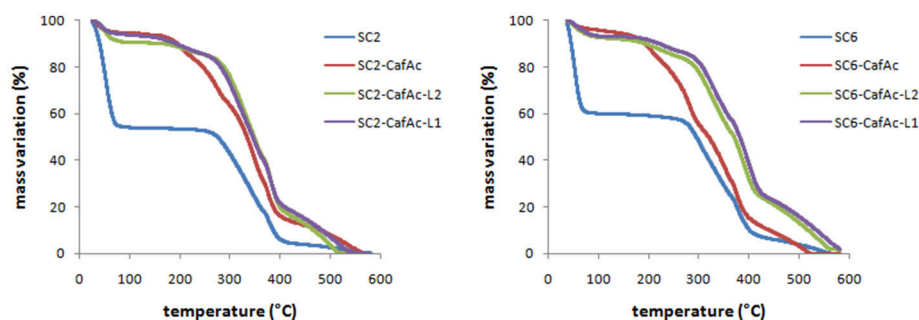


FIGURE 2 | TGA diagrams of the bio-composites (SC₂-CafAc-L₁/L₂ and SC₆-CafAc-L₁/L₂) related to original/functionalized support (SC₂, SC₆, SC₂-CafAc, SC₆-CafAc).

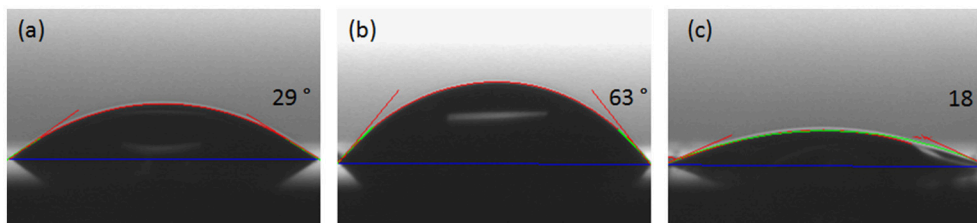


FIGURE 3 | Measurements of static contact angle of (a) S-CafAc, (b) S-CafAc-L₁, and (c) S-CafAc-L₂.

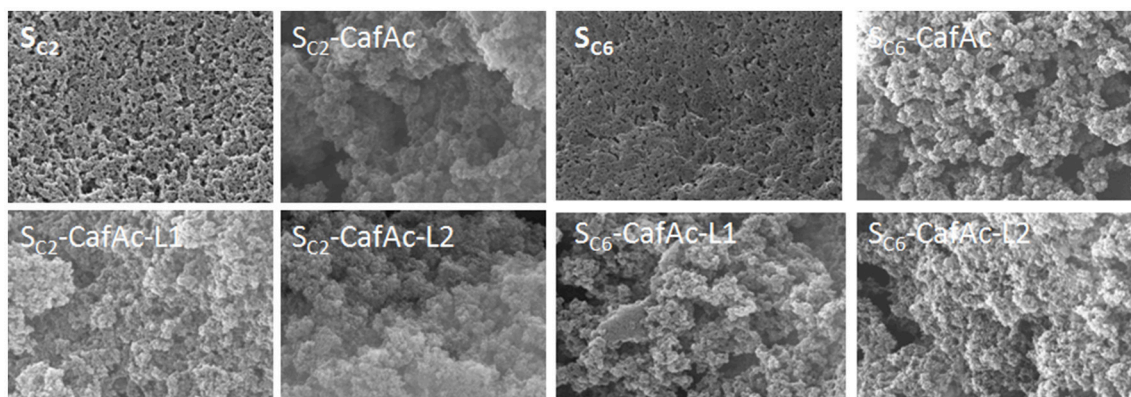


FIGURE 4 | SEM images of the particles with different composition: original particles (SC₂ and SC₆), CafAc-functionalized particles (SC₂/SC₆-CafAc), and bio-composites based on CA (SC₂/SC₆-CafAc-L₁), and SA (SC₂/SC₆-CafAc-L₂) oxi-copolymerization.

CONCLUSIONS

These results confirm the success of the one-pot approach for the production of lignin bio-composites via an enzyme oxi-copolymerization process. Monolignols such as SA and CA were easily attached on a support surface based on the interaction with immobilized CafAc leading to artificial lignin covering the support surface. SA allowed an advanced polymerization (L_2 polymer) and coverage compared to CA (L_1 polymer). Accordingly, L_1 -based bio-composites exhibited higher hydrophobicity than L_2 , while SA provided a more acidic bio-composite surface. Therefore, the developed protocol allows the synthesis of artificial lignin-based composites with predictable surface properties.

Based on these, the reported work offers a new alternative for the valorization of lignin residues with the production of new bio-composites following a green route. The versatility of the method may offer an easy control of the properties of the prepared bio-composites and an instrument to adjust them to different applications (e.g., support/ carrier for biomolecules).

AUTHOR CONTRIBUTIONS

All authors listed have made a substantial, direct and intellectual contribution to the work, and approved it for publication. SI and

CO performed the experiments for the preparation of the bio-composites and also UV-Vis/F-C analysis; BC performed TPD-NH₃ analysis; MT coordinated the research study and wrote the manuscript; IZ and AG characterized the bio-composites based on contact angle technique; AB performed FTIR analysis; ME and G-MM performed the SEM analysis and the interpretation of the corresponding results; VP revised and improved the manuscript.

ACKNOWLEDGMENTS

This work was financially supported by PN III TE program, contract no. 103/2015 and Core project PN-III-16-48-01 from MEN-UEFISCDI. We thank Puro-lite Life Sciences Company for Lifetech ECR8309F and Lifetech ECR8409F particles. Many thanks to dr. Miguel Alcalde (Institute of Catalysis, CSIC, Madrid, Spain) for 2-1B mutant of versatile peroxidase and dr. ing. Alexandru Branzan (Institute of Biology Bucharest of the Romanian Academy, Romania) for SEM analysis.

The authors are also grateful to the COST Action FP1306 for the financial support and transfer of knowledge.

SUPPLEMENTARY MATERIAL

The Supplementary Material for this article can be found online at: <https://www.frontiersin.org/articles/10.3389/fchem.2018.00124/full#supplementary-material>

REFERENCES

- Aro, T., and Fatehi, P. (2017). Production and application of lignosulfonates and sulfonated lignin. *ChemSusChem* 10, 1861–1877. doi: 10.1002/cssc.201700082
- Barzegari, M. R., Alemдар, A., Zhang, Y., and Rodrigue, D. (2013). Thermal analysis of highly filled composites of polystyrene with lignin. *Polym. Polymer Composites* 21, 357–366.
- Brebu, M., Tamminen, T., and Spiridon, I. (2013). Thermal degradation of various lignins by TG-MS/FTIR and Py-GC-MS. *J. Anal. Appl. Pyrolysis* 104, 531–539. doi: 10.1016/j.jaap.2013.05.016
- Brostow, W., Datashvili, T., Jiang, P., and Miller, H. (2016). Recycled HDPE reinforced with sol-gel silica modified wood sawdust. *Eur. Polym. J.* 76, 28–39. doi: 10.1016/j.eurpolymj.2016.01.015
- Buono, P., Duval, A., Verge, P., Averous, L., and Habibi, Y. (2016). New insights on the chemical modification of Lignin: acetylation versus Silylation. *ACS Sustain. Chem. Eng.* 4, 5212–5222. doi: 10.1021/acssuschemeng.6b00903
- Chung, Y. L., Olsson, J. V., Li, R. J., Frank, C. W., Waymouth, R. M., Billington, S. L., et al. (2013). A renewable lignin-lactide copolymer and application in biobased composites. *ACS Sustain. Chem. Eng.* 1, 1231–1238. doi: 10.1021/sc4000835
- Del Saz-Orozco, B., Oliet, M., Alonso, M. V., Rojo, E., and Rodríguez, F. (2012). Formulation optimization of unreinforced and lignin nanoparticle-reinforced phenolic foams using an analysis of variance approach. *Compos. Sci. Technol.* 72, 667–674. doi: 10.1016/j.compscitech.2012.01.013
- Duta, L., Popescu, A. C., Dorcioman, G., Mihailescu, I. N., Stan, G. E., Zgura, I., et al. (2012). “ZnO thin films deposited on textile material substrates for biomedical applications: ZnO thin films deposited on textiles,” in *NATO Science for Peace and Security Series A: Chemistry and Biology*, eds A. Vaseashta, E. Braman, and P. Susmann (Dordrecht: Springer), 207–210. doi: 10.1007/978-94-007-2488-4_20
- Fitigau, I. F., Boeriu, C. G., and Peter, F. (2015). Enzymatic modification of different lignins through oxidative coupling with hydrophilic compounds. *Macromol. Symp.* 352, 78–86. doi: 10.1002/masy.201400157
- García-Ruiz, E., González-Pérez, D., Ruiz-Dueñas, F. J., Martínez, A. T., and Alcalde, M. (2012). Directed evolution of a temperature-, peroxide- and alkaline pH-tolerant versatile peroxidase. *Biochem. J.* 441, 487–498. doi: 10.1042/BJ20111199
- Gosselink, R. J. A., Abächerli, A., Semke, H., Malherbe, R., Käuper, P., Nadif, A., et al. (2004a). Analytical protocols for characterisation of sulphur-free lignin. *Ind. Crops Prod.* 19, 271–281. doi: 10.1016/j.indcrop.2003.10.008
- Gosselink, R. J. A., de Jong, E., Guran, B., and Abächerli, A. (2004b). Co-ordination network for lignin—standardisation, production and applications adapted to market requirements (EUROLIGNIN). *Ind. Crops Prod.* 20, 121–129. doi: 10.1016/j.indcrop.2004.04.015
- Hao, D. C., Gu, X.-J., and Xiao, P. G. (eds.). (2015). “14 - Phytochemical and biological research of Salvia medicinal resources,” in *Medicinal Plants* (Cambridge: Woodhead Publishing), 587–639. doi: 10.1016/B978-0-08-100085-4.00001-3
- Hu, L., Pan, H., Zhou, Y., and Zhang, M. (2011). Methods to improve lignin's reactivity as a phenol substitute and as replacement for other phenolic compounds: a brief review. *Bioresources* 6, 3515–3525.
- Kramárová, Z., Alexy, P., Chodák, I., Špírk, E., Hudec, I., Košíková, B., et al. (2007). Biopolymers as fillers for rubber blends. *Polym. Adv. Technol.* 18, 135–140. doi: 10.1002/pat.803
- Lee, J. H., and Wendisch, V. F. (2017). Biotechnological production of aromatic compounds of the extended shikimate pathway from renewable biomass. *J. Biotechnol.* 257, 211–221. doi: 10.1016/j.jbiotec.2016.11.016
- Lee, R. A., Bédard, C., Berber, V., Beauchet, R., and Lavoie, J. M. (2013). UV-Vis as quantification tool for solubilized lignin following a single-shot steam process. *Bioresour. Technol.* 144(Suppl. C), 658–663. doi: 10.1016/j.biortech.2013.06.045
- Lora, J. H., and Glasser, W. G. (2002). Recent industrial applications of lignin: a sustainable alternative to nonrenewable materials. *J. Polym. Environ.* 10, 39–48. doi: 10.1023/A:1021070006895
- Luo, X., Mohanty, A., and Misra, M. (2013). Lignin as a reactive reinforcing filler for water-blown rigid biofoam composites from soy oil-based polyurethane. *Ind. Crops Prod.* 47, 13–19. doi: 10.1016/j.indcrop.2013.01.040

- Molina-Espeja, P., Garcia-Ruiz, E., Gonzalez-Perez, D., Ullrich, R., Hofrichter, M., and Alcalde, M. (2014). Directed evolution of unspecific peroxxygenase from *Agroclybe aegerita*. *Appl. Environ. Microbiol.* 80, 3496–3507. doi: 10.1128/AEM.00490-14
- Molina-Espeja, P., Ma, S., Mate, D. M., Ludwig, R., and Alcalde, M. (2015). Tandem-yeast expression system for engineering and producing unspecific peroxxygenase. *Enzyme Microb. Technol.* 73–74, 29–33. doi: 10.1016/j.enzmictec.2015.03.004
- Morandim-Giannetti, A. A., Agnelli, J. A. M., Lanças, B. Z., Magnabosco, R., Casarin, S. A., and Bettini, S. H. P. (2012). Lignin as additive in polypropylene/coir composites: thermal, mechanical and morphological properties. *Carbohydr. Polym.* 87, 2563–2568. doi: 10.1016/j.carbpol.2011.11.041
- Nair, S. S., Sharma, S., Pu, Y., Sun, Q., Pan, S., Zhu, J. Y., et al. (2014). High shear homogenization of lignin to nanolignin and thermal stability of nanolignin-polyvinyl alcohol blends. *ChemSusChem* 7, 3513–3520. doi: 10.1002/cssc.201402314
- Opris, C., Amanov, N., Parvulescu, V. I., and Tudorache, M. (2018). Peroxidase-based oxidative polymerization of monolignols. *Comp. Rendus Chim.* 21, 362–368. doi: 10.1016/j.crci.2017.09.002
- Opris, C., Cojocaru, B., Gheorghe, N., Tudorache, M., Coman, S. M., Parvulescu, V. I., et al. (2016). Lignin fragmentation over magnetically recyclable composite Co@Nb₂O₅@Fe₃O₄ catalysts. *J. Catal.* 339, 209–227. doi: 10.1016/j.jcat.2016.04.002
- Opris, C., Cojocaru, B., Gheorghe, N., Tudorache, M., Coman, S. M., Parvulescu, V. I., et al. (2017). Lignin fragmentation onto multifunctional Fe₃O₄@Nb₂O₅@Co@Re catalysts: the role of the composition and deposition route of rhenium. *ACS Catal.* 7, 3257–3267. doi: 10.1021/acscatal.6b02915
- Poletto, M., and Zattera, A. J. (2013). Materials produced from plant biomass: part III: degradation kinetics and hydrogen bonding in lignin. *Mater. Res.* 16, 1065–1070. doi: 10.1590/S1516-14392013005000112
- Popescu, A. C., Duta, L., Dorcioman, G., Mihailescu, I. N., Stan, G. E., Pasuk, I., et al. (2011). Radical modification of the wetting behavior of textiles coated with ZnO thin films and nanoparticles when changing the ambient pressure in the pulsed laser deposition process. *J. Appl. Phys.* 110:064321. doi: 10.1063/1.3639297
- Preda, N., Enculescu, M., Zgura, I., Socol, M., Matei, E., Vasilache, V., et al. (2013). Superhydrophobic properties of cotton fabrics functionalized with ZnO by electroless deposition. *Mater. Chem. Phys.* 138, 253–261. doi: 10.1016/j.matchemphys.2012.11.054
- Pucciariello, R., Villani, V., Bonini, C., D'Auria, M., and Vetere, T. (2004). Physical properties of straw lignin-based polymer blends. *Polymer* 45, 4159–4169. doi: 10.1016/j.polymer.2004.03.098
- Pupure, L., Varna, J., Joffe, R., and Pupurs, A. (2013). An analysis of the nonlinear behavior of lignin-based flax composites. *Mech. Composite Mater.* 49, 139–154. doi: 10.1007/s11029-013-9330-x
- Qian, Y., Deng, Y., Qiu, X., Li, H., and Yang, D. (2014). Formation of uniform colloidal spheres from lignin, a renewable resource recovered from pulping spent liquor. *Green Chem.* 16, 2156–2163. doi: 10.1039/c3gc42131g
- Qu, Y., Luo, H., Li, H., and Xu, J. (2015). Comparison on structural modification of industrial lignin by wet ball milling and ionic liquid pretreatment. *Biotechnol. Rep.* 6(Suppl. C), 1–7. doi: 10.1016/j.btre.2014.12.011
- Salanti, A., Zoia, L., Zanini, S., and Orlandi, M. (2016). Synthesis and characterization of lignin-silicone hybrid polymers as possible consolidants for decayed wood. *Wood Sci. Technol.* 50, 117–134. doi: 10.1007/s00226-015-0772-2
- Setua, D. K., Shukla, M. K., Nigam, V., Singh, H., and Mathur, G. N. (2000). Lignin reinforced rubber composites. *Polymer Composites* 21, 988–995. doi: 10.1002/pc.10252
- Singleton, V. L., Orthofer, R., and Lamuela-Raventos, R. M. (1999). Analysis of total phenols and other oxidation substrates and antioxidants by means of Folin-Ciocalteu Reagent. *Methods Enzymol.* 299, 152–178. doi: 10.1016/S0076-6879(99)90017-1
- Stanzione, J. F. III., Giangiulio, P. A., Sadler, J. M., La Scala, J. J., and Wool, R. P. (2013). Lignin-based bio-oil mimic as biobased resin for composite applications. *ACS Sustain. Chem. Eng.* 1, 419–426. doi: 10.1021/sc3001492
- Stewart, D. (2008). Lignin as a base material for materials applications: chemistry, application and economics. *Ind. Crops Prod.* 27, 202–207. doi: 10.1016/j.indcrop.2007.07.008
- Strzemieska, B., Klapiszewski, L., Jamrozik, A., Szalaty, T. J., Matykiewicz, D., Sterzynski, T., et al. (2016). Physicochemical characterization of functional lignin-silica hybrid fillers for potential application in abrasive tools. *Materials* 9:E517. doi: 10.3390/ma9070517
- Thakur, V. K., Thakur, M. K., Raghavan, P., and Kessler, M. R. (2014). Progress in green polymer composites from lignin for multifunctional applications: a review. *ACS Sustain. Chem. Eng.* 2, 1072–1092. doi: 10.1021/sc500087z
- Thanh Binh, N. T., Luong, N. D., Kim, D. O., Lee, S. H., Kim, B. J., Lee, Y. S., et al. (2009). Synthesis of lignin-based thermoplastic copolyester using kraft lignin as a macromonomer. *Composite Interfaces* 16, 923–935. doi: 10.1163/092764409X12477479344485
- Thomas, A., Allouche, M., Basyn, F., Brasseur, R., and Kerfelec, B. (2005). Role of the lid hydrophobicity pattern in pancreatic lipase activity. *J. Biol. Chem.* 280, 40074–40083. doi: 10.1074/jbc.M502123200
- Vinardell, M. P., Ugartondo, V., and Mitjans, M. (2008). Potential applications of antioxidant lignins from different sources. *Ind. Crops Prod.* 27, 220–223. doi: 10.1016/j.indcrop.2007.07.011
- Xiong, W., Yang, D., Zhong, R., Li, Y., Zhou, H., and Qiu, X. (2015). Preparation of lignin-based silica composite submicron particles from alkali lignin and sodium silicate in aqueous solution using a direct precipitation method. *Ind. Crops Prod.* 74, 285–292. doi: 10.1016/j.indcrop.2015.05.021
- Yamamoto, Y., Shirono, H., Kono, K., and Ohashi, Y. (1997). Immunopotentiating activity of the water-soluble lignin rich fraction prepared from lem—the extract of the solid culture medium of *Lentinus edodes* mycelia. *Biosci. Biotechnol. Biochem.* 61, 1909–1912. doi: 10.1271/bbb.61.1909
- Yin, Q., Yang, W., Sun, C., and Di, M. (2012). Preparation and properties of lignin-epoxy resin composite. *Bioresources* 7, 5737–5748. doi: 10.15376/biores.7.4.5737-5748
- Zakzeski, J., Bruijninx, P. C., Jongerius, A. L., and Weckhuysen, B. M. (2010). The Catalytic valorization of lignin for the production of renewable chemicals. *Chem. Rev.* 110, 3552–3599. doi: 10.1021/cr900354u
- Zgura, I., Beica, T., Mitrofan, I. L., Mateias, C. G., Pirvu, D., and Patrascu, I. (2010). Assessment of the impression materials by investigation of the hydrophilicity. *Digest. J. Nanomat. Biostruct.* 5, 749–755.
- Zgura, I., Moldovan, R., Negri, C. C., Frunza, S., Cotorobai, V. F., and Frunza, L. (2013). Surface free energy of smooth and dehydroxylated fused quartz from contact angle measurements using some particular organics as probe liquids. *J. Optoelectron. Adv. Mater.* 15, 627–634.
- Zou, H., Wu, S., and Shen, J. (2008). Polymer/silica nanocomposites: preparation, characterization, properties, and applications. *Chem. Rev.* 108, 3893–3957. doi: 10.1021/cr068035q

Conflict of Interest Statement: The authors declare that the research was conducted in the absence of any commercial or financial relationships that could be construed as a potential conflict of interest.

Copyright © 2018 Ion, Opris, Cojocaru, Tudorache, Zgura, Galca, Bodescu, Enache, Maria and Parvulescu. This is an open-access article distributed under the terms of the Creative Commons Attribution License (CC BY). The use, distribution or reproduction in other forums is permitted, provided the original author(s) and the copyright owner are credited and that the original publication in this journal is cited, in accordance with accepted academic practice. No use, distribution or reproduction is permitted which does not comply with these terms.



Efficient Mechanochemical Bifunctional Nanocatalysts for the Conversion of Isoeugenol to Vanillin

Somayeh Ostovar^{1,2}, Ana Franco², Alain R. Puente-Santiago², María Pinilla-de Dios², Daily Rodríguez-Padrón², Hamid R. Shaterian¹ and Rafael Luque^{2,3*}

¹ Department of Chemistry, University of Sistan and Baluchestan, Zahedan, Iran, ² Grupo FQM-383, Departamento de Química Orgánica, Universidad de Córdoba, Córdoba, Spain, ³ Peoples Friendship University of Russia, Moscow, Russia

OPEN ACCESS

Edited by:

Manoj B. Gawande,
Palacký University Olomouc, Czechia

Reviewed by:

Dinesh Nanaji Sawant,
Leibniz Institut für Katalyse (LG),
Germany

Carmen Moreno-Marrodan,
Istituto di Chimica dei Composti
OrganoMetallici (CNR), Italy

*Correspondence:

Rafael Luque
q62alsor@uco.es

Specialty section:

This article was submitted to
Green and Sustainable Chemistry,
a section of the journal
Frontiers in Chemistry

Received: 15 December 2017

Accepted: 08 March 2018

Published: 03 April 2018

Citation:

Ostovar S, Franco A,
Puente-Santiago AR, Pinilla-de
Dios M, Rodríguez-Padrón D,
Shaterian HR and Luque R (2018)
Efficient Mechanochemical
Bifunctional Nanocatalysts for the
Conversion of Isoeugenol to Vanillin.
Front. Chem. 6:77.
doi: 10.3389/fchem.2018.00077

A bifunctional nanocatalyst composed of iron containing SBA-15 material modified with sulfonic acid groups was synthesized by a mechanochemical approach. A full characterization of the obtained nanocatalyst was performed by N₂ physisorption isotherms analysis, transmission electron microscopy (TEM), X-ray powder diffraction (XRD) and Fourier-Infrared Spectroscopy (FT-IR). The mechanochemically synthesized nanocatalyst displays a high isoeugenol conversion to vanillin under mild conditions using H₂O₂ as oxidizing agent. Interestingly, this conversion resulted to be higher than that one obtained with the same material synthesized by an impregnation method. Additionally, the nanocatalyst showed excellent reusability over four successive runs under the studied reaction conditions.

Keywords: vanillin, nanocatalyst, catalytic oxidation, sulfonic groups, SBA-15

INTRODUCTION

Nowadays, in the field of Green Chemistry, the conversion of lignocellulosic biomass into value-added chemicals has become a challenging topic in both academic and industrial research areas (Zakzeski et al., 2010; Xu et al., 2014; Behling et al., 2016). Lignocellulosic biomass is composed by three major components (cellulose, hemicelluloses, and lignin), which offers specific opportunities to produce a myriad of valuable chemicals (Rinaldi et al., 2016). Among them, the highly functionalized and aromatic structure of lignin facilitates the designing of desired chemical platforms. In this sense, derived compounds of lignin such as eugenol, isoeugenol, and ferulic acid have been employed to obtain vanillin through a simple oxidation route (Gusevskaya et al., 2012). Vanillin (4-hydroxy-3-methoxybenzaldehyde) possesses a number of valuable applications for food, beverages, perfumery and pharmaceutical industries owed to it represent the principal flavor and aroma component in vanilla. Currently, the major amount of vanillin is obtained from petro-based compounds, especially guaiacol and glyoxylic acid by non-environmental friendly synthetic routes such as Riedel process, Huang et al. (2013) attaining low qualities of the final product. To overcome these drawbacks, greener strategies based on the catalytic oxidation of lignin model compounds have been developed using metal functionalized mesoporous silica material as efficient nanocatalysts (Augugliaro et al., 2012; Franco et al., 2017).

Noteworthy, it has been reported that the anchorage of organic functional moieties like –COOH and –SH can interact with silanol groups of the mesoporous silica framework and control

its surfaces properties and consequently its catalytic performance (Li and Yan, 2010; Rajabi et al., 2011). Among various functionalized groups, sulfonic acid group cause a remarkable increase on the catalytic performance of the catalysts due to its favored interactions with the metal active sites and its surface acid properties (Akiyama et al., 2011). Incorporation of sulfonic groups on the surface of ordered mesoporous such as SBA-15 and MCM-41 is performed generally by two step process (Kapoor et al., 2008): co-condensation or anchoring of -SH containing alkoxide precursors and the subsequence oxidation in the present of H_2O_2 , which are somewhat complicate and incomplete routes (Melero et al., 2006). In previous works, the lack of order in few domains of sulfonic groups at the pore surfaces have decreased the catalytic yields caused by the aggregation of nanoparticles on the outer surface of the nanocatalysts (Kim et al., 2009; Jackson et al., 2013). For these reasons, the designing of novel efficient synthetic routes toward the synthesis of high performance nanocatalysts composed of metal containing mesoporous silica modified with sulfonic acids groups is still a challenge.

In this work, we propose an unprecedented one-pot mechanochemical synthesis of bifunctional nanocatalysts (Figure 1) based on iron containing SBA-15 functionalized with sulfonic groups ($\text{Fe-SBA15-HSO}_3^{\text{BM}}$) for the selective oxidation of isoeugenol to vanillin. The methodology used represents a greener and innovative route to construct highly functionalized mesoporous silica nanomaterials taking advantage of their nanochannels with controllable pore size, high surface area and tunable reactivity. Also, we have compared the catalytic performance of the novel nanocatalysts with others synthesized

by conventional methods such as the ball milled/ impregnation method ($\text{Fe-SBA15-HSO}_3^{\text{BM-IM}}$).

EXPERIMENTAL

Materials

All chemicals chloride were obtained from Sigma–Aldrich with pure analytical degree.

Synthesis of SBA-15

The ordered mesoporous silica SBA-15 was synthesized following a procedure described in the literature (Jarry et al., 2006). The triblock copolymer Pluronic P123 (0.41 mmol) was dissolved in a HCl aqueous solution (2M) at 35°C . Subsequently, Tetraethyl ortho-silicate (TEOS) (25 mmol) was added drop wise to the solution mentioned above. The resulted solution was agitated for 24 h at 35°C . After that the mixture was subjected to a hydrothermal treatment in an oven at 100°C for 48 h. The resulting material was filtered and dried at 60°C . Finally, the template was calcined at 550°C for 8 h to remove it.

Preparation of $\text{Fe-SBA-HSO}_3^{\text{BM}}$ Nanocatalysts

$\text{Fe-SBA-HSO}_3^{\text{BM}}$ catalyst was prepared using 0.5 g of SBA-15 as silica support, 1.34 g of $\text{Fe}(\text{NO}_3)_3 \cdot 9\text{H}_2\text{O}$ as iron precursor, 0.25 mL of propionic acid and 0.5 mL of sulfuric acid in a planetary ball mill (Retsch PM-1000) at 350 rpm for 15 min, employing a 125 mL reaction chamber and eighteen 10 mm stainless steel balls (Pineda et al., 2012). Subsequently the

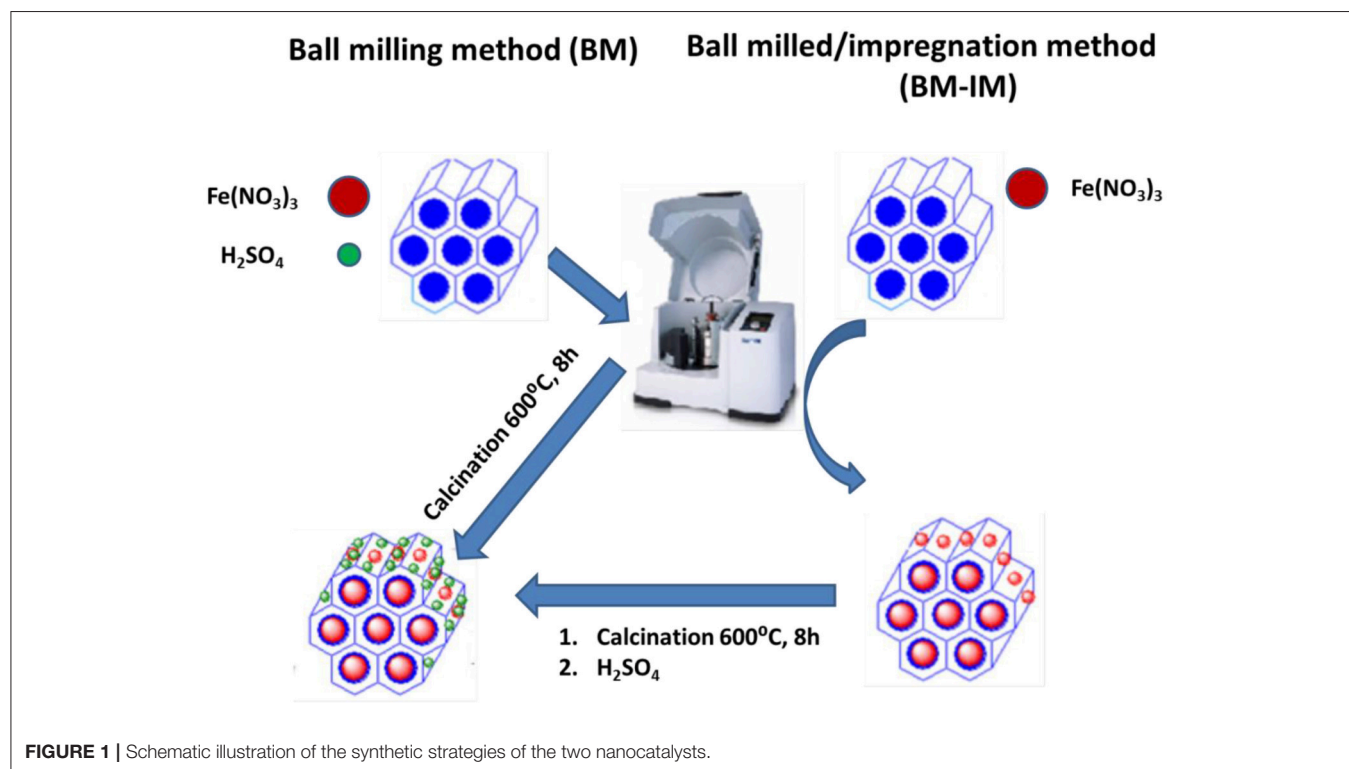


FIGURE 1 | Schematic illustration of the synthetic strategies of the two nanocatalysts.

obtained composite was heated up slowly to 800°C for 8 h using an extractor to remove the possible gases formed during the calcination process.

Preparation of Fe-SBA- $\text{HSO}_3^{\text{BM-IM}}$ Nanocatalysts

The Fe-SBA- HSO_3^{IM} catalyst was prepared by a two-step protocol. Firstly, 0.5 g of SBA-15, 1.34 g of $\text{Fe}(\text{NO}_3)_3 \cdot 9\text{H}_2\text{O}$ and 0.25 mL of propionic acid were milled in a planetary ball mill (Retsch PM-1000) at 350 rpm for 15 min. The obtained material was calcined

at 600°C for 8 h. Secondly, 10 mL of sulfuric acid was added drop wise to 1 g of the obtained Fe-SBA-15. After filtration, the solid was washed with distilled water, was heated up slowly to 800°C for 8 h using an extractor to remove the possible gases formed during the calcination process and dried overnight.

Catalyst Characterization

Low-angle XRD patterns were recorded on a Bruker D8 Discover diffractometer equipped with a goniometer Bragg Brentano θ/θ of high precision, and coupled to a Cu X-ray tube. The surface

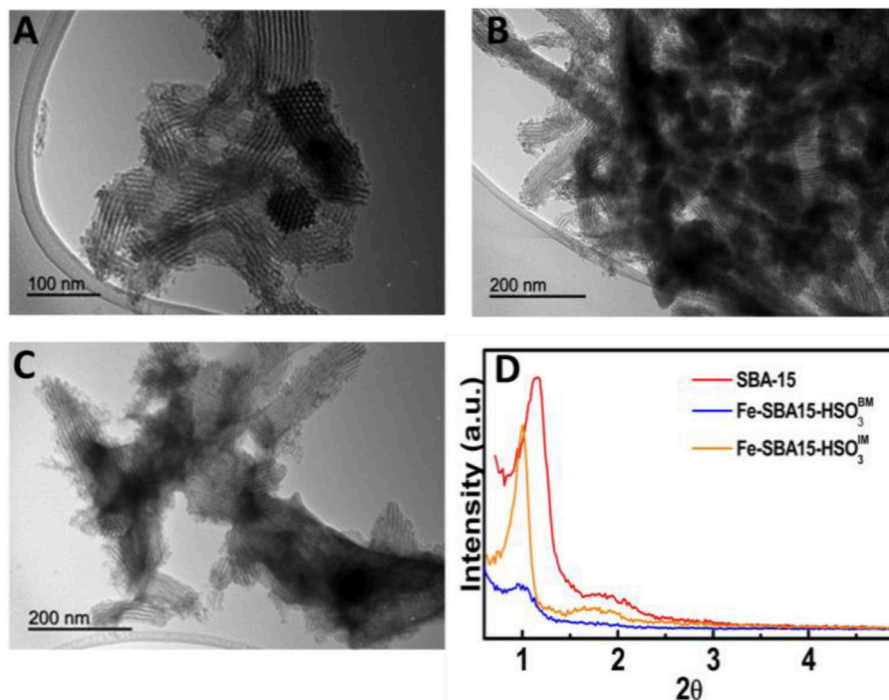


FIGURE 2 | TEM images of (A) SBA-15, (B) Fe-SBA15- HSO_3^{BM} nanocatalyst, (C) Fe-SBA15- $\text{HSO}_3^{\text{BM-IM}}$, and (D) small-angle XRD patterns of the nanocatalysts.

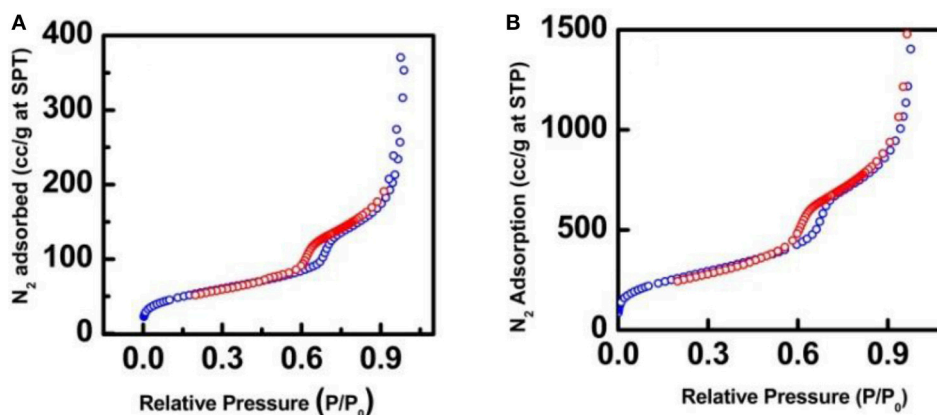


FIGURE 3 | N_2 adsorption-desorption isotherm for (A) Fe-SBA15- HSO_3^{BM} and (B) Fe-SBA15- $\text{HSO}_3^{\text{BM-IM}}$ nanocatalysts.

area and pore volume were calculated from N₂ adsorption-desorption isotherms at liquid nitrogen temperature (77 K) in a Micromeritics ASAP 2000 instrument. The samples were previously degassed for 24 h at 130°C at vacuum conditions ($p < 10^{-2}$ Pa).

TEM analysis was performed in the FEI Tecnai G2 system, integrated to a charge coupling device camera. To the preparation, the samples were diluted in ethanol and deposited on a copper grid.

The FT-IR spectra of both nanocatalysts were recorded on an infrared spectrophotometer (ABB MB3000 with Horizon MBTM software), equipped with an ATR PIKE MIRacleTM sampler and a ZnSe window employing 256 scans at a resolution of 16 cm⁻¹.

The metal content of the catalysts was obtained by ICP-MS in an Elan DRC-e (PerkinElmer SCIEX) spectrometer. Prior to the analysis, the samples (≈25 mg) were digested using an acid mixture of HF/HNO₃/HCl 1:1:1. Dilutions were performed with miliQ water up to a maximum of 1% of HF₂⁻ in acid solution.

Energy dispersive X-ray spectroscopy (EDX) of the obtained materials was carried out using a JEOL JSM-6300 Scanning

Microscope with energy-dispersive X-ray analysis (EDX) at 20 kV.

Oxidation of Isoeugenol to Vanillin

The oxidation reactions were carried in a carousel system using isoeugenol (0.8 mL, 5 mmol), 30% H₂O₂ solution (1.2 mL, 0.04 mmol), 0.10 g of catalyst and acetonitrile (8 mL) as solvent. The reaction mixture was heated at 90°C for 24 h. The progress of the reaction was monitored by withdrawing samples at 20, 40 min, and then every 1 h for 24 h. Samples were analyzed in a HP5890 Series II Gas Chromatograph (60 mL min⁻¹ N₂ carrier flow, 20 psi column top head pressure) using a flame ionization detector (FID). The capillary HP-101 column (25 m × 0.2 mm × 0.2 μm) was employed.

RESULTS AND DISCUSSION

The synthesized materials showed a typical diffraction pattern of SBA15-like hexagonal structure which displayed a high intensity (100) peaks at 0.95° and additional order (110) peaks at 1.76° (Figure 2D). The transmission electron microscopy (TEM) images (Figures 2B,C) depicted that Fe containing nanoparticles with size ranging between 4 and 5.7 nm were successfully incorporated inside the nanochannels of SBA-15 (Figure 2A) through the two synthetic routes. However, significant changes in the nanoparticles distribution patterns were observed for the two nanocatalysts. The Fe-SBA15-HSO₃^{BM} frameworks have a highly homogeneous and well-dispersed distribution (Figure 2B) which is in agreement with similar materials reported for our group (Pineda et al., 2011); while in the Fe-SBA15-HSO₃^{BM-IM} are highly aggregated. Also, the small shifts to lower diffraction angles of the (100) peaks suggest a slight disordering around the pores while maintaining the hexagonal pore structure upon the synthesis of both nanocatalysts.

The nitrogen adsorption/desorption isotherms were performed to investigate the surface area and pore size properties of the synthesized nanocatalysts. The nanocatalysts possess the typical type IV isotherms and H1 hysteresis loops between 0.6 and 0.75 P/P₀ (Figure 3), which is a representative behavior of mesoporous materials that contain uniform cylindrical pores (Gao et al., 2007). Interestingly, nitrogen adsorption/desorption experiments displayed a pronounced decay of the surface areas and pore volumes of the nanocatalysts in comparison with the SBA-15 (Table 1). These results can be attributed to the occupation of the SiO₂ nanochannels for the iron nanoparticles during the synthesis of the nanocatalysts and possible calcination

TABLE 1 | Textural properties of the synthesized nanocatalysts.

Material	S _{BET} ^a (m ² g ⁻¹)	D _{BJH} ^b (nm)	V _{BJH} ^c (cm ³ g ⁻¹)
SBA-15	629	5.9	0.75
Fe-SBA15-HSO ₃ ^{BM}	194	5.3	0.27
Fe-SBA15-HSO ₃ ^{BM-IM}	373	5.4	0.35

^aS_{BET}, specific surface area was estimated by the Brunauer-Emmett-Teller (BET) equation.

^bD_{BJH}, mean pore size diameter was estimated by the Barret-Joyner-Halenda (BJH) equation.

^cV_{BJH}, pore volume was estimated by the Barret-Joyner-Halenda (BJH) equation.

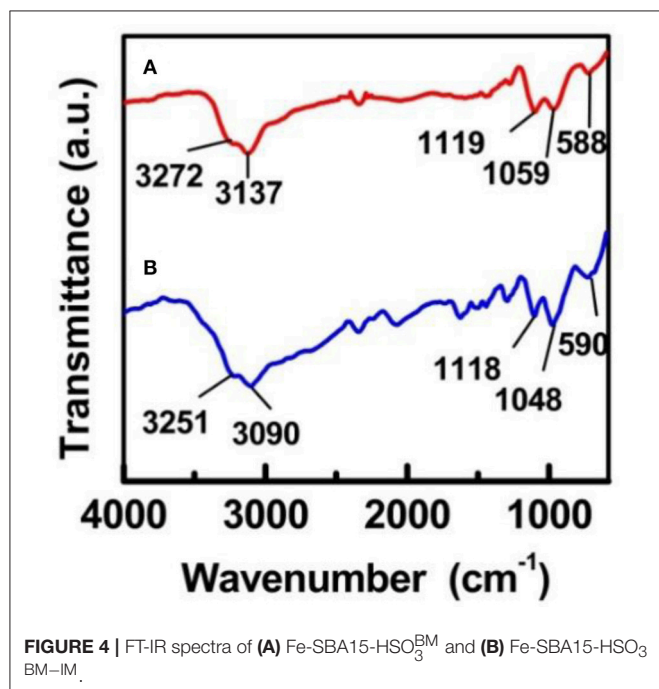


FIGURE 4 | FT-IR spectra of (A) Fe-SBA15-HSO₃^{BM} and (B) Fe-SBA15-HSO₃^{BM-IM}.

TABLE 2 | Elemental composition of the nanocatalysts.

	ICP-MS (wt%)		EDX (wt%)
	Fe	Fe	S
Fe-SBA15	22	21	–
Fe-SBA15-HSO ₃ ^{BM}	16	15	20
Fe-SBA15-HSO ₃ ^{BM-IM}	0.10	0.25	0.33

effects for the case of Fe-SBA15-HSO₃^{BM-IM} nanocatalysts (Zhang et al., 2015).

Figure 4 depicts the FT-IR results obtained for the Fe-SBA15-HSO₃^{BM} and Fe-SBA15-HSO₃^{IM} nanocatalysts respectively. In the high frequency regions the spectrum displays a broad band in the region of 2,700–3,600 cm⁻¹ which corresponds to -OH stretching absorption of the SO₃H groups. Bands appeared in the absorption ranges of 1,165–1,248 and 1,007–1,065 cm⁻¹ have been ascribed to the O=S=O asymmetric and symmetric stretching modes respectively. Also bands found in the range of 560–608 cm⁻¹ were assigned to the S-O stretching mode. All these IR bands strongly support the successful anchorage of the sulfonic groups on both nanocatalysts (Amoozadeh et al., 2016; Kolvari et al., 2016; Veisi et al., 2016).

The elemental composition of the Fe-SBA15-HSO₃^{BM} and Fe-SBA15-HSO₃^{IM} nanomaterials was determined by both, ICP-MS and EDX, as complementary techniques (**Table 2**). The ICP-MS

measurements of the Fe-SBA15-HSO₃^{BM} revealed an iron content of 16 wt%. This result was corroborated by EDX analysis, which displayed 15 and 20 wt% for iron and sulfur, respectively. These values strongly support the successful incorporation of sulfonic groups and iron in the SBA-15 by the applied mechanochemical protocol. Additionally, the elemental content of Fe-SBA15-HSO₃^{IM} was determined and compared with the values obtained for Fe-SBA15 before the impregnation process. It was observed a decrease in the iron content after the functionalization of the Fe-SBA15, which have been attributed to the leaching of iron. The high incorporation of iron oxide nanoparticles using the BM method suggests that this approach could represent a new option in the design of novel functionalized nanocatalysts.

The catalytic behavior of both nanocatalysts was subsequently investigated to get insights on the effects of their structural variations over the selective oxidation of isoeugenol (**Table 3**, **Figures 5**, **6**). Low activities were observed in the systems in the absence of the nanocatalysts and in the presence of the

TABLE 3 | Catalytic performances of the nanocatalysts toward the isoeugenol oxidation^a.

Entry	Catalyst	Time (h)	Conversion (% mol)	Selectivity (% mol)		
				vanillin	Diphenyl ether	Unidentified products
1	Blank	1	18	13	64	23
2	15-SBA	1	34	31	49	20
3	FeSBA-15HSO ₃ ^{BM}	1	93	50	1.8	47
4	FeSBA-15HSO ₃ ^{BM-IM}	1	22	20	63	11

^aReaction conditions: 0.1 g catalyst, 8 mL acetonitrile, 0.8 mL isoeugenol, 1.2 mL H₂O₂, T = 90°C, time: 1 h.

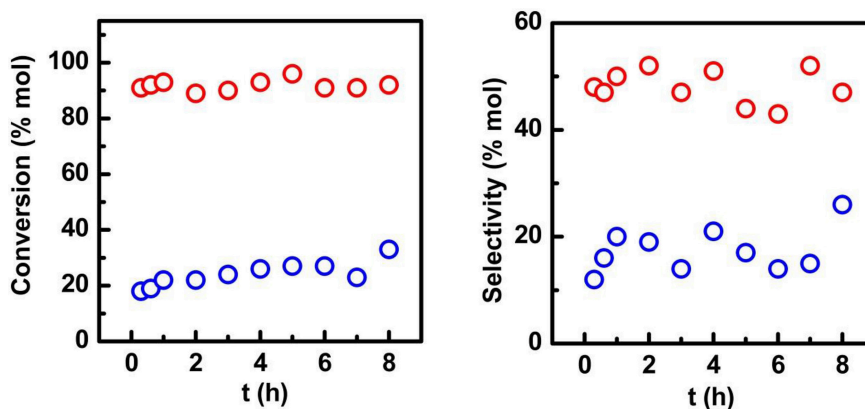


FIGURE 5 | Time dependent conversion and selectivity to vanillin profiles for (red circles) Fe-SBA15-HSO₃^{BM} and (blue circles) Fe-SBA15-HSO₃^{BM-IM} nanocatalysts. Reaction conditions: 0.1 g catalyst, 8 mL acetonitrile, 0.8 mL isoeugenol, 1.2 mL H₂O₂, T = 90°C, time: 1 h.

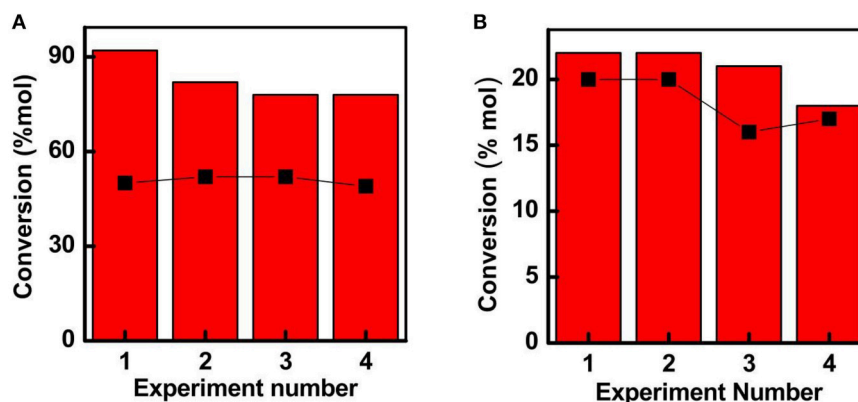


FIGURE 6 | Recycle activities obtained for **(A)** Fe-SBA15-HSO₃^{BM} and **(B)** Fe-SBA15-HSO₃^{BM-IM} toward the selective oxidation of isoeugenol to vanillin. Selectivity data for both nanocatalysts is inserted by the black squares representation. Reaction conditions: 0.1 g catalyst, 8 mL acetonitrile, 0.8 mL isoeugenol, 1.2 mL H₂O₂, *T* = 90°C, time: 1 h.

SBA-15 (Table 3 entry 1, 2). Under optimized reaction conditions (Table 3, entry 3), the Fe-SBA15-HSO₃^{BM} nanocatalyst showed a remarkable higher conversion and selectivity values of 93 and 51% respectively for the selective oxidation of the isoeugenol to vanillin. The lower conversion of the Fe-SBA15-HSO₃^{IM} (Table 3 entry 4) could be associated to both, the leaching of the Fe content during the synthesis of the material and the high aggregation of the nanoparticles on specific areas of the mesoporous silica materials which induces the disorganization of the sulfonic acid groups domains.

The time dependent conversion and selectivity profiles of the nanocatalysts are shown in the Figure 5. The nanocatalyst synthesized by the mechanochemistry approach displayed a high conversion and selectivity which validates its excellent catalytic performance, while the Fe-SBA15-HSO₃^{BM-IM} nanocatalyst achieved just a 33% after 8 h of reaction.

The reusability of the catalysts constitutes an important parameter to take into account for future applications. At the optimum conditions, the recycling experiments were performed to investigate the stability of the reused catalysts (Figure 6). Noteworthy, the Fe-SBA15-HSO₃^{BM} nanocatalyst could be reutilized for at least four catalytic runs without a substantial decay in the activity, suggesting that there is not leaching of the iron nanoparticles during the reaction process. In summary, it have been demonstrated that the iron containing sulfonic acid-functionalized mesoporous silica framework synthesized by a mechanochemical procedure induces a suitable stabilization of the small iron NPs homogeneously distributed inside of the mesoporous framework favoring the enhancement of the catalytic activity of the nanoreactor.

CONCLUSIONS

In summary, we have prepared an efficient heterogeneous nanocatalyst for the selective oxidation of the isoeugenol

to vanillin composed of sulfonic acid functionalized metal mesoporous silica framework using a one-step mechanochemical approach. The catalyst display a framework formed by a highly disperse small iron nanoparticles on the mesoporous silica stabilized by the sulfonic acids domains which induces the enhancement of the catalytic performance of the nanoreactors toward the selective oxidation of the isoeugenol. The work presented here constitutes a significant contribution, not only in the fabrication of effective bifunctional heterogeneous catalysts for the selective oxidation of the isoeugenol to vanillin, but also unraveling the structure,function relationship of the synthesized bifunctional catalysts.

AUTHOR CONTRIBUTIONS

SO conducted the catalytic reactions and wrote the first draft of the manuscript. AF conducted the synthesis of the catalyst. DR-P performed all the characterization of the materials. AP-S conducted interpretation of the materials and catalytic data. MP-dD revised the manuscript, discussed the results and improved the manuscript for submission. HS and RL conceived the concept of the paper, planned the experiments and revised, rewrote the final manuscript.

ACKNOWLEDGMENTS

RL gratefully acknowledges MINECO as well as FEDER funds for funding under project CTQ2016-78289-P and financial support from the University of Cordoba (Spain). HS gratefully acknowledges Sistan and Baluchestan University of Iran for the financial support of the research as well as Iran Nanotechnology Initiative Council for complementary financial supports. The publication has been prepared with support of RUDN University Program 5-100.

REFERENCES

- Akiyama, G., Matsuda, R., Sato, H., Takata, M., and Kitagawa, S. (2011). Cellulose hydrolysis by a new porous coordination polymer decorated with sulfonic acid functional groups. *Adv. Mater.* 23, 3294–3298. doi: 10.1002/adma.201101356
- Amoozadeh, A., Rahmani, S., Bitaraf, M., Abadi, F. B., and Tabrizian, E. (2016). Nano-zirconia as an excellent nano support for immobilization of sulfonic acid: a new, efficient and highly recyclable heterogeneous solid acid nanocatalyst for multicomponent reactions. *New J. Chem.* 40, 770–780. doi: 10.1039/C5NJ02430G
- Augugliaro, V., Camera-Roda, G., Loddo, V., Palmisano, V., Palmisano, L., Parrino, F., et al. (2012). Synthesis of vanillin in water by TiO₂ photocatalysis. *Appl. Catal. B Environ.* 111, 555–561. doi: 10.1016/j.apcatb.2011.11.007
- Behling, R., Valange, S., and Chatel, G. (2016). Heterogeneous catalytic oxidation for lignin valorization into valuable chemicals: what results? What limitations? What trends? *Green Chem.* 18, 1839–1854. doi: 10.1039/C5GC03061G
- Franco, A., De, S., Balu, A. M., Romero, A. A., and Luque, R. (2017). Selective oxidation of isoeugenol to vanillin over mechanochemically synthesized aluminosilicate supported transition metal catalysts. *Chem. Select.* 2, 9546–9551. doi: 10.1002/slct.201701273
- Gao, Z. F., Wang, L., Qi, T., Chu, J., and Zhang, Y. (2007). Synthesis, characterization, and cadmium(II) uptake of iminodiacetic acid-modified mesoporous SBA-15. *Colloids Surf. A Physicochem. Eng. Asp.* 304, 77–81. doi: 10.1016/j.colsurfa.2007.04.045
- Gusevskaya, E. V., Menini, L., Parreira, L. A., Mesquita, R. A., Kozlov, Y. N., Georgiy, B., et al. (2012). Oxidation of isoeugenol to vanillin by the “H₂O₂-vanadate-pyrazine-2-carboxylic acid” reagent. *J. Mol. Catal. A Chem.* 363, 140–147. doi: 10.1016/j.molcata.2012.06.001
- Huang, W. B., Du, C. Y., Jiang, J. A., and Ji, Y. F. (2013). Concurrent synthesis of vanillin and isovanillin. *Res. Chem. Intermed.* 39, 2849–2856. doi: 10.1007/s11164-012-0804-6
- Jackson, D. H. K., Wang, D., Gallo, J. M. R., Crisci, A. J., Scott, S. L., Dumesic, J. A., et al. (2013). Amine Catalyzed Atomic Layer Deposition of (3-Mercaptopropyl)trimethoxysilane for the Production of Heterogeneous Sulfonic Acid Catalysts. *Chem. Mater.* 25, 3844–3851. doi: 10.1021/cm401607g
- Jarry, B., Launay, F., Nogier, J. P., Montouillout, V., Gengembre, L., and Bonardet, J. L. (2006). Characterisation, acidity and catalytic activity of Ga-SBA-15 materials prepared following different synthesis procedures. *Appl. Catal. A* 309, 177–186. doi: 10.1016/j.apcata.2006.04.044
- Kapoor, M. P., Fujii, W., Kasama, Y., Yanagi, M., Nanbu, H., and Juneja, L. R. (2008). An alternate approach to the preparation of versatile sulfonic acid functionalized periodic mesoporous silicas with superior catalytic applications. *J. Mater. Chem. A* 18, 4683–4691. doi: 10.1039/b808248k
- Kim, H., Prakash, S., Mustain, W. E., and Kohl, P. A. (2009). Sol-gel based sulfonic acid-functionalized silica proton conductive membrane. *J. Power Sources* 193, 562–569. doi: 10.1016/j.jpowsour.2009.04.040
- Kolvári, E., Koukabi, N., Hosseini, M. M., Vahidian, M., and Ghobadi, E. (2016). Nano-ZrO₂ sulfuric acid: a heterogeneous solid acid nano catalyst for Biginelli reaction under solvent free conditions. *RSC Adv.* 6, 7419–7425. doi: 10.1039/C5RA19350H
- Li, Y., and Yan, B. (2010). Functionalized mesoporous SBA-15 with CeF₃: Eu³⁺ nanoparticle by three different methods: synthesis, characterization, and photoluminescence. *Nanoscale Res. Lett.* 5, 701–708. doi: 10.1007/s11671-010-9534-0
- Melero, J. A., van Grieken, R., and Morales, G. (2006). Advances in the synthesis and catalytic applications of organosulfonic-functionalized mesostructured materials. *Chem. Rev.* 106, 3790–3812. doi: 10.1021/cr050994h
- Pineda, A., Balu, A. M., Campelo, J. M., Romero, A. A., Carmona, D., Balas, F., et al. (2011). A dry milling approach for the synthesis of highly active nanoparticles supported on porous materials. *ChemSusChem* 4, 1561–1565. doi: 10.1002/cssc.201100265
- Pineda, A., Balu, A. M., Campelo, J. M., Luque, R., Romero, A. A., and Serrano-Ruiz, J. C. (2012). High alkylation activities of ball-milled synthesized low-load supported iron oxide nanoparticles on mesoporous aluminosilicates. *Catal. Today* 187, 65–69. doi: 10.1016/j.cattod.2012.02.028
- Rajabi, F., Naserian, S., Primo, A., and Luque, R. (2011). Efficient and highly selective aqueous oxidation of sulfides to sulfoxides at room temperature catalysed by supported iron oxide nanoparticles on SBA-15. *Adv. Synth. Catal.* 353, 2060–2066. doi: 10.1002/adsc.201100149
- Rinaldi, R., Jastrzebski, R., Clough, M. T., Ralph, J., Kennema, M., Bruijninx, P. C., et al. (2016). Paving the way for lignin valorisation: recent advances in bioengineering, biorefining and catalysis. *Angew. Chem. Int. Ed.* 55, 8164–8215. doi: 10.1002/anie.201510351
- Veisi, H., Taheri, S., and Hemmati, S. (2016). Preparation of polydopamine sulfamic acid-functionalized magnetic Fe₃O₄ nanoparticles with a core/shell nanostructure as heterogeneous and recyclable nanocatalysts for the acetylation of alcohols, phenols, amines and thiols under solvent-free conditions. *Green Chem.* 18, 6337–6348. doi: 10.1039/C6GC01975G
- Xu, C. P., Arancon, R. A., Labidi, J., and Luque, R. (2014). Lignin depolymerisation strategies: towards valuable chemicals and fuels. *Chem. Soc. Rev.* 43, 7485–7500. doi: 10.1039/C4CS00235K
- Zakzeski, J., Bruijninx, P. C., Jongerius, A. L., and Weckhuysen, B. M. (2010). The catalytic valorization of lignin for the production of renewable chemicals. *Chem. Rev.* 110, 3552–3599. doi: 10.1021/cr900354u
- Zhang, G. L., Qin, L., Wu, Y. J., Xu, Z., and Guo, X. (2015). Iron oxide nanoparticles immobilized to mesoporous NH₂-SiO₂ spheres by sulfonic acid functionalization as highly efficient catalysts. *Nanoscale* 7, 1102–1109. doi: 10.1039/C4NR05884D

Conflict of Interest Statement: The authors declare that the research was conducted in the absence of any commercial or financial relationships that could be construed as a potential conflict of interest.

Copyright © 2018 Ostovar, Franco, Puente-Santiago, Pinilla-de Dios, Rodríguez-Padrón, Shaterian and Luque. This is an open-access article distributed under the terms of the Creative Commons Attribution License (CC BY). The use, distribution or reproduction in other forums is permitted, provided the original author(s) and the copyright owner are credited and that the original publication in this journal is cited, in accordance with accepted academic practice. No use, distribution or reproduction is permitted which does not comply with these terms.

Advantages of publishing in Frontiers



OPEN ACCESS

Articles are free to read
for greatest visibility
and readership



FAST PUBLICATION

Around 90 days
from submission
to decision



HIGH QUALITY PEER-REVIEW

Rigorous, collaborative,
and constructive
peer-review



TRANSPARENT PEER-REVIEW

Editors and reviewers
acknowledged by name
on published articles

Frontiers

Avenue du Tribunal-Fédéral 34
1005 Lausanne | Switzerland

Visit us: www.frontiersin.org

Contact us: info@frontiersin.org | +41 21 510 17 00



REPRODUCIBILITY OF RESEARCH

Support open data
and methods to enhance
research reproducibility



DIGITAL PUBLISHING

Articles designed
for optimal readership
across devices



FOLLOW US

[@frontiersin](https://twitter.com/frontiersin)



IMPACT METRICS

Advanced article metrics
track visibility across
digital media



EXTENSIVE PROMOTION

Marketing
and promotion
of impactful research



LOOP RESEARCH NETWORK

Our network
increases your
article's readership